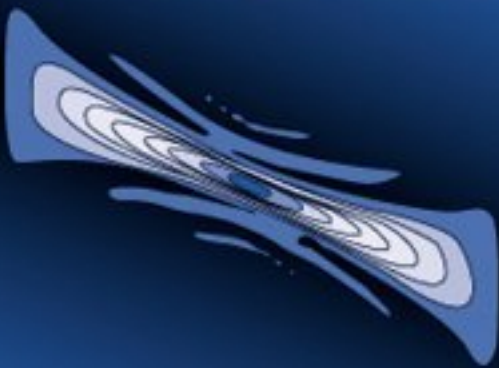


Radar Systems
Analysis *and* Design
Using
MATLAB



Bassem R. Mahafza

CHAPMAN & HALL/CRC

Radar Systems
Analysis and Design
Using
MATLAB

Radar Systems
Analysis and Design
Using
MATLAB

Bassem R. Mahafza, Ph.D.

COLSA Corporation
Huntsville, Alabama

CHAPMAN & HALL/CRC

Boca Raton London New York Washington, D.C.

Library of Congress Cataloging-in-Publication Data

Mahafza, Bassem R.

Radar systems & analysis and design using Matlab

p. cm.

Includes bibliographical references and index.

ISBN 1-58488-182-8 (alk. paper)

1. Radar. 2. System analysis—Data processing. 3. MATLAB. I. Title.

TK6575 .M27 2000

521.38484—dc21

00-026914

CIP

This book contains information obtained from authentic and highly regarded sources. Reprinted material is quoted with permission, and sources are indicated. A wide variety of references are listed. Reasonable efforts have been made to publish reliable data and information, but the author and the publisher cannot assume responsibility for the validity of all materials or for the consequences of their use.

Neither this book nor any part may be reproduced or transmitted in any form or by any means, electronic or mechanical, including photocopying, microfilming, and recording, or by any information storage or retrieval system, without prior permission in writing from the publisher.

The consent of CRC Press LLC does not extend to copying for general distribution, for promotion, for creating new works, or for resale. Specific permission must be obtained in writing from CRC Press LLC for such copying.

Direct all inquiries to CRC Press LLC, 2000 N.W. Corporate Blvd., Boca Raton, Florida 33431.

Trademark Notice: Product or corporate names may be trademarks or registered trademarks, and are used only for identification and explanation, without intent to infringe.

Visit the CRC Press Web site at www.crcpress.com

© 2000 by Chapman & Hall/CRC

No claim to original U.S. Government works

International Standard Book Number 1-58488-182-8

Library of Congress Card Number 00-026914

Printed in the United States of America 4 5 6 7 8 9 0

Printed on acid-free paper

Preface

Numerous books have been written on Radar Systems and Radar Applications. A limited set of these books provides companion software. There is need for a comprehensive reference book that can provide the reader with hands-on-like experience. The ideal radar book, in my opinion, should serve as a conclusive, detailed, and useful reference for working engineers as well as a textbook for students learning radar systems analysis and design. This book must assume few prerequisites and must stand on its own as a complete presentation of the subject. Examples and exercise problems must be included. User friendly software that demonstrates the theory needs to be included. This software should be reconfigurable to allow different users to vary the inputs in order to better analyze their relevant and unique requirements, and enhance understanding of the subject.

Radar Systems Analysis and Design Using MATLAB[®] concentrates on radar fundamentals, principles, and rigorous mathematical derivations. It also provides the user with a comprehensive set of MATLAB¹ 5.0 software that can be used for radar analysis and/or radar system design. All programs will accept user inputs or execute using the default set of parameters. This book will serve as a valuable reference to students and radar engineers in analyzing and understanding the many issues associated with radar systems analysis and design. It is written at the graduate level. Each chapter provides all the necessary mathematical and analytical coverage required for good understanding of radar theory. Additionally, dedicated MATLAB functions/programs have been developed for each chapter to further enhance the understanding of the theory, and provide a source for establishing radar system design requirements. This book includes over 1190 equations and over 230 illustrations and plots. There are over 200 examples and end-of-chapter problems. A solutions manual will be made available to professors using the book as a text. The philosophy behind *Radar Systems Analysis and Design Using MATLAB* is that radar systems should not be complicated to understand nor difficult to analyze and design.

All MATLAB programs and functions provided in this book can be downloaded from the CRC Press Web site (www.crcpress.com). For this purpose, create the following directory in your C-drive: C:\RSA. Copy all programs into this directory. The path tree should be as in Fig. F.1 in Appendix F. Users can execute a certain function/program GUI by typing: *file_name_driver*, where

1. All MATLAB functions and programs provided in this book were developed using MATLAB 5.0 - R11 with the Signal Processing Toolbox, on a PC with Windows 98 operating system.

file names are as indicated in Appendix F. The MATLAB functions and programs developed in this book include all forms of the radar equation: pulse compression, stretch processing, matched filter, probability of detection calculations with all Swerling models, High Range Resolution (HRR), stepped frequency waveform analysis, ghk tracking filter, Kalman filter, phased array antennas, and many more.

The first part of Chapter 1 describes the most common terms used in radar systems, such as range, range resolution, Doppler frequency, and coherency. The second part of this chapter develops the radar range equation in many of its forms. This presentation includes the low PRF, high PRF, search, bistatic radar, and radar equation with jamming. Radar losses are briefly addressed in this chapter. Chapter 2 discusses the Radar Cross Section (RCS). RCS dependency on aspect angle, frequency, and polarization are discussed. Target scattering matrix is developed. RCS formulas for many simple objects are presented. Complex object RCS is discussed, and target fluctuation models are introduced. Continuous wave radars and pulsed radars are discussed in Chapter 3. The CW radar equation is derived in this chapter. Resolving range and Doppler ambiguities is also discussed in detail.

Chapter 4 is intended to provide an overview of the radar probability of detection calculations and related topics. Detection of fluctuating targets including Swerling I, II, III, and IV models is presented and analyzed. Coherent and non-coherent integrations are also introduced. Cumulative probability of detecting analysis is in this chapter. Chapter 5 reviews radar waveforms, including CW, pulsed, and LFM. High Range Resolution (HRR) waveforms and stepped frequency waveforms are also analyzed.

The concept of the matched filter, and the radar ambiguity function constitute the topics of Chapter 6. Detailed derivations of many major results are presented in this chapter, including the coherent pulse train ambiguity function. Pulse compression is in Chapter 7. Analog and digital pulse compressions are also discussed in detail. This includes fast convolution and stretch processors. Binary phase codes and frequency codes are discussed.

Chapter 8 presents the phenomenology of radar wave propagation. Topics like multipath, refraction, diffraction, divergence, and atmospheric attenuation are included. Chapter 9 contains the concepts of clutter and Moving Target Indicator (MTI). Surface and volume clutter are defined and the relevant radar equations are derived. Delay line cancelers implementation to mitigate the effects of clutter is analyzed.

Chapter 10 has a brief discussion of radar antennas. The discussion includes linear and planar phased arrays. Conventional beamforming is in this chapter. Chapter 11 discusses target tracking radar systems. The first part of this chapter covers the subject of single target tracking. Topics such as sequential lobing, conical scan, monopulse, and range tracking are discussed in detail. The

second part of this chapter introduces multiple target tracking techniques. Fixed gain tracking filters such as the $\alpha\beta$ and the $\alpha\beta\gamma$ filters are presented in detail. The concept of the Kalman filter is introduced. Special cases of the Kalman filter are analyzed in depth.

Synthetic Aperture Radar (SAR) is the subject of Chapter 12. The topics of this chapter include: SAR signal processing, SAR design considerations, and the SAR radar equation. Arrays operated in sequential mode are discussed in this chapter. Chapter 13 presents an overview of signal processing. Finally, six appendices present discussion on the following: noise figure, decibel arithmetic, tables of the Fourier transform and Z-transform pairs, common probability density functions, and the MATLAB program and function name list.

MATLAB is a registered trademark
of The MathWorks, Inc.
For product information, please contact:
The MathWorks, Inc.
3 Apple Hill Drive
Natick, MA 01760-2098 USA
Tel: 508-647-7000
Fax: 508-647-7001
E-mail: info@mathworks.com
Web: www.mathworks.com

Bassem R. Mahafza
Huntsville, Alabama
January, 2000

Acknowledgment

I would like to acknowledge the following for help, encouragement, and support during the preparation of this book. First, I thank God for giving me the endurance and perseverance to complete this work. I could not have completed this work without the continuous support of my wife and four sons. The support and encouragement of all my family members and friends are appreciated. Special thanks to Dr. Andrew Ventre, Dr. Michael Dorsett, Mr. Edward Shamsi, and Mr. Skip Tornquist for reviewing and correcting different parts of the manuscript. Finally, I would like to thank Mr. Frank J. Collazo, the management, and the family of professionals at COLSA Corporation for their support.

To my sons:

*Zachary,
Joseph,
Jacob, and
Jordan*

To:

*My Wife,
My Mother,
and the memory of my Father*

Table of Contents

Preface

Acknowledgment

Chapter 1

Radar Fundamentals

1.1. Radar Classifications

1.2. Range

MATLAB Function “pulse_train.m”

1.3. Range Resolution

MATLAB Function “range_resolution.m”

1.4. Doppler Frequency

MATLAB Function “doppler_freq.m”

1.5. Coherence

1.6. The Radar Equation

MATLAB Function “radar_eq.m”

1.6.1. Low PRF Radar Equation

MATLAB Function “lprf_req.m”

1.6.2. High PRF Radar Equation

MATLAB Function “hprf_req.m”

1.6.3. Surveillance Radar Equation

MATLAB Function “power_aperture_eq.m”

1.6.4. Radar Equation with Jamming

Self-Screening Jammers (SSJ)

MATLAB Program “ssj_req.m”

Stand-Off Jammers (SOJ)

MATLAB Program “soj_req.m”

Range Reduction Factor

MATLAB Function “range_red_fac.m”

- 1.6.5. Bistatic Radar Equation
 - 1.7. Radar Losses
 - 1.7.1. Transmit and Receive Losses
 - 1.7.2. Antenna Pattern Loss and Scan Loss
 - 1.7.3. Atmospheric Loss
 - 1.7.4. Collapsing Loss
 - 1.7.5. Processing Losses
 - 1.7.6. Other Losses
 - 1.8. MATLAB Program and Function Listings
Problems
-

Chapter 2

Radar Cross Section (RCS)

- 2.1. RCS Definition
- 2.2. RCS Prediction Methods
- 2.3. RCS Dependency on Aspect Angle and Frequency
 - MATLAB Function "rcs_aspect.m"*
 - MATLAB Function "rcs-frequency.m"*
- 2.4. RCS Dependency on Polarization
 - 2.4.1. Polarization
 - 2.4.2. Target Scattering Matrix
- 2.5. RCS of Simple Objects
 - 2.5.1. Sphere
 - 2.5.2. Ellipsoid
 - MATLAB Function "rcs_ellipsoid.m"*
 - 2.5.3. Circular Flat Plate
 - MATLAB Function "rcs_circ_plate.m"*
 - 2.5.4. Truncated Cone (Frustum)
 - MATLAB Function "rcs_frustum.m"*
 - 2.5.5. Cylinder
 - MATLAB Function "rcs_cylinder.m"*
 - 2.5.6. Rectangular Flat Plate
 - MATLAB Function "rcs_rect_plate.m"*
 - 2.5.7. Triangular Flat Plate
 - MATLAB Function "rcs_isosceles.m"*
- 2.6. RCS of Complex Objects
- 2.7. RCS Fluctuations and Statistical Models
 - 2.7.1. RCS Statistical Models - Scintillation Models
 - Chi-Square of Degree 2m
 - Swerling I and II (Chi-Square of Degree 2)
 - Swerling III and IV (Chi-Square of Degree 4)
- 2.8. MATLAB Program/Function Listings
Problems

Chapter 3

Continuous Wave and Pulsed Radars

- 3.1. Functional Block Diagram
 - 3.2. CW Radar Equation
 - 3.3. Frequency Modulation
 - 3.4. Linear FM (LFM) CW Radar
 - 3.5. Multiple Frequency CW Radar
 - 3.6. Pulsed Radar
 - 3.7. Range and Doppler Ambiguities
 - 3.8. Resolving Range Ambiguity
 - 3.9. Resolving Doppler Ambiguity
 - 3.10. MATLAB Program “*range_calc.m*”
- Problems

Chapter 4

Radar Detection

- 4.1. Detection in the Presence of Noise
MATLAB Function “que_func.m”
- 4.2. Probability of False Alarm
- 4.3. Probability of Detection
MATLAB Function “marcumsq.m”
- 4.4. Pulse Integration
 - 4.4.1. Coherent Integration
 - 4.4.2. Non-Coherent Integration
MATLAB Function “improv_fac.m”
- 4.5. Detection of Fluctuating Targets
 - 4.5.1. Detection Probability Density Function
 - 4.5.2. Threshold Selection
MATLAB Function “incomplete_gamma.m”
MATLAB Function “threshold.m”
- 4.6. Probability of Detection Calculation
 - 4.6.1. Detection of Swerling V Targets
MATLAB Function “pd_swerling5.m”
 - 4.6.2. Detection of Swerling I Targets
MATLAB Function “pd_swerling1.m”
 - 4.6.3. Detection of Swerling II Targets
MATLAB Function “pd_swerling2.m”
 - 4.6.4. Detection of Swerling III Targets
MATLAB Function “pd_swerling3.m”
 - 4.6.5. Detection of Swerling IV Targets
MATLAB Function “pd_swerling4.m”
- 4.7. Cumulative Probability of Detection

- 4.8. Solving the Radar Equation
 - 4.9. Constant False Alarm Rate (CFAR)
 - 4.9.1. Cell-Averaging CFAR (Single Pulse)
 - 4.9.2. Cell-Averaging CFAR with
Non-Coherent Integration
 - 4.10. MATLAB Function and Program Listings
Problems
-

Chapter 5

Radar Waveforms Analysis

- 5.1. Low Pass, Band Pass Signals and Quadrature
Components
 - 5.2. CW and Pulsed Waveforms
 - 5.3. Linear Frequency Modulation Waveforms
 - 5.4. High Range Resolution
 - 5.5. Stepped Frequency Waveforms
 - 5.5.1. Range Resolution and Range Ambiguity
in SWF
MATLAB Function "hrr_profile.m"
 - 5.5.2. Effect of Target Velocity
 - 5.6. MATLAB Listings
Problems
-

Chapter 6

Matched Filter and the Radar Ambiguity Function

- 6.1. The Matched Filter SNR
- 6.2. The Replica
- 6.3. Matched Filter Response to LFM Waveforms
- 6.4. The Radar Ambiguity Function
- 6.5. Examples of the Ambiguity Function
 - 6.5.1. Single Pulse Ambiguity Function
MATLAB Function "single_pulse_ambg.m"
 - 6.5.2. LFM Ambiguity Function
MATLAB Function "lfm_ambg.m"
 - 6.5.3. Coherent Pulse Train Ambiguity Function
MATLAB Function "train_ambg.m"
- 6.6. Ambiguity Diagram Contours
- 6.7. MATLAB Listings
Problems

Chapter 7

Pulse Compression

- 7.1. Time-Bandwidth Product
 - 7.2. Radar Equation with Pulse Compression
 - 7.3. Analog Pulse Compression
 - 7.3.1. Correlation Processor
 - MATLAB Function “matched_filter.m”*
 - 7.3.2. Stretch Processor
 - MATLAB Function “stretch.m”*
 - 7.3.3. Distortion Due to Target Velocity
 - 7.3.4. Range Doppler Coupling
 - 7.4. Digital Pulse Compression
 - 7.4.1. Frequency Coding (Costas Codes)
 - 7.4.2. Binary Phase Codes
 - 7.4.3. Frank Codes
 - 7.4.4. Pseudo-Random (PRN) Codes
 - 7.5. MATLAB Listings
- Problems

Chapter 8

Radar Wave Propagation

- 8.1. Earth Atmosphere
 - 8.2. Refraction
 - 8.3. Ground Reflection
 - 8.3.1. Smooth Surface Reflection Coefficient
 - MATLAB Function “ref_coef.m”*
 - 8.3.2. Divergence
 - 8.3.3. Rough Surface Reflection
 - 8.4. The Pattern Propagation Factor
 - 8.4.1. Flat Earth
 - 8.4.2. Spherical Earth
 - 8.5. Diffraction
 - 8.6. Atmospheric Attenuation
 - 8.7. MATLAB Program “ref_coef.m”
- Problems

Chapter 9

Clutter and Moving Target Indicator (MTI)

- 9.1. Clutter Definition
- 9.2. Surface Clutter
 - 9.2.1. Radar Equation for Area Clutter

- 9.3. Volume Clutter
 - 9.3.1. Radar Equation for Volume Clutter
 - 9.4. Clutter Statistical Models
 - 9.5. Clutter Spectrum
 - 9.6. Moving Target Indicator (MTI)
 - 9.7. Single Delay Line Canceler
 - MATLAB Function “single_canceler.m”*
 - 9.8. Double Delay Line Canceler
 - MATLAB Function “double_canceler.m”*
 - 9.9. Delay Lines with Feedback (Recursive Filters)
 - 9.10. PRF Staggering
 - 9.11. MTI Improvement Factor
 - 9.12. Subclutter Visibility (SCV)
 - 9.13. Delay Line Cancelers with Optimal Weights
 - 9.14. MATLAB Program/Function Listings
- Problems
-

Chapter 10

Radar Antennas

- 10.1. Directivity, Power Gain, and Effective Aperture
 - 10.2. Near and Far Fields
 - 10.3. Circular Dish Antenna Pattern
 - MATLAB Function “circ_aperture.m”*
 - 10.4. Array Antennas
 - 10.4.1. Linear Array Antennas
 - MATLAB Function “linear_array.m”*
 - 10.5. Array Tapering
 - 10.6. Computation of the Radiation Pattern via the DFT
 - 10.7. Array Pattern for Rectangular Planar Array
 - MATLAB Function “rect_array.m”*
 - 10.8. Conventional Beamforming
 - 10.9. MATLAB Programs and Functions
- Problems
-

Chapter 11

Target Tracking

Part I: Single Target Tracking

- 11.1. Angle Tracking
 - 11.1.1. Sequential Lobing
 - 11.1.2. Conical Scan
- 11.2. Amplitude Comparison Monopulse

MATLAB Function “mono_pulse.m”

- 11.3. Phase Comparison Monopulse
- 11.4. Range Tracking

Part II: Multiple Target Tracking

- 11.5. Track-While-Scan (TWS)
- 11.6. State Variable Representation of an LTI System
- 11.7. The LTI System of Interest
- 11.8. Fixed-Gain Tracking Filters
 - 11.8.1. The $\alpha\beta$ Filter
 - 11.8.2. The $\alpha\beta\gamma$ Filter

MATLAB Function “ghk_tracker.m”

- 11.9. The Kalman Filter
 - 11.9.1. The Singer $\alpha\beta\gamma$ -Kalman Filter
 - 11.9.2. Relationship between Kalman and $\alpha\beta\gamma$ Filters

MATLAB Function “kalman_filter.m”

- 11.10. MATLAB Programs and Functions
- Problems

Chapter 12

Synthetic Aperture Radar

- 12.1. Introduction
- 12.2. Real Versus Synthetic Arrays
- 12.3. Side Looking SAR Geometry
- 12.4. SAR Design Considerations
- 12.5. SAR Radar Equation
- 12.6. SAR Signal Processing
- 12.7. Side Looking SAR Doppler Processing
- 12.8. SAR Imaging Using Doppler Processing
- 12.9. Range Walk
- 12.10. Case Study
- 12.11. Arrays in Sequential Mode Operation
 - 12.11.1. Linear Arrays
 - 12.11.2. Rectangular Arrays
- 12.12. MATLAB Programs
- Problems

Chapter 13

Signal Processing

- 13.1. Signal and System Classifications

- 13.2. The Fourier Transform
- 13.3. The Fourier Series
- 13.4. Convolution and Correlation Integrals
- 13.5. Energy and Power Spectrum Densities
- 13.6. Random Variables
- 13.7. Multivariate Gaussian Distribution
- 13.8. Random Processes
- 13.9. Sampling Theorem
- 13.10. The Z-Transform
- 13.11. The Discrete Fourier Transform
- 13.12. Discrete Power Spectrum
- 13.13. Windowing Techniques
- Problems

Appendix A

Noise Figure

Appendix B

Decibel Arithmetic

Appendix C

Fourier Transform Table

Appendix D

Some Common Probability Densities

- Chi-Square with N degrees of freedom
- Exponential
- Gaussian
- Laplace
- Log-Normal
- Rayleigh
- Uniform
- Weibull

Appendix E

Z - Transform Table

Appendix F

MATLAB Program and Function Name List

Bibliography

Bibliography

- Abramowitz, M. and Stegun, I. A., Editors, *Handbook of Mathematical Functions, with Formulas, Graphs, and Mathematical Tables*, Dover Publications, 1970.
- Balanis, C. A., *Antenna Theory, Analysis and Design*, Harper & Row, New York, 1982.
- Barkat, M., *Signal Detection and Estimation*, Artech House, Norwood, MA, 1991.
- Barton, D. K., *Modern Radar System Analysis*, Artech House, Norwood, MA, 1988.
- Benedict, T. and Bordner, G., Synthesis of an Optimal set of Radar Track-While-Scan Smoothing Equations, *IRE Transaction on Automatic Control*, Ac-7. July 1962, pp. 27-32.
- Beyer, W. H., *CRC Standard Mathematical Tables*, 26th edition, CRC Press, Boca Raton, FL, 1981.
- Billetter, D. R., *Multifunction Array Radar*, Artech House, Norwood, MA, 1989.
- Blackman, S. S., *Multiple-Target Tracking with Radar Application*, Artech House, Norwood, MA, 1986.
- Blake, L. V., *A Guide to Basic Pulse-Radar Maximum Range Calculation Part I Equations, Definitions, and Aids to Calculation*, Naval Res. Lab. Report 5868, 1969.
- Blake, L. V., *Radar-Range Performance Analysis*, Lexington Books, Lexington, MA, 1980.
- Boothe, R. R., *A Digital Computer Program for Determining the Performance of an Acquisition Radar Through Application of Radar Detection Probability Theory*, U.S. Army Missile Command: Report No. RD-TR-64-2. Redstone Arsenal, Alabama, 1964.
- Brookner, E., Editor, *Aspects of Modern Radar*, Artech House, Norwood, MA, 1988.
- Brookner, E., Editor, *Practical Phased Array Antenna System*, Artech House, Norwood, MA, 1991.
- Brookner, E., *Radar Technology*, Lexington Books, Lexington, MA, 1996.
- Burdic, W. S., *Radar Signal Analysis*, Prentice-Hall, Englewood Cliffs, NJ, 1968.
- Brookner, E., *Tracking and Kalman Filtering Made Easy*, John Wiley & Sons, New York, 1998.
- Cadzow, J. A., *Discrete-Time Systems, an Introduction with Interdisciplinary Applications*, Prentice-Hall, Englewood Cliffs, NJ, 1973.

- Carlson, A. B., *Communication Systems, An Introduction to Signals and Noise in Electrical Communication*, 3rd edition, McGraw-Hill, New York, 1986.
- Carpentier, M. H., *Principles of Modern Radar Systems*, Artech House, Norwood, MA, 1988.
- Compton, R. T., *Adaptive Antennas*, Prentice-Hall, Englewood Cliffs, NJ, 1988.
- Costas, J. P., A Study of a Class of Detection Waveforms Having Nearly Ideal Range-Doppler Ambiguity Properties, *Proc. IEEE* 72, 1984, pp. 996-1009.
- DiFranco, J. V. and Rubin, W. L., *Radar Detection*. Artech House, Norwood, MA, 1980.
- Dillard, R. A. and Dillard, G. M., *Detectability of Spread-Spectrum Signals*, Artech House, Norwood, MA, 1989.
- Edde, B., *Radar - Principles, Technology, Applications*, Prentice-Hall, Englewood Cliffs, NJ, 1993.
- Fielding, J. E. and Reynolds, G. D., *VCCALC: Vertical Coverage Calculation Software and Users Manual*, Artech House, Norwood, MA, 1988.
- Gabriel, W. F., Spectral Analysis and Adaptive Array Superresolution Techniques, *Proc. IEEE*, Vol. 68, June 1980, pp. 654-666.
- Gelb, A., Editor, *Applied Optimal Estimation*, MIT Press, Cambridge, MA, 1974.
- Hamming, R. W., *Digital Filters*, 2nd edition, Prentice-Hall, Englewood Cliffs, NJ, 1983.
- Hanselman, D. and Littlefield, B., *Mastering Matlab 5, A Complete Tutorial and Reference*, Malab Curriculum Series, Prentice-Hall, Englewood Cliffs, NJ, 1998.
- Hirsch, H. L. and Grove, D. C., *Practical Simulation of Radar Antennas and Radomes*, Artech House, Norwood, MA, 1987.
- Hovanessian, S. A., *Radar System Design and Analysis*, Artech House, Norwood, MA, 1984.
- James, D. A., *Radar Homing Guidance for Tactical Missiles*, John Wiley & Sons, New York, 1986.
- Klauder, J. R., Price, A. C., Darlington, S., and Albershiem, W. J., The Theory and Design of Chirp Radars, *The Bell System Technical Journal*, Vol. 39, No. 4, 1960.
- Knott, E. F., Shaeffner, J. F., and Tuley, M. T., *Radar Cross Section*, 2nd edition, Artech House, Norwood, MA, 1993.
- Lativa, J., Low-Angle Tracking Using Multifrequency Sampled Aperture Radar, *IEEE - AES Trans.*, Vol. 27, No. 5, September 1991, pp.797-805.
- Levanon, N., *Radar Principles*, John Wiley & Sons, New York, 1988.
- Lewis, B. L., Kretschmer, Jr., F. F., and Shelton, W. W., *Aspects of Radar Signal Processing*, Artech House, Norwood, MA, 1986.

- Long, M. W., *Radar Reflectivity of Land and Sea*, Artech House, Norwood, MA, 1983.
- Lothes, R. N., Szymanski, M. B., and Wiley, R. G., *Radar Vulnerability to Jamming*, Artech House, Norwood, MA, 1990.
- Mahafza, B. R. and Polge, R. J., Multiple Target Detection Through DFT Processing in a Sequential Mode Operation of Real Two-Dimensional Arrays, *Proc. of the IEEE Southeast Conf. '90*, New Orleans, LA, April 1990, pp. 168-170.
- Mahafza, B. R., Heifner, L.A., and Gracchi, V. C., Multitarget Detection Using Synthetic Sampled Aperture Radars (SSAMAR), *IEEE - AES Trans.*, Vol. 31, No. 3, July 1995, pp. 1127-1132.
- Mahafza, B. R. and Sajjadi, M., Three-Dimensional SAR Imaging Using a Linear Array in Transverse Motion, *IEEE - AES Trans.*, Vol. 32, No. 1, January 1996, pp. 499-510.
- Mahafza, B. R., *Introduction to Radar Analysis*, CRC Press, Boca Raton, FL, 1998.
- Marchand, P., *Graphics and GUIs with Matlab*, 2nd edition, CRC Press, Boca Raton, FL, 1999.
- Marcum, J. I., A Statistical Theory of Target Detection by Pulsed Radar, Mathematical Appendix, *IRE Trans.*, Vol. IT-6, April 1960, pp. 145-267.
- Meeks, M. L., *Radar Propagation at Low Altitudes*, Artech House, Norwood, MA, 1982.
- Melsa, J. L. and Cohn, D. L., *Decision and Estimation Theory*, McGraw-Hill, New York, 1978.
- Mensa, D. L., *High Resolution Radar Imaging*, Artech House, Norwood, MA, 1984.
- Meyer, D. P. and Mayer, H. A., *Radar Target Detection: Handbook of Theory and Practice*, Academic Press, New York, 1973.
- Monzingo, R. A. and Miller, T. W., *Introduction to Adaptive Arrays*, John Wiley & Sons, New York, 1980.
- Morchin, W., *Radar Engineer's Sourcebook*, Artech House, Norwood, MA, 1993.
- Morris, G. V., *Airborne Pulsed Doppler Radar*, Artech House, Norwood, MA, 1988.
- Nathanson, F. E., *Radar Design Principles*, 2nd edition, McGraw-Hill, New York, 1991.
- Navarro, Jr., A. M., *General Properties of Alpha Beta, and Alpha Beta Gamma Tracking Filters*, Physics Laboratory of the National Defense Research Organization TNO, Report PHL 1977-92, January 1977.
- North, D. O., An Analysis of the Factors which Determine Signal/Noise Discrimination in Pulsed Carrier Systems, *Proc. IEEE* 51, No. 7, July 1963, pp. 1015-1027.
- Oppenheim, A. V. and Schaffer, R. W., *Discrete-Time Signal Processing*, Prentice-Hall, Englewood Cliffs, NJ, 1989.

- Oppenheim, A. V., Willsky, A. S., and Young, I. T., *Signals and Systems*, Prentice-Hall, Englewood Cliffs, NJ, 1983.
- Orfanidis, S. J., *Optimum Signal Processing, an Introduction*, 2nd edition, McGraw-Hill, New York, 1988.
- Papoulis, A., *Probability, Random Variables, and Stochastic Processes*, second edition, McGraw-Hill, New York, 1984.
- Parl, S. A., New Method of Calculating the Generalized Q Function, *IEEE Trans. Information Theory*, Vol. IT-26, No. 1, January 1980, pp. 121-124.
- Peebles, Jr., P. Z., *Probability, Random Variables, and Random Signal Principles*, McGraw-Hill, New York, 1987.
- Peebles, Jr., P. Z., *Radar Principles*, John Wiley & Sons, New York, 1998.
- Pettit, R. H., *ECM and ECCM Techniques for Digital Communication Systems*, Lifetime Learning Publications, New York, 1982.
- Polge, R. J., Mahafza, B. R., and Kim, J. G., *Extension and Updating of the Computer Simulation of Range Relative Doppler Processing for MM Wave Seekers*, Interim Technical Report, Vol. I, prepared for the U.S. Army Missile Command, Redstone Arsenal, Alabama, January 1989.
- Polge, R. J., Mahafza, B. R., and Kim, J. G., Multiple Target Detection Through DFT Processing in a Sequential Mode Operation of Real or Synthetic Arrays, *IEEE 21th Southeastern Symposium on System Theory*, Tallahassee, FL, 1989, pp. 264-267.
- Poularikas, A. and Seely, S., *Signals and Systems*, PWS Publishers, Boston, MA, 1984.
- Rihaczek, A. W., *Principles of High Resolution Radars*, McGraw-Hill, New York, 1969.
- Ross, R. A., Radar Cross Section of Rectangular Flat Plate as a Function of Aspect Angle, *IEEE Trans. AP-14:320*, 1966.
- Ruck, G. T., Barrick, D. E., Stuart, W. D., and Krichbaum, C. K., *Radar Cross Section Handbook*, Volume 1, Plenum Press, New York, 1970.
- Ruck, G. T., Barrick, D. E., Stuart, W. D., and Krichbaum, C. K., *Radar Cross Section Handbook*, Volume 2, Plenum Press, New York, 1970.
- Rulf, B. and Robertshaw, G. A., *Understanding Antennas for Radar, Communications, and Avionics*, Van Nostrand Reinhold, 1987.
- Scanlan, M.J., Editor, *Modern Radar Techniques*, Macmillan, New York, 1987.
- Scheer, J. A. and Kurtz, J. L., Editors, *Coherent Radar Performance Estimation*, Artech House, Norwood, MA, 1993.
- Shanmugan, K. S. and Breipohl, A. M., *Random Signals: Detection, Estimation and Data Analysis*, John Wiley & Sons, New York, 1988.
- Singer, R. A., Estimating Optimal Tracking Filter Performance for Manned Maneuvering Targets, *IEEE Transaction on Aerospace and Electronics, AES-5*, July 1970, pp. 473-483.
- Skillman, W. A., *DETPROB: Probability of Detection Calculation Software and User's Manual*, Artech House, Norwood, MA, 1991.

- Skolnik, M. I., *Introduction to Radar Systems*, McGraw-Hill, New York, 1982.
- Skolnik, M. I., Editor, *Radar Handbook*, 2nd edition, McGraw-Hill, New York, 1990.
- Stearns, S. D. and David, R. A., *Signal Processing Algorithms*, Prentice-Hall, Englewood Cliffs, NJ, 1988.
- Stimson, G. W., *Introduction to Airborne Radar*, Hughes Aircraft Company, El Segundo, CA, 1983.
- Stratton, J. A., *Electromagnetic Theory*, McGraw-Hill, New York, 1941.
- Stremler, F. G., *Introduction to Communication Systems*, 3rd edition, Addison-Wesley, New York, 1990.
- Tzannes, N. S., *Communication and Radar Systems*, Prentice-Hall, Englewood Cliffs, NJ, 1985.
- Urkowitz, H., *Signal Theory and Random Processes*, Artech House, Norwood, MA, 1983.
- Urkowitz, H., *Decision and Detection Theory*, Unpublished Lecture Notes, Lockheed Martin Co., Moorestown, NJ.
- Vaughn, C. R., Birds and Insects as Radar Targets: A Review, *Proc. IEEE*, Vol. 73, No. 2, February 1985, pp. 205-227.
- Wehner, D. R., *High Resolution Radar*, Artech House, Norwood, MA, 1987.
- White, J. E., Mueller, D. D., and Bate, R. R., *Fundamentals of Astrodynamics*, Dover Publications, 1971.
- Ziemer, R. E. and Tranter, W. H., *Principles of Communications, Systems, Modulation, and Noise*, 2nd edition, Houghton Mifflin, Boston, MA, 1985.

1.1. Radar Classifications

The word radar is an abbreviation for RADio Detection And Ranging. In general, radar systems use modulated waveforms and directive antennas to transmit electromagnetic energy into a specific volume in space to search for targets. Objects (targets) within a search volume will reflect portions of this energy (radar returns or echoes) back to the radar. These echoes are then processed by the radar receiver to extract target information such as range, velocity, angular position, and other target identifying characteristics.

Radars can be classified as ground based, airborne, spaceborne, or ship based radar systems. They can also be classified into numerous categories based on the specific radar characteristics, such as the frequency band, antenna type, and waveforms utilized. Another classification is concerned with the mission and/or the functionality of the radar. This includes: weather, acquisition and search, tracking, track-while-scan, fire control, early warning, over the horizon, terrain following, and terrain avoidance radars. Phased array radars utilize phased array antennas, and are often called multifunction (multi-mode) radars. A phased array is a composite antenna formed from two or more basic radiators. Array antennas synthesize narrow directive beams that may be steered, mechanically or electronically. Electronic steering is achieved by controlling the phase of the electric current feeding the array elements, and thus the name phased arrays is adopted.

Radars are most often classified by the types of waveforms they use, or by their operating frequency. Considering the waveforms first, radars can be

Continuous Wave (CW) or Pulsed Radars (PR). CW radars are those that continuously emit electromagnetic energy, and use separate transmit and receive antennas. Unmodulated CW radars can accurately measure target radial velocity (Doppler shift) and angular position. Target range information cannot be extracted without utilizing some form of modulation. The primary use of unmodulated CW radars is in target velocity search and track, and in missile guidance. Pulsed radars use a train of pulsed waveforms (mainly with modulation). In this category, radar systems can be classified on the basis of the Pulse Repetition Frequency (PRF), as low PRF, medium PRF, and high PRF radars. Low PRF radars are primarily used for ranging where target velocity (Doppler shift) is not of interest. High PRF radars are mainly used to measure target velocity. Continuous wave as well as pulsed radars can measure both target range and radial velocity by utilizing different modulation schemes.

Table 1.1 has the radar classifications based on the operating frequency.

TABLE 1.1. Radar frequency bands.

Letter designation	Frequency (GHz)	New band designation (GHz)
<i>HF</i>	<i>0.003 - 0.03</i>	<i>A</i>
<i>VHF</i>	<i>0.03 - 0.3</i>	<i>A<0.25; B>0.25</i>
<i>UHF</i>	<i>0.3 - 1.0</i>	<i>B<0.5; C>0.5</i>
<i>L-band</i>	<i>1.0 - 2.0</i>	<i>D</i>
<i>S-band</i>	<i>2.0 - 4.0</i>	<i>E<3.0; F>3.0</i>
<i>C-band</i>	<i>4.0 - 8.0</i>	<i>G<6.0; H>6.0</i>
<i>X-band</i>	<i>8.0 - 12.5</i>	<i>I<10.0; J>10.0</i>
<i>Ku-band</i>	<i>12.5 - 18.0</i>	<i>J</i>
<i>K-band</i>	<i>18.0 - 26.5</i>	<i>J<20.0; K>20.0</i>
<i>Ka-band</i>	<i>26.5 - 40.0</i>	<i>K</i>
<i>MMW</i>	<i>Normally >34.0</i>	<i>L<60.0; M>60.0</i>

High Frequency (HF) radars utilize the electromagnetic waves' reflection off the ionosphere to detect targets beyond the horizon. Some examples include the United States Over The Horizon Backscatter (U.S. OTH/B) radar which operates in the frequency range of 5 – 28MHz, the U.S. Navy Relocatable Over The Horizon Radar (ROTHR), see Fig. 1.1, and the Russian Woodpecker radar. Very High Frequency (VHF) and Ultra High Frequency (UHF) bands are used for very long range Early Warning Radars (EWR). Some examples include the Ballistic Missile Early Warning System (BMEWS) search and track monopulse radar which operates at 245MHz (Fig. 1.2), the Perimeter and Acquisition Radar (PAR) which is a very long range multifunction phased

array radar, and the early warning PAVE PAWS multifunction UHF phased array radar. Because of the very large wavelength and the sensitivity requirements for very long range measurements, large apertures are needed in such radar systems.



Figure 1.1. U. S. Navy Over The Horizon Radar. Photograph obtained via the Internet.



Figure 1.2. Fylingdales BMEWS - United Kingdom. Photograph obtained via the Internet.

Radars in the L-band are primarily ground based and ship based systems that are used in long range military and air traffic control search operations. Most ground and ship based medium range radars operate in the S-band. For example, the Airport Surveillance Radar (ASR) used for air traffic control, and the ship based U.S. Navy AEGIS (Fig. 1.3) multifunction phased array are S-band radars. The Airborne Warning And Control System (AWACS) shown in Fig. 1.4 and the National Weather Service Next Generation Doppler Weather Radar (NEXRAD) are also S-band radars. However, most weather detection radar systems are C-band radars. Medium range search and fire control military radars and metric instrumentation radars are also C-band.



Figure 1.3. U. S. Navy AEGIS. Photograph obtained via the Internet.



Figure 1.4. U. S. Air Force AWACS. Photograph obtained via the Internet.

The X-band is used for radar systems where the size of the antenna constitutes a physical limitation; this includes most military multimode airborne radars. Radar systems that require fine target detection capabilities and yet cannot tolerate the atmospheric attenuation of higher frequency bands may also be X-band. The higher frequency bands (Ku, K, and Ka) suffer severe weather and atmospheric attenuation. Therefore, radars utilizing these frequency bands are limited to short range applications, such as the police traffic radars, short range terrain avoidance, and terrain following radars. Milli-Meter Wave (MMW) radars are mainly limited to very short range Radio Frequency (RF) seekers and experimental radar systems.

1.2. Range

Figure 1.5 shows a simplified pulsed radar block diagram. The time control box generates the synchronization timing signals required throughout the system. A modulated signal is generated and sent to the antenna by the modulator/transmitter block. Switching the antenna between the transmitting and receiving modes is controlled by the duplexer. The duplexer allows one antenna to be used to both transmit and receive. During transmission it directs the radar electromagnetic energy towards the antenna. Alternatively, on reception, it directs the received radar echoes to the receiver. The receiver amplifies the radar returns and prepares them for signal processing. Extraction of target information is performed by the signal processor block. The target's range, R , is computed by measuring the time delay, Δt ; it takes a pulse to travel the two-way path between the radar and the target. Since electromagnetic waves travel at the speed of light, $c = 3 \times 10^8$ m/sec, then

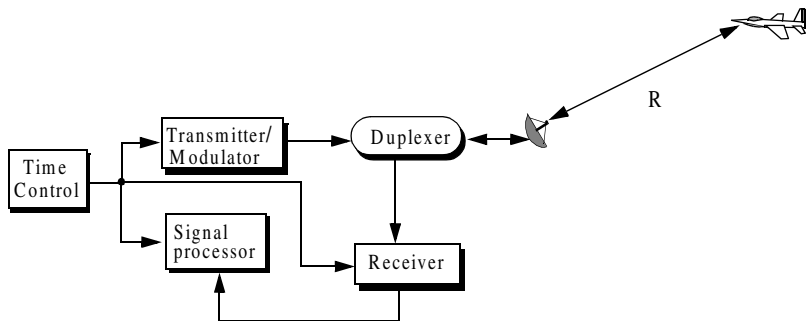


Figure 1.5. A simplified pulsed radar block diagram.

$$R = \frac{c\Delta t}{2} \quad (1.1)$$

where R is in meters and Δt is in seconds. The factor of $\frac{1}{2}$ is needed to account for the two-way time delay.

In general, a pulsed radar transmits and receives a train of pulses, as illustrated by Fig. 1.6. The Inter Pulse Period (IPP) is T , and the pulse width is τ . The IPP is often referred to as the Pulse Repetition Interval (PRI). The inverse of the PRI is the PRF, which is denoted by f_r ,

$$f_r = \frac{1}{PRI} = \frac{1}{T} \quad (1.2)$$

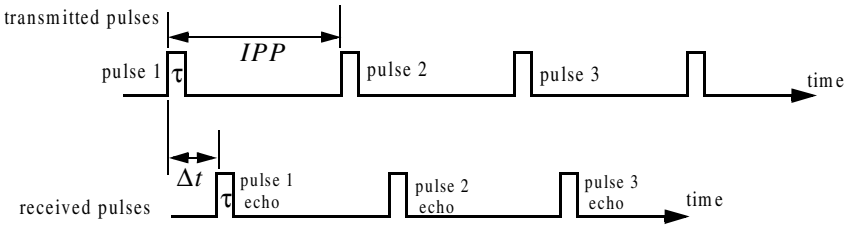


Figure 1.6. Train of transmitted and received pulses.

During each PRI the radar radiates energy only for τ seconds and listens for target returns for the rest of the PRI. The radar transmitting duty cycle (factor) d_t is defined as the ratio $d_t = \tau/T$. The radar average transmitted power is

$$P_{av} = P_t \times d_t, \quad (1.3)$$

where P_t denotes the radar peak transmitted power. The pulse energy is $E_p = P_t \tau = P_{av} T = P_{av} / f_r$.

The range corresponding to the two-way time delay T is known as the radar unambiguous range, R_u . Consider the case shown in Fig. 1.7. Echo 1 represents the radar return from a target at range $R_1 = c\Delta t/2$ due to pulse 1. Echo 2 could be interpreted as the return from the same target due to pulse 2, or it may be the return from a faraway target at range R_2 due to pulse 1 again. In this case,

$$R_2 = \frac{c\Delta t}{2} \quad \text{or} \quad R_2 = \frac{c(T + \Delta t)}{2} \quad (1.4)$$

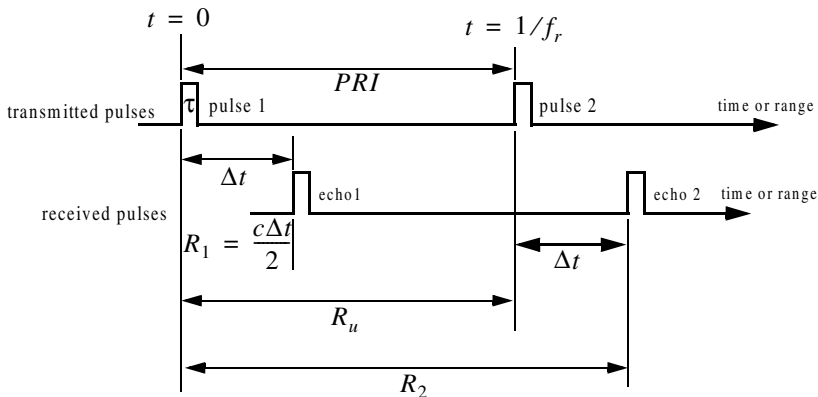


Figure 1.7. Illustrating range ambiguity.

Clearly, range ambiguity is associated with echo 2. Therefore, once a pulse is transmitted the radar must wait a sufficient length of time so that returns from targets at maximum range are back before the next pulse is emitted. It follows that the maximum unambiguous range must correspond to half of the PRI,

$$R_u = c \frac{T}{2} = \frac{c}{2f_r} \quad (1.5)$$

MATLAB Function “pulse_train.m”

The MATLAB function “pulse_train.m” computes the duty cycle, average transmitted power, pulse energy, and the pulse repetition frequency. It is given in Listing 1.1 in Section 1.8; its syntax is as follows:

$$[dt \text{ pav } ep \text{ prf } ru] = \text{pulse_train}(\text{tau}, \text{pri}, \text{p_peak})$$

where

Symbol	Description	Units	Status
<i>tau</i>	<i>pulse width</i>	<i>seconds</i>	<i>input</i>
<i>pri</i>	<i>PRI</i>	<i>seconds</i>	<i>input</i>
<i>p_peak</i>	<i>peak power</i>	<i>Watts</i>	<i>input</i>
<i>dt</i>	<i>duty cycle</i>	<i>none</i>	<i>output</i>
<i>pav</i>	<i>average transmitted power</i>	<i>Watts</i>	<i>output</i>
<i>ep</i>	<i>pulse energy</i>	<i>Joules</i>	<i>output</i>
<i>prf</i>	<i>PRF</i>	<i>Hz</i>	<i>output</i>
<i>ru</i>	<i>unambiguous range</i>	<i>Km</i>	<i>output</i>

Example 1.1: A certain airborne pulsed radar has peak power $P_t = 10\text{KW}$, and uses two PRFs, $f_{r1} = 10\text{KHz}$ and $f_{r2} = 30\text{KHz}$. What are the required pulse widths for each PRF so that the average transmitted power is constant and is equal to 1500Watts ? Compute the pulse energy in each case.

Solution: Since P_{av} is constant, then both PRFs have the same duty cycle. More precisely,

$$d_t = \frac{1500}{10 \times 10^3} = 0.15$$

The pulse repetition intervals are

$$T_1 = \frac{1}{10 \times 10^3} = 0.1\text{ms}$$

$$T_2 = \frac{1}{30 \times 10^3} = 0.0333\text{ms}$$

It follows that

$$\tau_1 = 0.15 \times T_1 = 15\mu\text{s}$$

$$\tau_2 = 0.15 \times T_2 = 5\mu\text{s}$$

$$E_{p1} = P_t \tau_1 = 10 \times 10^3 \times 15 \times 10^{-6} = 0.15\text{Joules}$$

$$E_{p2} = P_t \tau_2 = 10 \times 10^3 \times 5 \times 10^{-6} = 0.05\text{Joules}.$$

1.3. Range Resolution

Range resolution, denoted as ΔR , is a radar metric that describes its ability to detect targets in close proximity to each other as distinct objects. Radar systems are normally designed to operate between a minimum range R_{min} , and maximum range R_{max} . The distance between R_{min} and R_{max} is divided into M range bins (gates), each of width ΔR ,

$$M = \frac{R_{max} - R_{min}}{\Delta R} \tag{1.6}$$

Targets separated by at least ΔR will be completely resolved in range, as illustrated in Fig. 1.8. Targets within the same range bin can be resolved in cross range (azimuth) utilizing signal processing techniques.

Consider two targets located at ranges R_1 and R_2 , corresponding to time delays t_1 and t_2 , respectively. Denote the difference between those two ranges as ΔR :

$$\Delta R = R_2 - R_1 = c \frac{(t_2 - t_1)}{2} = c \frac{\delta t}{2} \quad (1.7)$$

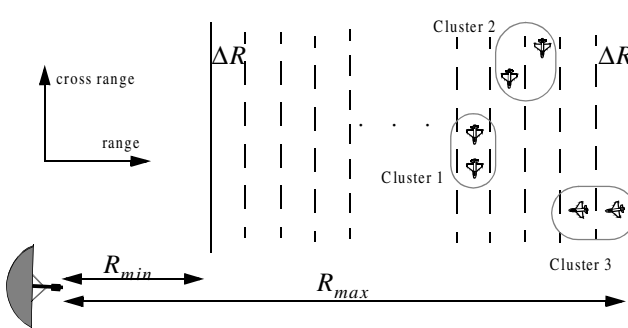


Figure 1.8. Resolving targets in range and cross range.

Now, try to answer the following question: What is the minimum δt such that target 1 at R_1 and target 2 at R_2 will appear completely resolved in range (different range bins)? In other words, what is the minimum ΔR ?

First, assume that the two targets are separated by $c\tau/4$, τ is the pulse width. In this case, when the pulse trailing edge strikes target 2 the leading edge would have traveled backwards a distance $c\tau$, and the returned pulse would be composed of returns from both targets (i.e., unresolved return), as shown in Fig. 1.9a. However, if the two targets are at least $c\tau/2$ apart, then as the pulse trailing edge strikes the first target the leading edge will start to return from target 2, and two distinct returned pulses will be produced, as illustrated by Fig. 1.9b. Thus, ΔR should be greater or equal to $c\tau/2$. And since the radar bandwidth B is equal to $1/\tau$, then

$$\Delta R = \frac{c\tau}{2} = \frac{c}{2B} \quad (1.8)$$

In general, radar users and designers alike seek to minimize ΔR in order to enhance the radar performance. As suggested by Eq. (1.8), in order to achieve fine range resolution one must minimize the pulse width. However, this will reduce the average transmitted power and increase the operating bandwidth. Achieving fine range resolution while maintaining adequate average transmitted power can be accomplished by using pulse compression techniques.

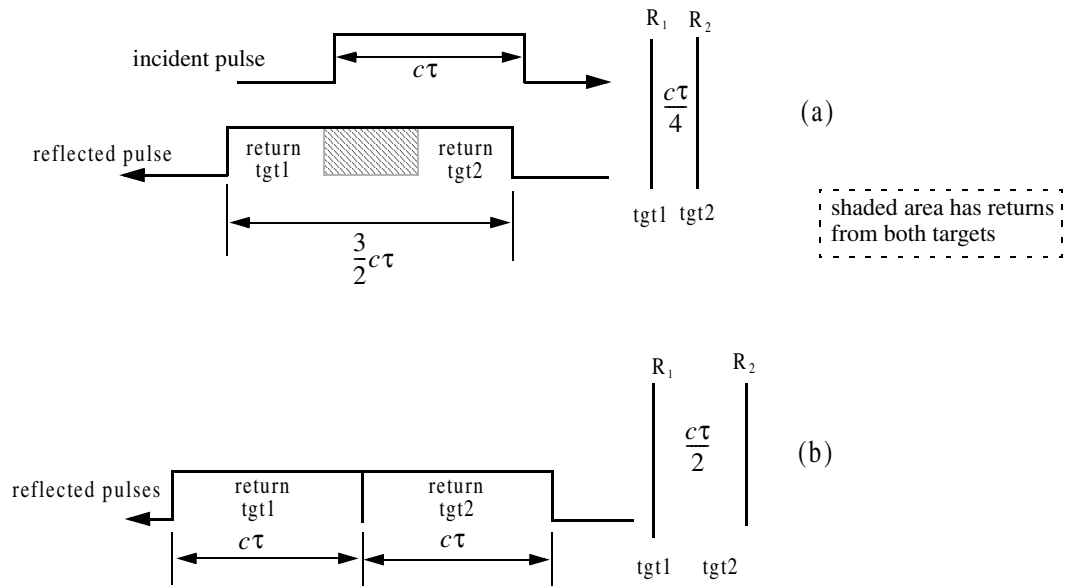


Figure 1.9. (a) Two unresolved targets. (b) Two resolved targets.

MATLAB Function “range_resolution.m”

The MATLAB function “range_resolution.m” computes range resolution. It is given in Listing 1.2 in Section 1.8; its syntax is as follows:

$$[\text{delta_R}] = \text{range_resolution}(\text{var}, \text{indicator})$$

where

Symbol	Description	Units	Status
<i>var, indicator</i>	<i>bandwidth, ‘hz’</i>	<i>Hz, none</i>	<i>inputs</i>
<i>var, indicator</i>	<i>pulse width, ‘s’</i>	<i>seconds, none</i>	<i>inputs</i>
<i>delta_R</i>	<i>range resolution</i>	<i>meters</i>	<i>output</i>

Example 1.2: A radar system with an unambiguous range of 100 Km, and a bandwidth 0.5 MHz. Compute the required PRF, PRI, ΔR, and τ.

Solution:

$$PRF = \frac{c}{2R_u} = \frac{3 \times 10^8}{2 \times 10^5} = 1500 \text{ Hz}$$

$$PRI = \frac{1}{PRF} = \frac{1}{1500} = 0.6667 \text{ ms}$$

Using the function “range_resolution” yields

$$\Delta R = \frac{c}{2B} = \frac{3 \times 10^8}{2 \times 0.5 \times 10^6} = 300 \text{ m}$$

$$\tau = \frac{2\Delta R}{c} = \frac{2 \times 300}{3 \times 10^8} = 2 \mu\text{s}.$$

1.4. Doppler Frequency

Radars use Doppler frequency to extract target radial velocity (range rate), as well as to distinguish between moving and stationary targets or objects such as clutter. The Doppler phenomenon describes the shift in the center frequency of an incident waveform due to the target motion with respect to the source of radiation. Depending on the direction of the target’s motion this frequency shift may be positive or negative. A waveform incident on a target has equiphase wavefronts separated by λ , the wavelength. A closing target will cause the reflected equiphase wavefronts to get closer to each other (smaller wavelength). Alternatively, an opening or receding target (moving away from the radar) will cause the reflected equiphase wavefronts to expand (larger wavelength), as illustrated in Fig. 1.10.

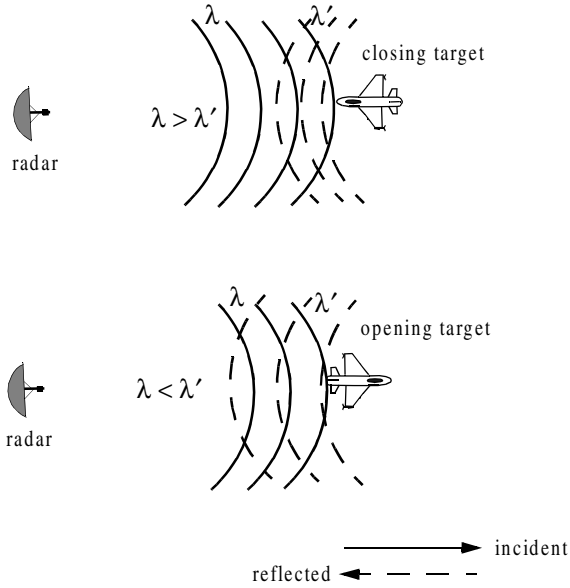


Figure 1.10. Effect of target motion on the reflected equiphase waveforms.

Consider a pulse of width τ (seconds) incident on a target which is moving towards the radar at velocity v , as shown in Fig. 1.11. Define d as the distance (in meters) that the target moves into the pulse during the interval Δt ,

$$d = v\Delta t \quad (1.9)$$

where Δt is equal to the time span between the pulse leading edge striking the target and the trailing edge striking the target. Since the pulse is moving at the speed of light and the trailing edge has moved distance $c\tau - d$, then

$$\Delta t = \frac{c\tau - d}{c} \quad (1.10)$$

Combining Eq. (1.9) and Eq. (1.10) yields

$$d = \frac{vc}{v + c}\tau \quad (1.11)$$

Now, in Δt seconds the pulse leading edge has moved in the direction of the radar a distance s ,

$$s = c\Delta t \quad (1.12)$$

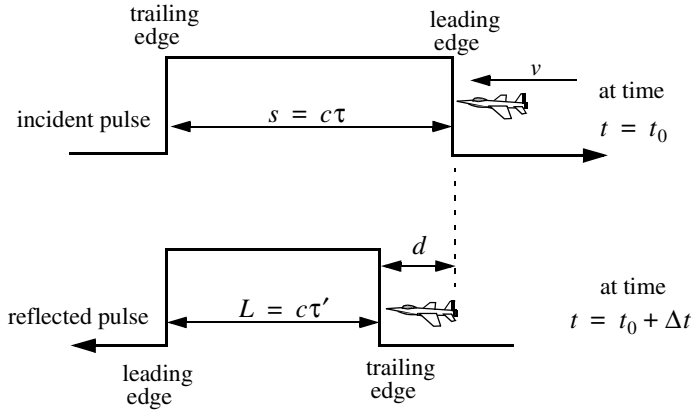


Figure 1.11. Illustrating the impact of target velocity on a single pulse.

Therefore, the reflected pulse width is now τ' seconds, or L meters,

$$L = c\tau' = s - d \quad (1.13)$$

Substituting Eq. (1.11) and Eq. (1.12) into Eq. (1.13) yields

$$c\tau' = c\Delta t - \frac{vc}{v+c}\tau \quad (1.14)$$

$$c\tau' = \frac{c^2}{v+c}\tau - \frac{vc}{v+c}\tau = \frac{c^2 - vc}{v+c}\tau \quad (1.15)$$

$$\tau' = \frac{c-v}{c+v}\tau \quad (1.16)$$

In practice, the factor $(c-v)/(c+v)$ is often referred to as the time dilation factor. Notice that if $v = 0$, then $\tau' = \tau$. In a similar fashion, one can compute τ' for an opening target. In this case,

$$\tau' = \frac{v+c}{c-v}\tau \quad (1.17)$$

To derive an expression for Doppler frequency, consider the illustration shown in Fig. 1.12. It takes the leading edge of pulse 2 Δt seconds to travel a distance $(c/f_r) - d$ to strike the target. Over the same time interval, the leading edge of pulse 1 travels the same distance $c\Delta t$. More precisely,

$$d = v\Delta t \quad (1.18)$$

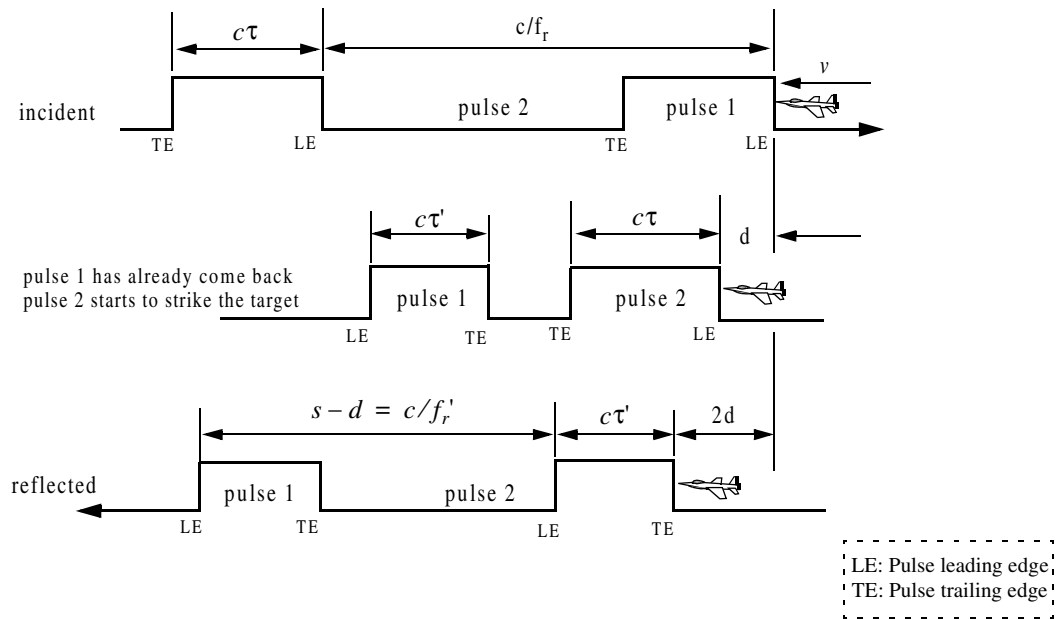


Figure 1.12. Illustration of target motion effects on the radar pulses.

$$\frac{c}{f_r} - d = c\Delta t \quad (1.19)$$

solving for Δt yields

$$\Delta t = \frac{c/f_r}{c+v} \quad (1.20)$$

$$d = \frac{cv/f_r}{c+v} \quad (1.21)$$

The reflected pulse spacing is now $s - d$ and the new PRF is f_r' , where

$$s - d = \frac{c}{f_r} = c\Delta t - \frac{cv/f_r}{c+v} \quad (1.22)$$

It follows that the new PRF is related to the original PRF by

$$f_r' = \frac{c+v}{c-v} f_r \quad (1.23)$$

However, since the number of cycles does not change, the frequency of the reflected signal will go up by the same factor. Denoting the new frequency by f_0' , it follows

$$f_0' = \frac{c+v}{c-v} f_0 \quad (1.24)$$

where f_0 is the carrier frequency of the incident signal. The Doppler frequency f_d is defined as the difference $f_0' - f_0$. More precisely,

$$f_d = f_0' - f_0 = \frac{c+v}{c-v} f_0 - f_0 = \frac{2v}{c-v} f_0 \quad (1.25)$$

but since $v \ll c$ and $c = \lambda f_0$, then

$$f_d \approx \frac{2v}{c} f_0 = \frac{2v}{\lambda} \quad (1.26)$$

Eq. (1.26) indicates that the Doppler shift is proportional to the target velocity, and thus, one can extract f_d from range rate and vice versa.

The result in Eq. (1.26) can also be derived using the following approach: Fig. 1.13 shows a closing target with velocity v . Let R_0 refer to the range at time t_0 (time reference), then the range to the target at any time t is

$$R(t) = R_0 - v(t - t_0) \quad (1.27)$$

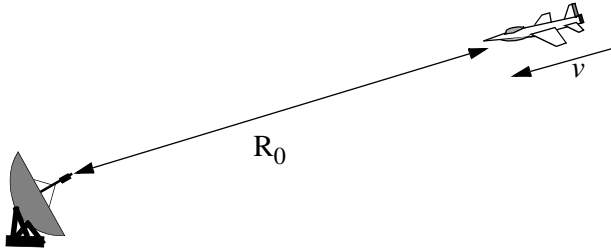


Figure 1.13. Closing target with velocity v .

The signal received by the radar is then given by

$$x_r(t) = x(t - \Psi(t)) \quad (1.28)$$

where $x(t)$ is the transmitted signal, and

$$\Psi(t) = \frac{2}{c}(R_0 - vt + vt_0) \quad (1.29)$$

Substituting Eq. (1.29) into Eq. (1.28) and collecting terms yield

$$x_r(t) = x\left(\left(1 + \frac{2v}{c}\right)t - \Psi_0\right) \quad (1.30)$$

the constant phase Ψ_0 is

$$\Psi_0 = \frac{2R_0}{c} + \frac{2v}{c} t_0 \quad (1.31)$$

Define the compression or scaling factor γ by

$$\gamma = 1 + \frac{2v}{c} \quad (1.32)$$

Note that for a receding target the scaling factor is $\gamma = 1 - (2v/c)$. Using Eq. (1.32) we can rewrite Eq. (1.30) as

$$x_r(t) = x(\gamma t - \Psi_0) \quad (1.33)$$

Eq. (1.33) is a time-compressed version of the returned signal from a stationary target ($v = 0$). Hence, based on the scaling property of the Fourier transform,

the spectrum of the received signal will be expanded in frequency by a factor of γ .

Consider the special case when

$$x(t) = y(t)\cos\omega_0t \quad (1.34)$$

where ω_0 is the radar center frequency in radians per second. The received signal $x_r(t)$ is then given by

$$x_r(t) = y(\gamma t - \psi_0)\cos(\gamma\omega_0t - \psi_0) \quad (1.35)$$

The Fourier transform of Eq. (1.35) is

$$X_r(\omega) = \frac{1}{2\gamma}\left(Y\left(\frac{\omega}{\gamma} - \omega_0\right) + Y\left(\frac{\omega}{\gamma} + \omega_0\right)\right) \quad (1.36)$$

where for simplicity the effects of the constant phase ψ_0 have been ignored in Eq. (1.36). Therefore, the band pass spectrum of the received signal is now centered at $\gamma\omega_0$ instead of ω_0 . The difference between the two values corresponds to the amount of Doppler shift incurred due to the target motion,

$$\omega_d = \omega_0 - \gamma\omega_0 \quad (1.37)$$

ω_d is the Doppler frequency in radians per second. Substituting the value of γ in Eq. (1.37) and using $2\pi f = \omega$ yield

$$f_d = \frac{2v}{c} f_0 = \frac{2v}{\lambda} \quad (1.38)$$

which is the same as Eq. (1.26). It can be shown that for a receding target the Doppler shift is $f_d = -2v/\lambda$. This is illustrated in Fig. 1.14.

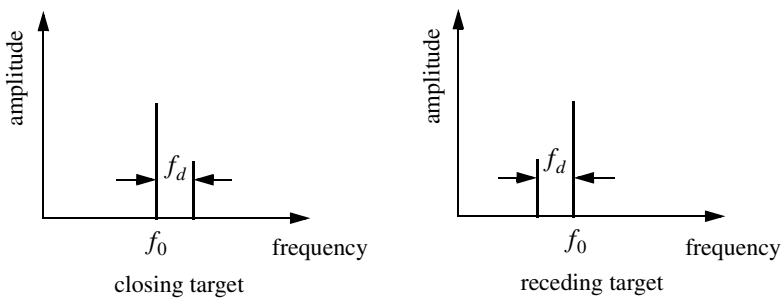


Figure 1.14. Spectra of radar received signal.

In both Eq. (1.38) and Eq. (1.26) the target radial velocity with respect to the radar is equal to v , but this is not always the case. In fact, the amount of Doppler frequency depends on the target velocity component in the direction of the radar (radial velocity). Fig. 1.15 shows three targets all having velocity v : target 1 has zero Doppler shift; target 2 has maximum Doppler frequency as defined in Eq. (1.38). The amount of Doppler frequency due to target 3 is $f_d = 2v\cos\theta/\lambda$, where $v\cos\theta$ is the radial velocity; and θ is the total angle between the radar line of sight and the target.

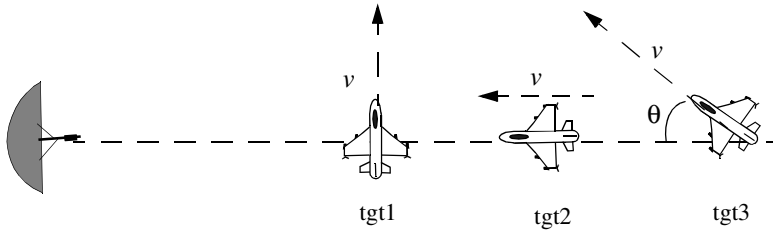


Figure 1.15. Target 1 generates zero Doppler. Target 2 generates maximum Doppler. Target 3 is in-between.

Thus, a more general expression for f_d that accounts for the total angle between the radar and the target is

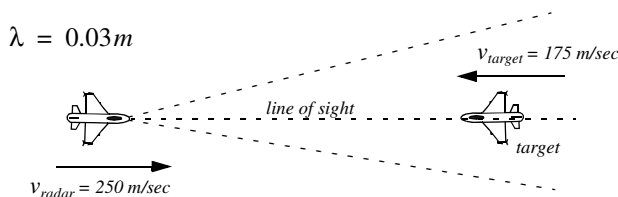
$$f_d = \frac{2v}{\lambda} \cos\theta \quad (1.39)$$

and for an opening target

$$f_d = \frac{-2v}{\lambda} \cos\theta \quad (1.40)$$

where $\cos\theta = \cos\theta_e \cos\theta_a$. The angles θ_e and θ_a are, respectively, the elevation and azimuth angles; see Fig. 1.16.

Example 1.3: Compute the Doppler frequency measured by the radar shown in the figure below.



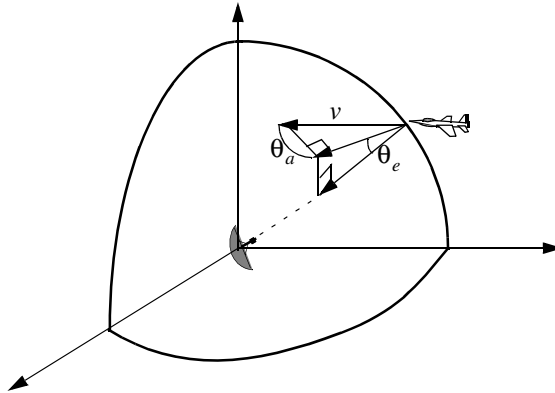


Figure 1.16. Radial velocity is proportional to the azimuth and elevation angles.

Solution: The relative radial velocity between the radar and the target is $v_{radar} + v_{target}$. Thus using Eq. (1.38), we get

$$f_d = 2 \frac{(250 + 175)}{0.03} = 28.3 \text{ KHz}$$

Similarly, if the target were opening the Doppler frequency is

$$f_d = 2 \frac{250 - 175}{0.03} = 5 \text{ KHz}.$$

MATLAB Function “doppler_freq.m”

The function “doppler_freq.m” computes Doppler frequency. It is given in Listing 1.3 in Section 1.8; its syntax is as follows:

$$[fd, tdr] = \text{doppler_freq}(freq, ang, tv, indicator)$$

where

Symbol	Description	Units	Status
<i>freq</i>	radar operating frequency	Hz	input
<i>ang</i>	aspect angle	degrees	input
<i>tv</i>	target velocity	m/sec	input
<i>indicator</i>	1 for closing target, 0 otherwise	none	input
<i>fd</i>	Doppler frequency	Hz	output
<i>tdr</i>	time dilation factor ratio τ' / τ	none	output

1.5. Coherence

A radar is said to be coherent if the phase of any two transmitted pulses is consistent, i.e., there is a continuity in the signal phase from one pulse to the next, as illustrated in Fig. 1.17a. One can view coherence as the radar's ability to maintain an integer multiple of wavelengths between the equiphase wavefront from the end of one pulse to the equiphase wavefront at the beginning of the next pulse, as illustrated by Fig. 1.17b. Coherency can be achieved by using a STABLE Local Oscillator (STALO). A radar is said to be coherent-on-receive or quasi-coherent if it stores in its memory a record of the phases of all transmitted pulses. In this case, the receiver phase reference is normally the phase of the most recent transmitted pulse.

Coherence also refers to the radar's ability to accurately measure (extract) the received signal phase. Since Doppler represents a frequency shift in the received signal, then only coherent or coherent-on-receive radars can extract Doppler information. This is because the instantaneous frequency of a signal is proportional to the time derivative of the signal phase. More precisely,

$$f_i = \frac{1}{2\pi} \frac{d}{dt} \phi(t) \quad (1.41)$$

where f_i is the instantaneous frequency, and $\phi(t)$ is the signal phase.

For example, consider the following signal:

$$x(t) = \cos(\gamma\omega_0 t - \psi_0) \quad (1.42)$$

where the scaling factor γ is defined in Eq. (1.32), and ψ_0 is a constant phase. It follows that the instantaneous frequency of $x(t)$ is

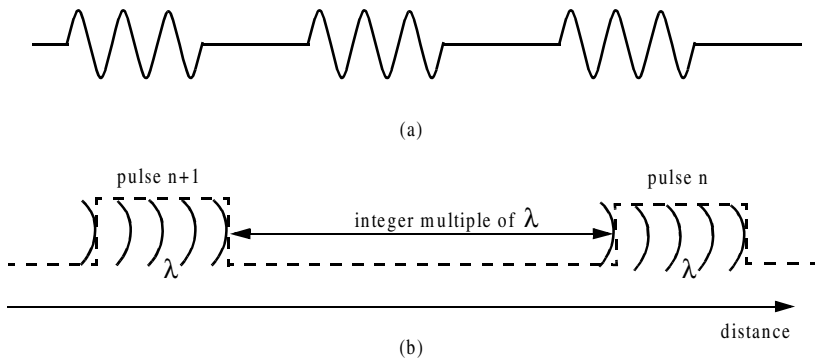


Figure 1.17. (a) Phase continuity between consecutive pulses. (b) Maintaining an integer multiple of wavelengths between the equiphase wavefronts of any two successive pulses guarantees coherence.

$$f_i = \gamma f_0 \quad (1.43)$$

where $\omega_0 = 2\pi f_0$. Substituting Eq. (1.32) into Eq. (1.43) yields

$$f_i = f_0 \left(1 + \frac{2v}{c} \right) = f_0 + \frac{2v}{\lambda} \quad (1.44)$$

where the relation $c = \lambda f$ is utilized. Note that the second term of the most right-hand side of Eq. (1.44) is a Doppler shift.

1.6. The Radar Equation

Consider a radar with an omni directional antenna (one that radiates energy equally in all directions). Since these kinds of antennas have a spherical radiation pattern, we can define the peak power density (power per unit area) at any point in space as

$$P_D = \frac{\text{Peak transmitted power}}{\text{area of a sphere}} \quad \frac{\text{watts}}{\text{m}^2} \quad (1.45)$$

The power density at range R away from the radar (assuming a lossless propagation medium) is

$$P_D = \frac{P_t}{4\pi R^2} \quad (1.46)$$

where P_t is the peak transmitted power and $4\pi R^2$ is the surface area of a sphere of radius R . Radar systems utilize directional antennas in order to increase the power density in a certain direction. Directional antennas are usually characterized by the antenna gain G and the antenna effective aperture A_e . They are related by

$$A_e = \frac{G\lambda^2}{4\pi} \quad (1.47)$$

where λ is the wavelength. The relationship between the antenna's effective aperture A_e and the physical aperture A is

$$\begin{aligned} A_e &= \rho A \\ 0 &\leq \rho \leq 1 \end{aligned} \quad (1.48)$$

ρ is referred to as the aperture efficiency, and good antennas require $\rho \rightarrow 1$. In this book we will assume, unless otherwise noted, that A and A_e are the same. We will also assume that antennas have the same gain in the transmitting and receiving modes. In practice, $\rho = 0.7$ is widely accepted.

The power density at a distance R away from a radar using a directive antenna of gain G is then given by

$$P_D = \frac{P_t G}{4\pi R^2} \quad (1.49)$$

When the radar radiated energy impinges on a target, the induced surface currents on that target radiate electromagnetic energy in all directions. The amount of the radiated energy is proportional to the target size, orientation, physical shape, and material, which are all lumped together in one target-specific parameter called the Radar Cross Section (RCS) and is denoted by σ .

The radar cross section is defined as the ratio of the power reflected back to the radar to the power density incident on the target,

$$\sigma = \frac{P_r}{P_D} m^2 \quad (1.50)$$

where P_r is the power reflected from the target. Thus, the total power delivered to the radar signal processor by the antenna is

$$P_{Dr} = \frac{P_t G \sigma}{(4\pi R^2)^2} A_e \quad (1.51)$$

substituting the value of A_e from Eq. (1.47) into Eq. (1.51) yields

$$P_{Dr} = \frac{P_t G^2 \lambda^2 \sigma}{(4\pi)^3 R^4} \quad (1.52)$$

Let S_{min} denote the minimum detectable signal power. It follows that the maximum radar range R_{max} is

$$R_{max} = \left(\frac{P_t G^2 \lambda^2 \sigma}{(4\pi)^3 S_{min}} \right)^{1/4} \quad (1.53)$$

Eq. (1.53) suggests that in order to double the radar maximum range, one must increase the peak transmitted power P_t sixteen times; or equivalently, one must increase the effective aperture four times.

In practical situations the returned signals received by the radar will be corrupted with noise, which introduces unwanted voltages at all radar frequencies. Noise is random in nature and can be described by its Power Spectral Density (PSD) function. The noise power N is a function of the radar operating bandwidth, B . More precisely

$$N = \text{Noise PSD} \times B \quad (1.54)$$

The input noise power to a lossless antenna is

$$N_i = kT_e B \quad (1.55)$$

where $k = 1.38 \times 10^{-23}$ joule/degree Kelvin is Boltzman's constant, and T_e is the effective noise temperature in degree Kelvin. It is always desirable that the minimum detectable signal (S_{min}) be greater than the noise power. The fidelity of a radar receiver is normally described by a figure of merit called the noise figure F (see Appendix A for details). The noise figure is defined as

$$F = \frac{(SNR)_i}{(SNR)_o} = \frac{S_i/N_i}{S_o/N_o} \quad (1.56)$$

$(SNR)_i$ and $(SNR)_o$ are, respectively, the Signal to Noise Ratios (SNR) at the input and output of the receiver. S_i is the input signal power, N_i is the input noise power, S_o and N_o are, respectively, the output signal and noise power. Substituting Eq. (1.55) into Eq. (1.56) and rearranging terms yield

$$S_i = kT_e B F (SNR)_o \quad (1.57)$$

Thus, the minimum detectable signal power can be written as

$$S_{min} = kT_e B F (SNR)_{o_{min}} \quad (1.58)$$

The radar detection threshold is set equal to the minimum output SNR, $(SNR)_{o_{min}}$. Substituting Eq. (1.58) in Eq. (1.53) gives

$$R_{max} = \left(\frac{P_t G^2 \lambda^2 \sigma}{(4\pi)^3 kT_e B F (SNR)_{o_{min}}} \right)^{1/4} \quad (1.59)$$

or equivalently,

$$(SNR)_o = \frac{P_t G^2 \lambda^2 \sigma}{(4\pi)^3 kT_e B F R^4} \quad (1.60)$$

Radar losses denoted as L reduce the overall SNR, and hence

$$(SNR)_o = \frac{P_t G^2 \lambda^2 \sigma}{(4\pi)^3 kT_e B F L R^4} \quad (1.61)$$

Although it may take on many different forms, Eq. (1.61) is what is widely known as the Radar Equation. It is a common practice to perform calculations

associated with the radar equation using decibel (dB) arithmetic. A review is presented in Appendix B.

MATLAB Function “radar_eq.m”

The function “radar_eq.m” implements Eq. (1.61); it is given in Listing 1.4 in Section 1.8. The outputs are either SNR in dB or range in Km where a different input setting is used for each case. The syntax is as follows:

$$[out_par] = radar_eq(pt, freq, g, sigma, te, b, nf, loss, input_par, option, rcs_delta1, rcs_delta2, pt_percent1, pt_percent2)$$

Symbol	Description	Units	Status
<i>pt</i>	<i>peak power</i>	<i>KW</i>	<i>input</i>
<i>freq</i>	<i>frequency</i>	<i>Hz</i>	<i>input</i>
<i>g</i>	<i>antenna gain</i>	<i>dB</i>	<i>input</i>
<i>sigma</i>	<i>target cross section</i>	<i>m²</i>	<i>input</i>
<i>te</i>	<i>effective temperature</i>	<i>Kelvin</i>	<i>input</i>
<i>b</i>	<i>bandwidth</i>	<i>Hz</i>	<i>input</i>
<i>nf</i>	<i>noise figure</i>	<i>dB</i>	<i>input</i>
<i>loss</i>	<i>radar losses</i>	<i>dB</i>	<i>input</i>
<i>input_par</i>	<i>SNR, or R_{max}</i>	<i>dB, or Km</i>	<i>input</i>
<i>option</i>	<i>1 means input_par = SNR 2 means input_par = R</i>	<i>none</i>	<i>input</i>
<i>rcs_delta1</i>	<i>rcs delta1 (sigma - delta1)</i>	<i>dB</i>	<i>input</i>
<i>rcs_delta2</i>	<i>rcs delta2 (sigma + delta2)</i>	<i>dB</i>	<i>input</i>
<i>pt_percent1</i>	<i>pt * pt_percent1%</i>	<i>none</i>	<i>input</i>
<i>pt_percent2</i>	<i>pt * pt_percent2%</i>	<i>none</i>	<i>input</i>
<i>out_par</i>	<i>R for option = 1 SNR for option = 2</i>	<i>Km, or dB</i>	<i>output</i>

If some of the inputs are not available in the proper format, the functions “dB_to_base10.m” and / or “base10_to_dB.m” can be used first. Plots of SNR versus range (or range versus SNR) for several choices of RCS and peak power are also generated by the function “radar_eq.m”. Typical plots utilizing Example 1.4 parameters are shown in Fig. 1.18. In this case, the default values are those listed in the example. Observation of these plots shows how doubling the peak power (3 dB) has little effect on improving the SNR. One should consider varying other radar parameters such as antenna gain to improve SNR, or detection range.

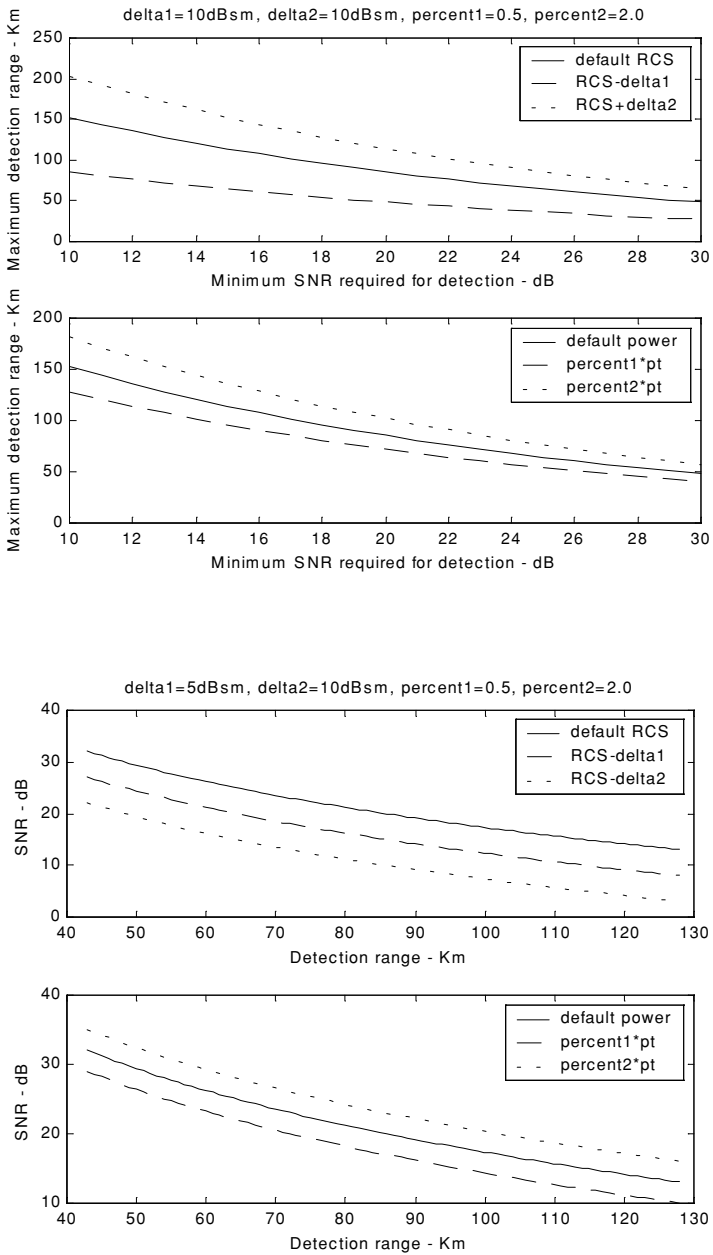


Figure 1.18. Typical outputs generated by the function “*radar_eq.m*”. Plots correspond to parameters from Example 1.4.

Example 1.4: A certain C-band radar with the following parameters: Peak power $P_t = 1.5\text{MW}$, operating frequency $f_0 = 5.6\text{GHz}$, antenna gain $G = 45\text{dB}$, effective temperature $T_e = 290\text{K}$, pulse width $\tau = 0.2\mu\text{sec}$. The radar threshold is $(\text{SNR})_{\min} = 20\text{dB}$. Assume target cross section $\sigma = 0.1\text{m}^2$. Compute the maximum range.

Solution: The radar bandwidth is

$$B = \frac{1}{\tau} = \frac{1}{0.2 \times 10^{-6}} = 5\text{MHz}$$

the wavelength is

$$\lambda = \frac{c}{f_0} = \frac{3 \times 10^8}{5.6 \times 10^9} = 0.054\text{m}$$

From Eq. (1.59) we have

$$(R^4)_{\text{dB}} = (P_t + G^2 + \lambda^2 + \sigma - (4\pi)^3 - kT_e B - F - (\text{SNR})_{\min})_{\text{dB}}$$

where, before summing, the dB calculations are carried out for each of the individual parameters on the right-hand side. We can now construct the following table with all parameters computed in dB:

P_t	λ^2	G^2	$kT_e B$	$(4\pi)^3$	F	$(\text{SNR})_{\min}$	σ
61.761	-25.421	90dB	-136.987	32.976	3dB	20dB	-10

It follows

$$R^4 = 61.761 + 90 - 25.352 - 10 - 32.976 + 136.987 - 3 - 20 = 197.420\text{dB}$$

$$R^4 = 10^{\frac{197.420}{10}} = 55.208 \times 10^{18} \text{m}^4$$

$$R = \sqrt[4]{55.208 \times 10^{18}} = 86.199\text{Km}$$

Thus, the maximum detection range is 86.2Km .

1.6.1. Low PRF Radar Equation

Consider a pulsed radar with pulse width τ , PRI T , and peak transmitted power P_t . The average transmitted power is $P_{av} = P_t d_t$, where $d_t = \tau/T$ is the transmission duty factor. We can define the receiving duty factor d_r as

$$d_r = \frac{T - \tau}{T} = 1 - \tau f_r \quad (1.62)$$

Thus, for low PRF radars ($T \gg \tau$) the receiving duty factor is $d_r \approx 1$.

Define the “time on target” T_i (the time that a target is illuminated by the beam) as

$$T_i = \frac{n_p}{f_r} \Rightarrow n_p = T_i f_r \quad (1.63)$$

where n_p is the total number of pulses that strikes the target, and f_r is the radar PRF. Assuming low PRF, the single pulse radar equation is given by

$$(SNR)_1 = \frac{P_i G^2 \lambda^2 \sigma}{(4\pi)^3 R^4 k T_e BFL} \quad (1.64)$$

and for n_p coherently integrated pulses we get

$$(SNR)_{n_p} = \frac{P_i G^2 \lambda^2 \sigma n_p}{(4\pi)^3 R^4 k T_e BFL} \quad (1.65)$$

Now by using Eq. (1.63) and using $B = 1/\tau$ the low PRF radar equation can be written as

$$(SNR)_{n_p} = \frac{P_i G^2 \lambda^2 \sigma T_i f_r \tau}{(4\pi)^3 R^4 k T_e FL} \quad (1.66)$$

MATLAB Function “lprf_req.m”

The function “lprf_req.m” implements the low PRF radar equation; it is given in Listing 1.5 in Section 1.8. Again when necessary the functions “dB_to_base10.m” and/or “base10_to_dB.m” can be used first. For a given set of input parameters, the function “lprf_req.m” computes $(SNR)_{np}$. Plots of SNR versus range for three sets of coherently integrated pulses are generated; see Fig. 1.19. Also, plots of SNR versus number of coherently integrated pulses for two choices of the default RCS and peak power are generated. Typical plots utilizing Example 1.4 parameters are shown in Fig. 1.20. As indicated by Fig. 1.20, integrating a limited number of pulses can significantly enhance the SNR; however, integrating large amount of pulses does not provide any further major improvement.

The syntax for function “lprf_req.m” is as follows:

$$[snr_out] = lprf_req(pt, freq, g, sigma, te, b, nf, loss, range, prf, np, rcs_delta, pt_percent, np1, np2)$$

Symbol	Description	Units	Status
<i>pt</i>	<i>peak power</i>	<i>KW</i>	<i>input</i>
<i>freq</i>	<i>frequency</i>	<i>Hz</i>	<i>input</i>
<i>g</i>	<i>antenna gain</i>	<i>dB</i>	<i>input</i>
<i>sigma</i>	<i>target cross section</i>	<i>m²</i>	<i>input</i>
<i>te</i>	<i>effective temperature</i>	<i>Kelvin</i>	<i>input</i>
<i>b</i>	<i>bandwidth</i>	<i>Hz</i>	<i>input</i>
<i>nf</i>	<i>noise figure</i>	<i>dB</i>	<i>input</i>
<i>loss</i>	<i>radar losses</i>	<i>dB</i>	<i>input</i>
<i>range</i>	<i>target range</i>	<i>Km</i>	<i>input</i>
<i>prf</i>	<i>PRF</i>	<i>Hz</i>	<i>input</i>
<i>np</i>	<i>number of pulses</i>	<i>none</i>	<i>input</i>
<i>np1</i>	<i>choice 1 for np</i>	<i>none</i>	<i>input</i>
<i>np2</i>	<i>choice 2 for np</i>	<i>none</i>	<i>input</i>
<i>rsc_delta</i>	<i>rsc delta1 (sigma - delta)</i>	<i>dB</i>	<i>input</i>
<i>pt_percent</i>	<i>pt * pt_percent%</i>	<i>none</i>	<i>input</i>
<i>snr_out</i>	<i>SNR</i>	<i>dB</i>	<i>output</i>

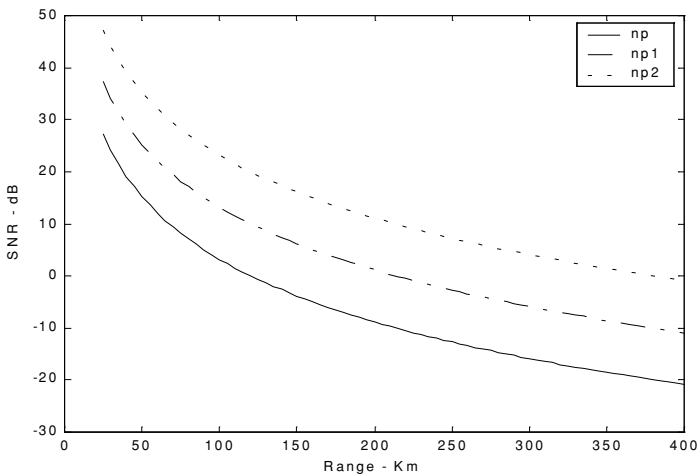


Figure 1.19. Typical output generated by the function “*lprf_req.m*”. Plots correspond to parameters from Example 1.4.

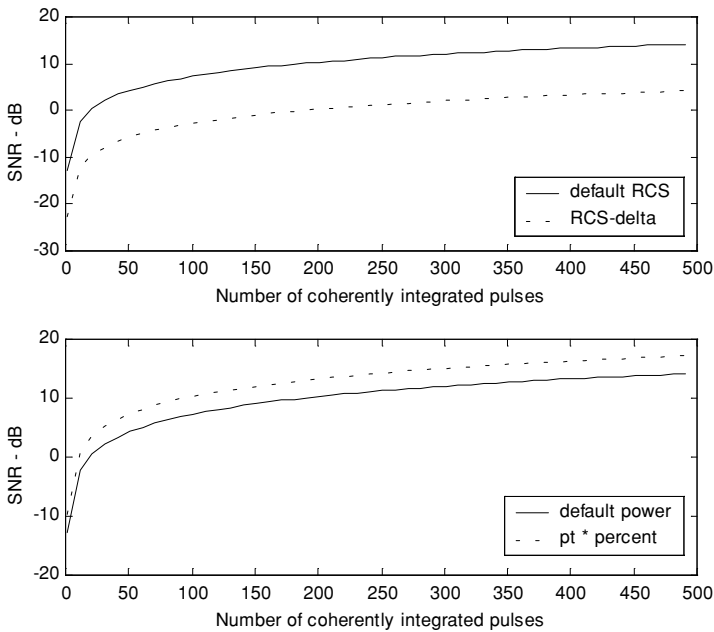


Figure 1.20. Typical outputs generated by the function “lprf_req.m”. Plots correspond to parameters from Example 1.4.

1.6.2. High PRF Radar Equation

Now, consider the high PRF radar case. The transmitted signal is a periodic train of pulses. The pulse width is τ and the period is T . This pulse train can be represented using an exponential Fourier series. The central power spectrum line (DC component) for this series contains most of the signal’s power. Its value is $(\tau/T)^2$, and it is equal to the square of the transmit duty factor. Thus, the single pulse radar equation for a high PRF radar (in terms of the DC spectral power line) is

$$SNR = \frac{P_t G^2 \lambda^2 \sigma d_r^2}{(4\pi)^3 R^4 k T_e B F L d_r} \quad (1.67)$$

where, in this case, we can no longer ignore the receive duty factor, since its value is comparable to the transmit duty factor. In fact, $d_r \approx d_t = \tau f_r$. Additionally, the operating radar bandwidth is now matched to the radar integration time (time on target), $B = 1/T_i$. It follows that

$$SNR = \frac{P_i \tau f_r T_i G^2 \lambda^2 \sigma}{(4\pi)^3 R^4 k T_e FL} \quad (1.68)$$

and finally,

$$SNR = \frac{P_{av} T_i G^2 \lambda^2 \sigma}{(4\pi)^3 R^4 k T_e FL} \quad (1.69)$$

where P_{av} was substituted for $P_i \tau f_r$. Note that the product $P_{av} T_i$ is a “kind of energy” product, which indicates that high PRF radars can enhance detection performance by using relatively low power and longer integration time.

MATLAB Function “hprf_req.m”

The function “hprf_req.m” implements the high PRF radar equation; it is given in Listing 1.6 in Section 1.8. Plots of SNR versus range for three duty cycle choices are generated. Figure 1.21 shows typical outputs generated by the function “hprf_req.m”. Its syntax is as follows:

$[snr_out] = hprf_req(pt, freq, g, sigma, dt, ti, range, te, nf, loss, prf, tau, dt1, dt2)$

where

Symbol	Description	Units	Status
<i>pt</i>	<i>peak power</i>	<i>KW</i>	<i>input</i>
<i>freq</i>	<i>frequency</i>	<i>Hz</i>	<i>input</i>
<i>g</i>	<i>antenna gain</i>	<i>dB</i>	<i>input</i>
<i>sigma</i>	<i>target cross section</i>	<i>m²</i>	<i>input</i>
<i>dt</i>	<i>duty cycle</i>	<i>none</i>	<i>input</i>
<i>ti</i>	<i>time on target</i>	<i>seconds</i>	<i>input</i>
<i>range</i>	<i>target range</i>	<i>Km</i>	<i>input</i>
<i>te</i>	<i>effective temperature</i>	<i>Kelvin</i>	<i>input</i>
<i>nf</i>	<i>noise figure</i>	<i>dB</i>	<i>input</i>
<i>loss</i>	<i>radar losses</i>	<i>dB</i>	<i>input</i>
<i>prf</i>	<i>PRF</i>	<i>Hz</i>	<i>input</i>
<i>tau</i>	<i>pulse width</i>	<i>seconds</i>	<i>input</i>
<i>dt1</i>	<i>duty cycle choice 1</i>	<i>none</i>	<i>input</i>
<i>dt2</i>	<i>duty cycle choice 2</i>	<i>none</i>	<i>input</i>
<i>snr_out</i>	<i>SNR</i>	<i>dB</i>	<i>output</i>

Note that either d_t or the combination of f_r and τ are needed. One should enter zero for d_t when f_r and τ are known and vice versa.

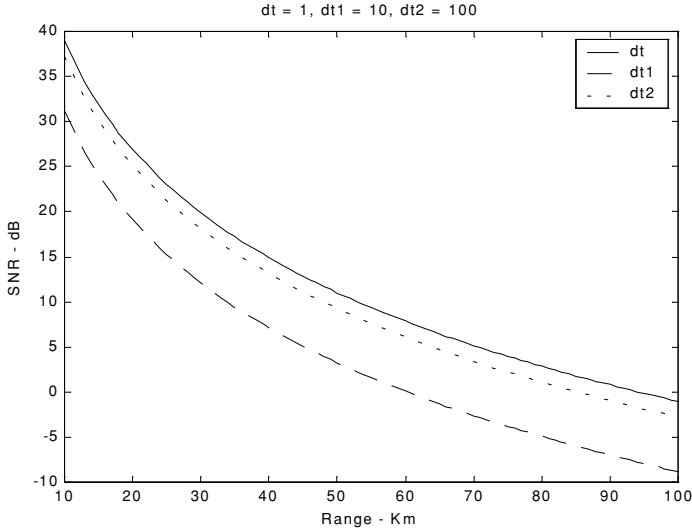


Figure 1.21. Typical output generated by the function “hprf_req.m”. Plots correspond to parameters from Example 1.5.

Example 1.5: Compute the single pulse SNR for a high PRF radar with the following parameters: peak power $P_t = 100\text{KW}$, antenna gain $G = 20\text{dB}$, operating frequency $f_0 = 5.6\text{GHz}$, losses $L = 8\text{dB}$, noise figure $F = 5\text{dB}$, effective temperature $T_e = 400\text{K}$, dwell interval $T_i = 2\text{s}$, duty factor $d_t = 0.3$. The range of interest is $R = 50\text{Km}$. Assume target RCS $\sigma = 0.01\text{m}^2$.

Solution: From Eq. (1.69) we have

$$(SNR)_{dB} = (P_{av} + G^2 + \lambda^2 + \sigma + T_i - (4\pi)^3 - R^4 - kT - F - L)_{dB}$$

The following table gives all parameters in dB:

P_{av}	λ^2	T_i	kT_e	$(4\pi)^3$	R^4	σ
44.771	-25.421	3.01	-202.581	32.976	187.959	-20

$$(SNR)_{dB} = 44.771 + 40 - 25.421 - 20 + 3.01 - 32.976 + 202.581 - 187.959 - 5 - 8 = 11.006\text{dB}$$

1.6.3. Surveillance Radar Equation

Surveillance or search radars continuously scan a specified volume in space searching for targets. They are normally used to extract target information such as range, angular position, and possibly target velocity. Depending on the radar design and antenna, different search patterns can be adopted. A two-dimensional (2-D) fan beam search pattern is shown in Fig.1.22a. In this case, the beam width is wide enough in elevation to cover the desired search volume along that coordinate; however, it has to be steered in azimuth. Fig. 1.22b shows a stacked beam search pattern; here the beam has to be steered in azimuth and elevation. This latter kind of search pattern is normally employed by phased array radars.

Search volumes are normally specified by a search solid angle Ω in steradians. The antenna $3dB$ beam width can be expressed in terms of its azimuth and elevation beam widths θ_a and θ_e , respectively. It follows that the antenna solid angle coverage is $\theta_a \theta_e$. In this book we will assume symmetrical antennas (circular apertures) so that $\theta_a = \theta_e$. Furthermore, when we refer to the antenna beam width we will always assume the $3dB$ beam width, θ_{3dB} .

The number of antenna beam positions n_B required to cover a solid angle Ω is (see Fig. 1.23)

$$n_B = \frac{\Omega}{\theta_a \theta_e} = \frac{\Omega}{\theta_{3dB}^2} \tag{1.70}$$

For a circular aperture of diameter D , the θ_{3dB} is

$$\theta_{3dB} \approx \frac{\lambda}{D} \tag{1.71}$$

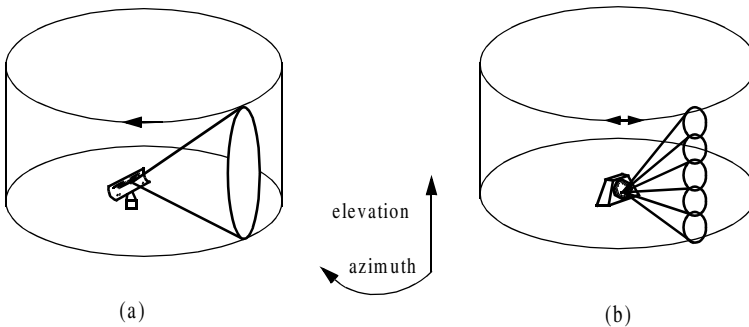


Figure 1.22. (a) 2-D fan search pattern; (b) stacked search pattern.

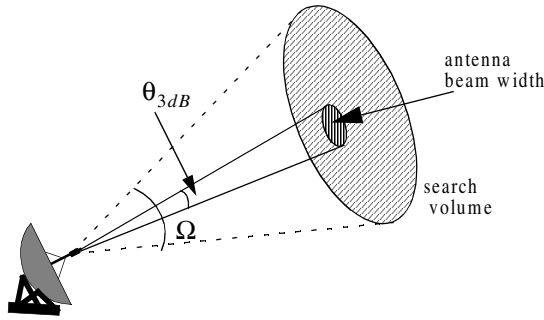


Figure 1.23. A cut in space showing the antenna beam width and the search volume.

and when aperture tapering is used, $\theta_{3dB} \approx 1.25\lambda/D$. Substituting Eq. (1.71) into Eq. (1.70) yields

$$n_B = \frac{D^2}{\lambda^2} \Omega \quad (1.72)$$

As a rule of thumb, the θ_{3dB} antenna beam width for a rectangular aperture of length a is $\theta_{3dB} \approx 2\lambda/a$.

Define the time it takes radar to search a volume defined by the solid angle Ω as the scan time T_{sc} . The time on target can then be expressed in terms of T_{sc} as

$$T_i = \frac{T_{sc}}{n_B} = \frac{T_{sc}\lambda^2}{D^2\Omega} \quad (1.73)$$

In order to define the search radar equation, start with Eq. (1.69) and use Eq. (1.73). More precisely,

$$SNR = \frac{P_{av}G^2\lambda^2\sigma}{(4\pi)^3 R^4 kT_e FL D^2\Omega} \frac{T_{sc}\lambda^2}{D^2\Omega} \quad (1.74)$$

and by using Eq. (1.47) in Eq. (1.74) we can define the search radar equation as

$$SNR = \frac{P_{av}A\sigma}{16R^4 kT_e LF} \frac{T_{sc}}{\Omega} \quad (1.75)$$

where the relation $A = \pi D^2/4$ (aperture area) was used.

The quantity $P_{av}A$ in Eq. (1.75) is known as the power aperture product. In practice, the power aperture product is widely used to categorize the radar ability to fulfill its search mission. Normally, a power aperture product is computed to meet predetermined SNR and radar cross section for a given search volume defined by Ω .

Example 1.6: Compute the power aperture product for an X-band radar with the following parameters: signal-to-noise ratio $SNR = 15dB$; losses $L = 8dB$; effective noise temperature $T_e = 900$ degree Kelvin; search volume $\Omega = 2^\circ$; scan time $T_{sc} = 2.5$ seconds; noise figure $F = 5dB$. Assume a $-10dBsm$ target cross section, and range $R = 250Km$. Also, compute the peak transmitted power corresponding to 30% duty factor, if the antenna gain is 45 dB.

Solution: The angular coverage is 2° in both azimuth and elevation. It follows that the solid angle coverage is

$$\Omega = \frac{2 \times 2}{(57.23)^2} = -29.132dB$$

Note that the factor $360/2\pi = 57.23$ converts angles into solid angles. From Eq. (1.75), we have

$$(SNR)_{dB} = (P_{av} + A + \sigma + T_{sc} - 16 - R^4 - kT_e - L - F - \Omega)_{dB}$$

σ	T_{sc}	16	R^4	kT_e
-10	3.979	12.041	215.918	-199.059

It follows that

$$15 = P_{av} + A - 10 + 3.979 - 12.041 - 215.918 + 199.054 - 5 - 8 + 29.133$$

Then the power aperture product is

$$P_{av} + A = 33.793dB$$

Now, assume the radar wavelength to be $\lambda = 0.03m$, then

$$A = \frac{G\lambda^2}{4\pi} = 3.550dB; P_{av} = -A + 33.793 = 30.243dB$$

$$P_{av} = 10^{3.0243} = 1057.548W$$

$$P_t = \frac{P_{av}}{d_t} = \frac{1057.548}{0.3} = 3.52516KW.$$

MATLAB Function “power_aperture_eq.m”

The function “power_aperture_req.m” implements the search radar equation given in Eq. (1.75); it is given in Listing 1.7 in Section 1.8. Plots of peak power versus aperture area and the power aperture product versus range for three range choices are generated. Figure 1.24 shows typical output using the parameters given in Example 1.6. The syntax is as follows:

$$[p_a_p, aperture, pt, pav] = power_aperture_req (snr, freq, tsc, sigma, dt, range, te, nf, loss, az_angle, el_angle, g, rcs_delta1, rcs_delta2)$$

where

Symbol	Description	Units	Status
<i>snr</i>	<i>sensitivity snr</i>	<i>dB</i>	<i>input</i>
<i>freq</i>	<i>frequency</i>	<i>Hz</i>	<i>input</i>
<i>tsc</i>	<i>scan time</i>	<i>seconds</i>	<i>input</i>
<i>sigma</i>	<i>target cross section</i>	<i>m²</i>	<i>input</i>
<i>dt</i>	<i>duty cycle</i>	<i>none</i>	<i>input</i>
<i>range</i>	<i>target range</i>	<i>Km</i>	<i>input</i>
<i>te</i>	<i>effective temperature</i>	<i>Kelvin</i>	<i>input</i>
<i>nf</i>	<i>noise figure</i>	<i>dB</i>	<i>input</i>
<i>loss</i>	<i>radar losses</i>	<i>dB</i>	<i>input</i>
<i>az_angle</i>	<i>search volume azimuth extent</i>	<i>degrees</i>	<i>input</i>
<i>el_angle</i>	<i>search volume elevation extent</i>	<i>degrees</i>	<i>input</i>
<i>g</i>	<i>antenna gain</i>	<i>dB</i>	<i>input</i>
<i>rcs_delta1</i>	<i>rcs delta 1 (sigma - delta1)</i>	<i>dB</i>	<i>input</i>
<i>rcs_delta2</i>	<i>rcs delta2 (sigma + delta2)</i>	<i>dB</i>	<i>input</i>
<i>p_a_p</i>	<i>power aperture product</i>	<i>dB</i>	<i>output</i>
<i>aperture</i>	<i>antenna aperture</i>	<i>m²</i>	<i>output</i>
<i>pt</i>	<i>peak power</i>	<i>KW</i>	<i>output</i>
<i>pav</i>	<i>average power</i>	<i>KW</i>	<i>output</i>

1.6.4. Radar Equation with Jamming

Any deliberate electronic effort intended to disturb normal radar operation is usually referred to as an Electronic Countermeasure (ECM). This may also include chaff, radar decoys, radar RCS alterations (e.g., radio frequency absorbing materials), and of course, radar jamming. Jammers can be categorized into two general types: (1) barrage jammers; and (2) deceptive jammers (repeaters).

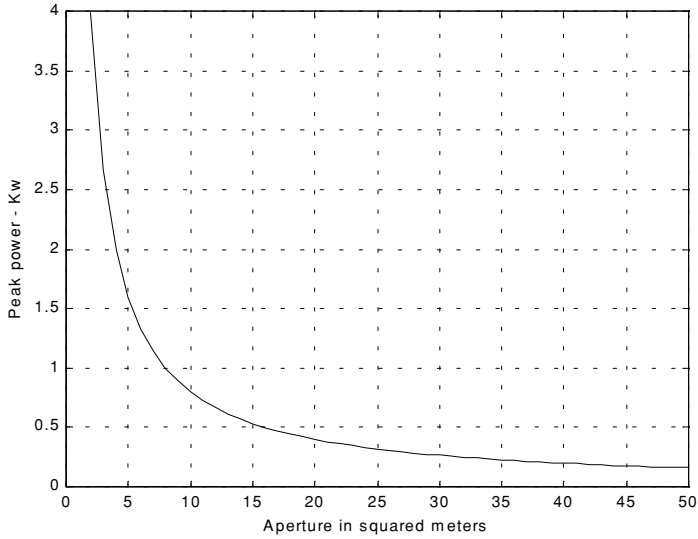
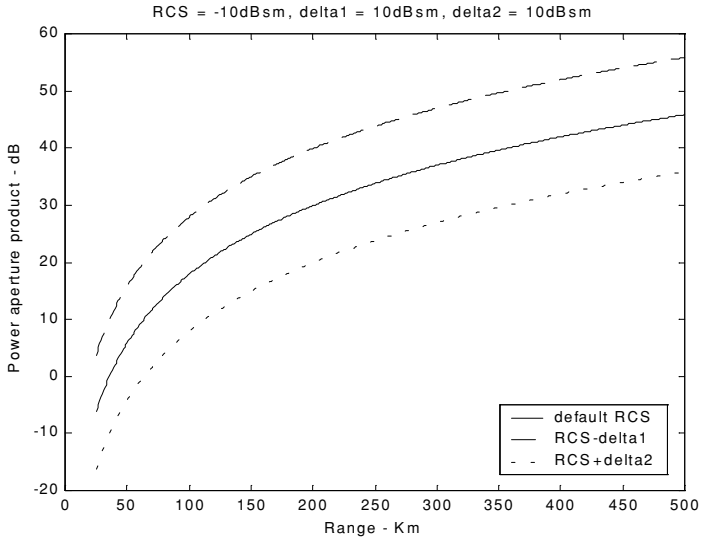


Figure 1.24. Typical outputs generated by the function “*power_aperture_req.m*”. Plots correspond to parameters from Example 1.6.

When strong jamming is present, detection capability is determined by receiver signal-to-noise plus interference ratio rather than SNR. And in most cases, detection is established based on the signal-to-interference ratio alone.

Barrage jammers attempt to increase the noise level across the entire radar operating bandwidth. Consequently, this lowers the receiver SNR, and, in turn, makes it difficult to detect the desired targets. This is the reason why barrage jammers are often called maskers (since they mask the target returns). Barrage jammers can be deployed in the main beam or in the side lobes of the radar antenna. If a barrage jammer is located in the radar main beam, it can take advantage of the antenna maximum gain to amplify the broadcasted noise signal. Alternatively, side lobe barrage jammers must either use more power, or operate at a much shorter range than main beam jammers. Main beam barrage jammers can be deployed either on-board the attacking vehicle, or act as an escort to the target. Side lobe jammers are often deployed to interfere with a specific radar, and since they do not stay close to the target, they have a wide variety of stand-off deployment options.

Repeater jammers carry receiving devices on board in order to analyze the radar's transmission, and then send back false target-like signals in order to confuse the radar. There are two common types of repeater jammers: spot noise repeaters and deceptive repeaters. The spot noise repeater measures the transmitted radar signal bandwidth and then jams only a specific range of frequencies. The deceptive repeater sends back altered signals that make the target appear in some false position (ghosts). These ghosts may appear at different ranges or angles than the actual target. Furthermore, there may be several ghosts created by a single jammer. By not having to jam the entire radar bandwidth, repeater jammers are able to make more efficient use of their jamming power. Radar frequency agility may be the only way possible to defeat spot noise repeaters.

Self-Screening Jammers (SSJ)

Self-screening jammers, also known as self-protecting jammers, are a class of ECM systems carried on the vehicle they are protecting. Escort jammers (carried on vehicles that accompany the attacking vehicles) can also be treated as SSJs if they appear at the same range as that of the target(s).

Assume a radar with an antenna gain G , wavelength λ , aperture A , bandwidth B , receiver losses L , and peak power P_t . The single pulse power received by the radar from a target of RCS σ , at range R , is

$$P_r = \frac{P_t G^2 \lambda^2 \sigma}{(4\pi)^3 R^4 L} \quad (1.76)$$

The power received by the radar from an SSJ jammer at the same range is

$$P_{SSJ} = \frac{P_J G_J}{4\pi R^2} \frac{AB}{B_J L_J} \quad (1.77)$$

where P_J, G_J, B_J, L_J are, respectively, the jammer's peak power, antenna gain, operating bandwidth, and losses. Substituting Eq. (1.47) into Eq. (1.77) yields

$$P_{SSJ} = \frac{P_J G_J}{4\pi R^2} \frac{\lambda^2 G}{4\pi} \frac{B}{B_J L_J} \quad (1.78)$$

The factor (B/B_J) (a ratio less than unity) is needed in order to compensate for the fact that the jammer bandwidth is usually larger than the operating bandwidth of the radar. This is because jammers are normally designed to operate against a wide variety of radar systems with different bandwidths. Thus, the radar equation for a SSJ case is obtained from Eqs. (1.76) and (1.78),

$$\frac{S}{S_{SSJ}} = \frac{P_t G \sigma B_J L_J}{4\pi P_J G_J R^2 B L} \quad (1.79)$$

where G_p is the radar processing gain.

The jamming power reaches the radar on a one-way transmission basis, whereas the target echoes involve two-way transmission. Thus, the jamming power is generally greater than the target signal power. In other words, the ratio S/S_{SSJ} is less than unity. However, as the target becomes closer to the radar, there will be a certain range such that the ratio S/S_{SSJ} is equal to unity. This range is known as the crossover or burn-through range. The range window where the ratio S/S_{SSJ} is sufficiently larger than unity is denoted as the detection range. In order to compute the crossover range R_{co} , set S/S_{SSJ} to unity in Eq. (1.79) and solve for range. It follows that

$$(R_{CO})_{SSJ} = \left(\frac{P_t G \sigma B_J L_J}{4\pi P_J G_J B L} \right)^{1/2} \quad (1.80)$$

MATLAB Program “ssj_req.m”

The program “ssj_req.m” implements Eqs. (1.76) through (1.80); it is given in Listing 1.8 in Section 1.8. This program calculates the crossover range and generates plots of relative S and S_{SSJ} versus range normalized to the crossover range, as illustrated in Fig. 1.25. In this example, the following parameters were utilized in producing this figure: radar peak power $p_t = 50KW$, jammer peak power $P_J = 200W$, radar operating bandwidth $B = 667KHz$, jammer bandwidth $B_J = 50MHz$, radar and jammer losses $L = L_J = 0.10dB$, target cross section $\sigma = 10.m^2$, radar antenna gain $G = 35dB$, jammer antenna gain $G_J = 10dB$.

The syntax is as follows:

$$[BR_range] = ssj_req (pt, g, freq, sigma, b, loss, pj, bj, gj, lossj)$$

where

Symbol	Description	Units	Status
<i>pt</i>	radar peak power	KW	input
<i>g</i>	radar antenna gain	dB	input
<i>sigma</i>	target cross section	m ²	input
<i>freq</i>	radar operating frequency	Hz	input
<i>b</i>	radar operating bandwidth	Hz	input
<i>loss</i>	radar losses	dB	input
<i>pj</i>	jammer peak power	KW	input
<i>bj</i>	jammer bandwidth	Hz	input
<i>gj</i>	jammer antenna gain	dB	input
<i>lossj</i>	jammer losses	dB	input
<i>BR_range</i>	burn-through range	Km	output

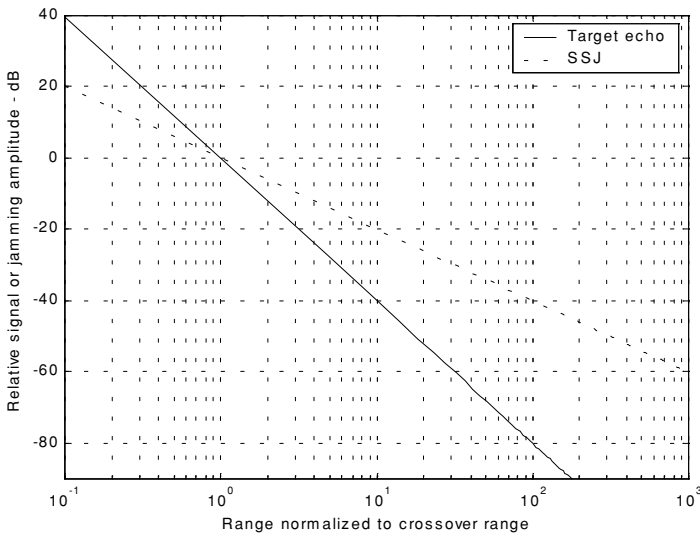


Figure 1.25. Target and jammer echo signals. Plots were generated using the program “*ssj_req.m*”.

Stand-Off Jammers (SOJ)

Stand-off jammers (SOJ) emit ECM signals from long ranges which are beyond the defense's lethal capability. The power received by the radar from an SOJ jammer at range R_J is

$$P_{SOJ} = \frac{P_J G_J}{4\pi R_J^2} \frac{\lambda^2 G'}{4\pi} \frac{B}{B_J L_J} \quad (1.81)$$

where all terms in Eq. (1.81) are the same as those for the SSJ case except for G' . The gain term G' represents the radar antenna gain in the direction of the jammer and is normally considered to be the side lobe gain.

The SOJ radar equation is then computed from Eqs. (1.81) and (1.76) as

$$\frac{S}{S_{SOJ}} = \frac{P_i G^2 R_J^2 \sigma B_J L_J}{4\pi P_J G_J G' R^4 B L} \quad (1.82)$$

Again, the crossover range is that corresponding to $S = S_{SOJ}$; it is given by

$$(R_{CO})_{SOJ} = \left(\frac{P_i G^2 R_J^2 \sigma B_J L_J}{4\pi P_J G_J G' B L} \right)^{1/4} \quad (1.83)$$

and the detection range is

$$R_D = \frac{(R_{co})_{SOJ}}{\sqrt[4]{(S/S_{SOJ})_{min}}} \quad (1.84)$$

where $(S/S_{SOJ})_{min}$ is the minimum value of the signal-to-jammer power ratio such that target detection can occur.

Note that in practice, the ratio S/S_{SOJ} is normally computed after pulse compression, and thus Eqs. (1.82) and (1.83) must be modified by multiplication with the compression gain G_{comp} . Plots in Figs. 1.25 and 1.26 were produced without regard to pulse compression gain.

MATLAB Program "soj_req.m"

The program "soj_req.m" implements Eqs. (1.82) and (1.83); it is given in Listing 1.9 in Section 1.8. The inputs to the program "soj_req.m" are the same as in the SSJ case, with two additional inputs: they are the radar antenna gain on the jammer G' and radar to jammer range R_J . This program generates the same type of plots as in the case of the SSJ. Typical output is in Fig. 1.26 utilizing the same parameters as those in the SSJ case, with jammer peak power $P_J = 5000W$, jammer antenna gain $G_J = 30dB$, radar antenna gain on the jammer $G' = 10dB$, and radar to jammer range $R_J = 22.2Km$.

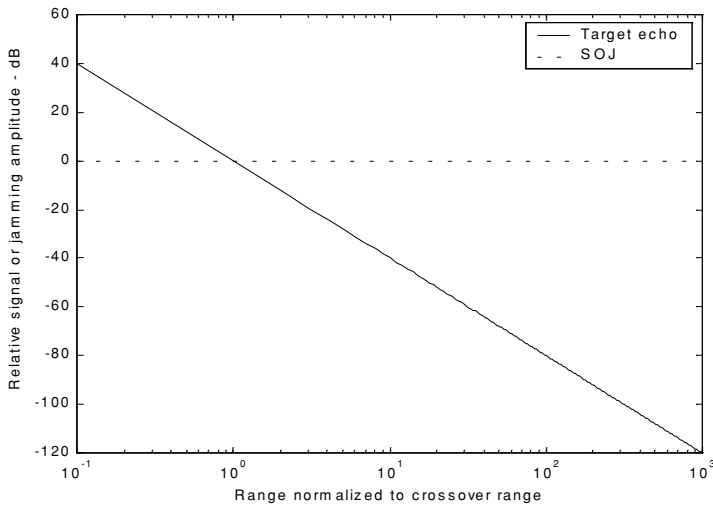


Figure 1.26. Target and jammer echo signals. Plots were generated using the program “*soj_req.m*”.

Range Reduction Factor

Consider a radar system whose detection range R in the absence of jamming is governed by Eq. (1.61), which is repeated here as Eq. (1.85):

$$(SNR)_o = \frac{P_t G^2 \lambda^2 \sigma}{(4\pi)^3 k T_e B F L R^4} \quad (1.85)$$

The term Range Reduction Factor (RRF) refers to the reduction in the radar detection range due to jamming. More precisely, in the presence of jamming the effective radar detection range is

$$R_{dj} = R \times RRF \quad (1.86)$$

In order to compute RRF, consider a radar characterized by Eq. (1.85), and a barrage jammer whose output power spectral density is J_o . Then, the amount of jammer power in the radar receiver is

$$P_j = J_o B = k T_j B \quad (1.87)$$

where k is Boltzman’s constant and T_j is the jammer effective temperature. It follows that the total jammer plus noise power in the radar receiver is given by

$$N_i + P_J = kT_e B + kT_J B \quad (1.88)$$

In this case, the radar detection range is now limited by the receiver signal-to-noise plus interference ratio rather than SNR. More precisely,

$$\left(\frac{S}{P_{SSJ} + N} \right) = \frac{P_i G^2 \lambda^2 \sigma}{(4\pi)^3 k(T_e + T_J) BFLR^4} \quad (1.89)$$

The amount of reduction in the signal-to-noise plus interference ratio because of the jammer effect can be computed from the difference between Eqs. (1.85) and (1.89). It is expressed (in dBs) by

$$\Upsilon = 10.0 \times \log \left(1 + \frac{T_J}{T_e} \right) \quad (1.90)$$

Consequently, the RRF is

$$RRF = 10^{\frac{-\Upsilon}{40}} \quad (1.91)$$

MATLAB Function “range_red_fac.m”

The function “range_red_factor.m” implements Eqs. (1.90) and (1.91); it is given in Listing 1.10 in Section 1.8. This function generates plots of RRF versus: (1) the radar operating frequency; (2) radar to jammer range; and (3) jammer power. Its syntax is as follows:

range_red_factor (te, pj, gj, g, freq, bj, rangej, lossj)

where

Symbol	Description	Units	Status
<i>te</i>	<i>radar effective temperature</i>	<i>K</i>	<i>input</i>
<i>pj</i>	<i>jammer peak power</i>	<i>KW</i>	<i>input</i>
<i>gj</i>	<i>jammer antenna gain</i>	<i>dB</i>	<i>input</i>
<i>g</i>	<i>radar antenna gain on jammer</i>	<i>dB</i>	<i>input</i>
<i>freq</i>	<i>radar operating frequency</i>	<i>Hz</i>	<i>input</i>
<i>bj</i>	<i>jammer bandwidth</i>	<i>Hz</i>	<i>input</i>
<i>rangej</i>	<i>radar to jammer range</i>	<i>Km</i>	<i>input</i>
<i>lossj</i>	<i>jammer losses</i>	<i>dB</i>	<i>input</i>

The following values were used to produce Figs. 1.27 through 1.29.

<i>te</i>	<i>pj</i>	<i>gj</i>	<i>g</i>	<i>freq</i>	<i>bj</i>	<i>rangej</i>	<i>lossj</i>
730K	150KW	3dB	40dB	10GHz	1MHz	400Km	1dB

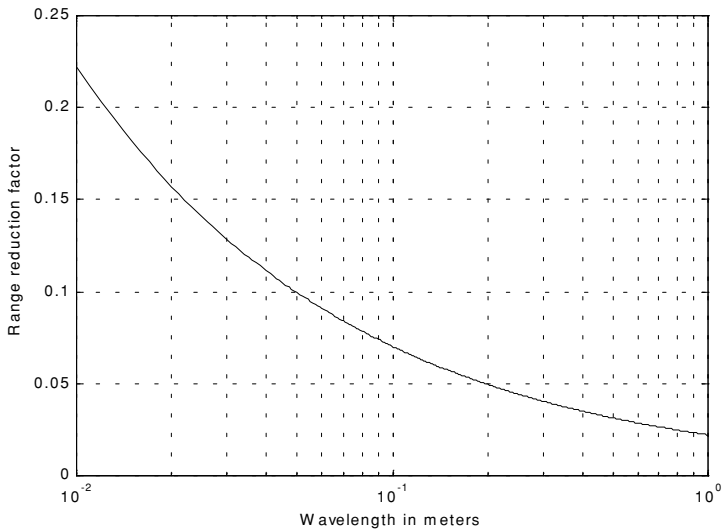


Figure 1.27. Range reduction factor versus radar operating wavelength. This plot was generated using the function “*range_red_factor.m*”.

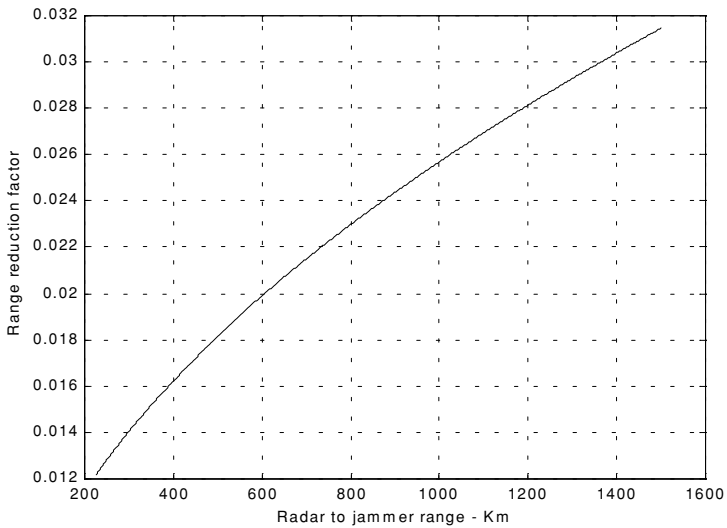


Figure 1.28. Range reduction factor versus radar to jammer range. This plot was generated using the function “*range_red_factor.m*”.

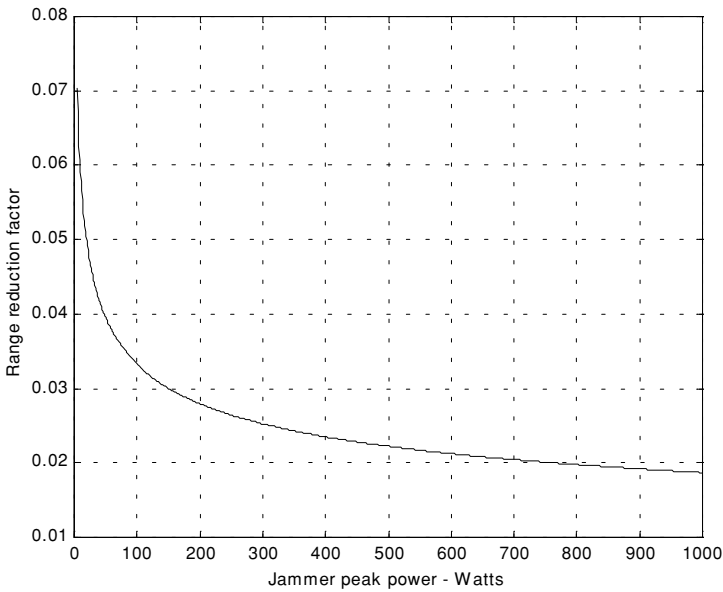


Figure 1.29. Range reduction factor versus jammer peak power. This plot was generated using the function “range_red_factor.m”.

1.6.5. Bistatic Radar Equation

Radar systems that use the same antenna for both transmitting and receiving are called monostatic radars. Bistatic radars use transmit and receive antennas that are placed in different locations. Under this definition CW radars, although they use separate transmit and receive antennas, are not considered bistatic radars unless the distance between the two antennas is considerable. Figure 1.30 shows the geometry associated with bistatic radars. The angle, β , is called the bistatic angle. A synchronization link between the transmitter and receiver is necessary in order to maximize the receiver’s knowledge of the transmitted signal so that it can extract maximum target information.

The synchronization link may provide the receiver with the following information: (1) the transmitted frequency in order to compute the Doppler shift; and (2) the transmit time or phase reference in order to measure the total scattered path ($R_t + R_r$). Frequency and phase reference synchronization can be maintained through line-of-sight communications between the transmitter and receiver. However, if this is not possible, the receiver may use a stable reference oscillator for synchronization.

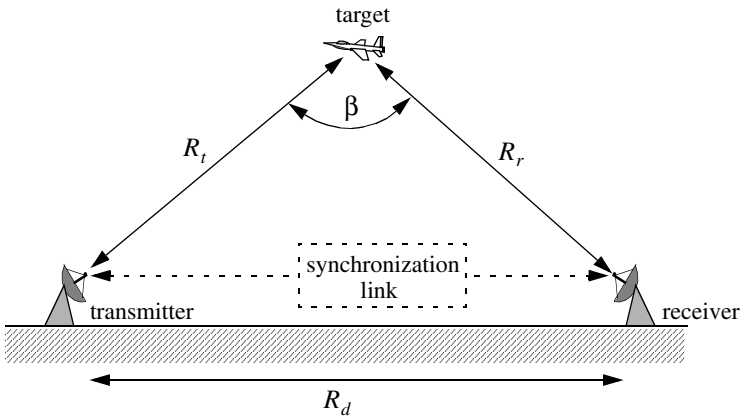


Figure 1.30. Bistatic radar geometry.

One major distinction between monostatic and bistatic radar operations has to do with the measured bistatic target RCS, denoted by σ_B . In the case of a small bistatic angle, the bistatic RCS is similar to the monostatic RCS: but, as the bistatic angle approaches 180° , the bistatic RCS becomes very large and can be approximated by

$$\sigma_{B_{max}} \approx \frac{4\pi A_t^2}{\lambda^2} \quad (1.92)$$

where λ is the wavelength and A_t is the target projected area.

The bistatic radar equation can be derived in a similar fashion to the monostatic radar equation. Referring to Fig. 1.30, the power density at the target is

$$P_D = \frac{P_t G_t}{4\pi R_t^2} \quad (1.93)$$

where P_t is the peak transmitted power, G_t is the gain of the transmitting antenna, and R_t is the range from the radar transmitter to the target.

The effective power scattered off a target with bistatic RCS σ_B is

$$P' = P_D \sigma_B \quad (1.94)$$

and the power density at the receiver antenna is

$$P_{refl} = \frac{P'}{4\pi R_r^2} = \frac{P_D \sigma_B}{4\pi R_r^2} \quad (1.95)$$

where R_r is the range from the target to the receiver. Substituting Eq. (1.93) into Eq. (1.95) yields

$$P_{refl} = \frac{P_t G_t \sigma_B}{(4\pi)^2 R_t^2 R_r^2} \quad (1.96)$$

The total power delivered to the signal processor by a receiver antenna with aperture A_e is

$$P_{Dr} = \frac{P_t G_t \sigma_B A_e}{(4\pi)^2 R_t^2 R_r^2} \quad (1.97)$$

Substituting $(G_r \lambda^2 / 4\pi)$ for A_e yields

$$P_{Dr} = \frac{P_t G_t G_r \lambda^2 \sigma_B}{(4\pi)^3 R_t^2 R_r^2} \quad (1.98)$$

where G_r is gain of the receive antenna. Finally, when transmitter and receiver losses, L_t and L_r , are taken into consideration, the bistatic radar equation can be written as

$$P_{Dr} = \frac{P_t G_t G_r \lambda^2 \sigma_B}{(4\pi)^3 R_t^2 R_r^2 L_t L_r L_p} \quad (1.99)$$

where L_p is the medium propagation loss.

1.7. Radar Losses

As indicated by the radar equation, the receiver SNR is inversely proportional to the radar losses. Hence, any increase in radar losses causes a drop in the SNR, thus decreasing the probability of detection, since it is a function of the SNR. Often, the principal difference between a good radar design and a poor radar design is the radar losses. Radar losses include ohmic (resistance) losses and statistical losses. In this section we will briefly summarize radar losses.

1.7.1. Transmit and Receive Losses

Transmit and receive losses occur between the radar transmitter and antenna input port, and between the antenna output port and the receiver front end, respectively. Such losses are often called plumbing losses. Typically, plumbing losses are on the order of 1 to 2 dBs.

1.7.2. Antenna Pattern Loss and Scan Loss

So far, when we used the radar equation we assumed maximum antenna gain. This is true only if the target is located along the antenna's boresight axis. However, as the radar scans across a target the antenna gain in the direction of the target is less than maximum, as defined by the antenna's radiation pattern. The loss in the SNR due to not having maximum antenna gain on the target at all times is called the antenna pattern (shape) loss. Once an antenna has been selected for a given radar, the amount of antenna pattern loss can be mathematically computed.

For example, consider a $\sin x/x$ antenna radiation pattern as shown in Fig. 1.31. It follows that the average antenna gain over an angular region of $\pm\theta/2$ about the boresight axis is

$$G_{av} \approx 1 - \left(\frac{\pi r}{\lambda}\right)^2 \frac{\theta^2}{36} \quad (1.100)$$

where r is the aperture radius and λ is the wavelength. In practice, Gaussian antenna patterns are often adopted. In this case, if θ_{3dB} denotes the antenna 3dB beam width, then the antenna gain can be approximated by

$$G(\theta) = \exp\left(-\frac{2.776\theta^2}{\theta_{3dB}^2}\right) \quad (1.101)$$

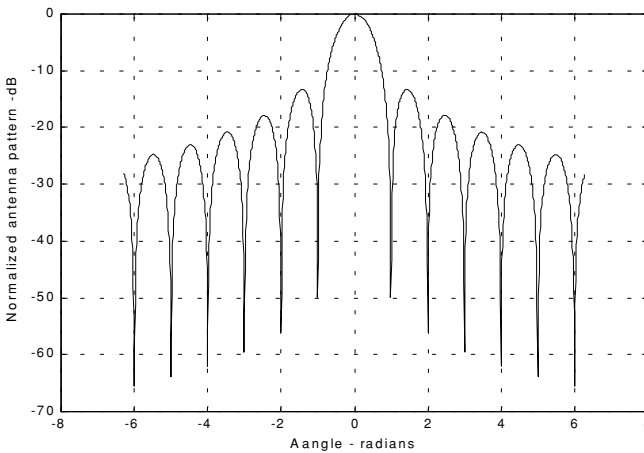


Figure 1.31. Normalized ($\sin x / x$) antenna pattern.

If the antenna scanning rate is so fast that the gain on receive is not the same as on transmit, additional scan loss has to be calculated and added to the beam shape loss. Scan loss can be computed in a similar fashion to beam shape loss. Phased array radars are often prime candidates for both beam shape and scan losses.

1.7.3. Atmospheric Loss

Detailed discussion of atmospheric loss and propagation effects is in a later chapter. Atmospheric attenuation is a function of the radar operating frequency, target range, and elevation angle. Atmospheric attenuation can be as high as a few dBs.

1.7.4. Collapsing Loss

When the number of integrated returned noise pulses is larger than the target returned pulses, a drop in the SNR occurs. This is called collapsing loss. The collapsing loss factor is defined as

$$\rho_c = \frac{n + m}{n} \tag{1.102}$$

where n is the number of pulses containing both signal and noise, while m is the number of pulses containing noise only. Radars detect targets in azimuth, range, and Doppler. When target returns are displayed in one coordinate, such as range, noise sources from azimuth cells adjacent to the actual target return converge in the target vicinity and cause a drop in the SNR. This is illustrated in Fig. 1.32.

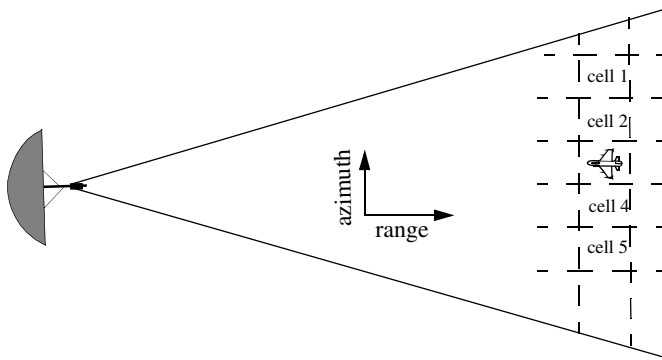


Figure 1.32. Illustration of collapsing loss. Noise sources in cells 1, 2, 4, and 5 converge to increase the noise level in cell 3.

1.7.5. Processing Losses

a. Detector Approximation:

The output voltage signal of a radar receiver that utilizes a linear detector is

$$v(t) = \sqrt{v_I^2(t) + v_Q^2(t)}$$

where (v_I, v_Q) are the in-phase and quadrature components. For a radar using a square law detector, we have $v^2(t) = v_I^2(t) + v_Q^2(t)$.

Since in real hardware the operations of squares and square roots are time consuming, many algorithms have been developed for detector approximation. This approximation results in a loss of the signal power, typically 0.5 to 1 dB.

b. Constant False Alarm Rate (CFAR) Loss:

In many cases the radar detection threshold is constantly adjusted as a function of the receiver noise level in order to maintain a constant false alarm rate. For this purpose, Constant False Alarm Rate (CFAR) processors are utilized in order to keep the number of false alarms under control in a changing and unknown background of interference. CFAR processing can cause a loss in the SNR level on the order of 1 dB.

Three different types of CFAR processors are primarily used. They are adaptive threshold CFAR, nonparametric CFAR, and nonlinear receiver techniques. Adaptive CFAR assumes that the interference distribution is known and approximates the unknown parameters associated with these distributions. Nonparametric CFAR processors tend to accommodate unknown interference distributions. Nonlinear receiver techniques attempt to normalize the root mean square amplitude of the interference.

c. Quantization Loss:

Finite word length (number of bits) and quantization noise cause an increase in the noise power density at the output of the Analog to Digital (A/D) converter. The A/D noise level is $q^2/12$, where q is the quantization level.

d. Range Gate Straddle:

The radar receiver is normally mechanized as a series of contiguous range gates (bins). Each range bin is implemented as an integrator matched to the transmitted pulse width. Since the radar receiver acts as a filter that smears (smooths), the received target echoes. The smoothed target return envelope is normally straddled to cover more than one range gate.

Typically, three gates are affected; they are called the early, on, and late gates. If a point target is located exactly at the center of a range gate, then the

early and late samples are equal. However, as the target starts to move into the next gate, the late sample becomes larger while the early sample gets smaller. In any case, the amplitudes of all three samples should always roughly add up to the same value. Fig. 1.33 illustrates the concept of range straddling. The envelope of the smoothed target echo is likely to be Gaussian shape. In practice, triangular shaped envelopes may be easier and faster to implement.

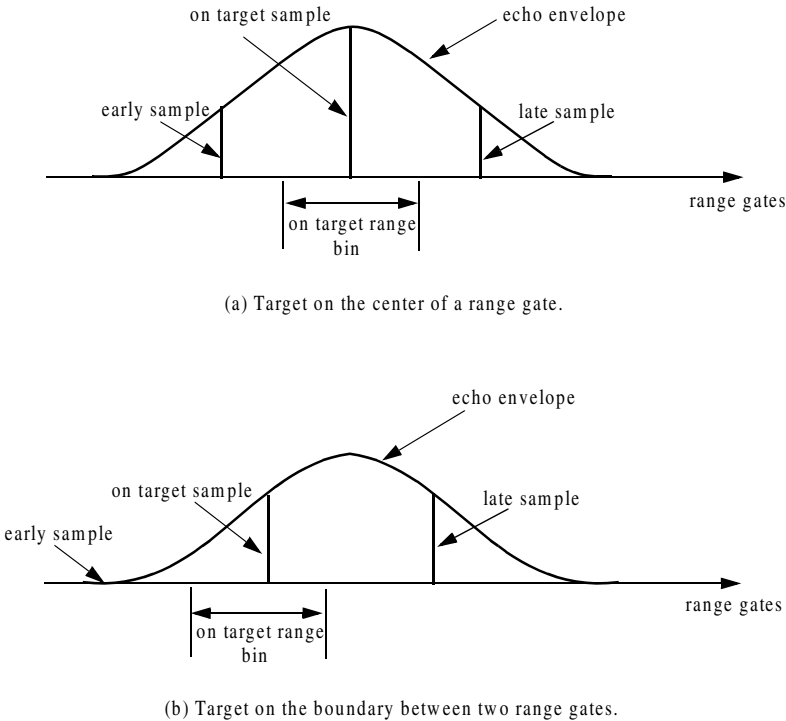
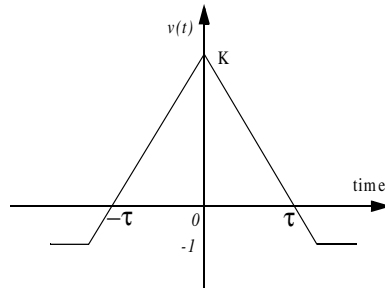


Figure 1.33. Illustration of range gate straddling.

Since the target is likely to fall anywhere between two adjacent range bins, a loss in the SNR occurs (per range gate). More specifically, a target's returned energy is split between three range bins. Typically, straddle loss of about 2 to 3 dBs is not unusual.

Example 1.7: Consider the smoothed target echo voltage shown below. Assume 1Ω resistance. Find the power loss due to range gate straddling over the interval $\{0, \tau\}$.



Solution: The smoothed voltage can be written as

$$v(t) = \begin{cases} K + \left(\frac{K+1}{\tau}\right)t & ; t < 0 \\ K - \left(\frac{K+1}{\tau}\right)t & ; t \geq 0 \end{cases}$$

The power loss due to straddle over the interval $\{0, \tau\}$ is

$$L_s = \frac{v^2}{K^2} = 1 - 2\left(\frac{K+1}{K\tau}\right)t + \left(\frac{K+1}{K\tau}\right)^2 t^2$$

The average power loss is then

$$\begin{aligned} \bar{L}_s &= \frac{2}{\tau} \int_0^{\tau/2} \left(1 - 2\left(\frac{K+1}{K\tau}\right)t + \left(\frac{K+1}{K\tau}\right)^2 t^2\right) dt \\ &= 1 - \frac{K+1}{2K} + \frac{(K+1)^2}{12K^2} \end{aligned}$$

and, for example, if $K = 15$, then $\bar{L}_s = 2.5dB$.

e. Doppler Filter Straddle:

Doppler filter straddle is similar to range gate straddle. However, in this case the Doppler filter spectrum is spread (widened) due to weighting functions. Weighting functions are normally used to reduce the side lobe levels. Since the target Doppler frequency can fall anywhere between two Doppler filters, signal loss occurs. This is illustrated in Fig. 1.34, where due to weighting, the crossover frequency f_{co} is smaller than the filter cutoff frequency f_c which normally corresponds to the 3dB power point.

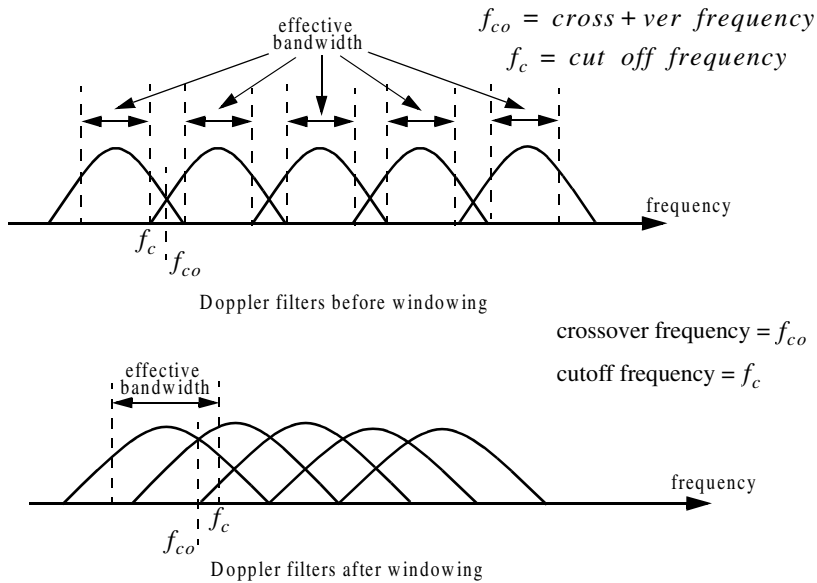


Figure 1.34. Due to windowing, the crossover frequency may become smaller than the cutoff frequency.

1.7.6. Other Losses

Other losses may include equipment losses due to aging radar hardware, matched filter loss, and antenna efficiency loss. Tracking radars suffer from crossover (squint) loss (see Chapter 11).

1.8. MATLAB Program and Function Listings

This section presents listings for all MATLAB functions and programs used in this chapter. Users are encouraged to vary the input parameters and rerun these programs in order to enhance their understanding of the theory presented in the text. All selected parameters and variables follow the same naming notation used in the text, thus, understanding the structure and hierarchy of the presented code should be an easy task once the user has read the theory.

For almost each MATLAB function or program provided in this book, there is a companion file designated as “filename_driver.m”. These “driver” files utilize MATLAB-based Graphical User Interface (GUI). For example, the

companion “*driver*” file for the function “*lprf_req.m*” is “*lprf_req_driver.m*”. When a “*driver*” file is executed, it opens a GUI work space which can be used by the user to enter values to parameters and produce the relevant plots. Figure 1.35 shows the GUI work space for the function “*lprf_req_driver.m*”. Note that all MATLAB programs and functions developed in this book can be downloaded from CRC Press Web Site “www.crcpress.com”.

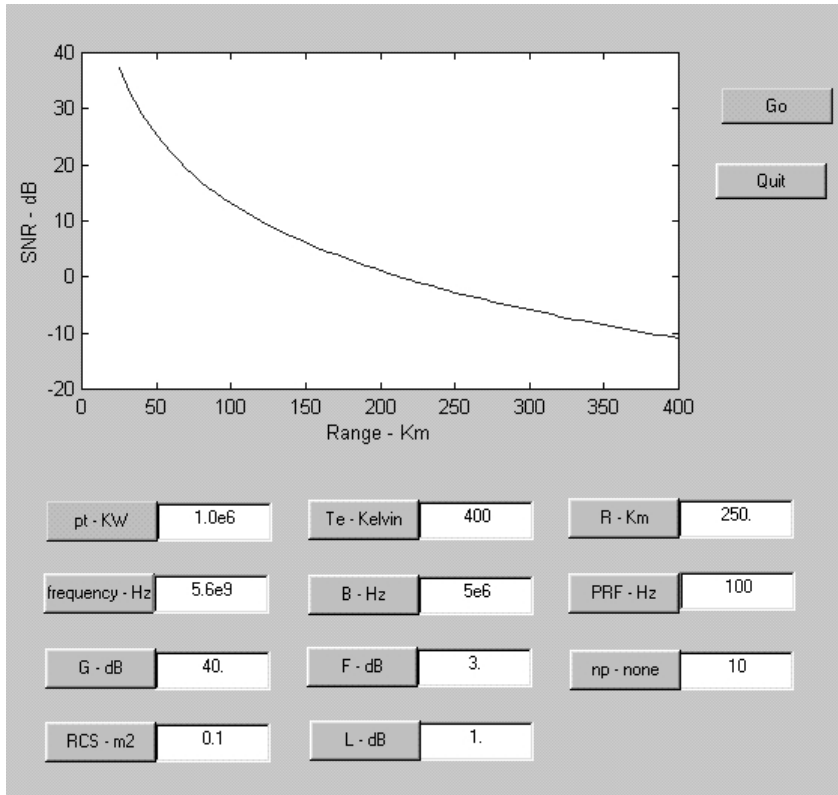


Figure 1.35 GUI work space related to the function “*lprf_req.m*”. Note that this GUI was designed on a Windows 98 Personal Computer (PC) using MATLAB 5 - Release 11 and thus, it may appear different on Apple or Unix based machines, or PC systems using earlier versions of MATLAB.

Listing 1.1. MATLAB Function “pulse_train.m”

```
function [dt, prf, pav, ep, ru] = pulse_train(tau, pri, p_peak)
% This function is described in Section 1.2.
c = 3.0e+8;
dt = tau / pri;
prf = 1. / pri;
pav = p_peak * dt;
ep = p_peak * tau;
ru = 1.0e-3 * c * pri / 2.0;
return
```

Listing 1.2. MATLAB Function “range_resolution.m”

```
function [delta_R] = range_resolution(bandwidth,indicator)
% This function computes radar range resolution in meters
% the bandwidth must be in Hz ==> indicator = Hz.
% Bandwidth may be equal to (1/pulse width)==> indicator = seconds
c = 3.e+8;
if(indicator == 'hz')
    delta_R = c / (2.0 * bandwidth);
else
    delta_R = c * bandwidth / 2.0;
end
return
```

Listing 1.3. MATLAB Function “doppler_freq.m”

```
function [fd, tdr] = doppler_freq(freq, ang, tv, indicator)
% This function computes Doppler frequency and time dilation factor ratio
% tau_prime / tau
format long
c = 3.0e+8;
ang_rad = ang * pi / 180.;
lambda = c / freq;
if (indicator == 1)
    fd = 2.0 * tv * cos(ang_rad) / lambda;
    tdr = (c - tv) / (c + tv);
else
    fd = -2.0 * c * tv * cos(ang_rad) / lambda;
    tdr = (c + tv) / (c -tv);
end
return
```

Listing 1.4. MATLAB Function “radar_eq.m”

```
function [out_par] = radar_eq(pt, freq, g, sigma, te, b, nf, loss, input_par, option,
    rcs_delta1, rcs_delta2, pt_percent1, pt_percent2)
```

% This function implements Eq. (1.161). Parameters description is in Section 1.6.

```

c = 3.0e+8;
lambda = c / freq;
p_peak = base10_to_dB(pt);
lambda_sq = lambda^2;
lambda_sqdb = base10_to_dB(lambda_sq);
sigmadb = base10_to_dB(sigma);
for_pi_cub = base10_to_dB((4.0 * pi)^3);
k_db = base10_to_dB(1.38e-23);
te_db = base10_to_dB(te);
b_db = base10_to_dB(b);
if (option == 1)
    temp = p_peak + 2. * g + lambda_sqdb + sigmadb - ...
        for_pi_cub - k_db - te_db - b_db - nf - loss - input_par;
    out_par = dB_to_base10(temp)^(1/4)
    % calculate sigma(+/-)10dB (rcs +- rcs_delta1,2)
    sigmap = rcs_delta1 + sigmadb;
    sigmam = sigmadb - rcs_delta2.;
    % calculate.pt_percent1 * pt and pt_percent2% * pt
    pt05 = p_peak + base10_to_dB(pt_percent1);
    pt200 = p_peak + base10_to_dB(pt_percent2);
    index = 0;
    % vary snr from .5 to 1.5 of default value
    for snrvar = input_par*.5: 1: input_par*1.5
        index = index + 1;
        range1(index) = dB_to_base10(p_peak + 2. * g + lambda_sqdb + ...
            sigmam - for_pi_cub - k_db - te_db - b_db - nf - loss - snrvar) ...
            ^(1/4) / 1000.0;
        range2(index) = dB_to_base10(p_peak + 2. * g + lambda_sqdb + ...
            sigmadb - for_pi_cub - k_db - te_db - b_db - nf - loss - snrvar) ...
            ^(1/4) / 1000.0;
        range3(index) = dB_to_base10(p_peak + 2. * g + lambda_sqdb + ...
            sigmap - for_pi_cub - k_db - te_db - b_db - nf - loss - snrvar) ...
            ^(1/4) / 1000.0;
    end
    index = 0;
    for snrvar = input_par*.5: 1: input_par*1.5;
        index = index + 1;
        rangp1(index) = dB_to_base10(pt05 + 2. * g + lambda_sqdb + ...
            sigmadb - for_pi_cub - k_db - te_db - b_db - nf - loss - snrvar) ...
            ^(1/4) / 1000.0;
        rangp2(index) = dB_to_base10(p_peak + 2. * g + lambda_sqdb + ...
            sigmadb - for_pi_cub - k_db - te_db - b_db - nf - loss - snrvar) ...
            ^(1/4) / 1000.0;
        rangp3(index) = dB_to_base10(pt200 + 2. * g + lambda_sqdb + ...
            sigmadb - for_pi_cub - k_db - te_db - b_db - nf - loss - snrvar) ...
            ^(1/4) / 1000.0;
    end
end

```

```

snrvar = input_par*.5: 1: input_par*1.5;
figure (1)
subplot (2,1,1)
plot (snrvar,range2,snrvar,range1,snrvar,range3)
legend ('default RCS','RCS-rcs_delta1','RCS+rcs_delta2')
xlabel ('Minimum SNR required for detection - dB');
ylabel ('Detection range - Km');
%title ('Plots correspond to input parameters from example 1.4');
subplot (2,1,2)
plot (snrvar,rangp2,snrvar,rangp1,snrvar,rangp3)
legend ('default power','.pt_percent1*pt', 'pt_percent2*pt')
xlabel ('Minimum SNR required for detection - dB');
ylabel ('Detection range - Km')
else
range_db = base10_to_dB(input_par * 1000.0);
out_par = p_peak + 2. * g + lambda_sqdb + sigmadb - ...
    for_pi_cub - k_db - te_db - b_db - nf - loss - 4.0 * range_db
% calculate sigma -- rcs_delta1,2 dB
sigma5 = sigmadb - rcs_delta1;
sigma10 = sigmadb - rcs_delta2;
% calculate pt_percent1 % * pt and pt_percent2*pt
pt05 = p_peak + base10_to_dB(pt_percent1);
pt200 = p_peak + base10_to_dB(pt_percent2);
index = 0;
% vary snr from .5 to 1.5 of default value
for rangvar = input_par*.5 : 1 : input_par*1.5
    index = index + 1;
    var = 4.0 * base10_to_dB(rangvar * 1000.0);
    snr1(index) = p_peak + 2. * g + lambda_sqdb + sigmadb - ...
        for_pi_cub - k_db - te_db - b_db - nf - loss - var;
    snr2(index) = p_peak + 2. * g + lambda_sqdb + sigma5 - ...
        for_pi_cub - k_db - te_db - b_db - nf - loss - var;
    snr3(index) = p_peak + 2. * g + lambda_sqdb + sigma10 - ...
        for_pi_cub - k_db - te_db - b_db - nf - loss - var;
end
index = 0;
for rangvar = input_par*.5 : 1 : input_par*1.5;
    index = index + 1;
    var = 4.0 * base10_to_dB(rangvar * 1000.0);
    snrp1(index) = pt05 + 2. * g + lambda_sqdb + sigmadb - ...
        for_pi_cub - k_db - te_db - b_db - nf - loss - var;
    snrp2(index) = p_peak + 2. * g + lambda_sqdb + sigmadb - ...
        for_pi_cub - k_db - te_db - b_db - nf - loss - var;
    snrp3(index) = pt200 + 2. * g + lambda_sqdb + sigmadb - ...
        for_pi_cub - k_db - te_db - b_db - nf - loss - var;
end
end
rangvar = input_par*.5 : 1 : input_par*1.5;

```

```

figure (2)
subplot (2,1,1)
plot (rangvar,snr1,rangvar,snr2,rangvar,snr3)
legend ('default RCS','RCS-rcs_delta1','RCS-rcs_delta2')
xlabel ('Detection range - Km');
ylabel ('SNR - dB');
%title ('Plots correspond to input parameters from example 1.4');
subplot (2,1,2)
plot (rangvar,snrp2,rangvar,snrp1,rangvar,snrp3)
legend ('default power','pt_percent1*pt','pt_percent2*pt')
xlabel ('Detection range - Km');
ylabel ('SNR - dB');

```

Input file “radar_reqi.m”

```

% Use this input file to reproduce Fig. 1.18
clear all
pt = 1.5e+6;      % peak power in Watts
freq = 5.6e+9;   % radar operating frequency in Hz
g = 45.0;        % antenna gain in dB
sigma = 0.1;     % radar cross section in m square
te = 290.0;     % effective noise temperature in Kelvins
b = 5.0e+6;     % radar operating bandwidth in Hz
nf = 3.0;       % noise figure in dB
loss = 0.0;     % radar losses in dB
option = 1;     % 1 ==> input_par = SNR in dB
                % 2 ==> input_par = Range in Km

input_par = 20;
rcs_delta1 = 5.0; % rcs variation choice 1
rcs_delta2 = 10.0; % rcs variation choice2
pt_percent1 = 0.5; % peak power variation choice 1
pt_percent2 = 2.0; % peak power variation choice 2

```

Listing 1.5. MATLAB Function “lprf_req.m”

```

function [snr_out] = lprf_req (pt, freq, g, sigma, te, b, nf, loss, range, prf, np, rcs_delta,
                             pt_percent, np1, np2)
% This program implements the LOW PRF radar equation.
c = 3.0e+8;
lambda = c / freq;
p_peak = base10_to_dB(pt);
lambda_sq = lambda^2;
lambda_sqdb = base10_to_dB(lambda_sq);
sigmadb = base10_to_dB(sigma);
for_pi_cub = base10_to_dB((4.0 * pi)^3);
k_db = base10_to_dB(1.38e-23);
te_db = base10_to_dB(te)
b_db = base10_to_dB(b);

```

```

np_db = base10_to_dB(np);
range_db = base10_to_dB(range * 1000.0);
% Implement Eq. (1.65)
snr_out = p_peak + 2. * g + lambda_sqdb + sigmadb + np_db - ...
    for_pi_cub - k_db - te_db - b_db - nf - loss - 4.0 * range_db
% Generate plots in Fig. 1.19
index = 0;
n1 = np_db;
n2 = base10_to_dB(np1);
n3 = base10_to_dB(np2)
for range_var = 25:5:400 % 25 - 400 Km
    index = index + 1;
    rangevar_db = base10_to_dB(range_var * 1000.0);
    snr1(index) = p_peak + 2. * g + lambda_sqdb + sigmadb + n1 - ...
        for_pi_cub - k_db - te_db - b_db - nf - loss - 4.0 * rangevar_db;
    snr2(index) = p_peak + 2. * g + lambda_sqdb + sigmadb + n2 - ...
        for_pi_cub - k_db - te_db - b_db - nf - loss - 4.0 * rangevar_db;
    snr3(index) = p_peak + 2. * g + lambda_sqdb + sigmadb + n3 - ...
        for_pi_cub - k_db - te_db - b_db - nf - loss - 4.0 * rangevar_db;
end
figure(1)
var = 25:5:400;
plot(var,snr1,'k',var,snr2,'k--',var,snr3,'k-.')
legend('np = 1','np1','np2')
xlabel('Range - Km');
ylabel('SNR - dB');
%title('np = 1, np1 = 10, np2 =100');
% Generate plots in Fig. 1.20
sigma5 = sigmadb - rcs_delta.;
pt05 = p_peak + base10_to_dB(pt_percent);
index = 0;
for nvar =1:10:500 % 500 pulses
    index = index + 1;
    ndb = base10_to_dB(nvar);
    snrs(index) = p_peak + 2. * g + lambda_sqdb + sigmadb + ndb - ...
        for_pi_cub - k_db - te_db - b_db - nf - loss - 4.0 * range_db;
    snrs5(index) = p_peak + 2. * g + lambda_sqdb + sigma5 + ndb - ...
        for_pi_cub - k_db - te_db - b_db - nf - loss - 4.0 * range_db;
end
index = 0;
for nvar =1:10:500 % 500 pulses
    index = index + 1;
    ndb = base10_to_dB(nvar);
    snrp(index) = p_peak + 2. * g + lambda_sqdb + sigmadb + ndb - ...
        for_pi_cub - k_db - te_db - b_db - nf - loss - 4.0 * range_db;
    snrp5(index) = pt05 + 2. * g + lambda_sqdb + sigmadb + ndb - ...
        for_pi_cub - k_db - te_db - b_db - nf - loss - 4.0 * range_db;
end
end

```



```

nvar =1:10:500;
figure (2)
subplot (2,1,1)
plot (nvar,snrs,'k',nvar,snrs5,'k --')
legend ('default RCS','RCS-delta')
xlabel ('Number of coherently integrated pulses');
ylabel ('SNR - dB');
%title ('delta = 10, percent = 2');
subplot (2,1,2)
plot (nvar,snrp,'k',nvar,snrp5,'k --')
legend ('default power','pt * percent')
xlabel ('Number of coherently integrated pulses');
ylabel ('SNR - dB');

```

Input file “lprf_reqi.m”

```

% Use this input file to reproduce Fig.s 1.19 and 1.20
pt = 1.5e+6;      % peak power in Watts
freq = 5.6e+9;   % radar operating frequency in Hz
g = 45.0;        % antenna gain in dB
sigma = 0.1;     % radar cross section in m square
te = 290.0;     % effective noise temperature in Kelvins
b = 5.0e+6;     % radar operating bandwidth in Hz
nf = 3.0;       % noise figure in dB
loss = 0.0;     % radar losses in dB
np = 1;        % 1 number of coherently integrated pulses
prf = 100 ;    % PRF in Hz
range = 250.0; % target range in Km
np1 = 10;     % choice 1 of np
np2 = 100;    % choice 2 of np
rcs_delta = 10.0; % rcs variation
pt_percent = 2.0; % pt variation

```

Listing 1.6. MATLAB Function “hprf_req.m”

```

function [snr_out] = hprf_req (pt, freq, g, sigma, dt, ti, range, te, nf, loss, prf, tau, dt1,
                             dt2)
% This program implements the High PRF radar equation.
c = 3.0e+8;
lambda = c / freq;
% Compute the duty cycle
if (dt == 0)
    dt = tau * prf;
end
pav_db = base10_to_dB(pt * dt);
lambda_sqdb = base10_to_dB(lambda^2);
sigmadb = base10_to_dB(sigma);
for_pi_cub = base10_to_dB((4.0 * pi)^3);

```

```

k_db = base10_to_dB(1.38e-23);
te_db = base10_to_dB(te);
ti_db = base10_to_dB(ti);
range_db = base10_to_dB(range * 1000.0);
% Implement Eq. (1.69)
snr_out = pav_db + 2. * g + lambda_sqdb + sigmadb + ti_db - ...
    for_pi_cub - k_db - te_db - nf - loss - 4.0 * range_db
% Generate Plots in Figure 1.21
index = 0;
pav10 = base10_to_dB(pt * dt1);
pav20 = base10_to_dB(pt * dt2);
for range_var = 10:1:100
    index = index + 1;
    rangevar_db = base10_to_dB(range_var * 1000.0);
    snr1(index) = pav_db + 2. * g + lambda_sqdb + sigmadb + ti_db - ...
        for_pi_cub - k_db - te_db - nf - loss - 4.0 * rangevar_db;
    snr2(index) = pav10 + 2. * g + lambda_sqdb + sigmadb + ti_db - ...
        for_pi_cub - k_db - te_db - nf - loss - 4.0 * rangevar_db;
    snr3(index) = pav20 + 2. * g + lambda_sqdb + sigmadb + ti_db - ...
        for_pi_cub - k_db - te_db - nf - loss - 4.0 * rangevar_db;
end
figure (1)
var = 10:1:100;
plot (var,snr1,'k',var,snr2,'k--',var,snr3,'k:')
grid
legend ('dt','dt1','dt2')
xlabel ('Range - Km');
ylabel ('SNR - dB');
%title ('dt = 30%, dt1 = 5%, dt2 = 20%');

```

Input file “hprf_reqi.m”

```

% Use this input file to reproduce Fig. 1.21
clear all
pt = 100.0e+3;      % peak power in Watts
freq = 5.6e+9;     % radar operating frequency in Hz
g = 20.0;          % antenna gain in dB
sigma = 0.01;     % radar cross section in m square
ti = 2.0;         % time on target in seconds
dt = 0.3;        % radar duty cycle
%% %% %% %% %% %% %% %% enter dt = 0 when PRF and Tau are given %% %% %% %%
prf = 0.0;       % PRF
%% %% %% %% %% %% %% %% enter fr = 0 when duty cycle is known %% %% %%
tau = 0.0;      % pulse width in seconds
%% %% %% %% %% %% %% %% enter tau = 0 when duty cycle is known %% %% %%
te = 400.0;     % effective noise temperature in Kelvins
nf = 5.0;      % noise figure in dB
loss = 8.0;    % radar losses in dB

```

```

range =50.0;          % target range in Km
dt1 = 0.05;
dt2 = 0.2;

```

Listing 1.7. MATLAB Function “power_aperture_req.m”

```

function [p_a_p, aperture, pt, pav] = power_aperture_req (snr, freq, tsc, sigma, dt,
                range, te, nf, loss, az_angle, el_angle, g, rcs_delta1, rcs_delta2)
% This program implements the search radar equation.
c = 3.0e+8;
% Compute Omega in steradians
omega = (az_angle / 57.23) * (el_angle /57.23);
omega_db = base10_to_dB(omega);
lambda = c / freq;
lambda_sqdb = base10_to_dB(lambda^2);
sigmadb = base10_to_dB(sigma);
k_db = base10_to_dB(1.38e-23);
te_db = base10_to_dB(te);
tsc_db = base10_to_dB(tsc);
factor = base10_to_dB(16.0);
range_db = base10_to_dB(range * 1000.);
p_a_p = snr - sigmadb - tsc_db + factor + 4.0 * range_db + ...
    k_db + te_db + nf + loss + omega_db
aperture = g + lambda_sqdb - base10_to_dB(4.0 * pi)
pav = p_a_p - aperture;
pav = dB_to_base10(pav) / 1000.0
pt = pav / dt
% Calculate sigma(+-) rcs_delta1,2 dB
sigmap = rcs_delta1 + sigmadb;
sigmam = sigmadb - rcs_delta2.;
index = 0;
% vary range from 10% to 200% of input range
for rangevar = range*.1 : 1 : range*2.0
    index = index + 1;
    rangedb = base10_to_dB(rangevar * 1000.0);
    pap1(index) = snr - sigmadb - tsc_db + factor + 4.0 * rangedb + ...
        k_db + te_db + nf + loss + omega_db;
    papm(index) = snr - sigmam - tsc_db + factor + 4.0 * rangedb + ...
        k_db + te_db + nf + loss + omega_db;
    papp(index) = snr - sigmap - tsc_db + factor + 4.0 * rangedb + ...
        k_db + te_db + nf + loss + omega_db;
end
var = range*.1 : 1 : range*2.0;
figure (1)
plot (var,pap1,'k',var,papm,'k --',var,papp,'k:')
legend ('default RCS','RCS-delta1','RCS+1delta2')
xlabel ('Range - Km');
ylabel ('Power aperture product - dB');

```

```

%title ('delta1 = 10dBsm, delta2 = 10dBsm');
index = 0;
% Vary aperture from 2 msq to 50 msq
for apervar = 2:1:50
    aperdb = base10_to_dB(apervar);
    index = index + 1;
    pav = p_a_p - aperdb;
    pav = dB_to_base10(pav) / 1000.0;
    pt(index) = pav / dt;
end
figure (2)
apervar = 2:1:50;
plot (apervar, pt,'k')
grid
xlabel ('Aperture in squared meters')
ylabel ('Peak power - Kw')

```

Input file “power_aperture_reqi.m”

```

% Use this input file to reproduce plots in Fig. 1.24
clear all
snr = 15.0;           % sensitivity SNR in dB
freq = 10.0e+9;      % radar operating frequency in Hz
tsc = 2.5;           % antenna scan time in seconds
sigma = 0.1;         % radar cross section in m square
dt = 0.3;            % radar duty cycle
range = 250.0;       % sensitivity range in Km
te = 900.0;          % effective noise temperature in Kelvins
nf = 5.0;            % noise figure in dB
loss = 8.0;          % radar losses in dB
az_angle = 2.0;     % search volume azimuth extent in degrees
el_angle = 2.0;     % search volume elevation extent in degrees
g = 45.0;            % antenna gain in dB
rcs_delta1 = 10.0;
rcs_delta2 = 10.0;

```

Listing 1.8. MATLAB Program “ssj_req.m”

```

function [BR_range] = ssj_req (pt, g, freq, sigma, b, loss, ...
    pj, bj, gj, lossj)
% This function implements Eq.s (1.76) through (1.80)
c = 3.0e+8;
lambda = c / freq;
lambda_db = base10_to_dB(lambda^2);
if (loss == 0.0)
    loss = 0.000001;
end
if (lossj == 0.0)

```

```

    lossj = 0.000001;
end
% Compute Omega in steradians
sigmadb = base10_to_dB(sigma);
pt_db = base10_to_dB(pt);
b_db = base10_to_dB(b);
bj_db = base10_to_dB(bj);
pj_db = base10_to_dB(pj);
factor = base10_to_dB(4.0 *pi);
BR_range = sqrt((pt * (dB_to_base10(g)) * sigma * bj * (dB_to_base10(lossj))) / ...
    (4.0 * pi * pj * (dB_to_base10(gj)) * b * ...
    (dB_to_base10(lossj)))) / 1000.0
s_at_br = pt_db + 2.0 * g + lambda_db + sigmadb - ...
    3.0 * factor - 4.* base10_to_dB(BR_range) - loss
% prepare to plot Figure 1.25
index =0;
for ran_var = .1:10:10000
    index = index + 1;
    ran_db = base10_to_dB(ran_var * 1000.0);
    ssj(index) = pj_db + gj + lambda_db + g + b_db - 2.0 * factor - ...
        2.0 * ran_db - bj_db - lossj + s_at_br ;
    s(index) = pt_db + 2.0 * g + lambda_db + sigmadb - ...
        3.0 * factor - 4.* ran_db - loss + s_at_br ;
end
ranvar = .1:10:10000;
ranvar = ranvar ./ BR_range;
semilogx (ranvar,s,'k',ranvar,ssj,'k-');
% axis([.1 1000 -90 40]); % This line is specific to Fig. 1.25
xlabel ('Range normalized to cross-over range');
legend ('Target echo','SSJ')
ylabel ('Relative signal or jamming amplitude - dB');
grid

```

Input file “ssj_reqi.m”

```

% Use this input file to reproduce Fig. 1.25
clear all
pt = 50.0e+3;      % peak power in Watts
g = 35.0;         % antenna gain in dB
freq = 3.2e+9;    % radar operating frequency in Hz
sigma = 10.0 ;    % radar cross section in m square
b = 667.0e+3;     % radar operating bandwidth in Hz
loss = 0.000;    % radar losses in dB
pj = 200.0;      % jammer peak power in Watts
bj = 50.0e+6;    % jammer operating bandwidth in Hz
gj = 10.0;      % jammer antenna gain in dB
lossj = 0.0;    % jammer losses in dB

```

Listing 1.9. MATLAB Program “soj_req.m”

```
function [BR_range] = soj_req (pt, g, sigma, b, freq, loss, range, ...
    pj, bj,gj, lossj, gprime, rangej)
% This function implements equations for SOJs
c = 3.0e+8;
lambda = c / freq;
lambda_db = base10_to_dB(lambda^2)
if (loss == 0.0)
    loss = 0.000001;
end
if (lossj == 0.0)
    lossj = 0.000001;
end
% Compute Omega in steradians
sigmadb = base10_to_dB(sigma);
range_db = base10_to_dB(range * 1000.);
rangej_db = base10_to_dB(rangej * 1000.);
pt_db = base10_to_dB(pt);
b_db = base10_to_dB(b);
bj_db = base10_to_dB(bj);
pj_db = base10_to_dB(pj);
factor = base10_to_dB(4.0 * pi);
BR_range = ((pt * dB_to_base10(2.0*g) * sigma * bj * dB_to_base10(lossj) * ...
    (rangej)^2) / (4.0 * pi * pj * dB_to_base10(gj) * dB_to_base10(gprime) * ...
    b * dB_to_base10(loss)))^0.25 / 1000.
%* (dB_to_base10(16))^0.25)
s_at_br = pt_db + 2.0 * g + lambda_db + sigmadb - ...
    3.0 * factor - 4.0 * base10_to_dB(BR_range) - loss
% prepare to plot Figure 1.27
index = 0;
for ran_var = .1:1:1000;
    index = index + 1;
    ran_db = base10_to_dB(ran_var * 1000.0);
    s(index) = pt_db + 2.0 * g + lambda_db + sigmadb - ...
        3.0 * factor - 4.0 * ran_db - loss + s_at_br;
    soj(index) = s_at_br - s_at_br;
end
ranvar = .1:1:1000;
%ranvar = ranvar ./BR_range;
semilogx (ranvar,s,'k',ranvar,soj,'k-');
xlabel ('Range normalized to cross-over range');
legend ('Target echo','SOJ')
ylabel ('Relative signal or jamming amplitude - dB');
```

Input file “soj_reqi.m”

```
% Use this input file to reproduce Fig. 1.26
clear all
pt = 50.0e+3;      % peak power in Watts
g = 35.0;          % antenna gain in dB
freq = 3.6e+9;    % radar operating frequency in Hz
sigma = 10 ;      % radar cross section in m square
b = 667.0e+3;     % radar operating bandwidth in Hz
range = 20*1852;  % radar to target range
gprime = 10.0;    % radar antenna gain on jammer
loss = 0.01;      % radar losses in dB
rangej = 12*1852; % range to jammer in Km
pj = 5.0e+3;      % jammer peak power in Watts
bj = 50.0e+6;     % jammer operating bandwidth in Hz
gj = 30.0;        % jammer antenna gain in dB
lossj = 0.01;     % jammer losses in dB
rangej = 12*1852; % range to jammer in Km
```

Listing 1.10. MATLAB Function “range_red_factor.m”

```
function RRF = range_red_factor (te, pj, gj, g, freq, bj, rangej, lossj)
% This function computes the range reduction factor and produce
% plots of RRF versus wavelength, radar to jammer range, and jammer power
c = 3.0e+8;
k = 1.38e-23;
lambda = c / freq;
gj_10 = dB_to_base10(gj);
g_10 = dB_to_base10(g);
lossj_10 = dB_to_base10(lossj);
index = 0;
for wavelength = .01:.001:1
    index = index + 1;
    jamer_temp = (pj * gj_10 * g_10 * wavelength^2) / ...
        (4.0^2 * pi^2 * k * bj * lossj_10 * (rangej * 1000.0)^2);
    delta = 10.0 * log10(1.0 + (jamer_temp / te));
    rrf(index) = 10^(-delta / 40.0);
end
w = 0.01:.001:1;
figure (1)
semilogx (w,rrf,'k')
grid
xlabel ('Wavelength in meters')
ylabel ('Range reduction factor')
index = 0;
for ran =rangej*.3:1:rangej*2
    index = index + 1;
    jamer_temp = (pj * gj_10 * g_10 * wavelength^2) / ...
```

```

    (4.0^2 * pi^2 * k * bj * lossj_10 * (ran * 1000.0)^2);
    delta = 10.0 * log10(1.0 + (jamer_temp / te));
    rrf1(index) = 10^(-delta / 40.0);
end
figure(2)
ranvar = rangej*.3:1:rangej*2 ;
plot (ranvar,rrf1,'k')
grid
xlabel ('Radar to jammer range - Km')
ylabel ('Range reduction factor')
index = 0;
for pjvar = pj*.01:1:pj*2
    index = index + 1;
    jamer_temp = (pjvar * gj_10 * g_10 * wavelength^2) / ...
        (4.0^2 * pi^2 * k * bj * lossj_10 * (rangej * 1000.0)^2);
    delta = 10.0 * log10(1.0 + (jamer_temp / te));
    rrf2(index) = 10^(-delta / 40.0);
end
figure(3)
pjvar = pj*.01:1:pj*2;
plot (pjvar,rrf2,'k')
grid
xlabel ('Jammer peak power - Watts')
ylabel ('Range reduction factor')

```

Input file “range_red_factori.m”

```

% Use this input file to reproduce Fig.s 1.27 through 1.29
clear all
te = 500.0;           % radar effective temperature in Kelvin
pj = 500;             % jammer peak power in W
gj = 3.0;             % jammer antenna gain in dB
g = 45.0;            % radar antenna gain
freq = 10.0e+9;      % radar operating frequency in Hz
bj = 10.0e+6;        % radar operating bandwidth in Hz
rangej = 750.0;     % radar to jammer range in Km
lossj = 1.0;         % jammer losses in dB

```

Problems

1.1. (a) Calculate the maximum unambiguous range for a pulsed radar with PRF of 200Hz and 750Hz ; (b) What are the corresponding PRIs?

1.2. For the same radar in Problem 1.1, assume a duty cycle of 30% and peak power of 5KW . Compute the average power and the amount of radiated energy during the first 20ms .

- 1.3. A certain pulsed radar uses pulse width $\tau = 1\mu s$. Compute the corresponding range resolution.
- 1.4. An X-band radar uses PRF of $3KHz$. Compute the unambiguous range, and the required bandwidth so that the range resolution is $30m$. What is the duty cycle?
- 1.5. Compute the Doppler shift associated with a closing target with velocity 100, 200, and 350 meters per second. In each case compute the time dilation factor. Assume that $\lambda = 0.3m$.
- 1.6. A certain L-band radar has center frequency $1.5GHz$, and PRF $f_r = 10KHz$. What is the maximum Doppler shift that can be measured by this radar?
- 1.7. Starting with a modified version of Eq. (1.27), derive an expression for the Doppler shift associated with a receding target.
- 1.8. In reference to Fig. 1.16, compute the Doppler frequency for $v = 150m/s$, $\theta_a = 30^\circ$, and $\theta_e = 15^\circ$. Assume that $\lambda = 0.1m$.
- 1.9. A pulsed radar system has a range resolution of $30cm$. Assuming sinusoid pulses at $45KHz$, determine the pulse width and the corresponding bandwidth.
- 1.10. (a) Develop an expression for the minimum PRF of a pulsed radar; (b) compute $f_{r,min}$ for a closing target whose velocity is $400m/s$; (c) what is the unambiguous range? Assume that $\lambda = 0.2m$.
- 1.11. An L-band pulsed radar is designed to have an unambiguous range of $100Km$ and range resolution $\Delta R \leq 100m$. The maximum resolvable Doppler frequency corresponds to $v_{target} \leq 350m/sec$. Compute the maximum required pulse width, the PRF, and the average transmitted power if $P_t = 500W$.
- 1.12. Compute the aperture size for an X-band antenna at $f_0 = 9GHz$. Assume antenna gain $G = 10, 20, 30 dB$.
- 1.13. An L-band radar (1500 MHz) uses an antenna whose gain is $G = 30dB$. Compute the aperture size. If the radar duty cycle is $d_t = 0.2$ and the average power is $25KW$, compute the power density at range $R = 50Km$.
- 1.14. For the radar described in Problem 1.13, assume the minimum detectable signal is $5dBm$. Compute the radar maximum range for $\sigma = 1.0, 10.0, 20.0m^2$.

1.15. Consider an L-band radar with the following specifications: operating frequency $f_0 = 1500\text{MHz}$, bandwidth $B = 5\text{MHz}$, and antenna gain $G = 5000$. Compute the peak power, the pulse width, and the minimum detectable signal for this radar. Assume target RCS $\sigma = 10\text{m}^2$, the single pulse SNR is 15.4dB , noise figure $F = 5\text{dB}$, temperature $T_0 = 290\text{K}$, and maximum range $R_{max} = 150\text{Km}$.

1.16. Repeat Example 1.4 with $P_t = 1\text{MW}$, $G = 40\text{dB}$, and $\sigma = 0.5\text{m}^2$.

1.17. Show that the DC component is the dominant spectral line for high PRF waveforms.

1.18. Repeat Example 1.5 with $L = 5\text{dB}$, $F = 10\text{dB}$, $T = 500\text{K}$, $T_i = 1.5\text{s}$, $d_t = 0.25$, and $R = 75\text{Km}$.

1.19. Consider a low PRF C-band radar operating at $f_0 = 5000\text{MHz}$. The antenna has a circular aperture with radius 2m . The peak power is $P_t = 1\text{MW}$ and the pulse width is $\tau = 2\mu\text{s}$. The PRF is $f_r = 250\text{Hz}$, and the effective temperature is $T_0 = 600\text{K}$. Assume radar losses $L = 15\text{dB}$ and target RCS $\sigma = 10\text{m}^2$. (a) Calculate the radar's unambiguous range; (b) calculate the range R_0 that corresponds to $\text{SNR} = 0\text{dB}$; (c) calculate the SNR at $R = 0.75R_0$.

1.20. The atmospheric attenuation can be included in the radar equation as another loss term. Consider an X-band radar whose detection range at 20Km includes a 0.25dB/Km atmospheric loss. Calculate the corresponding detection range with no atmospheric attenuation.

1.21. Let the maximum unambiguous range for a low PRF radar be R_{max} . (a) Calculate the SNR at $(1/2)R_{max}$ and $(3/4)R_{max}$. (b) If a target with $\sigma = 10\text{m}^2$ exists at $R = (1/2)R_{max}$, what should the target RCS be at $R = (3/4)R_{max}$ so that the radar has the same signal strength from both targets.

1.22. A Milli-Meter Wave (MMW) radar has the following specifications: operating frequency $f_0 = 94\text{GHz}$, PRF $f_r = 15\text{KHz}$, pulse width $\tau = 0.05\text{ms}$, peak power $P_t = 10\text{W}$, noise figure $F = 5\text{dB}$, circular antenna with diameter $D = 0.254\text{m}$, antenna gain $G = 30\text{dB}$, target RCS $\sigma = 1\text{m}^2$, system losses $L = 8\text{dB}$, radar scan time $T_{sc} = 3\text{s}$, radar angular

coverage 200° , and atmospheric attenuation $3\text{dB}/\text{Km}$. Compute the following: (a) wavelength λ ; (b) range resolution ΔR ; (c) bandwidth B ; (d) the SNR as a function of range; (e) the range for which $\text{SNR} = 15\text{dB}$; (f) antenna beam width; (g) antenna scan rate; (h) time on target; (i) the effective maximum range when atmospheric attenuation is considered.

1.23. Repeat Example 1.5 with $\Omega = 4^\circ$, $\sigma = 1\text{m}^2$, and $R = 400\text{Km}$.

1.24. Using Eq. (1.80), compute (as a function of B_J/B) the crossover range for the radar in Problem 1.22. Assume $P_J = 100\text{W}$, $G_J = 10\text{dB}$, and $L_J = 2\text{dB}$.

1.25. Using Eq. (1.80), compute (as a function of B_J/B) the crossover range for the radar in Problem 1.22. Assume $P_J = 200\text{W}$, $G_J = 15\text{dB}$, and $L_J = 2\text{dB}$. Assume $G' = 12\text{dB}$ and $R_J = 25\text{Km}$.

1.26. A certain radar is subject to interference from an SSJ jammer. Assume the following parameters: radar peak power $P_t = 55\text{KW}$, radar antenna gain $G = 30\text{dB}$, radar pulse width $\tau = 2\mu\text{s}$, radar losses $L = 10\text{dB}$, jammer power $P_J = 150\text{W}$, jammer antenna gain $G_J = 12\text{dB}$, jammer bandwidth $B_J = 50\text{MHz}$, and jammer losses $L_J = 1\text{dB}$. Compute the crossover range for a 5m^2 target.

1.27. A radar with antenna gain G is subject to a repeater jammer whose antenna gain is G_J . The repeater illuminates the radar with three fourths of the incident power on the jammer. (a) Find an expression for the ratio between the power received by the jammer and the power received by the radar; (b) what is this ratio when $G = G_J = 200$ and $R/\lambda = 10^5$?

1.28. Using Fig. 1.30 derive an expression for R_r . Assume 100% synchronization between the transmitter and receiver.

1.29. An X-band airborne radar transmitter and an air-to-air missile receiver act as a bistatic radar system. The transmitter guides the missile toward its target by continuously illuminating the target with a CW signal. The transmitter has the following specifications: peak power $P_t = 4\text{KW}$; antenna gain $G_t = 25\text{dB}$; operating frequency $f_0 = 9.5\text{GHz}$. The missile receiver has the following characteristics: aperture $A_r = 0.01\text{m}^2$; bandwidth $B = 750\text{Hz}$;

noise figure $F = 7dB$; and losses $L_r = 2dB$. Assume that the bistatic RCS is $\sigma_B = 3m^2$. Assume $R_r = 35Km$; $R_t = 17Km$. Compute the SNR at the missile.

1.30. Repeat the previous problem when there is $0.1dB/Km$ atmospheric attenuation.

1.31. Consider an antenna with a $\sin x/x$ pattern. Let $x = (\pi r \sin \theta)/\lambda$, where r is the antenna radius, λ is the wavelength, and θ is the off-boresight angle. Derive Eq. (1.100). Hint: Assume small x , and expand $\sin x/x$ as an infinite series.

1.32. Compute the amount of antenna pattern loss for a phased array antenna whose two-way pattern is approximated by

$$f(y) = [\exp(-2 \ln 2 (y/\theta_{3dB})^2)]^4$$

where θ_{3dB} is the $3dB$ beam width. Assume circular symmetry.

1.33. A certain radar has a range gate size of $30m$. Due to range gate straddle, the envelope of a received pulse can be approximated by a triangular spread over three range bins. A target is detected in range bin 90. You need to find the exact target position with respect to the center of the range cell. (a) Develop an algorithm to determine the position of a target with respect to the center of the cell; (b) assuming that the early, on, and late measurements are, respectively, equal to $4/6$, $5/6$, and $1/6$, compute the exact target position.

1.34. Compute the amount of Doppler filter straddle loss for the filter defined by

$$H(f) = \frac{1}{1 + a^2 f^2}$$

Assume half-power frequency $f_{3dB} = 500Hz$ and crossover frequency $f_c = 350Hz$.

In Chapter 1, the term Radar Cross Section (RCS) was used to describe the amount of scattered power from a target towards the radar, when the target is illuminated by RF energy. At that time, RCS was referred to as a target-specific constant. This was only a simplification and, in practice, it is rarely the case. In this chapter, the phenomenon of target scattering and methods of RCS calculation are examined. Target RCS fluctuations due to aspect angle, frequency, and polarization are presented. Radar cross section characteristics of some simple and complex targets are also introduced. The analysis of extended RCS due to volume and surface clutter will be explored in a later chapter.

2.1. RCS Definition

Electromagnetic waves, with any specified polarization, are normally diffracted or scattered in all directions when incident on a target. These scattered waves are broken down into two parts. The first part is made of waves that have the same polarization as the receiving antenna. The other portion of the scattered waves will have a different polarization to which the receiving antenna does not respond. The two polarizations are orthogonal and are referred to as the Principle Polarization (PP) and Orthogonal Polarization (OP), respectively. The intensity of the *backscattered* energy that has the same polarization as the radar's receiving antenna is used to define the target RCS. When a target is illuminated by RF energy, it acts like an antenna, and will have near and far fields. Waves reflected and measured in the near field are, in general, spherical. Alternatively, in the far field the wavefronts are decomposed into a linear combination of plane waves.

Assume the power density of a wave incident on a target located at range R away from the radar is P_{Di} . The amount of reflected power from the target is

$$P_r = \sigma P_{Di} \quad (2.1)$$

σ denotes the target cross section. Define P_{Dr} as the power density of the scattered waves at the receiving antenna. It follows that

$$P_{Dr} = P_r / (4\pi R^2) \quad (2.2)$$

Equating Eqs. (2.1) and (2.2) yields

$$\sigma = 4\pi R^2 \left(\frac{P_{Dr}}{P_{Di}} \right) \quad (2.3)$$

and in order to ensure that the radar receiving antenna is in the far field (i.e., scattered waves received by the antenna are planar), Eq. (2.3) is modified

$$\sigma = 4\pi R^2 \lim_{R \rightarrow \infty} \left(\frac{P_{Dr}}{P_{Di}} \right) \quad (2.4)$$

The RCS defined by Eq. (2.4) is often referred to as either the monostatic RCS, the backscattered RCS, or simply target RCS.

The backscattered RCS is measured from all waves scattered in the direction of the radar and has the same polarization as the receiving antenna. It represents a portion of the total scattered target RCS σ_t , where $\sigma_t > \sigma$. Assuming spherical coordinate system defined by (ρ, θ, ϕ) , then at range ρ the target scattered cross section is a function of (θ, ϕ) . Let the angles (θ_i, ϕ_i) define the direction of propagation of the incident waves. Also, let the angles (θ_s, ϕ_s) define the direction of propagation of the scattered waves. The special case, when $\theta_s = \theta_i$ and $\phi_s = \phi_i$, defines the monostatic RCS. The RCS measured by the radar at angles $\theta_s \neq \theta_i$ and $\phi_s \neq \phi_i$ is called the bistatic RCS.

The total target scattered RCS is given by

$$\sigma_t = \frac{1}{4\pi} \int_{\phi_s = 0}^{2\pi} \int_{\theta_s = 0}^{\pi} \sigma(\theta_s, \phi_s) \sin\theta_s \, d\theta \, d\phi_s \quad (2.5)$$

The amount of backscattered waves from a target is proportional to the ratio of the target extent (size) to the wavelength, λ , of the incident waves. In fact, a radar will not be able to detect targets much smaller than its operating wavelength. For example, if weather radars use L-band frequency, rain drops become nearly invisible to the radar since they are much smaller than the

wavelength. RCS measurements in the frequency region, where the target extent and the wavelength are comparable, are referred to as the Rayleigh region. Alternatively, the frequency region where the target extent is much larger than the radar operating wavelength is referred to as the optical region. In practice, the majority of radar applications falls within the optical region.

The analysis presented in this book assumes far field monostatic RCS measurements in the optical region. Near field RCS, bistatic RCS, and RCS measurements in the Rayleigh region will not be considered since their treatment falls beyond this book's intended scope. Additionally, RCS treatment in this chapter is mainly concerned with Narrow Band (NB) cases. In other words, the extent of the target under consideration falls within a single range bin of the radar. Wide Band (WB) RCS measurements will be briefly addressed in a later section. Wide band radar range bins are small (typically 10 - 50 cm), hence, the target under consideration may cover many range bins. The RCS value in an individual range bin corresponds to the portion of the target falling within that bin.

2.2. RCS Prediction Methods

Before presenting the different RCS calculation methods, it is important to understand the significance of RCS prediction. Most radar systems use RCS as a means of discrimination. Therefore, accurate prediction of target RCS is critical in order to design and develop robust discrimination algorithms. Additionally, measuring and identifying the scattering centers (sources) for a given target aid in developing RCS reduction techniques. Another reason of lesser importance is that RCS calculations require broad and extensive technical knowledge, thus many scientists and scholars find the subject challenging and intellectually motivating. Two categories of RCS prediction methods are available: exact and approximate.

Exact methods of RCS prediction are very complex even for simple shape objects. This is because they require solving either differential or integral equations that describe the scattered waves from an object under the proper set of boundary conditions. Such boundary conditions are governed by Maxwell's equations. Even when exact solutions are achievable, they are often difficult to interpret and to program using digital computers.

Due to the difficulties associated with the exact RCS prediction, approximate methods become the viable alternative. The majority of the approximate methods are valid in the optical region, and each has its own strengths and limitations. Most approximate methods can predict RCS within few dBs of the truth. In general, such a variation is quite acceptable by radar engineers and designers. Approximate methods are usually the main source for predicting

RCS of complex and extended targets such as aircrafts, ships, and missiles. When experimental results are available, they can be used to validate and verify the approximations.

Some of the most commonly used approximate methods are Geometrical Optics (GO), Physical Optics (PO), Geometrical Theory of Diffraction (GTD), Physical Theory of Diffraction (PTD), and Method of Equivalent Currents (MEC). Interested readers may consult Knott or Ruck (see bibliography) for more details on these and other approximate methods.

2.3. RCS Dependency on Aspect Angle and Frequency

Radar cross section fluctuates as a function of radar aspect angle and frequency. For the purpose of illustration, isotropic point scatterers are considered. An isotropic scatterer is one that scatters incident waves equally in all directions. Consider the geometry shown in Fig. 2.1. In this case, two unity ($1m^2$) isotropic scatterers are aligned and placed along the radar line of sight (zero aspect angle) at a far field range R . The spacing between the two scatterers is 1 meter. The radar aspect angle is then changed from zero to 180 degrees, and the composite RCS of the two scatterers measured by the radar is computed.

This composite RCS consists of the superposition of the two individual radar cross sections. At zero aspect angle, the composite RCS is $2m^2$. Taking scatterer-1 as a phase reference, when the aspect angle is varied, the composite RCS is modified by the phase that corresponds to the electrical spacing between the two scatterers. For example, at aspect angle 10° , the electrical spacing between the two scatterers is

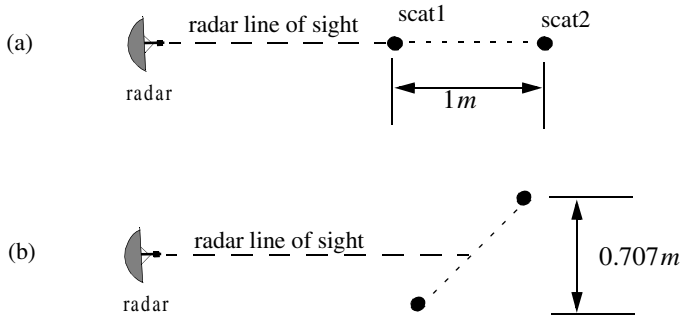


Figure 2.1. RCS dependency on aspect angle. (a) Zero aspect angle, zero electrical spacing. (b) 45° aspect angle, 1.414λ electrical spacing.

$$elec\text{-}spacing = \frac{2 \times (1.0 \times \cos(10))}{\lambda} \quad (2.6)$$

λ is the radar operating wavelength.

Fig. 2.2 shows the composite RCS corresponding to this experiment. This plot can be reproduced using MATLAB function “*rcs_aspect.m*” given in Listing 2.1 in Section 2.8. As indicated by Fig. 2.1, RCS is dependent on the radar aspect angle. Knowledge of this constructive and destructive interference between the individual scatterers can be very critical when a radar tries to extract RCS of complex or maneuvering targets. This is true because of two reasons. First, the aspect angle may be continuously changing. Second, complex target RCS can be viewed to be made up from contributions of many individual scattering points distributed on the target surface. These scattering points are often called scattering centers. Many approximate RCS prediction methods generate a set of scattering centers that define the back-scattering characteristics of such complex targets.

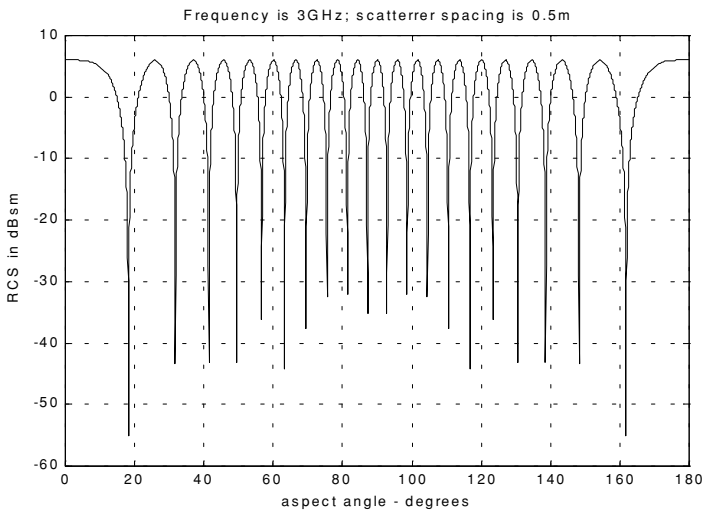


Figure 2.2. Illustration of RCS dependency on aspect angle.

MATLAB Function “rcs_aspect.m”

The function “*rcs_aspect.m*” computes and plots the RCS dependency on aspect angle. Its syntax is as follows:

$$[rcs] = rcs_aspect(scatter_spacing, freq)$$

Symbol	Description	Units	Status
<i>scat_spacing</i>	<i>scatterer spacing</i>	<i>meters</i>	<i>input</i>
<i>freq</i>	<i>radar frequency</i>	<i>Hz</i>	<i>input</i>
<i>rsc</i>	<i>array of RCS versus aspect angle</i>	<i>dBsm</i>	<i>output</i>

Next, to demonstrate RCS dependency on frequency, consider the experiment shown in Fig. 2.3. In this case, two far field unity isotropic scatterers are aligned with radar line of sight, and the composite RCS is measured by the radar as the frequency is varied from 8 GHz to 12.5 GHz (X-band). Figs. 2.4 and 2.5 show the composite RCS versus frequency for scatterer spacing of 0.1 and 0.7 meters.

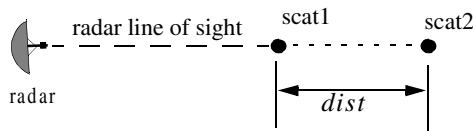


Figure 2.3. Experiment setup which demonstrates RCS dependency on frequency; $dist = 0.1$, or 0.7 m.

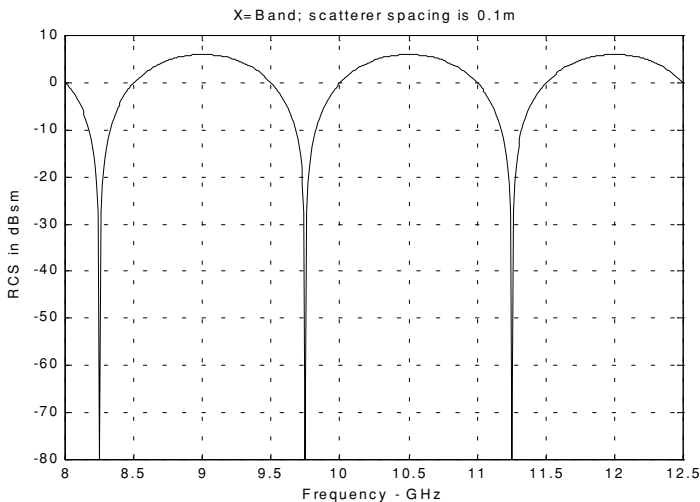


Figure 2.4. Illustration of RCS dependency on frequency.

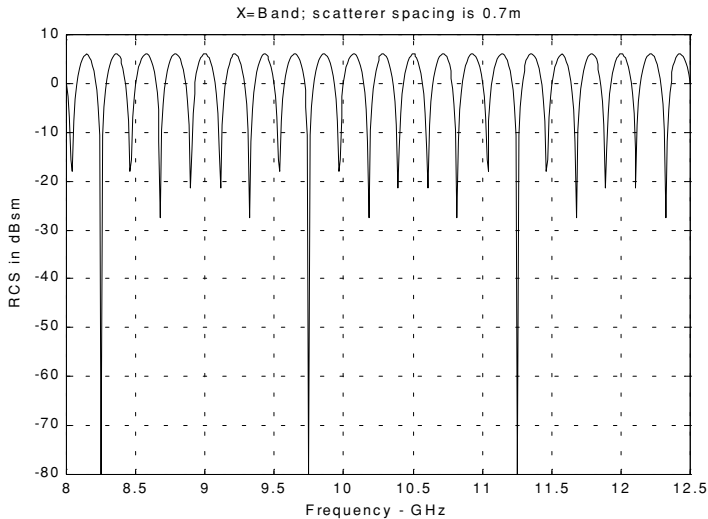


Figure 2.5. Illustration of RCS dependency on frequency.

The plots shown in Figs. 2.4 and 2.5 can be reproduced using MATLAB function “*rcs_frequency.m*” given in Listing 2.2 in Section 2.8. From those two figures, RCS fluctuation as a function of frequency is evident. Little frequency change can cause serious RCS fluctuation when the scatterer spacing is large. Alternatively, when scattering centers are relatively close, it requires more frequency variation to produce significant RCS fluctuation.

MATLAB Function “*rcs_frequency.m*”

The function “*rcs_frequency.m*” computes and plots the RCS dependency on frequency. Its syntax is as follows:

$$[rcs] = rcs_frequency(scatter_spacing, frequ, freql)$$

where

Symbol	Description	Units	Status
<i>scatter_spacing</i>	<i>scatterer spacing</i>	<i>meters</i>	<i>input</i>
<i>freql</i>	<i>start of frequency band</i>	<i>Hz</i>	<i>input</i>
<i>frequ</i>	<i>end of frequency band</i>	<i>Hz</i>	<i>input</i>
<i>rcs</i>	<i>array of RCS versus aspect angle</i>	<i>dBsm</i>	<i>output</i>

2.4. RCS Dependency on Polarization

The material in this section covers two topics. First, a review of polarization fundamentals is presented. Second, the concept of target scattering matrix is introduced.

2.4.1. Polarization

The x and y electric field components for a wave traveling along the positive z direction are given by

$$E_x = E_1 \sin(\omega t - kz) \quad (2.7)$$

$$E_y = E_2 \sin(\omega t - kz + \delta) \quad (2.8)$$

where $k = 2\pi/\lambda$, ω is the wave frequency, the angle δ is the time phase angle which E_y leads E_x , and finally, E_1 and E_2 are, respectively, the wave amplitudes along the x and y directions. When two or more electromagnetic waves combine, their electric fields are integrated vectorially at each point in space for any specified time. In general, the combined vector traces an ellipse when observed in the x-y plane. This is illustrated in [Fig. 2.6](#).

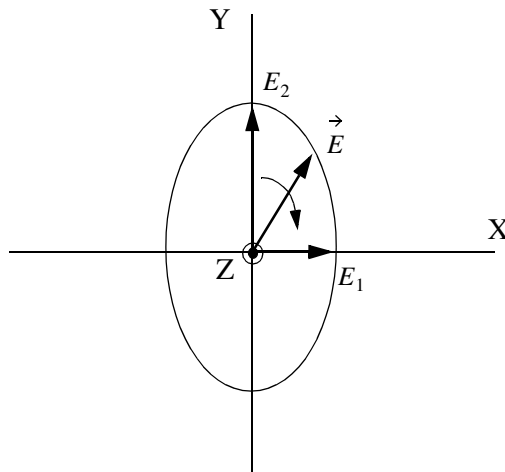


**Figure 2.6. Electric field components along the x and y directions.
The positive z direction is out of the page.**

The ratio of the major to the minor axes of the polarization ellipse is called the Axial Ratio (AR). When AR is unity, the polarization ellipse becomes a circle, and the resultant wave is then called circularly polarized. Alternatively, when $E_1 = 0$ and $AR = \infty$ the wave becomes linearly polarized.

Eqs. (2.7) and (2.8) can be combined to give the instantaneous total electric field,

$$\vec{E} = \hat{a}_x E_1 \sin(\omega t - kz) + \hat{a}_y E_2 \sin(\omega t - kz + \delta) \quad (2.9)$$

where \hat{a}_x and \hat{a}_y are unit vectors along the x and y directions, respectively. At $z = 0$, $E_x = E_1 \sin(\omega t)$ and $E_y = E_2 \sin(\omega t + \delta)$, then by replacing $\sin(\omega t)$ by the ratio E_x/E_1 and by using trigonometry properties Eq. (2.9) can be rewritten as

$$\frac{E_x^2}{E_1^2} - \frac{2E_x E_y \cos \delta}{E_1 E_2} + \frac{E_y^2}{E_2^2} = (\sin \delta)^2 \quad (2.10)$$

Note that Eq. (2.10) has no dependency on ωt .

In the most general case, the polarization ellipse may have any orientation, as illustrated in Fig. 2.7. The angle ξ is called the tilt angle of the ellipse. In this case, AR is given by

$$AR = \frac{OA}{OB} \quad (1 \leq AR \leq \infty) \quad (2.11)$$

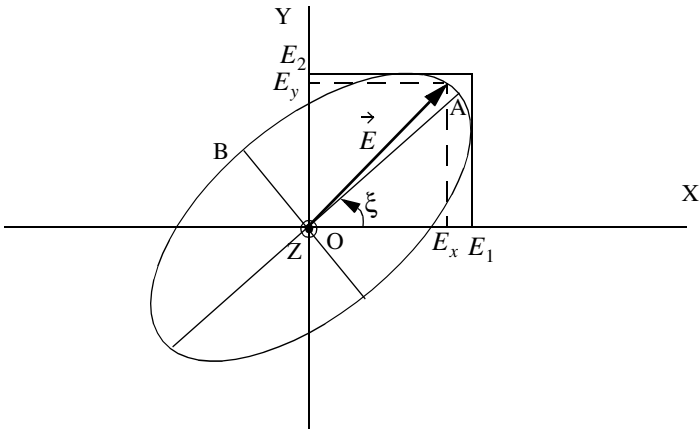


Figure 2.7. Polarization ellipse in the general case.

When $E_1 = 0$, the wave is said to be linearly polarized in the y direction, while if $E_2 = 0$ the wave is said to be linearly polarized in the x direction. Polarization can also be linear at an angle of 45° when $E_1 = E_2$ and $\xi = 45^\circ$. When $E_1 = E_2$ and $\delta = 90^\circ$, the wave is said to be Left Circularly Polarized (LCP), while if $\delta = -90^\circ$ the wave is said to be Right Circularly Polarized (RCP). It is a common notation to call the linear polarizations along the x and y directions by the names horizontal and vertical polarizations, respectively.

In general, an arbitrarily polarized electric field may be written as the sum of two circularly polarized fields. More precisely,

$$\vec{E} = \vec{E}_R + \vec{E}_L \quad (2.12)$$

where \vec{E}_R and \vec{E}_L are the RCP and LCP fields, respectively. Similarly, the RCP and LCP waves can be written as

$$\vec{E}_R = \vec{E}_V + j\vec{E}_H \quad (2.13)$$

$$\vec{E}_L = \vec{E}_V - j\vec{E}_H \quad (2.14)$$

where \vec{E}_V and \vec{E}_H are the fields with vertical and horizontal polarizations, respectively. Combining Eqs. (2.13) and (2.14) yields

$$E_R = \frac{E_H - jE_V}{\sqrt{2}} \quad (2.15)$$

$$E_L = \frac{E_H + jE_V}{\sqrt{2}} \quad (2.16)$$

Using matrix notation Eqs. (2.15) and (2.16) can be rewritten as

$$\begin{bmatrix} E_R \\ E_L \end{bmatrix} = \frac{1}{\sqrt{2}} \begin{bmatrix} 1 & -j \\ 1 & j \end{bmatrix} \begin{bmatrix} E_H \\ E_V \end{bmatrix} = [T] \begin{bmatrix} E_H \\ E_V \end{bmatrix} \quad (2.17)$$

$$\begin{bmatrix} E_H \\ E_V \end{bmatrix} = \frac{1}{\sqrt{2}} \begin{bmatrix} 1 & 1 \\ j & -j \end{bmatrix} \begin{bmatrix} E_R \\ E_L \end{bmatrix} = [T]^{-1} \begin{bmatrix} E_R \\ E_L \end{bmatrix} \quad (2.18)$$

For many targets the scattered waves will have different polarization than the incident waves. This phenomenon is known as depolarization or cross-polarization. However, perfect reflectors reflect waves in such a fashion that an incident wave with horizontal polarization remains horizontal, and an incident

wave with vertical polarization remains vertical but is phase shifted 180° . Additionally, an incident wave which is RCP becomes LCP when reflected, and a wave which is LCP becomes RCP after reflection from a perfect reflector. Therefore, when a radar uses LCP waves for transmission, the receiving antenna needs to be RCP polarized in order to capture the PP RCS, and LCR to measure the OP RCS.

2.4.2. Target Scattering Matrix

Target backscattered RCS is commonly described by a matrix known as the scattering matrix, and is denoted by $[S]$. When an arbitrarily linearly polarized wave is incident on a target, the backscattered field is then given by

$$\begin{bmatrix} E_1^s \\ E_2^s \end{bmatrix} = [S] \begin{bmatrix} E_1^i \\ E_2^i \end{bmatrix} = \begin{bmatrix} s_{11} & s_{12} \\ s_{21} & s_{22} \end{bmatrix} \begin{bmatrix} E_1^i \\ E_2^i \end{bmatrix} \quad (2.19)$$

The superscripts i and s denote incident and scattered fields. The quantities s_{ij} are in general complex and the subscripts 1 and 2 represent any combination of orthogonal polarizations. More precisely, $1 = H, R$, and $2 = V, L$. From Eq. (2.3), the backscattered RCS is related to the scattering matrix components by the following relation:

$$\begin{bmatrix} \sigma_{11} & \sigma_{12} \\ \sigma_{21} & \sigma_{22} \end{bmatrix} = 4\pi R^2 \begin{bmatrix} |s_{11}|^2 & |s_{12}|^2 \\ |s_{21}|^2 & |s_{22}|^2 \end{bmatrix} \quad (2.20)$$

It follows that once a scattering matrix is specified, the target backscattered RCS can be computed for any combination of transmitting and receiving polarizations. The reader is advised to see Ruck for ways to calculate the scattering matrix $[S]$.

Rewriting Eq. (2.20) in terms of the different possible orthogonal polarizations yields

$$\begin{bmatrix} E_H^s \\ E_V^s \end{bmatrix} = \begin{bmatrix} s_{HH} & s_{HV} \\ s_{VH} & s_{VV} \end{bmatrix} \begin{bmatrix} E_H^i \\ E_V^i \end{bmatrix} \quad (2.21)$$

$$\begin{bmatrix} E_R^s \\ E_L^s \end{bmatrix} = \begin{bmatrix} s_{RR} & s_{RL} \\ s_{LR} & s_{LL} \end{bmatrix} \begin{bmatrix} E_R^i \\ E_L^i \end{bmatrix} \quad (2.22)$$

By using the transformation matrix $[T]$ in Eq. (2.17), the circular scattering elements can be computed from the linear scattering elements

$$\begin{bmatrix} s_{RR} & s_{RL} \\ s_{LR} & s_{LL} \end{bmatrix} = [T] \begin{bmatrix} s_{HH} & s_{HV} \\ s_{VH} & s_{VV} \end{bmatrix} \begin{bmatrix} 1 & 0 \\ 0 & -1 \end{bmatrix} [T]^{-1} \quad (2.23)$$

and the individual components are

$$\begin{aligned} s_{RR} &= \frac{-s_{VV} + s_{HH} - j(s_{HV} + s_{VH})}{2} \\ s_{RL} &= \frac{s_{VV} + s_{HH} + j(s_{HV} - s_{VH})}{2} \\ s_{LR} &= \frac{s_{VV} + s_{HH} - j(s_{HV} - s_{VH})}{2} \\ s_{LL} &= \frac{-s_{VV} + s_{HH} + j(s_{HV} + s_{VH})}{2} \end{aligned} \quad (2.24)$$

Similarly, the linear scattering elements are given by

$$\begin{bmatrix} s_{HH} & s_{HV} \\ s_{VH} & s_{VV} \end{bmatrix} = [T]^{-1} \begin{bmatrix} s_{RR} & s_{RL} \\ s_{LR} & s_{LL} \end{bmatrix} \begin{bmatrix} 1 & 0 \\ 0 & -1 \end{bmatrix} [T] \quad (2.25)$$

and the individual components are

$$\begin{aligned} s_{HH} &= \frac{-s_{RR} + s_{RL} + s_{LR} - s_{LL}}{2} \\ s_{VH} &= \frac{j(s_{RR} - s_{LR} + s_{RL} - s_{LL})}{2} \\ s_{HV} &= \frac{-j(s_{RR} + s_{LR} - s_{RL} - s_{LL})}{2} \\ s_{VV} &= \frac{s_{RR} + s_{LL} + js_{RL} + s_{LR}}{2} \end{aligned} \quad (2.26)$$

2.5. RCS of Simple Objects

This section presents examples of backscattered radar cross section for a number of simple shape objects. In all cases, except for the perfectly conducting sphere, only optical region approximations are presented. Radar designers and RCS engineers consider the perfectly conducting sphere to be the simplest target to examine. Even in this case, the complexity of the exact solution, when

compared to the optical region approximation, is overwhelming. Most formulas presented are Physical Optics (PO) approximation for the backscattered RCS measured by a far field radar in the direction (θ, φ) , as illustrated in Fig. 2.8.

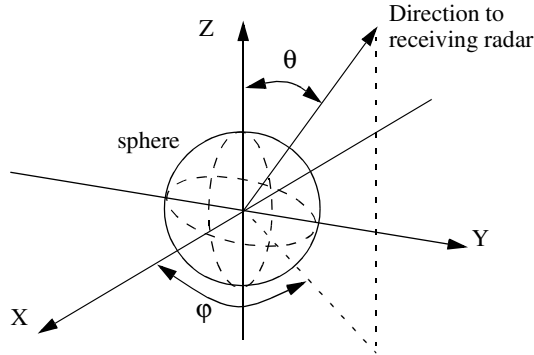


Figure 2.8. Direction of antenna receiving backscattered waves.

2.5.1. Sphere

Due to symmetry, waves scattered from a perfectly conducting sphere are co-polarized (have the same polarization) with the incident waves. This means that the cross-polarized backscattered waves are practically zero. For example, if the incident waves were Left Circularly Polarized (LCP), then the backscattered waves will also be LCP. However, because of the opposite direction of propagation of the backscattered waves, they are considered to be Right Circularly Polarized (RCP) by the receiving antenna. Therefore, the PP backscattered waves from a sphere are LCP, while the OP backscattered waves are negligible.

The normalized exact backscattered RCS for a perfectly conducting sphere is a Mie series given by

$$\frac{\sigma}{\pi r^2} = \left(\frac{j}{kr}\right) \sum_{n=1}^{\infty} (-1)^n (2n+1) \left[\left(\frac{krJ_{n-1}(kr) - nJ_n(kr)}{krH_{n-1}^{(1)}(kr) - nH_n^{(1)}(kr)} \right) - \left(\frac{J_n(kr)}{H_n^{(1)}(kr)} \right) \right] \quad (2.27)$$

where r is the radius of the sphere, $k = 2\pi/\lambda$, λ is the wavelength, J_n is the spherical Bessel of the first kind of order n , and $H_n^{(1)}$ is the Hankel function of order n , and is given by

$$H_n^{(1)}(kr) = J_n(kr) + jY_n(kr) \quad (2.28)$$

Y_n is the spherical Bessel function of the second kind of order n . Plots of the normalized perfectly conducting sphere RCS as a function of its circumference in wavelength units are shown in Figs. 2.9a and 2.9b. These plots can be reproduced using the function “*rsc_sphere.m*” given in Listing 2.3 in Section 2.8.

In Fig. 2.9, three regions are identified. First is the optical region (corresponds to a large sphere). In this case,

$$\sigma = \pi r^2 \quad r \gg \lambda \quad (2.29)$$

Second is the Rayleigh region (small sphere). In this case,

$$\sigma \approx 9\pi r^2 (kr)^4 \quad r \ll \lambda \quad (2.30)$$

The region between the optical and Rayleigh regions is oscillatory in nature and is called the Mie or resonance region.

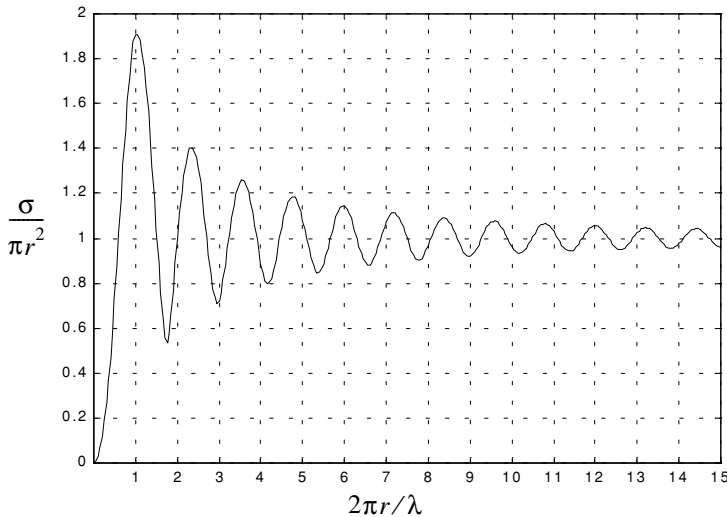


Figure 2.9a. Normalized backscattered RCS for a perfectly conducting sphere.

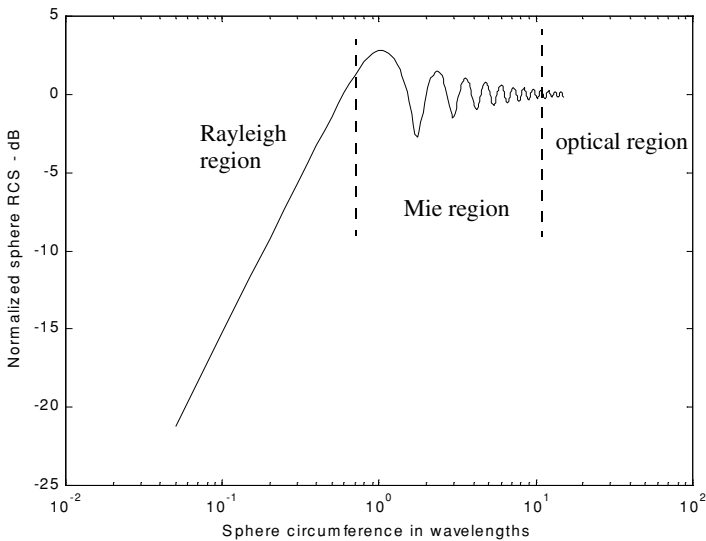


Figure 2.9b. Normalized backscattered RCS for a perfectly conducting sphere using semi-log scale.

The backscattered RCS for a perfectly conducting sphere is constant in the optical region. For this reason, radar designers typically use spheres of known cross sections to experimentally calibrate radar systems. For this purpose, spheres are flown attached to balloons. In order to obtain Doppler shift, spheres of known RCS are dropped out of an airplane and towed behind the airplane whose velocity is known to the radar.

2.5.2. Ellipsoid

An ellipsoid centered at (0,0,0) is shown in Fig. 2.10. It is defined by the following equation:

$$\left(\frac{x}{a}\right)^2 + \left(\frac{y}{b}\right)^2 + \left(\frac{z}{c}\right)^2 = 1 \quad (2.31)$$

One widely accepted approximation for the ellipsoid backscattered RCS is given by

$$\sigma = \frac{\pi a^2 b^2 c^2}{(a^2 (\sin \theta)^2 (\cos \phi)^2 + b^2 (\sin \theta)^2 (\sin \phi)^2 + c^2 (\cos \theta)^2)^2} \quad (2.32)$$

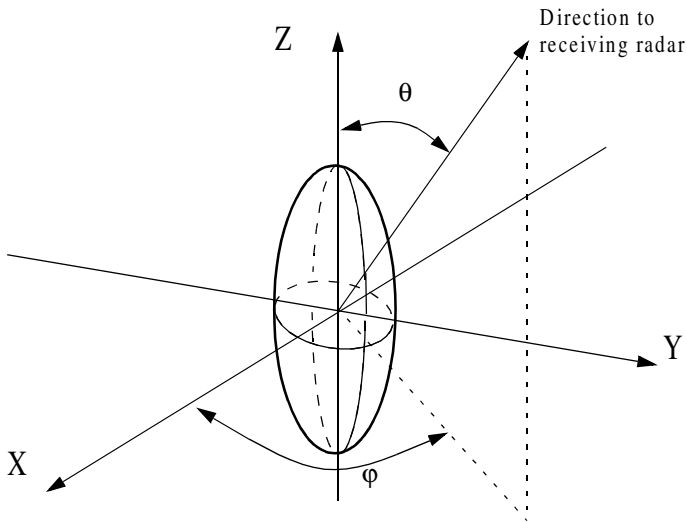


Figure 2.10. Ellipsoid.

When $a = b$, the ellipsoid becomes roll symmetric. Thus, the RCS is independent of ϕ , and Eq. (2.32) is reduced to

$$\sigma = \frac{\pi b^4 c^2}{(a^2 (\sin \theta)^2 + c^2 (\cos \theta)^2)^2} \quad (2.33)$$

and for the case when $a = b = c$,

$$\sigma = \pi c^2 \quad (2.34)$$

Note that Eq. (2.34) defines the backscattered RCS of a sphere. This should be expected, since under the condition $a = b = c$ the ellipsoid becomes a sphere. Fig. 2.11 shows the backscattered RCS for an ellipsoid versus θ for $\phi = 45^\circ$. This plot can be generated using MATLAB function “*rcs_ellipsoid.m*” given in Listing 2.4 in Section 2.8. Note that at normal incidence ($\theta = 90^\circ$) the RCS corresponds to that of a sphere of radius c , and is often referred to as the broadside specular RCS value.

MATLAB Function “*rcs_ellipsoid.m*”

The function “*rcs_ellipsoid.m*” computes and plots the RCS of an ellipsoid versus aspect angle. It utilizes Eq. (2.32) and its syntax is as follows:

$$[rcs] = rcs_ellipsoid(a, b, c, phi)$$

where

Symbol	Description	Units	Status
a	<i>ellipsoid a-radius</i>	<i>meters</i>	<i>input</i>
b	<i>ellipsoid b-radius</i>	<i>meters</i>	<i>input</i>
c	<i>ellipsoid c-radius</i>	<i>meters</i>	<i>input</i>
ϕ	<i>ellipsoid roll angle</i>	<i>degrees</i>	<i>input</i>
r_{cs}	<i>array of RCS versus aspect angle</i>	<i>dBsm</i>	<i>output</i>

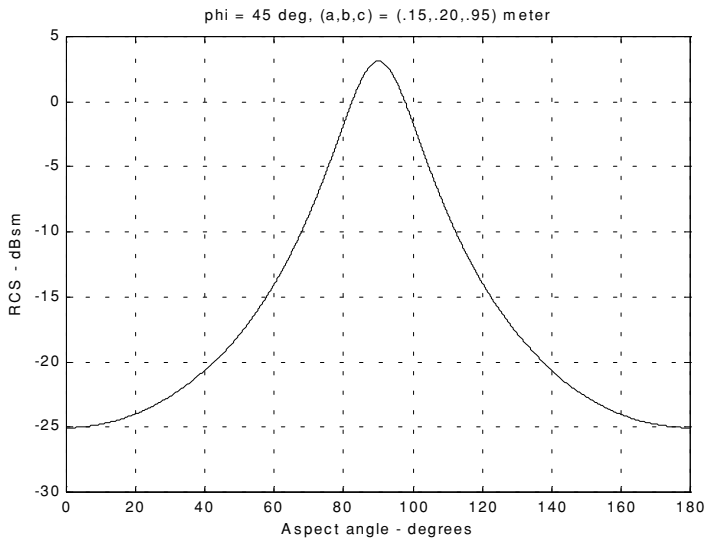


Figure 2.11. Ellipsoid backscattered RCS versus aspect angle, $\phi = 45^\circ$.

2.5.3. Circular Flat Plate

Fig. 2.12 shows a circular flat plate of radius r , centered at the origin. Due to the circular symmetry, the backscattered RCS of a circular flat plate has no dependency on ϕ . The RCS is only aspect angle dependent. For normal incidence (i.e., zero aspect angle) the backscattered RCS for a circular flat plate is

$$\sigma = \frac{4\pi^3 r^4}{\lambda^2} \quad \theta = 0^\circ \quad (2.35)$$

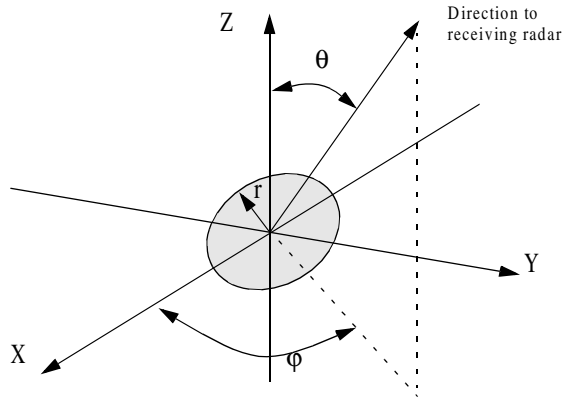


Figure 2.12. Circular flat plate.

For non-normal incidence, two approximations for the circular flat plate backscattered RCS for any linearly polarized incident wave are

$$\sigma = \frac{\lambda r}{8\pi \sin\theta (\tan(\theta))^2} \quad (2.36)$$

$$\sigma = \pi k^2 r^4 \left(\frac{2J_1(2kr \sin\theta)}{2kr \sin\theta} \right)^2 (\cos\theta)^2 \quad (2.37)$$

where $k = 2\pi/\lambda$, and $J_1(\beta)$ is the first order spherical Bessel function evaluated at β . The RCS corresponding to Eqs. (2.35) through (2.37) is shown in Fig. 2.13. These plots can be reproduced using MATLAB function “*rcs_circ_plate.m*” given in Listing 2.5 in Section 2.8.

MATLAB Function “*rcs_circ_plate.m*”

The function “*rcs_circ_plate.m*” calculates and plots the backscattered RCS from a circular plate. Its syntax is as follows:

$$[rcs] = rcs_circ_plate(r, freq)$$

where

Symbol	Description	Units	Status
<i>r</i>	<i>radius of circular plate</i>	<i>meters</i>	<i>input</i>
<i>freq</i>	<i>frequency</i>	<i>Hz</i>	<i>input</i>
<i>rcs</i>	<i>array of RCS versus aspect angle</i>	<i>dBsm</i>	<i>output</i>

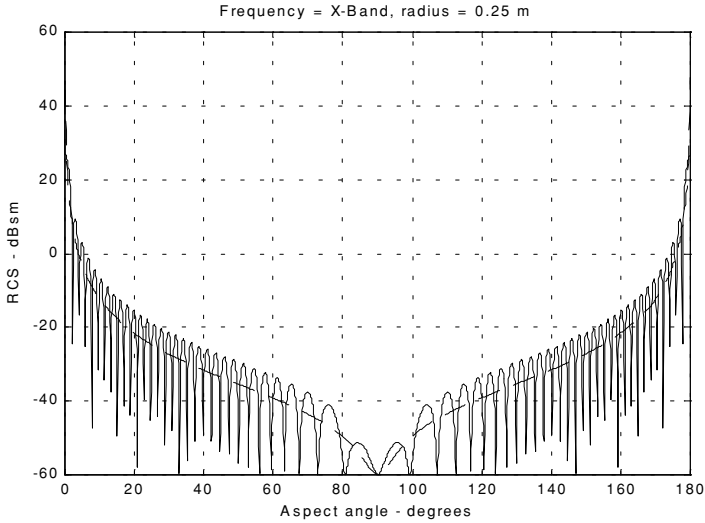


Figure 2.13. Backscattered RCS for a circular flat plate. Solid line corresponds to Eq. (2.37). Dashed line corresponds to Eq. (2.36).

2.5.4. Truncated Cone (Frustum)

Figs. 2.14 and 2.15 show the geometry associated with a frustum. The half cone angle α is given by

$$\tan \alpha = \frac{(r_2 - r_1)}{H} = \frac{r_2}{L} \quad (2.38)$$

Define the aspect angle at normal incidence (broadside) as θ_n . Thus, when a frustum is illuminated by a radar located at the same side as the cone's small end, the angle θ_n is

$$\theta_n = 90^\circ - \alpha \quad (2.39)$$

Alternatively, normal incidence occurs at

$$\theta_n = 90^\circ + \alpha \quad (2.40)$$

At normal incidence, one approximation for the backscattered RCS of a truncated cone due to a linearly polarized incident wave is

$$\sigma_{\theta_n} = \frac{8\pi(z_2^{3/2} - z_1^{3/2})^2}{9\lambda \sin \theta_n} \tan \alpha (\sin \theta_n - \cos \theta_n \tan \alpha)^2 \quad (2.41)$$

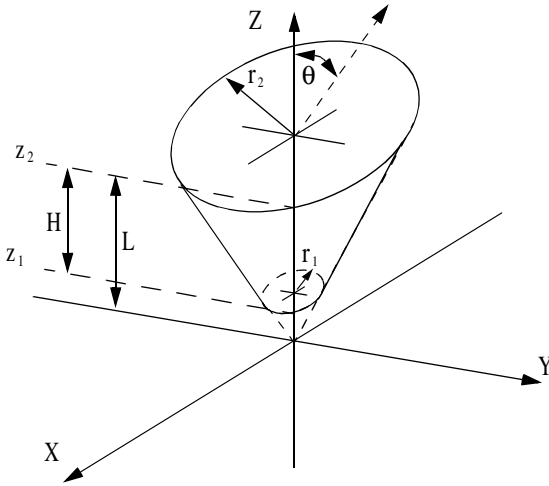


Figure 2.14. Truncated cone (frustum).

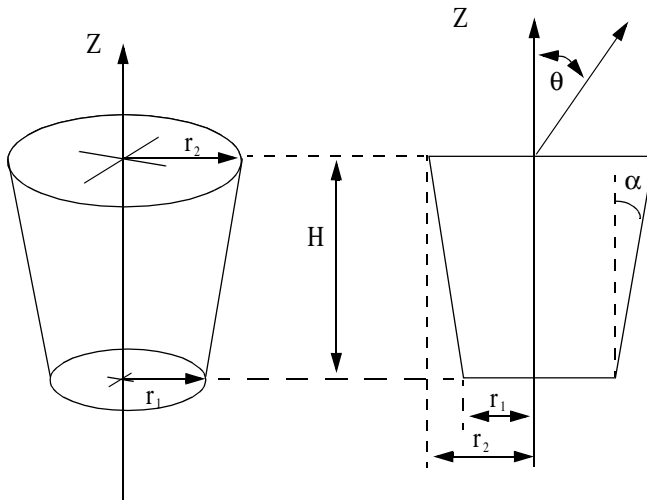


Figure 2.15. Definition of half cone angle.

where λ is the wavelength, and z_1, z_2 are defined in Fig. 2.14. Using trigonometric identities, Eq. (2.41) can be reduced to

$$\sigma_{\theta_n} = \frac{8\pi(z_2^{3/2} - z_1^{3/2})^2}{9\lambda} \frac{\sin\alpha}{(\cos\alpha)^4} \quad (2.42)$$

For non-normal incidence, the backscattered RCS due to a linearly polarized incident wave is

$$\sigma = \frac{\lambda z \tan\alpha}{8\pi \sin\theta} \left(\frac{\sin\theta - \cos\theta \tan\alpha}{\sin\theta \tan\alpha + \cos\theta} \right)^2 \quad (2.43)$$

where z is equal to either z_1 or z_2 depending on whether the RCS contribution is from the small or the large end of the cone. Again, using trigonometric identities Eq. (2.43) (assuming the radar illuminates the frustum starting from the large end) is reduced to

$$\sigma = \frac{\lambda z \tan\alpha}{8\pi \sin\theta} (\tan(\theta - \alpha))^2 \quad (2.44)$$

When the radar illuminates the frustum starting from the small end (i.e., the radar is in the negative z direction in Fig. (2.14)), Eq. (2.44) should be modified to

$$\sigma = \frac{\lambda z \tan\alpha}{8\pi \sin\theta} (\tan(\theta + \alpha))^2 \quad (2.45)$$

For example, consider a frustum defined by $H = 20.945\text{ cm}$, $r_1 = 2.057\text{ cm}$, $r_2 = 5.753\text{ cm}$. It follows that the half cone angle is 10° . Fig. 2.16 (top) shows a plot of its RCS when illuminated by a radar in the positive z direction. Fig. 2.16 (bottom) shows the same thing, except in this case, the radar is in the negative z direction. Note that for the first case, normal incidence occur at 100° , while for the second case it occurs at 80° . These plots can be reproduced using MATLAB function “*rsc_frustum.m*” given in Listing 2.6 in Section 2.8.

MATLAB Function “*rsc_frustum.m*”

The function “*rsc_frustum.m*” computes and plots the backscattered RCS of a truncated conic section. The syntax is as follows:

$$[rsc] = rsc_frustum(r1, r2, freq, indicator)$$

where

Symbol	Description	Units	Status
$r1$	<i>small end radius</i>	<i>meters</i>	<i>input</i>
$r2$	<i>large end radius</i>	<i>meters</i>	<i>input</i>
$freq$	<i>frequency</i>	<i>Hz</i>	<i>input</i>
$indicator$	<i>indicator = 1 when viewing from large end</i> <i>indicator = 0 when viewing from small end</i>	<i>none</i>	<i>input</i>
r_{cs}	<i>array of RCS versus aspect angle</i>	<i>dBsm</i>	<i>output</i>

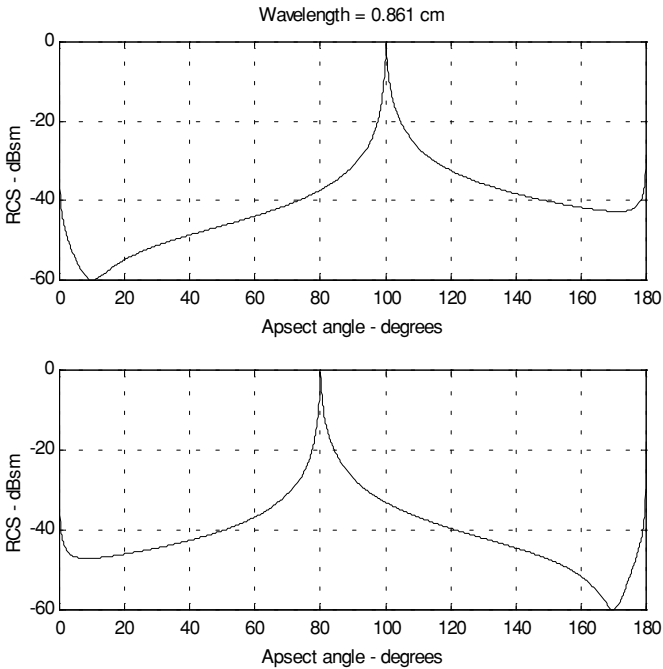


Figure 2.16. Backscattered RCS for a frustum.

2.5.5. Cylinder

Fig. 2.17 shows the geometry associated with a cylinder. Two cases are presented: first, the general case of an elliptical cylinder; second, the case of a circular cylinder. The normal and non-normal incidence backscattered RCS for an

elliptical cylinder due a linearly polarized incident wave are, respectively, given by

$$\sigma_{\theta_n} = \frac{2\pi H^2 r_2^2 r_1^2}{\lambda(r_1^2(\cos\varphi)^2 + r_2^2(\sin\varphi)^2)^{1.5}} \quad (2.46)$$

$$\sigma = \frac{\lambda r_2^2 r_1^2 \sin\theta}{8\pi(\cos\theta)^2(r_1^2(\cos\varphi)^2 + r_2^2(\sin\varphi)^2)^{1.5}} \quad (2.47)$$

For a circular cylinder of radius r , then due to roll symmetry, Eqs. (2.46) and (2.47), respectively, reduce to

$$\sigma_{\theta_n} = \frac{2\pi H^2 r}{\lambda} \quad (2.48)$$

$$\sigma = \frac{\lambda r \sin\theta}{8\pi(\cos\theta)^2} \quad (2.49)$$

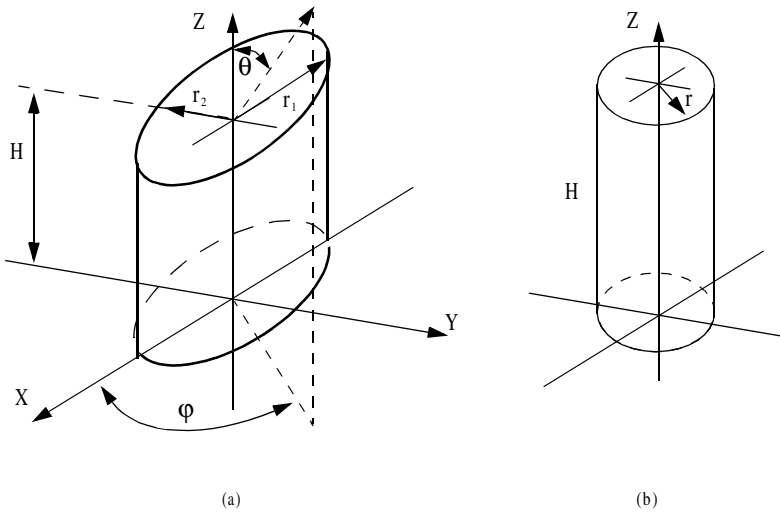


Figure 2.17. (a) Elliptical cylinder; (b) circular cylinder.

Fig. 2.18 shows a plot of the cylinder backscattered RCS using Eqs. (2.48) and (2.49). This plot can be reproduced using MATLAB function “*rcs_cylinder.m*” given in Listing 2.7 in Section 2.8. Note that the broadside specular occurs at aspect angle of 90° .

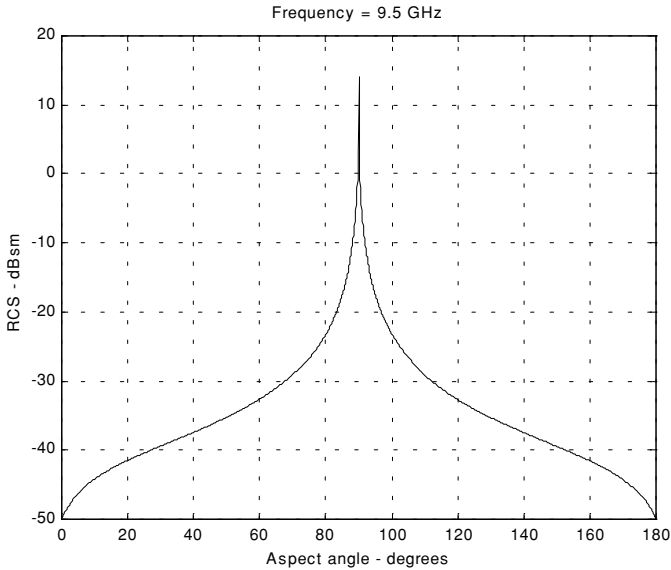


Figure 2.18. Backscattered RCS for a cylinder, $r = 0.125m$ and $H = 1m$.

MATLAB Function “*rcs_cylinder.m*”

The function “*rcs_cylinder.m*” computes and plots the backscattered RCS of a cylinder. The syntax is as follows:

$$[rcs] = rcs_cylinder(r, h, freq)$$

where

Symbol	Description	Units	Status
<i>r</i>	<i>radius</i>	<i>meters</i>	<i>input</i>
<i>h</i>	<i>length of cylinder</i>	<i>meters</i>	<i>input</i>
<i>freq</i>	<i>frequency</i>	<i>Hz</i>	<i>input</i>
<i>rcs</i>	<i>array of RCS versus aspect angle</i>	<i>dBsm</i>	<i>output</i>

2.5.6. Rectangular Flat Plate

Consider a perfectly conducting rectangular thin flat plate in the x-y plane as shown in Fig. 2.19. The two sides of the plate are denoted by $2a$ and $2b$. For a linearly polarized incident wave in the x-z plane, the horizontal and vertical backscattered RCS are, respectively, given by

$$\sigma_V = \frac{b^2}{\pi} \left| \sigma_{1V} - \sigma_{2V} \left[\frac{1}{\cos \theta} + \frac{\sigma_{2V}}{4} (\sigma_{3V} + \sigma_{4V}) \right] \sigma_{5V}^{-1} \right|^2 \quad (2.50)$$

$$\sigma_H = \frac{b^2}{\pi} \left| \sigma_{1H} - \sigma_{2H} \left[\frac{1}{\cos \theta} - \frac{\sigma_{2H}}{4} (\sigma_{3H} + \sigma_{4H}) \right] \sigma_{5H}^{-1} \right|^2 \quad (2.51)$$

where $k = 2\pi/\lambda$ and

$$\sigma_{1V} = \cos(k a \sin \theta) - j \frac{\sin(k a \sin \theta)}{\sin \theta} = (\sigma_{1H})^* \quad (2.52)$$

$$\sigma_{2V} = \frac{e^{j(ka - \pi/4)}}{\sqrt{2\pi}(ka)^{3/2}} \quad (2.53)$$

$$\sigma_{3V} = \frac{(1 + \sin \theta) e^{-jk a \sin \theta}}{(1 - \sin \theta)^2} \quad (2.54)$$

$$\sigma_{4V} = \frac{(1 - \sin \theta) e^{jk a \sin \theta}}{(1 + \sin \theta)^2} \quad (2.55)$$

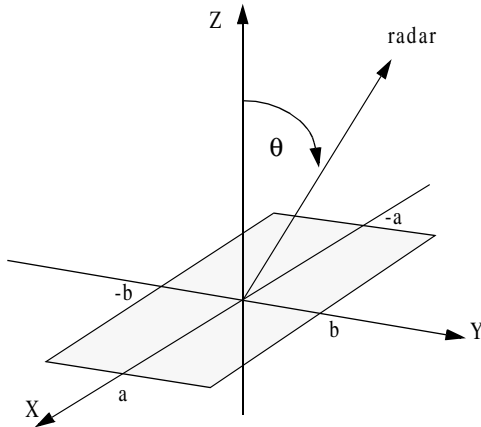


Figure 2.19. Rectangular flat plate.

$$\sigma_{5V} = 1 - \frac{e^{j(2ka - \pi/2)}}{8\pi(ka)^3} \quad (2.56)$$

$$\sigma_{2H} = \frac{4e^{j(ka + \pi/4)}}{\sqrt{2\pi}(ka)^{1/2}} \quad (2.57)$$

$$\sigma_{3H} = \frac{e^{-jk a \sin \theta}}{1 - \sin \theta} \quad (2.58)$$

$$\sigma_{4H} = \frac{e^{jk a \sin \theta}}{1 + \sin \theta} \quad (2.59)$$

$$\sigma_{5H} = 1 - \frac{e^{j(2ka + (\pi/2))}}{2\pi(ka)} \quad (2.60)$$

Eqs. (2.50) and (2.51) are valid and quite accurate for aspect angles $0^\circ \leq \theta \leq 80^\circ$. For aspect angles near 90° , Ross¹ obtained by extensive fitting of measured data an empirical expression for the RCS. It is given by

$$\sigma_H \rightarrow 0$$

$$\sigma_V = \frac{ab^2}{\lambda} \left\{ \left[1 + \frac{\pi}{2(2a/\lambda)^2} \right] + \left[1 - \frac{\pi}{2(2a/\lambda)^2} \right] \cos \left(2ka - \frac{3\pi}{5} \right) \right\} \quad (2.61)$$

The backscattered RCS for a perfectly conducting thin rectangular plate for incident waves at any θ, φ can be approximated by

$$\sigma = \frac{4\pi a^2 b^2}{\lambda^2} \left(\frac{\sin(ak \sin \theta \cos \varphi)}{ak \sin \theta \cos \varphi} \frac{\sin(bk \sin \theta \sin \varphi)}{bk \sin \theta \sin \varphi} \right)^2 (\cos \theta)^2 \quad (2.62)$$

Eq. (2.62) is independent of the polarization, and is only valid for aspect angles $\theta \leq 20^\circ$. Fig. 2.20, shows an example for the backscattered RCS of a rectangular flat plate, for both vertical (Fig. 2.20a) and horizontal (Fig. 2.20b) polarizations, using Eqs. (2.50), (2.51) and (2.62). In this example, $a = b = 10.16 \text{ cm}$ and wavelength $\lambda = 3.25 \text{ cm}$. This plot can be reproduced using MATLAB function “*rcs_rect_plate*” given in Listing 2.8 in Section 2.8.

MATLAB Function “*rcs_rect_plate.m*”

The function “*rcs_rect_plate.m*” calculates and plots the backscattered RCS of a rectangular flat plate. Its syntax is as follows:

1. Ross, R. A. Radar Cross Section of Rectangular Flat Plate as a Function of Aspect Angle, *IEEE Trans. AP-14:320*, 1966.

$$[rcs] = rcs_rect_plate(a, b, freq)$$

where

Symbol	Description	Units	Status
<i>a</i>	<i>short side of plate</i>	<i>meters</i>	<i>input</i>
<i>b</i>	<i>long side of plate</i>	<i>meters</i>	<i>input</i>
<i>freq</i>	<i>frequency</i>	<i>Hz</i>	<i>input</i>
<i>rcs</i>	<i>array of RCS versus aspect angle</i>	<i>dBsm</i>	<i>output</i>

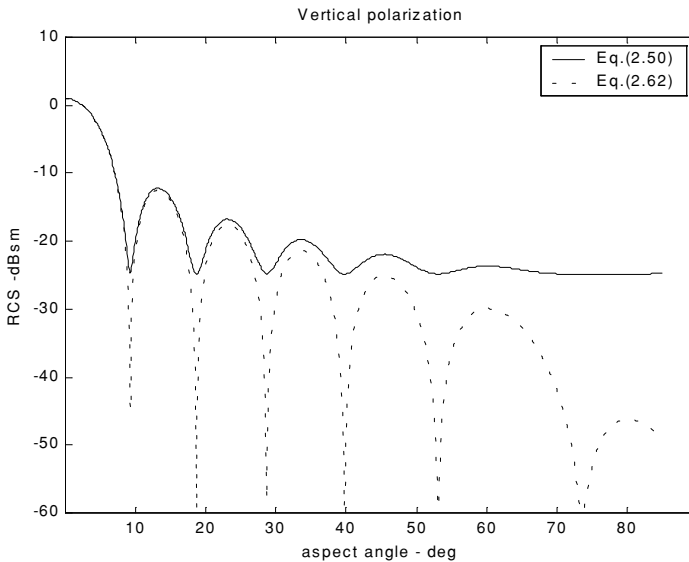


Figure 2.20a. Backscattered RCS for a rectangular flat plate.

2.5.7. *Triangular Flat Plate*

Consider the triangular flat plate defined by the isosceles triangle as oriented in Fig. 2.21. The backscattered RCS can be approximated for small aspect angles (less than 30°) by

$$\sigma = \frac{4\pi A^2}{\lambda^2} (\cos \theta)^2 \sigma_0 \quad (2.63)$$

$$\sigma_0 = \frac{[(\sin\alpha)^2 - (\sin(\beta/2))^2]^2 + \sigma_{01}}{\alpha^2 - (\beta/2)^2} \quad (2.64)$$

$$\sigma_{01} = 0.25(\sin\phi)^2[(2a/b)\cos\phi\sin\beta - \sin\phi\sin 2\alpha]^2 \quad (2.65)$$

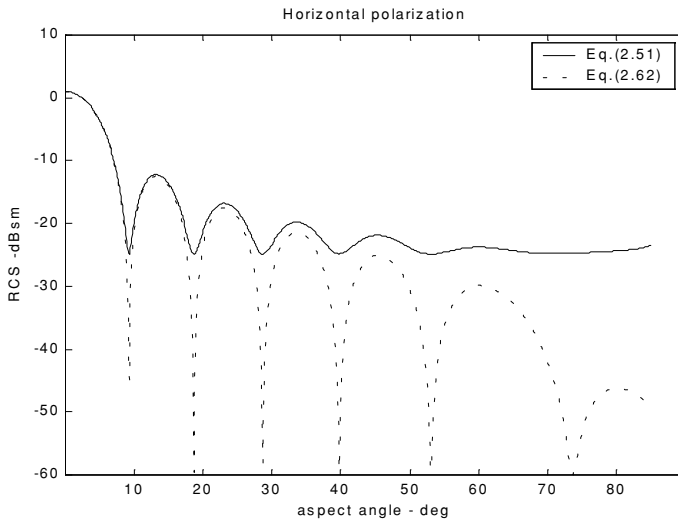


Figure 2.20b. Backscattered RCS for a rectangular flat plate.

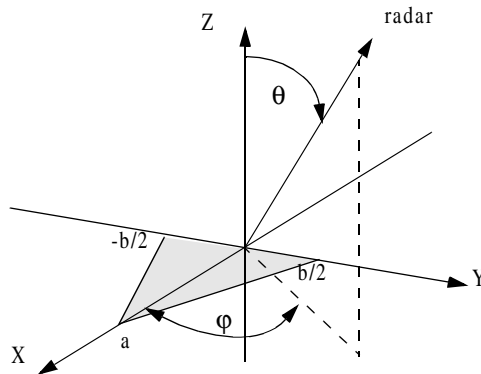


Figure 2.21. Coordinates for a perfectly conducting isosceles triangular plate.

where $\alpha = k a \sin \theta \cos \varphi$, $\beta = k b \sin \theta \sin \varphi$, and $A = ab/2$. For waves incident in the plane $\varphi = 0$, the RCS reduces to

$$\sigma = \frac{4\pi A^2}{\lambda^2} (\cos \theta)^2 \left[\frac{(\sin \alpha)^4}{\alpha^4} + \frac{(\sin 2\alpha - 2\alpha)^2}{4\alpha^4} \right] \quad (2.66)$$

and for incidence in the plane $\varphi = \pi/2$

$$\sigma = \frac{4\pi A^2}{\lambda^2} (\cos \theta)^2 \left[\frac{(\sin(\beta/2))^4}{(\beta/2)^4} \right] \quad (2.67)$$

Fig. 2.22 shows a plot for the normalized backscattered RCS from a perfectly conducting isosceles triangular flat plate. In this example $a = 0.2m$, $b = 0.75m$, and $\varphi = 0, \pi/2$. This plot can be reproduced using MATLAB function “*rcs_isosceles.m*” given in Listing 2.9 in Section 2.8.

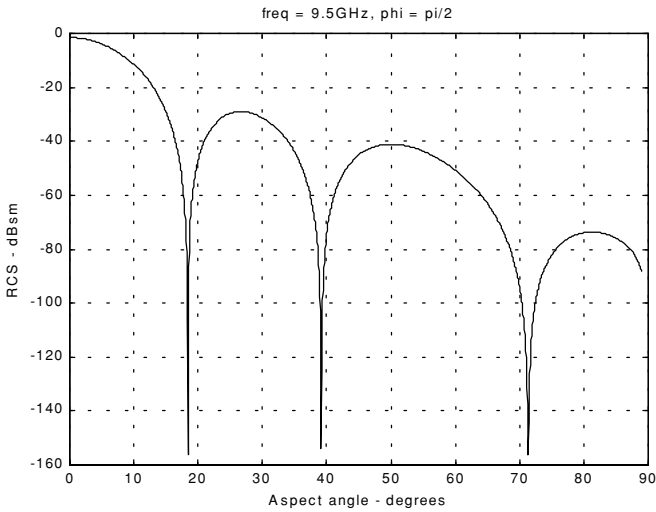


Figure 2.22. Backscattered RCS for a perfectly conducting triangular flat plate, $a = 20cm$ and $b = 75cm$.

MATLAB Function “*rcs_isosceles.m*”

The function “*rcs_isosceles.m*” calculates and plots the backscattered RCS of a triangular flat plate. Its syntax is as follows:

$$[rcs] = rcs_isosceles(a, b, freq, phi)$$

where

Symbol	Description	Units	Status
a	<i>height of plate</i>	<i>meters</i>	<i>input</i>
b	<i>base of plate</i>	<i>meters</i>	<i>input</i>
$freq$	<i>frequency</i>	<i>Hz</i>	<i>input</i>
phi	<i>roll angle</i>	<i>degrees</i>	<i>input</i>
rsc	<i>array of RCS versus aspect angle</i>	<i>dBsm</i>	<i>output</i>

2.6. RCS of Complex Objects

A complex target RCS is normally computed by coherently combining the cross sections of the simple shapes that make that target. In general, a complex target RCS can be modeled as a group of individual scattering centers distributed over the target. The scattering centers can be modeled as isotropic point scatterers (N-point model) or as simple shape scatterers (N-shape model). In any case, knowledge of the scattering centers' locations and strengths is critical in determining complex target RCS. This is true, because as seen in Section 2.3, relative spacing and aspect angles of the individual scattering centers drastically influence the overall target RCS. Complex targets that can be modeled by many equal scattering centers are often called Swerling 1 or 2 targets. Alternatively, targets that have one dominant scattering center and many other smaller scattering centers are known as Swerling 3 or 4 targets.

In NB radar applications, contributions from all scattering centers combine coherently to produce a single value for the target RCS at every aspect angle. However, in WB applications, a target may straddle over many range bins. For each range bin, the average RCS extracted by the radar represents the contributions from all scattering centers that fall within that bin.

As an example, consider a circular cylinder with two perfectly conducting circular flat plates on both ends. Assume linear polarization and let $H = 1m$ and $r = 0.125m$. The backscattered RCS for this object versus aspect angle is shown in Fig. 2.23. Note that at aspect angles close to 0° and 180° the RCS is mainly dominated by the circular plate, while at aspect angles close to normal incidence, the RCS is dominated by the cylinder broadside specular return. This plot can be reproduced using MATLAB program "*rsc_cylinder_complex.m*" given in Listing 2.10 in Section 2.8.

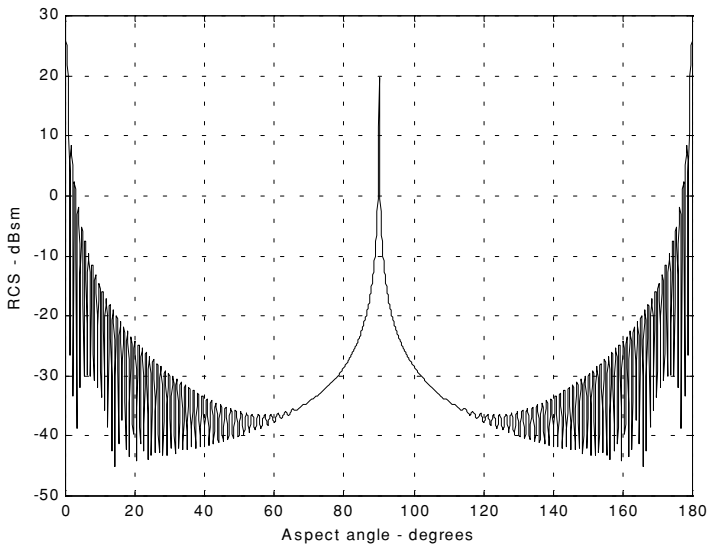


Figure 2.23. Backscattered RCS for a cylinder with flat plates.

2.7. RCS Fluctuations and Statistical Models

In most practical radar systems there is relative motion between the radar and an observed target. Therefore, the RCS measured by the radar fluctuates over a period of time as a function of frequency and the target aspect angle. This observed RCS is referred to as the radar dynamic cross section. Up to this point, all RCS formulas discussed in this chapter assumed stationary target, where in this case, the backscattered RCS is often called static RCS.

Dynamic RCS may fluctuate in amplitude and/or in phase. Phase fluctuation is called glint, while amplitude fluctuation is called scintillation. Glint causes the far field backscattered wavefronts from a target to be non-planar. For most radar applications, glint introduces linear errors in the radar measurements, and thus it is not of a major concern. However, cases where high precision and accuracy are required, glint can be detrimental. Examples include precision instrumentation tracking radar systems, missile seekers, and automated aircraft landing systems. For more details on glint, the reader is advised to visit cited references listed in the bibliography.

Radar cross-section scintillation can vary slowly or rapidly depending on the target size, shape, dynamics, and its relative motion with respect to the radar.

Thus, due to the wide variety of RCS scintillation sources changes in the radar cross section are modeled statistically as random processes. The value of an RCS random process at any given time defines a random variable at that time. Many of the RCS scintillation models were developed and verified by experimental measurements.

2.7.1. RCS Statistical Models - Scintillation Models

This section presents the most commonly used RCS statistical models. Statistical models that apply to sea, land, and volume clutter, such as the Weibull and Log-normal distributions, will be discussed in a later chapter. The choice of a particular model depends heavily on the nature of the target under examination.

Chi-Square of Degree $2m$

The Chi-square distribution applies to a wide range of targets; its *pdf* is given by

$$f(\sigma) = \frac{m}{\Gamma(m)\sigma_{av}} \left(\frac{m\sigma}{\sigma_{av}}\right)^{m-1} e^{-m\sigma/\sigma_{av}} \quad \sigma \geq 0 \quad (2.68)$$

where $\Gamma(m)$ is the gamma function with argument m , and σ_{av} is the average value. As the degree gets larger the distribution corresponds to constrained RCS values (narrow range of values). The limit $m \rightarrow \infty$ corresponds to a constant RCS target (steady-target case).

Swerling I and II (Chi-Square of Degree 2)

In Swerling I, the RCS samples measured by the radar are correlated throughout an entire scan, but are uncorrelated from scan to scan (slow fluctuation). In this case, the *pdf* is

$$f(\sigma) = \frac{1}{\sigma_{av}} \exp\left(-\frac{\sigma}{\sigma_{av}}\right) \quad \sigma \geq 0 \quad (2.69)$$

where σ_{av} denotes the average RCS overall target fluctuation. Swerling II target fluctuation is more rapid than Swerling I, but the measurements are pulse to pulse uncorrelated. This is illustrated in Fig. 2.24. Swerling II RCS distribution is also defined by Eq. (2.69). Swerlings I and II apply to targets consisting of many independent fluctuating point scatterers of approximately equal physical dimensions.

Swerling III and IV (Chi-Square of Degree 4)

Swerlings III and IV have the same *pdf*, and it is given by

$$f(\sigma) = \frac{4\sigma}{\sigma_{av}^2} \exp\left(-\frac{2\sigma}{\sigma_{av}}\right) \quad \sigma \geq 0 \quad (2.70)$$

The fluctuations in Swerling III are similar to Swerling I; while in Swerling IV they are similar to Swerling II fluctuations (see Fig. 2.24). Swerlings III and IV are more applicable to targets that can be represented by one dominant scatterer and many other small reflectors. Fig. 2.25 shows a typical plot of the *pdfs* for Swerling cases. This plot can be reproduced using MATLAB program “*Swerling_models.m*” given in Listing 2.11 in Section 2.8.

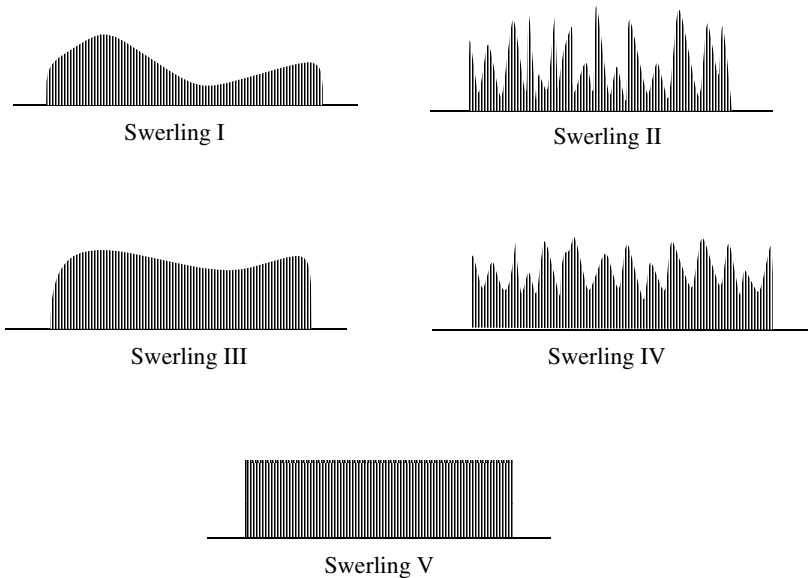


Figure 2.24. Radar returns from targets with different Swerling fluctuations. Swerling V corresponds to a steady RCS target case.

2.8. MATLAB Program/Function Listings

This section presents listings for all MATLAB programs/functions used in this chapter. The user is advised to rerun these programs with different input parameters. All functions have companion MATLAB “*filename_driver.m*” files that utilize MATLAB Graphical User Interface (GUI). Figure 2.26 shows a typical GUI screen capture associated with the cylinder case.

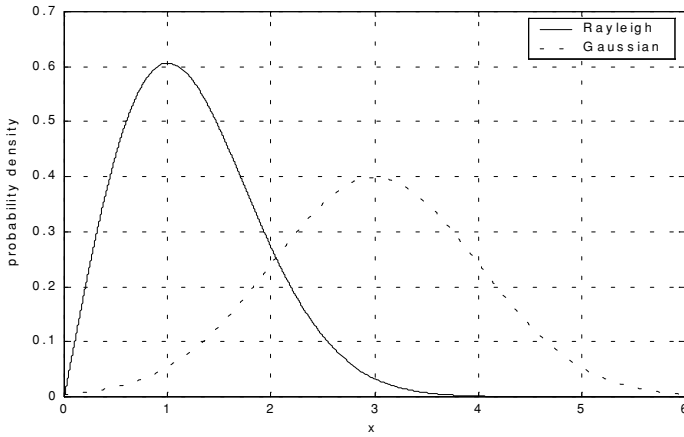


Figure 2.25. Probability densities for Swerling targets.

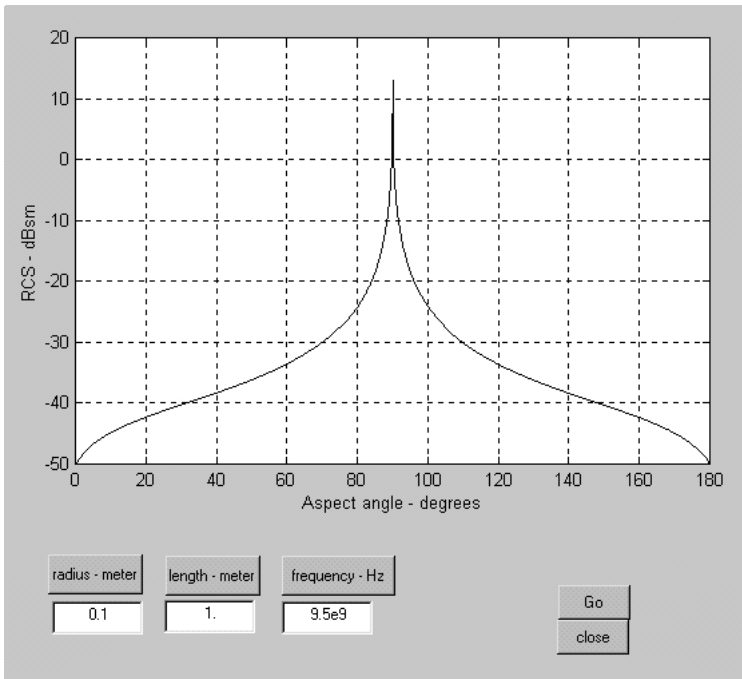


Figure 2.26. GUI work space associated with the function “*rsc_cylinder.m*”.

Listing 2.1. MATLAB Function “rcs_aspect.m”

```
function [rcs] = rcs_aspect (scat_spacing, freq)
% This function demonstrates the effect of aspect angle on RCS.
% Poit scatterers separated by scat_spacing meter. Initially the two scatterers
% are aligned with radar line of sight. The aspect angle is changed from
% 0 degrees to 180 degrees and the equivalent RCS is computed.
% Plot of RCS versus aspect is generated.
eps = 0.00001;
wavelength = 3.0e+8 / freq;
% Compute aspect angle vector
aspect_degrees = 0.:05:180.;
aspect_radians = (pi/180) .* aspect_degrees;
% Compute electrical scatterer spacing vector in wavelength units
elec_spacing = (2.0 * scat_spacing / wavelength) .* cos(aspect_radians);
% Compute RCS (rcs = RCS_scatter1 + RCS_scatter2)
% Scatter1 is taken as phase reference point
rcs = abs(1.0 + cos((2.0 * pi) .* elec_spacing) ...
    + i * sin((2.0 * pi) .* elec_spacing));
rcs = rcs + eps;
rcs = 20.0*log10(rcs); % RCS in dBsm
% Plot RCS versus aspect angle
figure (1);
plot (aspect_degrees,rcs,'k');
grid;
xlabel ('aspect angle - degrees');
ylabel ('RCS in dBsm');
%title (' Frequency is 3GHz; scatterer spacing is 0.5m');
```

Listing 2.2. MATLAB Function “rcs_frequency.m”

```
function [rcs] = rcs_frequency (scat_spacing, frequ, freql)
% This program demonstrates the dependency of RCS on wavelength
eps = 0.0001;
freq_band = frequ - freql;
delfreq = freq_band / 500.;
index = 0;
for freq = freql: delfreq: frequ
    index = index +1;
    wavelength(index) = 3.0e+8 / freq;
end
elec_spacing = 2.0 * scat_spacing ./ wavelength;
rcs = abs ( 1 + cos((2.0 * pi) .* elec_spacing) ...
    + i * sin((2.0 * pi) .* elec_spacing));
rcs = rcs + eps;
rcs = 20.0*log10(rcs); % RCS ins dBsm
% Plot RCS versus frequency
freq = freql:delfreq:frequ;
```

```

plot(freq,rsc);
grid;
xlabel('Frequency');
ylabel('RCS in dBsm');

```

Listing 2.3. MATLAB Program “rsc_sphere.m”.

```

% This program calculates the back-scattered RCS for a perfectly
% conducting sphere using Eq.(2.7), and produce plots similar to Fig.2.9
% Spherical Bessel functions are computed using series approximation and recursion.
clear all
eps = 0.00001;
index = 0;
% kr limits are [0.05 - 15] ==> 300 points
for kr = 0.05:0.05:15
    index = index + 1;
    sphere_rcs = 0. + 0.*i;
    f1 = 0. + 1.*i;
    f2 = 1. + 0.*i;
    m = 1.;
    n = 0.;
    q = -1.;
    % initially set del to huge value
    del = 100000+100000*i;
    while(abs(del) > eps)
        q = -q;
        n = n + 1;
        m = m + 2;
        del = (2.*n-1) * f2 / kr-f1;
        f1 = f2;
        f2 = del;
        del = q * m / (f2 * (kr * f1 - n * f2));
        sphere_rcs = sphere_rcs + del;
    end
    rcs(index) = abs(sphere_rcs);
    sphere_rcsdb(index) = 10. * log10(rcs(index));
end
figure(1);
n=0.05:.05:15;
plot (n,rsc,'k');
set (gca,'xtick',[1 2 3 4 5 6 7 8 9 10 11 12 13 14 15]);
%xlabel ('Sphere circumference in wavelengths');
%ylabel ('Normalized sphere RCS');
grid;
figure (2);
plot (n,sphere_rcsdb,'k');
set (gca,'xtick',[1 2 3 4 5 6 7 8 9 10 11 12 13 14 15]);
xlabel ('Sphere circumference in wavelengths');

```



```

ylabel ('Normalized sphere RCS - dB');
grid;
figure (3);
semilogx (n,sphere_rcsdb,'k');
xlabel ('Sphere circumference in wavelengths');
ylabel ('Normalized sphere RCS - dB');

```

Listing 2.4. MATLAB Function “rcs_ellipsoid.m”

```

function [rcs] = rcs_ellipsoid (a, b, c, phi)
% This function computes and plots the ellipsoid RCS versus aspect angle.
% The roll angle angle phi is fixed,
eps = 0.00001;
sin_phi_s = sin(phi)^2;
cos_phi_s = cos(phi)^2;
% Generate aspect angle vector
theta = 0.:05:180.0;
theta = (theta .* pi) ./ 180.;
if(a ~= b & a ~= c)
    rcs = (pi * a^2 * b^2 * c^2) ./ (a^2 * cos_phi_s .* (sin(theta).^2) + ...
        b^2 * sin_phi_s .* (sin(theta).^2) + ...
        c^2 .* (cos(theta).^2)).^2 ;
else
    if(a == b & a ~= c)
        rcs = (pi * b^4 * c^2) ./ ( b^2 .* (sin(theta).^2) + ...
            c^2 .* (cos(theta).^2)).^2 ;
    else
        if (a == b & a ==c)
            rcs = pi * c^4;
        end
    end
end
rcs_db = 10.0 * log10(rcs);
figure (1);
plot ((theta * 180.0 / pi),rcs_db,'k');
xlabel ('Aspect angle - degrees');
ylabel ('RCS - dBsm');
%title ('phi = 45 deg, (a,b,c) = (.15,.20,.95) meter')
grid;

```

Listing 2.5. MATLAB Function “rcs_circ_plate.m”

```

function [rcs] = rcs_circ_plate (r, freq)
% This function calculates and plots the RCS of a circular flat plate of radius r.
eps = 0.000001;
% Compute wavelength
lambda = 3.e+8 / freq; % X-Band
index = 0;

```

```

for aspect_deg = 0.:1:180
    index = index + 1;
    aspect = (pi / 180.) * aspect_deg;
% Compute RCS using Eq. (2.35)
    if (aspect == 0 | aspect == pi)
        rcs_po(index) = (4.0 * pi^3 * r^4 / lambda^2) + eps;
        rcs_mu(index) = rcs_po(1);
    else
% Compute RCS using Eq. (2.36)
        x = (4. * pi * r / lambda) * sin(aspect);
        val1 = 4. * pi^3 * r^4 / lambda^2;
        val2 = 2. * besselj(1,x) / x;
        rcs_po(index) = val1 * (val2 * cos(aspect))^2 + eps;
% Compute RCS using Eq. (2.36)
        val1m = lambda * r;
        val2m = 8. * pi * sin(aspect) * (tan(aspect)^2);
        rcs_mu(index) = val1m / val2m + eps;
    end
end
rcsdb_po = 10. * log10(rcs_po);
rcsdb_mu = 10 * log10(rcs_mu);
angle = 0.:1:180;
plot(angle,rcsdb_po,'k',angle,rcsdb_mu,'k--')
grid;
xlabel ('Aspect angle - degrees');
ylabel ('RCS - dBsm');
%title ('Frequency = X-Band, radius = 0.25 m');

```

Listing 2.6. MATLAB Function “rcs_frustum.m”

```

function [rcs] = rcs_frustum (r1, r2, h, freq, indicator)
% This program computes the monostatic RCS for a frustum.
% Incident linear Polarization is assumed. To compute RCP or LCP RCS
% one must use Eq. (2.24)
% Normal incidence is according to Eq.s (2.39) and (2.40)
index = 0;
eps = 0.000001;
lambda = 3.0e+8 / freq;
% Comput half cone angle, alpha
alpha = atan(( r2 - r1)/h);
% Compute z1 and z2
z2 = r2 / tan(alpha);
z1 = r1 / tan(alpha);
delta = (z2^1.5 - z1^1.5)^2;
factor = (8. * pi * delta) / (9. * lambda);
large_small_end = indicator;
if (large_small_end == 1)
    % Compute normal incidence, large end

```

```

normal_incidence = (180./pi) * ((pi /2) + alpha)
% Compute RCS from zero aspect to normal incidence
for theta = 0.001:.1:normal_incidence-.5
    index = index +1;
    theta = theta * pi /180.;
    rcs(index) = (lambda * z1 * tan(alpha) *(tan(theta - alpha))^2) / ...
        (8. * pi *sin(theta)) + eps;
end
%Compute broadside RCS
index = index +1;
rcs_normal = factor * sin(alpha) / ((cos(alpha))^4) + eps;
rcs(index) = rcs_normal;
% Compute RCS from broad side to 180 degrees
for theta = normal_incidence+.5:.1:180
    index = index + 1;
    theta = theta * pi / 180. ;
    rcs(index) = (lambda * z2 * tan(alpha) *(tan(theta - alpha))^2) / ...
        (8. * pi *sin(theta)) + eps;
end
else
% Compute normal incidence, small end
normal_incidence = (180./pi) * ((pi /2) - alpha)
% Compute RCS from zero aspect to normal incidence (large end)
for theta = 0.001:.1:normal_incidence-.5
    index = index +1;
    theta = theta * pi /180.;
    rcs(index) = (lambda * z1 * tan(alpha) *(tan(theta + alpha))^2) / ...
        (8. * pi *sin(theta)) + eps;
end
%Compute broadside RCS
index = index +1;
rcs_normal = factor * sin(alpha) / ((cos(alpha))^4) + eps;
rcs(index) = rcs_normal;
% Compute RCS from broad side to 180 degrees (small end of frustum)
for theta = normal_incidence+.5:.1:180
    index = index + 1;
    theta = theta * pi / 180. ;
    rcs(index) = (lambda * z2 * tan(alpha) *(tan(theta + alpha))^2) / ...
        (8. * pi *sin(theta)) + eps;
end
end
% Plot RCS versus aspect angle
delta = 180 /index;
angle = 0.001:delta:180;
plot (angle,10*log10(rcs),'k');
grid;
xlabel ('Aspect angle - degrees');
ylabel ('RCS - dBsm');

```

```
%title ('Wavelength = .861 cm');
```

Listing 2.7. MATLAB Function “rcs_cylinder.m”

```
function [rcs] = rcs_cylinder (r, h, freq)
% This program computes RCS for a cylinder. Circular symmetry is assumed.
% Plot of RCS versus aspect angle is produced
index = 0;
eps =0.00001;
% Compute wavelength
lambda = 3.0e+8 / freq;
% Compute RCS from zero aspect to broadside
for theta = 0.0:1:90-.5
    index = index +1;
    theta = theta * pi /180.;
    rcs(index) = (lambda * r * sin(theta) / ...
        (8. * pi * (cos(theta))^2)) + eps;
end
% Compute RCS for broadside specular
theta = pi/2;
index = index +1;
rcs(index) = (2. * pi * h^2 * r / lambda )+ eps;
% Compute RCS from 90 to 180 degrees
for theta = 90+.5:1:180.
    index = index + 1;
    theta = theta * pi / 180.;
    rcs(index) = ( lambda * r * sin(theta) / ...
        (8. * pi * (cos(theta))^2)) + eps;
end
% Plot results
delta= 180/(index-1)
angle = 0:delta:180;
plot(angle,10*log10(rcs),'k');
grid;
xlabel ('Aspect angle - degrees');
ylabel ('RCS - dBsm');
%title ('Frequency = 9.5 GHz');
```

Listing 2.8. MATLAB Function “rcs_rect_plate.m”

```
function [rcs] = rcs_rect_plate (a, b, freq)
% This function computes the backscattered RCS for a rectangular flat plate.
% The RCS is computed for vertical and horizontal polarization based on
% Eq.s(2.50)through (2.60). Also Physical Optics approximation Eq.(2.62)
% is computed.
eps = 0.000001;
lambda = 3.0e+8 / freq;
ka = 2. * pi * a / lambda;
```

```

% Compute aspect angle vector
theta_deg = 0.05:0.1:85;
theta = (pi/180.) .* theta_deg;
sigma1v = cos(ka .* sin(theta)) - i .* sin(ka .* sin(theta)) ./ sin(theta);
sigma2v = exp(i * ka - (pi / 4)) / (sqrt(2 * pi) *(ka)^1.5);
sigma3v = (1. + sin(theta)) .* exp(-i * ka .* sin(theta)) ./ ...
    (1. - sin(theta)).^2;
sigma4v = (1. - sin(theta)) .* exp(i * ka .* sin(theta)) ./ ...
    (1. + sin(theta)).^2;
sigma5v = 1. - (exp(i * 2. * ka - (pi / 2)) / (8. * pi * (ka)^3));
sigma1h = cos(ka .* sin(theta)) + i .* sin(ka .* sin(theta)) ./ sin(theta);
sigma2h = 4. * exp(i * ka * (pi / 4.)) / (sqrt(2 * pi * ka));
sigma3h = exp(-i * ka .* sin(theta)) ./ (1. - sin(theta));
sigma4h = exp(i * ka * sin(theta)) ./ (1. + sin(theta));
sigma5h = 1. - (exp(j * 2. * ka + (pi / 4.)) / 2. * pi * ka);
% Compute vertical polarization RCS
rcs_v = (b^2 / pi) .* (abs(sigma1v - sigma2v .*((1. / cos(theta)) ...
    + .25 * sigma2v .* (sigma3v + sigma4v)) .* (sigma5v).^-1)).^2 + eps;
% compute horizontal polarization RCS
rcs_h = (b^2 / pi) .* (abs(sigma1h - sigma2h .*((1. / cos(theta)) ...
    - .25 * sigma2h .* (sigma3h + sigma4h)) .* (sigma5h).^-1)).^2 + eps;
% Compute RCS from Physical Optics, Eq.(2.62)
angle = ka .* sin(theta);
rcs_po = (4. * pi* a^2 * b^2 / lambda^2) .* (cos(theta)).^2 .* ...
    ((sin(angle) ./ angle).^2) + eps;
rcsdb_v = 10. .*log10(rcs_v);
rcsdb_h = 10. .*log10(rcs_h);
rcsdb_po = 10. .*log10(rcs_po);
subplot(1,2,1)
plot(theta_deg, rcsdb_v,'k',theta_deg,rcsdb_po,'k --');
set(gca,'xtick',[10:10:85]);
title('Vertical polarization');
ylabel('RCS -dBsm');
xlabel('aspect angle - deg');
legend('Solid Eq.(2.51)', 'Dashed Eq.(2.62)');
subplot(1,2,2)
plot(theta_deg, rcsdb_h,'k',theta_deg,rcsdb_po,'k --');
set(gca,'xtick',[10:10:85]);
title('Horizontal polarization');
ylabel('RCS -dBsm');
xlabel('aspect angle - deg');
xlabel('aspect angle - deg');
legend('Solid eq.(2.50)', 'Dashed eq.(2.62)');

```

Listing 2.9. MATLAB Function “rcs_isosceles.m”

```

function [rcs] = rcs_isosceles (a, b, freq, phi)
% This program calculates the backscattered RCS for a perfectly

```

```

% conducting triangular flat plate, using Eq.s (2.63) through (2.65)
% The default case is to assume phi = pi/2. These equations are
% valid for aspect angles less than 30 degrees
% compute area of plate
A = a * b / 2.;
lambda = 3.e+8 / 9.5e+8;
phi = pi / 2.;
ka = 2. * pi / lambda;
kb = 2. * pi / lambda;
% Compute theta vector
theta_deg = 0.01:.05:89;
theta = (pi / 180.) .* theta_deg;
alpha = ka * cos(phi) .* sin(theta);
beta = kb * sin(phi) .* sin(theta);
if (phi == pi / 2)
    rcs = (4. * pi * A^2 / lambda^2) .* cos(theta).^2 .* (sin(beta ./ 2)).^4 ...
        ./ (beta./2).^4 + eps;
end
if (phi == 0)
    rcs = (4. * pi * A^2 / lambda^2) .* cos(theta).^2 .* ...
        ((sin(alpha).^4 ./ alpha.^4) + (sin(2 .* alpha) - 2.*alpha).^2 ...
        ./ (4 .* alpha.^4)) + eps;
end
if (phi ~= 0 & phi ~= pi/2)
    sigmao1 = 0.25 * sin(phi)^2 .* ((2. * a / b) * cos(phi) .* ...
        sin(beta) - sin(phi) .* sin(2. .* alpha)).^2;
    fact1 = (alpha).^2 - (.5 .* beta).^2;
    fact2 = (sin(alpha).^2 - sin(.5 .* beta).^2).^2;
    sigmao = (fact2 + sigmao1) ./ fact1;
    rcs = (4. * pi * A^2 / lambda^2) .* cos(theta).^2 .* sigmao + eps;
end
rcsdb = 10. * log10(rcs);
plot(theta_deg,rcsdb,'k')
xlabel ('Aspect angle - degrees');
ylabel ('RCS - dBsm')
%title ('freq = 9.5GHz, phi = pi/2');
grid;

```

Listing 2.10. MATLAB Program “rcs_cylinder_complex.m”

% This program computes the backscattered RCS for a cylinder
% with flat plates.

```

clear all
index = 0;
eps = 0.00001;
a1 = 125;
h = 1.;

```

```

lambda = 3.0e+8 / 9.5e+9;
lambda = 0.00861;
index = 0;
for theta = 0.0:1:90-.1
    index = index + 1;
    theta = theta * pi / 180.;
    rcs(index) = (lambda * a1 * sin(theta) / ...
        (8 * pi * (cos(theta))^2)) + eps;
end
theta*180/pi;
theta = pi/2;
index = index + 1;
rcs(index) = (2 * pi * h^2 * a1 / lambda) + eps;
for theta = 90+.1:1:180.
    index = index + 1;
    theta = theta * pi / 180.;
    rcs(index) = ( lambda * a1 * sin(theta) / ...
        (8 * pi * (cos(theta))^2)) + eps;
end
r = a1;
index = 0;
for aspect_deg = 0.:1:180
    index = index + 1;
    aspect = (pi / 180.) * aspect_deg;
% Compute RCS using Eq. (2.37)
if (aspect == 0 | aspect == pi)
    rcs_po(index) = (4.0 * pi^3 * r^4 / lambda^2) + eps;
    rcs_mu(index) = rcs_po(1);
else
    x = (4. * pi * r / lambda) * sin(aspect);
    val1 = 4. * pi^3 * r^4 / lambda^2;
    val2 = 2. * besselj(1,x) / x;
    rcs_po(index) = val1 * (val2 * cos(aspect))^2 + eps;
end
end
rcs_t=(rcs_po + rcs);
angle = 0:1:180;
plot(angle,10*log10(rcs_t(1:1801)), 'k');
grid;
xlabel ('Aspect angle -degrees');
ylabel ('RCS -dBsm');

```

Listing 2.11. MATLAB Program “Swerling_models.m”

```

% This program computes and plots Swerling statistical models
% sigma_bar = 1.5;
clear all

```

```

sigma = 0:0.001:6;
sigma_bar = 1.5;
swer_3_4 = (4. / sigma_bar^2) .* sigma .* ...
    exp(-2. * (sigma ./ sigma_bar));
%t.*exp(-(t.^2)/2.
swer_1_2 = (1. / sigma_bar) .* exp(-sigma ./ sigma_bar);
plot(sigma,swer_1_2,'k',sigma,swer_3_4,'k');
grid;
gtext ('Swerling I,II');
gtext ('Swerling III,IV');
xlabel ('sigma');
ylabel ('Probability density');
title ('sigma-bar = 1.5');

```

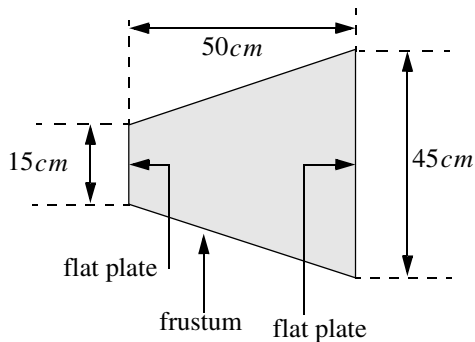
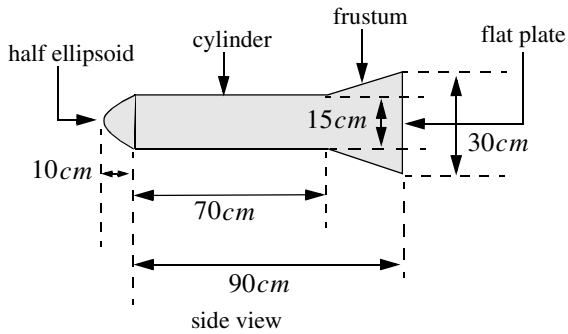
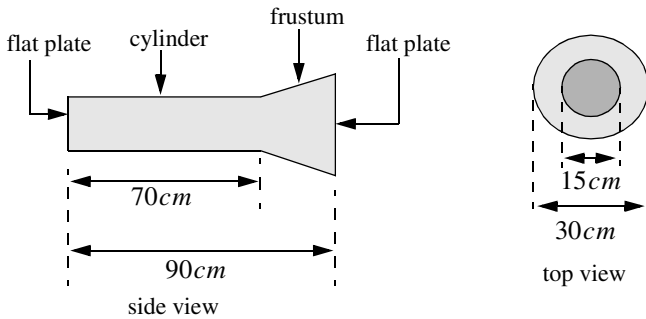
Problems

2.1. Design a cylindrical RCS calibration target such that its broadside RCS (cylinder) and end (flat plate) RCS are equal to $10m^2$ at $f = 9.5GHz$. The RCS for a flat plate of area A is $\sigma_{fp} = 4\pi f^2 A^2 / c^2$.

2.2. The following table is constructed from a radar cross-section measurement experiment. Calculate the mean and standard deviation of the radar cross section.

Number of samples	RCS, m²
2	55
6	67
12	73
16	90
20	98
24	110
26	117
19	126
13	133
8	139
5	144
3	150

2.3. Develop a MATLAB simulation to compute and plot the backscattered RCS for the following objects. Utilize the simple shape MATLAB functions developed in this chapter. Assume that the radar is located on the left side of the page and that its line of sight is aligned with the target body axis. Assume an X-band radar.

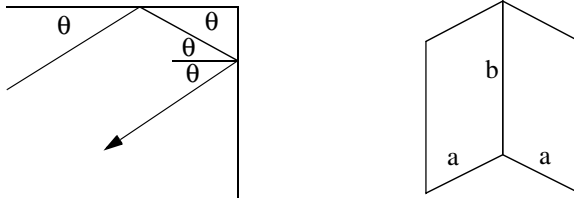


2.4. The backscattered RCS for a corner reflector is given by

$$\sigma = \left[\sqrt{\frac{16\pi a^4}{\lambda^2} (\sin \theta)^2} + \sqrt{\frac{4\pi a^4}{\lambda^2} \left(\frac{\sin\left(\frac{2\pi a}{\lambda} \sin \theta\right)}{\frac{2\pi a}{\lambda} \sin \theta} \right)^2} \right]^2 \quad 0^\circ \leq \theta \leq 45^\circ$$

This RCS is symmetric about the angle $\theta = 45^\circ$. Develop a MATLAB program to compute and plot the RCS for a corner reflector. The RCS at the $\theta = 45^\circ$ is

$$\sigma = \frac{8\pi a^2 b^2}{\lambda^2}$$



corner reflector

Continuous Wave (CW) radars utilize CW waveforms, which may be considered to be a pure sinewave of the form $\cos 2\pi f_0 t$. Spectra of the radar echo from stationary targets and clutter will be concentrated at f_0 . The center frequency for the echoes from moving targets will be shifted by f_d , the Doppler frequency. Thus by measuring this frequency difference CW radars can very accurately extract target radial velocity. Because of the continuous nature of CW emission, range measurement is not possible without some modifications to the radar operations and waveforms, which will be discussed later.

3.1. Functional Block Diagram

In order to avoid interruption of the continuous radar energy emission, two antennas are used in CW radars, one for transmission and one for reception. Fig. 3.1 shows a simplified CW radar block diagram. The appropriate values of the signal frequency at different locations are noted on the diagram. The individual Narrow Band Filters (NBF) must be as narrow as possible in bandwidth in order to allow accurate Doppler measurements and minimize the amount of noise power.

In theory, the operating bandwidth of a CW radar is infinitesimal (since it corresponds to an infinite duration continuous sinewave). However, systems with infinitesimal bandwidths cannot physically exist, and thus the bandwidth of CW radars is assumed to correspond to that of a gated CW waveform (see Chapter 5).

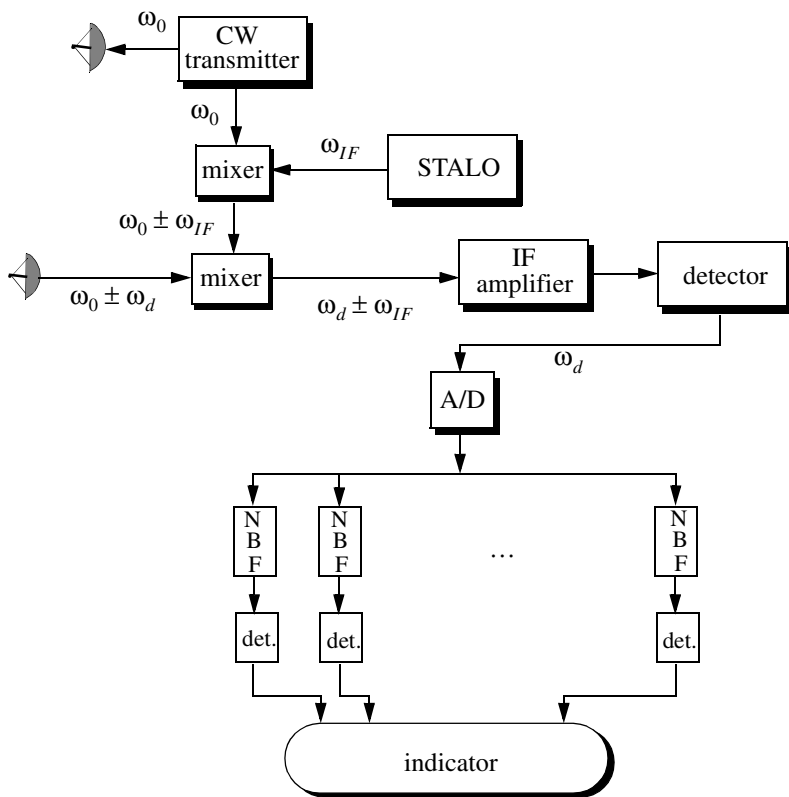


Figure 3.1. CW radar block diagram.

The NBF bank (Doppler filter bank) can be implemented using a Fast Fourier Transform (FFT). If the Doppler filter bank is implemented using an FFT of size N_{FFT} , and if the individual NBF bandwidth (FFT bin) is Δf , then the effective radar Doppler bandwidth is $N_{FFT}\Delta f/2$. The reason for the one-half factor is to account for both negative and positive Doppler shifts.

Since range is computed from the radar echoes by measuring a two-way time delay, then single frequency CW radars cannot measure target range. In order for CW radars to be able to measure target range, the transmit and receive waveforms must have some sort of timing marks. By comparing the timing marks at transmit and receive, CW radars can extract target range.

The timing mark can be implemented by modulating the transmit waveform, and one commonly used technique is Linear Frequency Modulation (LFM). Before we discuss LFM signals, we will first introduce the CW radar equation and briefly address the general Frequency Modulated (FM) waveforms using sinusoidal modulating signals.

3.2. CW Radar Equation

As indicated by Fig. 3.1, the CW radar receiver declares detection at the output of a particular Doppler bin if that output value passes the detection threshold within the detector box. Since the NBF bank is implemented by an FFT, only finite length data sets can be processed at a time. The length of such blocks is normally referred to as the dwell time or dwell interval. The dwell interval determines the frequency resolution or the bandwidth of the individual NBFs. More precisely,

$$\Delta f = 1/T_{Dwell} \quad (3.1)$$

T_{Dwell} is the dwell interval. Therefore, once the maximum resolvable frequency by the NBF bank is chosen the size of the NBF bank is computed as

$$N_{FFT} = 2B/\Delta f \quad (3.2)$$

B is the maximum resolvable frequency by the FFT. The factor 2 is needed to account for both positive and negative Doppler shifts. It follows that

$$T_{Dwell} = N_{FFT}/2B \quad (3.3)$$

The CW radar equation can now be derived from the high PRF radar equation given in Eq. (1.69) and repeated here as Eq. (3.4)

$$SNR = \frac{P_{av} T_i G^2 \lambda^2 \sigma}{(4\pi)^3 R^4 k T_e FL} \quad (3.4)$$

In the case of CW radars, P_{av} is replaced by the CW average transmitted power over the dwell interval P_{CW} , and T_i must be replaced by T_{Dwell} . Thus, the CW radar equation can be written as

$$SNR = \frac{P_{CW} T_{Dwell} G_t G_r \lambda^2 \sigma}{(4\pi)^3 R^4 k T_e F L L_{win}} \quad (3.5)$$

where G_t and G_r are the transmit and receive antenna gains, respectively. The factor L_{win} is a loss term associated with the type of window (weighting) used in computing the FFT. Other terms in Eq. (3.5) have been defined earlier.

3.3. Frequency Modulation

The discussion presented in this section will be restricted to sinusoidal modulating signals. In this case, the general formula for an FM waveform can be expressed by

$$s(t) = A \cos \left(2\pi f_0 t + k_f \int_0^t \cos 2\pi f_m u du \right) \quad (3.6)$$

f_0 is the radar operating frequency (carrier frequency), $\cos 2\pi f_m t$ is the modulating signal, A is a constant, and $k_f = 2\pi \Delta f_{peak}$, where Δf_{peak} is the peak frequency deviation. The phase is given by

$$\psi(t) = 2\pi f_0 t + 2\pi \Delta f_{peak} \int_0^t \cos 2\pi f_m u du = 2\pi f_0 t + \beta \sin 2\pi f_m t \quad (3.7)$$

where β is the FM modulation index given by

$$\beta = \frac{\Delta f_{peak}}{f_m} \quad (3.8)$$

Let $s_r(t)$ be the received radar signal from a target at range R . It follows that

$$s_r(t) = A_r \cos(2\pi f_0(t - \Delta t) + \beta \sin 2\pi f_m(t - \Delta t)) \quad (3.9)$$

where the delay Δt is

$$\Delta t = \frac{2R}{c} \quad (3.10)$$

c is the speed of light. CW radar receivers utilize phase detectors in order to extract target range from the instantaneous frequency, as illustrated in Fig. 3.2. A good measurement of the phase detector output $o(t)$ implies a good measurement of Δt , and hence range.

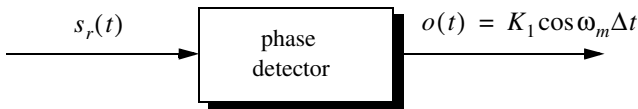


Figure 3.2. Extracting range from an FM signal return.
 K_1 is a constant.

Consider the FM waveform $s(t)$ given by

$$s(t) = A \cos(2\pi f_0 t + \beta \sin 2\pi f_m t) \quad (3.11)$$

which can be written as

$$s(t) = A \operatorname{Re}\{e^{j2\pi f_0 t} e^{j\beta \sin 2\pi f_m t}\} \quad (3.12)$$

where $\operatorname{Re}\{\cdot\}$ denotes the real part. Since the signal $\exp(j\beta \sin 2\pi f_m t)$ is periodic with period $T = 1/f_m$, it can be expressed using the complex exponential Fourier series as

$$e^{j\beta \sin 2\pi f_m t} = \sum_{n=-\infty}^{\infty} C_n e^{jn2\pi f_m t} \quad (3.13)$$

where the Fourier series coefficients C_n are given by

$$C_n = \frac{1}{2\pi} \int_{-\pi}^{\pi} e^{j\beta \sin 2\pi f_m t} e^{-jn2\pi f_m t} dt \quad (3.14)$$

Make the change of variable $u = 2\pi f_m t$, and recognize that the Bessel function of the first kind of order n is

$$J_n(\beta) = \frac{1}{2\pi} \int_{-\pi}^{\pi} e^{j(\beta \sin u - nu)} du \quad (3.15)$$

Thus, the Fourier series coefficients are $C_n = J_n(\beta)$, and consequently Eq. (3.13) can now be written as

$$e^{j\beta \sin 2\pi f_m t} = \sum_{n=-\infty}^{\infty} J_n(\beta) e^{jn2\pi f_m t} \quad (3.16)$$

which is known as the Bessel-Jacobi equation. Fig. 3.3 shows a plot of Bessel functions of the first kind for $n = 0, 1, 2, 3$.

The total power in the signal $s(t)$ is

$$P = \frac{1}{2} A^2 \sum_{n=-\infty}^{\infty} |J_n(\beta)|^2 = \frac{1}{2} A^2 \quad (3.17)$$

Substituting Eq. (3.16) into Eq. (3.12) yields

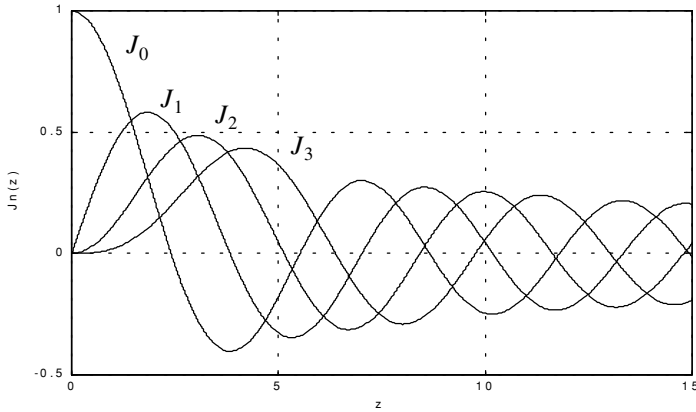


Figure 3.3. Plot of Bessel functions of order 0, 1, 2, and 3.

$$s(t) = ARe \left\{ e^{j2\pi f_0 t} \sum_{n=-\infty}^{\infty} J_n(\beta) e^{jn2\pi f_m t} \right\} \quad (3.18)$$

Expanding Eq. (3.18) yields

$$s(t) = A \sum_{n=-\infty}^{\infty} J_n(\beta) \cos(2\pi f_0 + n2\pi f_m)t \quad (3.19)$$

Finally, since $J_n(\beta) = J_{-n}(\beta)$ for n odd and $J_n(\beta) = -J_{-n}(\beta)$ for n even we can rewrite Eq. (3.19) as

$$\begin{aligned} s(t) = A \{ & J_0(\beta) \cos 2\pi f_0 t + \\ & J_1(\beta) [\cos(2\pi f_0 + 2\pi f_m)t - \cos(2\pi f_0 - 2\pi f_m)t] \\ & + J_2(\beta) [\cos(2\pi f_0 + 4\pi f_m)t + \cos(2\pi f_0 - 4\pi f_m)t] \\ & + J_3(\beta) [\cos(2\pi f_0 + 6\pi f_m)t - \cos(2\pi f_0 - 6\pi f_m)t] \\ & + J_4(\beta) [\cos((2\pi f_0 + 8\pi f_m)t + \cos(2\pi f_0 - 8\pi f_m)t)] + \dots \} \end{aligned} \quad (3.20)$$

The spectrum of $s(t)$ is composed of pairs of spectral lines centered at f_0 , as sketched in Fig. 3.4. The spacing between adjacent spectral lines is f_m . The central spectral line has an amplitude equal to $AJ_0(\beta)$, while the amplitude of the n th spectral line is $AJ_n(\beta)$.

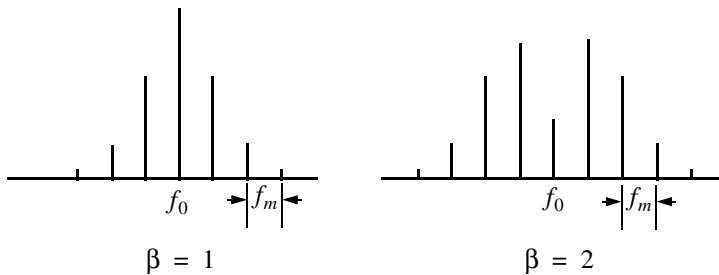


Figure 3.4. Amplitude line spectra sketch for FM signal.

As indicated by Eq. (3.20) the bandwidth of FM signals is infinite. However, the magnitudes of spectral lines of the higher orders are small, and thus the bandwidth can be approximated using Carson's rule,

$$B \approx 2(\beta + 1)f_m \quad (3.21)$$

When β is small, only $J_0(\beta)$ and $J_1(\beta)$ have significant values. Thus, we may approximate Eq. (3.20) by

$$s(t) \approx A \{ J_0(\beta) \cos 2\pi f_0 t + J_1(\beta) [\cos(2\pi f_0 + 2\pi f_m)t - \cos(2\pi f_0 - 2\pi f_m)t] \} \quad (3.22)$$

Finally, for small β , the Bessel functions can be approximated by

$$J_0(\beta) \approx 1 \quad (3.23)$$

$$J_1(\beta) \approx \frac{1}{2}\beta \quad (3.24)$$

Thus, Eq. (3.22) may be approximated by

$$s(t) \approx A \left\{ \cos 2\pi f_0 t + \frac{1}{2}\beta [\cos(2\pi f_0 + 2\pi f_m)t - \cos(2\pi f_0 - 2\pi f_m)t] \right\} \quad (3.25)$$

Example 3.1: If the modulation index is $\beta = 0.5$, give an expression for the signal $s(t)$.

Solution: From Bessel function tables we get $J_0(0.5) = 0.9385$ and $J_1(0.5) = 0.2423$; then using Eq. (3.17) we get

$$s(t) \approx A \{ (0.9385) \cos 2\pi f_0 t + (0.2423) [\cos(2\pi f_0 + 2\pi f_m)t - \cos(2\pi f_0 - 2\pi f_m)t] \}$$

Example 3.2: Consider an FM transmitter with output signal $s(t) = 100 \cos(2000\pi t + \varphi(t))$. The frequency deviation is 4Hz, and the modulating waveform is $x(t) = 10 \cos 16\pi t$. Determine the FM signal bandwidth. How many spectral lines will pass through a band pass filter whose bandwidth is 58Hz centered at 1000Hz?

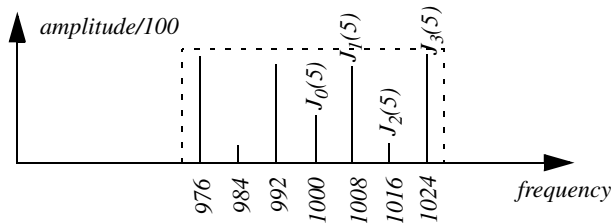
Solution: The peak frequency deviation is $\Delta f_{peak} = 4 \times 10 = 40\text{Hz}$. It follows that

$$\beta = \frac{\Delta f_{peak}}{f_m} = \frac{40}{8} = 5$$

Using Eq. (3.16) we get

$$B \approx 2(\beta + 1)f_m = 2 \times (5 + 1) \times 8 = 96\text{Hz}$$

However, only seven spectral lines pass through the band pass filter as illustrated in the figure shown below.



3.4. Linear FM (LFM) CW Radar

CW radars may use LFM waveforms so that both range and Doppler information can be measured. In practical CW radars, the LFM waveform cannot be continually changed in one direction, and thus periodicity in the modulation is normally utilized. Fig. 3.5 shows a sketch of a triangular LFM waveform. The modulation does not need to be triangular; it may be sinusoidal, saw-tooth, or some other form. The dashed line in Fig 3.5 represents the return waveform from a stationary target at range R . The beat frequency f_b is also sketched in Fig. 3.5. It is defined as the difference (due to heterodyning) between the transmitted and received signals. The time delay Δt is a measure of target range, as defined in Eq. (3.10).

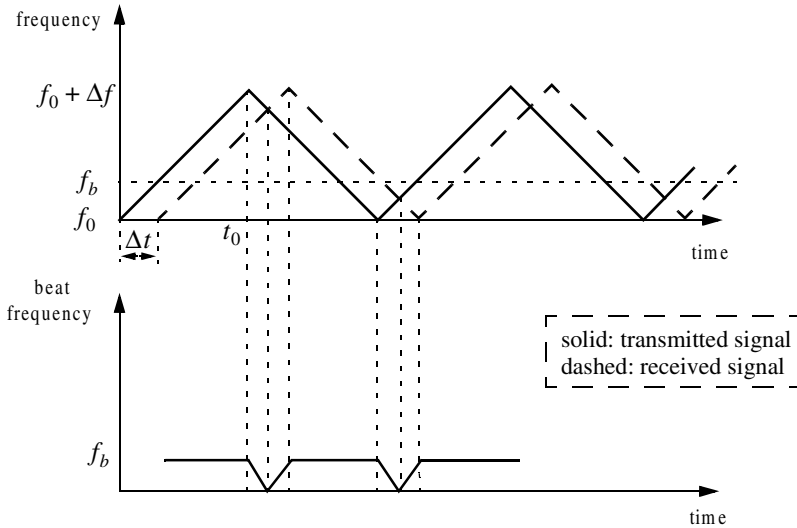


Figure 3.5. Transmitted and received triangular LFM signals and beat frequency for stationary target.

In practice, the modulating frequency f_m is selected such that

$$f_m = \frac{1}{2t_0} \quad (3.26)$$

The rate of frequency change, \dot{f} , is

$$\dot{f} = \frac{\Delta f}{t_0} = \frac{\Delta f}{(1/2f_m)} = 2f_m \Delta f \quad (3.27)$$

where Δf is the peak frequency deviation. The beat frequency f_b is given by

$$f_b = \Delta t \dot{f} = \frac{2R}{c} \dot{f} \quad (3.28)$$

Eq. (3.28) can be rewritten as

$$\dot{f} = \frac{c}{2R} f_b \quad (3.29)$$

Equating Eqs. (3.27) and (3.29) and solving for f_b yield

$$f_b = \frac{4Rf_m \Delta f}{c} \quad (3.30)$$

Now consider the case when Doppler is present (i.e., non-stationary target). The corresponding triangular LFM transmitted and received waveforms are

sketched in Fig. 3.6, along with the corresponding beat frequency. As before the beat frequency is defined as

$$f_b = f_{received} - f_{transmitted} \quad (3.31)$$

When the target is not stationary the received signal will contain a Doppler shift term in addition to the frequency shift due to the time delay Δt . In this case, the Doppler shift term subtracts from the beat frequency during the positive portion of the slope. Alternatively, the two terms add up during the negative portion of the slope. Denote the beat frequency during the positive (up) and negative (down) portions of the slope, respectively, as f_{bu} and f_{bd} .

It follows that

$$f_{bu} = \frac{2R}{c}\dot{f} - \frac{2\dot{R}}{\lambda} \quad (3.32)$$

where \dot{R} is the range rate or the target radial velocity as seen by the radar. The first term of the right-hand side of Eq. (3.32) is due to the range delay defined by Eq. (3.28), while the second term is due to the target Doppler. Similarly,

$$f_{bd} = \frac{2R}{c}\dot{f} + \frac{2\dot{R}}{\lambda} \quad (3.33)$$

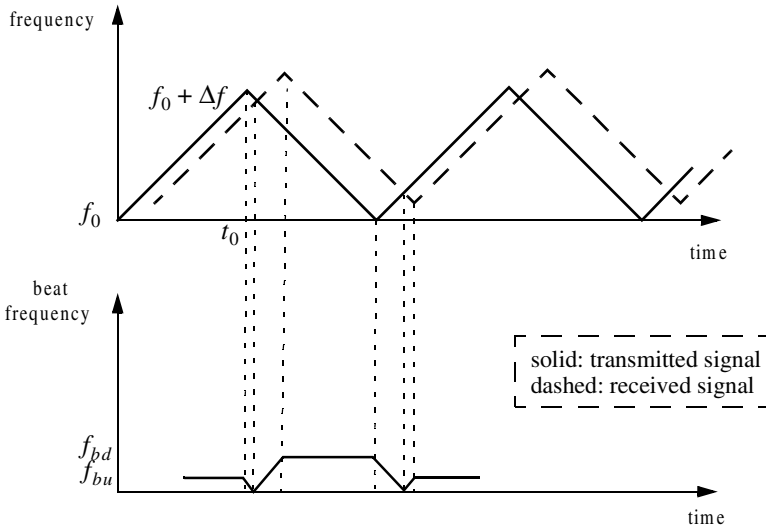


Figure 3.6. Transmitted and received LFM signals and beat frequency, for a moving target.

Range is computed by adding Eq. (3.32) and Eq. (3.33). More precisely,

$$R = \frac{c}{4f_i}(f_{bu} + f_{bd}) \quad (3.34)$$

The range rate is computed by subtracting Eq. (3.33) from Eq. (3.32),

$$\dot{R} = \frac{\lambda}{4}(f_{bd} - f_{bu}) \quad (3.35)$$

As indicated by Eq. (3.34) and Eq. (3.35), CW radars utilizing triangular LFM can extract both range and range rate information. In practice, the maximum time delay Δt_{max} is normally selected as

$$\Delta t_{max} = 0.1t_0 \quad (3.36)$$

Thus, the maximum range is given by

$$R_{max} = \frac{0.1ct_0}{2} = \frac{0.1c}{4f_m} \quad (3.37)$$

and the maximum unambiguous range will correspond to a shift equal to $2t_0$.

3.5. Multiple Frequency CW Radar

CW radars do not have to use LFM waveforms in order to obtain good range measurements. Multiple frequency schemes allow CW radars to compute very adequate range measurements, without using frequency modulation. In order to illustrate this concept, first consider a CW radar with the following waveform:

$$s(t) = A \sin 2\pi f_0 t \quad (3.38)$$

The received signal from a target at range R is

$$s_r(t) = A_r \sin(2\pi f_0 t - \varphi) \quad (3.39)$$

where the phase φ is equal to

$$\varphi = 2\pi f_0 \frac{2R}{c} \quad (3.40)$$

Solving for R we obtain

$$R = \frac{c\varphi}{4\pi f_0} = \frac{\lambda}{4\pi} \varphi \quad (3.41)$$

Clearly, the maximum unambiguous range occurs when φ is maximum, i.e., $\varphi = 2\pi$. Therefore, even for relatively large radar wavelengths, R is limited to impractical small values.

Next, consider a radar with two CW signals, denoted by $s_1(t)$ and $s_2(t)$. More precisely,

$$s_1(t) = A_1 \sin 2\pi f_1 t \quad (3.42)$$

$$s_2(t) = A_2 \sin 2\pi f_2 t \quad (3.43)$$

The received signals from a moving target are

$$s_{1r}(t) = A_{r1} \sin(2\pi f_1 t - \varphi_1) \quad (3.44)$$

and

$$s_{2r}(t) = A_{r2} \sin(2\pi f_2 t - \varphi_2) \quad (3.45)$$

where $\varphi_1 = (4\pi f_1 R)/c$ and $\varphi_2 = (4\pi f_2 R)/c$. After heterodyning (mixing) with the carrier frequency, the phase difference between the two received signals is

$$\varphi_2 - \varphi_1 = \Delta\varphi = \frac{4\pi R}{c}(f_2 - f_1) = \frac{4\pi R}{c}\Delta f \quad (3.46)$$

Again R is maximum when $\Delta\varphi = 2\pi$; it follows that the maximum unambiguous range is now

$$R = \frac{c}{2\Delta f} \quad (3.47)$$

and since $\Delta f \ll c$, the range computed by Eq. (3.47) is much greater than that computed by Eq. (3.41).

3.6. Pulsed Radar

Pulsed radars transmit and receive a train of modulated pulses. Range is extracted from the two-way time delay between a transmitted and received pulse. Doppler measurements can be made in two ways. If accurate range measurements are available between consecutive pulses, then Doppler frequency can be extracted from the range rate $\dot{R} = \Delta R/\Delta t$. This approach works fine as long as the range is not changing drastically over the interval Δt . Otherwise, pulsed radars utilize a Doppler filter bank.

Pulsed radar waveforms can be completely defined by the following: (1) carrier frequency which may vary depending on the design requirements and

radar mission; (2) pulse width, which is closely related to the bandwidth and defines the range resolution; (3) modulation; and finally (4) the pulse repetition frequency. Different modulation techniques are usually utilized to enhance the radar performance, or to add more capabilities to the radar that otherwise would not have been possible. The PRF must be chosen to avoid Doppler and range ambiguities as well as maximize the average transmitted power.

Radar systems employ low, medium, and high PRF schemes. Low PRF waveforms can provide accurate, long, unambiguous range measurements, but exert severe Doppler ambiguities. Medium PRF waveforms must resolve both range and Doppler ambiguities; however, they provide adequate average transmitted power as compared to low PRFs. High PRF waveforms can provide superior average transmitted power and excellent clutter rejection capabilities. Alternatively, high PRF waveforms are extremely ambiguous in range. Radar systems utilizing high PRFs are often called Pulsed Doppler Radars (PDR). Range and Doppler ambiguities for different PRFs are summarized in [Table 3.1](#).

Distinction of a certain PRF as low, medium, or high PRF is almost arbitrary and depends on the radar mode of operations. For example, a 3KHz PRF is considered low if the maximum detection range is less than 30Km . However, the same PRF would be considered medium if the maximum detection range is well beyond 30Km .

Radars can utilize constant and varying (agile) PRFs. For example, Moving Target Indicator (MTI) radars use PRF agility to avoid blind speeds. This kind of agility is known as PRF staggering. PRF agility is also used to avoid range and Doppler ambiguities, as will be explained in the next three sections. Additionally, PRF agility is also used to prevent jammers from locking onto the radar's PRF. These two latter forms of PRF agility are sometimes referred to as PRF jitter.

TABLE 3.1. PRF ambiguities.

PRF	Range Ambiguous	Doppler Ambiguous
Low PRF	No	Yes
Medium PRF	Yes	Yes
High PRF	Yes	No

[Fig. 3.7](#) shows a simplified pulsed radar block diagram. The range gates can be implemented as filters that open and close at time intervals that correspond to the detection range. The width of such an interval corresponds to the desired range resolution. The radar receiver is often implemented as a series of contiguous (in time) range gates, where the width of each gate is matched to the radar pulse width. The NBF bank is normally implemented using an FFT, where

bandwidth of the individual filters corresponds to the FFT frequency resolution.

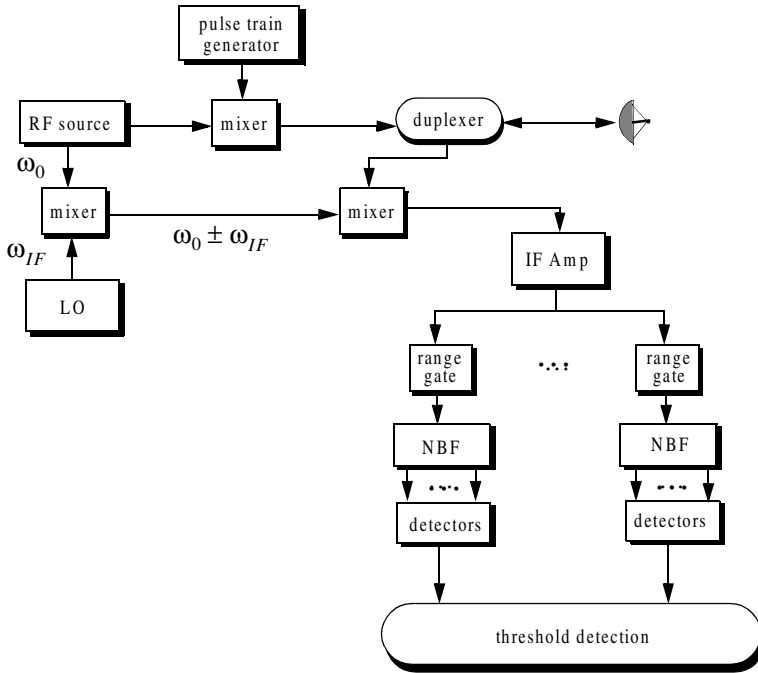


Figure 3.7. Pulsed radar block diagram.

3.7. Range and Doppler Ambiguities

As explained earlier, a pulsed radar can be range ambiguous if a second pulse is transmitted prior to the return of the first pulse. In general, the radar PRF is chosen such that the unambiguous range is large enough to meet the radar's operational requirements. Therefore, long-range search (surveillance) radars would require relatively low PRFs.

The line spectrum of a train of pulses has $\sin x/x$ envelope, and the line spectra are separated by the PRF, f_r , as illustrated in Fig. 3.8. The Doppler filter bank is capable of resolving target Doppler as long as the anticipated Doppler shift is less than one half the bandwidth of the individual filters (i.e., one half the width of an FFT bin). Thus, pulsed radars are designed such that

$$f_r = 2f_{dmax} = \frac{2v_{rmax}}{\lambda} \quad (3.48)$$

where f_{dmax} is the maximum anticipated target Doppler frequency, v_{rmax} is the maximum anticipated target radial velocity, and λ is the radar wavelength.

If the Doppler frequency of the target is high enough to make an adjacent spectral line move inside the Doppler band of interest, the radar can be Doppler ambiguous. Therefore, in order to avoid Doppler ambiguities, radar systems require high PRF rates when detecting high speed targets. When a long-range radar is required to detect a high speed target, it may not be possible to be both range and Doppler unambiguous. This problem can be resolved by using multiple PRFs. Multiple PRF schemes can be incorporated sequentially within each dwell interval (scan or integration frame) or the radar can use a single PRF in one scan and resolve ambiguity in the next. The latter technique, however, may have problems due to changing target dynamics from one scan to the next.

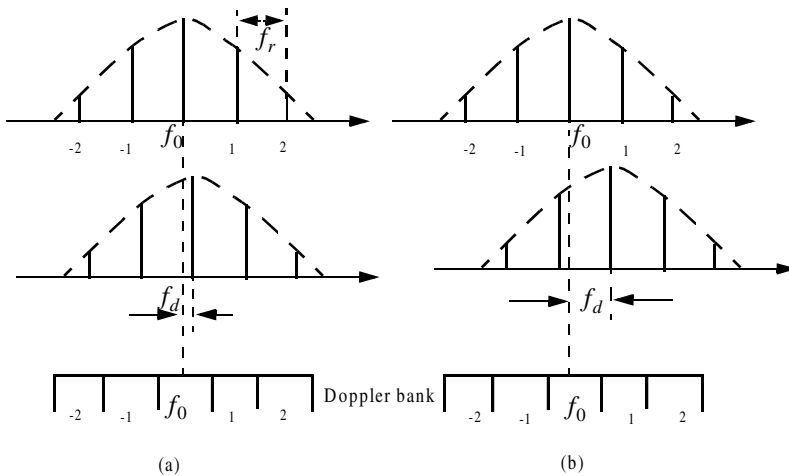


Figure 3.8. Spectra of transmitted and received waveforms, and Doppler bank. (a) Doppler is resolved. (b) Spectral lines have moved into the next Doppler filter. This results in an ambiguous Doppler measurement.

3.8. Resolving Range Ambiguity

Consider a radar that uses two PRFs, f_{r1} and f_{r2} , on transmit to resolve range ambiguity, as shown in Fig. 3.9. Denote R_{u1} and R_{u2} as the unambiguous ranges for the two PRFs, respectively. Normally, these unambiguous

ranges are relatively small and are short of the desired radar unambiguous range R_u (where $R_u \gg R_{u1}, R_{u2}$). Denote the radar desired PRF that corresponds to R_u as f_{rd} .

We choose f_{r1} and f_{r2} such that they are relatively prime with respect to one another. One choice is to select $f_{r1} = Nf_{rd}$ and $f_{r2} = (N + 1)f_{rd}$ for some integer N . Within one period of the desired PRI ($T_d = 1/f_{rd}$) the two PRFs f_{r1} and f_{r2} coincide only at one location, which is the true unambiguous target position. The time delay T_d establishes the desired unambiguous range. The time delays t_1 and t_2 correspond to the time between the transmit of a pulse on each PRF and receipt of a target return due to the same pulse.

Let M_1 be the number of PRF1 intervals between transmit of a pulse and receipt of the true target return. The quantity M_2 is similar to M_1 except it is for PRF2. It follows that, over the interval 0 to T_d , the only possible results are $M_1 = M_2 = M$ or $M_1 + 1 = M_2$. The radar needs only to measure t_1 and t_2 . First, consider the case when $t_1 < t_2$. In this case,

$$t_1 + \frac{M}{f_{r1}} = t_2 + \frac{M}{f_{r2}} \tag{3.49}$$

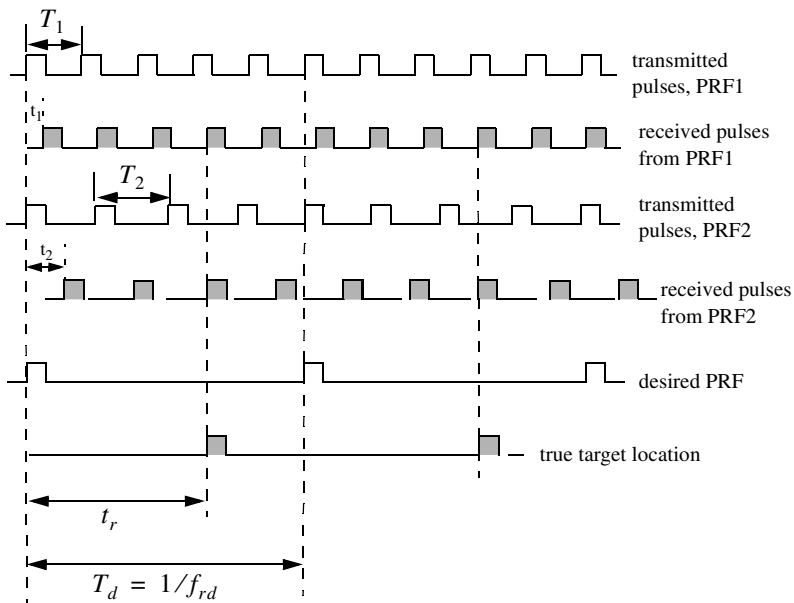


Figure 3.9. Resolving range ambiguity.

for which we get

$$M = \frac{t_2 - t_1}{T_1 - T_2} \quad (3.50)$$

where $T_1 = 1/f_{r1}$ and $T_2 = 1/f_{r2}$. It follows that the round trip time to the true target location is

$$\begin{aligned} t_r &= MT_1 + t_1 \\ t_r &= MT_2 + t_2 \end{aligned} \quad (3.51)$$

and the true target range is

$$R = ct_r/2 \quad (3.52)$$

Now if $t_1 > t_2$, then

$$t_1 + \frac{M}{f_{r1}} = t_2 + \frac{M+1}{f_{r2}} \quad (3.53)$$

Solving for M we get

$$M = \frac{(t_2 - t_1) + T_2}{T_1 - T_2} \quad (3.54)$$

and the round-trip time to the true target location is

$$t_{r1} = MT_1 + t_1 \quad (3.55)$$

and in this case, the true target range is

$$R = \frac{ct_{r1}}{2} \quad (3.56)$$

Finally, if $t_1 = t_2$, then the target is in the first ambiguity. It follows that

$$t_{r2} = t_1 = t_2 \quad (3.57)$$

and

$$R = ct_{r2}/2 \quad (3.58)$$

Since a pulse cannot be received while the following pulse is being transmitted, these times correspond to blind ranges. This problem can be resolved by using a third PRF. In this case, once an integer N is selected, then in order to guarantee that the three PRFs are relatively prime with respect to one another, we may choose $f_{r1} = N(N+1)f_{rd}$, $f_{r2} = N(N+2)f_{rd}$, and $f_{r3} = (N+1)(N+2)f_{rd}$.

3.9. Resolving Doppler Ambiguity

The Doppler ambiguity problem is analogous to that of range ambiguity. Therefore, the same methodology can be used to resolve Doppler ambiguity. In this case, we measure the Doppler frequencies f_{d1} and f_{d2} instead of t_1 and t_2 .

If $f_{d1} > f_{d2}$, then we have

$$M = \frac{(f_{d2} - f_{d1}) + f_{r2}}{f_{r1} - f_{r2}} \quad (3.59)$$

And if $f_{d1} < f_{d2}$,

$$M = \frac{f_{d2} - f_{d1}}{f_{r1} - f_{r2}} \quad (3.60)$$

and the true Doppler is

$$\begin{aligned} f_d &= Mf_{r1} + f_{d1} \\ f_d &= Mf_{r2} + f_{d2} \end{aligned} \quad (3.61)$$

Finally, if $f_{d1} = f_{d2}$, then

$$f_d = f_{d1} = f_{d2} \quad (3.62)$$

Again, blind Dopplers can occur, which can be resolved using a third PRF.

Example 3.3: A certain radar uses two PRFs to resolve range ambiguities. The desired unambiguous range is $R_u = 100\text{Km}$. Choose $N = 59$. Compute f_{r1} , f_{r2} , R_{u1} , and R_{u2} .

Solution: First let us compute the desired PRF, f_{rd}

$$f_{rd} = \frac{c}{2R_u} = \frac{3 \times 10^8}{200 \times 10^3} = 1.5\text{KHz}$$

It follows that

$$\begin{aligned} f_{r1} &= Nf_{rd} = (59)(1500) = 88.5\text{KHz} \\ f_{r2} &= (N + 1)f_{rd} = (59 + 1)(1500) = 90\text{KHz} \\ R_{u1} &= \frac{c}{2f_{r1}} = \frac{3 \times 10^8}{2 \times 88.5 \times 10^3} = 1.695\text{Km} \end{aligned}$$

$$R_{u2} = \frac{c}{2f_{r2}} = \frac{3 \times 10^8}{2 \times 90 \times 10^3} = 1.667 \text{ Km.}$$

Example 3.4: Consider a radar with three PRFs; $f_{r1} = 15\text{KHz}$, $f_{r2} = 18\text{KHz}$, and $f_{r3} = 21\text{KHz}$. Assume $f_0 = 9\text{GHz}$. Calculate the frequency position of each PRF for a target whose velocity is 550m/s . Calculate f_d (Doppler frequency) for another target appearing at 8KHz , 2KHz , and 17KHz for each PRF.

Solution: The Doppler frequency is

$$f_d = 2 \frac{vf_0}{c} = \frac{2 \times 550 \times 9 \times 10^9}{3 \times 10^8} = 33\text{KHz}$$

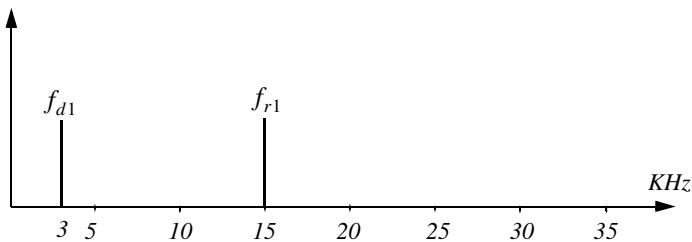
Then by using Eq. (3.61) $n_i f_{ri} + f_{di} = f_d$ where $i = 1, 2, 3$, we can write

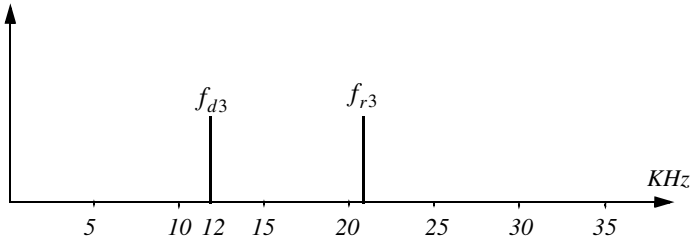
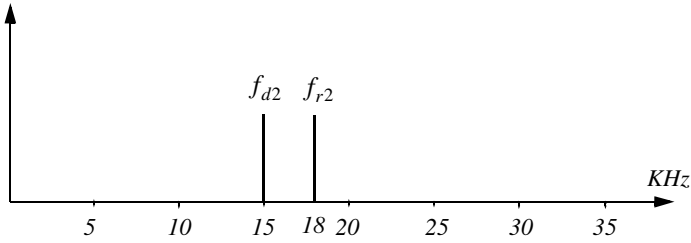
$$n_1 f_{r1} + f_{d1} = 15n_1 + f_{d1} = 33$$

$$n_2 f_{r2} + f_{d2} = 18n_2 + f_{d2} = 33$$

$$n_3 f_{r3} + f_{d3} = 21n_3 + f_{d3} = 33$$

We will show here how to compute n_1 , and leave the computations of n_2 and n_3 to the reader. First, if we choose $n_1 = 0$, that means $f_{d1} = 33\text{KHz}$, which cannot be true since f_{d1} cannot be greater than f_{r1} . Choosing $n_1 = 1$ is also invalid since $f_{d1} = 18\text{KHz}$ cannot be true either. Finally, if we choose $n_1 = 2$ we get $f_{d1} = 3\text{KHz}$, which is an acceptable value. It follows that the minimum n_1, n_2, n_3 that may satisfy the above three relations are $n_1 = 2$, $n_2 = 1$, and $n_3 = 1$. Thus, the apparent Doppler frequencies are $f_{d1} = 2\text{KHz}$, $f_{d2} = 15\text{KHz}$, and $f_{d3} = 12\text{KHz}$.





Now for the second part of the problem. Again by using Eq. (3.61) we have

$$n_1 f_{r1} + f_{d1} = f_d = 15n_1 + 8$$

$$n_2 f_{r2} + f_{d2} = f_d = 18n_2 + 2$$

$$n_3 f_{r3} + f_{d3} = f_d = 21n_3 + 17$$

We can now solve for the smallest integers n_1, n_2, n_3 that satisfy the above three relations. See the table below.

n	0	1	2	3	4
f_d from f_{r1}	8	23	<u>38</u>	53	68
f_d from f_{r2}	2	20	<u>38</u>	56	
f_d from f_{r3}	17	<u>38</u>	39		

Thus, $n_1 = 2 = n_2$, and $n_3 = 1$, and the true target Doppler is $f_d = 38\text{KHz}$. It follows that

$$v_r = 38000 \times \frac{0.0333}{2} = 632.7 \frac{m}{\text{sec}}$$

3.10. MATLAB Program “range_calc.m”

The program “range_calc.m” solves the radar range equation of the form

$$R = \left(\frac{P_t \tau f_r T_i G_t G_r \lambda^2 \sigma}{(4\pi)^3 k T_e FL (SNR)_o} \right)^{\frac{1}{4}} \quad (3.63)$$

where P_t is peak transmitted power, τ is pulse width, f_r is PRF, G_t is transmitting antenna gain, G_r receiving antenna gain, λ is wavelength, σ is target cross section, k is Boltzman’s constant, T_e effective noise temperature, F is system noise figure, L is total system losses, and $(SNR)_o$ is the minimum SNR required for detection. This equation applies for both CW and pulsed radars. In the case of CW radars, the terms $P_t \tau f_r$ must be replaced by the average CW power P_{CW} . Additionally, the term T_i refers to the dwell interval; alternatively, in the case of pulse radars T_i denotes the time on target. MATLAB-based GUI is utilized in inputting and editing all input parameters. The outputs include the maximum detection range versus minimum SNR plots. This program can be executed by typing “range_calc_driver” which is included in this book’s companion software. This software can be downloaded from CRC Press Web site “www.crcpress.com”. The related MATLAB GUI workspace associated with this program is illustrated in Fig. 3.10.

Problems

3.1. Prove that

$$\sum_{n=-\infty}^{\infty} J_n(z) = 1.$$

3.2. Show that $J_{-n}(z) = (-1)^n J_n(z)$. Hint: You may utilize the relation

$$J_n(z) = \frac{1}{\pi} \int_0^{\pi} \cos(z \sin y - ny) dy.$$

3.3. In a multiple frequency CW radar, the transmitted waveform consists of two continuous sinewaves of frequencies $f_1 = 105\text{KHz}$ and $f_2 = 115\text{KHz}$. Compute the maximum unambiguous detection range.

3.4. Consider a radar system using linear frequency modulation. Compute the range that corresponds to $\dot{f} = 20, 10\text{MHz}$. Assume a beat frequency $f_b = 1200\text{Hz}$.

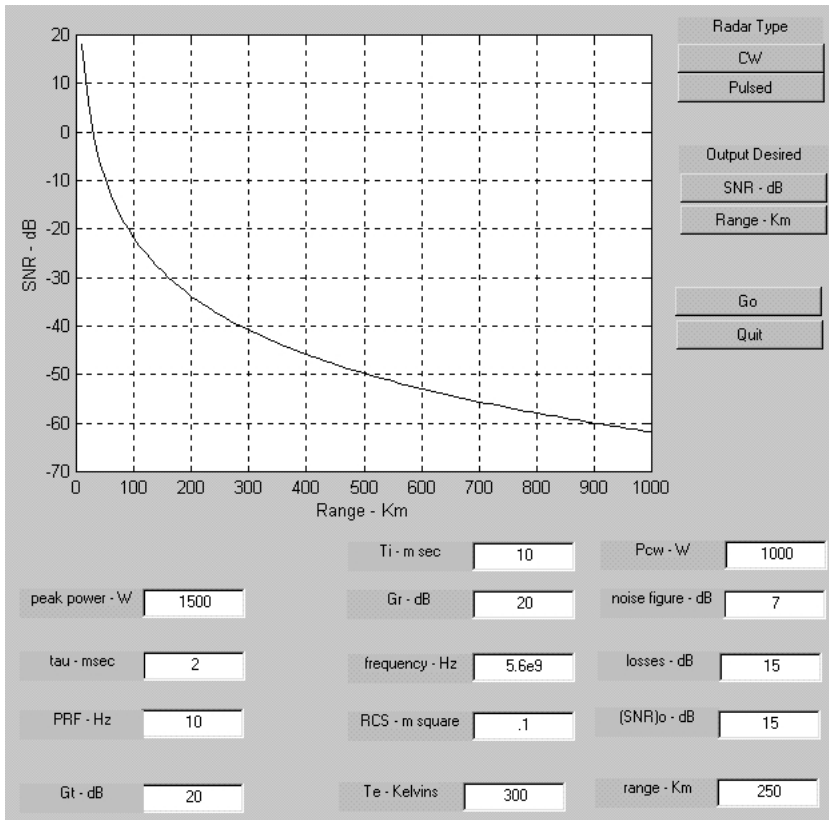
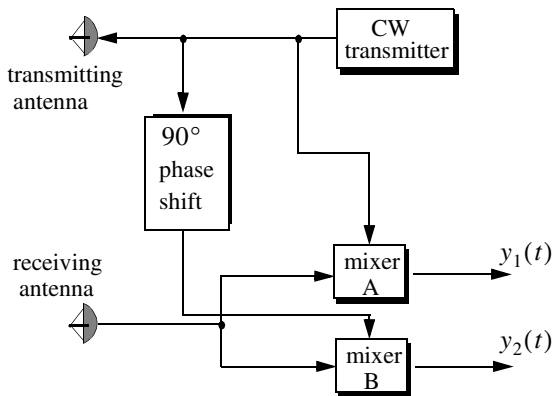


Figure 3.10. GUI work space associated with the program *"range_calc.m"*.

3.5. A certain radar using linear frequency modulation has a modulation frequency $f_m = 300\text{Hz}$, and frequency sweep $\Delta f = 50\text{MHz}$. Calculate the average beat frequency differences that correspond to range increments of 10 and 15 meters.

3.6. A CW radar uses linear frequency modulation to determine both range and range rate. The radar wavelength is $\lambda = 3\text{cm}$, and the frequency sweep is $\Delta f = 200\text{kHz}$. Let $t_0 = 20\text{ms}$. (a) Calculate the mean Doppler shift; (b) compute f_{bu} and f_{bd} corresponding to a target at range $R = 350\text{Km}$, which is approaching the radar with radial velocity of 250m/s .

3.7. In Chapter 1 we developed an expression for the Doppler shift associated with a CW radar (i.e., $f_d = \pm 2v/\lambda$, where the plus sign is used for closing targets and the negative sign is used for receding targets). CW radars can use the system shown below to determine whether the target is closing or receding. Assuming that the emitted signal is $A \cos \omega_0 t$ and the received signal is $kA \cos((\omega_0 \pm \omega_d)t + \phi)$, show that the direction of the target can be determined by checking the phase shift difference in the outputs $y_1(t)$ and $y_2(t)$.



3.8. Consider a medium PRF radar on board an aircraft moving at a speed of 350 m/s with PRFs $f_{r1} = 10\text{KHz}$, $f_{r2} = 15\text{KHz}$, and $f_{r3} = 20\text{KHz}$; the radar operating frequency is 9.5GHz . Calculate the frequency position of a nose-on target with a speed of 300 m/s . Also calculate the closing rate of a target appearing at 6 , 5 , and 18KHz away from the center line of PRF 10 , 15 , and 20KHz , respectively.

3.9. Repeat Problem 3.8 when the target is 15° off the radar line of sight.

3.10. A certain radar operates at two PRFs, f_{r1} and f_{r2} , where $T_{r1} = (1/f_{r1}) = T/5$ and $T_{r2} = (1/f_{r2}) = T/6$. Show that this multiple PRF scheme will give the same range ambiguity as that of a single PRF with PRI T .

3.11. Consider an X-band radar with wavelength $\lambda = 3\text{ cm}$ and bandwidth $B = 10\text{ MHz}$. The radar uses two PRFs, $f_{r1} = 50\text{ kHz}$ and $f_{r2} = 55.55\text{ kHz}$. A target is detected at range bin 46 for f_{r1} and at bin 12 for f_{r2} . Determine the actual target range.

3.12. A certain radar uses two PRFs to resolve range ambiguities. The desired unambiguous range is $R_u = 150\text{ km}$. Select a reasonable value for N . Compute the corresponding f_{r1} , f_{r2} , R_{u1} , and R_{u2} .

3.13. A certain radar uses three PRFs to resolve range ambiguities. The desired unambiguous range is $R_u = 250\text{ km}$. Select $N = 43$. Compute the corresponding f_{r1} , f_{r2} , f_{r3} , R_{u1} , R_{u2} , and R_{u3} .

4.1. Detection in the Presence of Noise

A simplified block diagram of a radar receiver that employs an envelope detector followed by a threshold decision is shown in Fig. 4.1. The input signal to the receiver is composed of the radar echo signal $s(t)$ and additive zero mean white Gaussian noise $n(t)$, with variance ψ^2 . The input noise is assumed to be spatially incoherent and uncorrelated with the signal.

The output of the band pass IF filter is the signal $v(t)$, which can be written as

$$\begin{aligned}v(t) &= v_I(t)\cos\omega_0t + v_Q(t)\sin\omega_0t = r(t)\cos(\omega_0t - \varphi(t)) \\v_I(t) &= r(t)\cos\varphi(t) \\v_Q(t) &= r(t)\sin\varphi(t)\end{aligned}\tag{4.1}$$

where $\omega_0 = 2\pi f_0$ is the radar operating frequency, $r(t)$ is the envelope of $v(t)$, the phase is $\varphi(t) = \text{atan}(v_Q/v_I)$, and the subscripts I, Q , respectively, refer to the in-phase and quadrature components.

A target is detected when $r(t)$ exceeds the threshold value V_T , where the decision hypotheses are

$$\begin{aligned}s(t) + n(t) &> V_T && \text{Detection} \\n(t) &> V_T && \text{False alarm}\end{aligned}$$

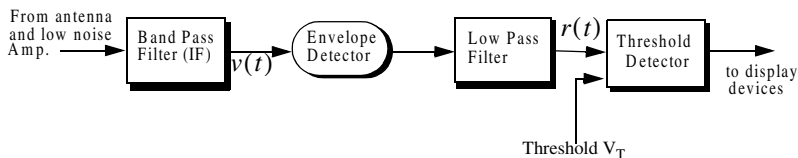


Figure 4.1. Simplified block diagram of an envelope detector and threshold receiver.

The case when the noise subtracts from the signal (while a target is present) to make $r(t)$ smaller than the threshold is called a miss. Radar designers seek to maximize the probability of detection for a given probability of false alarm.

The IF filter output is a complex random variable that is composed of either noise alone or noise plus target return signal (sine wave of amplitude A). The quadrature components corresponding to the first case are

$$\begin{aligned} v_I(t) &= n_I(t) \\ v_Q(t) &= n_Q(t) \end{aligned} \tag{4.2}$$

and for the second case,

$$\begin{aligned} v_I(t) &= A + n_I(t) = r(t) \cos \varphi(t) \Rightarrow n_I(t) = r(t) \cos \varphi(t) - A \\ v_Q(t) &= n_Q(t) = r(t) \sin \varphi(t) \end{aligned} \tag{4.3}$$

where the noise quadrature components $n_I(t)$ and $n_Q(t)$ are uncorrelated zero mean low pass Gaussian noise with equal variances, ψ^2 . The joint Probability Density Function (*pdf*) of the two random variables $n_I; n_Q$ is

$$\begin{aligned} f(n_I, n_Q) &= \frac{1}{2\pi\psi^2} \exp\left(-\frac{n_I^2 + n_Q^2}{2\psi^2}\right) \\ &= \frac{1}{2\pi\psi^2} \exp\left(-\frac{(r \cos \varphi - A)^2 + (r \sin \varphi)^2}{2\psi^2}\right) \end{aligned} \tag{4.4}$$

The *pdfs* of the random variables $r(t)$ and $\varphi(t)$, respectively, represent the modulus and phase of $v(t)$. The joint *pdf* for the two random variables $r(t); \varphi(t)$ is given by

$$f(r, \varphi) = f(n_I, n_Q) |J| \tag{4.5}$$

where $[J]$ is a matrix of derivatives defined by

$$[J] = \begin{bmatrix} \frac{\partial n_I}{\partial r} & \frac{\partial n_I}{\partial \varphi} \\ \frac{\partial n_Q}{\partial r} & \frac{\partial n_Q}{\partial \varphi} \end{bmatrix} = \begin{bmatrix} \cos \varphi & -r \sin \varphi \\ \sin \varphi & r \cos \varphi \end{bmatrix} \quad (4.6)$$

The determinant of the matrix of derivatives is called the Jacobian, and in this case it is equal to

$$|J| = r(r) \quad (4.7)$$

Substituting Eqs. (4.4) and (4.7) into Eq. (4.5) and collecting terms yield

$$f(r, \varphi) = \frac{r}{2\pi\psi^2} \exp\left(-\frac{r^2 + A^2}{2\psi^2}\right) \exp\left(\frac{rA \cos \varphi}{\psi^2}\right) \quad (4.8)$$

The *pdf* for r alone is obtained by integrating Eq. (4.8) over φ

$$f(r) = \int_0^{2\pi} f(r, \varphi) d\varphi = \frac{r}{\psi^2} \exp\left(-\frac{r^2 + A^2}{2\psi^2}\right) \frac{1}{2\pi} \int_0^{2\pi} \exp\left(\frac{rA \cos \varphi}{\psi^2}\right) d\varphi \quad (4.9)$$

where the integral inside Eq. (4.9) is known as the modified Bessel function of zero order,

$$I_0(\beta) = \frac{1}{2\pi} \int_0^{2\pi} e^{\beta \cos \theta} d\theta \quad (4.10)$$

Thus,

$$f(r) = \frac{r}{\psi^2} I_0\left(\frac{rA}{\psi^2}\right) \exp\left(-\frac{r^2 + A^2}{2\psi^2}\right) \quad (4.11)$$

which is the Rice probability density function. If $A/\psi^2 = 0$ (noise alone), then Eq. (4.11) becomes the Rayleigh probability density function

$$f(r) = \frac{r}{\psi^2} \exp\left(-\frac{r^2}{2\psi^2}\right) \quad (4.12)$$

Also, when (A/ψ^2) is very large, Eq. (4.11) becomes a Gaussian probability density function of mean A and variance ψ^2 :

$$f(r) \approx \frac{1}{\sqrt{2\pi}\psi^2} \exp\left(-\frac{(r-A)^2}{2\psi^2}\right) \quad (4.13)$$

Fig. 4.2 shows plots for the Rayleigh and Gaussian densities.

The density function for the random variable φ is obtained from

$$f(\varphi) = \int_0^r f(r, \varphi) dr \quad (4.14)$$

While the detailed derivation is left as an exercise, the result of Eq. (4.14) is

$$f(\varphi) = \frac{1}{2\pi} \exp\left(\frac{-A^2}{2\psi^2}\right) + \frac{A \cos \varphi}{\sqrt{2\pi}\psi^2} \exp\left(\frac{-(A \sin \varphi)^2}{2\psi^2}\right) F\left(\frac{A \cos \varphi}{\psi}\right) \quad (4.15)$$

where

$$F(x) = \int_{-\infty}^x \frac{1}{\sqrt{2\pi}} e^{-\xi^2/2} d\xi \quad (4.16)$$

The function $F(x)$ can be found tabulated in most mathematical formulas and tables reference books. Note that for the case of noise alone ($A = 0$), Eq. (4.15) collapses to a uniform *pdf* over the interval $\{0, 2\pi\}$.

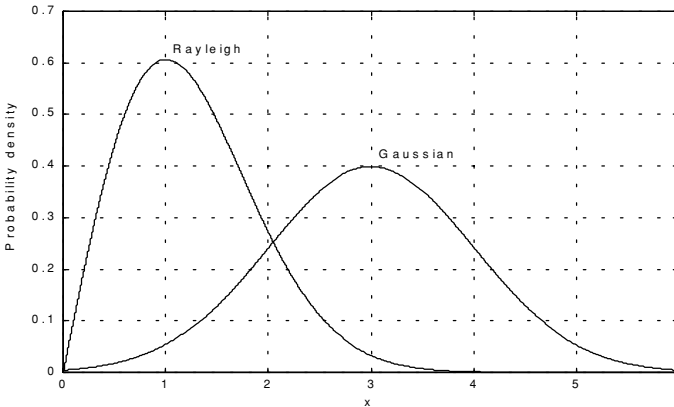


Figure 4.2. Gaussian and Rayleigh probability densities.

One excellent approximation for the function $F(x)$ is

$$F(x) = 1 - \left(\frac{1}{0.661x + 0.339\sqrt{x^2 + 5.51}} \right) \frac{1}{\sqrt{2\pi}} e^{-x^2/2} \quad x \geq 0 \quad (4.17)$$

and for negative values of x

$$F(-x) = 1 - F(x) \quad (4.18)$$

MATLAB Function “que_func.m”

The function “que_func.m” computes $F(x)$ using Eqs. (4.17) and (4.18) and is given in Listing 4.1 in Section 4.10. The syntax is as follows:

$$fofx = que_func(x)$$

4.2. Probability of False Alarm

The probability of false alarm P_{fa} is defined as the probability that a sample R of the signal $r(t)$ will exceed the threshold voltage V_T when noise alone is present in the radar,

$$P_{fa} = \int_{V_T}^{\infty} \frac{r}{\Psi^2} \exp\left(-\frac{r^2}{2\Psi^2}\right) dr = \exp\left(\frac{-V_T^2}{2\Psi^2}\right) \quad (4.19a)$$

$$V_T = \sqrt{2\Psi^2 \ln\left(\frac{1}{P_{fa}}\right)} \quad (4.19b)$$

Fig. 4.3 shows a plot of the normalized threshold versus the probability of false alarm. It is evident from this figure that P_{fa} is very sensitive to small changes in the threshold value.

The false alarm time T_{fa} is related to the probability of false alarm by

$$T_{fa} = \frac{t_{int}}{P_{fa}} \quad (4.20)$$

where t_{int} represents the radar integration time, or the average time that the output of the envelope detector will pass the threshold voltage. Since the radar operating bandwidth B is the inverse of t_{int} , then by substituting Eq. (4.19) into Eq. (4.20) we can write T_{fa} as

$$T_{fa} = \frac{1}{B} \exp\left(\frac{V_T^2}{2\Psi^2}\right) \quad (4.21)$$

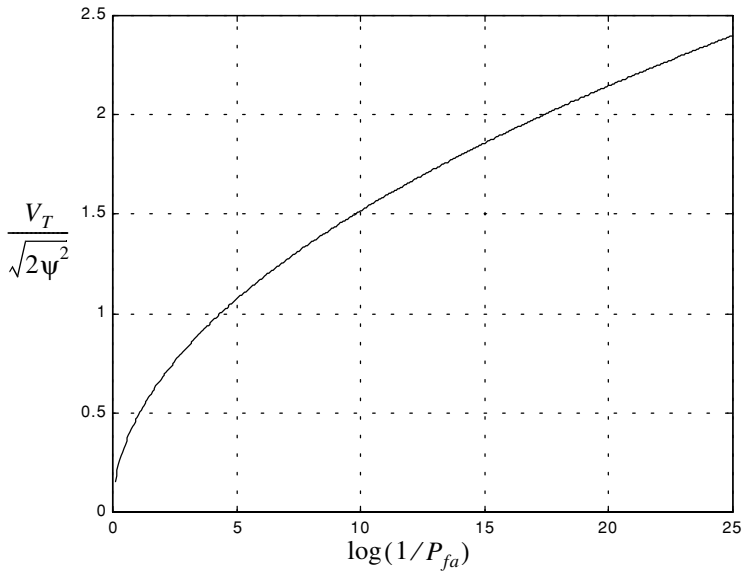


Figure 4.3. Normalized detection threshold versus probability of false alarm.

Minimizing T_{fa} means increasing the threshold value, and as a result the radar maximum detection range is decreased. Therefore, the choice of an acceptable value for T_{fa} becomes a compromise depending on the radar mode of operation. The false alarm number n_{fa} was defined by Marcum (see bibliography) as the reciprocal of P_{fa} . Using Marcum's definition of the false alarm number, the probability of false alarm is given by $P_{fa} \approx \ln(2)(n_p/n_{fa})$, where $n_p > 1$ is the number of pulses and $P_{fa} < 0.007$.

4.3. Probability of Detection

The probability of detection P_D is the probability that a sample R of $r(t)$ will exceed the threshold voltage in the case of noise plus signal,

$$P_D = \int_{V_T}^{\infty} \frac{r}{\psi^2} I_0\left(\frac{rA}{\psi^2}\right) \exp\left(-\frac{r^2 + A^2}{2\psi^2}\right) dr \quad (4.22)$$

If we assume that the radar signal is a sine waveform with amplitude A , then its power is $A^2/2$. Now, by using $SNR = A^2/2\psi^2$ (single-pulse SNR) and $(V_T^2/2\psi^2) = \ln(1/P_{fa})$, then Eq. (4.22) can be rewritten as

$$P_D = \int_{\sqrt{2\Psi^2 \ln(1/P_{fa})}}^{\infty} \frac{r}{\Psi^2} I_0\left(\frac{rA}{\Psi^2}\right) \exp\left(-\frac{r^2 + A^2}{2\Psi^2}\right) dr = Q\left[\sqrt{\frac{A^2}{\Psi^2}}, \sqrt{2\ln\left(\frac{1}{P_{fa}}\right)}\right] \quad (4.23)$$

$$Q[\alpha, \beta] = \int_{\beta}^{\infty} \zeta I_0(\alpha\zeta) e^{-(\zeta^2 + \alpha^2)/2} d\zeta \quad (4.24)$$

Q is called Marcum's Q-function. When P_{fa} is small and P_D is relatively large so that the threshold is also large, Eq. (4.24) can be approximated by

$$P_D \approx F\left(\frac{A}{\Psi} - \sqrt{2\ln\left(\frac{1}{P_{fa}}\right)}\right) \quad (4.25)$$

where $F(x)$ is given by Eq. (4.16).

Many approximations for computing Eq. (4.23) can be found throughout the literature. One very accurate approximation presented by North (see bibliography) is given by

$$P_D \approx 0.5 \times \operatorname{erfc}(\sqrt{-\ln P_{fa}} - \sqrt{\operatorname{SNR} + 0.5}) \quad (4.26)$$

where the complementary error function is

$$\operatorname{erfc}(z) = 1 - \frac{2}{\sqrt{\pi}} \int_0^z e^{-v^2} dv \quad (4.27)$$

Table 4.1 gives samples of the single pulse SNR corresponding to few values of P_D and P_{fa} , using Eq. (4.26). For example, if $P_D = 0.99$ and $P_{fa} = 10^{-10}$, then the minimum single pulse SNR required to accomplish this combination of P_D and P_{fa} is $\operatorname{SNR} = 16.12\text{dB}$.

MATLAB Function “marcumsg.m”

The integral given in Eq. (4.23) is complicated and can be computed using numerical integration techniques. Parl¹ developed an excellent algorithm to numerically compute this integral. It is summarized as follows:

$$Q[a, b] = \left\{ \begin{array}{ll} \frac{\alpha_n}{2\beta_n} \exp\left(\frac{(a-b)^2}{2}\right) & a < b \\ 1 - \left(\frac{\alpha_n}{2\beta_n} \exp\left(\frac{(a-b)^2}{2}\right)\right) & a \geq b \end{array} \right\} \quad (4.28)$$

1. Parl, S., A New Method of Calculating the Generalized Q Function, *IEEE Trans. Information Theory*, Vol. IT-26, No. 1, January 1980, pp. 121-124.

TABLE 4.1. Single pulse SNR (dB).

P_D	P_{fa}									
	10^{-3}	10^{-4}	10^{-5}	10^{-6}	10^{-7}	10^{-8}	10^{-9}	10^{-10}	10^{-11}	10^{-12}
.1	4.00	6.19	7.85	8.95	9.94	10.44	11.12	11.62	12.16	12.65
.2	5.57	7.35	8.75	9.81	10.50	11.19	11.87	12.31	12.85	13.25
.3	6.75	8.25	9.50	10.44	11.10	11.75	12.37	12.81	13.25	13.65
.4	7.87	8.85	10.18	10.87	11.56	12.18	12.75	13.25	13.65	14.00
.5	8.44	9.45	10.62	11.25	11.95	12.60	13.11	13.52	14.00	14.35
.6	8.75	9.95	11.00	11.75	12.37	12.88	13.50	13.87	14.25	14.62
.7	9.56	10.50	11.50	12.31	12.75	13.31	13.87	14.20	14.59	14.95
.8	10.18	11.12	12.05	12.62	13.25	13.75	14.25	14.55	14.87	15.25
.9	10.95	11.85	12.65	13.31	13.85	14.25	14.62	15.00	15.45	15.75
.95	11.50	12.40	13.12	13.65	14.25	14.64	15.10	15.45	15.75	16.12
.98	12.18	13.00	13.62	14.25	14.62	15.12	15.47	15.85	16.25	16.50
.99	12.62	13.37	14.05	14.50	15.00	15.38	15.75	16.12	16.47	16.75
.995	12.85	13.65	14.31	14.75	15.25	15.71	16.06	16.37	16.65	17.00
.998	13.31	14.05	14.62	15.06	15.53	16.05	16.37	16.7	16.89	17.25
.999	13.62	14.25	14.88	15.25	15.85	16.13	16.50	16.85	17.12	17.44
.9995	13.84	14.50	15.06	15.55	15.99	16.35	16.70	16.98	17.35	17.55
.9999	14.38	14.94	15.44	16.12	16.50	16.87	17.12	17.35	17.62	17.87

$$\alpha_n = d_n + \frac{2n}{ab}\alpha_{n-1} + \alpha_{n-2} \quad (4.29)$$

$$\beta_n = 1 + \frac{2n}{ab}\beta_{n-1} + \beta_{n-2} \quad (4.30)$$

$$d_{n+1} = d_n d_1 \quad (4.31)$$

$$\alpha_0 = \begin{cases} 1 & a < b \\ 0 & a \geq b \end{cases} \quad (4.32)$$

$$d_1 = \begin{cases} a/b & a < b \\ b/a & a \geq b \end{cases} \quad (4.33)$$

$\alpha_{-1} = 0.0$, $\beta_0 = 0.5$, and $\beta_{-1} = 0$. The recursive Eqs. (4.29) through (4.31) are computed continuously until $\beta_n > 10^p$ for some value $p \geq 3$. The accuracy of the algorithm is enhanced as the value of p is increased. The MATLAB function “*marcumsq.m*” given in Listing 4.2 in Section 4.10 implements Parl’s

algorithm to compute the probability of detection defined in Eq. (4.23). The syntax is as follows:

$$Pd = \text{marcumsq}(\alpha, \beta)$$

where α and β are from Eq. (4.24). Fig. 4.4 shows plots of the probability of detection, P_D , versus the single pulse SNR, with the P_{fa} as a parameter. This figure can be reproduced using the MATLAB program “*prob_snr1.m*” given in Listing 4.3 in Section 4.10. This program uses the function “*marcumsq.m*”.

Example 4.1: A pulsed radar has the following specification: time of false alarm $T_{fa} = 16.67$ minutes; probability of detection $P_D = 0.9$ and bandwidth $B = 1$ GHz. Find the radar integration time t_{int} , the probability of false alarm P_{fa} , and the SNR of a single pulse.

Solution:

$$t_{int} = \frac{1}{B} = \frac{1}{10^9} = 1 \text{ nsec}$$

$$P_{fa} = \frac{1}{T_{fa}B} = \frac{1}{10^9 \times 16.67 \times 60} \approx 10^{-12}$$

and from Table 4.1 or from Fig. 4.4, we read

$$(SNR)_1 \approx 15.75 \text{ dB.}$$

4.4. Pulse Integration

When a target is illuminated by the radar beam it normally reflects numerous pulses. The radar probability of detection is normally enhanced by summing all (or most) of the returned pulses. The process of adding radar echoes from many pulses is called radar pulse integration. Pulse integration can be performed on the quadrature components prior to the envelope detector. This is called coherent integration or pre-detection integration. Coherent integration preserves the phase relationship between the received pulses, thus a build up in the signal amplitude is achieved. Alternatively, pulse integration performed after the envelope detector (where the phase relation is destroyed) is called non-coherent or post-detection integration.

4.4.1. Coherent Integration

In coherent integration, if a perfect integrator is used (100% efficiency), then integrating n_p pulses would improve the SNR by the same factor. Otherwise, integration loss occurs which is always the case for non-coherent integration. In order to demonstrate this signal buildup, consider the case where the radar return signal contains both signal plus additive noise. The m^{th} pulse is

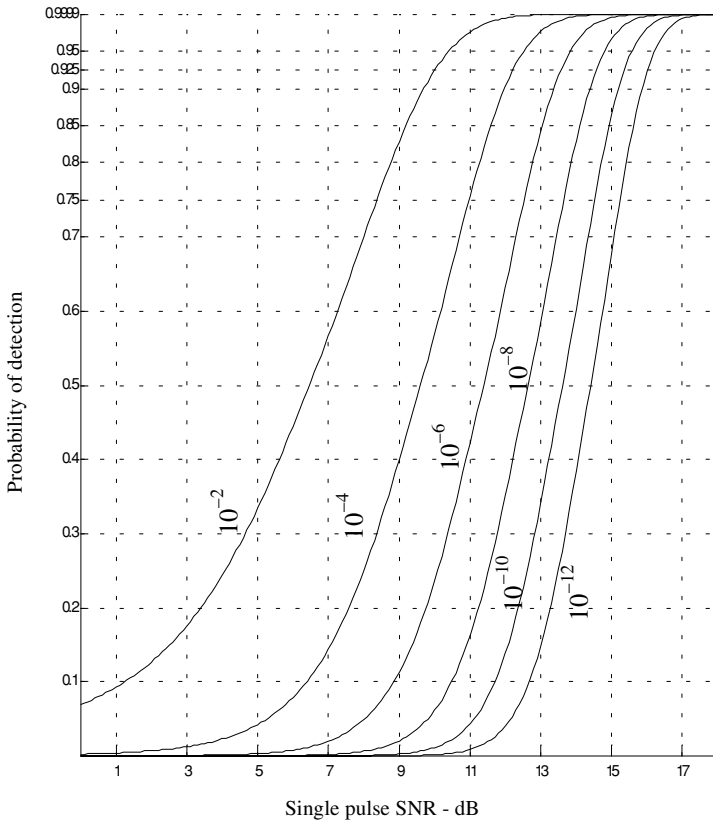


Figure 4.4. Probability of detection versus single pulse SNR, for several values of P_{fa} .

$$y_m(t) = s(t) + n_m(t) \quad (4.34)$$

where $s(t)$ is the radar return of interest and $n_m(t)$ is white uncorrelated additive noise signal. Coherent integration of n_p pulses yields

$$z(t) = \frac{1}{n_p} \sum_{m=1}^{n_p} y_m(t) = \sum_{m=1}^{n_p} \frac{1}{n_p} [s(t) + n_m(t)] = s(t) + \sum_{m=1}^{n_p} \frac{1}{n_p} n_m(t) \quad (4.35)$$

The total noise power in $z(t)$ is equal to the variance. More precisely,

$$\Psi_{nz}^2 = E \left[\left(\sum_{m=1}^{n_p} \frac{1}{n_p} n_m(t) \right) \left(\sum_{l=1}^{n_p} \frac{1}{n_p} n_l(t) \right)^* \right] \quad (4.36)$$

where $E[\]$ is the expected value operator. It follows that

$$\Psi_{nz}^2 = \frac{1}{n_p^2} \sum_{m,l=1}^{n_p} E[n_m(t)n_l^*(t)] = \frac{1}{n_p^2} \sum_{m,l=1}^{n_p} \Psi_{ny}^2 \delta_{ml} = \frac{1}{n_p} \Psi_{ny}^2 \quad (4.37)$$

where Ψ_{ny}^2 is the single pulse noise power and δ_{ml} is equal to zero for $m \neq l$ and unity for $m = l$. Observation of Eqs. (4.35) and (4.37) shows that the desired signal power after coherent integration is unchanged, while the noise power is reduced by the factor $1/n_p$. Thus, the SNR after coherent integration is improved by n_p .

Denote the single pulse SNR required to produce a given probability of detection as $(SNR)_1$. Also, denote $(SNR)_{n_p}$ as the SNR required to produce the same probability of detection when n_p pulses are integrated. It follows that

$$(SNR)_{n_p} = \frac{1}{n_p} (SNR)_1 \quad (4.38)$$

The requirements of remembering the phase of each transmitted pulse as well as maintaining coherency during propagation is very costly and challenging to achieve. In practice, most radar systems utilize non-coherent integration.

4.4.2. Non-Coherent Integration

Non-coherent integration is often implemented after the envelope detector, also known as the quadratic detector. A block diagram of radar receiver utilizing a square law detector and non-coherent integration is illustrated in Fig. 4.5. In practice, the square law detector is normally used as an approximation to the optimum receiver.

The *pdf* for the signal $r(t)$ was derived earlier and it is given in Eq. (4.11). Define a new dimensionless variable y as

$$y_n = r_n / \Psi \quad (4.39)$$

and also define

$$\mathfrak{R}_p = \frac{A^2}{\Psi^2} = 2SNR \quad (4.40)$$

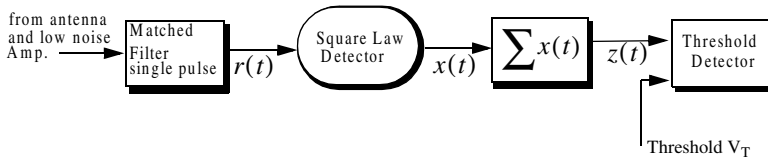


Figure 4.5. Simplified block diagram of a square law detector and non-coherent integration.

It follows that the *pdf* for the new variable is then given by

$$f(y_n) = f(r_n) \left| \frac{dr_n}{dy_n} \right| = y_n I_0(y_n \sqrt{\mathfrak{R}_p}) \exp\left(\frac{-(y_n^2 + \mathfrak{R}_p)}{2}\right) \quad (4.41)$$

The output of a square law detector for the n^{th} pulse is proportional to the square of its input, which, after the change of variable in Eq. (4.39), is proportional to y_n . Thus, it is convenient to define a new change variable,

$$x_n = \frac{1}{2}y_n^2 \quad (4.42)$$

The *pdf* for the variable at the output of the square law detector is given by

$$f(x_n) = f(y_n) \left| \frac{dy_n}{dx_n} \right| = \exp\left(-\left(x_n + \frac{\mathfrak{R}_p}{2}\right)\right) I_0(\sqrt{2x_n \mathfrak{R}_p}) \quad (4.43)$$

Non-coherent integration of n_p pulses is implemented as

$$z = \sum_{n=1}^{n_p} x_n \quad (4.44)$$

Since the random variables x_n are independent, the *pdf* for the variable z is

$$f(z) = f(x_1) \bullet f(x_2) \bullet \dots \bullet f(x_{n_p}) \quad (4.45)$$

the operator \bullet symbolically indicates convolution. The characteristic functions for the individual *pdfs* can then be used to compute the joint *pdf* in Eq. (4.45). The details of this development are left as an exercise. The result is

$$f(z) = \left(\frac{2z}{n_p \mathfrak{R}_p}\right)^{(n_p-1)/2} \exp\left(-z - \frac{1}{2}n_p \mathfrak{R}_p\right) I_{n_p-1}(\sqrt{2n_p z \mathfrak{R}_p}) \quad (4.46)$$

where I_{n_p-1} is the modified Bessel function of order $n_p - 1$. Therefore, the probability of detection is obtained by integrating $f(z)$ from the threshold value to infinity. Alternatively, the probability of false alarm is obtained by letting \mathfrak{R}_p be zero and integrating the *pdf* from the threshold value to infinity. Closed form solutions to these integrals are not easily available. Therefore, numerical techniques are often utilized to generate tables for the probability of detection.

The non-coherent integration efficiency $E(n_p)$ is defined as

$$E(n_p) = \frac{(SNR)_1}{n_p(SNR)_{n_p}} \leq 1 \quad (4.47)$$

The integration improvement factor $I(n_p)$ for a specific P_{fa} is defined as the ratio of $(SNR)_1$ to $(SNR)_{n_p}$

$$I(n_p) = \frac{(SNR)_1}{(SNR)_{n_p}} = n_p E(n_p) \leq n_p \quad (4.48)$$

Note that $(SNR)_{n_p}$ corresponds to the SNR needed to produce the same P_D as in the case of a single pulse when n_p pulses are used. It follows that $(SNR)_{n_p} < (SNR)_1$.

An empirically derived expression for the improvement factor that is accurate within 0.8dB is reported in Peebles¹ as

$$[I(n_p)]_{dB} = 6.79(1 + 0.235P_D) \left(1 + \frac{\log(1/P_{fa})}{46.6} \right) \log(n_p) \quad (4.49)$$

$$(1 - 0.140\log(n_p) + 0.018310(\log n_p)^2)$$

Fig. 4.6 shows plots of the integration improvement factor as a function of the number of integrated pulses with P_D and P_{fa} as parameters, using Eq. (4.49). This plot can be reproduced using the MATLAB program “fig4_5.m” given in Listing 4.4 in Section 4.10.

Example 4.2: Consider the same radar defined in Example 4.1. Assume non-coherent integration of 10 pulses. Find the reduction in the SNR.

Solution: The integration improvement factor is calculated using the function “improv_fac.m”. It is $I(10) \cong 9.20dB$, and from Eq. (4.48) we get

$$(SNR)_{n_p} = \frac{(SNR)_1}{I(n_p)} \Rightarrow (SNR)_{n_p} = 15.75 - 9.20 = 6.55dB$$

1. Peebles Jr., P. Z., *Radar Principles*, John Wiley & Sons, Inc., 1998.

Thus, non-coherent integration of 10 pulses where $(SNR)_{10} = 6.55\text{dB}$ provides the same detection performance as $(SNR)_1 = 15.75\text{dB}$ of a single pulse and no integration.

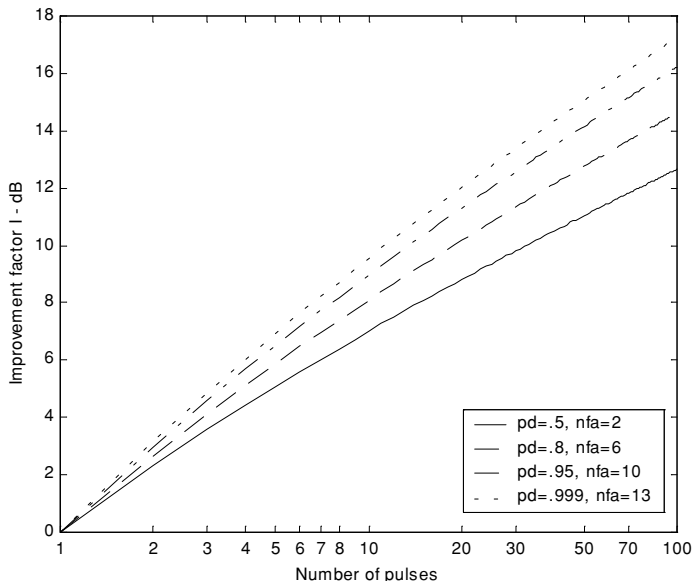


Figure 4.6. Improvement factor versus number of pulses (non-coherent integration). These plots were generated using the empirical approximation in Eq. (4.49).

MATLAB Function “improv_fac.m”

The function “improv_fac.m” calculates the improvement factor using Eq. (4.49). It is given in Listing 4.5 in Section 4.10. The syntax is as follows:

$$[impr_of_np] = improv_fac(np, pfa, pd)$$

where

Symbol	Description	Units	Status
np	number of integrated pulses	none	input
pfa	probability of false alarm	none	input
pd	probability of detection	none	input
$impr_of_np$	improvement factor	output	dB

4.5. Detection of Fluctuating Targets

So far when we addressed the probability of detection, we assumed a constant target cross section (non-fluctuating target). However, when target scintillation is present, the probability of detection decreases, or equivalently the SNR is reduced.

4.5.1. Detection Probability Density Function

The probability density functions for fluctuating targets were given in Chapter 2. And for convenience, they are repeated here as Eqs. (4.50) and (4.51):

$$f(A) = \frac{1}{A_{av}} \exp\left(-\frac{A}{A_{av}}\right) \quad A \geq 0 \quad (4.50)$$

for Swerling I and II type targets, and

$$f(A) = \frac{4A}{A_{av}^2} \exp\left(-\frac{2A}{A_{av}}\right) \quad A \geq 0 \quad (4.51)$$

for Swerling III and IV type targets, where A_{av} denotes the average RCS over all target fluctuations.

The probability of detection for a scintillating target is computed in a similar fashion to Eq. (4.22), except in this case $f(r)$ is replaced by the conditional *pdf* $f(r/A)$. Performing the analysis for the general case (i.e., using Eq. (4.46)) yields

$$f(z/A) = \left(\frac{2z}{n_p A^2 / \Psi^2}\right)^{(n_p - 1)/2} \exp\left(-z - \frac{1}{2} n_p \frac{A^2}{\Psi^2}\right) I_{n_p - 1} \left(\sqrt{2 n_p z \frac{A^2}{\Psi^2}}\right) \quad (4.52)$$

To obtain $f(z)$ use the relations

$$f(z, A) = f(z/A)f(A) \quad (4.53)$$

$$f(z) = \int f(z, A) dA \quad (4.54)$$

Finally, using Eq. (4.54) in Eq. (4.53) produces

$$f(z) = \int f(z/A)f(A) dA \quad (4.55)$$

where $f(z/A)$ is defined in Eq. (4.52) and $f(A)$ is in either Eq. (4.50) or (4.51). The probability of detection is obtained by integrating the *pdf* derived from Eq. (4.55) from the threshold value to infinity. Performing the integration in Eq. (4.55) leads to the incomplete Gamma function.

4.5.2. Threshold Selection

In practice, the detection threshold, V_T , is found from the probability of false alarm P_{fa} . DiFranco and Rubin¹ give a general form relating the threshold and P_{fa} for any number of pulses and non-coherent integration,

$$P_{fa} = 1 - \Gamma_I\left(\frac{V_T}{\sqrt{n_p}}, n_p - 1\right) \quad (4.56)$$

where Γ_I is used to denote the incomplete Gamma function, and it is given by

$$\Gamma_I\left(\frac{V_T}{\sqrt{n_p}}, n_p - 1\right) = \int_0^{V_T/\sqrt{n_p}} \frac{e^{-\gamma} \gamma^{n_p-1-1}}{(n_p-1-1)!} d\gamma \quad (4.57)$$

For our purposes, the incomplete Gamma function can be approximated by

$$\Gamma_I\left(\frac{V_T}{\sqrt{n_p}}, n_p - 1\right) = 1 - \frac{V_T^{n_p-1} e^{-V_T}}{(n_p-1)!} \left[1 + \frac{n_p-1}{V_T} + \frac{(n_p-1)(n_p-2)}{V_T^2} + \dots + \frac{(n_p-1)!}{V_T^{n_p-1}} \right] \quad (4.58)$$

The threshold value V_T can then be approximated by the recursive formula used in the Newton-Raphson method. More precisely,

$$V_{T,m} = V_{T,m-1} - \frac{G(V_{T,m-1})}{G'(V_{T,m-1})} \quad ; \quad m = 1, 2, 3, \dots \quad (4.59)$$

The iteration is terminated when $|V_{T,m} - V_{T,m-1}| < V_{T,m-1}/10000.0$. The functions G and G' are

$$G(V_{T,m}) = (0.5)^{n_p/n_{fa}} - \Gamma_I(V_T, n_p) \quad (4.60)$$

$$G'(V_{T,m}) = - \frac{e^{-V_T} V_T^{n_p-1}}{(n_p-1)!} \quad (4.61)$$

The initial value for the recursion is

$$V_{T,0} = n_p - \sqrt{n_p} + 2.3 \sqrt{-\log P_{fa}} (\sqrt{-\log P_{fa}} + \sqrt{n_p} - 1) \quad (4.62)$$

1. DiFranco, J. V. and Rubin, W. L., *Radar Detection*. Artech House, 1980.

MATLAB Function “incomplete_gamma.m”

In general, the incomplete Gamma function for some integer N is

$$\Gamma_I(x, N) = \int_0^x \frac{e^{-v} v^{N-1}}{(N-1)!} dv \tag{4.63}$$

The function “incomplete_gamma.m” implements Eq. (4.63). It is given in Listing 4.6 in Section 4.10. The syntax for this function is as follows:

$$[value] = incomplete_gamma (x, N)$$

where

Symbol	Description	Units	Status
x	variable input to $\Gamma_I(x, N)$	units of x	input
N	variable input to $\Gamma_I(x, N)$	none / integer	input
value	$\Gamma_I(x, N)$	none	output

Fig. 4.7 shows the incomplete Gamma function for $N = 1, 3, 10$. Note that the limiting values for the incomplete Gamma function are

$$\Gamma_I(0, N) = 0 \quad \Gamma_I(\infty, N) = 1 \tag{4.64}$$

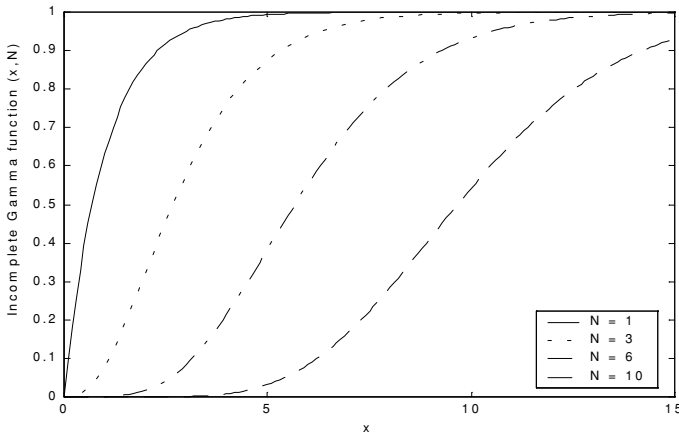


Figure 4.7. The incomplete Gamma function for four values of N .

MATLAB Function “*threshold.m*”

The function “*threshold.m*” calculates the threshold using the recursive formula used in the Newton-Raphson method. It is given in Listing 4.7 in Section 4.10. The syntax is as follows:

$$[pfa, vt] = threshold (nfa, np)$$

where

Symbol	Description	Units	Status
<i>nfa</i>	Marcum’s false alarm number	none	input
<i>np</i>	number of integrated pulses	none	input
<i>pfa</i>	probability of false alarm	none	output
<i>vt</i>	threshold value	none	output

Fig. 4.8 shows plots for the threshold value versus the number of integrated pulses for several values of n_{fa} ; remember that $P_{fa} \approx \ln(2)(n_p/n_{fa})$.

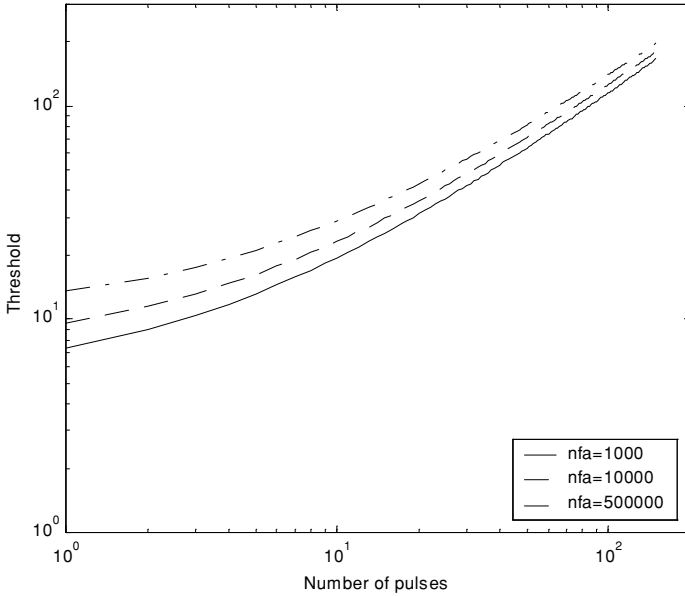


Figure 4.8. Threshold V_T versus n_p for several values of n_{fa} .

4.6. Probability of Detection Calculation

Denote the range at which the single pulse SNR is unity (0 dB) as R_0 , and refer to it as the reference range. Then, for a specific radar, the single pulse SNR at R_0 is defined by the radar equation and is given by

$$(SNR)_{R_0} = \frac{P_t G^2 \lambda^2 \sigma}{(4\pi)^3 k T_0 B F L R_0^4} = 1 \quad (4.65)$$

The single pulse SNR at any range R is

$$SNR = \frac{P_t G^2 \lambda^2 \sigma}{(4\pi)^3 k T_0 B F L R^4} \quad (4.66)$$

Dividing Eq. (4.66) by Eq. (4.65) yields

$$\frac{SNR}{(SNR)_{R_0}} = \left(\frac{R_0}{R}\right)^4 \quad (4.67)$$

Therefore, if the range R_0 is known then the SNR at any other range R is

$$(SNR)_{dB} = 40 \log\left(\frac{R_0}{R}\right) \quad (4.68)$$

Also, define the range R_{50} as the range at which the probability of detection is $P_D = 0.5 = P_{50}$. Normally, the radar unambiguous range R_u is set equal to $2R_{50}$.

4.6.1. Detection of Swerling V Targets

Marcum defined the probability of false alarm for the case when $n_p > 1$ as

$$P_{fa} = 1 - (P_{50})^{n_p/n_{fa}} \approx \ln(2)(n_p/n_{fa}) \quad (4.69)$$

The single pulse probability of detection for non-fluctuating targets is given in Eq. (4.23). When $n_p > 1$, the probability of detection is computed using the Gram-Charlier series. In this case, the probability of detection is

$$P_D \cong \frac{\operatorname{erfc}(V/\sqrt{2})}{2} - \frac{e^{-V^2/2}}{\sqrt{2\pi}} [C_3(V^2 - 1) + C_4 V(3 - V^2) - C_6 V(V^4 - 10V^2 + 15)] \quad (4.70)$$

where the constants C_3 , C_4 , and C_6 are the Gram-Charlier series coefficients, and the variable V is

$$V = \frac{V_T - n_p(1 + SNR)}{\varpi} \quad (4.71)$$

In general, values for C_3 , C_4 , C_6 , and ϖ vary depending on the target fluctuation type. In the case of Swerling V targets, they are

$$C_3 = -\frac{SNR + 1/3}{\sqrt{n_p}(2SNR + 1)^{1.5}} \quad (4.72)$$

$$C_4 = \frac{SNR + 1/4}{n_p(2SNR + 1)^2} \quad (4.73)$$

$$C_6 = C_3^2/2 \quad (4.74)$$

$$\varpi = \sqrt{n_p(2SNR + 1)} \quad (4.75)$$

MATLAB Function “pd_swerling5.m”

The function “pd_swerling5.m” calculates the probability of detection for Swerling V targets using Eq. (4.70). It is given in Listing 4.8 in Section 4.10. The syntax is as follows:

$$[pd] = pd_swerling5(input1, indicator, np, snr)$$

where

Symbol	Description	Units	Status
<i>input1</i>	P_{fa} , or n_{fa}	none	input
<i>indicator</i>	1 when $input1 = P_{fa}$ 2 when $input1 = n_{fa}$	none	input
<i>np</i>	number of integrated pulses	none	input
<i>snr</i>	SNR	dB	input
<i>pd</i>	probability of detection	none	output

Fig. 4.9 shows a plot for the probability of detection versus SNR for cases $n_p = 1, 10$. Note that it requires less SNR, with ten pulses integrated non-coherently, to achieve the same probability of detection as in the case of a single pulse. Hence, for any given P_D the SNR improvement can be read from the plot. Equivalently, using the function “improv_fac.m” leads to about the same result. For example, when $P_D = 0.8$ the function “improv_fac.m” gives

an SNR improvement factor of $I(10) \approx 8.55 \text{ dB}$. Observation of Fig. 4.9 shows that the ten pulse SNR is about 5.03 dB . Therefore, the single pulse SNR is about (from Eq. (4.48)) 14.5 dB , which can be read from the figure. This figure can be reproduced using MATLAB program “fig4_9.m”, which is part of the companion software of this book.

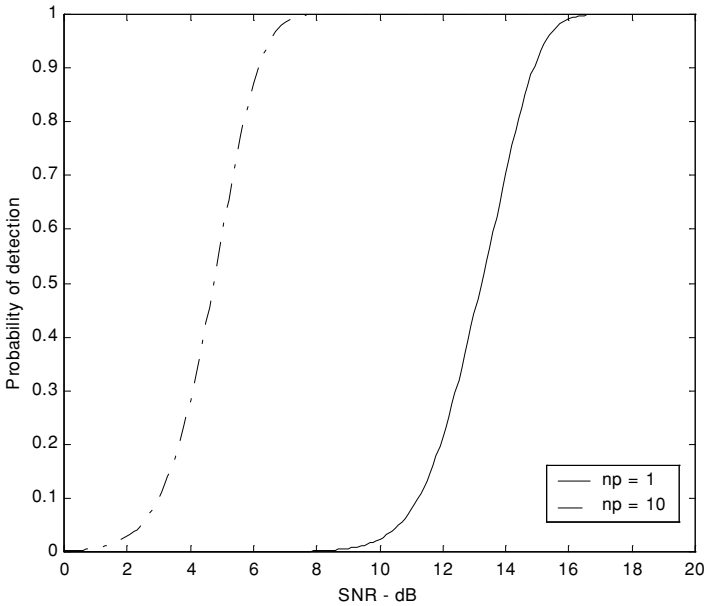


Figure 4.9. Probability of detection versus SNR, $P_{fa} = 10^{-9}$, and non-coherent integration.

4.6.2. Detection of Swerling I Targets

The exact formula for the probability of detection for Swerling I type targets was derived by Swerling. It is

$$P_D = e^{-V_T/(1+SNR)} \quad ; \quad n_p = 1 \quad (4.76)$$

$$P_D = 1 - \Gamma_I(V_T, n_p - 1) + \left(1 + \frac{1}{n_p SNR}\right)^{n_p - 1} \Gamma_I\left(\frac{V_T}{1 + \frac{1}{n_p SNR}}, n_p - 1\right) \quad (4.77)$$

$$\times e^{-V_T/(1+n_p SNR)} \quad ; \quad n_p > 1$$

MATLAB Function “pd_swerling1.m”

The function “pd_swerling1.m” calculates the probability of detection for Swerling I type targets. It is given in Listing 4.9 in Section 4.10. The syntax is as follows:

$$[pd] = pd_swerling1(nfa, np, snr)$$

where

Symbol	Description	Units	Status
<i>nfa</i>	<i>Marcum’s false alarm number</i>	<i>none</i>	<i>input</i>
<i>np</i>	<i>number of integrated pulses</i>	<i>none</i>	<i>input</i>
<i>snr</i>	<i>SNR</i>	<i>dB</i>	<i>input</i>
<i>pd</i>	<i>probability of detection</i>	<i>none</i>	<i>output</i>

Fig. 4.10 shows a plot of the probability of detection as a function of SNR for $n_p = 1$ and $P_{fa} = 10^{-9}$ for both Swerling I and V type fluctuating. Note that it requires more SNR, with fluctuation, to achieve the same P_D as in the case with no fluctuation. Fig. 4.11a shows a plot of the probability of detection versus SNR for $n_p = 1, 10, 50, 100$, where $P_{fa} = 10^{-6}$. Fig. 4.11b is similar to Fig. 4.11a; in this case $P_{fa} = 10^{-12}$.

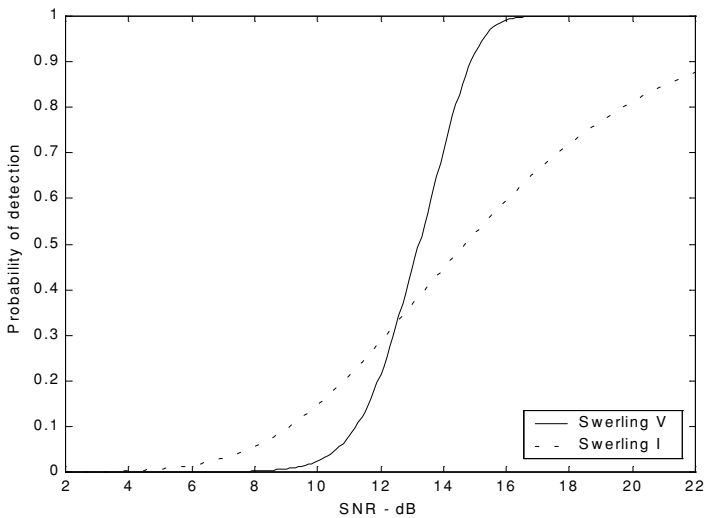


Figure 4.10. Probability of detection versus SNR, single pulse. $P_{fa} = 10^{-9}$.

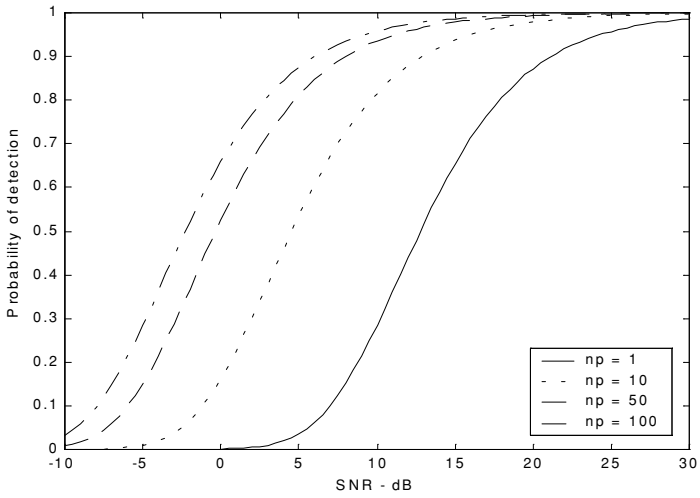


Figure 4.11a. Probability of detection versus SNR. Swerling I. $P_{fa} = 10^{-6}$.

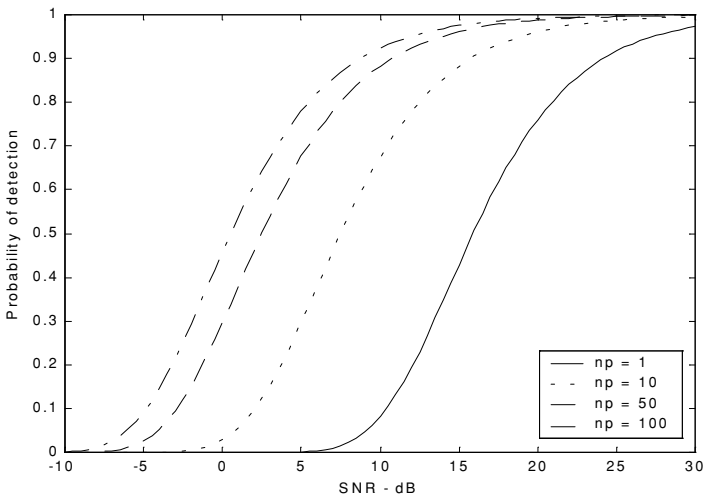


Figure 4.11b. Probability of detection versus SNR. Swerling I. $P_{fa} = 10^{-12}$.

4.6.3. Detection of Swerling II Targets

In the case of Swerling II targets, the probability of detection is given by

$$P_D = 1 - \Gamma_I\left(\frac{V_T}{(1 + SNR)}, n_p\right) \quad ; \quad n_p \leq 50 \quad (4.78)$$

For the case when $n_p > 50$ Eq. (4.70) is used to compute the probability of detection. In this case,

$$C_3 = -\frac{1}{3\sqrt{n_p}} \quad , \quad C_6 = \frac{C_3^2}{2} \quad (4.79)$$

$$C_4 = \frac{1}{4n_p} \quad (4.80)$$

$$\bar{\sigma} = \sqrt{n_p} (1 + SNR) \quad (4.81)$$

MATLAB Function “pd_swerling2.m”

The function “pd_swerling2.m” calculates P_D for Swerling II type targets. It is given in Listing 4.10 in Section 4.10. The syntax is as follows:

$$[pd] = pd_swerling2(nfa, np, snr)$$

where

Symbol	Description	Units	Status
<i>nfa</i>	<i>Marcum's false alarm number</i>	<i>none</i>	<i>input</i>
<i>np</i>	<i>number of integrated pulses</i>	<i>none</i>	<i>input</i>
<i>snr</i>	<i>SNR</i>	<i>dB</i>	<i>input</i>
<i>pd</i>	<i>probability of detection</i>	<i>none</i>	<i>output</i>

Fig. 4.12 shows a plot of the probability of detection as a function of SNR for $n_p = 1, 10, 50, 100$, where $P_{fa} = 10^{-9}$.

4.6.4. Detection of Swerling III Targets

The exact formula, developed by Marcum, for the probability of detection for Swerling III type targets when $n_p = 1, 2$ is

$$P_D = \exp\left(\frac{-V_T}{1 + n_p SNR/2}\right) \left(1 + \frac{2}{n_p SNR}\right)^{n_p - 2} \times \left(1 + \frac{V_T}{1 + n_p SNR/2} - \frac{2}{n_p SNR}(n_p - 2)\right) = K_0 \quad (4.82)$$

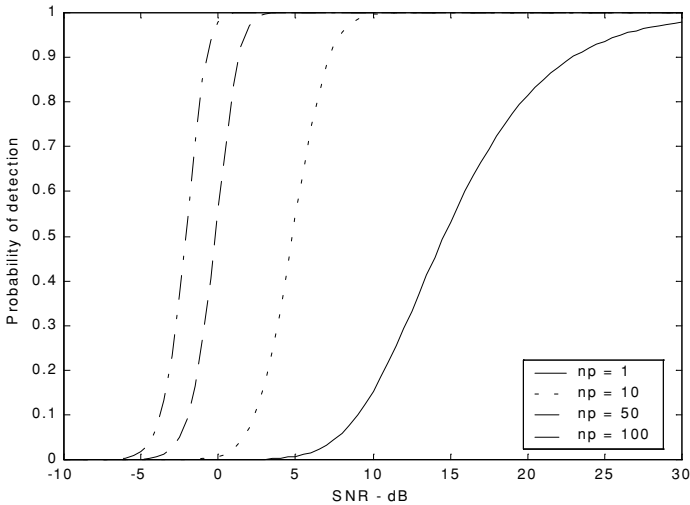


Figure 4.12. Probability of detection versus SNR. Swerling II. $P_{fa} = 10^{-9}$.

For $n_p > 2$ the expression is

$$P_D = \frac{V_T^{n_p-1} e^{-V_T}}{(1 + n_p SNR/2)(n_p - 2)!} + 1 - \Gamma_I(V_T, n_p - 1) + K_0 \Gamma_I\left(\frac{V_T}{1 + 2/n_p SNR}, n_p - 1\right) \quad (4.83)$$

MATLAB Function “pd_swerling3.m”

The function “pd_swerling3.m” calculates P_D for Swerling II type targets. It is given in Listing 4.11 in Section 4.10. The syntax is as follows:

$$[pd] = pd_swerling3(nfa, np, snr)$$

where

Symbol	Description	Units	Status
<i>nfa</i>	<i>Marcum’s false alarm number</i>	<i>none</i>	<i>input</i>
<i>np</i>	<i>number of integrated pulses</i>	<i>none</i>	<i>input</i>
<i>snr</i>	<i>SNR</i>	<i>dB</i>	<i>input</i>
<i>pd</i>	<i>probability of detection</i>	<i>none</i>	<i>output</i>

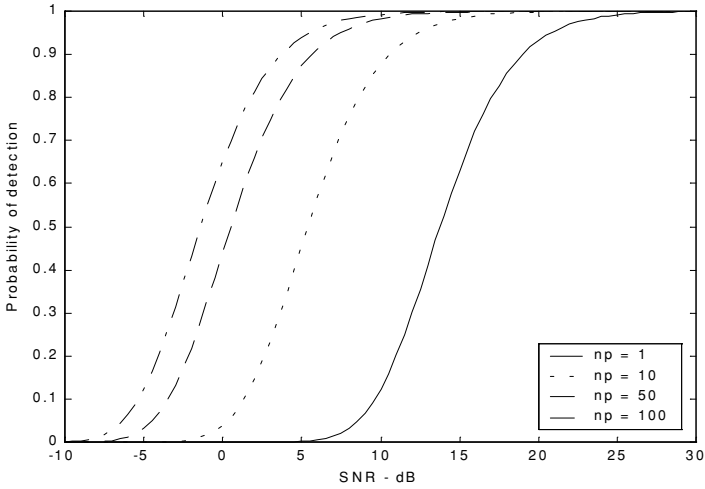


Figure 4.13. Probability of detection versus SNR. Swerling III. $P_{fa} = 10^{-9}$.

Fig. 4.13 shows a plot of the probability of detection as a function of SNR for $n_p = 1, 10, 50, 100$, where $P_{fa} = 10^{-9}$.

4.6.5. Detection of Swerling IV Targets

The expression for the probability of detection for Swerling IV targets for $n_p < 50$ is

$$P_D = 1 - \left[\gamma_0 + \left(\frac{SNR}{2} \right) n_p \gamma_1 + \left(\frac{SNR}{2} \right)^2 \frac{n_p (n_p - 1)}{2!} \gamma_2 + \dots + \left(\frac{SNR}{2} \right)^{n_p} \gamma_{n_p} \right] \left(1 + \frac{SNR}{2} \right)^{-n_p} \quad (4.84)$$

where

$$\gamma_i = \Gamma_I \left(\frac{V_T}{1 + (SNR)/2}, n_p + i \right) \quad (4.85)$$

By using the recursive formula

$$\Gamma_I(x, i + 1) = \Gamma_I(x, i) - \frac{x^i}{i! \exp(x)} \quad (4.86)$$

then only γ_0 needs to be calculated using Eq. (4.85) and the rest of γ_i are calculated from the following recursion:

$$\gamma_i = \gamma_{i-1} - A_i \quad ; i > 0 \quad (4.87)$$

$$A_i = \frac{V_T / (1 + (SNR) / 2)}{n_p + i - 1} A_{i-1} \quad ; i > 1 \quad (4.88)$$

$$A_1 = \frac{(V_T / (1 + (SNR) / 2))^{n_p}}{n_p! \exp(V_T / (1 + (SNR) / 2))} \quad (4.89)$$

$$\gamma_0 = \Gamma_I\left(\frac{V_T}{(1 + (SNR) / 2)}, n_p\right) \quad (4.90)$$

For the case when $n_p \geq 50$, the Gram-Charlier series and Eq. (4.70) can be used to calculate the probability of detection. In this case,

$$C_3 = \frac{1}{3\sqrt{n_p}} \frac{2\beta^3 - 1}{(2\beta^2 - 1)^{1.5}} \quad ; \quad C_6 = \frac{C_3^2}{2} \quad (4.91)$$

$$C_4 = \frac{1}{4n_p} \frac{2\beta^4 - 1}{(2\beta^2 - 1)^2} \quad (4.92)$$

$$\varpi = \sqrt{n_p(2\beta^2 - 1)} \quad (4.93)$$

$$\beta = 1 + \frac{SNR}{2} \quad (4.94)$$

MATLAB Function “pd_swerling4.m”

The function “pd_swerling4.m” calculates P_D for Swerling II type targets. It is given in Listing 4.12 in Section 4.10. The syntax is as follows:

$$[pd] = pd_swerling4(nfa, np, snr)$$

where

Symbol	Description	Units	Status
<i>nfa</i>	<i>Marcum's false alarm number</i>	<i>none</i>	<i>input</i>
<i>np</i>	<i>number of integrated pulses</i>	<i>none</i>	<i>input</i>
<i>snr</i>	<i>SNR</i>	<i>dB</i>	<i>input</i>
<i>pd</i>	<i>probability of detection</i>	<i>none</i>	<i>output</i>

Fig. 4.14 shows a plot of the probability of detection as a function of SNR for $n_p = 1, 10, 50, 100$, where $P_{fa} = 10^{-9}$.

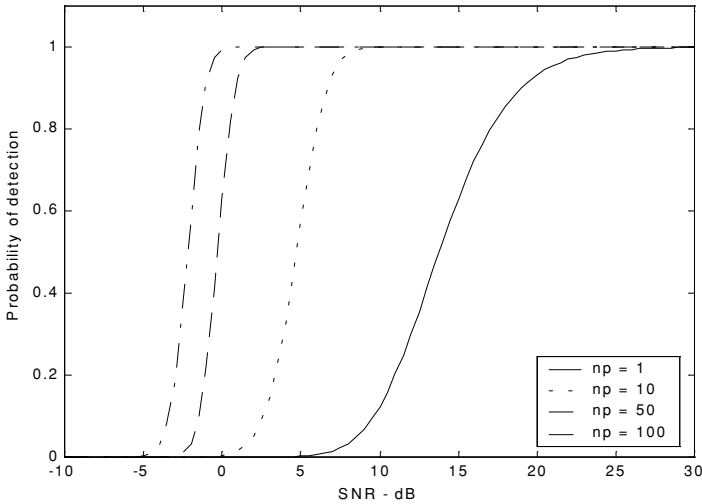


Figure 4.14. Probability of detection versus SNR. Swerling IV. $P_{fa} = 10^{-9}$.

4.7. Cumulative Probability of Detection

The cumulative probability of detection refers to detecting the target at least once by the time it is range R . More precisely, consider a target closing on a scanning radar, where the target is illuminated only during a scan (frame). As the target gets closer to the radar, its probability of detection increases since the SNR is also increased. Suppose that the probability of detection during the n th frame is P_{D_n} ; then, the cumulative probability of detecting the target at least once during the n th frame (see Fig. 4.15) is given by

$$P_{C_n} = 1 - \prod_{i=1}^n (1 - P_{D_i}) \quad (4.95)$$

P_{D_1} is usually selected to be very small. Clearly, the probability of not detecting the target during the n th frame is $1 - P_{C_n}$. The probability of detection for the i th frame, P_{D_i} , is computed as discussed in the previous section.

Example 4.3: A radar detects a closing target at $R = 10\text{Km}$, with probability of detection equal to 0.5. Assume $P_{fa} = 10^{-7}$. Compute and sketch the single look probability of detection as a function of normalized range (with respect to

$R = 10\text{Km}$), over the interval $(2 - 20)\text{Km}$. If the range between two successive frames is 1Km , what is the cumulative probability of detection at $R = 8\text{Km}$?

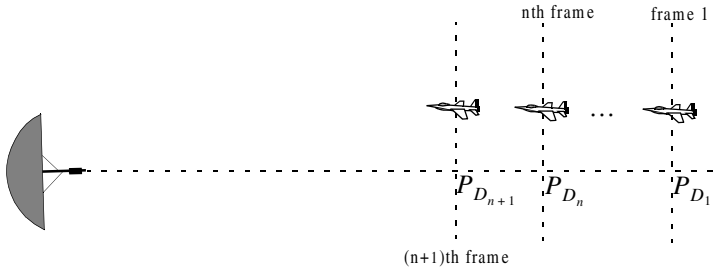


Figure 4.15. Detecting a target in many frames.

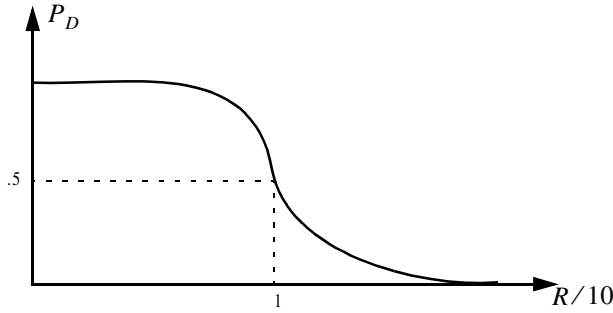
Solution: From the function “marcumsg.m” or from [Table 4.1](#) the SNR corresponding to $P_D = 0.5$ and $P_{fa} = 10^{-7}$ is approximately 12dB . By using a similar analysis to that which led to Eq. (4.68), we can express the SNR at any range R as

$$(SNR)_R = (SNR)_{10} + 40 \log \frac{10}{R} = 52 - 40 \log R$$

Then with the help of the function “marcumsg.m” we can construct the following table:

R Km	(SNR) dB	P_D
2	39.09	0.999
4	27.9	0.999
6	20.9	0.999
8	15.9	0.999
9	13.8	0.9
10	12.0	0.5
11	10.3	0.25
12	8.8	0.07
14	6.1	0.01
16	3.8	ϵ
20	0.01	ϵ

where ϵ is very small. Below is a sketch of P_D versus normalized range.



The cumulative probability of detection is given in Eq. (4.95), where the probability of detection of the first frame is selected to be very small. Thus, we can arbitrarily choose frame 1 to be at $R = 16\text{Km}$. Note that selecting a different starting point for frame 1 would have a negligible effect on the cumulative probability (we only need P_{D_1} to be very small). Below is a range listing for frames 1 through 9, where frame 9 corresponds to $R = 8\text{Km}$.

frame	1	2	3	4	5	6	7	8	9
range in Km	16	15	14	13	12	11	10	9	8

The cumulative probability of detection at 8 Km is then

$$P_{C_9} = 1 - (1 - 0.999)(1 - 0.9)(1 - 0.5)(1 - 0.25)(1 - 0.07)(1 - 0.01)(1 - \epsilon)^3 \approx 0.9998$$

4.8. Solving the Radar Equation

The radar equation was developed in Chapter 1. It is given by

$$R = \left(\frac{P_t \tau f_r T_i G_t G_r \lambda^2 \sigma}{(4\pi)^3 k T_e F L (SNR)_o} \right)^{\frac{1}{4}} \quad (4.96)$$

where P_t is peak transmitted power, τ is pulse width, f_r is PRF, T_i is dwell interval, G_t is transmitting antenna gain, G_r is receiving antenna gain, λ is wavelength, σ is target cross section, k is Boltzman's constant, T_e is effective noise temperature, F is system noise figure, L is total system losses, and $(SNR)_o$ is the minimum SNR required for detection.

Assuming that the radar parameters such as power, antenna gain, wavelength, losses, bandwidth, effective temperature, and noise figure are known, the steps one should follow to solve for range are shown in Fig. 4.16. Note that both sides of the bottom half of Fig. 4.16 are identical. Nevertheless, we purposely show two paths so that a distinction between scintillating and non-fluctuating targets is made.

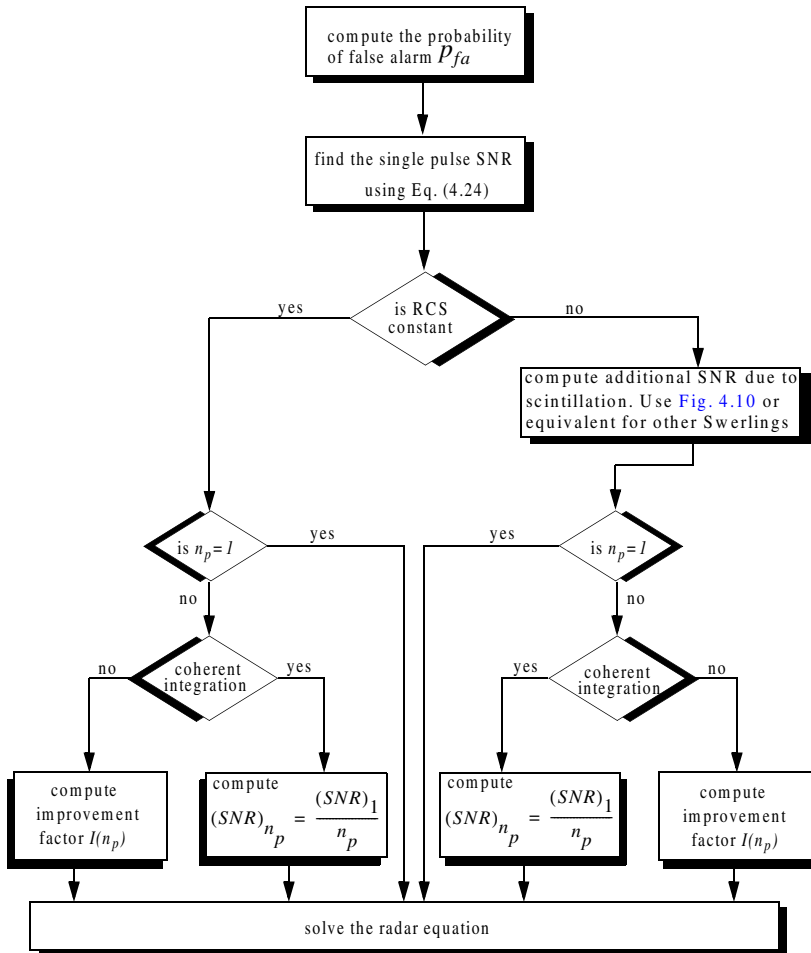


Figure 4.16. Solving the radar equation.

4.9. Constant False Alarm Rate (CFAR)

The detection threshold is computed so that the radar receiver maintains a constant pre-determined probability of false alarm. Eq. (4.19b) gives the relationship between the threshold value V_T and the probability of false alarm P_{fa} , and for convenience is repeated here as Eq. (4.97):

$$V_T = \sqrt{2\psi^2 \ln\left(\frac{1}{P_{fa}}\right)} \quad (4.97)$$

If the noise power ψ^2 is assumed to be constant, then a fixed threshold can satisfy Eq. (4.97). However, due to many reasons this condition is rarely true. Thus, in order to maintain a constant probability of false alarm the threshold value must be continuously updated based on the estimates of the noise variance. The process of continuously changing the threshold value to maintain a constant probability of false alarm is known as Constant False Alarm Rate (CFAR).

Three different types of CFAR processors are primarily used. They are adaptive threshold CFAR, nonparametric CFAR, and nonlinear receiver techniques. Adaptive CFAR assumes that the interference distribution is known and approximates the unknown parameters associated with these distributions. Nonparametric CFAR processors tend to accommodate unknown interference distributions. Nonlinear receiver techniques attempt to normalize the root mean square amplitude of the interference.

In this book only analog Cell-Averaging CFAR (CA-CFAR) technique is examined. The analysis presented in this section closely follows Urkowitz¹.

4.9.1. Cell-Averaging CFAR (Single Pulse)

The CA-CFAR processor is shown in Fig. 4.17. Cell averaging is performed on a series of range and/or Doppler bins (cells). The echo return for each pulse is detected by a square law detector. In analog implementation these cells are obtained from a tapped delay line. The Cell Under Test (CUT) is the central cell. The immediate neighbors of the CUT are excluded from the averaging process due to possible spillover from the CUT. The output of M reference cells ($M/2$ on each side of the CUT) is averaged. The threshold value is obtained by multiplying the averaged estimate from all reference cells by a constant K_0 (used for scaling). A detection is declared in the CUT if

$$Y_1 \geq K_0 Z \quad (4.98)$$

1. Urkowitz, H., Decision and Detection Theory, unpublished lecture notes. Lockheed Martin Co., Moorestown, NJ.

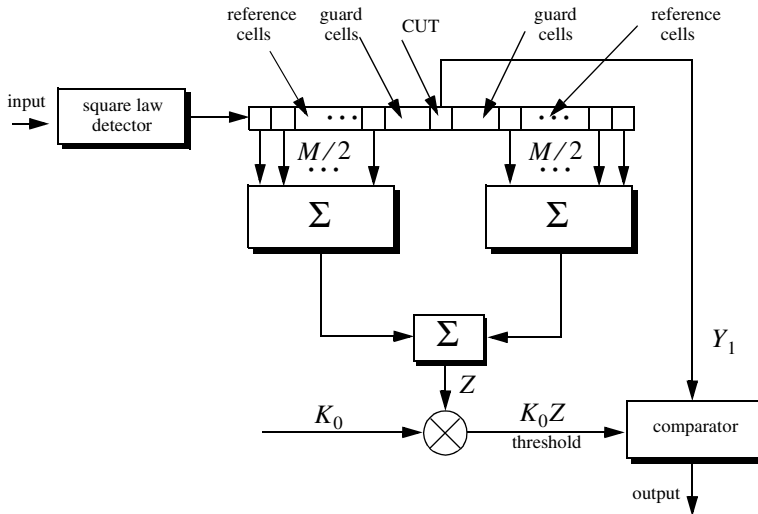


Figure 4.17. Conventional CA-CFAR.

Cell-averaging CFAR assumes that the target of interest is in the CUT and all reference cells contain zero mean independent Gaussian noise of variance ψ^2 . Therefore, the output of the reference cells, Z , represents a random variable with gamma probability density function (special case of the Chi-square) with $2M$ degrees of freedom. In this case, the gamma *pdf* is

$$f(z) = \frac{z^{(M/2)-1} e^{(-z/2\psi^2)}}{2^{M/2} \psi^M \Gamma(M/2)} \quad ; \quad z > 0 \quad (4.99)$$

The probability of false alarm corresponding to a fixed threshold was derived earlier. When CA-CFAR is implemented, then the probability of false alarm can be derived from the conditional false alarm probability, which is averaged over all possible values of the threshold in order to achieve an unconditional false alarm probability. The conditional probability of false alarm when $y = V_T$ can be written as

$$P_{fa}(V_T = y) = e^{-y/2\psi^2} \quad (4.100)$$

It follows that the unconditional probability of false alarm is

$$P_{fa} = \int_0^{\infty} P_{fa}(V_T = y) f(y) dy \quad (4.101)$$

where $f(y)$ is the *pdf* of the threshold, which except for the constant K_0 is the same as that defined in Eq. (4.99). Therefore,

$$f(y) = \frac{y^{M-1} e^{(-y/2K_0\Psi^2)}}{(2K_0\Psi^2)^M \Gamma(M)} \quad ; \quad y \geq 0 \quad (4.102)$$

Substituting Eqs. (4.102) and (4.100) into Eq. (4.101) yields

$$P_{fa} = \frac{1}{(1 + K_0)^M} \quad (4.103)$$

Observation of Eq. (4.103) shows that the probability of false alarm is now independent of the noise power, which is the objective of CFAR processing.

4.9.2. Cell-Averaging CFAR with Non-Coherent Integration

In practice, CFAR averaging is often implemented after non-coherent integration, as illustrated in Fig. 4.18. Now, the output of each reference cell is the sum of n_p squared envelopes. It follows that the total number of summed reference samples is Mn_p . The output Y_1 is also the sum of n_p squared envelopes. When noise alone is present in the CUT, Y_1 is random variable whose *pdf* is a gamma distribution with $2n_p$ degrees of freedom. Additionally, the summed output of the reference cells is the sum of Mn_p squared envelopes. Thus, Z is also a random variable who has a gamma *pdf* with $2Mn_p$ degrees of freedom.

The probability of false alarm is then equal to the probability that the ratio Y_1/Z exceeds the threshold. More precisely,

$$P_{fa} = Prob\{Y_1/Z > K_1\} \quad (4.104)$$

Eq. (4.104) implies that one must first find the joint *pdf* for the ratio Y_1/Z . However, this can be avoided if P_{fa} is first computed for a fixed threshold value V_T , then averaged over all possible value of the threshold. Therefore, let the conditional probability of false when $y = V_T$ be $P_{fa}(V_T = y)$. It follows that the unconditional false alarm probability is given by

$$P_{fa} = \int_0^{\infty} P_{fa}(V_T = y) f(y) dy \quad (4.105)$$

where $f(y)$ is the *pdf* of the threshold. In view of this, the probability density function describing the random variable $K_1 Z$ is given by

$$f(y) = \frac{(y/K_1)^{Mn_p-1} e^{(-y/2K_0\Psi^2)}}{(2\Psi^2)^{Mn_p} K_1 \Gamma(Mn_p)} \quad ; \quad y \geq 0 \quad (4.106)$$

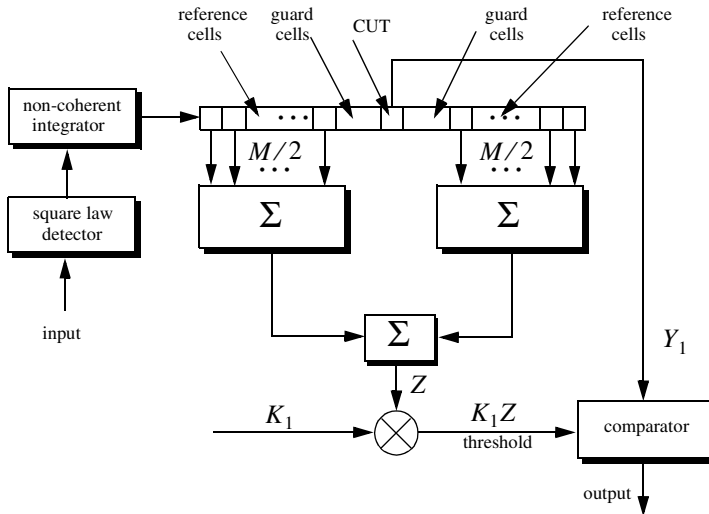


Figure 4.18. Conventional CA-CFAR with non-coherent integration.

It can be shown (see problems) that in this case the probability of false alarm is independent of the noise power and is given by

$$P_{fa} = \frac{1}{(1 + K_1)^{Mn_p}} \sum_{k=0}^{n_p - 1} \frac{1}{k!} \frac{\Gamma(Mn_p + k)}{\Gamma(Mn_p)} \left(\frac{K_1}{1 + K_1} \right)^k \quad (4.107)$$

which is identical to Eq. (4.103) when $K_1 = K_0$ and $n_p = 1$.

4.10. MATLAB Function and Program Listings

This section presents listings for all MATLAB programs/functions used in this chapter. The user is advised to rerun these programs with different input parameters. All functions have companion MATLAB “filename_driver.m” files that utilize MATLAB Graphical User Interface (GUI).

Listing 4.1. MATLAB Function “que_func.m”

```
function fofx = que_func(x)
% This function computes the value of the Q-function
% listed in Eq.(4.16). It uses the approximation in Eq.s (4.17) and (4.18)
if (x >= 0)
denom = 0.661 * x + 0.339 * sqrt(x^2 + 5.51);
```

```

expo = exp(-x^2 / 2.0);
fofx = 1.0 - (1.0 / sqrt(2.0 * pi)) * (1.0 / denom) * expo;
else
denom = 0.661 * x + 0.339 * sqrt(x^2 + 5.51);
expo = exp(-x^2 / 2.0);
value = 1.0 - (1.0 / sqrt(2.0 * pi)) * (1.0 / denom) * expo;
fofx = 1.0 - value;
end

```

Listing 4.2. MATLAB Function “marcumsq.m”

```

function PD = marcumsq (a,b)
% This function uses Parl's method to compute PD
max_test_value = 1000.; % increase to more than 1000 for better results
if (a < b)
    alphan0 = 1.0;
    dn = a / b;
else
    alphan0 = 0.;
    dn = b / a;
end
alphan_1 = 0.;
betan0 = 0.5;
betan_1 = 0.;
d1 = dn;
n = 0;
ratio = 2.0 / (a * b);
r1 = 0.0;
betan = 0.0;
alphan = 0.0;
while betan < max_test_value,
    n = n + 1;
    alphan = dn + ratio * n * alphan0 + alphan;
    betan = 1.0 + ratio * n * betan0 + betan;
    alphan_1 = alphan0;
    alphan0 = alphan;
    betan_1 = betan0;
    betan0 = betan;
    dn = dn * D1;
end
PD = (alphan0 / (2.0 * betan0)) * exp( -(a-b)^2 / 2.0);
if ( a >= b)
    PD = 1.0 - PD;
end
return

```

Listing 4.3. MATLAB Program “prob_snr1.m”

```
% This program is used to produce Fig. 4.3
clear all
for nfa = 2:2:12
    b = sqrt(-2.0 * log(10^(-nfa)));
    index = 0;
    hold on
    for snr = 0:.1:18
        index = index + 1;
        a = sqrt(2.0 * 10^(.1*snr));
        pro(index) = marcumsg(a,b);
    end
    x = 0:.1:18;
    set(gca,'ytick',[.1 .2 .3 .4 .5 .6 .7 .75 .8 .85 .9 .95 .9999])
    set(gca,'xtick',[1 2 3 4 5 6 7 8 9 10 11 12 13 14 15 16 17 18])

    loglog(x, pro,'k');
end
hold off
xlabel ('Single pulse SNR - dB')
ylabel ('Probability of detection')
grid
```

Listing 4.4. MATLAB Program “fig4_5.m”

```
% This program is used to produce Fig. 4.5
% It uses the function "improv_fac"
pfa1 = 1.0e-2;
pfa2 = 1.0e-6;
pfa3 = 1.0e-10;
pfa4 = 1.0e-13;
pd1 = .5;
pd2 = .8;
pd3 = .95;
pd4 = .999;
index = 0;
for np = 1:1:100
    index = index + 1;
    I1(index) = improv_fac (np, pfa1, pd1);
    I2(index) = improv_fac (np, pfa2, pd2);
    I3(index) = improv_fac (np, pfa3, pd3);
    I4(index) = improv_fac (np, pfa4, pd4);
end
np = 1:1:100;
semilogx (np, I1, 'k', np, I2, 'k--', np, I3, 'k-', np, I4, 'k:')
set (gca,'xtick',[1 2 3 4 5 6 7 8 10 20 30 50 70 100]);
xlabel ('Number of pulses');
```

```
ylabel ('Improvement factor I - dB')
legend ('pd=.5, nfa=2','pd=.8, nfa=6','pd=.95, nfa=10','pd=.999, nfa=13');
```

Listing 4.5. MATLAB Function “improv_fac.m”

```
function impr_of_np = improv_fac (np, pfa, pd)
% This function computes the non-coherent integration improvement
% factor using the empirical formula defined in Eq. (4.49)
fact1 = 1.0 + log10( 1.0 / pfa) / 46.6;
fact2 = 6.79 * (1.0 + 0.253 * pd);
fact3 = 1.0 - 0.14 * log10(np) + 0.0183 * (log10(np)^2);
impr_of_np = fact1 * fact2 * fact3 * log10(np);
return
```

Listing 4.6. MATLAB Function “incomplete_gamma.m”

```
function [value] = incomplete_gamma ( vt, np)
% This function implements Eq. (4.63) to compute the Incomplete Gamma Function
format long
eps = 1.000000001;
% Test to see if np = 1
if (np == 1)
    value1 = vt * exp(-vt);
    value = 1.0 - exp(-vt);
    return
end
sumold = 1.0;
sumnew =1.0;
calc1 = 1.0;
calc2 = np;
xx = np * log(vt) - vt - factor(calc2);
temp1 = exp(xx);
temp2 = np / vt;
diff = .0;
ratio = 1000.0;
if (vt >= np)
    while (ratio >= eps)
        diff = diff + 1.0;
        calc1 = calc1 * (calc2 - diff) / vt ;
        sumnew = sumold + calc1;
        ratio = sumnew / sumold;
        sumold = sumnew;
    end
    value = 1.0 - temp1 * sumnew * temp2;
    return
else
    diff = 0.;
    sumold = 1.;
```



```

ratio = 1000.;
calc1 = 1.;
while(ratio >= eps)
    diff = diff + 1.0;
    calc1 = calc1 * vt / (calc2 + diff);
    sumnew = sumold + calc1;
    ratio = sumnew / sumold;
    sumold = sumnew;
end
value = temp1 * sumnew;
end

```

Listing 4.7. MATLAB Function “threshold.m”

```

function [pfa, vt] = threshold (nfa, np)
% This function calculates the threshold value from nfa and np.
% The newton-Raphson recursive formula is used (Eq. (4.59)
% This function uses "incomplete_gamma.m".
delmax = .00001;
eps = 0.000000001;
delta =10000.;
pfa = np * log(2) / nfa;
sqrtpfa = sqrt(-log10(pfa));
sqrtnp = sqrt(np);
vt0 = np - sqrtnp + 2.3 * sqrtpfa * (sqrtpfa + sqrtnp - 1.0);
vt = vt0;
while (abs(delta) >= vt0)
    igf = incomplete_gamma(vt0,np);
    num = 0.5^(np/nfa) - igf;
    temp = (np-1) * log(vt0+eps) - vt0 - factor(np-1);
    deno = exp(temp);
    vt = vt0 + (num / deno);
    delta = abs(vt - vt0) * 10000.0;
    vt0 = vt;
end

```

Listing 4.8. MATLAB Function “pd_swerling5.m”

```

function pd = pd_swerling5 (input1, indicator, np, snrbar)
% This function is used to calculate the probability of
% for Swerling 5 or 0 targets for np>1.
if(np == 1)
    'Stop, np must be greater than 1'
    return
end
format long
snrbar = 10.0^(snrbar/10.);
eps = 0.00000001;

```

```

delmax = .00001;
delta =10000.;
% Calculate the threshold Vt
if (indicator ~=1)
    nfa = input1;
    pfa = np * log(2) / nfa;
else
    pfa = input1;
    nfa = np * log(2) / pfa;
end
sqrtpfa = sqrt(-log10(pfa));
sqrtnp = sqrt(np);
vt0 = np - sqrtnp + 2.3 * sqrtpfa * (sqrtpfa + sqrtnp - 1.0);
vt = vt0;
while (abs(delta) >= vt0)
    igf = incomplete_gamma(vt0,np);
    num = 0.5^(np/nfa) - igf;
    temp = (np-1) * log(vt0+eps) - vt0 - factor(np-1);
    deno = exp(temp);
    vt = vt0 + (num / (deno+eps));
    delta = abs(vt - vt0) * 10000.0;
    vt0 = vt;
end
% Calculate the Gram-Chrlier coefficients
temp1 = 2.0 * snrbar + 1.0;
omegabar = sqrt(np * temp1);
c3 = -(snrbar + 1.0 / 3.0) / (sqrt(np) * temp1^1.5);
c4 = (snrbar + 0.25) / (np * temp1^2.);
c6 = c3 * c3 / 2.0;
V = (vt - np * (1.0 + 2.*snrbar)) / omegabar;
Vsqr = V * V;
val1 = exp(-Vsqr / 2.0) / sqrt( 2.0 * pi);
val2 = c3 * (V^2 -1.0) + c4 * V * (3.0 - V^2) -...
    c6 * V * (V^4 - 10. * V^2 + 15.0);
q = 0.5 * erfc (V/sqrt(2.0));
pd = q - val1 * val2;

```

Listing 4.9. MATLAB Function “pd_swerling1.m”

```

function pd = pd_swerling1 (nfa, np, snrbar)
% This function is used to calculate the probability of
% for Swerling 1 targets.
format long
snrbar = 10.0^(snrbar/10.);
eps = 0.00000001;
delmax = .00001;
delta =10000.;
% Calculate the threshold Vt

```

```

pfa = np * log(2) / nfa;
sqrtpfa = sqrt(-log10(pfa));
sqrtnp = sqrt(np);
vt0 = np - sqrtnp + 2.3 * sqrtpfa * (sqrtpfa + sqrtnp - 1.0);
vt = vt0;
while (abs(delta) >= vt0)
    igf = incomplete_gamma(vt0,np);
    num = 0.5^(np/nfa) - igf;
    temp = (np-1) * log(vt0+eps) - vt0 - factor(np-1);
    deno = exp(temp);
    vt = vt0 + (num / (deno+eps));
    delta = abs(vt - vt0) * 10000.0;
    vt0 = vt;
end
if (np == 1)
    temp = -vt / (1.0 + snrbar);
    pd = exp(temp);
    return
end
temp1 = 1.0 + np * snrbar;
temp2 = 1.0 / (np * snrbar);
temp = 1.0 + temp2;
val1 = temp^(np-1.);
igf1 = incomplete_gamma(vt,np-1);
igf2 = incomplete_gamma(vt/temp,np-1);
pd = 1.0 - igf1 + val1 * igf2 * exp(-vt/temp1);

```

Listing 4.10. MATLAB Function “pd_swering2.m”

```

function pd = pd_swering2 (nfa, np, snrbar)
% This function is used to calculate the probability of
% for Swerling 2 targets.
format long
snrbar = 10.0^(snrbar/10.);
eps = 0.00000001;
delmax = .00001;
delta =10000.;
% Calculate the threshold Vt
pfa = np * log(2) / nfa;
sqrtpfa = sqrt(-log10(pfa));
sqrtnp = sqrt(np);
vt0 = np - sqrtnp + 2.3 * sqrtpfa * (sqrtpfa + sqrtnp - 1.0);
vt = vt0;
while (abs(delta) >= vt0)
    igf = incomplete_gamma(vt0,np);
    num = 0.5^(np/nfa) - igf;
    temp = (np-1) * log(vt0+eps) - vt0 - factor(np-1);
    deno = exp(temp);

```

```

    vt = vt0 + (num / (deno+eps));
    delta = abs(vt - vt0) * 10000.0;
    vt0 = vt;
end
if (np <= 50)
    temp = vt / (1.0 + snrbar);
    pd = 1.0 - incomplete_gamma(temp,np);
    return
else
    temp1 = snrbar + 1.0;
    omegabar = sqrt(np) * temp1;
    c3 = -1.0 / sqrt(9.0 * np);
    c4 = 0.25 / np;
    c6 = c3 * c3 / 2.0;
    V = (vt - np * temp1) / omegabar;
    Vsqr = V * V;
    val1 = exp(-Vsqr / 2.0) / sqrt( 2.0 * pi);
    val2 = c3 * (V^2 - 1.0) + c4 * V * (3.0 - V^2) - ...
        c6 * V * (V^4 - 10. * V^2 + 15.0);
    q = 0.5 * erfc (V/sqrt(2.0));
    pd = q - val1 * val2;
end

```

Listing 4.11. MATLAB Function “pd_swerling3.m”

```

function pd = pd_swerling3 (nfa, np, snrbar)
% This function is used to calculate the probability of
% for Swerling 2 targets.
format long
snrbar = 10.0^(snrbar/10.);
eps = 0.00000001;
delmax = .00001;
delta =10000.;
% Calculate the threshold Vt
pfa = np * log(2) / nfa;
sqrtpfa = sqrt(-log10(pfa));
sqrtnp = sqrt(np);
vt0 = np - sqrtnp + 2.3 * sqrtpfa * (sqrtpfa + sqrtnp - 1.0);
vt = vt0;
while (abs(delta) >= vt0)
    igf = incomplete_gamma(vt0,np);
    num = 0.5^(np/nfa) - igf;
    temp = (np-1) * log(vt0+eps) - vt0 - factor(np-1);
    deno = exp(temp);
    vt = vt0 + (num / (deno+eps));
    delta = abs(vt - vt0) * 10000.0;
    vt0 = vt;
end

```

```

temp1 = vt / (1.0 + 0.5 * np * snrbar);
temp2 = 1.0 + 2.0 / (np * snrbar);
temp3 = 2.0 * (np - 2.0) / (np * snrbar);
ko = exp(-temp1) * temp2^(np-2.) * (1.0 + temp1 - temp3);
if (np <= 2)
    pd = ko;
    return
else
    temp4 = vt^(np-1.) * exp(-vt) / (temp1 * exp(factor(np-2.)));
    temp5 = vt / (1.0 + 2.0 / (np * snrbar));
    pd = temp4 + 1.0 - incomplete_gamma(vt,np-1.) + ko * ...
        incomplete_gamma(temp5,np-1.);
end

```

Listing 4.12. MATLAB Function “pd_swerling4.m”

```

function pd = pd_swerling4(nfa, np, snrbar)
% This function is used to calculate the probability of
% for Swerling 2 targets.
format long
snrbar = 10.0^(snrbar/10.);
eps = 0.00000001;
delmax = .00001;
delta = 10000.;
% Calculate the threshold Vt
pfa = np * log(2) / nfa;
sqrtpfa = sqrt(-log10(pfa));
sqrtnp = sqrt(np);
vt0 = np - sqrtnp + 2.3 * sqrtpfa * (sqrtpfa + sqrtnp - 1.0);
vt = vt0;
while (abs(delta) >= vt0)
    igf = incomplete_gamma(vt0,np);
    num = 0.5^(np/nfa) - igf;
    temp = (np-1) * log(vt0+eps) - vt0 - factor(np-1);
    deno = exp(temp);
    vt = vt0 + (num / (deno+eps));
    delta = abs(vt - vt0) * 10000.0;
    vt0 = vt;
end
h8 = snrbar / 2.0;
beta = 1.0 + h8;
beta2 = 2.0 * beta^2 - 1.0;
beta3 = 2.0 * beta^3;
if (np >= 50)
    temp1 = 2.0 * beta - 1;
    omegabar = sqrt(np * temp1);
    c3 = (beta3 - 1.) / 3.0 / beta2 / omegabar;
    c4 = (beta3 * beta3 - 1.0) / 4. / np / beta2 / beta2;;

```

```

c6 = c3 * c3 / 2.0;
V = (vt - np * (1.0 + snrbar)) / omegabar;
Vsqr = V * V;
val1 = exp(-Vsqr / 2.0) / sqrt( 2.0 * pi);
val2 = c3 * (V^2 - 1.0) + c4 * V * (3.0 - V^2) - ...
    c6 * V * (V^4 - 10. * V^2 + 15.0);
q = 0.5 * erfc (V/sqrt(2.0));
pd = q - val1 * val2;
return
else
snr = 1.0;
gamma0 = incomplete_gamma(vt/beta,np);
a1 = (vt / beta)^np / (exp(factor(np)) * exp(vt/beta));
sum = gamma0;
for i = 1:1:np
    temp1 = 1;
    if (i == 1)
        ai = a1;
    else
        ai = (vt / beta) * a1 / (np + i - 1);
    end
    a1 = ai;
    gammai = gamma0 - ai;
    gamma0 = gammai;
    a1 = ai;

    for ii = 1:1:i
        temp1 = temp1 * (np + 1 - ii);
    end
    term = (snrbar / 2.0)^i * gammai * temp1 / exp(factor(i));
    sum = sum + term;
end
pd = 1.0 - sum / beta^np;
end
pd = max(pd,0.);

```

Problems

4.1. In the case of noise alone, the quadrature components of a radar return are independent Gaussian random variables with zero mean and variance ψ^2 . Assume that the radar processing consists of envelope detection followed by threshold decision. (a) Write an expression for the *pdf* of the envelope; (b) determine the threshold V_T as a function of ψ that ensures a probability of false alarm $P_{fa} \leq 10^{-8}$.

4.2. (a) Derive Eq. (4.13); (b) derive Eq. (4.15).

4.3. A pulsed radar has the following specifications: time of false alarm $T_{fa} = 10 \text{ minutes}$, probability of detection $P_D = 0.95$, operating bandwidth $B = 1\text{MHz}$. (a) What is the probability of false alarm P_{fa} ? (b) What is the single pulse SNR? (c) Assuming non-coherent integration of 100 pulses, what is the SNR reduction so that P_D and P_{fa} remain unchanged?

4.4. An L-band radar has the following specifications: operating frequency $f_0 = 1.5\text{GHz}$, operating bandwidth $B = 2\text{MHz}$, noise figure $F = 8\text{dB}$, system losses $L = 4\text{dB}$, time of false alarm $T_{fa} = 12 \text{ minutes}$, detection range $R = 12\text{Km}$, probability of detection $P_D = 0.5$, antenna gain $G = 5000$, and target RCS $\sigma = 1\text{m}^2$. (a) Determine the PRF f_r , the pulse width τ , the peak power P_t , the probability of false alarm P_{fa} , and the minimum detectable signal level S_{min} . (b) How can you reduce the transmitter power to achieve the same performance when 10 pulses are integrated non-coherently? (c) If the radar operates at a shorter range in the single pulse mode, find the new probability of detection when the range decreases to 9Km .

4.5. (a) Show how you can use the radar equation to determine the PRF f_r , the pulse width τ , the peak power P_t , the probability of false alarm P_{fa} , and the minimum detectable signal level S_{min} . Assume the following specifications: operating frequency $f_0 = 1.5\text{MHz}$, operating bandwidth $B = 1\text{MHz}$, noise figure $F = 10\text{dB}$, system losses $L = 5\text{dB}$, time of false alarm $T_{fa} = 20 \text{ minutes}$, detection range $R = 12\text{Km}$, probability of detection $P_D = 0.5$ (three pulses). (b) If post detection integration is assumed, determine the SNR.

4.6. Show that when computing the probability of detection at the output of an envelope detector, it is possible to use Gaussian probability approximation when the SNR is very large.

4.7. A radar system uses a threshold detection criterion. The probability of false alarm $P_{fa} = 10^{-10}$. (a) What must be the average SNR at the input of a linear detector so that the probability of miss is $P_m = 0.15$? Assume large SNR approximation (see Problem 4.6). (b) Write an expression for the *pdf* at the output of the envelope detector.

- 4.8.** An X-band radar has the following specifications: received peak power $10^{-10}W$, probability of detection $P_D = 0.95$, time of false alarm $T_{fa} = 8 \text{ minutes}$, pulse width $\tau = 2\mu s$, operating bandwidth $B = 2MHz$, operating frequency $f_0 = 10GHz$, and detection range $R = 100Km$. Assume single pulse processing. (a) Compute the probability of false alarm P_{fa} . (b) Determine the SNR at the output of the IF amplifier. (c) At what SNR would the probability of detection drop to 0.9 (P_{fa} does not change)? (d) What is the increase in range that corresponds to this drop in the probability of detection?
- 4.9.** A certain radar utilizes 10 pulses for non-coherent integration. The single pulse SNR is $15dB$ and the probability of miss is $P_m = 0.15$. (a) Compute the probability of false alarm P_{fa} . (b) Find the threshold voltage V_T .
- 4.10.** Consider a scanning low PRF radar. The antenna half-power beam width is 1.5° , and the antenna scan rate is 35° per second. The pulse width is $\tau = 2\mu s$, and the PRF is $f_r = 400Hz$. (a) Compute the radar operating bandwidth. (b) Calculate the number of returned pulses from each target illumination. (c) Compute the SNR improvement due to post-detection integration (assume 100% efficiency). (d) Find the number of false alarms per minute for a probability of false alarm $P_{fa} = 10^{-6}$.
- 4.11.** Using the equation

$$P_D = 1 - e^{-SNR} \int_{P_{fa}}^1 I_0(\sqrt{4SNR \ln u}) du$$

calculate P_D when $SNR = 10dB$ and $P_{fa} = 0.01$. Perform the integration numerically.

- 4.12.** Repeat Example 4.3 with $P_D = 0.8$ and $P_{fa} = 10^{-5}$.
- 4.13.** Derive Eq. (4.107).
- 4.14.** Write a MATLAB program to compute the CA-CFAR threshold value. Use similar approach to that used in the case of a fixed threshold.
- 4.15.** A certain radar has the following specifications: single pulse SNR corresponding to a reference range $R_0 = 200Km$ is $10dB$. The probability of detection at this range is $P_D = 0.95$. Assume a Swerling I type target. Use the radar equation to compute the required pulse widths at ranges $R = 220Km, 250Km, 175Km$ so that the probability of detection is maintained.

- 4.16. Repeat Problem 4.15 for swerling IV type target.
- 4.17. Utilizing the MATLAB functions presented in this chapter, plot the actual value for the improvement factor versus the number of integrated pulses. Pick three different values for the probability of false alarm.
- 4.18. Reproduce [Fig. 4.10](#) for Swerling II, III, and IV type targets.
- 4.19. Develop a MATLAB program to calculate the cumulative probability of detection.

Choosing a particular waveform type and a signal processing technique in a radar system depends heavily on the radar's specific mission and role. The cost and complexity associated with a certain type of waveform hardware and software implementation constitute a major factor in the decision process. Radar systems can use Continuous Waveforms (CW) or pulsed waveforms with or without modulation. Modulation techniques can be either analog or digital. Range and Doppler resolutions are directly related to the specific waveform frequency characteristics. Thus, knowledge of the power spectrum density of a waveform is very critical. In general, signals or waveforms can be analyzed using time domain or frequency domain techniques. This chapter introduces many of the most commonly used radar waveforms. Relevant uses of a specific waveform will be addressed in the context of its time and frequency domain characteristics. In this book, the terms waveform and signal are being used interchangeably to mean the same thing.

5.1. Low Pass, Band Pass Signals and Quadrature Components

Signals that contain significant frequency composition at a low frequency band that includes DC are called Low Pass (LP) signals. Signals that have significant frequency composition around some frequency away from the origin are called Band Pass (BP) signals. A real BP signal $x(t)$ can be represented mathematically by

$$x(t) = r(t) \cos(2\pi f_0 t + \psi_x(t)) \quad (5.1)$$

where $r(t)$ is the amplitude modulation or envelope, $\psi_x(t)$ is the phase modulation, f_0 is the carrier frequency, and both $r(t)$ and $\psi_x(t)$ have frequency components significantly smaller than f_0 . The frequency modulation is

$$f_m(t) = \frac{1}{2\pi} \frac{d}{dt} \psi_x(t) \quad (5.2)$$

and the instantaneous frequency is

$$f_i(t) = \frac{1}{2\pi} \frac{d}{dt} (2\pi f_0 t + \psi_x(t)) = f_0 + f_m(t) \quad (5.3)$$

If the signal bandwidth is B , and if f_0 is very large compared to B , the signal $x(t)$ is referred to as a narrow band pass signal.

Band pass signals can also be represented by two low pass signals known as the quadrature components; in this case Eq. (5.1) can be rewritten as

$$x(t) = x_I(t) \cos 2\pi f_0 t - x_Q(t) \sin 2\pi f_0 t \quad (5.4)$$

where $x_I(t)$ and $x_Q(t)$ are real LP signals referred to as the quadrature components and are given, respectively, by

$$\begin{aligned} x_I(t) &= r(t) \cos \psi_x(t) \\ x_Q(t) &= r(t) \sin \psi_x(t) \end{aligned} \quad (5.5)$$

Fig. 5.1 shows how the quadrature components are extracted.

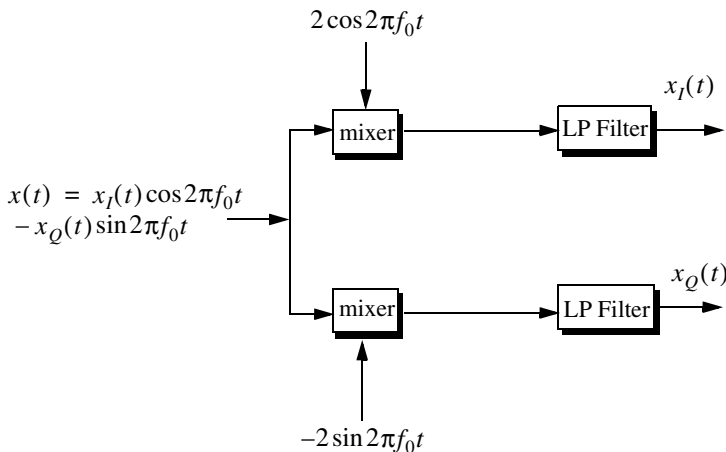


Figure 5.1. Extraction of quadrature components.

5.2. CW and Pulsed Waveforms

The spectrum of a given signal describes the spread of its energy in the frequency domain. An energy signal (finite energy) can be characterized by its Energy Spectrum Density (ESD) function, while a power signal (finite power) is characterized by the Power Spectrum Density (PSD) function. The units of the ESD are Joules per Hertz, while the PSD has units Watts per Hertz.

The signal bandwidth is the range of frequency over which the signal has a nonzero spectrum. In general, any signal can be defined using its duration (time domain) and bandwidth (frequency domain). A signal is said to be band-limited if it has finite bandwidth. Signals that have finite durations (time-limited) will have infinite bandwidths, while band-limited signals have infinite durations. The extreme case is being a continuous sine wave, whose bandwidth is infinitesimal.

A time domain signal $f(t)$ has a Fourier Transform (FT) $F(\omega)$ given by

$$F(\omega) = \int_{-\infty}^{\infty} f(t)e^{-j\omega t} dt \quad (5.6)$$

where the Inverse FT (IFT) is

$$f(t) = \frac{1}{2\pi} \int_{-\infty}^{\infty} F(\omega)e^{j\omega t} d\omega \quad (5.7)$$

The signal autocorrelation function $R_f(\tau)$ is

$$R_f(\tau) = \int_{-\infty}^{\infty} f^*(t)f(t+\tau) dt \quad (5.8)$$

The asterisk indicates complex conjugate. The signal amplitude spectrum is $|F(\omega)|$. If $f(t)$ were an energy signal, then its ESD is $|F(\omega)|^2$; and if it were a power signal, then its PSD is $S_f(\omega)$ which is the FT of the autocorrelation function,

$$\bar{S}_f(\omega) = \int_{-\infty}^{\infty} \bar{R}_f(\tau)e^{-j\omega\tau} d\tau \quad (5.9)$$

First, consider a CW waveform given by

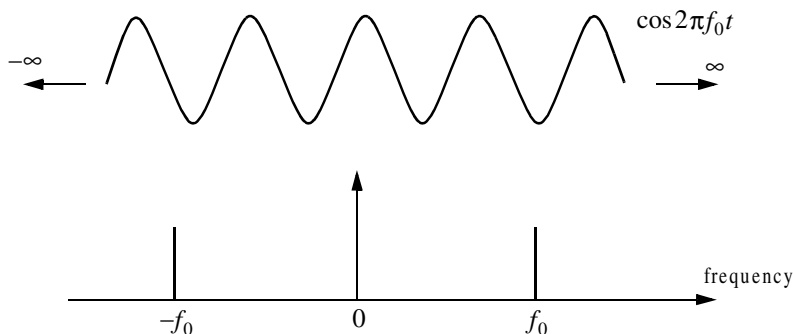


Figure 5.2. Amplitude spectrum for a continuous sine wave.

$$f_1(t) = A \cos \omega_0 t \quad (5.10)$$

The FT of $f_1(t)$ is

$$F_1(\omega) = A\pi[\delta(\omega - \omega_0) + \delta(\omega + \omega_0)] \quad (5.11)$$

where $\delta(\cdot)$ is the Dirac delta function, and $\omega_0 = 2\pi f_0$. As indicated by the amplitude spectrum shown in Fig. 5.2, the signal $f_1(t)$ has infinitesimal bandwidth, located at $\pm f_0$.

Next consider the time domain signal $f_2(t)$ given by

$$f_2(t) = A \text{Rect}\left(\frac{t}{\tau}\right) = \begin{cases} A & -\frac{\tau}{2} \leq t \leq \frac{\tau}{2} \\ 0 & \text{otherwise} \end{cases} \quad (5.12)$$

It follows that the FT is

$$F_2(\omega) = A\tau \text{Sinc}\left(\frac{\omega\tau}{2}\right) \quad (5.13)$$

where

$$\text{Sinc}(x) = \frac{\sin(\pi x)}{\pi x} \quad (5.14)$$

The amplitude spectrum of $f_2(t)$ is shown in Fig. 5.3. In this case, the bandwidth is infinite. Since infinite bandwidths cannot be physically implemented, the signal bandwidth is approximated by $2\pi/\tau$ radians per second or $1/\tau$ Hertz. In practice, this approximation is widely accepted since it accounts for most of the signal energy.

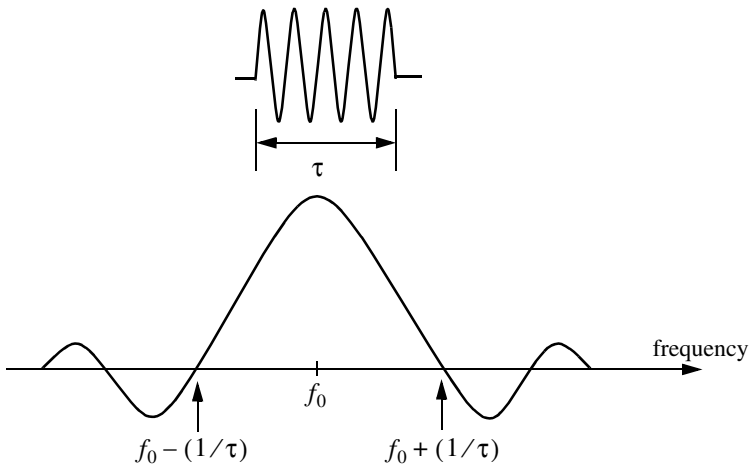


Figure 5.3. Amplitude spectrum for a single pulse, or a train of non-coherent pulses.

Now consider the coherent gated CW waveform $f_3(t)$ given by

$$f_3(t) = \sum_{n=-\infty}^{\infty} f_2(t - nT) \quad (5.15)$$

Clearly $f_3(t)$ is periodic, where T is the period (recall that $f_r = 1/T$ is the PRF). Using the complex exponential Fourier series we can rewrite $f_3(t)$ as

$$f_3(t) = \sum_{n=-\infty}^{\infty} F_n e^{j\frac{2\pi n t}{T}} \quad (5.16)$$

where the Fourier series coefficients F_n are given by

$$F_n = \frac{A\tau}{T} \text{Sinc}\left(\frac{n\tau\pi}{T}\right) \quad (5.17)$$

It follows that the FT of $f_3(t)$ is

$$F_3(\omega) = 2\pi \sum_{n=-\infty}^{\infty} F_n \delta(\omega - 2n\pi f_r) \quad (5.18)$$

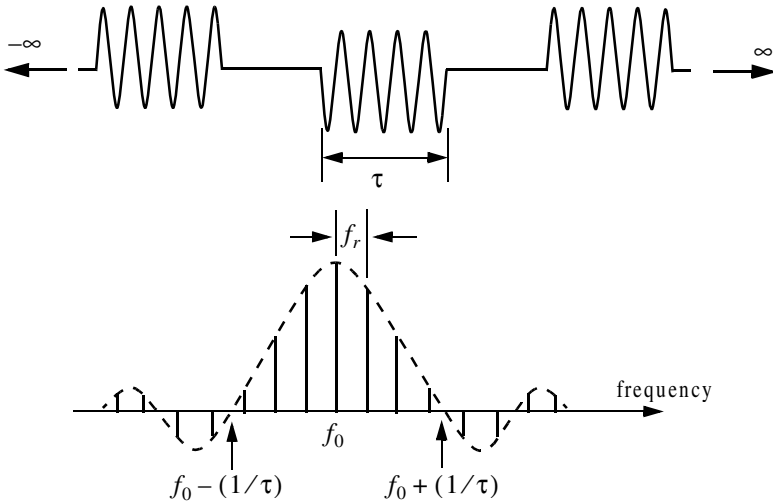


Figure 5.4. Amplitude spectrum for a coherent pulse train of infinite length.

The amplitude spectrum of $f_3(t)$ is shown in Fig. 5.4. In this case, the spectrum has a $\text{sinc}(x)$ envelope that corresponds to F_n . The spacing between the spectral lines is equal to the radar PRF, f_r .

Finally, define the function $f_4(t)$ as

$$f_4(t) = \sum_{n=0}^N f_2(t - nT) \quad (5.19)$$

Note that $f_4(t)$ is a limited duration $f_3(t)$. The FT of $f_4(t)$ is

$$F_4(\omega) = AN\tau \left(\text{Sinc}\left(\frac{\omega NT}{2}\right) \bullet \sum_{n=-\infty}^{\infty} \text{Sinc}(n\pi\tau f_r) \delta(\omega - 2n\pi f_r) \right) \quad (5.20)$$

where the operator (\bullet) indicates convolution. The spectrum in this case is shown in Fig. 5.5. The envelope is still a $\text{sinc}(x)$ which corresponds to the pulse width. But the spectral lines are replaced by $\text{sinc}(x)$ spectra that correspond to the duration NT .

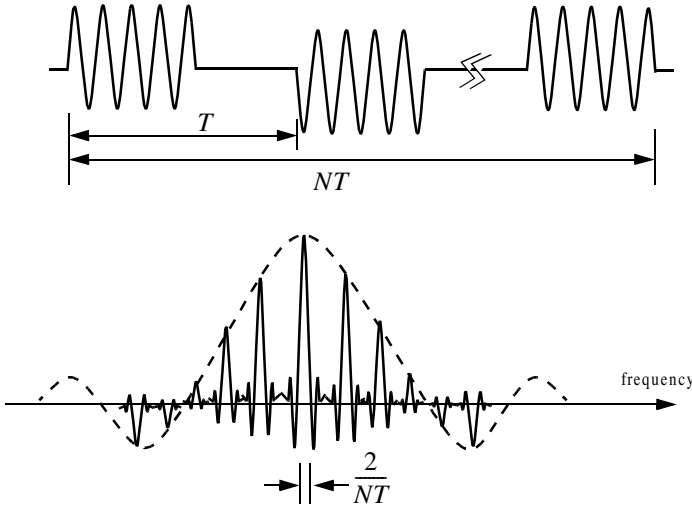


Figure 5.5. Amplitude spectrum for a coherent pulse train of finite length.

5.3. Linear Frequency Modulation Waveforms

Frequency or phase modulated waveforms can be used to achieve much wider operating bandwidths. Linear Frequency Modulation (LFM) is commonly used. In this case, the frequency is swept linearly across the pulse width, either upward (up-chirp) or downward (down-chirp). The matched filter bandwidth is proportional to the sweep bandwidth, and is independent of the pulse width. Fig. 5.6 shows a typical example of an LFM waveform. The pulse width is τ , and the bandwidth is B .

The LFM up-chirp instantaneous phase can be expressed by

$$\psi(t) = 2\pi\left(f_0 t + \frac{\mu}{2} t^2\right) \quad -\frac{\tau}{2} \leq t \leq \frac{\tau}{2} \quad (5.21)$$

where f_0 is the radar center frequency, and $\mu = (2\pi B)/\tau$ is the LFM coefficient. Thus, the instantaneous frequency is

$$f(t) = \frac{1}{2\pi} \frac{d}{dt} \psi(t) = f_0 + \mu t \quad -\frac{\tau}{2} \leq t \leq \frac{\tau}{2} \quad (5.22)$$

Similarly, the down-chirp instantaneous phase and frequency are given, respectively, by

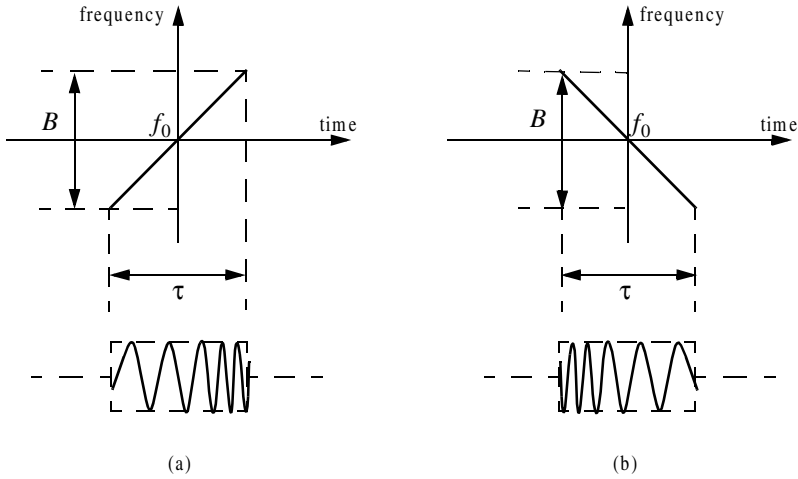


Figure 5.6. Typical LFM waveforms. (a) up-chirp; (b) down-chirp.

$$\psi(t) = 2\pi\left(f_0 t - \frac{\mu}{2} t^2\right) \quad -\frac{\tau}{2} \leq t \leq \frac{\tau}{2} \quad (5.23)$$

$$f(t) = \frac{1}{2\pi} \frac{d}{dt} \psi(t) = f_0 - \mu t \quad -\frac{\tau}{2} \leq t \leq \frac{\tau}{2} \quad (5.24)$$

A typical LFM waveform can be expressed in complex notation by

$$s_1(t) = \text{Rect}\left(\frac{t}{\tau}\right) e^{j2\pi\left(f_0 t + \frac{\mu}{2} t^2\right)} \quad (5.25)$$

where $\text{Rect}(t/\tau)$ denotes a rectangular pulse of width τ . Eq. (5.25) can be written as

$$s_1(t) = e^{j2\pi f_0 t} s(t) \quad (5.26)$$

where

$$s(t) = \text{Rect}\left(\frac{t}{\tau}\right) e^{j\pi\mu t^2} \quad (5.27)$$

is the complex envelope function of $s_1(t)$.

The spectrum of the signal $s_1(t)$ is determined from its complex envelope $s(t)$. The complex exponential term in Eq. (5.26) introduces a frequency shift about the center frequency f_0 . Taking the FT of $s(t)$ yields

$$S(\omega) = \int_{-\infty}^{\infty} \text{Rect}\left(\frac{t}{\tau}\right) e^{j\pi\mu t^2} e^{-j\omega t} dt = \int_{-\frac{\tau}{2}}^{\frac{\tau}{2}} \exp\left(\frac{j2\pi\mu t^2}{2}\right) e^{-j\omega t} dt \quad (5.28)$$

Let $\mu' = 2\pi\mu = 2\pi B/\tau$, and perform the change of variable

$$x = \sqrt{\frac{\mu'}{\pi}}\left(t - \frac{\omega}{\mu'}\right) \quad ; \quad dx = \sqrt{\frac{\mu'}{\pi}} dt \quad (5.29)$$

Thus, Eq. (5.28) can be written as

$$S(\omega) = \sqrt{\frac{\pi}{\mu'}} e^{-j\omega^2/2\mu'} \int_{-x_1}^{x_2} e^{j\pi x^2/2} dx \quad (5.30)$$

$$S(\omega) = \sqrt{\frac{\pi}{\mu'}} e^{-j\omega^2/2\mu'} \left\{ \int_0^{x_2} e^{j\pi x^2/2} dx - \int_0^{-x_1} e^{j\pi x^2/2} dx \right\} \quad (5.31)$$

where

$$x_1 = \sqrt{\frac{\mu'}{\pi}}\left(\frac{\tau}{2} + \frac{\omega}{\mu'}\right) = \sqrt{\frac{B\tau}{2}}\left(1 + \frac{f}{B/2}\right) \quad (5.32)$$

$$x_2 = \sqrt{\frac{\mu'}{\pi}}\left(\frac{\tau}{2} - \frac{\omega}{\mu'}\right) = \sqrt{\frac{B\tau}{2}}\left(1 - \frac{f}{B/2}\right) \quad (5.33)$$

The Fresnel integrals, denoted by $C(x)$ and $S(x)$, are defined by

$$C(x) = \int_0^x \cos\left(\frac{\pi v^2}{2}\right) dv \quad (5.34)$$

$$S(x) = \int_0^x \sin\left(\frac{\pi v^2}{2}\right) dv \quad (5.35)$$

Fresnel integrals are approximated by

$$C(x) = \frac{1}{2} + \frac{1}{\pi x} \sin\left(\frac{\pi}{2}x^2\right) \quad ; \quad x \gg 1 \quad (5.36)$$

$$S(x) = \frac{1}{2} - \frac{1}{\pi x} \cos\left(\frac{\pi}{2}x^2\right) \quad ; \quad x \gg 1 \quad (5.37)$$

Note that, $C(-x) = -C(x)$ and $S(-x) = -S(x)$. Fig. 5.7 shows a plot for both $C(x)$ and $S(x)$ for $0 \leq x \leq 10$. This figure can be reproduced using MATLAB function “*fresnel_int.m*” given in Listing 5.1 in Section 5.6.

Using Eqs. (5.34) and (5.35) into (5.31) and performing the integration yield,

$$S(\omega) = \tau \sqrt{\frac{1}{B\tau}} e^{-j\omega^2/(4\pi B)} \left\{ \frac{[C(x_2) + C(x_1)] + j[S(x_2) + S(x_1)]}{\sqrt{2}} \right\} \quad (5.38)$$

Fig. 5.8 shows a typical plot for the amplitude spectrum of an LFM waveform. The square-like spectrum is widely known as the Fresnel spectrum.

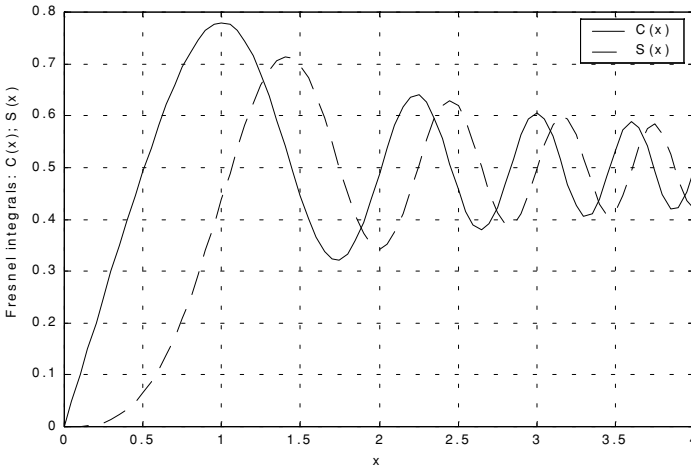


Figure 5.7. Fresnel integrals.

5.4. High Range Resolution

An expression for range resolution ΔR in terms of the pulse width τ was derived in Chapter 1. When pulse compression is not used, the instantaneous bandwidth B of radar receiver is normally matched to the pulse bandwidth, and in most radar applications this is done by setting $B = 1/\tau$. Therefore, range resolution is given by

$$\Delta R = \frac{c\tau}{2} = \frac{c}{2B} \quad (5.39)$$

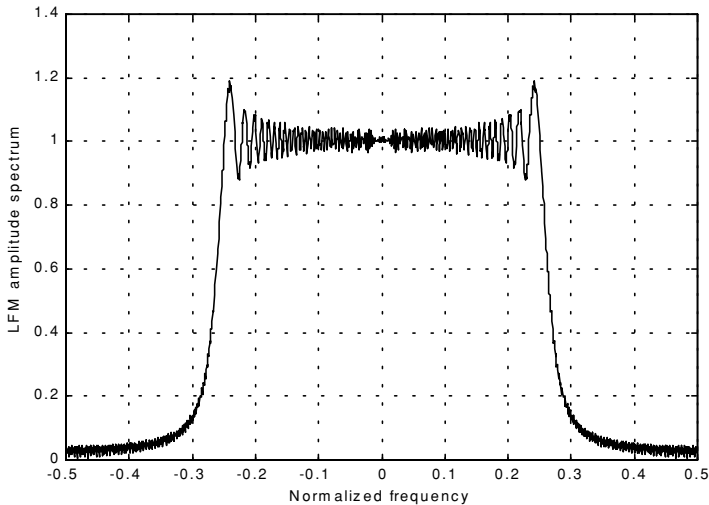


Figure 5.8. Typical spectrum for an LFM waveform.

Radar users and designers alike seek to accomplish High Range Resolution (HRR) by minimizing ΔR . However, as suggested by Eq. (5.39) in order to achieve HRR one must use very short pulses and consequently reduce the average transmitted power, and impose severe operating bandwidth requirements.

Achieving fine range resolution while maintaining adequate average transmitted power can be accomplished by using pulse compression techniques, which will be discussed in Chapter 7. By means of frequency or phase modulation, pulse compression allows us to achieve the average transmitted power of a relatively long pulse, while obtaining the range resolution corresponding to a very short pulse. As an example, consider an LFM waveform whose bandwidth is B and uncompressed pulse width (transmitted) is τ . After pulse compression the compressed pulse width is denoted by τ' , where $\tau' \ll \tau$, and the HRR is

$$\Delta R = \frac{c\tau'}{2} \ll \frac{c\tau}{2} \quad (5.40)$$

Linear frequency modulation and Frequency-Modulated (FM) CW waveforms are commonly used to achieve HRR. High range resolution can also be synthesized using a class of waveforms known as the “Stepped Frequency Waveforms (SFW).” Stepped frequency waveforms require more complex hardware implementation as compared to LFM or FM-CW; however, the radar operating bandwidth requirements are less restrictive. This is true, because the

receiver instantaneous bandwidth is matched to the SFW sub-pulse bandwidth which is much smaller than an LFM or FM-CW bandwidth. A brief discussion of SFW waveforms is presented in the following section.

5.5. Stepped Frequency Waveforms

Stepped Frequency Waveforms (SFW) produce Synthetic HRR target profiles because the target range profile is computed by means of Inverse Discrete Fourier Transformation (IDFT) of frequency domain samples of the actual target range profile. The process of generating a synthetic HRR profile is described in Wehner¹. It is summarized as follows:

1. A series of n narrow-band pulses are transmitted. The frequency from pulse to pulse is stepped by a fixed frequency step Δf . Each group of n pulses is referred to as a burst.
2. The received signal is sampled at a rate that coincides to the center of each pulse.
3. The quadrature components for each burst are collected and stored.
4. Spectral weighting (to reduce the range sidelobe levels) is applied on the quadrature components. Corrections for target velocity, phase, and amplitude variations are applied.
5. The IDFT of the weighted quadrature components of each burst is calculated to synthesize a range profile for that burst. The process is repeated for N bursts to obtain consecutive synthetic HRR profiles.

Fig. 5.9 shows a typical SFW burst. The Pulse Repetition Interval (PRI) is T , and the pulse width is τ' . Each pulse can have its own LFM, or other type of modulation; in this book LFM is assumed. The center frequency for the i^{th} step is

$$f_i = f_0 + i\Delta f \quad ; \quad i = 0, n - 1 \quad (5.41)$$

Within a burst, the transmitted waveform for the i^{th} step can be described as

$$s_i(t) = \begin{cases} C_i \cos 2\pi f_i t + \theta_i & ; \quad iT \leq t \leq iT + \tau' \\ 0 & ; \quad \text{elsewhere} \end{cases} \quad (5.42)$$

where θ_i are the relative phases and C_i are constants. The received signal from a target located at range R_0 at time $t = 0$ is then given by

$$s_{ri}(t) = C_i' \cos(2\pi f_i(t - \tau(t)) + \theta_i) \quad ; \quad iT + \tau(t) \leq t \leq iT + \tau' + \tau(t) \quad (5.43)$$

1. Wehner, D. R., *High Resolution Radar, second edition*. Artech House, 1995.

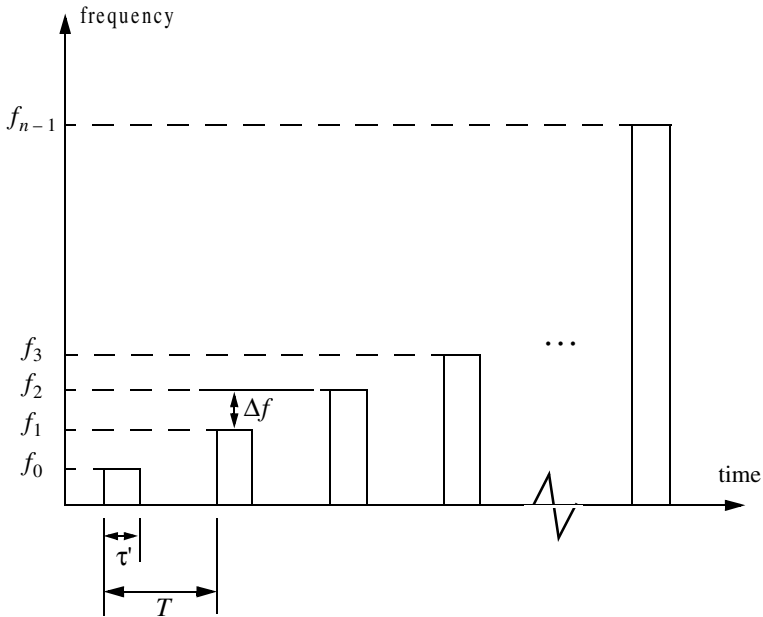


Figure 5.9. Stepped frequency waveform burst.

where C_i' are constant and the round trip delay $\tau(t)$ is given by

$$\tau(t) = \frac{R_0 - vt}{c/2} \quad (5.44)$$

c is the speed of light and v is the target radial velocity.

The received signal is down converted to base-band in order to extract the quadrature components. More precisely, $s_{r_i}(t)$ is mixed with the signal

$$y_i(t) = C \cos(2\pi f_i t + \theta_i) \quad ; \quad iT \leq t \leq iT + \tau' \quad (5.45)$$

After low pass filtering, the quadrature components are given by

$$\begin{pmatrix} x_I(t) \\ x_Q(t) \end{pmatrix} = \begin{pmatrix} A_i \cos \psi_i(t) \\ A_i \sin \psi_i(t) \end{pmatrix} \quad (5.46)$$

where A_i are constants, and

$$\psi_i(t) = -2\pi f_i \left(\frac{2R_0}{c} - \frac{2vt}{c} \right) \quad (5.47)$$

where now $f_i = \Delta f$. For each pulse, the quadrature components are then sampled at

$$t_i = iT + \tau_r + \frac{2R_0}{c} \quad (5.48)$$

τ_r is the time delay associated with range that corresponds to the start of the range profile.

The quadrature components can then be expressed in complex form as

$$X_i = A_i e^{j\psi_i} \quad (5.49)$$

Eq. (5.49) represents samples of the target reflectivity, due to a single burst, in the frequency domain. This information can then be transformed into a series of range delay reflectivity (i.e., range profile) values by using the IDFT. It follows that

$$H_l = \frac{1}{n} \sum_{i=0}^{n-1} X_i \exp\left(j\frac{2\pi li}{n}\right) \quad ; \quad 0 \leq l \leq n-1 \quad (5.50)$$

Substituting Eqs. (5.49) and (5.47) into (5.50) and collecting terms yield

$$H_l = \frac{1}{n} \sum_{i=0}^{n-1} A_i \exp\left\{j\left(\frac{2\pi li}{n} - 2\pi f_i \left(\frac{2R_0}{c} - \frac{2vt_i}{c}\right)\right)\right\} \quad (5.51)$$

By normalizing with respect to n and by assuming that $A_i = 1$ and that the target is stationary (i.e., $v = 0$), then Eq. (5.51) can be written as

$$H_l = \sum_{i=0}^{n-1} \exp\left\{j\left(\frac{2\pi li}{n} - 2\pi f_i \frac{2R_0}{c}\right)\right\} \quad (5.52)$$

Using $f_i = i\Delta f$ inside Eq. (5.52) yields

$$H_l = \sum_{i=0}^{n-1} \exp\left\{j\frac{2\pi i}{n} \left(-\frac{2nR_0\Delta f}{c} + l\right)\right\} \quad (5.53)$$

which can be simplified to (see problems)

$$H_l = \frac{\sin \pi \chi}{\sin \frac{\pi \chi}{n}} \exp\left(j \frac{n-1}{2} \frac{2\pi \chi}{n}\right) \quad (5.54)$$

where

$$\chi = \frac{-2nR_0\Delta f}{c} + l \quad (5.55)$$

Finally, the synthesized range profile is

$$|H_l| = \left| \frac{\sin \pi \chi}{\sin \frac{\pi \chi}{n}} \right| \quad (5.56)$$

5.5.1. Range Resolution and Range Ambiguity in SFW

As usual, range resolution is determined from the overall system bandwidth. Assuming a SFW with n steps, and step size Δf , then the corresponding range resolution is equal to

$$\Delta R = \frac{c}{2n\Delta f} \quad (5.57)$$

Range ambiguity associated with a SFW can be determined by examining the phase term that corresponds to a point scatterer located range R_0 . More precisely,

$$\psi_i(t) = 2\pi f_i \frac{2R_0}{c} \quad (5.58)$$

It follows that

$$\frac{\Delta \psi}{\Delta f} = \frac{4\pi(f_{i+1} - f_i)R_0}{(f_{i+1} - f_i)c} = \frac{4\pi R_0}{c} \quad (5.59)$$

or equivalently,

$$R_0 = \frac{\Delta \psi}{\Delta f} \frac{c}{4\pi} \quad (5.60)$$

It is clear from Eq. (5.60) that range ambiguity exists for $\Delta \psi = \Delta \psi + 2n\pi$. Therefore,

$$R_0 = \frac{\Delta \psi + 2n\pi}{\Delta f} \frac{c}{4\pi} = R_0 + n \left(\frac{c}{2\Delta f} \right) \quad (5.61)$$

and the unambiguous range window is

$$R_u = \frac{c}{2\Delta f} \quad (5.62)$$

Hence, a range profile synthesized using a particular SFW represents the relative range reflectivity for all scatterers within the unambiguous range window, with respect to the absolute range that corresponds to the burst time delay. Additionally, if a specific target extent is larger than R_u , then all scatterers falling outside the unambiguous range window will fold over and appear in the synthesized profile. This foldover problem is identical to the spectral foldover that occurs when using a Fourier Transform (FFT) to resolve certain signal frequency contents. For example, consider an FFT with frequency resolution $\Delta f = 50\text{Hz}$, and size $N_{FFT} = 64$. In this case, this FFT can resolve frequency tones between -1600Hz and 1600Hz . When this FFT is used to resolve the frequency content of a sine-wave tone equal to 1800Hz , foldover occurs and a spectral line at the fourth FFT bin (i.e., 200Hz) appears. Therefore, in order to avoid foldover in the synthesized range profile, the frequency step Δf must be (from Eq. (5.62))

$$\Delta f \leq \frac{c}{2E} \quad (5.63)$$

where E is the target extent in meters.

Additionally, the pulse width must also be large enough to contain the whole target extent. Thus,

$$\Delta f \leq \frac{1}{\tau} \quad (5.64)$$

and in practice,

$$\Delta f \leq \frac{1}{2\tau} \quad (5.65)$$

This is necessary in order to reduce the amount of contamination of the synthesized range profile caused by the clutter surrounding the target under consideration.

MATLAB Function “hrr_profile.m”

The function “*hrr_profile.m*” computes and plots the synthetic HRR profile for a specific SFW. It is given in Listing 5.2 in Section 5.6. This function utilizes an IDFT of size equal to twice the number of steps. Hamming window of the same size is also assumed. The syntax is as follows:

$[hl] = hrr_profile (nscat, scat_range, scat_rcs, n, deltaf, prf, v, rnote)$

where

Symbol	Description	Units	Status
<i>nscat</i>	<i>number of scatterers that make up the target</i>	<i>none</i>	<i>input</i>
<i>scat_range</i>	<i>vector containing range to individual scatterers</i>	<i>meters</i>	<i>input</i>
<i>scat_rcs</i>	<i>vector containing RCS of individual scatterers</i>	<i>meter square</i>	<i>input</i>
<i>n</i>	<i>number of steps</i>	<i>none</i>	<i>input</i>
<i>deltaf</i>	<i>frequency step</i>	<i>Hz</i>	<i>input</i>
<i>prf</i>	<i>PRF of SFW</i>	<i>Hz</i>	<i>input</i>
<i>v</i>	<i>target velocity</i>	<i>meter/second</i>	<i>input</i>
<i>rnote</i>	<i>profile starting range</i>	<i>meters</i>	<i>input</i>
<i>hl</i>	<i>range profile</i>	<i>dB</i>	<i>output</i>

For example, assume that the range profile starts at $R_0 = 900m$ and that

<i>nscat</i>	<i>tau</i>	<i>n</i>	<i>deltaf</i>	<i>prf</i>	<i>v</i>
3	100μsec	64	10MHz	10KHz	0.0

In this case,

$$\Delta R = \frac{3 \times 10^8}{2 \times 64 \times 10 \times 10^6} = 0.235m$$

$$R_u = \frac{3 \times 10^8}{2 \times 10 \times 10^6} = 15m$$

Thus, scatterers that are more than 0.235 meters apart will appear as distinct peaks in the synthesized range profile. Assume two cases, where in the first case,

$$[scat_range] = [908, 910, 912] \text{ meters}$$

and in the second case,

$$[scat_range] = [908, 910, 910.4] \text{ meters}$$

In both cases, let

$$[scat_rcs] = [100, 10, 1] \text{ meter square}$$

Fig. 5.10 shows the synthesized range profiles generated using the function “*hrr_profile.m*” and the first case when the Hamming window is not used. Fig. 5.11 is similar to Fig. 5.10, except in this case the Hamming window is used.

Fig. 5.12 shows the synthesized range profile that corresponds to the second case (Hamming window is used). Note that all three scatterers were resolved in Figs. 5.10 and 5.11; however, the last two yesteryears are not resolved in Fig. 5.12, since they are separated by less than ΔR .

Next, consider another case where

$$[scat_range] = [908, 912, 916] \text{ meters}$$

Fig. 5.13 shows the corresponding range profile. In this case, foldover occurs, and the last Scatterer appears at the lower portion of the synthesized range profile. Also, consider the case where

$$[scat_range] = [908, 912, 923] \text{ meters}$$

Fig. 5.14 shows the corresponding range profile. In this case, ambiguity is associated with the first and third scatterers since they are separated by $15m$. Both appear at the same FFT bin.

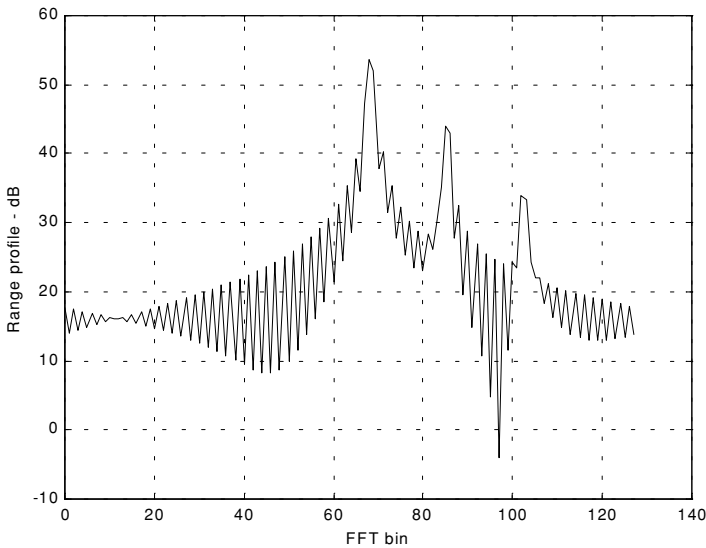


Figure 5.10. Synthetic range profile for three resolved scatterers. No window.

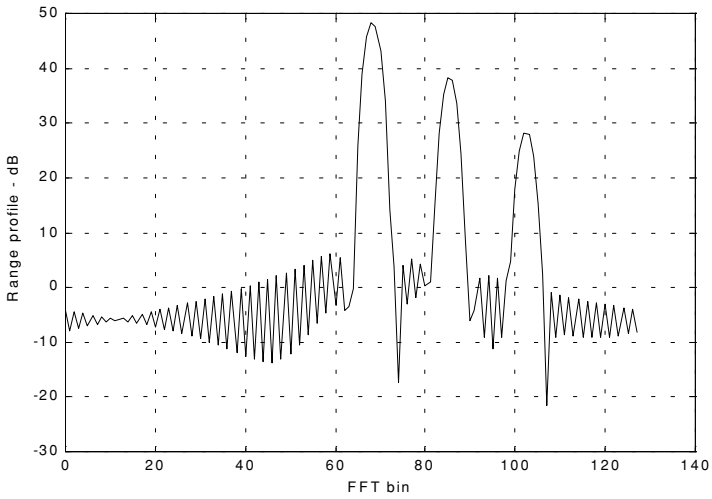


Figure 5.11. Synthetic range profile for three scatterers. Hamming window.

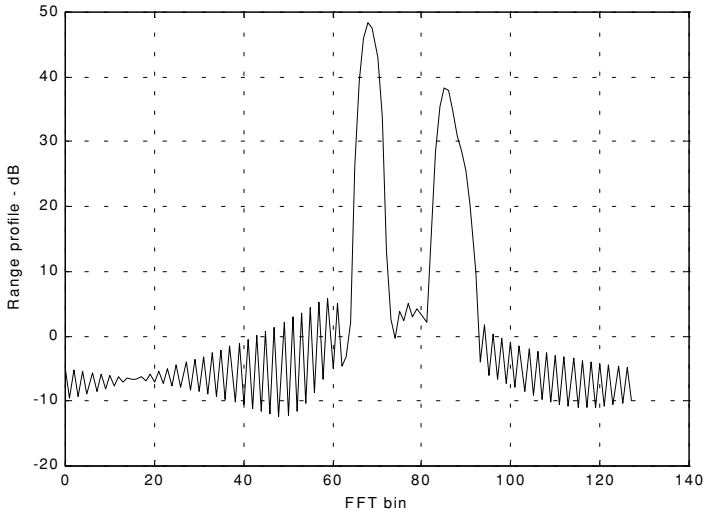


Figure 5.12. Synthetic range profile for three scatterers. Two are unresolved.

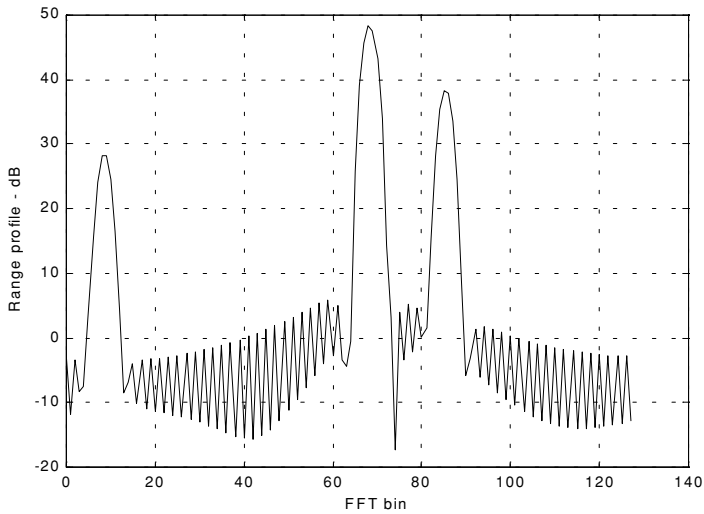


Figure 5.13. Synthetic range profile for three scatterers. Third scatterer folds over.

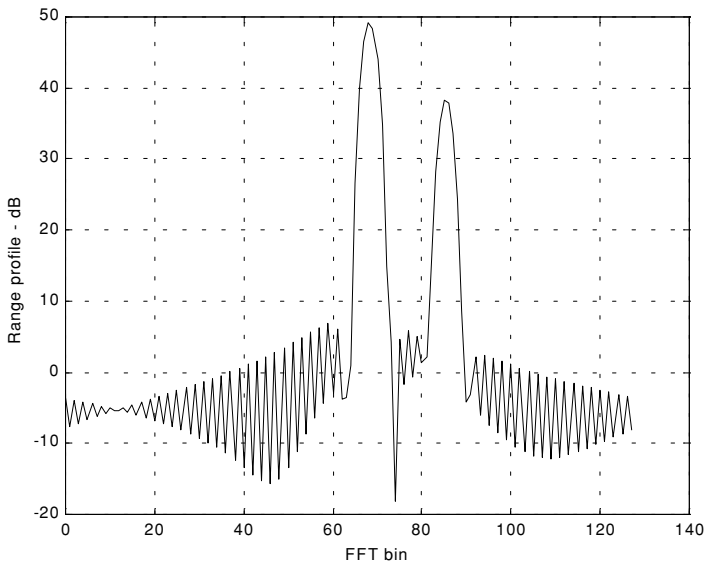


Figure 5.14. Synthetic range profile for three scatterers. The first and third scatterers appear at the same FFT bin.

5.5.2. Effect of Target Velocity

The range profile defined in Eq. (5.56) was obtained by assuming that the target under examination was stationary. The effect of target velocity on the synthesized range profile can be determined by substituting Eqs. (5.47) and (5.48) into Eq. (5.50), which after normalization yields

$$H_l = \sum_{i=0}^{n-1} \exp \left\{ j \frac{2\pi l i}{n} - j 2\pi f_i \left[\frac{2R}{c} - \frac{2v}{c} \left(iT + \frac{\tau_1}{2} + \frac{2R}{c} \right) \right] \right\} \quad (5.66)$$

The additional phase term present in Eq. (5.66) distorts the synthesized range profile. In order to illustrate this distortion, consider the SFW described in the previous section, and assume the three scatterers of the first case. Also, assume that $v = 200 \text{ m/s}$. Fig. 5.15 shows the synthesized range profile for this case. Comparisons of Figs. 5.11 and 5.15 clearly show the distortion effects caused by the uncompensated target velocity.

This distortion can be eliminated by multiplying the complex received data at each pulse by the phase term

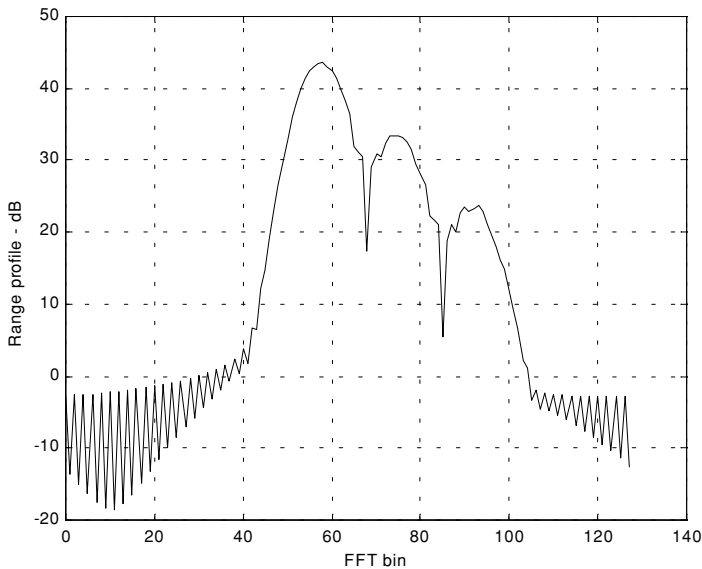


Figure 5.15. Illustration of range profile distortion due to target velocity.

$$\Phi = \exp\left(-j2\pi f_i \left[\frac{2v}{c} \left(iT + \frac{\tau_1}{2} + \frac{2R}{c} \right) \right] \right) \quad (5.67)$$

where v and R are, respectively, estimates of the target velocity and range. This process of modifying the phase of the quadrature components is often referred to as “phase rotation.” In practice, when good estimates of v and R are not available, then the effects of target velocity are reduced by using frequency hopping between the consecutive pulses within the SFW. In this case, the frequency of each individual pulse is chosen according to a predetermined code. Waveforms of this type are often called Frequency Coded Waveforms (FCW). Costas waveforms or signals, which will be discussed in Chapter 7, are a good example of this type of waveform.

5.6. MATLAB Listings

This section presents listings for all MATLAB programs/functions used in this chapter. The user is advised to rerun these programs with different input parameters.

Listing 5.1. MATLAB Program “fresnel_int.m”

```
clear all
n = 0;
for x = 0:.05:4
    n = n+1;
    sx(n) = quad8('fresnels',0,x);
    cx(n) = quad8('fresnelc',0,x);
end
plot(cx)
x=0:.05:4;
plot(x,cx,'k',x,sx,'k--')
grid
xlabel('x')
ylabel('Fresnel integrals: C(x); S(x)')
%
function cx = fresnelc(x)
cx = cos(pi * .5 * x.^2);
%
function cx = fresnels(x)
cx = sin(pi * .5 * x.^2);
```

Listing 5.2. MATLAB Function “hrr_profile.m”

```
function [hl] = hrr_profile (nscat, scat_range, scat_rcs, n, deltaf, prf, v, rnote)
% Range or Time domain Profile
% Range_Profile returns the Range or Time domain plot of a simulated
% HRR SFW returning from a predetermined number of targets with a prede-
% termined
c=3.0e8; % speed of light (m/s)
num_pulses = n;
SNR_dB = 40;
%carrier_freq = 9.5e9; %Hz (10GHz)
freq_step = deltaf; %Hz (10MHz)
V = v; % radial velocity (m/s) -- (+)=towards radar (-)=away
PRI = 1. / prf; % (s)
Inphase = zeros((2*num_pulses),1);
Quadrature = zeros((2*num_pulses),1);
Inphase_tgt = zeros(num_pulses,1);
Quadrature_tgt = zeros(num_pulses,1);
IQ_freq_domain = zeros((2*num_pulses),1);
Weighted_I_freq_domain = zeros((num_pulses),1);
Weighted_Q_freq_domain = zeros((num_pulses),1);
Weighted_IQ_time_domain = zeros((2*num_pulses),1);
Weighted_IQ_freq_domain = zeros((2*num_pulses),1);
abs_Weighted_IQ_time_domain = zeros((2*num_pulses),1);
dB_abs_Weighted_IQ_time_domain = zeros((2*num_pulses),1);
taur = 2. * rnote / c;
for jscat = 1:nscat
    ii = 0;
    for i = 1:num_pulses
        ii = ii+1;
        rec_freq = ((i-1)*freq_step);
        Inphase_tgt(ii) = Inphase_tgt(ii) + sqrt(scat_rcs(jscat)) * ...
            cos(-2*pi*rec_freq*(2.*scat_range(jscat)/c - 2*(V/c)* ...
                ((i-1)*PRI + taur/2 + 2*scat_range(jscat)/c)));
        Quadrature_tgt(ii) = Quadrature_tgt(ii) + sqrt(scat_rcs(jscat))* ...
            sin(-2*pi*rec_freq*(2*scat_range(jscat)/c - 2*(V/c)* ...
                ((i-1)*PRI + taur/2 + 2*scat_range(jscat)/c)));
    end
end
Inphase = Inphase_tgt;
Quadrature = Quadrature_tgt;
Weighted_I_freq_domain(1:num_pulses) = Inphase(1:num_pulses)...
    *(hamming(num_pulses));
Weighted_Q_freq_domain(1:num_pulses) = Quadrature(1:num_pulses).* ...
```



```

    (hamming(num_pulses));
    Weighted_IQ_freq_domain(1:num_pulses)= Weighted_I_freq_domain + ...
    Weighted_Q_freq_domain*j;
    Weighted_IQ_freq_domain(num_pulses:2*num_pulses)=0.+0.i;
    Weighted_IQ_time_domain = (ifft(Weighted_IQ_freq_domain));
    abs_Weighted_IQ_time_domain = (abs(Weighted_IQ_time_domain));
    dB_abs_Weighted_IQ_time_domain =
    20.0*log10(abs_Weighted_IQ_time_domain)+SNR_dB;

    plot((0:(2*num_pulses-1)), dB_abs_Weighted_IQ_time_domain,'k')
    xlabel ('FFT bin')
    ylabel ('Range profile - dB')
    grid

```

Problems

- 5.1. Derive Eq. (5.17).
- 5.2. Derive Eq. (5.66).
- 5.3. Derive Eq. (5.54).
- 5.4. Write a MATLAB program to perform HRR synthesis for frequency coded waveforms.
- 5.5. Reproduce [Fig. 5.5](#) for $v = 10, 50, 100, 150, 250$ m/s. Compare your outputs. What are your conclusions?

***Matched Filter and
the Radar Ambiguity
Function***

6.1. The Matched Filter SNR

The most unique characteristic of the matched filter is that it produces the maximum achievable instantaneous SNR at its output when a signal plus additive white noise are present at the input. The noise does not need to be Gaussian. The peak instantaneous SNR at the receiver output can be achieved by matching the radar receiver transfer function to the received signal. We will show that the peak instantaneous signal power divided by the average noise power at the output of a matched filter is equal to twice the input signal energy divided by the input noise power, regardless of the waveform used by the radar. This is the reason why matched filters are often referred to as optimum filters in the SNR sense. Note that the peak power used in the derivation of the radar equation (SNR) represents the average signal power over the duration of the pulse, not the peak instantaneous signal power as in the case of a matched filter. In practice, it is sometimes difficult to achieve perfect matched filtering. In such cases, sub-optimum filters may be used. Due to this mismatch, degradation in the output SNR occurs.

Consider a radar system that uses a finite duration energy signal $s_i(t)$. Denote the pulse width as τ , and assume that a matched filter receiver is utilized. The main question that we need to answer is: What is the impulse, or frequency, response of the filter that maximizes the instantaneous SNR at the output of the receiver when a delayed version of the signal $s_i(t)$ plus additive white noise is at the input?

The matched filter input signal can then be represented by

$$x(t) = C s_i(t - t_1) + n_i(t) \quad (6.1)$$

where C is a constant, t_1 is an unknown time delay proportional to the target range, and $n_i(t)$ is input white noise. Since the input noise is white, its corresponding autocorrelation and Power Spectral Density (PSD) functions are given, respectively, by

$$\bar{R}_{n_i}(t) = \frac{N_0}{2} \delta(t) \quad (6.2)$$

$$\bar{S}_{n_i}(\omega) = \frac{N_0}{2} \quad (6.3)$$

where N_0 is a constant. Denote $s_o(t)$ and $n_o(t)$ as the signal and noise filter outputs. More precisely, we can define

$$y(t) = C s_o(t - t_1) + n_o(t) \quad (6.4)$$

where

$$s_o(t) = s_i(t) \bullet h(t) \quad (6.5)$$

$$n_o(t) = n_i(t) \bullet h(t) \quad (6.6)$$

The operator (\bullet) indicates convolution, and $h(t)$ is the filter impulse response (the filter is assumed to be linear time invariant).

Let $R_h(t)$ denote the filter autocorrelation function. It follows that the output noise autocorrelation and PSD functions are

$$\bar{R}_{n_o}(t) = \bar{R}_{n_i}(t) \bullet R_h(t) = \frac{N_0}{2} \delta(t) \bullet R_h(t) = \frac{N_0}{2} R_h(t) \quad (6.7)$$

$$\bar{S}_{n_o}(\omega) = \bar{S}_{n_i}(\omega) |H(\omega)|^2 = \frac{N_0}{2} |H(\omega)|^2 \quad (6.8)$$

where $H(\omega)$ is the Fourier transform for the filter impulse response, $h(t)$. The total average output noise power is equal to $\bar{R}_{n_o}(t)$ evaluated at $t = 0$. More precisely,

$$\bar{R}_{n_o}(0) = \frac{N_0}{2} \int_{-\infty}^{\infty} |h(u)|^2 du \quad (6.9)$$

The output signal power evaluated at time t is $|C s_o(t - t_1)|^2$, and by using Eq. (6.5) we get

$$s_o(t-t_1) = \int_{-\infty}^{\infty} s_i(t-t_1-u) h(u) du \quad (6.10)$$

A general expression for the output SNR at time t can be written as

$$SNR(t) = \frac{|Cs_o(t-t_1)|^2}{\overline{R_{n_o}(0)}} \quad (6.11)$$

Substituting Eqs. (6.9) and (6.10) into Eq. (6.11) yields

$$SNR(t) = \frac{C^2 \left| \int_{-\infty}^{\infty} s_i(t-t_1-u) h(u) du \right|^2}{\frac{N_0}{2} \int_{-\infty}^{\infty} |h(u)|^2 du} \quad (6.12)$$

The Schwartz inequality states that

$$\left| \int_{-\infty}^{\infty} P(x)Q(x)dx \right|^2 \leq \int_{-\infty}^{\infty} |P(x)|^2 dx \int_{-\infty}^{\infty} |Q(x)|^2 dx \quad (6.13)$$

where the equality applies only when $P = kQ^*$, where k is a constant and can be assumed to be unity. Then by applying Eq. (6.13) on the numerator of Eq. (6.12), we get

$$\begin{aligned} SNR(t) &\leq \frac{C^2 \int_{-\infty}^{\infty} |s_i(t-t_1-u)|^2 du \int_{-\infty}^{\infty} |h(u)|^2 du}{\frac{N_0}{2} \int_{-\infty}^{\infty} |h(u)|^2 du} \\ &= \frac{2C^2 \int_{-\infty}^{\infty} |s_i(t-t_1-u)|^2 du}{N_0} \end{aligned} \quad (6.14)$$

Eq. (6.14) tells us that the peak instantaneous SNR occurs when equality is achieved (i.e., from Eq. (6.13) $h = ks_i^*$). More precisely, if we assume that equality occurs at $t = t_0$, and that $k = 1$, then

$$h(u) = s_i^*(t_0 - t_1 - u) \quad (6.15)$$

and the maximum instantaneous SNR is

$$SNR(t_0) = \frac{2C^2 \int_{-\infty}^{\infty} |s_i(t_0 - t_1 - u)|^2 du}{N_0} \quad (6.16)$$

Eq. (6.16) can be simplified using Parseval's theorem,

$$E = C^2 \int_{-\infty}^{\infty} |s_i(t_0 - t_1 - u)|^2 du \quad (6.17)$$

where E denotes the energy of the input signal; consequently we can write the output peak instantaneous SNR as

$$SNR(t_0) = \frac{2E}{N_0} \quad (6.18)$$

Thus, we can draw the conclusion that the peak instantaneous SNR depends only on the signal energy and input noise power, and is independent of the waveform utilized by the radar.

Finally, we can define the impulse response for the matched filter from Eq. (6.15). If we desire the peak to occur at $t_0 = t_1$, we get the non-causal matched filter impulse response,

$$h_{nc}(t) = s_i^*(-t) \quad (6.19)$$

Alternatively, the causal impulse response is

$$h_c(t) = s_i^*(\tau - t) \quad (6.20)$$

where in this case, the peak occurs at $t_0 = t_1 + \tau$. It follows that the Fourier transforms of $h_{nc}(t)$ and $h_c(t)$ are given, respectively, by

$$H_{nc}(\omega) = S_i^*(\omega) \quad (6.21)$$

$$H_c(\omega) = S_i^*(\omega)e^{-j\omega\tau} \quad (6.22)$$

where $S_i(\omega)$ is the Fourier transform of $s_i(t)$. Thus, the moduli of $H(\omega)$ and $S_i(\omega)$ are identical; however, the phase responses are opposite of each other.

Example 6.1: Compute the maximum instantaneous SNR at the output of a linear filter whose impulse response is matched to the signal $x(t) = \exp(-t^2/2T)$.

Solution: The signal energy is

$$E = \int_{-\infty}^{\infty} |x(t)|^2 dt = \int_{-\infty}^{\infty} e^{(-t^2)/T} dt = \sqrt{\pi T} \text{ Joules}$$

It follows that the maximum instantaneous SNR is

$$SNR = \frac{\sqrt{\pi T}}{N_0/2}$$

where $N_0/2$ is the input noise power spectrum density.

6.2. The Replica

Again, consider a radar system that uses a finite duration energy signal $s_i(t)$, and assume that a matched filter receiver is utilized. The input signal is given in Eq. (6.1) and is repeated here as Eq. (6.23),

$$x(t) = C s_i(t - t_1) + n_i(t) \quad (6.23)$$

The matched filter output $y(t)$ can be expressed by the convolution integral between the filter's impulse response and $x(t)$,

$$y(t) = \int_{-\infty}^{\infty} x(u)h(t-u)du \quad (6.24)$$

Substituting Eq. (6.20) into Eq. (6.24) yields

$$y(t) = \int_{-\infty}^{\infty} x(u)s_i^*(\tau - t + u)du = \bar{R}_{x s_i}(t - \tau) \quad (6.25)$$

where $\bar{R}_{x s_i}(t - \tau)$ is a cross-correlation between $x(t)$ and $s_i(\tau - t)$. Therefore, the matched filter output can be computed from the cross-correlation between the radar received signal and a delayed replica of the transmitted waveform. If the input signal is the same as the transmitted signal, the output of the matched

filter would be the autocorrelation function of the received (or transmitted) signal. In practice, replicas of the transmitted waveforms are normally computed and stored in memory for use by the radar signal processor when needed.

6.3. Matched Filter Response to LFM Waveforms

In order to develop a general expression for the matched filter output when an LFM waveform is utilized, we will consider the case when the radar is tracking a closing target with velocity v . The transmitted signal is

$$s_1(t) = \text{Rect}\left(\frac{t}{\tau'}\right) e^{j2\pi\left(f_0 t + \frac{\mu}{2} t^2\right)} \quad (6.26)$$

The received signal is then given by

$$s_{r_1}(t) = s_1(t - \Delta(t)) \quad (6.27)$$

$$\Delta(t) = t_0 - \frac{2v}{c}(t - t_0) \quad (6.28)$$

where t_0 is the time corresponding to the target initial detection range, and c is the speed of light. Using Eq. (6.28) we can rewrite Eq. (6.27) as

$$s_{r_1}(t) = s_1\left(t - t_0 + \frac{2v}{c}(t - t_0)\right) = s_1(\gamma(t - t_0)) \quad (6.29)$$

and

$$\gamma = 1 + 2\frac{v}{c} \quad (6.30)$$

is the scaling coefficient. Substituting Eq. (6.26) into Eq. (6.29) yields

$$s_{r_1}(t) = \text{Rect}\left(\frac{\gamma(t - t_0)}{\tau'}\right) e^{j2\pi f_0 \gamma(t - t_0)} e^{j\pi \mu \gamma^2 (t - t_0)^2} \quad (6.31)$$

which is the analytical signal representation for $s_{r_1}(t)$. The complex envelope of the signal $s_{r_1}(t)$ is obtained by multiplying Eq. (6.31) by $\exp(-j2\pi f_0 t)$. Denote the complex envelope by $s_r(t)$, then after some manipulation we get

$$s_r(t) = e^{-j2\pi f_0 t_0} \text{Rect}\left(\frac{\gamma(t - t_0)}{\tau'}\right) e^{j2\pi f_0 (\gamma - 1)(t - t_0)} e^{j\pi \mu \gamma^2 (t - t_0)^2} \quad (6.32)$$

The Doppler shift due to the target motion is

$$f_d = \frac{2v}{c}f_0 \quad (6.33)$$

and since $\gamma - 1 = 2v/c$, we get

$$f_d = (\gamma - 1)f_0 \quad (6.34)$$

Using the approximation $\gamma \approx 1$ and Eq. (6.34), Eq. (6.32) is rewritten as

$$s_r(t) \approx e^{j2\pi f_d(t-t_0)} s(t-t_0) \quad (6.35)$$

where

$$s(t-t_0) = e^{-j2\pi f_0 t} s_1(t-t_0) \quad (6.36)$$

$s_1(t)$ is given in Eq. (6.26). The matched filter response is given by the convolution integral

$$s_o(t) = \int_{-\infty}^{\infty} h(u)s_r(t-u)du \quad (6.37)$$

For a non-causal matched filter the impulse response $h(u)$ is equal to $s^*(-t)$; it follows that

$$s_o(t) = \int_{-\infty}^{\infty} s^*(-u)s_r(t-u)du \quad (6.38)$$

Substituting Eq. (6.36) into Eq. (6.38), and performing some algebraic manipulations, we get

$$s_o(t) = \int_{-\infty}^{\infty} s^*(u) e^{j2\pi f_d(t+u-t_0)} s(t+u-t_0)du \quad (6.39)$$

Finally, making the change of variable $t' = t + u$ yields

$$s_o(t) = \int_{-\infty}^{\infty} s^*(t'-t)s(t'-t_0)e^{j2\pi f_d(t'-t_0)} dt' \quad (6.40)$$

It is customary to set $t_0 = 0$, and it follows that

$$s_o(t;f_d) = \int_{-\infty}^{\infty} s(t')s^*(t'-t)e^{j2\pi f_d t'} dt' \quad (6.41)$$

where we used the notation $s_o(t;f_d)$ to indicate that the output is a function of both time and Doppler frequency.

The two-dimensional (2-D) correlation function for the signal $s(t)$ is obtained from the matched filter response by replacing t by $-\tau$, then

$$\chi(\tau;f_d) = \int_{-\infty}^{\infty} s(t')s^*(t'+\tau)e^{j2\pi f_d t'} dt' \quad (6.42)$$

6.4. The Radar Ambiguity Function

The radar ambiguity function represents the output of the matched filter, and it describes the interference caused by range and/or Doppler of a target when compared to a reference target of equal RCS. The ambiguity function evaluated at $(\tau, f_d) = (0, 0)$ is equal to the matched filter output that is matched perfectly to the signal reflected from the target of interest. In other words, returns from the nominal target are located at the origin of the ambiguity function. Thus, the ambiguity function at nonzero τ and f_d represents returns from some range and Doppler different from those for the nominal target.

The radar ambiguity function is normally used by radar designers as a means of studying different waveforms. It can provide insight about how different radar waveforms may be suitable for the various radar applications. It is also used to determine the range and Doppler resolutions for a specific radar waveform. The three-dimensional (3-D) plot of the ambiguity function versus frequency and time delay is called the radar ambiguity diagram. The radar ambiguity function for the signal $s(t)$ is defined as the modulus squared of its 2-D correlation function, i.e., $|\chi(\tau;f_d)|^2$. More precisely,

$$|\chi(\tau;f_d)|^2 = \left| \int_{-\infty}^{\infty} s(t)s^*(t+\tau)e^{j2\pi f_d t} dt \right|^2 \quad (6.43)$$

In this notation, the target of interest is located at $(\tau, f_d) = (0, 0)$, and the ambiguity diagram is centered at the same point. Note that some authors define the ambiguity function as $|\chi(\tau;f_d)|$. In this book, $|\chi(\tau;f_d)|$ is called the uncertainty function. Denote E as the energy of the signal $s(t)$,

$$E = \int_{-\infty}^{\infty} |s(t)|^2 dt \quad (6.44)$$

We will now list the properties for the radar ambiguity function:

1) The maximum value for the ambiguity function occurs at $(\tau, f_d) = (0, 0)$ and is equal to $4E^2$,

$$\max\{|\chi(\tau;f_d)|^2\} = |\chi(0;0)|^2 = (2E)^2 \quad (6.45)$$

$$|\chi(\tau;f_d)|^2 \leq |\chi(0;0)|^2 \quad (6.46)$$

2) The ambiguity function is symmetric,

$$|\chi(\tau;f_d)|^2 = |\chi(-\tau;-f_d)|^2 \quad (6.47)$$

3) The total volume under the ambiguity function is constant,

$$\iint |\chi(\tau;f_d)|^2 d\tau df_d = (2E)^2 \quad (6.48)$$

4) If the function $S(f)$ is the Fourier transform of the signal $s(t)$, then by using Parseval's theorem we get

$$|\chi(\tau;f_d)|^2 = \left| \int S^*(f)S(f-f_d)e^{-j2\pi f\tau} df \right|^2 \quad (6.49)$$

6.5. Examples of the Ambiguity Function

The ideal radar ambiguity function is represented by a spike of infinitesimal width that peaks at the origin and is zero everywhere else, as illustrated in Fig. 6.1. An ideal ambiguity function provides perfect resolution between neighboring targets regardless of how close they may be with respect to each other. Unfortunately, an ideal ambiguity function cannot physically exist. This is because the ambiguity function must have finite peak value equal to $(2E)^2$ and a finite volume also equal to $(2E)^2$. Clearly, the ideal ambiguity function cannot meet those two requirements.

6.5.1. Single Pulse Ambiguity Function

Consider the normalized rectangular pulse $s(t)$ defined by

$$s(t) = \frac{1}{\sqrt{\tau}} \text{Rect}\left(\frac{t}{\tau}\right) \quad (6.50)$$

From Eq. (6.42) we have

$$\chi(\tau;f_d) = \int_{-\infty}^{\infty} s(t)s^*(t+\tau)e^{j2\pi f_d t} dt \quad (6.51)$$

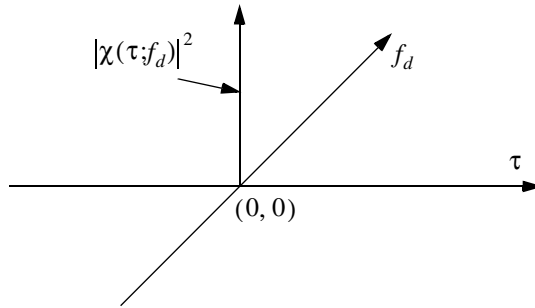


Figure 6.1. Ideal ambiguity function.

Substituting Eq. (6.50) into Eq. (6.51) and performing the integration yield,

$$|\chi(\tau; f_d)|^2 = \left| \left(1 - \frac{|\tau|}{\tau'} \right) \frac{\sin(\pi f_d(\tau' - |\tau|))}{\pi f_d(\tau' - |\tau|)} \right|^2 \quad |\tau| \leq \tau' \quad (6.52)$$

MATLAB Function “single_pulse_ambg.m”

The function “single_pulse_ambg.m” implements Eq. (6.52). It is given in Listing 6.1 in Section 6.7. The syntax is as follows:

single_pulse_ambg [taup]

taup is the pulse width. Fig. 6.2 (a-d) shows 3-D and contour plots of single pulse uncertainty and ambiguity functions. These plots can be reproduced using MATLAB program “fig6_2.m” given in Listing 6.2 in Section 6.7.

The ambiguity function cut along the time delay axis τ is obtained by setting $f_d = 0$. More precisely,

$$|\chi(\tau; 0)|^2 = \left(1 - \frac{|\tau|}{\tau'} \right)^2 \quad |\tau| \leq \tau' \quad (6.53)$$

Note that the time autocorrelation function of the signal $s(t)$ is equal to $\chi(\tau; 0)$. Similarly, the cut along the Doppler axis is

$$|\chi(0; f_d)|^2 = \left| \frac{\sin \pi \tau' f_d}{\pi \tau' f_d} \right|^2 \quad (6.54)$$

Figs. 6.3 and 6.4, respectively, show the plots of the uncertainty function cuts defined by Eqs. (6.53) and (6.54). Since the zero Doppler cut along the time delay axis extends between $-\tau'$ and τ' , then, close targets would be unambiguous if they are at least τ' seconds apart.

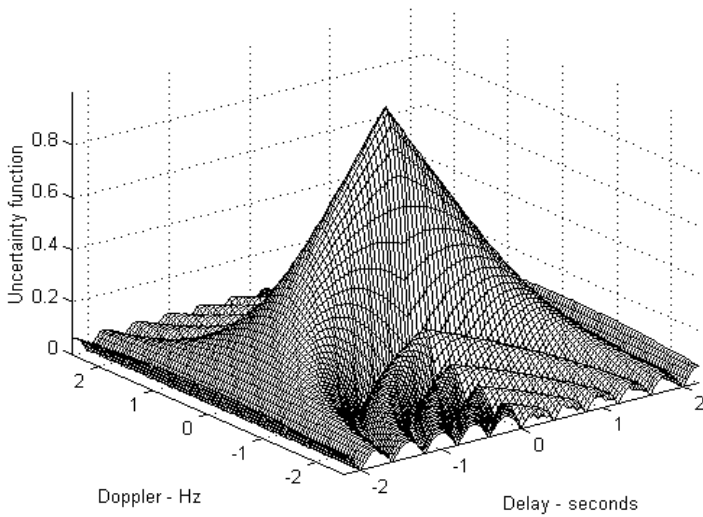


Figure 6.2a. Single pulse 3-D uncertainty plot. Pulse width is 2 seconds.

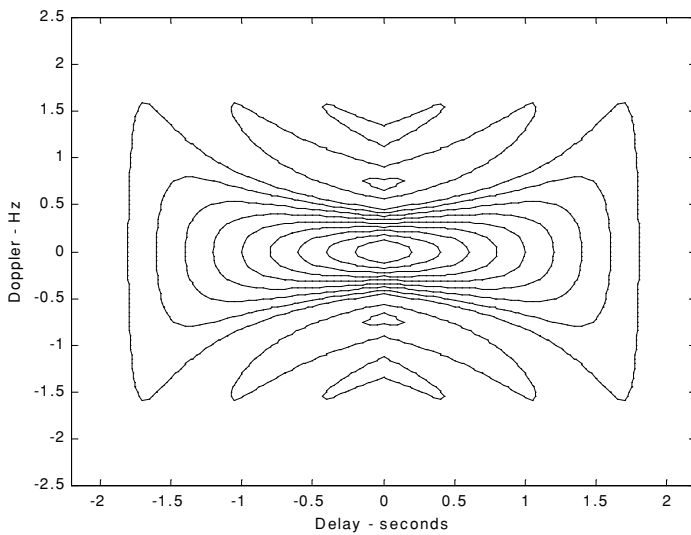


Figure 6.2b. Contour plot corresponding to [Fig. 6.2a](#).

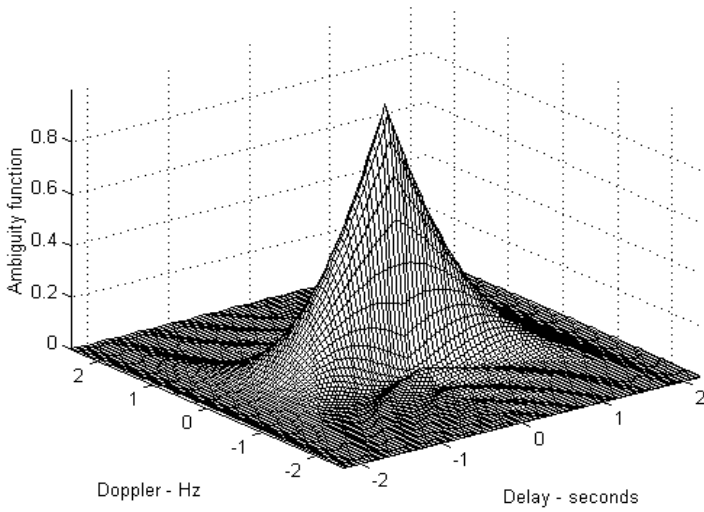


Figure 6.2c. Single pulse 3-D ambiguity plot. Pulse width is 2 seconds.

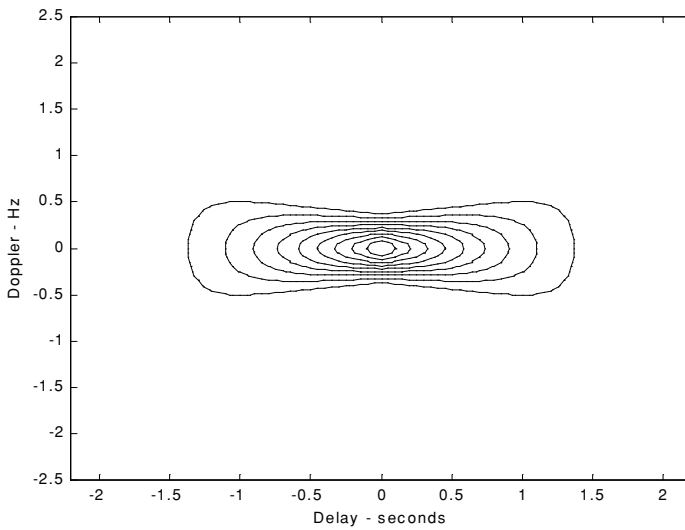


Figure 6.2d. Contour plot corresponding to [Fig. 6.2c](#).

The zero time cut along the Doppler frequency axis has a $(\sin x/x)^2$ shape. It extends from $-\infty$ to ∞ . The first null occurs at $f_d = \pm 1/\tau'$. Hence, it is possible to detect two targets that are shifted by $1/\tau'$, without any ambiguity.

We conclude that a single pulse range and Doppler resolutions are limited by the pulse width τ' . Fine range resolution requires that a very short pulse be used. Unfortunately, using very short pulses requires very large operating bandwidths, and may limit the radar average transmitted power to impractical values.

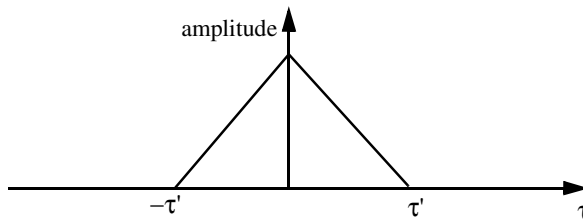


Figure 6.3. Zero Doppler uncertainty function cut along the time delay axis.

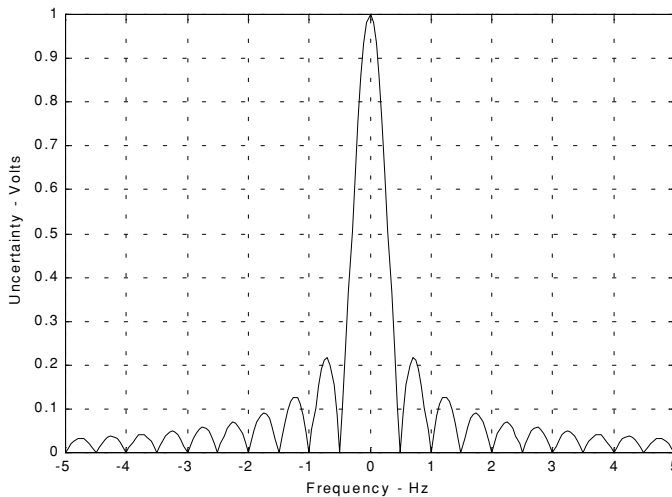


Figure 6.4. Uncertainty function of a single frequency pulse (zero delay). This plot can be reproduced using MATLAB program “Fig6_4.m” given in Listing 6.3 in Section 6.7.

6.5.2. LFM Ambiguity Function

Consider the LFM complex envelope signal defined by

$$s(t) = \frac{1}{\sqrt{\tau'}} \text{Rect}\left(\frac{t}{\tau'}\right) e^{j\pi\mu t^2} \quad (6.55)$$

In order to compute the ambiguity function for the LFM complex envelope, we will first consider the case when $0 \leq \tau \leq \tau'$. In this case the integration limits are from $-\tau'/2$ to $(\tau'/2) - \tau$. Substituting Eq. (6.55) into Eq. (6.51) yields

$$\chi(\tau; f_d) = \frac{1}{\tau'} \int_{-\infty}^{\infty} \text{Rect}\left(\frac{t}{\tau'}\right) \text{Rect}\left(\frac{t+\tau}{\tau'}\right) e^{j\pi\mu t^2} e^{-j\pi\mu(t+\tau)^2} dt \quad (6.56)$$

It follows that

$$\chi(\tau; f_d) = \frac{e^{-j\pi\mu\tau^2}}{\tau'} \int_{\frac{-\tau'}{2}}^{\frac{\tau'}{2} - \tau} e^{-j2\pi(\mu\tau - f_d)t} dt \quad (6.57)$$

We will leave the rest of the integration process to the reader. Finishing the integration process in Eq. (6.57) yields

$$\chi(\tau; f_d) = e^{j\pi\tau f_d} \left(1 - \frac{\tau}{\tau'}\right) \frac{\sin\left(\pi\tau'(\mu\tau + f_d)\left(1 - \frac{\tau}{\tau'}\right)\right)}{\pi\tau'(\mu\tau + f_d)\left(1 - \frac{\tau}{\tau'}\right)} \quad 0 \leq \tau \leq \tau' \quad (6.58)$$

Similar analysis for the case when $-\tau' \leq \tau \leq 0$ can be carried out, where in this case the integration limits are from $(-\tau'/2) - \tau$ to $\tau'/2$. The same result can be obtained by using the symmetry property of the ambiguity function ($|\chi(-\tau, -f_d)| = |\chi(\tau, f_d)|$). It follows that an expression for $\chi(\tau; f_d)$ that is valid for any τ is given by

$$\chi(\tau; f_d) = e^{j\pi\tau f_d} \left(1 - \frac{|\tau|}{\tau'}\right) \frac{\sin\left(\pi\tau'(\mu\tau + f_d)\left(1 - \frac{|\tau|}{\tau'}\right)\right)}{\pi\tau'(\mu\tau + f_d)\left(1 - \frac{|\tau|}{\tau'}\right)} \quad |\tau| \leq \tau' \quad (6.59)$$

and the LFM ambiguity function is

$$|\chi(\tau; f_d)|^2 = \left| \left(1 - \frac{|\tau|}{\tau'}\right) \frac{\sin\left(\pi\tau'(\mu\tau + f_d)\left(1 - \frac{|\tau|}{\tau'}\right)\right)}{\pi\tau'(\mu\tau + f_d)\left(1 - \frac{|\tau|}{\tau'}\right)} \right|^2 \quad |\tau| \leq \tau' \quad (6.60)$$

Again the time autocorrelation function is equal to $\chi(\tau, 0)$. The reader can verify that the ambiguity function for a down-chirp LFM waveform is given by

$$|\chi(\tau; f_d)|^2 = \left| \left(1 - \frac{|\tau|}{\tau'}\right) \frac{\sin\left(\pi\tau'(\mu\tau - f_d)\left(1 - \frac{|\tau|}{\tau'}\right)\right)}{\pi\tau'(\mu\tau - f_d)\left(1 - \frac{|\tau|}{\tau'}\right)} \right|^2 \quad |\tau| \leq \tau' \quad (6.61)$$

MATLAB Function “lfn_ambg.m”

The function “lfn_ambg.m” implements Eqs. (6.60) and (6.61). It is given in Listing 6.4 in Section 6.7. The syntax is as follows:

lfn_ambg [taup, b, up_down]

where

Symbol	Description	Units	Status
<i>taup</i>	<i>pulse width</i>	<i>seconds</i>	<i>input</i>
<i>b</i>	<i>bandwidth</i>	<i>Hz</i>	<i>input</i>
<i>up_down</i>	<i>up_down = 1 for up chirp</i> <i>up_down = -1 for down chirp</i>	<i>none</i>	<i>input</i>

Fig. 6.5 (a-d) shows 3-D and contour plots for the LFM uncertainty and ambiguity functions for

<i>taup</i>	<i>b</i>	<i>up_down</i>
<i>1</i>	<i>10</i>	<i>1</i>

These plots can be reproduced using MATLAB program “fig6_5.m” given in Listing 6.5 in Section 6.7. This function generates 3-D and contour plots of an LFM ambiguity function.

The up-chirp ambiguity function cut along the time delay axis τ is

$$|\chi(\tau; 0)|^2 = \left| \left(1 - \frac{|\tau|}{\tau'}\right) \frac{\sin\left(\pi\mu\tau\tau'\left(1 - \frac{|\tau|}{\tau'}\right)\right)}{\pi\mu\tau\tau'\left(1 - \frac{|\tau|}{\tau'}\right)} \right|^2 \quad |\tau| \leq \tau' \quad (6.62)$$

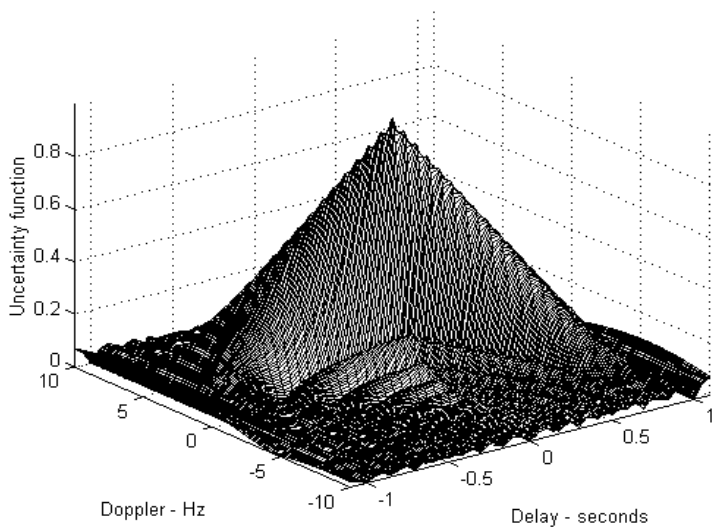


Figure 6.5a. Up-chirp LFM 3-D uncertainty plot. Pulse width is 1 second; and bandwidth is 10 Hz.

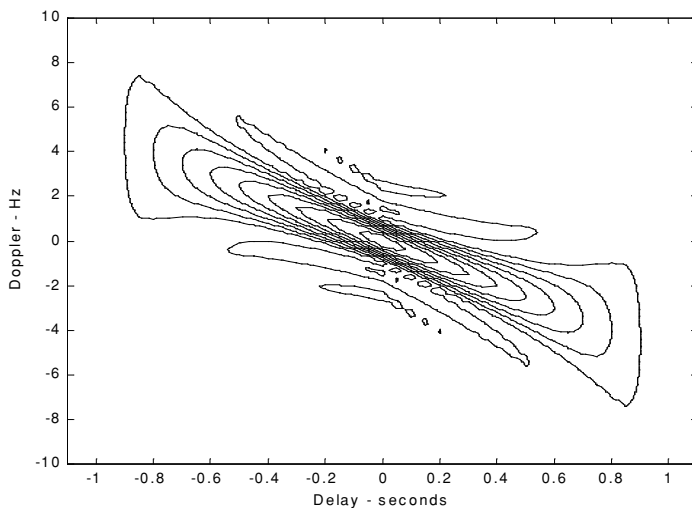


Figure 6.5b. Contour plot corresponding to [Fig. 6.5a](#).

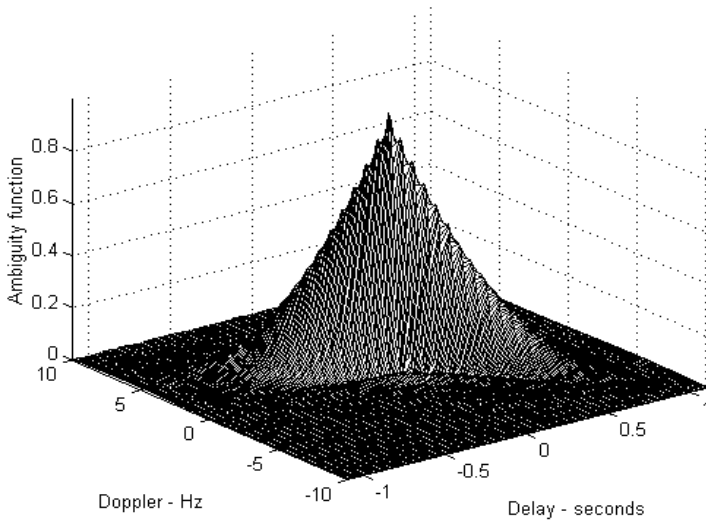


Figure 6.5c. Up-chirp LFM 3-D ambiguity plot. Pulse width is 1 second; and bandwidth is 10 Hz.

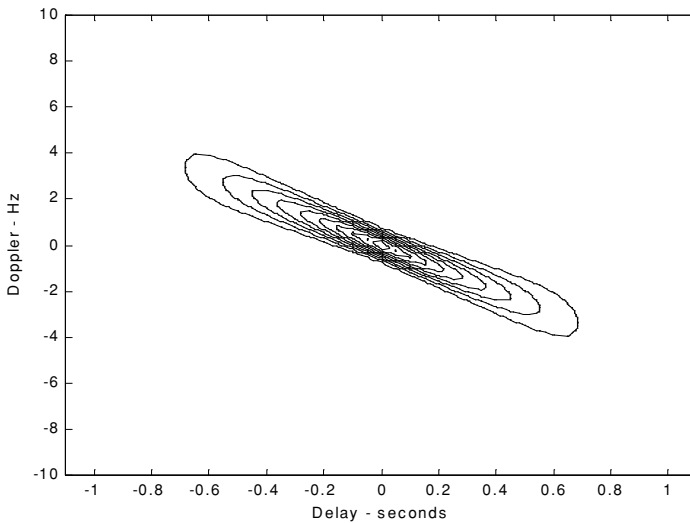


Figure 6.5d. Contour plot corresponding to [Fig. 6.5c](#).

Fig. 6.6 shows a plot for a cut in the uncertainty function corresponding to Eq. (6.62). Note that the LFM ambiguity function cut along the Doppler frequency axis is similar to that of the single pulse. This should not be surprising since the pulse shape has not changed (we only added frequency modulation). However, the cut along the time delay axis changes significantly. It is now much narrower compared to the unmodulated pulse cut. In this case, the first null occurs at

$$\tau_{n1} \approx 1/B \tag{6.63}$$

which indicates that the effective pulse width (compressed pulse width) of the matched filter output is completely determined by the radar bandwidth. It follows that the LFM ambiguity function cut along the time delay axis is narrower than that of the unmodulated pulse by a factor

$$\xi = \frac{\tau'}{(1/B)} = \tau' B \tag{6.64}$$

ξ is referred to as the compression ratio (also called time-bandwidth product and compression gain). All three names can be used interchangeably to mean the same. As indicated by Eq. (6.64) the compression ratio also increases as the radar bandwidth is increased.

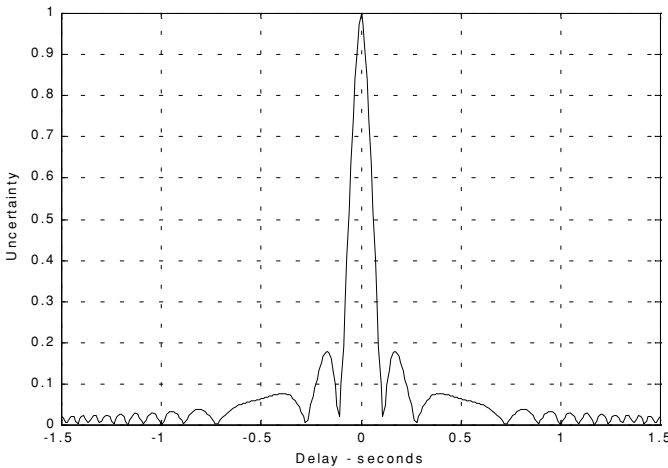


Figure 6.6. Zero Doppler Ambiguity function of an LFM pulse ($\tau' = 1$, $b = 20$). This plot can be reproduced using MATLAB program “fig6_6.m” given in Listing 6.6 in Section 6.7.

Example 6.2: Compute the range resolution before and after pulse compression corresponding to an LFM waveform with the following specifications: Bandwidth $B = 1\text{GHz}$; and pulse width $\tau' = 10\text{ms}$.

Solution: The range resolution before pulse compression is

$$\Delta R_{uncomp} = \frac{c\tau'}{2} = \frac{10 \times 10^{-3} \times 3 \times 10^8}{2} = 1.5 \times 10^6 \text{ meters}$$

Using Eq. (6.63) yields

$$\tau_{n1} = \frac{1}{1 \times 10^9} = 1 \text{ ns}$$

$$\Delta R_{comp} = \frac{c\tau_{n1}}{2} = \frac{3 \times 10^8 \times 1 \times 10^{-9}}{2} = 15 \text{ cm}.$$

6.5.3. Coherent Pulse Train Ambiguity Function

Fig. 6.7 shows a plot of coherent pulse train. The pulse width is denoted as τ' and the PRI is T . The number of pulses in the train is N ; hence, the train's length is $(N - 1)T$ seconds. A normalized individual pulse $s(t)$ is defined by

$$s_1(t) = \frac{1}{\sqrt{\tau'}} \text{Rect}\left(\frac{t}{\tau'}\right) \quad (6.65)$$

When coherency is maintained between the consecutive pulses, then an expression for the normalized train is

$$s(t) = \frac{1}{\sqrt{N}} \sum_{i=0}^{N-1} s_1(t - iT) \quad (6.66)$$

The output of the matched filter is

$$\chi(\tau; f_d) = \int_{-\infty}^{\infty} s(t) s^*(t + \tau) e^{j2\pi f_d t} dt \quad (6.67)$$

Substituting Eq. (6.66) into Eq. (6.67) and interchanging the summations and integration yield,

$$\chi(\tau; f_d) = \frac{1}{N} \sum_{i=0}^{N-1} \sum_{j=0}^{N-1} \int_{-\infty}^{\infty} s_1(t - iT) s_1^*(t - jT - \tau) e^{j2\pi f_d t} dt \quad (6.68)$$

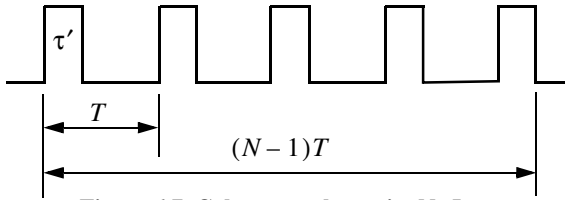


Figure 6.7. Coherent pulse train. N=5.

Making the change of variable $t_1 = t - iT$ yields

$$\chi(\tau; f_d) = \frac{1}{N} \sum_{i=0}^{N-1} e^{j2\pi f_d iT} \sum_{j=0}^{N-1} \int_{-\infty}^{\infty} s_1(t_1) s_1^*(t_1 - [\tau - (i-j)T]) e^{j2\pi f_d t_1} dt_1 \quad (6.69)$$

The integral inside Eq. (6.69) represents the output of the matched filter for a single pulse, and is denoted by χ_1 . It follows that

$$\chi(\tau; f_d) = \frac{1}{N} \sum_{i=0}^{N-1} e^{j2\pi f_d iT} \sum_{j=0}^{N-1} \chi_1[\tau - (i-j)T; f_d] \quad (6.70)$$

When the relation $q = i - j$ is used, then the following relation is true¹:

$$\sum_{i=0}^N \sum_{m=0}^N = \sum_{q=-(N-1)}^0 \sum_{i=0}^{N-1-|q|} \left[\text{for } j = i - q \right] + \sum_{q=1}^{N-1} \sum_{j=0}^{N-1-|q|} \left[\text{for } i = j + q \right] \quad (6.71)$$

Using Eq. (6.71) into Eq. (6.70) gives

$$\chi(\tau; f_d) = \frac{1}{N} \sum_{q=-(N-1)}^0 \left\{ \chi_1(\tau - qT; f_d) \sum_{i=0}^{N-1-|q|} e^{j2\pi f_d iT} \right\} + \frac{1}{N} \sum_{q=1}^{N-1} \left\{ e^{j2\pi f_d qT} \chi_1(\tau - qT; f_d) \sum_{j=0}^{N-1-|q|} e^{j2\pi f_d jT} \right\} \quad (6.72)$$

1. Rihaczek, A. W., *Principles of High Resolution Radar*, Artech House, 1996.

Setting $z = \exp(j2\pi f_d T)$, and using the relation

$$\sum_{j=0}^{N-1-|q|} z^j = \frac{1-z^{N-|q|}}{1-z} \quad (6.73)$$

yield

$$\sum_{i=0}^{N-1-|q|} e^{j2\pi f_d iT} = e^{[j\pi f_d(N-1-|q|)T]} \frac{\sin[\pi f_d(N-1-|q|)T]}{\sin(\pi f_d T)} \quad (6.74)$$

Using Eq. (6.74) into Eq. (6.72) yields two complementary sums for positive and negative q . Both sums can be combined as

$$\chi(\tau; f_d) = \frac{1}{N} \sum_{q=-(N-1)}^{N-1} \chi_1(\tau - qT; f_d) e^{[j\pi f_d(N-1+q)T]} \frac{\sin[\pi f_d(N-|q|)T]}{\sin(\pi f_d T)} \quad (6.75)$$

Finally, the ambiguity function associated with the coherent pulse train is computed as the modulus square of Eq. (6.75). For $\tau' < T/2$, the ambiguity function reduces to

$$\chi(\tau; f_d) = \frac{1}{N} \sum_{q=-(N-1)}^{N-1} |\chi_1(\tau - qT; f_d)| \left| \frac{\sin[\pi f_d(N-|q|)T]}{\sin(\pi f_d T)} \right| \quad (6.76)$$

Thus, the ambiguity function for a coherent pulse train is the superposition of the individual pulse's ambiguity functions. The ambiguity function cuts along the time delay and Doppler axes are, respectively, given by

$$|\chi(\tau; 0)|^2 = \left[\sum_{q=-(N-1)}^{N-1} \left(1 - \frac{|q|}{N}\right) \left(1 - \frac{|\tau - qT|}{\tau'}\right) \right]^2 \quad ; \quad |\tau - qT| < \tau' \quad (6.77)$$

$$|\chi(0; f_d)|^2 = \left[\frac{1}{N} \frac{\sin(\pi f_d \tau')}{\pi f_d \tau'} \frac{\sin(\pi f_d NT)}{\sin(\pi f_d T)} \right]^2 \quad (6.78)$$

MATLAB Function “train_ambg.m”

The function “train_ambg.m” implements Eq. (6.76). It is given in Listing 6.7 in Section 6.7. The syntax is as follows:

train_ambg [taup, n, pri]

where

Symbol	Description	Units	Status
<i>taup</i>	<i>pulse width</i>	<i>seconds</i>	<i>input</i>
<i>n</i>	<i>number of pulses in train</i>	<i>none</i>	<i>input</i>
<i>pri</i>	<i>pulse repetition interval</i>	<i>seconds</i>	<i>input</i>

Fig. 6.8 (a-d) shows typical outputs of this function, for

<i>taup</i>	<i>n</i>	<i>pri</i>
0.2	5	1

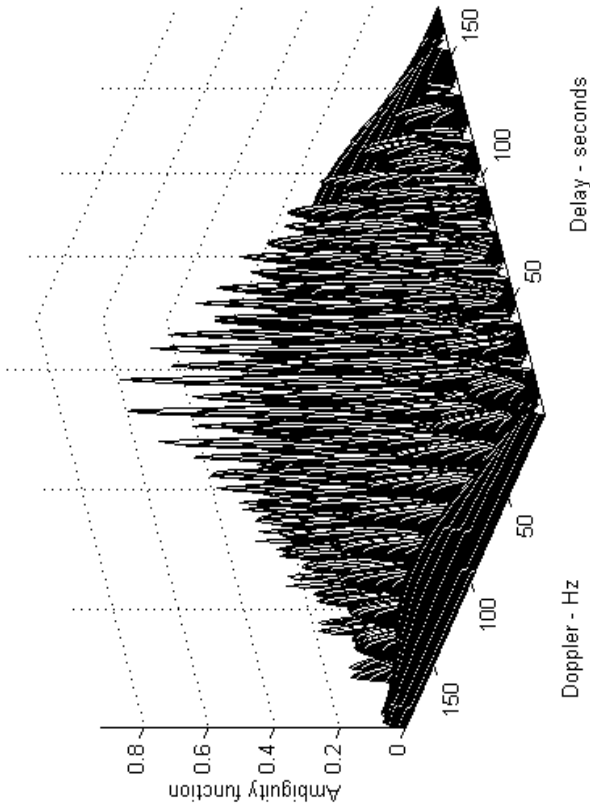


Figure 6.8a. Three-dimensional ambiguity plot for a five pulse equal amplitude coherent train. Pulse width is 0.2 seconds; and PRI is 1 second, $N=5$. This plot can be reproduced using MATLAB program “fig6_8a.m” given in Listing 6.8 in Section 6.7.

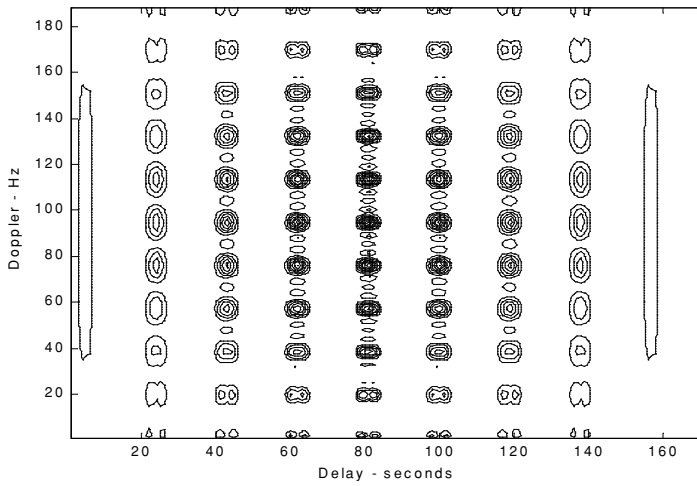


Figure 6.8b. Contour plot corresponding to Fig. 6.8a.

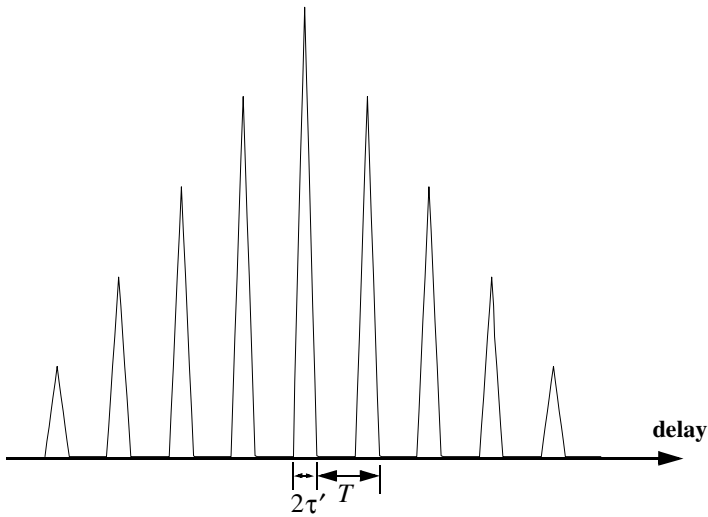


Figure 6.8c. Zero Doppler cut corresponding to Fig. 6.8a.

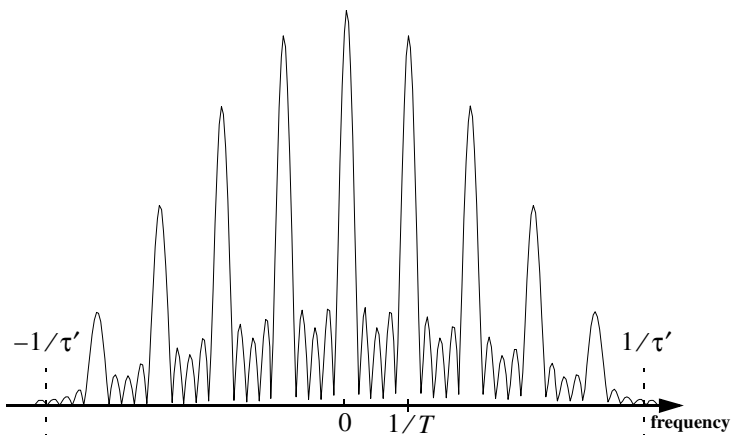


Figure 6.8d. Zero delay cut corresponding to Fig. 6.8a.

6.6. Ambiguity Diagram Contours

Plots of the ambiguity function are called ambiguity diagrams. For a given waveform, the corresponding ambiguity diagram is normally used to determine the waveform properties such as the target resolution capability, measurements (time and frequency) accuracy and its response to clutter. Three-dimensional ambiguity diagrams are difficult to plot and interpret. This is the reason why contour plots of the 3-D ambiguity diagram are often used to study the characteristics of a waveform. An ambiguity contour is a 2-D plot (frequency/time) of a plane intersecting the 3-D ambiguity diagram that corresponds to some threshold value. The resultant plots are ellipses. It is customary to display the ambiguity contour plots that correspond to one half of the peak autocorrelation value.

Fig. 6.9 shows a sketch of typical ambiguity contour plots associated with a gated CW pulse. It indicates that narrow pulses provide better range accuracy than long pulses. Alternatively, the Doppler accuracy is better for a wider pulse than it is for a short one. This trade-off between range and Doppler measurements comes from the uncertainty associated with the time-bandwidth product of a single sinusoidal pulse, where the product of uncertainty in time (range) and uncertainty in frequency (Doppler) cannot be much smaller than unity. Note that an exact plot for Fig. 6.9 can be obtained using the function “*single_pulse_ambg.m*” and the MATLAB command *contour*.

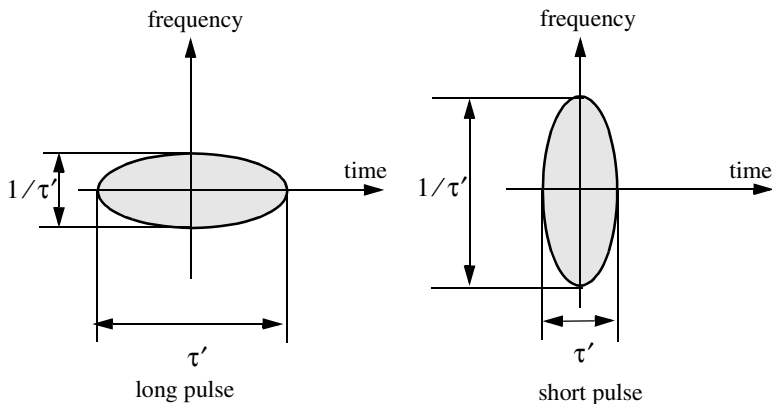


Figure 6.9. Ambiguity contour plot associated with a sinusoid modulated gated CW pulse. See Fig. 6.2.

Multiple ellipses in an ambiguity contour plot indicate the presence of multiple targets. Thus, it seems that one may improve the radar resolution by increasing the ambiguity diagram threshold value. This is illustrated in Fig. 6.10. However, in practice this is not possible for two reasons. First, in the presence of noise we lack knowledge of the peak correlation value; and second, targets in general will have different amplitudes.

Now consider the case of a coherent pulse train described in Fig. 6.7. For a pulse train, range accuracy is still determined by the pulse width, the same way as in the case of a single pulse, while Doppler accuracy is determined by the train length. Thus, time and frequency measurements can be made independently of each other. However, additional peaks appear in the ambiguity diagram which may cause range and Doppler uncertainties. This is illustrated in Fig. 6.11.

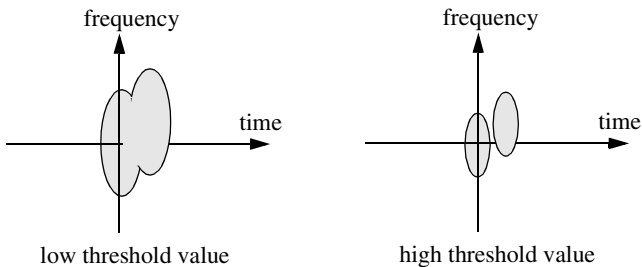


Figure 6.10. Effect of threshold value on resolution.

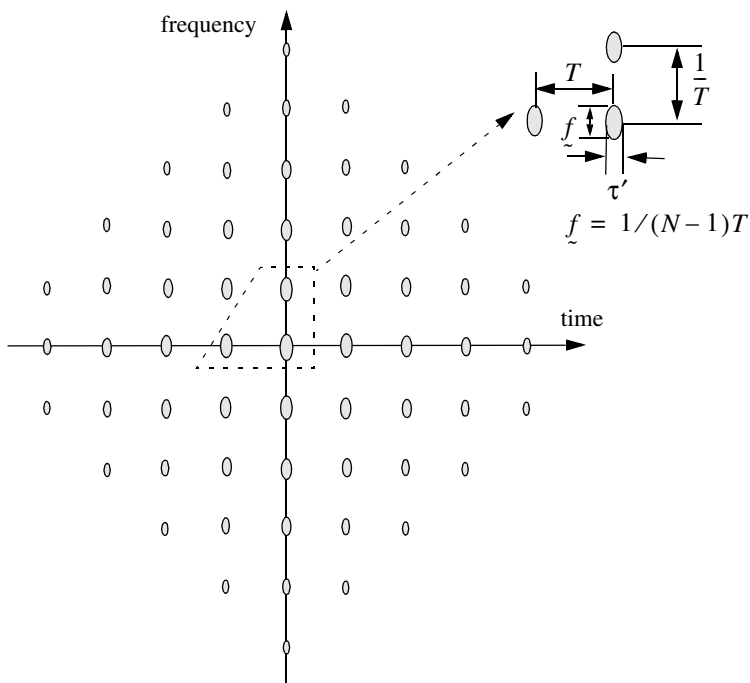


Figure 6.11. Ambiguity contour plot corresponding to Fig. 6.7. For an exact plot see Fig. 6.8b.

As one would expect, high PRF pulse trains (i.e., small T) lead to extreme uncertainty in range, while low PRF pulse trains have extreme ambiguity in Doppler, as shown in Fig. 6.12. Medium PRF pulse trains have moderate ambiguity in both range and Doppler, which can be overcome by using multiple PRFs, as illustrated in Fig. 6.13 for two medium PRFs. Note that the two diagrams (in Fig. 6.13) agree only in one location (center of the plot) which corresponds to the true target location.

It is possible to avoid ambiguities caused by pulse trains and still have reasonable independent control on both range and Doppler accuracies by using a single modulated pulse with a time-bandwidth product that is much larger than unity. Figure 6.14 shows the ambiguity contour plot associated with an LFM waveform. In this case, τ' is the pulse width and B is the pulse bandwidth. In this case, exact plots can be obtained using the function “*lfm_ambg.m*”.

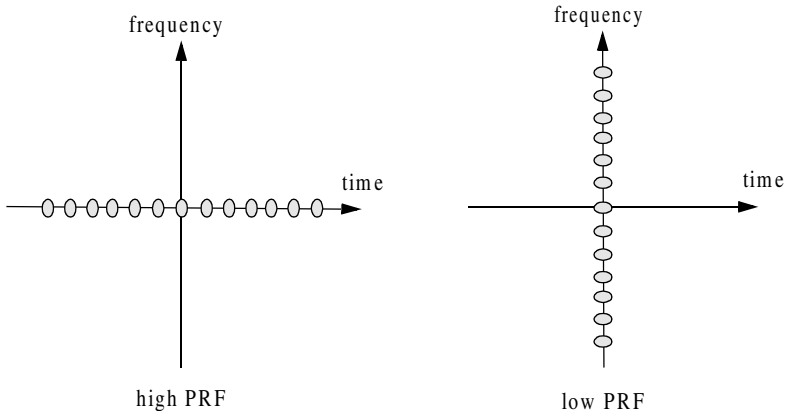


Figure 6.12. Uncertainty associated with low and high PRFs.

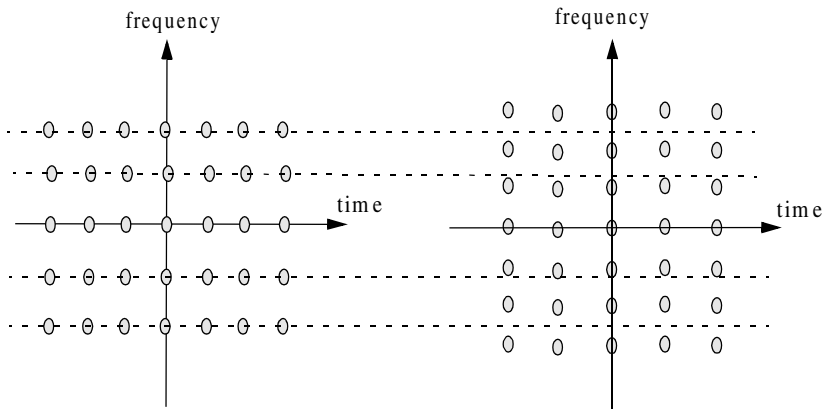


Figure 6.13. Uncertainty of two medium PRFs.

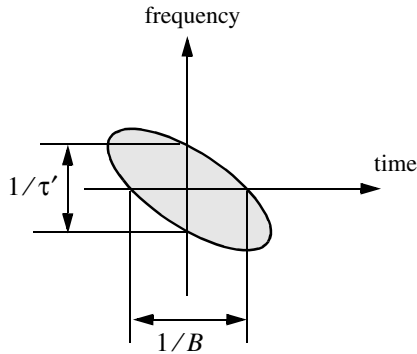


Figure 6.14. Ambiguity contour plot associated with an up-chirp LFM waveform. For an exact plot see [Fig. 6.5b](#).

6.7. MATLAB Listings

This section presents listings for all MATLAB programs/functions used in this chapter. The user is strongly advised to rerun the MATLAB programs in order to enhance their understanding of this chapter's material.

Listing 6.1. MATLAB Function “single_pulse_ambg.m”

```
function x = single_pulse_ambg (taup)
colormap (gray(1))
eps = 0.000001;
i = 0;
taumax = 1.1 * taup;
taumin = -taumax;
for tau = taumin:.05:taumax
    i = i + 1;
    j = 0;
    for fd = -5/taup:.05:5/taup
        j = j + 1;
        val1 = 1. - abs(tau) / taup;
        val2 = pi * taup * (1.0 - abs(tau) / taup) * fd;
        x(j,i) = abs( val1 * sin(val2+eps)/(val2+eps));
    end
end
end
```

Listing 6.2. MATLAB Program “fig6_2.m”

```
clear all
eps = 0.000001;
```

```

taup = 2.;
taumin = -1.1 * taup;
taumax = -taumin;
x = single_pulse_ambg(taup);
taux = taumin:.05:taumax;
fdy = -5/taup:.05:5/taup;
figure(1)
mesh(taux,fdy,x);
xlabel ('Delay - seconds')
ylabel ('Doppler - Hz')
zlabel ('Ambiguity function')
figure(2)
contour(taux,fdy,x);
xlabel ('Delay - seconds')
ylabel ('Doppler - Hz')
y = x.^2;
figure(3)
mesh(taux,fdy,y);
xlabel ('Delay - seconds')
ylabel ('Doppler - Hz')
zlabel ('Ambiguity function')
figure(4)
contour(taux,fdy,y);
xlabel ('Delay - seconds')
ylabel ('Doppler - Hz')

```

Listing 6.3. MATLAB Program “fig6_4.m”

```

clear all
eps = 0.0001;
taup = 2.;
fd = -10./taup:.05:10./taup;
uncer = abs( sinc(taup .* fd));
ambg = uncer.^2;
plot(fd, ambg)
xlabel ('Frequency - Hz')
ylabel ('Ambiguity - Volts')
grid
figure(2)
plot (fd, uncer);
xlabel ('Frequency - Hz')
ylabel ('Uncertainty - Volts')
grid

```

Listing 6.4. MATLAB Function “lfm_ambg.m”

```

function x = lfm_ambg(taup, b, up_down)
eps = 0.000001;

```

```

i = 0;
mu = up_down * b / 2. / taup;
for tau = -1.1*taup:.05:1.1*taup
    i = i + 1;
    j = 0;
    for fd = -b:.05:b
        j = j + 1;
        val1 = 1. - abs(tau) / taup;
        val2 = pi * taup * (1.0 - abs(tau) / taup);
        val3 = (fd + mu * tau);
        val = val2 * val3;
        x(j,i) = abs( val1 * (sin(val+eps)/(val+eps))).^2;
    end
end
end

```

Listing 6.5. MATLAB Program “fig6_5.m”

```

clear all
eps = 0.0001;
taup = 1.;
b = 10.;
up_down = 1.;
x = lfm_ambg(taup, b, up_down);
taux = -1.1*taup:.05:1.1*taup;
fdy = -b:.05:b;
figure(1)
mesh(taux,fdy,x)
xlabel ('Delay - seconds')
ylabel ('Doppler - Hz')
zlabel ('Ambiguity function')
figure(2)
contour(taux,fdy,x)
xlabel ('Delay - seconds')
ylabel ('Doppler - Hz')
y = sqrt(x);
figure(3)
mesh(taux,fdy,y)
xlabel ('Delay - seconds')
ylabel ('Doppler - Hz')
zlabel ('Uncertainty function')
figure(4)
contour(taux,fdy,y)
xlabel ('Delay - seconds')
ylabel ('Doppler - Hz')

```

Listing 6.6. MATLAB Program “fig6_6.m”

```

clear all

```

```

taup = 1;
b =20.;
up_down = 1.;
taux = -1.5*taup:.01:1.5*taup;
fd = 0.;
mu = up_down * b / 2. / taup;
ii = 0.;
for tau = -1.5*taup:.01:1.5*taup
    ii = ii + 1;
    val1 = 1. - abs(tau) / taup;
    val2 = pi * taup * (1.0 - abs(tau) / taup);
    val3 = (fd + mu * tau);
    val = val2 * val3;
    x(ii) = abs( val1 * (sin(val+eps)/(val+eps)));
end
figure(1)
plot(taux,x)
grid
xlabel ('Delay - seconds')
ylabel ('Uncertaunty')
figure(2)
plot(taux,x.^2)
grid
xlabel ('Delay - seconds')
ylabel ('Ambiguity')

```

Listing 6.7. MATLAB Function “train_ambg.m”

```

function x = train_ambg (taup, n, pri)
if( taup > pri / 2.)
    'ERROR. Pulse width must be less than the PRI/2.'
    break
end
gap = pri - 2.*taup;
eps = 0.000001;
b = 1. / taup;
ii = 0.;
for q = -(n-1):1:n-1
    tauo = q - taup ;
    index = -1.;
    for tau1 = tauo:0.0533:tauo+gap+2.*taup
        index = index + 1;
        tau = -taup + index*.0533;
        ii = ii + 1;
        j = 0.;
        for fd = -b:.0533:b
            j = j + 1;
            if (abs(tau) <= taup)

```



```

    val1 = 1. -abs(tau) / taup;
    val2 = pi * taup * fd * (1.0 - abs(tau) / taup);
    val3 = abs(val1 * sin(val2+eps) / (val2+eps));
    val4 = abs((sin(pi*fd*(n-abs(q))*pri+eps)) / (sin(pi*fd*pri+eps)));
    x(j,ii) = val3 * val4 / n;
else
    x(j,ii) = 0.;
end
end
end
end
end

```

Listing 6.8. MATLAB Program “fig6_8a.m”

```

clear all
taup = 0.2;
pri = 1;
n = 5;
x = train_ambg (taup, n, pri);
figure(1)
mesh(x)
xlabel ('Delay - seconds')
ylabel ('Doppler - Hz')
zlabel ('Ambiguity function')
figure(2)
contour(x);
xlabel ('Delay - seconds')
ylabel ('Doppler - Hz')

```

Problems

6.1. Define $\{x_I(n) = 1, -1, 1\}$ and $\{x_Q(n) = 1, 1, -1\}$. (a) Compute the discrete correlations: R_{x_I} , R_{x_Q} , $R_{x_I x_Q}$, and $R_{x_Q x_I}$. (b) A certain radar transmits the signal $s(t) = x_I(t) \cos 2\pi f_0 t - x_Q(t) \sin 2\pi f_0 t$. Assume that the autocorrelation $s(t)$ is equal to $y(t) = y_I(t) \cos 2\pi f_0 t - y_Q(t) \sin 2\pi f_0 t$. Compute and sketch $y_I(t)$ and $y_Q(t)$.

6.2. Compute the frequency response for the filter matched to the signal

$$(a) x(t) = \exp\left(\frac{-t^2}{2T}\right); (b) x(t) = u(t) \exp(-\alpha t),$$

where α is a positive constant.

6.3. Repeat Example 6.1 for $x(t) = u(t) \exp(-\alpha t)$.

- 6.4. Derive Eq. (6.43).
- 6.5. Prove the properties of the radar ambiguity function.
- 6.6. Starting with Eq. (6.61) derive Eq. (6.62).
- 6.7. A radar system uses LFM waveforms. The received signal is of the form $s_r(t) = As(t - \tau) + n(t)$, where τ is a time delay that depends on range, $s(t) = \text{Rect}(t/\tau') \cos(2\pi f_0 t - \psi(t))$, and $\psi(t) = -\pi B t^2 / \tau'$. Assume that the radar bandwidth is $B = 5\text{MHz}$, and the pulse width is $\tau' = 5\mu\text{s}$. (a) Give the quadrature components of the matched filter response that matched to $s(t)$. (b) Write an expression for the output of the matched filter. (c) Compute the increase in SNR produced by the matched filter.
- 6.8. (a) Write an expression for the ambiguity function of an LFM waveform, where $\tau' = 6.4\mu\text{s}$, and the compression ratio is 32. (b) Give an expression for the matched filter impulse response.
- 6.9. Repeat Example 6.2 for $B = 2, 5$, and 10GHz .
- 6.10. (a) Write an expression for the ambiguity function of a LFM signal with bandwidth $B = 10\text{MHz}$, pulse width $\tau' = 1\mu\text{s}$, and wavelength $\lambda = 1\text{cm}$. (b) Plot the zero Doppler cut of the ambiguity function. (c) Assume a target moving towards the radar with radial velocity $v_r = 100\text{m/s}$. What is the Doppler shift associated with this target? (d) Plot the ambiguity function for the Doppler cut in part (c). (e) Assume that three pulses are transmitted with PRF $f_r = 2000\text{Hz}$. Repeat part b.
- 6.11. (a) Give an expression for the ambiguity function for a pulse train consisting of 4 pulses, where the pulse width is $\tau' = 1\mu\text{s}$ and the pulse repetition interval is $T = 10\mu\text{s}$. Assume a wavelength of $\lambda = 1\text{cm}$. (b) Sketch the ambiguity function contour.
- 6.12. Hyperbolic frequency modulation (HFM) is better than LFM for high radial velocities. The HFM phase is

$$\psi_h(t) = \frac{\omega_0^2}{\mu_h} \ln \left(1 + \frac{\mu_h \alpha t}{\omega_0} \right)$$

where μ_h is an HFM coefficient and α is a constant. (a) Give an expression for the instantaneous frequency of a HFM pulse of duration τ'_h . (b) Show that HFM can be approximated by LFM. Express the LFM coefficient μ_l in terms of μ_h and in terms of B and τ' .

- 6.13. Consider a Sonar system with range resolution $\Delta R = 4\text{cm}$. (a) A sinusoidal pulse at frequency $f_0 = 100\text{KHz}$ is transmitted. What is the pulse width, and what is the bandwidth? (b) By using an up-chirp LFM, centered at

f_0 , one can increase the pulse width for the same range resolution. If you want to increase the transmitted energy by a factor of 20, give an expression for the transmitted pulse. (c) Give an expression for the causal filter matched to the LFM pulse in part b.

6.14. A pulse train $y(t)$ is given by

$$y(t) = \sum_{n=0}^2 w(n)x(t - n\tau')$$

where $x(t) = \exp(-t^2/2)$ is a single pulse of duration τ' and the weighting sequence is $\{w(n)\} = \{0.5, 1, 0.7\}$. Find and sketch the correlations R_x , R_w , and R_y .

6.15. Repeat the previous problem for $x(t) = \exp(-t^2/2)\cos 2\pi f_0 t$.

6.16. Modify the function “*train_ambg.m*” to accommodate the case $\tau' = T$.

6.17. Using the MATLAB functions presented in this chapter, generate the exact plots that correspond to [Figs. 6.13](#) and [6.14](#).

6.18. Using the function “*lfm_ambg.m*” reproduce [Fig. 6.6b](#) for a down-chirp LFM pulse.

Range resolution for a given radar can be significantly improved by using very short pulses. Unfortunately, utilizing short pulses decreases the average transmitted power, which can hinder the radar's normal modes of operation, particularly for multi-function and surveillance radars. Since the average transmitted power is directly linked to the receiver SNR, it is often desirable to increase the pulse width (i.e., increase the average transmitted power) while simultaneously maintaining adequate range resolution. This can be made possible by using pulse compression techniques. Pulse compression allows us to achieve the average transmitted power of a relatively long pulse, while obtaining the range resolution corresponding to a short pulse. In this chapter, we will analyze analog and digital pulse compression techniques.

Two analog pulse compression techniques are discussed in this chapter. The first technique is known as "correlation processing" which is dominantly used for narrow band and some medium band radar operations. The second technique is called "stretch processing" and is normally used for extremely wide band radar operations. Digital pulse compression will also be briefly presented.

7.1. Time-Bandwidth Product

Consider a radar system that employs a matched filter receiver. Let the matched filter receiver bandwidth be denoted as B . Then, the noise power available within the matched filter bandwidth is given by

$$N_i = 2 \frac{N_0}{2} B \quad (7.1)$$

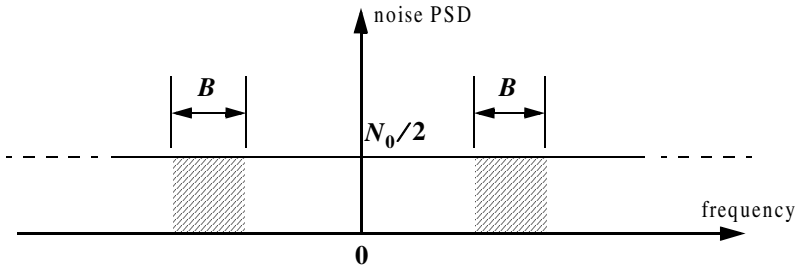


Figure 7.1. Input noise power.

where the factor of two is used to account for both negative and positive frequency bands, as illustrated in Fig. 7.1. The average input signal power over a pulse duration τ' is

$$S_i = \frac{E}{\tau'} \quad (7.2)$$

E is the signal energy. Consequently, the matched filter input SNR is given by

$$(SNR)_i = \frac{S_i}{N_i} = \frac{E}{N_0 B \tau'} \quad (7.3)$$

Using Eqs. (6.18) (from Chapter 6) and (7.3), one may compute the output peak instantaneous SNR to the input SNR ratio as

$$\frac{SNR(t_0)}{(SNR)_i} = 2B\tau' \quad (7.4)$$

The quantity $B\tau'$ is referred to as the “time-bandwidth product” for a given waveform, or its corresponding matched filter. The factor $B\tau'$ by which the output SNR is increased over that at the input is called the matched filter gain, or simply the compression gain.

In general, the time-bandwidth product of an unmodulated pulse approaches unity. The time-bandwidth product of a pulse can be made much greater than unity by using frequency or phase modulation. If the radar receiver transfer function is perfectly matched to that of the input waveform, then the compression gain is equal to $B\tau'$. Clearly, the compression gain becomes smaller than $B\tau'$ as the spectrum of the matched filter deviates from that of the input signal.

7.2. Radar Equation with Pulse Compression

The radar equation for a pulsed radar can be written as

$$SNR = \frac{P_i \tau' G^2 \lambda^2 \sigma}{(4\pi)^3 R^4 k T_e FL} \quad (7.5)$$

where P_i is peak power, τ' is pulse width, G is antenna gain, σ is target RCS, R is range, k is Boltzman's constant, T_e is effective noise temperature, F is noise figure, and L is total radar losses.

Pulse compression radars transmit relatively long pulses (with modulation) and process the radar echo into very short pulses (compressed). One can view the transmitted pulse to be composed of a series of very short subpulses (duty is 100%), where the width of each subpulse is equal to the desired compressed pulse width. Denote the compressed pulse width as τ_c . Thus, for an individual subpulse, Eq. (7.5) can be written as

$$(SNR)_{\tau_c} = \frac{P_i \tau_c G^2 \lambda^2 \sigma}{(4\pi)^3 R^4 k T_e FL} \quad (7.6)$$

The SNR for the uncompressed pulse is then derived from Eq. (7.6) as

$$SNR = \frac{P_i (\tau' = n\tau_c) G^2 \lambda^2 \sigma}{(4\pi)^3 R^4 k T_e FL} \quad (7.7)$$

where n is the number of subpulses. Equation (7.7) is denoted as the radar equation with pulse compression.

Observation of Eqs. (7.5) and (7.7) indicates the following (note that both equations have the same form): For a given set of radar parameters, and as long as the transmitted pulse remains unchanged, then the SNR is also unchanged regardless of the signal bandwidth. More precisely, when pulse compression is used, the detection range is maintained while the range resolution is drastically improved by keeping the pulse width unchanged and by increasing the bandwidth. Remember that range resolution is proportional to the inverse of the signal bandwidth,

$$\Delta R = c/2B \quad (7.8)$$

7.3. Analog Pulse Compression

Correlation and stretch pulse compression techniques are discussed in this section. Two MATLAB programs which execute digital implementation of both techniques (using the FFT) are also presented.

7.3.1. Correlation Processor

In this case, pulse compression is accomplished by adding frequency modulation to a long pulse at transmission, and by using a matched filter receiver in order to compress the received signal. As an example, we saw in Chapter 6 that using LFM within a rectangular pulse compresses the matched filter output by a factor $\xi = B\tau$, which is directly proportional to the pulse width and bandwidth. Thus, by using long pulses and wideband LFM modulation we can achieve large compression ratios. This form of pulse compression is known as “correlation processing.”

Fig. 7.2 illustrates the advantage of pulse compression. In this example, an LFM waveform is used. Two targets with RCS $\sigma_1 = 1m^2$ and $\sigma_2 = 0.5m^2$ are detected. The two targets are not separated enough in time to be resolved. Fig. 7.2a shows the composite echo signal from those targets. Clearly, the target returns overlap and, thus, they are not resolved. However, after pulse compression the two pulses are completely separated and are resolved as two targets. In fact, when using LFM, returns from neighboring targets are resolved as long as they are separated, in time, by τ_{n1} , the compressed pulse width.

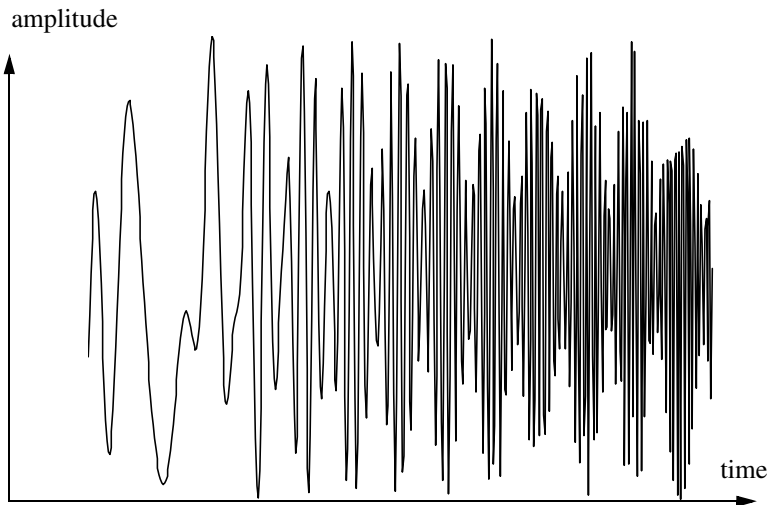


Figure 7.2a. Composite echo signal for two unresolved targets.

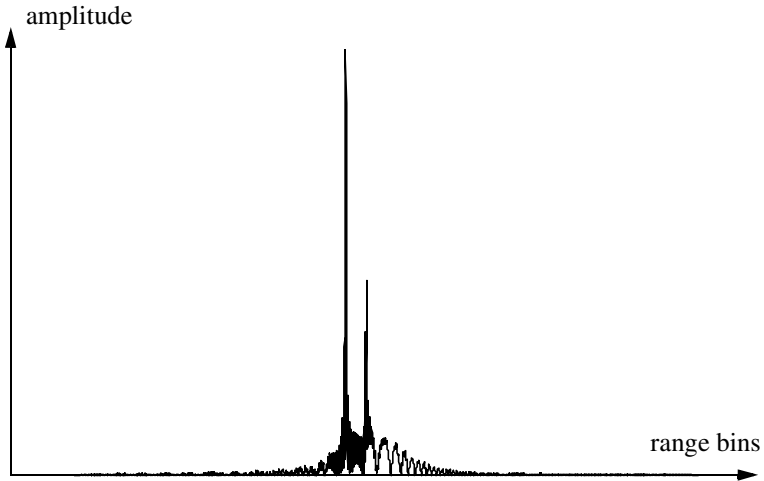


Figure 7.2b. Composite echo signal corresponding to Fig. 7.2a, after pulse compression.

Radar operations (search, track, etc.) are usually carried out over a specified range window, referred to as the receive window and defined by the difference between the radar maximum and minimum range. Returns from all targets within the receive window are collected and passed through a matched filter circuitry to perform pulse compression. One implementation of such analog processors is the Surface Acoustic Wave (SAW) devices. Because of the recent advances in digital computer development, the correlation processor is often performed digitally using the FFT. This digital implementation is called Fast Convolution Processing (FCP) and can be implemented at base-band. The fast convolution process is illustrated in Fig. 7.3

Since the matched filter is a linear time invariant system, its output can be described mathematically by the convolution between its input and its impulse response,

$$y(t) = s(t) \bullet h(t) \quad (7.9)$$

where $s(t)$ is the input signal, $h(t)$ is the matched filter impulse response (replica), and the \bullet operator symbolically represents convolution. From the Fourier transform properties,

$$FFT\{s(t) \bullet h(t)\} = S(f) \cdot H(f) \quad (7.10)$$

And when both signals are sampled properly, the compressed signal $y(t)$ can be computed from

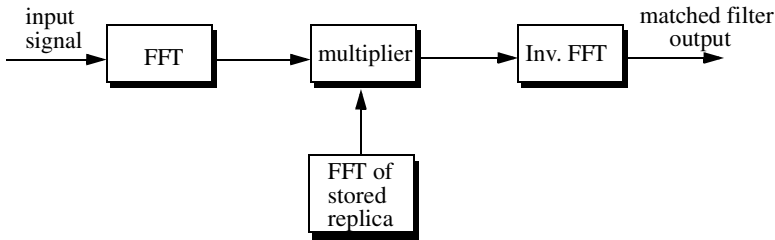


Figure 7.3. Computing the matched filter output using an FFT.

$$y = FFT^{-1}\{S \cdot H\} \quad (7.11)$$

where FFT^{-1} is the inverse FFT. When using pulse compression, it is desirable to use modulation schemes that can accomplish a maximum pulse compression ratio, and can significantly reduce the side lobe levels of the compressed waveform. For the LFM case the first side lobe is approximately $13.4dB$ below the main peak, and for most radar applications this may not be sufficient. In practice, high side lobe levels are not preferable because noise and/or jammers located at the side lobes may interfere with target returns in the main lobe.

Weighting functions (windows) can be used on the compressed pulse spectrum in order to reduce the side lobe levels. The cost associated with such an approach is a loss in the main lobe resolution, and a reduction in the peak value (i.e., loss in the SNR), as illustrated in Fig. 7.4. Weighting the time domain transmitted or received signal instead of the compressed pulse spectrum will theoretically achieve the same goal. However, this approach is rarely used, since amplitude modulating the transmitted waveform introduces extra burdens on the transmitter.

Consider a radar system that utilizes a correlation processor receiver (i.e., matched filter). The receive window in meters is defined by

$$R_{rec} = R_{max} - R_{min} \quad (7.12)$$

where R_{max} and R_{min} , respectively, define the maximum and minimum range over which the radar performs detection. Typically R_{rec} is limited to the extent of the target complex. The normalized complex transmitted signal has the form

$$s(t) = \exp\left(j2\pi\left(f_0 t + \frac{\mu}{2} t^2\right)\right) \quad 0 \leq t \leq \tau' \quad (7.13)$$

τ' is the pulse width, $\mu = B/\tau'$, and B is the bandwidth. Note that this definition of the LFM pulse is different from that in Chapter 6. Earlier, f_0 denoted the chirp center frequency and in Eq. (7.13) it denotes the chirp start frequency.

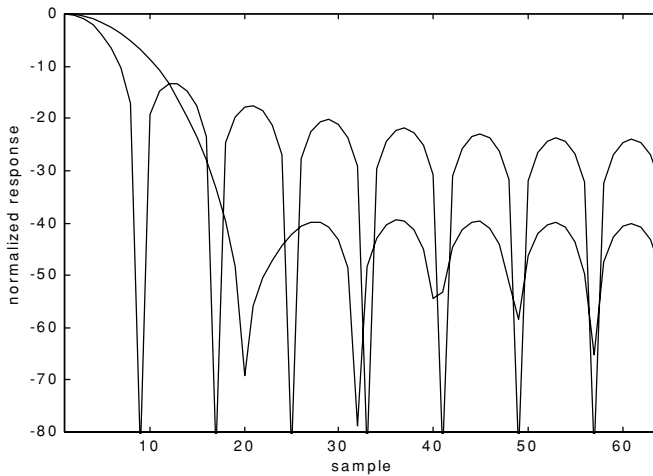


Figure 7.4. Reducing the first sidelobe to -42 dB doubles the main lobe width.

The radar echo signal is similar to the transmitted one with the exception of a time delay and an amplitude change that correspond to the target RCS. Consider a target at range R_1 . The echo received by the radar from this target is

$$s_r(t) = a_1 \exp\left(j2\pi\left(f_0(t - \tau_1) + \frac{\mu}{2}(t - \tau_1)^2\right)\right) \quad (7.14)$$

where a_1 is proportional to target RCS, antenna gain, and range attenuation. The time delay τ_1 is given by

$$\tau_1 = 2R_1/c \quad (7.15)$$

The first step of the processing consists of removing the frequency f_0 . This is accomplished by mixing $s_r(t)$ with a reference signal whose phase is $2\pi f_0 t$. The phase of the resultant signal, after low pass filtering, is then given by

$$\psi(t) = 2\pi\left(-f_0\tau_i + \frac{\mu}{2}(t - \tau_i)^2\right) \quad (7.16)$$

and the instantaneous frequency is

$$f_i(t) = \frac{1}{2\pi} \frac{d}{dt}\psi(t) = \mu(t - \tau_i) = \frac{B}{\tau'}\left(t - \frac{2R_1}{c}\right) \quad (7.17)$$

The quadrature components are

$$\begin{pmatrix} x_I(t) \\ x_Q(t) \end{pmatrix} = \begin{pmatrix} \cos \psi(t) \\ \sin \psi(t) \end{pmatrix} \quad (7.18)$$

Sampling the quadrature components is performed next. The number of samples, N , must be chosen so that foldover (ambiguity) in the spectrum is avoided. For this purpose, the sampling frequency, f_s (based on the Nyquist sampling rate), must be

$$f_s \geq 2B \quad (7.19)$$

and the sampling interval is

$$\Delta t \leq 1/2B \quad (7.20)$$

Using Eq. (7.17) it can be shown that (the proof is left as an exercise) the frequency resolution of the FFT is

$$\Delta f = 1/\tau' \quad (7.21)$$

The minimum required number of samples is

$$N = \frac{1}{\Delta f \Delta t} = \frac{\tau'}{\Delta t} \quad (7.22)$$

Equating Eqs. (7.20) and (7.22) yields

$$N \geq 2B\tau' \quad (7.23)$$

Consequently, a total of $2B\tau'$ real samples, or $B\tau'$ complex samples, is sufficient to completely describe an LFM waveform of duration τ' and bandwidth B . For example, an LFM signal of duration $\tau = 20 \mu s$ and bandwidth $B = 5 \text{ MHz}$ requires 200 real samples to determine the input signal (100 samples for the I-channel and 100 samples for the Q-channel).

For better implementation of the FFT N is extended by zero padding, to the next power of two. Thus, the total number of samples, for some positive integer m , is

$$N_{FFT} = 2^m \geq N \quad (7.24)$$

The final steps of the FCP processing include: (1) taking the FFT of the sampled sequence; (2) multiplying the frequency domain sequence of the signal with the FFT of the matched filter impulse response; and (3) performing the inverse FFT of the composite frequency domain sequence in order to generate the time domain compressed pulse (HRR profile). Of course, weighting, antenna gain, and range attenuation compensation must also be performed.

Assume that I targets at ranges R_1, R_2, \dots and so forth are within the receive window. From superposition, the phase of the down converted signal is

$$\psi(t) = \sum_{i=1}^I 2\pi \left(-f_0 \tau_i + \frac{\mu}{2} (t - \tau_i)^2 \right) \quad (7.25)$$

The times $\{\tau_i = (2R_i/c); i = 1, 2, \dots, I\}$ represent the two-way time delays, where τ_1 coincides with the start of the receive window.

MATLAB Function “*matched_filter.m*”

The function “*matched_filter.m*” performs fast convolution processing. It is given in Listing 7.1 in Section 7.5. The syntax is as follows:

$[y] = \text{matched_filter}(nscat, \text{taup}, f0, b, \text{rmin}, \text{rrec}, \text{scat_range}, \text{scat_rcs}, \text{win})$

where

Symbol	Description	Units	Status
<i>nscat</i>	<i>number of point scatterers within the received window</i>	<i>none</i>	<i>input</i>
<i>rmin</i>	<i>minimum range of receive window</i>	<i>Km</i>	<i>input</i>
<i>rrec</i>	<i>receive window size</i>	<i>m</i>	<i>input</i>
<i>taup</i>	<i>uncompressed pulse width</i>	<i>seconds</i>	<i>input</i>
<i>f0</i>	<i>chirp start frequency</i>	<i>Hz</i>	<i>input</i>
<i>b</i>	<i>chirp bandwidth</i>	<i>Hz</i>	<i>input</i>
<i>scat_range</i>	<i>vector of scatterers range</i>	<i>Km</i>	<i>input</i>
<i>scat_rsc</i>	<i>vector of scatterers RCS</i>	<i>m²</i>	<i>input</i>
<i>win</i>	<i>0 = no window</i> <i>1 = Hamming</i> <i>2 = Kaiser with parameter pi</i> <i>3 = Chebychev - sidelobes at -60dB</i>	<i>none</i>	<i>input</i>
<i>y</i>	<i>compressed output</i>	<i>volts</i>	<i>output</i>

The user can access this function either by a MATLAB function call, or by executing the MATLAB program “*matched_filter_driver.m*” which utilizes MATLAB based GUI. The outputs of this function are the complex array y and plots of the uncompressed and compressed signal versus relative. This function utilizes the function “*power_integer_2.m*” which implements Eq. (7.24):

```

function n = power_integer_2(x)
m = 0.;
for j = 1:30
    m = m + 1.;
    delta = x - 2.^m;
    if(delta < 0.)
        n = m;
        return
    else
        end
end
end

```

As an example, consider the case where

<i>nscat</i>	2	<i>b</i>	16 MHz
<i>rmin</i>	150 Km	<i>scat_range</i>	<i>rmin</i> in Km + {0, 50} meters
<i>rrec</i>	200 m	<i>scat_rsc</i>	{1, 1} m ²
<i>taup</i>	0.005 ms	<i>win</i>	2 (Kaiser)
<i>f0</i>	14 MHz		

Note that the compressed pulsed range resolution, without using a window, is $\Delta R = 9.3m$. [Figs. 7.5](#) and [7.6](#), respectively, show the uncompressed and compressed echo signal corresponding to this example.

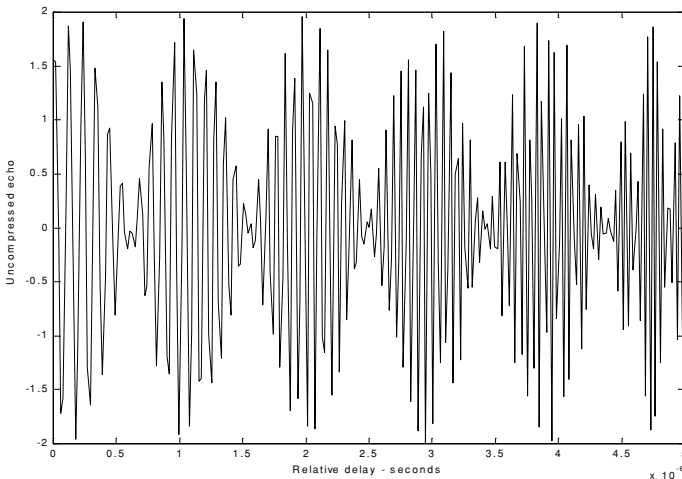


Figure 7.5. Uncompressed echo signal. Scatterers are unresolved.

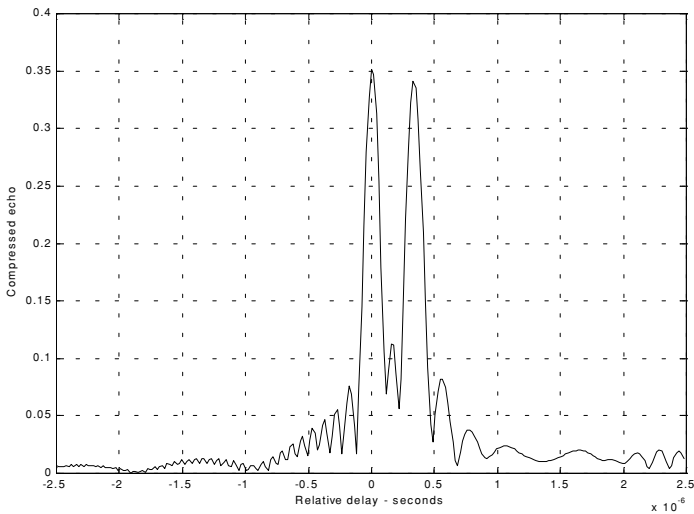


Figure 7.6. Compressed echo signal. Scatterers are resolved.

7.3.2. Stretch Processor

Stretch processing, also known as “active correlation,” is normally used to process extremely high bandwidth LFM waveforms. This processing technique consists of the following steps: First, the radar returns are mixed with a replica (reference signal) of the transmitted waveform. This is followed by Low Pass Filtering (LPF) and coherent detection. Next, Analog to Digital (A/D) conversion is performed; and finally, a bank of Narrow Band Filters (NBFs) is used in order to extract the tones that are proportional to target range, since stretch processing effectively converts time delay into frequency. All returns from the same range bin produce the same constant frequency. Fig. 7.7 shows a block diagram for a stretch processing receiver. The reference signal is an LFM waveform that has the same LFM slope as the transmitted LFM signal. It exists over the duration of the radar “receive-window,” which is computed from the difference between the radar maximum and minimum range. Denote the start frequency of the reference chirp as f_r .

Consider the case when the radar receives returns from a few close (in time or range) targets, as illustrated in Fig. 7.7. Mixing with the reference signal and performing low pass filtering are effectively equivalent to subtracting the return frequency chirp from the reference signal. Thus, the LPF output consists of constant tones corresponding to the targets’ positions. The normalized transmitted signal can be expressed by

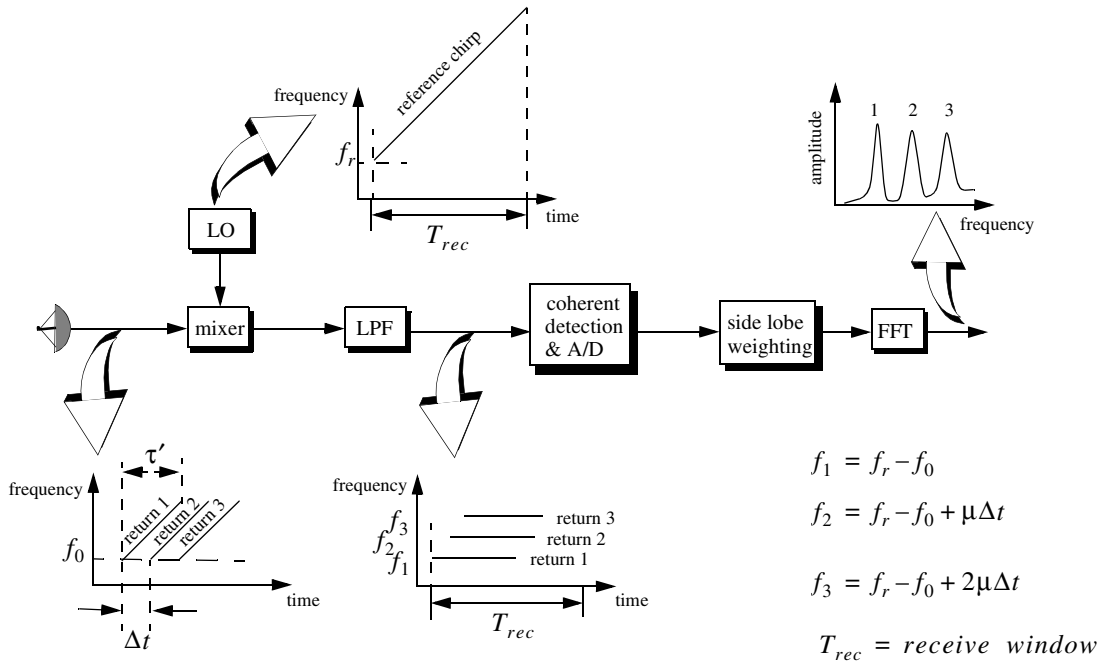


Figure 7.7. Stretch processing block diagram.

$$s_1(t) = \cos\left(2\pi\left(f_0 t + \frac{\mu}{2} t^2\right)\right) \quad 0 \leq t \leq \tau' \quad (7.26)$$

where $\mu = B/\tau'$ is the LFM coefficient and f_0 is the chirp start frequency. Assume a point scatterer at range R . The received signal by the radar is

$$s_r(t) = a \cos\left[2\pi\left(f_0(t - \Delta\tau) + \frac{\mu}{2}(t - \Delta\tau)^2\right)\right] \quad (7.27)$$

where a is proportional to target RCS, antenna gain, and range attenuation. The time delay $\Delta\tau$ is

$$\Delta\tau = 2R/c \quad (7.28)$$

The reference signal is

$$s_{ref}(t) = 2 \cos\left(2\pi\left(f_r t + \frac{\mu}{2} t^2\right)\right) \quad 0 \leq t \leq T_{rec} \quad (7.29)$$

The received window in seconds is

$$T_{rec} = \frac{2(R_{max} - R_{min})}{c} = \frac{2R_{rec}}{c} \quad (7.30)$$

It is customary to let $f_r = f_0$. The output of the mixer is made of the product of the received and reference signals. After low pass filtering the signal is

$$s_0(t) = a \cos(2\pi f_0 t \Delta\tau + 2\pi\mu\Delta\tau t - \pi\mu(\Delta\tau)^2) \quad (7.31)$$

Substituting Eq. (7.28) into (7.31) and collecting terms yield

$$s_0(t) = a \cos\left[\left(\frac{4\pi BR}{c\tau'}\right)t + \frac{2R}{c}\left(2\pi f_0 - \frac{2\pi BR}{c\tau'}\right)\right] \quad (7.32)$$

and since $\tau' \gg 2R/c$, Eq. (7.32) is approximated by

$$s_0(t) \approx a \cos\left[\left(\frac{4\pi BR}{c\tau'}\right)t + \frac{4\pi R}{c}f_0\right] \quad (7.33)$$

The instantaneous frequency is

$$f_{inst} = \frac{1}{2\pi} \frac{d}{dt} \left(\frac{4\pi BR}{c\tau'} t + \frac{4\pi R}{c} f_0 \right) = \frac{2BR}{c\tau'} \quad (7.34)$$

which clearly indicates that target range is proportional to the instantaneous frequency. Therefore, proper sampling of the LPF output and taking the FFT of

the sampled sequence lead to the following conclusion: a peak at some frequency f_1 indicates presence of a target at range

$$R_1 = f_1 c \tau' / 2B \quad (7.35)$$

Assume I close targets at ranges R_1, R_2, \dots and so forth ($R_1 < R_2 < \dots < R_I$). From superposition, the total signal is

$$s_r(t) = \sum_{i=1}^I a_i(t) \cos \left[2\pi \left(f_0(t - \tau_i) + \frac{\mu}{2}(t - \tau_i)^2 \right) \right] \quad (7.36)$$

where $\{a_i(t); i = 1, 2, \dots, I\}$ are proportional to the targets' cross sections, antenna gain, and range. The times $\{\tau_i = (2R_i/c); i = 1, 2, \dots, I\}$ represent the two-way time delays, where τ_1 coincides with the start of the receive window. Using Eq. (7.32) the overall signal at the output of the LPF can then be described by

$$s_o(t) = \sum_{i=1}^I a_i \cos \left[\left(\frac{4\pi B R_i}{c \tau'} \right) t + \frac{2R_i}{c} \left(2\pi f_0 - \frac{2\pi B R_i}{c \tau'} \right) \right] \quad (7.37)$$

And hence, target returns appear at constant frequency tones that can be resolved using the FFT. Consequently, determining the proper sampling rate and FFT size is very critical. The rest of this section presents a methodology for computing the proper FFT parameters required for stretch processing.

Assume a radar system using a stretch processor receiver. The pulse width is τ' and the chirp bandwidth is B . Since stretch processing is normally used in extreme bandwidth cases (i.e., very large B), the receive window over which radar returns will be processed is typically limited to few meters to possibly less than 100 meters. The compressed pulse range resolution is computed from Eq. (7.8). Declare the FFT size by N and its frequency resolution by Δf . The frequency resolution can be computed using the following procedure: consider two adjacent point scatterers at range R_1 and R_2 . The minimum frequency separation, Δf , between those scatterers so that they are resolved can be computed from Eq. (7.34). More precisely,

$$\Delta f = f_2 - f_1 = \frac{2B}{c \tau'} (R_2 - R_1) = \frac{2B}{c \tau'} \Delta R \quad (7.38)$$

Substituting Eq. (7.8) into Eq. (7.38) yields

$$\Delta f = \frac{2B}{c \tau'} \frac{c}{2B} = \frac{1}{\tau'} \quad (7.39)$$

The maximum resolvable frequency by the FFT is limited to the region $\pm N\Delta f/2$. Thus, the maximum resolvable frequency is

$$\frac{N\Delta f}{2} > \frac{2B(R_{max} - R_{min})}{c\tau'} = \frac{2BR_{rec}}{c\tau'} \quad (7.40)$$

Using Eqs. (7.30) and (7.39) into Eq. (7.40) and collecting terms yield

$$N > 2BT_{rec} \quad (7.41)$$

For better implementation of the FFT, choose an FFT of size

$$N_{FFT} \geq N = 2^m \quad (7.42)$$

m is a nonzero positive integer. The sampling interval is then given by

$$\Delta f = \frac{1}{T_s N_{FFT}} \Rightarrow T_s = \frac{1}{\Delta f N_{FFT}} \quad (7.43)$$

MATLAB Function “stretch.m”

The function “*stretch.m*” presents a digital implementation of stretch processing. It is given in Listing 7.2 in Section 7.5. The syntax is as follows:

$$[y] = stretch(nscat, \tau_{aup}, f_0, b, rmin, rrec, scat_range, scat_rcs, win)$$

where

Symbol	Description	Units	Status
<i>nscat</i>	<i>number of point scatterers within the received window</i>	<i>none</i>	<i>input</i>
<i>rmin</i>	<i>minimum range of receive window</i>	<i>Km</i>	<i>input</i>
<i>rrec</i>	<i>range receive window</i>	<i>m</i>	<i>input</i>
<i>taup</i>	<i>uncompressed pulse width</i>	<i>seconds</i>	<i>input</i>
<i>f0</i>	<i>chirp start frequency</i>	<i>Hz</i>	<i>input</i>
<i>b</i>	<i>chirp bandwidth</i>	<i>Hz</i>	<i>input</i>
<i>scat_range</i>	<i>vector of scatterers range</i>	<i>Km</i>	<i>input</i>
<i>scat_rsc</i>	<i>vector of scatterers RCS</i>	<i>m²</i>	<i>input</i>
<i>win</i>	<i>0 = no window 1 = Hamming 2 = Kaiser with parameter pi 3 = Chebychev - sidelobes at -60dB</i>	<i>none</i>	<i>input</i>
<i>y</i>	<i>compressed output</i>	<i>volts</i>	<i>output</i>

The user can access this function either by a MATLAB function call or by executing the MATLAB program “*stretch_driver.m*” which utilizes MATLAB based GUI. The outputs of this function are the complex array y and plots of the uncompressed and compressed echo signal versus time. As an example, consider the case where

<i>nscat</i>	3
<i>rmin</i>	150 Km
<i>rrec</i>	30 m
<i>taup</i>	10 ms
<i>f0</i>	5.6 GHz
<i>b</i>	1 GHz
<i>scat_range</i>	<i>rmin</i> in Km+ {1.5, 7.5, 15.5} m
<i>scat_rsc</i>	{1, 1, 2} m ²
<i>win</i>	2 (Kaiser)

Note that the compressed pulse range resolution, without using a window, is $\Delta R = 0.15\text{cm}$. Figs. 7.8 and 7.9, respectively, show the uncompressed and compressed echo signals corresponding to this example.

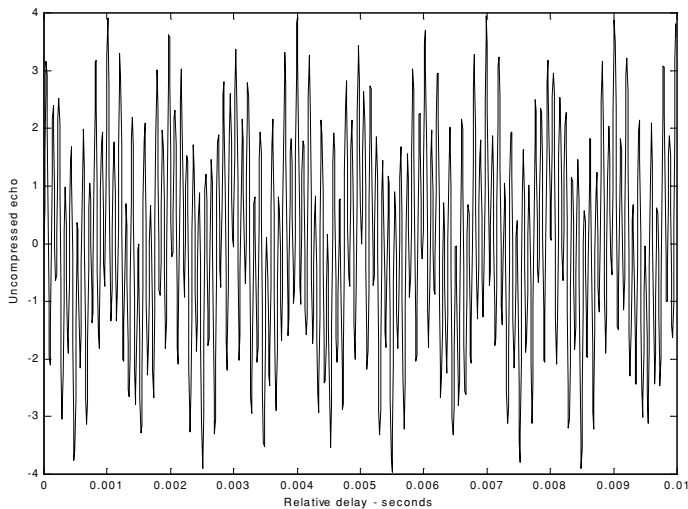


Figure 7.8. Uncompressed echo signal. Three targets are unresolved.

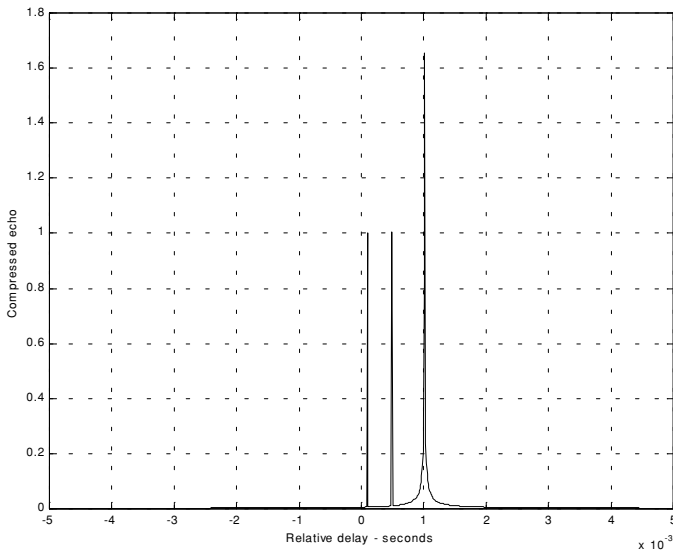


Figure 7.9. Compressed echo signal. Three targets are resolved.

7.3.3. Distortion Due to Target Velocity

Up to this point, we have analyzed pulse compression with no regards to target velocity. In fact, all analyses provided assumed stationary targets. Uncompensated target radial velocity, or equivalently Doppler shift, degrades the quality of the HRR profile generated by pulse compression. In Chapter 5, the effects of radial velocity on SFW were analyzed; similar distortion in the HRR profile is also present with LFM waveforms when target radial velocity is not compensated for.

The two effects of target radial velocity (Doppler frequency) on the radar received pulse were developed in Chapter 1. When the target radial velocity is not zero, the received pulse width is expanded (or compressed) by the time dilation factor. Additionally, the received pulse center frequency is shifted by the amount of Doppler frequency. When these effects are not compensated for, the pulse compression processor output is distorted. This is illustrated in Fig. 7.10. Fig. 7.10a shows a typical output of the pulse compression processor with no distortion. Alternatively, Figs. 7.10b, 7.10c, and 7.10d show the output of the pulse compression processor when 5% shift of the chirp center frequency and 10% time dilation are present.

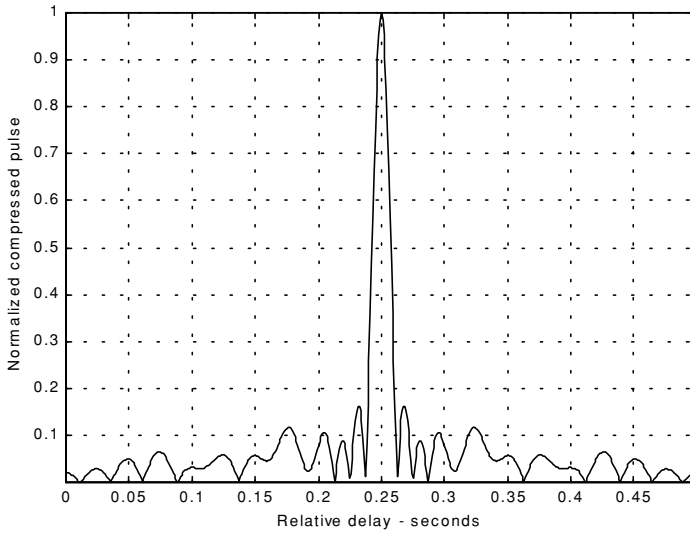


Figure 7.10a. Compressed pulse output of a pulse compression processor. No distortion is present. This figure can be reproduced using MATLAB program “fig7_10” given in Listing 7.3 in Section 7.5.

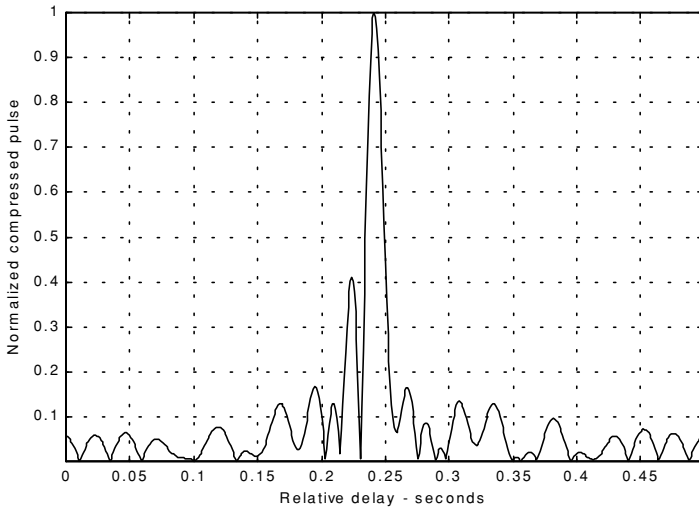


Figure 7.10b. Mismatched compressed pulse; 5% Doppler shift.

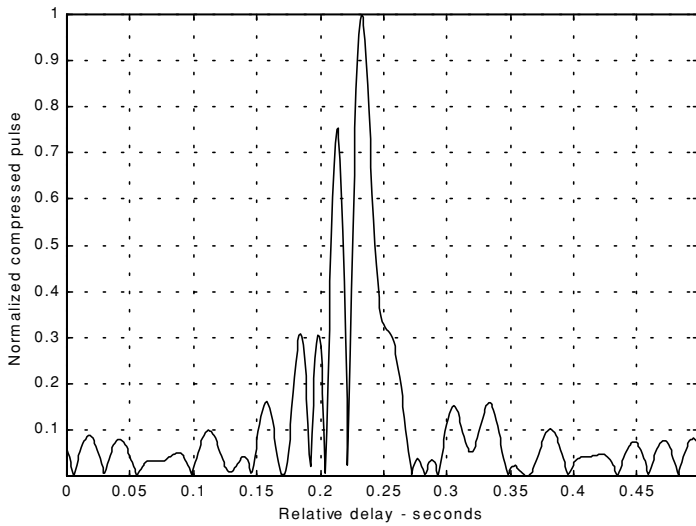


Figure 7.10c. Mismatched compressed pulse; 10% time dilation.

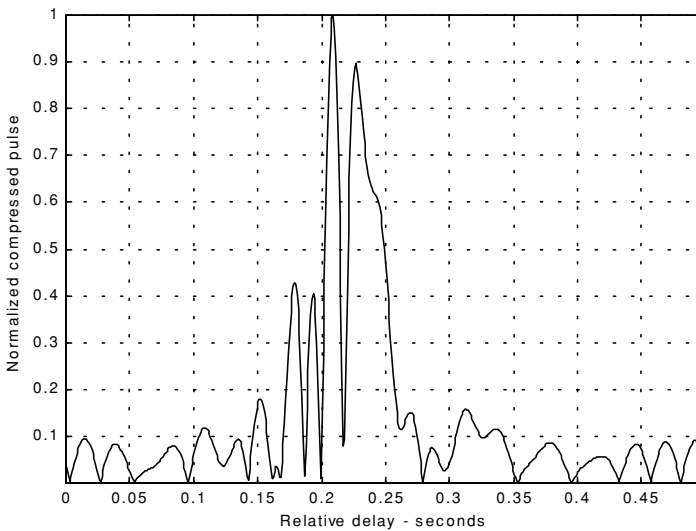


Figure 7.10d. Mismatched compressed pulse; 10% time dilation and 5% Doppler shift.

Correction for the distortion caused by the target radial velocity can be overcome by using the following approach. Over a period of few pulses, the radar data processor estimates the radial velocity of the target under track. Then, the chirp slope and pulse width of the next transmitted pulse are changed to account for the estimated Doppler frequency and time dilation.

7.3.4. Range Doppler Coupling

Plots and characteristics of the ambiguity function for an LFM waveform were presented in Chapter 6. However, the distinctive property of range Doppler coupling associated with LFM was not presented. Range Doppler coupling is a phrase used to describe the shift in the delay/range response of an LFM ambiguity function due to the presence of a Doppler shift. The nature of range Doppler coupling can be better understood by analyzing the LFM ambiguity function. An expression for an LFM ambiguity function was developed in Chapter 6, and is repeated here as Eq. (7.44):

$$|\chi(\tau; f_d)|^2 = \left| \frac{\sin\left(\pi\tau'(\mu\tau + f_d)\left(1 - \frac{|\tau|}{\tau'}\right)\right)}{\pi\tau'(\mu\tau + f_d)\left(1 - \frac{|\tau|}{\tau'}\right)} \right|^2 \quad |\tau| \leq \tau' \quad (7.44)$$

For this purpose, consider the sketch of an LFM ambiguity function shown in Fig. 7.11.

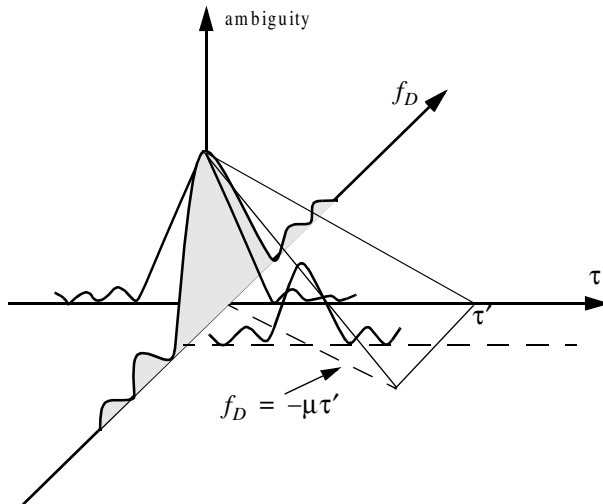


Figure 7.11. Illustration of range Doppler coupling for an LFM pulse.

The ambiguity surface extends from $-\tau'$ to τ' in range and from $-\infty$ to ∞ in Doppler. The response has a maximum at the point $(\tau, f_D) = (0, 0)$. Profiles parallel to the Doppler axis have maxima above the line $f_D = -\mu\tau$ which passes through the origin. The presence of radial velocity forces the peak of the ambiguity surface to a point that has a peak value smaller than the maximum that occurs at the origin. However, as long as the shift is less than the line $f_D = 1/\tau'$, the ambiguity function response exerts acceptable reduction in peak values, as illustrated in Fig. 7.11. This is the reason why some times LFM waveforms are called Doppler invariant.

7.4. Digital Pulse Compression

In this section we will briefly discuss three digital pulse compression techniques. They are frequency codes, binary phase codes, and poly-phase codes. Costas codes, Barker Codes, and Frank codes will be presented to illustrate, respectively, frequency, binary phase, and poly-phase coding. We will determine the pulse compression goodness of a code, based on its autocorrelation function since in the absence of noise, the output of the matched filter is proportional to the code autocorrelation. Given the autocorrelation function of a certain code, the main lobe width (compressed pulse width) and the side lobe levels are the two factors that need to be considered in order to evaluate the code's pulse compression characteristics.

7.4.1. Frequency Coding (Costas Codes)

Construction of Costas codes can be understood from the construction process of Stepped Frequency Waveforms (SFW) described in Chapter 5. In SFW, a relatively long pulse of length τ' is divided into N subpulses, each of width τ_1 ($\tau' = N\tau_1$). Each group of N subpulses is called a burst. Within each burst the frequency is increased by Δf from one subpulse to the next. The overall burst bandwidth is $N\Delta f$. More precisely,

$$\tau_1 = \tau'/N \quad (7.45)$$

and the frequency for the i th subpulse is

$$f_i = f_0 + i\Delta f \quad ; \quad i = 1, N \quad (7.46)$$

where f_0 is a constant frequency and $f_0 \gg \Delta f$. It follows that the time-bandwidth product of this waveform is

$$\Delta f\tau' = N^2 \quad (7.47)$$

Costas signals (or codes) are similar to SFW, except that the frequencies for the subpulses are selected in a random fashion, according to some predetermined rule or logic. For this purpose, consider the $N \times N$ matrix shown in Fig. 7.12. In this case, the rows are indexed from $i = 1, 2, \dots, N$ and the columns are indexed from $j = 0, 1, 2, \dots, (N - 1)$. The rows are used to denote the subpulses and the columns are used to denote the frequency. A “dot” indicates the frequency value assigned to the associated subpulse. In this fashion, Fig. 7.12a shows the frequency assignment associated with a SFW. Alternatively, the frequency assignments in Fig. 7.12b are chosen randomly. For a matrix of size $N \times N$, there are a total of $N!$ possible ways of assigning the “dots” (i.e., $N!$ possible codes).

The sequences of “dots” assignment for which the corresponding ambiguity function approaches an ideal or a “thumbtack” response are called Costas codes. A near thumbtack response was obtained by Costas¹ by using the following logic: only one frequency per time slot (row) and per frequency slot (column). Therefore, for an $N \times N$ matrix the number of possible Costas codes is drastically less than $N!$. For example, there are $N_c = 4$ possible Costas codes for $N = 3$, and $N_c = 40$ possible codes for $N = 5$. It can be shown that the code density, defined as the ratio $N_c/N!$, significantly gets smaller as N becomes larger.

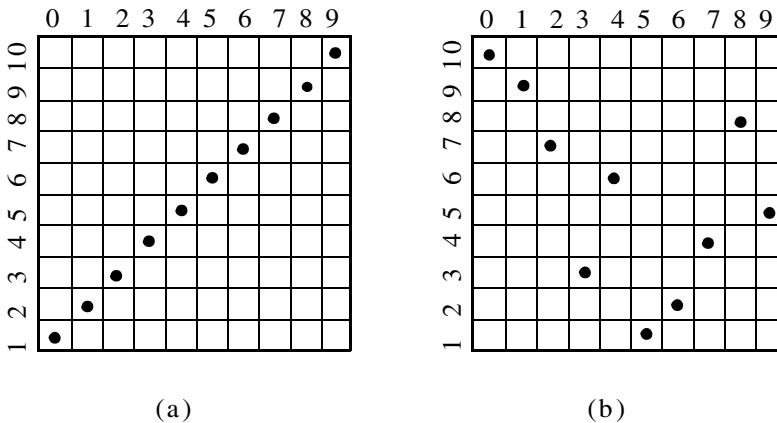


Figure 7.12. Frequency assignment for a burst of N subpulses. (a) SFW (stepped LFM); (b) Costas code of length $N_c = 10$.

1. Costas, J. P., A study of a Class of Detection Waveforms Having Nearly Ideal Range-Doppler Ambiguity Properties, *Proc. IEEE* 72, 1984, pp. 996-1009.

There are numerous analytical ways to generate Costas codes. In this section we will describe two of these methods. First, let q be an odd prime number, and choose the number of subpulses as

$$N = q - 1 \quad (7.48)$$

Define γ as the primitive root of q . A primitive root of q (an odd prime number) is defined as γ such that the powers $\gamma, \gamma^2, \gamma^3, \dots, \gamma^{q-1}$ modulo q generate every integer from 1 to $q - 1$.

In the first method, for an $N \times N$ matrix, label the rows and columns, respectively, as

$$\begin{aligned} i &= 0, 1, 2, \dots, (q - 2) \\ j &= 1, 2, 3, \dots, (q - 1) \end{aligned} \quad (7.49)$$

Place a dot in the location (i, j) corresponding to the frequency f_i (from Eq. (7.46)) if and only if

$$i = (\gamma)^j \pmod{q} \quad (7.50)$$

In the next method, Costas code is first obtained from the logic described above; then by deleting the first row and first column from the matrix a new code is generated. This method produces a Costas code of length $N = q - 2$.

Define the normalized complex envelope of the Costas signal as

$$s(t) = \frac{1}{\sqrt{N\tau_1}} \sum_{l=0}^{N-1} s_l(t - l\tau_1) \quad (7.51)$$

$$s_l(t) = \begin{cases} \exp(j2\pi f_l t) & 0 \leq t \leq \tau_1 \\ 0 & \text{elsewhere} \end{cases} \quad (7.52)$$

Costas showed that the output of the matched filter is

$$\chi(\tau, f_D) = \frac{1}{N} \sum_{l=0}^{N-1} \exp(j2\pi l f_D \tau) \left\{ \Phi_{ll}(\tau, f_D) + \sum_{\substack{q=0 \\ q \neq l}}^{N-1} \Phi_{lq}(\tau - (l - q)\tau_1, f_D) \right\} \quad (7.53)$$

$$\Phi_{lq}(\tau, f_D) = \left(\tau_1 - \frac{|\tau|}{\tau_1} \right) \frac{\sin \alpha}{\alpha} \exp(-j\beta - j2\pi f_q \tau) \quad , \quad |\tau| \leq \tau_1 \quad (7.54)$$

$$\alpha = \pi(f_l - f_q - f_D)(\tau_1 - |\tau|) \quad (7.55)$$

$$\beta = \pi(f_l - f_q - f_D)(\tau_1 + |\tau|) \quad (7.56)$$

Three-dimensional plots for the ambiguity function of Costas signals show the near thumbtack response of the ambiguity function. All sidelobes, except for few around the origin, have amplitude $1/N$. Few sidelobes close to the origin have amplitude $2/N$, which is typical of Costas codes. The compression ratio of a Costas code is approximately N .

7.4.2. Binary Phase Codes

In this case, a relatively long pulse of width τ' is divided into N smaller pulses; each is of width $\Delta\tau = \tau'/N$. Then, the phase of each sub-pulse is randomly chosen as either 0 or π radians relative to some CW reference signal. It is customary to characterize a sub-pulse that has 0 phase (amplitude of +1 Volt) as either “1” or “+.” Alternatively, a sub-pulse with phase equal to π (amplitude of -1 Volt) is characterized by either “0” or “-.” The compression ratio associated with binary phase codes is equal to $\xi = \tau'/\Delta\tau$, and the peak value is N times larger than that of the long pulse. The goodness of a compressed binary phase code waveform depends heavily on the random sequence of the phase for the individual sub-pulses.

One family of binary phase codes that produce compressed waveforms with constant side lobe levels equal to unity is the Barker code. Fig. 7.13 illustrates this concept for a Barker code of length seven. A Barker code of length n is denoted as B_n . There are only seven known Barker codes that share this unique property; they are listed in Table 7.1. Note that B_2 and B_4 have complementary forms that have the same characteristics. Since there are only seven Barker codes, they are not used when radar security is an issue.

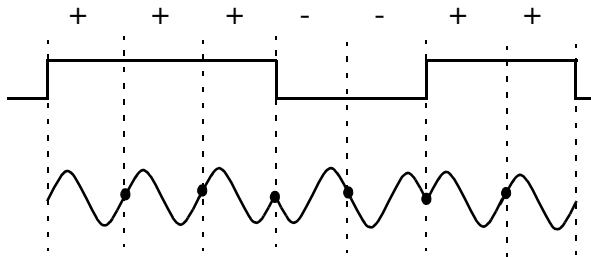


Figure 7.13. Binary phase code of length 7.

TABLE 7.1. Barker codes.

Code symbol	Code length	Code elements	Side lobe reduction (dB)
B_2	2	+ -	6.0
		+ +	
B_3	3	+ + -	9.5
B_4	4	+ + - +	12.0
		+ + + -	
B_5	5	+ + + - +	14.0
B_7	7	+ + + - - + -	16.9
B_{11}	11	+ + + - - + - - + -	20.8
B_{13}	13	+ + + + + - - + + - - + -	22.3

In general, the autocorrelation function (which is an approximation for the matched filter output) for a B_N Barker code will be $2N\Delta\tau$ wide. The main lobe is $2\Delta\tau$ wide; the peak value is equal to N . There are $(N-1)/2$ side lobes on either side of the main lobe; this is illustrated in Fig. 7.14 for a B_{13} . Notice that the main lobe is equal to 13, while all side lobes are unity.

The most side lobe reduction offered by a Barker code is -22.3dB , which may not be sufficient for the desired radar application. However, Barker codes can be combined to generate much longer codes. In this case, a B_m code can be used within a B_n code (m within n) to generate a code of length mn . The compression ratio for the combined B_{mn} code is equal to mn . As an example, a combined B_{54} is given by

$$B_{54} = \{11101, 11101, 00010, 11101\} \quad (7.57)$$

and is illustrated in Fig. 7.15. Unfortunately, the side lobes of a combined Barker code autocorrelation function are no longer equal to unity.

Some side lobes of a Barker code autocorrelation function can be reduced to zero if the matched filter is followed by a linear transversal filter with impulse response given by

$$h(t) = \sum_{k=-N}^N \beta_k \delta(t - 2k\Delta\tau) \quad (7.58)$$

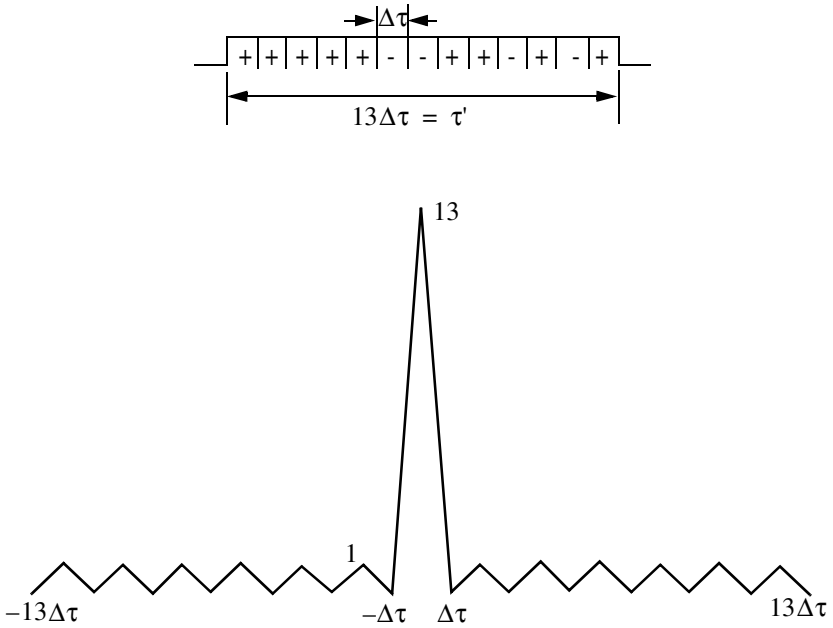


Figure 7.14. Barker code of length 13, and its corresponding autocorrelation function.

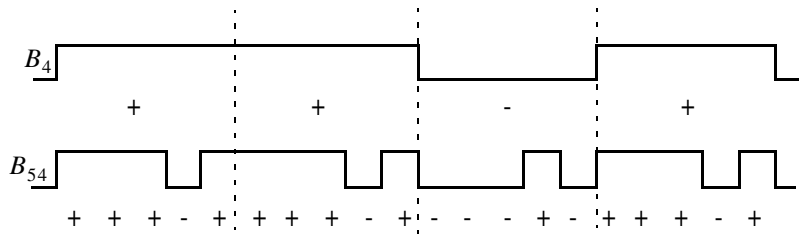


Figure 7.15. A combined B_{54} Barker code.

where N is the filter's order, the coefficients β_k ($\beta_k = \beta_{-k}$) are to be determined, $\delta(\cdot)$ is the delta function, and $\Delta\tau$ is the Barker code sub-pulse width. A filter of order N produces N zero side lobes on either side of the main lobe. The main lobe amplitude and width do not change. This is illustrated in Fig. 7.16.

In order to illustrate this approach further, consider the case where the input to the matched filter is B_{11} , and assume $N = 4$. The autocorrelation for a B_{11} code is

$$\phi_{11} = \{-1, 0, -1, 0, -1, 0, -1, 0, -1, 0, 11, 0, -1, 0, -1, 0, -1, 0, -1, 0, -1\} \quad (7.59)$$

The output of the transversal filter is the discrete convolution between its impulse response and the sequence ϕ_{11} . At this point we need to compute the coefficients β_k that guarantee the desired filter output (i.e., unchanged main lobe and four zero side lobe levels). Performing the discrete convolution as defined in Eq. (7.58), and collecting equal terms ($\beta_k = \beta_{-k}$) yield the following set of five linearly independent equations:

$$\begin{bmatrix} 11 & -2 & -2 & -2 & -2 \\ -1 & 10 & -2 & -2 & -1 \\ -1 & -2 & 10 & -2 & -1 \\ -1 & -2 & -1 & 11 & -1 \\ -1 & -1 & -1 & -1 & 11 \end{bmatrix} \begin{bmatrix} \beta_0 \\ \beta_1 \\ \beta_2 \\ \beta_3 \\ \beta_4 \end{bmatrix} = \begin{bmatrix} 11 \\ 0 \\ 0 \\ 0 \\ 0 \end{bmatrix} \quad (7.60)$$

The solution of Eq. (7.60) is left as an exercise. Note that by setting the first equation equal to 11 and all other equations to 0 and then solving for β_k guarantees that the main peak remains unchanged, and that the next four side lobes are zeros. So far we have assumed that coded pulses have rectangular shapes. Using other pulses of other shapes, such as Gaussian, may produce better side lobe reduction and a larger compression ratio.

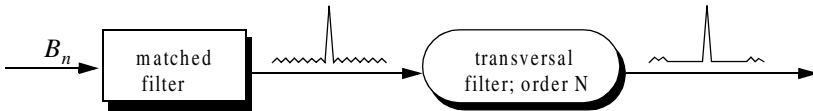


Figure 7.16. A linear transversal filter of order N can be used to produce N zero side lobes in the autocorrelation function. In this figure, $N = 4$.

7.4.3. Frank Codes

Codes that use any harmonically related phases based on a certain fundamental phase increment are called poly-phase codes. We will demonstrate this coding technique using Frank codes. In this case, a single pulse of width τ is divided into N equal groups; each group is subsequently divided into other N sub-pulses each of width $\Delta\tau$. Therefore, the total number of sub-pulses within each pulse is N^2 , and the compression ratio is $\xi = N^2$. As before, the phase within each sub-pulse is held constant with respect to some CW reference signal.

A Frank code of N^2 sub-pulses is referred to as an N-phase Frank code. The first step in computing a Frank code is to divide 360° by N , and define the result as the fundamental phase increment $\Delta\phi$. More precisely,

$$\Delta\phi = \frac{360^\circ}{N} \tag{7.61}$$

Note that the size of the fundamental phase increment decreases as the number of groups is increased, and because of phase stability, this may degrade the performance of very long Frank codes. For N-phase Frank code the phase of each sub-pulse is computed from

$$\begin{pmatrix} 0 & 0 & 0 & 0 & \dots & 0 \\ 0 & 1 & 2 & 3 & \dots & N-1 \\ 0 & 2 & 4 & 6 & \dots & 2(N-1) \\ \dots & \dots & \dots & \dots & \dots & \dots \\ \dots & \dots & \dots & \dots & \dots & \dots \\ 0 & (N-1) & 2(N-1) & 3(N-1) & \dots & (N-1)^2 \end{pmatrix} \Delta\phi \tag{7.62}$$

where each row represents a group, and a column represents the sub-pulses for that group. For example, a 4-phase Frank code has $N = 4$, and the fundamental phase increment is $\Delta\phi = (360^\circ/4) = 90^\circ$. It follows that

$$\begin{pmatrix} 0 & 0 & 0 & 0 \\ 0 & 90^\circ & 180^\circ & 270^\circ \\ 0 & 180^\circ & 0 & 180^\circ \\ 0 & 270^\circ & 180^\circ & 90^\circ \end{pmatrix} \Rightarrow \begin{pmatrix} 1 & 1 & 1 & 1 \\ 1 & j & -1 & -j \\ 1 & -1 & 1 & -1 \\ 1 & -j & -1 & j \end{pmatrix} \tag{7.63}$$

Therefore, a Frank code of 16 elements is given by

$$F_{16} = \{1 \ 1 \ 1 \ 1 \ 1 \ j \ -1 \ -j \ 1 \ -1 \ 1 \ -1 \ 1 \ -j \ -1 \ j\} \tag{7.64}$$

The phase increments within each row represent a stepwise approximation of an up-chirp LFM waveform. The phase increments for subsequent rows increase linearly versus time. Thus, the corresponding LFM chirp slopes also increase linearly for subsequent rows. This is illustrated in Fig. 7.17, for F_{16} .

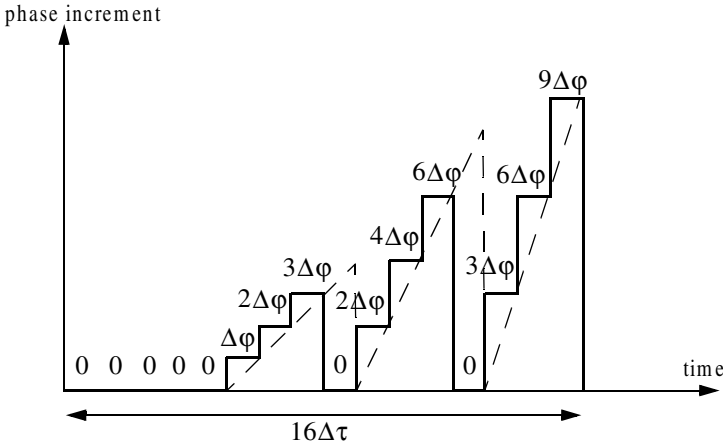


Figure 7.17. Stepwise approximation of an up-chirp waveform, using a Frank code of 16 elements.

7.4.4. Pseudo-Random (PRN) Codes

Pseudo-random (PRN) codes are also known as Maximal Length Sequences (MLS) codes. These codes are called pseudo-random because the statistics associated with their occurrence is similar to that associated with the coin-toss sequences. Maximum length sequences are periodic with period L and the code values take on two binary values (+1 and -1). The MLS correlation function is

$$\phi(n) = \begin{cases} L & n = 0, \pm L, \pm 2L, \dots \\ -1 & \text{elsewhere} \end{cases} \quad (7.65)$$

Fig. 7.18 shows a typical sketch for an MLS autocorrelation function. Clearly these codes have the advantage that the compression ratio becomes very large as the period is increased. Additionally, adjacent peaks (grating lobes) become farther apart.

Maximum length sequences exist for all integer values m , with a period equal to $2^m - 1$. They can be generated using shift register circuits with the proper feedback connections, where the sum is a modulo-2 operation. This is

illustrated in Fig. 7.19 for $m = 4$ (i.e., $L = 15$). Note that the circuit shown in Fig. 7.19 is not the only one that can produce this code.

In radar applications, long codes are very desirable. However, having very long codes presents many possibilities for the feedback connections through the modulo-2 adder. For example, for $m = 80$, the period is $L = 2^{80} - 1$, which is very huge and may take years to produce the corresponding code. Therefore, there is a need for a more systematic method for producing MLS codes.

In practice, typical MLS codes are produced by using the primitive polynomials with the proper degree that corresponds to the code, and the feedback connections are made according to the chosen polynomial, as illustrated in Fig. 7.19 for $m = 4$. In this example the primitive polynomial is $x^4 + x + 1$. Of course the initial loading for the registers must be different from all zeros. More details on primitive polynomials can be found in many cited references.

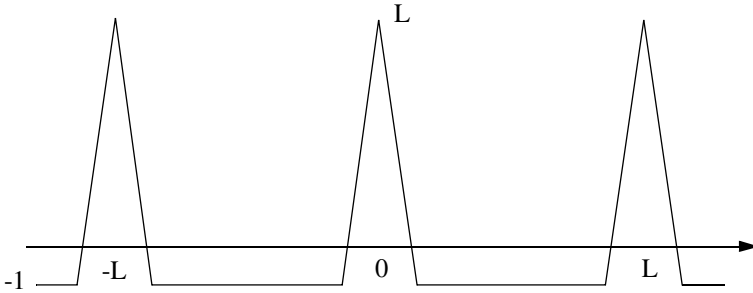


Figure 7.18. Typical autocorrelation of an MLS code of length L .

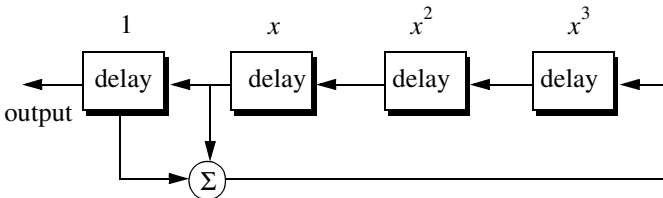


Figure 7.19. Circuit for generating an MLS sequence of length $L = 15$.
The primitive polynomial is $x^4 + x + 1$.

7.5. MATLAB Listings

This section presents listings for all MATLAB programs/functions used in this chapter. The user is advised to rerun these programs with different input parameters.

Listing 7.1. MATLAB Function “matched_filter.m”

```
function [y] = matched_filter(nscat, taup, f0, b, rmin, rrec, scat_range,
scat_rcs, winid)
%
eps = 1.0e-16;
htau = taup / 2.;
c = 3.e8;
n = fix(2. * taup * b);
m = power_integer_2(n);
nfft = 2.^m;
x(nscat,1:nfft) = 0.;
y(1:nfft) = 0.;
replica(1:nfft) = 0.;
if( winid == 0.)
    win(1:nfft) = 1.;
    win = win';
else
    if(winid == 1.)
        win = hamming(nfft);
    else
        if( winid == 2.)
            win = kaiser(nfft,pi);
        else
            if(winid == 3.)
                win = chebwin(nfft,60);
            end
        end
    end
end
end
deltar = c / 2. / b;
max_rrec = deltar * nfft / 2.;
maxr = max(scat_range) - rmin;
if(rrec > max_rrec | maxr >= rrec )
    'Error. Receive window is too large; or scatterers fall outside window'
    break
end
trec = 2. * rrec / c;
```

```

deltat = taup / nfft;
t = 0: deltat:taup-eps;
uplimit = max(size(t));
replica(1:uplimit) = exp(i * 2.* pi * (.5 * (b/taup) .* t.^2));
figure(3)
subplot(2,1,1)
plot(real(replica))
title('Matched filter time domain response')
subplot(2,1,2)
plot(fftshift(abs(fft(replica))));
title('Matched filter frequency domain response')
for j = 1:1:nscat
    t_tgt = 2. * (scat_range(j) - rmin) / c + htau;
    x(j,1:uplimit) = scat_rcs(j) .* exp(i * 2.* pi * ...
        (.5 * (b/taup) .* (t+t_tgt).^2));
    y = y + x(j,:);
end
figure(1)
plot(t,real(y),'k')
xlabel ('Relative delay - seconds')
ylabel ('Uncompressed echo')
title ('Zero delay coincide with minimum range')
rfft = fft(replica,nfft);
yfft = fft(y,nfft);
out= abs(iff((rfft .* conj(yfft)) .* win' )) ./ (nfft);
figure(2)
time = -htau:deltat:htau-eps;
plot(time,out,'k')
xlabel ('Relative delay - seconds')
ylabel ('Compressed echo')
title ('Zero delay coincide with minimum range')
grid

```

Listing 7.2. MATLAB Function “stretch.m”

```

function [y] = stretch(nscat,taup,f0,b,rmin,rrec,scat_range,scat_rcs,winid)
eps = 1.0e-16;
htau = taup / 2.;
c = 3.e8;
trec = 2. * rrec / c;
n = fix(2. * trec * b);
m = power_integer_2(n);
nfft = 2.^m;
x(nscat,1:nfft) = 0.;

```

```

y(1:nfft) = 0.;
if( winid == 0.)
    win(1:nfft) = 1.;
    win = win';
else
    if(winid == 1.)
        win = hamming(nfft);
    else
        if( winid == 2.)
            win = kaiser(nfft,pi);
        else
            if(winid == 3.)
                win = chebwin(nfft,60);
            end
        end
    end
end
deltar = c / 2. / b;
max_rrec = deltar * nfft / 2.;
rrec = max(scatterers_range) - rmin;
if(rrec > max_rrec | max_rrec >= rrec )
    'Error. Receive window is too large; or scatterers fall outside window'
    break
end
deltat = taup / nfft;
t = 0: deltat:taup-eps;
uplimit = max(size(t));
for j = 1:1:nscat
    psi1 = 4. * pi * scatterers_range(j) * f0 / c - ...
        4. * pi * b * scatterers_range(j) * scatterers_range(j) / c / taup;
    psi2 = (4. * pi * b * scatterers_range(j) / c / taup) .* t;
    x(j,1:uplimit) = scatterers_rcs(j) .* exp(i * psi1 + i .* psi2);
    y = y + x(j,:);
end
figure(1)
plot(t,real(y),'k')
xlabel ('Relative delay - seconds')
ylabel ('Uncompressed echo')
title ('Zero delay coincide with minimum range')
ywin = y .* win';
yfft = fft(y,nfft) ./ nfft;
out = fftshift(abs(yfft));
figure(2)
time = -htau:deltat:htau-eps;

```

```

plot(time,out,'k')
xlabel ('Relative delay - seconds')
ylabel ('Compressed echo')
title ('Zero delay coincide with minimum range')
grid

```

Listing 7.3. MATLAB Program “fig7_10.m”

```

clear all
eps = 1.5e-5;
t = 0:0.001:.5;
y = chirp(t,0,.25,20);
figure(1)
plot(t,y);
yfft = fft(y,512);
ycomp = fftshift(abs(iff(yfft .* conj(yfft))));
maxval = max (ycomp);
ycomp = eps + ycomp ./ maxval;
figure(1)
del = .5 /512.;
tt = 0:del:.5-eps;
plot (tt,ycomp,'k')
xlabel ('Relative delay - seconds');
ylabel('Normalized compressed pulse')
grid
%change center frequency
y1 = chirp (t,0,.25,21);
y1fft = fft(y1,512);
y1comp = fftshift(abs(iff(y1fft .* conj(y1fft))));
maxval = max (y1comp);
y1comp = eps + y1comp ./ maxval;
figure(2)
plot (tt,y1comp,'k')
xlabel ('Relative delay - seconds');
ylabel('Normalized compressed pulse')
grid
%change pulse width
t = 0:0.001:.45;
y2 = chirp (t,0,.225,20);
y2fft = fft(y2,512);
y2comp = fftshift(abs(iff(y2fft .* conj(y2fft))));
maxval = max (y2comp);
y2comp = eps + y2comp ./ maxval;
figure(3)

```

```

plot(tt,y2comp,'k')
xlabel('Relative delay - seconds');
ylabel('Normalized compressed pulse')
grid

```

Problems

- 7.1.** Starting with Eq. (7.17), prove Eq. (7.21).
- 7.2.** The smallest positive primitive root of $q = 11$ is $\gamma = 2$; for $N = 10$ generate the corresponding Costas matrix.
- 7.3.** Develop a MATLAB program to plot the ambiguity function associated with Costas codes. Use Eqs. (7.53) through (7.56). Your program should generate 3-D plots, contour plots, and zero delay/Doppler cuts. Verify the side lobe behaviour and the compression ratio of Costas codes.
- 7.4.** Consider the 7-bit Barker code, designated by the sequence $x(n)$. (a) Compute and plot the autocorrelation of this code. (b) A radar uses binary phase coded pulses of the form $s(t) = r(t)\cos(2\pi f_0 t)$, where $r(t) = x(0)$, for $0 < t < \Delta t$, $r(t) = x(n)$, for $n\Delta t < t < (n+1)\Delta t$, and $r(t) = 0$, for $t > 7\Delta t$. Assume $\Delta t = 0.5\mu s$. (a) Give an expression for the autocorrelation of the signal $s(t)$, and for the output of the matched filter when the input is $s(t - 10\Delta t)$; (b) compute the time bandwidth product, the increase in the peak SNR, and the compression ratio.
- 7.5.** (a) Perform the discrete convolution between the sequence ϕ_{11} defined in Eq. (7.59), and the transversal filter impulse response (i.e., derive Eq. (7.60)). (b) Solve Eq. (7.60), and sketch the corresponding transversal filter output.
- 7.6.** Repeat the previous problem for $N = 13$ and $k = 6$. Use Barker code of length 13.
- 7.7.** Develop a Barker code of length 35. Consider both B_{75} and B_{57} .
- 7.8.** Write a computer program to calculate the discrete correlation between any two finite length sequences. Verify your code by comparing your results to the output of the MATLAB function “*xcorr*”.
- 7.9.** Compute the discrete autocorrelation for an F_{16} Frank code.
- 7.10.** Generate a Frank code of length 8, F_8 .

In the earlier chapters, radar systems were analyzed with the assumption that the radar waves which traveled to and from targets are in free space. Signal interference due to the earth and its atmosphere was not considered. Despite the fact that “*free space analysis*” may be adequate to provide a general understanding of radar systems, it is only an approximation. In order to accurately predict radar performance, we must modify free space analysis to include the effects of the earth and its atmosphere. This modification should account for ground reflections from the surface of the earth, diffraction of electromagnetic waves, bending or refraction of radar waves due to the earth atmosphere, and attenuation or absorption of radar energy by the gases constituting the atmosphere.

8.1. Earth Atmosphere

The earth atmosphere is comprised of several layers, as illustrated in [Fig. 8.1](#). The first layer which extends in altitude to about 20 Km is known as the troposphere. Electromagnetic waves refract (bend downward) as they travel in the troposphere. The troposphere refractive effect is related to its dielectric constant which is a function of the pressure, temperature, water vapor, and gaseous content. Additionally, due to gases and water vapor in the atmosphere radar energy suffers a loss. This loss is known as the atmospheric attenuation. Atmospheric attenuation increases significantly in the presence of rain, fog, dust, and clouds.

The region above the troposphere (altitude from 20 to 50 Km) behaves like free space, and thus little refraction occurs in this region. This region is known as the interference zone.

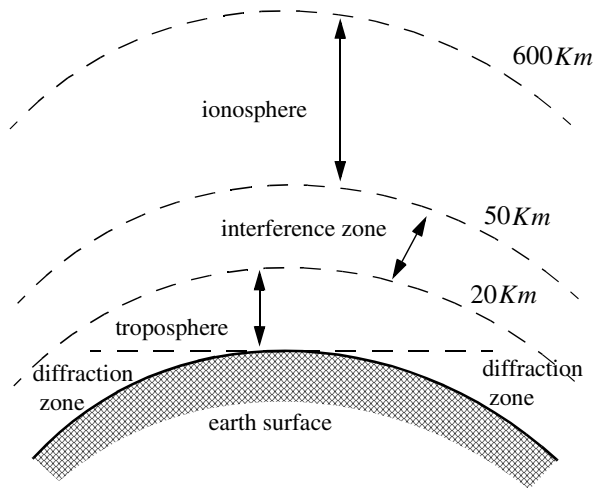


Figure 8.1. Earth atmosphere geometry.

The ionosphere extends from about 50 Km to about 600 Km. It has very low gas density compared to the troposphere. It contains a significant amount of ionized free electrons. The ionization is primarily caused by the sun's ultraviolet and X-rays. This presence of free electrons in the ionosphere affects electromagnetic wave propagation in different ways. These effects include refraction, absorption, noise emission, and polarization rotation. The degree of degradation depends heavily on the frequency of the incident waves. For example, frequencies lower than about 4 to 6 MHz are completely reflected from the lower region of the ionosphere. Frequencies higher than 30 MHz may penetrate the ionosphere with some level of attenuation. In general, as the frequency is increased the ionosphere's effects become less prominent.

The region below the horizon, close to the earth's surface, is called the diffraction region. Diffraction is a term used to describe the bending of radar waves around physical objects. Two types of diffraction are common. They are knife edge and cylinder edge diffraction.

8.2. Refraction

In free space, electromagnetic waves travel in straight lines. However, in the presence of the earth atmosphere, they bend (refract). Refraction is a term used

to describe the deviation of radar wave propagation from straight lines. The deviation from straight line propagation is caused by the variation of the index of refraction. The index of refraction is defined as

$$n = c/v \quad (8.1)$$

where c is the velocity of electromagnetic waves in free space and v is the wave velocity in the medium. Close to the earth's surface the index of refraction is almost unity; however, with increasing altitude the index of refraction decreases gradually. The discussion presented in this chapter assumes a well mixed atmosphere, where the index of refraction decreases in a smooth monotonic fashion with height. The rate of change of the earth's index of refraction n with altitude h is normally referred to as the refractivity gradient, dn/dh . As a result of the negative rate of change in dn/dh , electromagnetic waves travel at slightly higher velocities in the upper troposphere than the lower part. As a result of this, waves traveling horizontally in the troposphere gradually bend downward. In general, since the rate of change in the refractivity index is very slight, waves do not curve downward appreciably unless they travel very long distances through the troposphere.

Refraction affects radar waves in two different ways depending on height. For targets that have altitudes, typically above 100 meters, the effect of refraction is illustrated in Fig. 8.2. In this case, refraction imposes limitations on the radar's capability to measure target position. Refraction introduces an error in measuring the elevation angle.

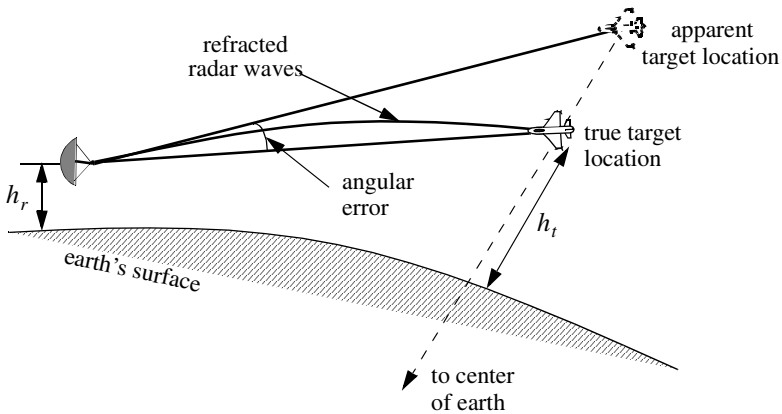


Figure 8.2. Refraction high altitude effect on electromagnetic waves.

In a well mixed atmosphere, the refractivity gradient close to the earth's surface is almost constant. However, temperature changes and humidity lapses close to the earth's surface may cause serious changes in the refractivity profile. When the refractivity index becomes large enough electromagnetic waves bend around the curve of the earth. Consequently, the radar's range to the horizon is extended. This phenomenon is called ducting, and is illustrated in Fig. 8.3. Ducting can be serious over the sea surface, particularly during the hot summertime.

Using ray tracing (geometric optics) an integral-relating range-to-target height with the elevation angle as a parameter can be derived and calculated. However, such computations are complex and numerically intensive. Thus, in practice, radar systems deal with refraction in two different ways, depending on height. For altitudes higher than 3 Km, actual target heights are estimated from look-up tables or from charts of target height versus range for different elevation angles.

Simpler methods that are valid for altitude less than 3 Km, for calculating target height, can also be employed. In this case, the most common way of dealing with refraction is to replace the actual earth with an imaginary earth whose effective radius is $r_e = kr_0$, where r_0 is the actual earth radius, and k is

$$k = \frac{1}{1 + r_0(dn/dh)} \tag{8.2}$$

When the refractivity gradient is assumed to be constant with altitude and is equal to 39×10^{-9} per meter, then $k = 4/3$. Using an effective earth radius $r_e = (4/3)r_0$ produces what is known as the "four third earth model." In general, choosing

$$r_e = r_0(1 + 6.37 \times 10^{-3}(dn/dh)) \tag{8.3}$$

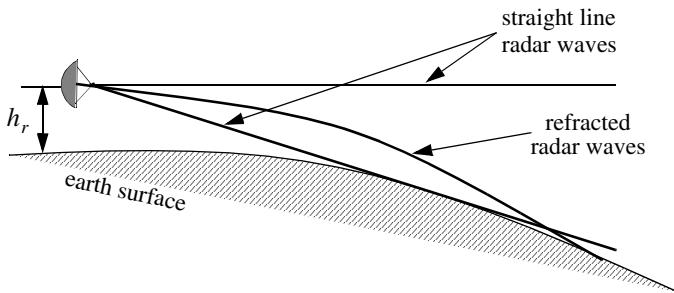


Figure 8.3. Refraction low altitude effect on electromagnetic waves.

produces a propagation model where waves travel in straight lines. Selecting the correct value for k depends heavily on the region's meteorological conditions. Blake¹ derives the "height-finding equation" for the 4/3 earth. It is

$$h = h_r + 6076R \sin \theta + 0.6625R^2 (\cos \theta)^2 \quad (8.4)$$

where h and h_r are in feet and R is nautical miles. All variables are defined in Fig. 8.4.

The distance to the horizon for a radar located at height h_r can be calculated with the help of Fig. 8.5. For the right-angle triangle OBA we get

$$r_h = \sqrt{(r_0 + h_r)^2 - r_0^2} \quad (8.5)$$

where r_h is the distance to the horizon. By expanding Eq. (8.5) and collecting terms we can derive the expression for the distance to the horizon as

$$r_h^2 = 2r_0h_r + h_r^2 \quad (8.6)$$

Finally, since $r_0 \gg h_r$ Eq. (8.6) is approximated by

$$r_h \approx \sqrt{2r_0h_r} \quad (8.7)$$

and when refraction is accounted for, Eq. (8.7) becomes

$$r_h \approx \sqrt{2r_e h_r} \quad (8.8)$$

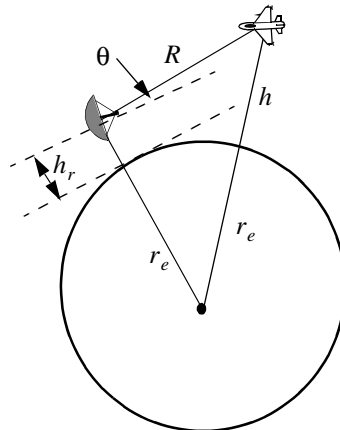


Figure 8.4. Measuring target height for 4/3 earth.

1. Blake, L. V., *Radar Range-Performance Analysis*, Artech House, 1986.

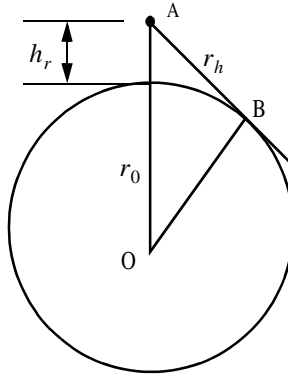


Figure 8.5. Measuring the distance to the horizon.

8.3. Ground Reflection

When radar waves are reflected from the earth's surface, they suffer a loss in amplitude and a change in phase. Three factors that contribute to these changes that are the overall ground reflection coefficient are the reflection coefficient for a flat surface, the divergence factor due to earth curvature, and the surface roughness.

8.3.1. Smooth Surface Reflection Coefficient

The smooth surface reflection coefficient depends on the frequency, on the surface dielectric coefficient, and on the radar grazing angle. The vertical polarization and the horizontal polarization reflection coefficients are

$$\Gamma_v = \frac{\epsilon \sin \psi_g - \sqrt{\epsilon - (\cos \psi_g)^2}}{\epsilon \sin \psi_g + \sqrt{\epsilon - (\cos \psi_g)^2}} \quad (8.9)$$

$$\Gamma_h = \frac{\sin \psi_g - \sqrt{\epsilon - (\cos \psi_g)^2}}{\sin \psi_g + \sqrt{\epsilon - (\cos \psi_g)^2}} \quad (8.10)$$

where ψ_g is the grazing angle (incident angle) and ϵ is the complex dielectric constant of the surface, and are given by

$$\epsilon = \epsilon' - j\epsilon'' \quad (8.11)$$

Typical values of ϵ' and ϵ'' can be found tabulated in the literature. For example, seawater at 28°C has $\epsilon' = 65$ and $\epsilon'' = 30.7$ at X-band. Fig. 8.6 shows the corresponding magnitude plots for Γ_h and Γ_v , while Fig. 8.7 shows the phase plots. The plots shown in those figures show the general typical behavior of the reflection coefficient.

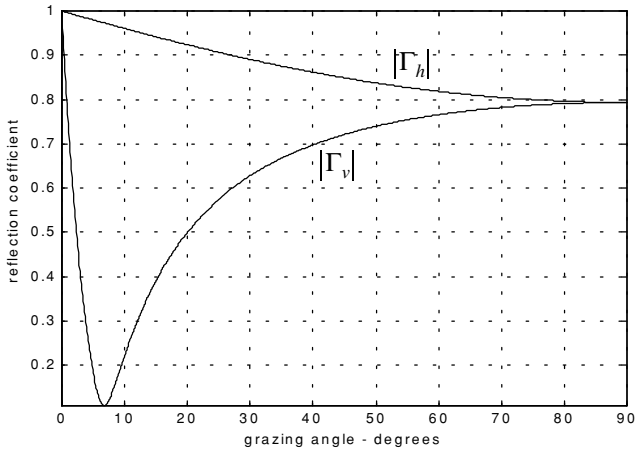


Figure 8.6. Reflection coefficient magnitude.

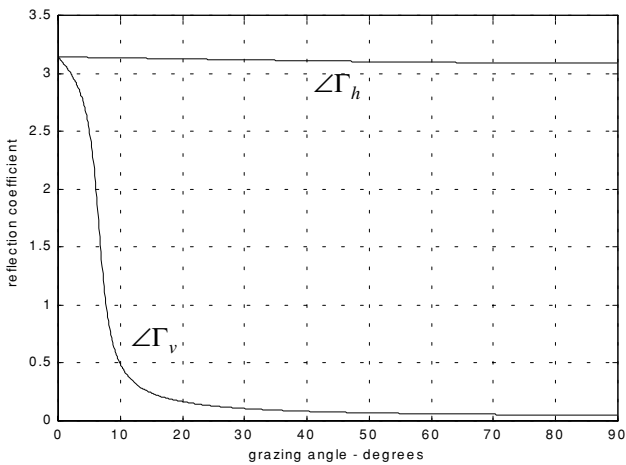


Figure 8.7. Reflection coefficient phase.

Note that when $\psi_g = 90^\circ$ we get

$$\Gamma_h = \frac{1 - \sqrt{\epsilon}}{1 + \sqrt{\epsilon}} = -\frac{\epsilon - \sqrt{\epsilon}}{\epsilon + \sqrt{\epsilon}} = -\Gamma_v \quad (8.12)$$

while when the grazing angle is very small ($\psi_g \approx 0$), we have

$$\Gamma_h = -1 = \Gamma_v \quad (8.13)$$

Observation of Figs. 8.6 and 8.7 yield the following conclusions: (1) The magnitude of the reflection coefficient with horizontal polarization is equal to unity at very small grazing angles and it decreases monotonically as the angle is increased. (2) The magnitude of the vertical polarization has a well defined minimum. The angle that corresponds to this condition is called Brewster's polarization angle. For this reason, airborne radars in the look-down mode utilize mainly vertical polarization to significantly reduce the terrain bounce reflections. (3) For horizontal polarization the phase is almost π ; however, for vertical polarization the phase changes to zero around the Brewster's angle. (4) For very small angles (less than 2°) both $|\Gamma_h|$ and $|\Gamma_v|$ are nearly one; $\angle\Gamma_h$ and $\angle\Gamma_v$ are nearly π . Thus, little difference in the propagation of horizontally or vertically polarized waves exists at low grazing angles.

MATLAB Function "ref_coef.m"

The function "ref_coef.m" calculates and plots the horizontal and vertical magnitude and phase response of the reflection coefficient. It is given in Section 8.7. The syntax is as follows

$$[rh,rv,ph,pv] = ref_coef(eps,epspp)$$

where

Symbol	Description	Status
<i>eps</i>	ϵ'	<i>input</i>
<i>epspp</i>	ϵ''	<i>input</i>
<i>rh</i>	vector of $ \Gamma_h $	<i>output</i>
<i>rv</i>	vector of $ \Gamma_v $	<i>output</i>
<i>ph</i>	vector of $\angle\Gamma_h$	<i>output</i>
<i>vh</i>	vector of $\angle\Gamma_v$	<i>output</i>

8.3.2. Divergence

The overall reflection coefficient is also affected by the round earth divergence factor, D . When an electromagnetic wave is incident on a round earth surface, the reflected wave diverges because of the earth's curvature. This is illustrated in Fig. 8.8a. Due to divergence the reflected energy is defocused, and the radar power density is reduced. The divergence factor can be derived using geometrical considerations. A widely accepted approximation for the divergence factor is given by

$$D \approx \frac{1}{\sqrt{1 + \frac{2r_1 r_2}{r_e r \sin \psi_g}}} \quad (8.14)$$

where all variables in Eq. (8.14) are defined in Fig. 8.8b.

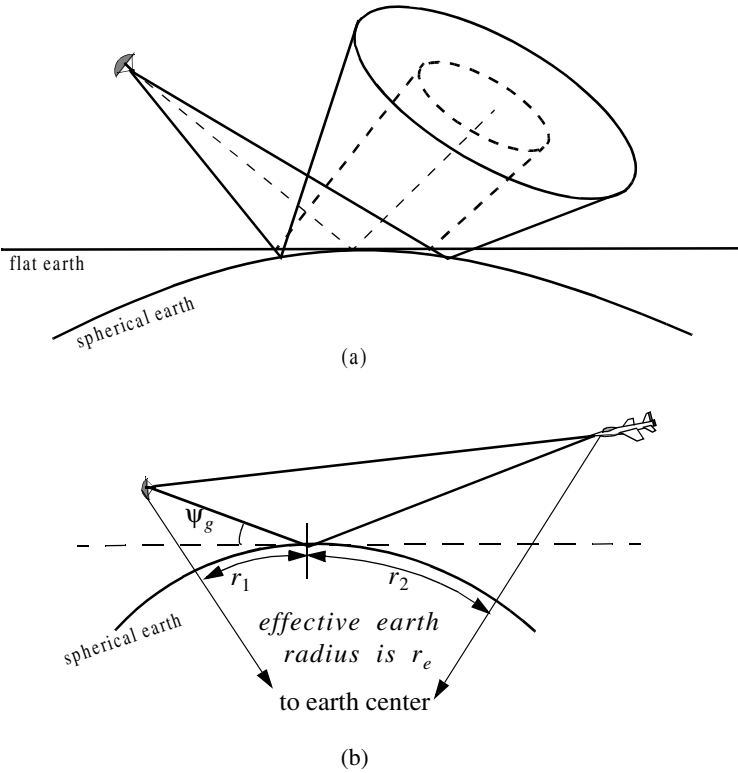


Figure 8.8. Illustration of divergence. (a) Solid line: Ray perimeter for spherical earth. Dashed line: Ray perimeter for flat earth. (b) Definition of variables in Eq. (8.14)

8.3.3. Rough Surface Reflection

In addition to divergence, surface roughness also affects the reflection coefficient. Surface roughness is given by

$$S_r = e^{-2\left(\frac{2\pi h_{rms} \sin \Psi_g}{\lambda}\right)^2} \quad (8.15)$$

where h_{rms} is the rms surface height irregularity. In general, rays reflected from rough surfaces undergo changes in phase and amplitude, which results in the diffused (non-coherent) portion of the reflected signal. Combining the above three factors, we can express the total reflection coefficient Γ_t as

$$\Gamma_t = \Gamma_{(h,v)} DS_r \quad (8.16)$$

$\Gamma_{(h,v)}$ is the horizontal or vertical smoothed surface reflection coefficient.

8.4. The Pattern Propagation Factor

In general, the pattern propagation factor is a term used to describe the wave propagation when free space conditions are not met. This factor is defined separately for the transmitting and receiving paths. The propagation factor also accounts for the radar antenna pattern effects. The basic definition of the propagation factor is

$$F = |E/E_0| \quad (8.17)$$

where E is the electric field in the medium and E_0 is the free space electric field.

Near the surface of the earth, multipath propagation effects dominate the formation of the propagation factor. In this section, a general expression for the propagation factor due to multipath will be developed. In this sense, the propagation factor describes the constructive/destructive interference of the electromagnetic waves diffracted from the earth surface (which can be either flat or curved). The subsequent sections derive the specific forms of the propagation factor due to flat and curved earth.

Consider the geometry shown in Fig. 8.9. The radar is located at height h_r . The target is at range R , and is located at a height h_t . The grazing angle is Ψ_g . The radar energy emanating from its antenna will reach the target via two paths: the “direct path” AB and the “indirect path” ACB . The lengths of the paths AB and ACB are normally very close to one another and thus, the difference between the two paths is very small. Denote the direct path as R_d , the indirect path as R_i , and the difference as $\Delta R = R_i - R_d$. It follows that the phase difference between the two paths is given by

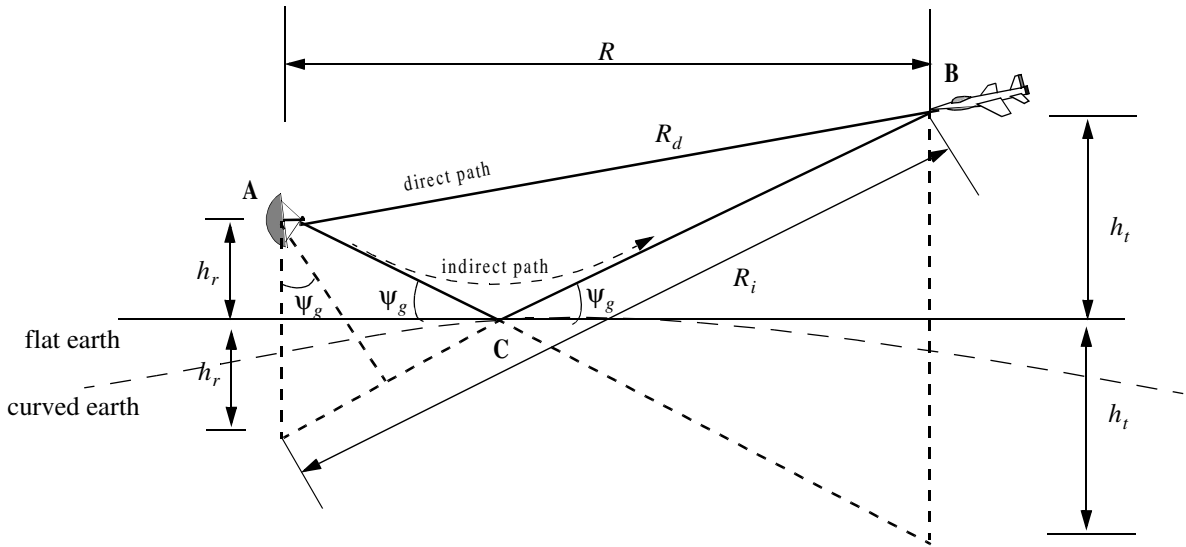


Figure 8.9. Geometry for multipath propagation.

$$\Delta\Phi = \frac{2\pi}{\lambda}\Delta R \quad (8.18)$$

where λ is the radar wavelength.

The indirect signal amplitude arriving at the target is less than the signal amplitude arriving via the direct path. This is because the antenna gain in the direction of the indirect path is less than that along the direct path, and because the signal reflected from the earth surface at point C is modified in amplitude and phase in accordance to the earth's reflection coefficient, Γ . The earth reflection coefficient is given by

$$\Gamma = \rho e^{j\phi} \quad (8.19)$$

where ρ is less than unity and ϕ describes the phase shift induced on the indirect path signal due to surface roughness.

The direct signal (in volts) arriving at the target via the direct path can be written as

$$E_d = e^{j\omega_0 t} e^{j\frac{2\pi}{\lambda}R_d} \quad (8.20)$$

where the time harmonic term $\exp(j\omega_0 t)$ represents the signal's time dependency, and the exponential term $\exp(j(2\pi/\lambda)R_d)$ represents the signal spatial phase. The indirect signal at the target is

$$E_i = \rho e^{j\phi} e^{j\omega_0 t} e^{j\frac{2\pi}{\lambda}R_i} \quad (8.21)$$

where $\rho \exp(j\phi)$ is the surface reflection coefficient. Therefore, the overall signal arriving at the target is

$$E = E_d + E_i = e^{j\omega_0 t} e^{j\frac{2\pi}{\lambda}R_d} \left(1 + \rho e^{j\left(\phi + \frac{2\pi}{\lambda}(R_i - R_d)\right)} \right) \quad (8.22)$$

Due to reflections from the earth surface, the overall signal strength is then modified at the target by the ratio of the signal strength in the presence of earth to the signal strength at the target in free space. From Eq. (8.17) the modulus of this ratio is the propagation factor. By using Eqs. (8.20) and (8.22) the propagation factor is computed as

$$F = \left| \frac{E_d}{E_d + E_i} \right| = \left| 1 + \rho e^{j\phi} e^{j\Delta\Phi} \right| \quad (8.23)$$

which can be rewritten as

$$F = |1 + \rho e^{j\alpha}| \quad (8.24)$$

where $\alpha = \Delta\Phi + \varphi$. Using Euler's identity ($e^{j\alpha} = \cos\alpha + j\sin\alpha$), Eq. (8.24) can be written as

$$F = \sqrt{1 + \rho^2 + 2\rho\cos\alpha} \quad (8.25)$$

It follows that the signal power at the target is modified by the factor F^2 . By using reciprocity, the signal power at the radar is computed by multiplying the radar equation by the factor F^4 . In the following two sections we will develop exact expressions for the propagation factor for flat and curved earth.

The propagation factor for free space and no multipath is $F = 1$. Denote the radar detection range in free space (i.e., $F = 1$) as R_0 . It follows that the detection range in the presence of the atmosphere and multipath interference is

$$R = \frac{R_0 F}{(L_a)^{1/4}} \quad (8.26)$$

where L_a is the two-way atmospheric loss at range R . Atmospheric attenuation will be discussed in a later section. Thus, for the purpose of illustrating the effect of multipath interference on the propagation factor, assume that $L_a = 1$. In this case, Eq. (8.26) is modified to

$$R = R_0 F \quad (8.27)$$

Fig. 8.10 shows the general effects of multipath interference on the propagation factor. Note that, due to the presence of surface reflections, the antenna elevation coverage is transformed into a lobed pattern structure. The lobe widths are directly proportional to λ , and inversely proportional to h_r . A target located at a maxima will be detected at twice its free space range. Alternatively, at other angles, the detection range will be less than that in free space.

8.4.1. Flat Earth

Using the geometry of Fig. 8.9, the direct and indirect paths are computed as

$$R_d = \sqrt{R^2 + (h_t - h_r)^2} \quad (8.28)$$

$$R_i = \sqrt{R^2 + (h_t + h_r)^2} \quad (8.29)$$

Eqs. (8.28) and (8.29) can be approximated using the truncated binomial series expansion as

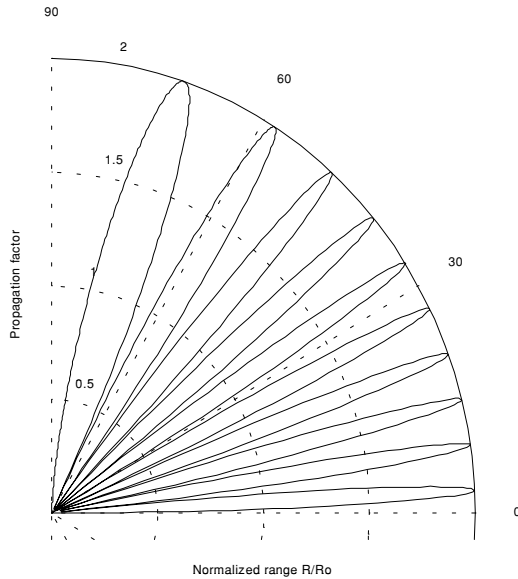


Figure 8.10. Vertical lobe structure due to the reflecting surface as a function of the elevation angle.

$$R_d \approx R + \frac{(h_t - h_r)^2}{2R} \quad (8.30)$$

$$R_i \approx R + \frac{(h_t + h_r)^2}{2R} \quad (8.31)$$

This approximation is valid for low grazing angles, where $R \gg h_t, h_r$. It follows that

$$\Delta R = R_i - R_d \approx \frac{2h_t h_r}{R} \quad (8.32)$$

Substituting Eq. (8.32) into Eq. (8.18) yields the phase difference due to multi-path propagation between the two signals (direct and indirect) arriving at the target. More precisely,

$$\Delta\Phi = \frac{2\pi}{\lambda} \Delta R \approx \frac{4\pi h_t h_r}{\lambda R} \quad (8.33)$$

At this point assume smooth surface with reflection coefficient $\Gamma = -1$. This assumption means that waves reflected from the surface suffer no amplitude loss, and that the induced surface phase shift is equal to 180° . Using Eq. (8.18) and Eq. (8.25) along with these assumptions yield

$$F^2 = 2 - 2 \cos \Delta\Phi = 4(\sin(\Delta\Phi/2))^2 \quad (8.34)$$

Substituting Eq. (8.33) into Eq. (8.34) yields

$$F^2 = 4\left(\sin\frac{2\pi h_t h_r}{\lambda R}\right)^2 \quad (8.35)$$

By using reciprocity, the expression for the propagation factor at the radar is then given by

$$F^4 = 16\left(\sin\frac{2\pi h_t h_r}{\lambda R}\right)^4 \quad (8.36)$$

Finally, the signal power at the radar is computed by multiplying the radar equation by the factor F^4 ,

$$P_r = \frac{P_t G^2 \lambda^2 \sigma}{(4\pi)^3 R^4} 16\left(\sin\frac{2\pi h_t h_r}{\lambda R}\right)^4 \quad (8.37)$$

Since the sine function varies between 0 and 1, the signal power will then vary between 0 and 16. Therefore, the fourth power relation between signal power and the target range results in varying the target range from 0 to twice the actual range in free space. In addition to that, the field strength at the radar will now have holes that correspond to the nulls of the propagation factor.

The nulls of the propagation factor occur when the sine is equal to zero. More precisely,

$$\frac{2h_r h_t}{\lambda R} = n \quad (8.38)$$

where $n = \{0, 1, 2, \dots\}$. The maxima occur at

$$\frac{4h_r h_t}{\lambda R} = n + 1 \quad (8.39)$$

The target heights that produce nulls in the propagation factor are $\{h_t = n(\lambda R/2h_r); n = 0, 1, 2, \dots\}$, and the peaks are produced from target heights $\{h_t = n(\lambda R/4h_r); n = 1, 2, \dots\}$. Therefore, due to the presence of surface reflections, the antenna elevation coverage is transformed into a lobed pattern structure as illustrated by Fig. 8.10. A target located at a maxima will be detected at twice its free space range. Alternatively, at other angles, the

detection range will be less than that in free space. At angles defined by Eq. (8.38) there would be no measurable target returns.

For small angles, Eq. (8.37) can be approximated by

$$P_r \approx \frac{4\pi P_t G^2 \sigma}{\lambda^2 R^8} (h_t h_r)^4 \quad (8.40)$$

Thus, the received signal power varies as the eighth power of the range instead of the fourth power. Also, the factor $G\lambda$ is now replaced by G/λ .

8.4.2. Spherical Earth

In order to model the effects of multipath propagation on radar performance more accurately, we need to remove the flat earth condition and account for the earth's curvature. When considering round earth, electromagnetic waves travel in curved paths because of the atmospheric refraction. And as mentioned earlier, the most commonly used approach to mitigating the effects of atmospheric refraction is to replace the actual earth by an imaginary earth such that electromagnetic waves travel in straight lines. The effective radius of the imaginary earth is

$$r_e = kr_0 \quad (8.41)$$

where k is a constant and r_0 is the actual earth radius (6371 Km). Using the geometry in Fig. 8.11, the direct and indirect path difference is

$$\Delta R = R_1 + R_2 - R_d \quad (8.42)$$

The propagation factor is computed by using ΔR from Eq. (8.42) in Eq. (8.18) and substituting the result in Eq. (8.25). To compute (R_1 , R_2 , and R_d) the following cubic equation must first be solved for r_1 :

$$2r_1^3 - 3rr_1^2 + (r^2 - 2r_e(h_r + h_t))r_1 + 2r_e h_r r = 0 \quad (8.43)$$

The solution is

$$r_1 = \frac{r}{2} - p \sin \frac{\xi}{3} \quad (8.44)$$

where

$$p = \frac{2}{\sqrt{3}} \sqrt{r_e(h_t + h_r) + \frac{r^2}{4}} \quad (8.45)$$

$$\xi = \operatorname{asin}\left(\frac{2r_e r(h_t - h_r)}{p^3}\right) \quad (8.46)$$

Next, we solve for R_1 , R_2 , and R_d . From Fig. 8.11,

$$\phi_1 = r_1/r_e \quad (8.47)$$

$$\phi_2 = r_2/r_e \quad (8.48)$$

Using the law of cosines to the triangles ABO and BOC yields

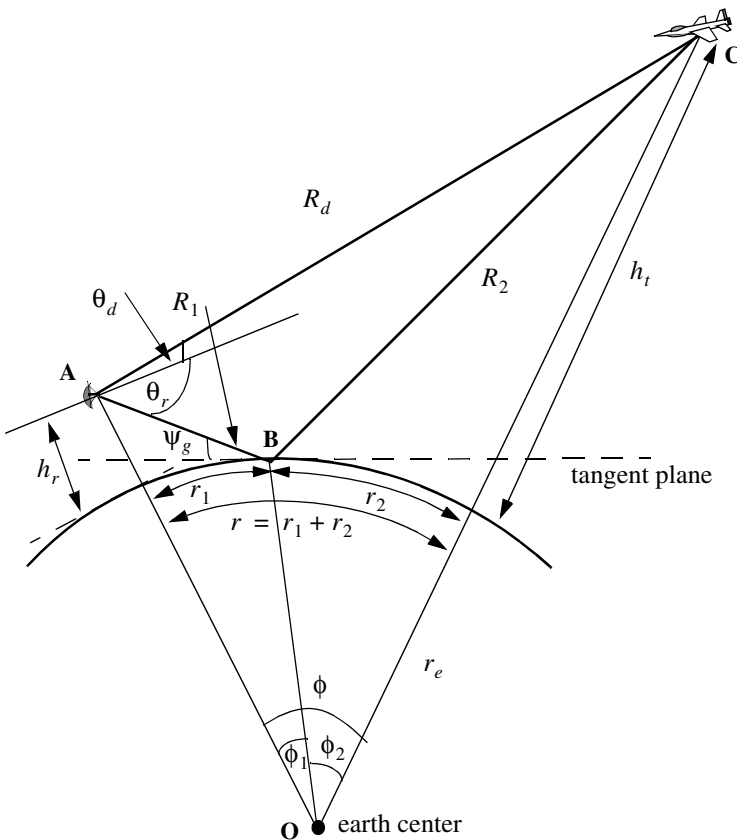


Figure 8.11. Geometry associated with multipath propagation over round earth.

$$R_1 = \sqrt{r_e^2 + (r_e + h_r)^2 - 2r_e(r_e + h_r)\cos\phi_1} \quad (8.49)$$

$$R_2 = \sqrt{r_e^2 + (r_e + h_t)^2 - 2r_e(r_e + h_t)\cos\phi_2} \quad (8.50)$$

Eqs. (8.49) and (8.50) can be written in the following simpler forms:

$$R_1 = \sqrt{h_r^2 + 4r_e(r_e + h_r)(\sin(\phi_1/2))^2} \quad (8.51)$$

$$R_2 = \sqrt{h_t^2 + 4r_e(r_e + h_t)(\sin(\phi_2/2))^2} \quad (8.52)$$

Using the law of cosines on the triangle AOC yields

$$R_d = \sqrt{(h_t - h_r)^2 + 4(r_e + h_t)(r_e + h_r)\left(\sin\left(\frac{\phi_1 + \phi_2}{2}\right)\right)^2} \quad (8.53)$$

Substituting Eqs. (8.51) through (8.53) directly into Eq. (8.42) may not be conducive to numerical accuracy. A more suitable form for the computation of ΔR is then derived. The detailed derivation is in Blake. The results are listed below. For better numerical accuracy use the following expression to compute ΔR :

$$\Delta R = \frac{4R_1R_2(\sin\psi_g)^2}{R_1 + R_2 + R_d} \quad (8.54)$$

where

$$\psi_g \approx \text{asin}\left(\frac{h_t}{R_1} - \frac{R_1}{2r_e}\right) \quad (8.55)$$

8.5. Diffraction

Diffraction is a term used to describe the phenomenon of electromagnetic waves bending around obstacles. It is of major importance to radar systems operating at very low altitudes. Hills and ridges diffract radio energy and make it possible to perform detection in regions that are physically shadowed. In practice, experimental data measurements provide the dominant source of information available on this phenomenon. Some theoretical analyses of diffraction are also available. However, in these cases many assumptions are made, and perhaps the most important assumption is that obstacles are chosen to be perfect conductors.

The problem of propagation over a knife edge on a plane can be described with help of Fig. 8.12. The target and radar heights are denoted, respectively,

by h_t and h_r . The edge height is h_e . Denote the distance by which the radar rays clear (or do not clear) the tip of the edge by δ . As a matter of notation δ is assumed to be positive when the direct rays clear the edge, and is negative otherwise. Because of the fact that ground reflection occurs on both sides of the edge, then the propagation factor is composed of four distinct rays, as illustrated in Fig. 8.13. An expression for the propagation factor corresponding to the four rays is reported in Meeks (see Bibliography).

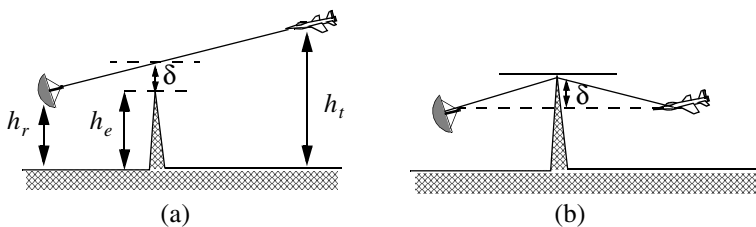


Figure 8.12. Diffraction over a knife edge. (a) Positive δ . (b) Negative δ .

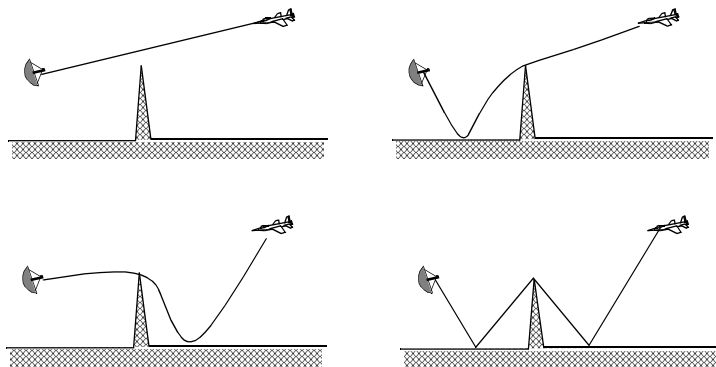


Figure 8.13. Four ray formation.

8.6. Atmospheric Attenuation

Electromagnetic waves travel in free space without suffering any energy loss. Alternatively, due to gases and water vapor in the atmosphere radar

energy suffers a loss. This loss is known as the atmospheric attenuation. Atmospheric attenuation increases significantly in the presence of rain, fog, dust, and clouds. Most of the lost radar energy is normally absorbed by gases and water vapor and transformed into heat, while a small portion of this lost energy is used in molecular transformation of the atmosphere particles.

The two-way atmospheric attenuation over a range R can be expressed as

$$L_{atmosphere} = e^{-2\alpha R} \tag{8.56}$$

where α is the one-way attenuation coefficient. Water vapor attenuation peaks at about 22.3GHz , while attenuation due to oxygen peaks at between 60 and 118GHz . Atmospheric attenuation is severe for frequencies higher than 35GHz . This is the reason why ground-based radars rarely use frequencies higher than 35GHz .

Atmospheric attenuation is a function range, frequency, and elevation angle. Fig. 8.14 shows a typical two-way atmospheric attenuation plot versus range at 3GHz , with the elevation angle as a parameter. Fig. 8.15 is similar to Fig. 8.14, except it is for 10GHz . For further details on this subject the reader is advised to visit Blake.

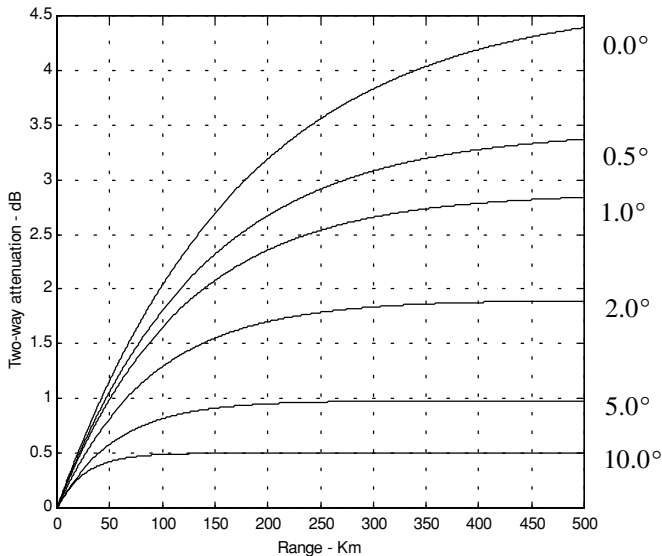


Figure 8.14. Attenuation versus range; frequency is 3 GHz.

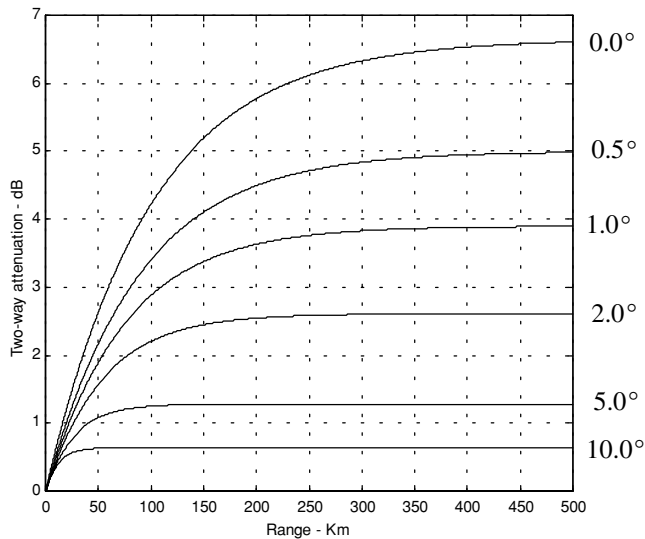


Figure 8.15. Attenuation versus range; frequency is 10 GHz.

8.7. MATLAB Program “ref_coef.m”

```
function [rh,rv,ph,pv] = ref_coef(eps,epspp)
eps = eps - i * epspp; %65.0-30.7i;
psi = 0:0.1:90;
psirad = psi.*(pi/180.);
arg1 = eps-(cos(psirad).^2);
arg2 = sqrt(arg1);
arg3 = sin(psirad);
arg4 = eps.*arg3;
rv = (arg4-arg2)./(arg4+arg2);
rh = (arg3-arg2)./(arg3+arg2);
gamamodv = abs(rv);
gamamodh = abs(rh);
figure(1)
plot(psi,gamamodv,'k',psi,gamamodh,'k-.');
axis tight
grid
xlabel('grazing angle - degrees');
ylabel('reflection coefficient - amplitude')
```

```

legend ('Vertical Polarization','Horizontal Polarization')
pv = -angle(rv);
ph = angle(rh);
figure(2)
plot(psi,pv,'k',psi,ph,'k -');
grid
xlabel('grazing angle - degrees');
ylabel('reflection coefficient - phase')
legend ('Vertical Polarization','Horizontal Polarization')

```

Problems

8.1. Using Eq. (8.4), determine h when $h_r = 15m$ and $R = 35Km$.

8.2. An exponential expression for the index of refraction is given by

$$n = 1 + 315 \times 10^{-6} \exp(-0.136h)$$

where the altitude h is in Km. Calculate the index of refraction for a well mixed atmosphere at 10% and 50% of the troposphere.

8.3. Rederive Eq. (8.34) assuming vertical polarization.

8.4. Reproduce Figs. 8.6 and 8.7 by using $f = 8GHz$ and (a) $\epsilon' = 2.8$ and $\epsilon'' = 0.032$ (dry soil); (b) $\epsilon' = 47$ and $\epsilon'' = 19$ (sea water at $0^\circ C$); (c) $\epsilon' = 50.3$ and $\epsilon'' = 18$ (lake water at $0^\circ C$).

8.5. In reference to Fig. 8.9, assume a radar height of $h_r = 100m$ and a target height of $h_t = 500m$. The range is $R = 20Km$. (a) Calculate the lengths of the direct and indirect paths. (b) Calculate how long it will take a pulse to reach the target via the direct and indirect paths.

8.6. In the previous problem, assuming that you may be able to use the small grazing angle approximation: (a) Calculate the ratio of the direct to the indirect signal strengths at the target. (b) If the target is closing on the radar with velocity $v = 300m/s$, calculate the Doppler shift along the direct and indirect paths. Assume $\lambda = 3cm$.

8.7. Utilizing the plots generated in solving Problem 8.4, derive an empirical expression for the Brewster's angle.

8.8. A radar at altitude $h_r = 10m$ and a target at altitude $h_t = 300m$, and assuming a spherical earth, calculate r_1 , r_2 , and ψ_g .

8.9. Derive an asymptotic form for Γ_h and Γ_v when the grazing angle is very small.

- 8.10.** In reference to [Fig. 8.8](#), assume a radar height of $h_r = 100m$ and a target height of $h_t = 500m$. The range is $R = 20Km$. (a) Calculate the lengths of the direct and indirect paths. (b) Calculate how long it will take a pulse to reach the target via the direct and indirect paths.
- 8.11.** Using the law of cosines, derive Eqs. (8.51) through (8.53).
- 8.12.** In the previous problem, assuming that you may be able to use the small grazing angle approximation: (a) Calculate the ratio of the direct to the indirect signal strengths at the target. (b) If the target is closing on the radar with velocity $v = 300m/s$, calculate the Doppler shift along the direct and indirect paths. Assume $\lambda = 3cm$.
- 8.13.** In the previous problem, assuming that you may be able to use the small grazing angle approximation: (a) Calculate the ratio of the direct to the indirect signal strengths at the target. (b) If the target is closing on the radar with velocity $v = 300m/s$, calculate the Doppler shift along the direct and indirect paths. Assume $\lambda = 3cm$.
- 8.14.** Calculate the range to the horizon corresponding to a radar at $5Km$ and $10Km$ of altitude. Assume $4/3$ earth.
- 8.15.** Develop a mathematical expression that can be used to reproduce [Figs. 8.14](#) and [8.15](#).

9.1. Clutter Definition

Clutter is a term used to describe any object that may generate unwanted radar returns that may interfere with normal radar operations. Parasitic returns that enter the radar through the antenna's main lobe are called main lobe clutter; otherwise they are called side lobe clutter. Clutter can be classified in two main categories: surface clutter and airborne or volume clutter. Surface clutter includes trees, vegetation, ground terrain, man-made structures, and sea surface (sea clutter). Volume clutter normally has large extent (size) and includes chaff, rain, birds, and insects. Chaff consists of a large number of small dipole reflectors that have large RCS values. It is released by hostile aircraft or missiles as a means of ECM in an attempt to confuse the defense. Surface clutter changes from one area to another, while volume clutter may be more predictable.

Clutter echoes are random and have thermal noise-like characteristics because the individual clutter components (scatterers) have random phases and amplitudes. In many cases, the clutter signal level is much higher than the receiver noise level. Thus, the radar's ability to detect targets embedded in high clutter background depends on the Signal-to-Clutter Ratio (SCR) rather than the SNR.

White noise normally introduces the same amount of noise power across all radar range bins, while clutter power may vary within a single range bin. And since clutter returns are target-like echoes, the only way a radar can distinguish target returns from clutter echoes is based on the target RCS σ_t , and the anticipated clutter RCS σ_c (via clutter map). Clutter RCS can be defined as the equivalent radar cross section attributed to reflections from a clutter area, A_c . The average clutter RCS is given by

$$\sigma_c = \sigma^0 A_c \quad (9.1)$$

where $\sigma^0 (m^2/m^2)$ is the clutter scattering coefficient, a dimensionless quantity that is often expressed in dB. Some radar engineers express σ^0 in terms of squared centimeters per squared meter. In these cases, σ^0 is 40dB higher than normal.

The term that describes the constructive/destructive interference of the electromagnetic waves diffracted from an object (target or clutter) is called the propagation factor (see Chapter 8 for more details). Since target and clutter returns have different angles of arrival (different propagation factors), we can define the SCR as

$$SCR = \frac{\sigma_t F_t^2 F_r^2}{\sigma_c F_c^2} \quad (9.2)$$

where F_c is the clutter propagation factor, F_t and F_r are, respectively, the transmit and receive propagation factors for the target. In many cases $F_t = F_r$.

9.2. Surface Clutter

Surface clutter includes both land and sea clutter, and is often called area clutter. Area clutter manifests itself in airborne radars in the look-down mode. It is also a major concern for ground-based radars when searching for targets at low grazing angles. The grazing angle ψ_g is the angle from the surface of the earth to the main axis of the illuminating beam, as illustrated in Fig. 9.1.

Three factors affect the amount of clutter in the radar beam. They are the grazing angle, surface roughness, and the radar wavelength. Typically, the clutter scattering coefficient σ^0 is larger for smaller wavelengths. Fig. 9.2 shows a sketch describing the dependency of σ^0 on the grazing angle. Three regions are identified; they are the low grazing angle region, flat or plateau region, and the high grazing angle region.

The low grazing angle region extends from zero to about the critical angle. The critical angle is defined by Rayleigh as the angle below which a surface is considered to be smooth, and above which a surface is considered to be rough. Denote the root mean square (rms) of a surface height irregularity as h_{rms} , then according to the Rayleigh criteria the surface is considered to be smooth if

$$\frac{4\pi h_{rms}}{\lambda} \sin \psi_g < \frac{\pi}{2} \quad (9.3)$$

Consider a wave incident on a rough surface, as shown in Fig. 9.3. Due to surface height irregularity (surface roughness), the “rough path” is longer than the “smooth path” by a distance $2h_{rms} \sin \psi_g$. This path difference translates into a phase differential $\Delta\psi$:

$$\Delta\psi = \frac{2\pi}{\lambda} 2h_{rms} \sin \psi_g \quad (9.4)$$

The critical angle ψ_{gc} is then computed when $\Delta\psi = \pi$ (first null), thus

$$\frac{4\pi h_{rms}}{\lambda} \sin \psi_{gc} = \pi \quad (9.5)$$

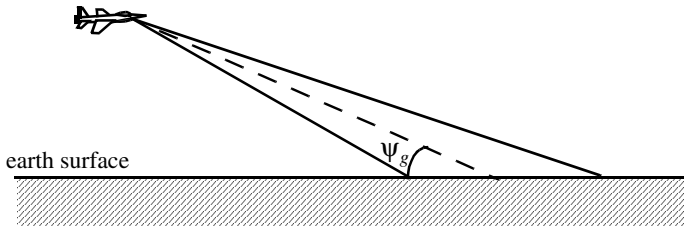


Figure 9.1. Definition of grazing angle.

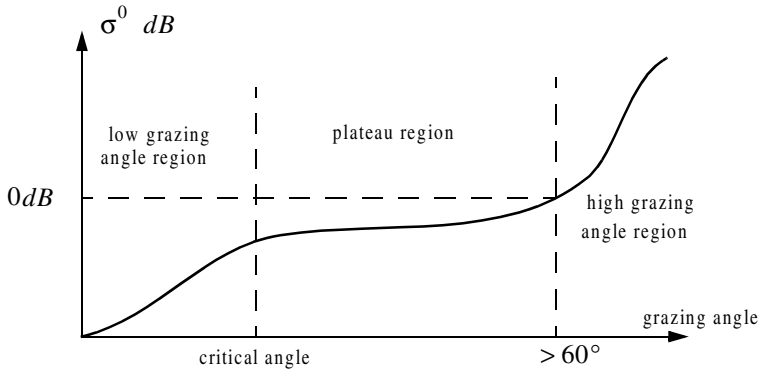


Figure 9.2. Clutter regions.

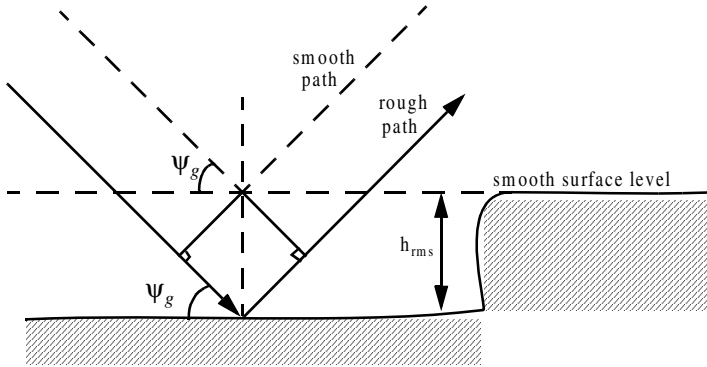


Figure 9.3. Rough surface definition.

or equivalently,

$$\Psi_{gc} = \text{asin} \frac{\lambda}{4h_{rms}} \quad (9.6)$$

In the case of sea clutter, for example, the rms surface height irregularity is

$$h_{rms} \approx 0.025 + 0.046 S_{state}^{1.72} \quad (9.7)$$

where S_{state} is the sea state, which is tabulated in several cited references. The sea state is characterized by the wave height, period, length, particle velocity, and wind velocity. For example, $S_{state} = 3$ refers to a moderate sea state, where in this case the wave height is approximately equal to between 0.9144 to 1.2192 m, the wave period 3.5 to 4.5 seconds, wave length 1.9812 to 33.528 m, wave velocity 20.372 to 25.928 Km/hr, and wind velocity 22.224 to 29.632 Km/hr.

Clutter at low grazing angles is often referred to as diffused clutter, where there are a large number of clutter returns in the radar beam (non-coherent reflections). In the flat region the dependency of σ^0 on the grazing angle is minimal. Clutter in the high grazing angle region is more specular (coherent reflections) and the diffuse clutter components disappear. In this region the smooth surfaces have larger σ^0 than rough surfaces, opposite of the low grazing angle region.

9.2.1. Radar Equation for Area Clutter

Consider an airborne radar in the look-down mode shown in Fig. 9.4. The intersection of the antenna beam with ground defines an elliptically shaped footprint. The size of the footprint is a function of the grazing angle and the antenna 3dB beam width θ_{3dB} , as illustrated in Fig. 9.5. The footprint is divided into many ground range bins each of size $(c\tau/2)\sec\psi_g$, where τ is the pulse width.

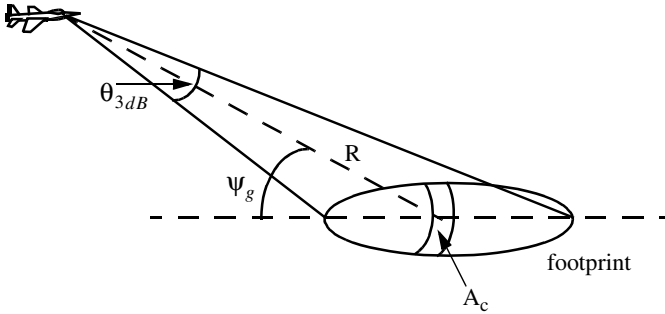


Figure 9.4. Airborne radar in the look-down mode.

From Fig. 9.5, the clutter area A_c is

$$A_c \approx R\theta_{3dB}\frac{c\tau}{2}\sec\psi_g \quad (9.8)$$

The power received by the radar from a scatterer within A_c is given by the radar equation as

$$S_t = \frac{P_t G^2 \lambda^2 \sigma_t}{(4\pi)^3 R^4} \quad (9.9)$$

where as usual, P_t is the peak transmitted power, G is the antenna gain, λ is the wavelength, and σ_t is the target RCS. Similarly, the received power from clutter is

$$S_{A_c} = \frac{P_t G^2 \lambda^2 \sigma_c}{(4\pi)^3 R^4} \quad (9.10)$$

where the subscript A_c is used for area clutter. Substituting Eq. (9.1) for σ_c into Eq. (9.10), we can then obtain the SCR for area clutter by dividing Eq. (9.9) by Eq. (9.10). More precisely,

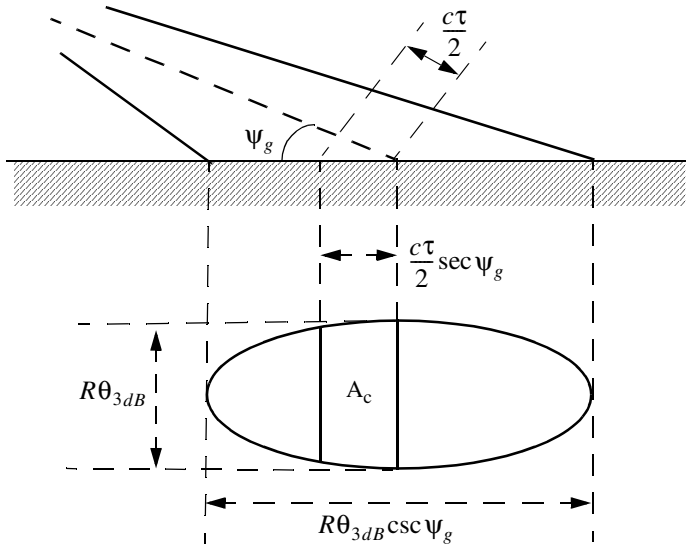


Figure 9.5. Footprint definition.

$$(SCR)_{Ac} = \frac{2\sigma_t \cos \psi_g}{\sigma^0 \theta_{3dB} R c \tau} \quad (9.11)$$

Example 9.1: Consider an airborne radar shown in Fig. 9.4. Let the antenna 3dB beam width be $\theta_{3dB} = 0.02 \text{ rad}$, the pulse width $\tau = 2 \mu\text{s}$, range $R = 20 \text{ Km}$, and grazing angle $\psi_g = 20^\circ$. Assume target RCS $\sigma_t = 1 \text{ m}^2$, and clutter reflection coefficient $\sigma^0 = 0.0136 \text{ m}^2/\text{m}^2$. Compute the SCR.

Solution: The SCR is given by Eq. (9.11) as

$$(SCR)_{Ac} = \frac{2\sigma_t \cos \psi_g}{\sigma^0 \theta_{3dB} R c \tau} \Rightarrow$$

$$(SCR)_{Ac} = \frac{(2)(1)(\cos 20)}{(0.0136)(0.02)(20000)(3 \times 10^8)(2 \times 10^{-6})} = 2.48 \times 10^{-4}$$

It follows that

$$(SCR)_{Ac} = -36.06 \text{ dB}$$

Thus, for reliable detection the radar must somehow increase its SCR by at least $(36 + X) \text{ dB}$, where X is on the order of 10 dB or better.

9.3. Volume Clutter

Volume clutter has large extents and includes rain (weather), chaff, birds, and insects. The volume clutter coefficient is normally expressed in squared meters (RCS per resolution volume). Birds, insects, and other flying particles are often referred to as angel clutter or biological clutter. The average RCS for individual birds or insects as a function of the weight of the bird or insect is reported in the literature¹ as

$$(\sigma_b)_{dBsm} \approx -46 + 5.8 \log W_b \quad (9.12)$$

where W_b is the individual bird or insect weight in grams. Bird and insect RCSs are also a function of frequency; for example, a pigeon's average RCS is $-26dBsm$ at S-band, and is equal to $-27dBsm$ at X-band.

As mentioned earlier, chaff is used as an ECM technique by hostile forces. It consists of a large number of dipole reflectors with large RCS values. Historically, chaff was made of aluminum foil; however, in recent years most chaff is made of the more rigid fiber glass with conductive coating. The maximum chaff RCS occurs when the dipole length L is one half the radar wavelength. The average RCS for a single dipole when viewed broadside is

$$\sigma_{chaff1} \approx 0.88\lambda^2 \quad (9.13)$$

and for an average aspect angle, it drops to

$$\sigma_{chaff1} \approx 0.15\lambda^2 \quad (9.14)$$

where the subscript *chaff1* is used to indicate a single dipole, and λ is the radar wavelength. The total chaff RCS within a radar resolution volume is

$$\sigma_{chaff} \approx 0.15\lambda^2 N_D \quad (9.15)$$

where N_D is the total number of dipoles in the resolution volume.

Weather or rain clutter is easier to suppress than chaff, since rain droplets can be viewed as perfect small spheres. We can use the Rayleigh approximation of perfect sphere to estimate the rain droplets' RCS. The Rayleigh approximation, without regard to the propagation medium index of refraction, is given in Eq. (2.30) and is repeated here as Eq. (9.16):

$$\sigma = 9\pi r^2 (kr)^4 \quad r \ll \lambda \quad (9.16)$$

where $k = 2\pi/\lambda$, and r is radius of a rain droplet.

1. Edde, B., *Radar - Principles, Technology, Applications*, Prentice-Hall, 1993.

Electromagnetic waves when reflected from a perfect sphere become strongly co-polarized (have the same polarization as the incident waves). Consequently, if the radar transmits, say, a right-hand-circularly (RHC) polarized wave, then the received waves are left-hand-circularly (LHC) polarized, because it is propagating in the opposite direction. Therefore, the back-scattered energy from rain droplets retains the same wave rotation (polarization) as the incident wave, but has a reversed direction of propagation. It follows that radars can suppress rain clutter by co-polarizing the radar transmit and receive antennas.

Defining η as RCS per unit resolution volume V_W , it is computed as the sum of all individual scatterers RCS within the volume,

$$\eta = \sum_{i=1}^N \sigma_i \quad (9.17)$$

where N is the total number of scatterers within the resolution volume. Thus, the total RCS of a single resolution volume is

$$\sigma_W = \sum_{i=1}^N \sigma_i V_W \quad (9.18)$$

A resolution volume is shown in Fig. 9.6, and is approximated by

$$V_W \approx \frac{\pi}{8} \theta_a \theta_e R^2 c \tau \quad (9.19)$$

where θ_a , θ_e are, respectively, the antenna beam width in azimuth and elevation, τ is the pulse width in seconds, c is speed of light, and R is range.

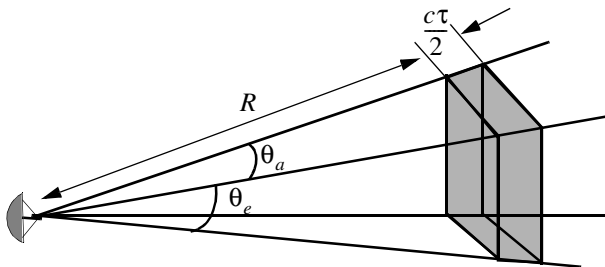


Figure 9.6. Definition of a resolution volume.

Consider a propagation medium with an index of refraction m . The i th rain droplet RCS approximation in this medium is

$$\sigma_i \approx \frac{\pi^5}{\lambda^4} K^2 D_i^6 \quad (9.20)$$

where

$$K^2 = \left| \frac{m^2 - 1}{m^2 + 2} \right|^2 \quad (9.21)$$

and D_i is the i th droplet diameter. For example, temperatures between $32^\circ F$ and $68^\circ F$ yield

$$\sigma_i \approx 0.93 \frac{\pi^5}{\lambda^4} D_i^6 \quad (9.22)$$

and for ice Eq. (9.20) can be approximated by

$$\sigma_i \approx 0.2 \frac{\pi^5}{\lambda^4} D_i^6 \quad (9.23)$$

Substituting Eq. (9.20) into Eq. (9.17) yields

$$\eta = \frac{\pi^5}{\lambda^4} K^2 Z \quad (9.24)$$

where the weather clutter coefficient Z is defined as

$$Z = \sum_{i=1}^N D_i^6 \quad (9.25)$$

In general, a rain droplet diameter is given in millimeters and the radar resolution volume is expressed in cubic meters, thus the units of Z are often expressed in *millimeter*⁶/*m*³.

9.3.1. Radar Equation for Volume Clutter

The radar equation gives the total power received by the radar from a σ_t target at range R as

$$S_t = \frac{P_t G^2 \lambda^2 \sigma_t}{(4\pi)^3 R^4} \quad (9.26)$$

where all parameters in Eq. (9.26) have been defined earlier. The weather clutter power received by the radar is

$$S_W = \frac{P_t G^2 \lambda^2 \sigma_W}{(4\pi)^3 R^4} \quad (9.27)$$

Using Eq. (9.18) and Eq. (9.19) into Eq. (9.27) and collecting terms yield

$$S_W = \frac{P_t G^2 \lambda^2}{(4\pi)^3 R^4} \frac{\pi}{8} R^2 \theta_a \theta_e c \tau \sum_{i=1}^N \sigma_i \quad (9.28)$$

The SCR for weather clutter is then computed by dividing Eq. (9.26) by Eq. (9.28). More precisely,

$$(SCR)_V = \frac{S_t}{S_W} = \frac{8\sigma_t}{\pi \theta_a \theta_e c \tau R^2 \sum_{i=1}^N \sigma_i} \quad (9.29)$$

where the subscript V is used to denote volume clutter.

Example 9.2: A certain radar has target RCS $\sigma_t = 0.1m^2$, pulse width $\tau = 0.2\mu s$, antenna beam width $\theta_a = \theta_e = 0.02radians$. Assume the detection range to be $R = 50Km$, and compute the SCR if $\sum \sigma_i = 1.6 \times 10^{-8}(m^2/m^3)$.

Solution: From Eq. (9.29) we have

$$(SCR)_V = \frac{8\sigma_t}{\pi \theta_a \theta_e c \tau R^2 \sum_{i=1}^N \sigma_i}$$

substituting the proper values we get

$$(SCR)_V = \frac{(8)(0.1)}{\pi(0.02)^2(3 \times 10^8)(0.2 \times 10^{-6})(50 \times 10^3)^2(1.6 \times 10^{-8})} = 0.265$$

$$(SCR)_V = -5.768dB.$$

9.4. Clutter Statistical Models

Since clutter within a resolution cell (or volume) is composed of a large number of scatterers with random phases and amplitudes, it is statistically described by a probability distribution function. The type of distribution depends on the nature of clutter itself (sea, land, volume), the radar operating frequency, and the grazing angle.

If sea or land clutter is composed of many small scatterers when the probability of receiving an echo from one scatterer is statistically independent of the echo received from another scatterer, then the clutter may be modeled using a Rayleigh distribution,

$$f(x) = \frac{2x}{x_0} \exp\left(-\frac{x^2}{x_0}\right) ; x \geq 0 \quad (9.30)$$

where x_0 is the mean squared value of x .

The log-normal distribution best describes land clutter at low grazing angles. It also fits sea clutter in the plateau region. It is given by

$$f(x) = \frac{1}{\sigma\sqrt{2\pi} x} \exp\left(-\frac{(\ln x - \ln x_m)^2}{2\sigma^2}\right) ; x > 0 \quad (9.31)$$

where x_m is the median of the random variable x , and σ is the standard deviation of the random variable $\ln(x)$.

The Weibull distribution is used to model clutter at low grazing angles (less than five degrees) for frequencies between 1 and 10GHz. The Weibull probability density function is determined by the Weibull slope parameter a (often tabulated) and a median scatter coefficient $\bar{\sigma}_0$, and is given by

$$f(x) = \frac{bx^{b-1}}{\bar{\sigma}_0} \exp\left(-\frac{x^b}{\bar{\sigma}_0}\right) ; x \geq 0 \quad (9.32)$$

where $b = 1/a$ is known as the shape parameter. Note that when $b = 2$ the Weibull distribution becomes a Rayleigh distribution.

9.5. Clutter Spectrum

The power spectrum of stationary clutter (zero Doppler) can be represented by a delta function. However, clutter is not always stationary; it actually exhibits some Doppler frequency spread because of wind speed and motion of the radar scanning antenna. In general, the clutter spectrum is concentrated around

$f = 0$ and integer multiples of the radar PRF f_r , and may exhibit some small spreading.

The clutter power spectrum can be written as the sum of fixed (stationary) and random (due to frequency spreading) components. For most cases, the random component is Gaussian. If we denote the fixed to the random power ratio by W^2 , then we can write the clutter spectrum as

$$S_c(\omega) = \bar{\sigma}_0 \left(\frac{W^2}{1 + W^2} \right) \delta(\omega_0) + \frac{\bar{\sigma}_0}{(1 + W^2) \sqrt{2\pi\sigma_\omega^2}} \exp\left(-\frac{(\omega - \omega_0)^2}{2\sigma_\omega^2}\right) \quad (9.33)$$

where $\omega_0 = 2\pi f_0$ is the radar operating frequency in radians per second, σ_ω is the rms frequency spread component (determines the Doppler frequency spread), and $\bar{\sigma}_0$ is the Weibull parameter.

The first term of the right-hand side of Eq. (9.33) represents the PSD for stationary clutter, while the second term accounts for the frequency spreading. Nevertheless, since most of the clutter power is concentrated around zero Doppler with some spreading (typically less than 100 Hz), it is customary to model clutter using a Gaussian-shaped power spectrum (which is easier to analyze than Eq. (9.33)). More precisely,

$$S_c(\omega) = \frac{P_c}{\sqrt{2\pi\sigma_\omega^2}} \exp\left(-\frac{(\omega - \omega_0)^2}{2\sigma_\omega^2}\right) \quad (9.34)$$

where P_c is the total clutter power; σ_ω^2 and ω_0 were defined earlier. Fig. 9.7 shows a typical PSD sketch of radar returns when both target and clutter are present. Note that the clutter power is concentrated around DC and integer multiples of the PRF.

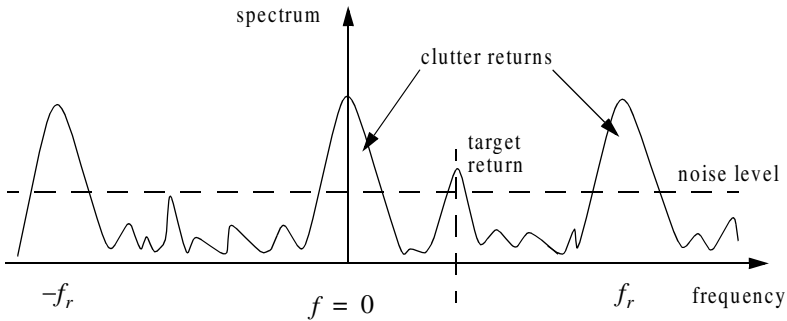


Figure 9.7. Typical radar return PSD when clutter and target are present.

9.6. Moving Target Indicator (MTI)

Clutter spectrum is normally concentrated around DC ($f = 0$) and multiple integers of the radar PRF f_r , as illustrated in Fig. 9.8a. In CW radars, clutter is avoided or suppressed by ignoring the receiver output around DC, since most of the clutter power is concentrated about the zero frequency band. Pulsed radar systems may utilize special filters that can distinguish between slowly moving or stationary targets and fast moving ones. This class of filters is known as the Moving Target Indicator (MTI). In simple words, the purpose of an MTI filter is to suppress target-like returns produced by clutter, and allow returns from moving targets to pass through with little or no degradation. In order to effectively suppress clutter returns, an MTI filter needs to have a deep stop-band at DC and at integer multiples of the PRF. Fig. 9.8b shows a typical sketch of an MTI filter response, while Fig. 9.8c shows its output when the PSD shown in Fig. 9.8a is the input.

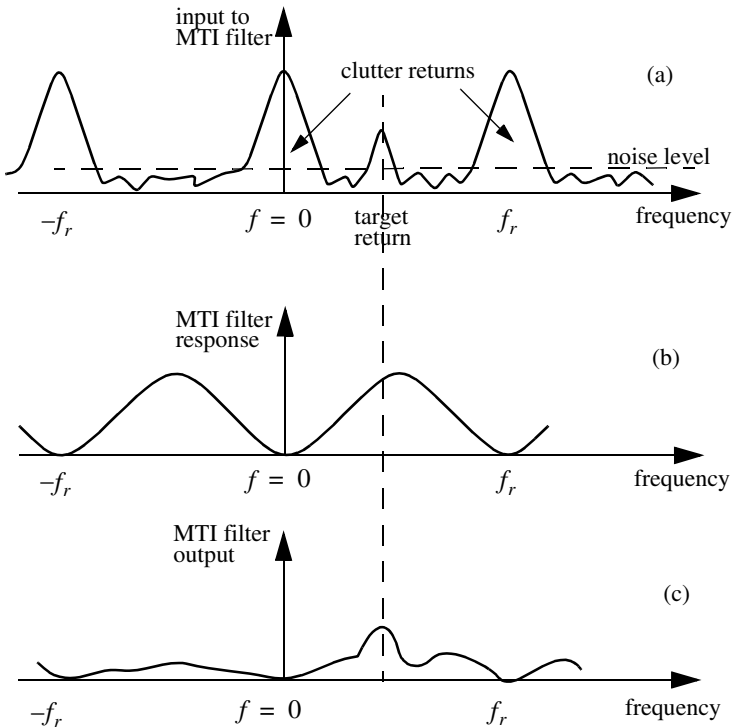


Figure 9.8. (a) Typical radar return PSD when clutter and target are present. (b) MTI filter frequency response. (c) Output from an MTI filter.

MTI filters can be implemented using delay line cancelers. As we will show later in this chapter, the frequency response of this class of MTI filters is periodic, with nulls at integer multiples of the PRF. Thus, targets with Doppler frequencies equal to nf_r are severely attenuated. And since Doppler is proportional to target velocity ($f_d = 2v/\lambda$), target speeds that produce Doppler frequencies equal to integer multiples of f_r are known as blind speeds. More precisely,

$$v_{blind} = \frac{\lambda f_r}{2} ; n \geq 0 \tag{9.35}$$

Radar systems can minimize the occurrence of blind speeds by either employing multiple PRF schemes (PRF staggering) or by using high PRFs where in this case the radar may become range ambiguous. The main difference between PRF staggering and PRF agility is that the pulse repetition interval (within an integration interval) can be changed between consecutive pulses for the case of PRF staggering.

Fig. 9.9 shows a block diagram of a coherent MTI radar. Coherent transmission is controlled by the STABLE Local Oscillator (STALO). The outputs of the STALO, f_{LO} , and the COHERENT Oscillator (COHO), f_C , are mixed to produce the transmission frequency, $f_{LO} + f_C$. The Intermediate Frequency (IF), $f_C \pm f_d$, is produced by mixing the received signal with f_{LO} . After the IF amplifier, the signal is passed through a phase detector and is converted into a base band. Finally, the video signal is inputted into an MTI filter.

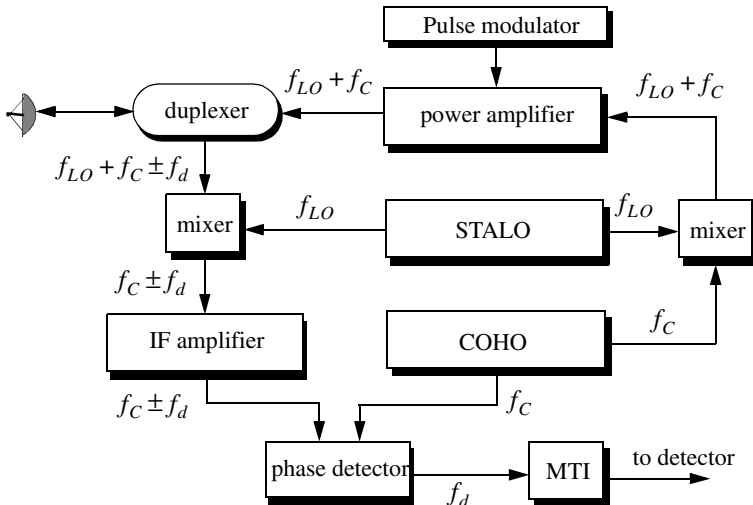


Figure 9.9. Coherent MTI radar block diagram.

9.7. Single Delay Line Canceler

A single delay line canceler can be implemented as shown in Fig. 9.10. The canceler's impulse response is denoted as $h(t)$. The output $y(t)$ is equal to the convolution between the impulse response $h(t)$ and the input $x(t)$. The single delay canceler is often called a "two-pulse canceler" since it requires two distinct input pulses before an output can be read.

The delay T is equal to the PRI of the radar ($1/f_r$). The output signal $y(t)$ is

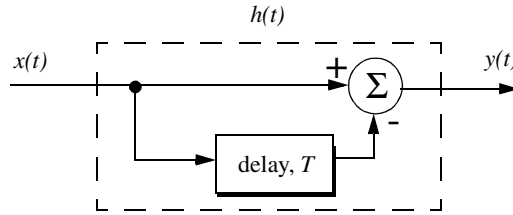


Figure 9.10. Single delay line canceler.

$$y(t) = x(t) - x(t - T) \quad (9.36)$$

The impulse response of the canceler is given by

$$h(t) = \delta(t) - \delta(t - T) \quad (9.37)$$

where $\delta(\cdot)$ is the delta function. It follows that the Fourier transform (FT) of $h(t)$ is

$$H(\omega) = 1 - e^{-j\omega T} \quad (9.38)$$

where $\omega = 2\pi f$.

In the z-domain, the single delay line canceler response is

$$H(z) = 1 - z^{-1} \quad (9.39)$$

The power gain for the single delay line canceler is given by

$$|H(\omega)|^2 = H(\omega)H^*(\omega) = (1 - e^{-j\omega T})(1 - e^{j\omega T}) \quad (9.40)$$

It follows that

$$|H(\omega)|^2 = 1 + 1 - (e^{j\omega T} + e^{-j\omega T}) = 2(1 - \cos \omega T) \quad (9.41)$$

and using the trigonometric identity $(2 - 2\cos 2\vartheta) = 4(\sin \vartheta)^2$ yields

$$|H(\omega)|^2 = 4(\sin(\omega T/2))^2 \quad (9.42)$$

MATLAB Function “single_canceler.m”

The function “single_canceler.m” computes and plots (as a function of f/f_r) the amplitude response for a single delay line canceler. It is given in Listing 9.1 in Section 9.14. The syntax is as follows:

$$[resp] = single_canceler(fofr)$$

where $fofr$ is the number of periods desired. Typical output of the function “single_canceler.m” is shown in Fig. 9.11. Clearly, the frequency response of a single canceler is periodic with a period equal to f_r . The peaks occur at $f = (2n + 1)/(2f_r)$, and the nulls are at $f = nf_r$, where $n \geq 0$.

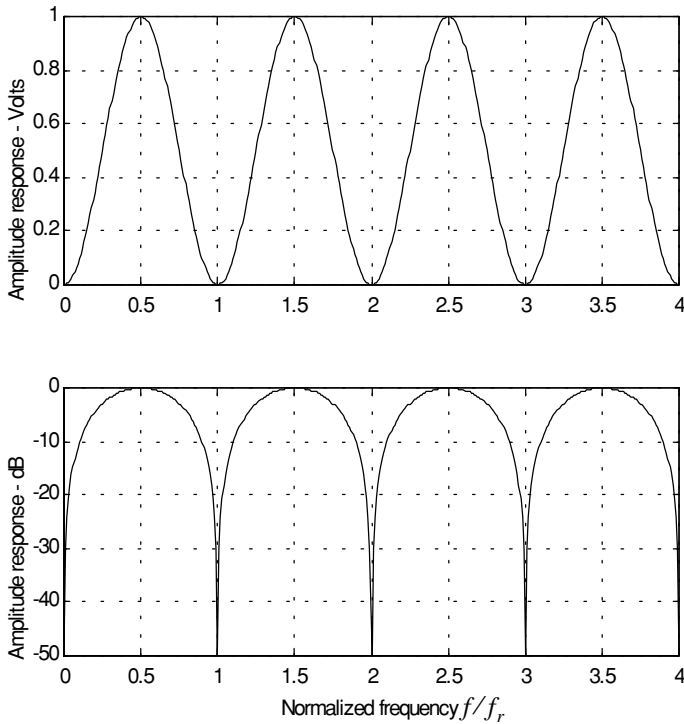


Figure 9.11. Single canceler frequency response.

In most radar applications the response of a single canceler is not acceptable since it does not have a wide notch in the stop-band. A double delay line canceler has better response in both the stop- and pass-bands, and thus it is more frequently used than a single canceler. In this book, we will use the names “single delay line canceler” and “single canceler” interchangeably.

9.8. Double Delay Line Canceler

Two basic configurations of a double delay line canceler are shown in Fig. 9.12. Double cancelers are often called “three-pulse cancelers” since they require three distinct input pulses before an output can be read. The double line canceler impulse response is given by

$$h(t) = \delta(t) - 2\delta(t - T) + \delta(t - 2T) \quad (9.43)$$

Again, the names “double delay line” canceler and “double canceler” will be used interchangeably. The power gain for the double delay line canceler is

$$|H(\omega)|^2 = |H_1(\omega)|^2 |H_1(\omega)|^2 \quad (9.44)$$

where $|H_1(\omega)|^2$ is the single line canceler power gain given in Eq. (9.42). It follows that

$$|H(\omega)|^2 = 16 \left(\sin\left(\frac{\omega T}{2}\right) \right)^4 \quad (9.45)$$

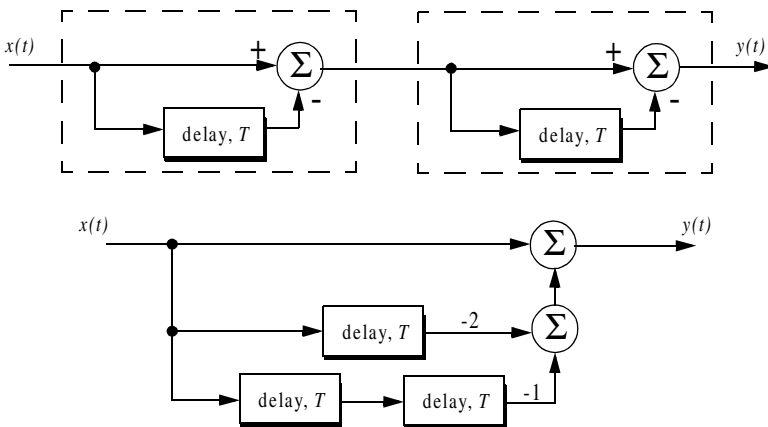


Figure 9.12. Two configurations for a double delay line canceler.

And in the z-domain, we have

$$H(z) = (1 - z^{-1})^2 = 1 - 2z^{-1} + z^{-2} \tag{9.46}$$

MATLAB Function “double_canceler.m”

The function “single_canceler.m” computes and plots (as a function of f/f_r) the amplitude response for a single delay line canceler. It is given in Listing 9.2 in Section 9.14. The syntax is as follows:

$$[resp] = double_canceler(fofr)$$

where $fofr$ is the number of periods desired.

Fig. 9.13 shows typical output from this function. Note that the double canceler has a better response than the single canceler (deeper notch and flatter pass-band response).

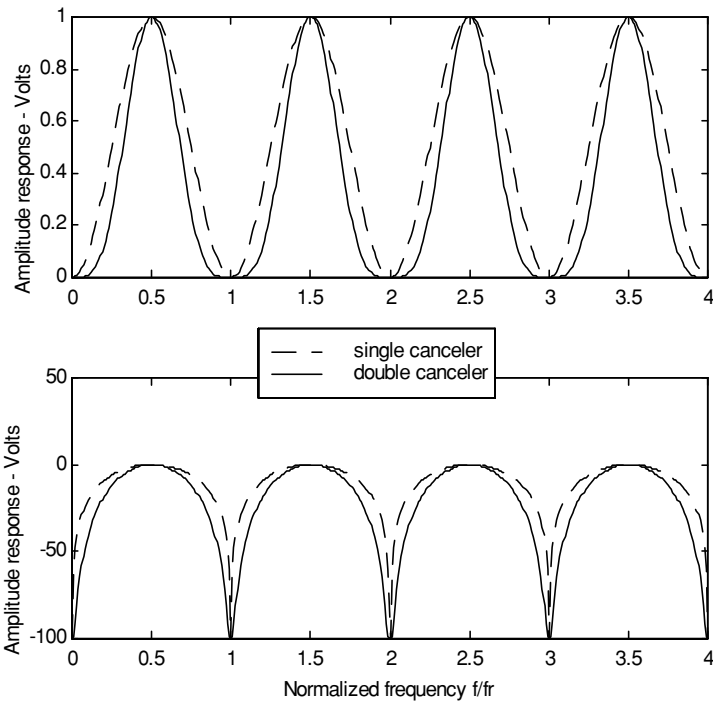


Figure 9.13. Normalized frequency responses for single and double cancelers.

9.9. Delay Lines with Feedback (Recursive Filters)

Delay line cancelers with feedback loops are known as recursive filters. The advantage of a recursive filter is that through a feedback loop we will be able to shape the frequency response of the filter. As an example, consider the single canceler shown in Fig. 9.14. From the figure we can write

$$y(t) = x(t) - (1 - K)w(t) \quad (9.47)$$

$$v(t) = y(t) + w(t) \quad (9.48)$$

$$w(t) = v(t - T) \quad (9.49)$$

Applying the z-transform to the above three equations yields

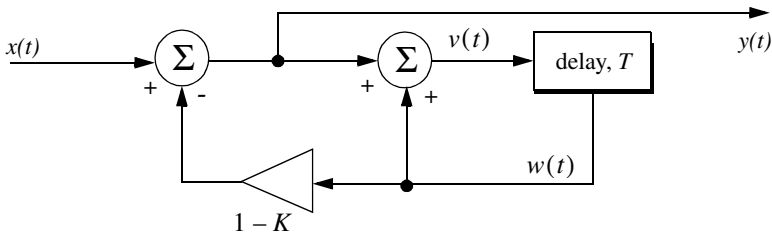


Figure 9.14. MTI recursive filter.

$$Y(z) = X(z) - (1 - K)W(z) \quad (9.50)$$

$$V(z) = Y(z) + W(z) \quad (9.51)$$

$$W(z) = z^{-1}V(z) \quad (9.52)$$

Solving for the transfer function $H(z) = Y(z)/X(z)$ yields

$$H(z) = \frac{1 - z^{-1}}{1 - Kz^{-1}} \quad (9.53)$$

The modulus square of $H(z)$ is then equal to

$$|H(z)|^2 = \frac{(1 - z^{-1})(1 - z)}{(1 - Kz^{-1})(1 - Kz)} = \frac{2 - (z + z^{-1})}{(1 + K^2) - K(z + z^{-1})} \quad (9.54)$$

Using the transformation $z = e^{j\omega T}$ yields

$$z + z^{-1} = 2 \cos \omega T \quad (9.55)$$

Thus, Eq. (54) can now be rewritten as

$$|H(e^{j\omega T})|^2 = \frac{2(1 - \cos \omega T)}{(1 + K^2) - 2K \cos(\omega T)} \quad (9.56)$$

Note that when $K = 0$, Eq. (9.56) collapses to Eq. (9.42) (single line canceler). Fig. 9.15 shows a plot of Eq. (9.56) for $K = 0.25, 0.7, 0.9$. Clearly, by changing the gain factor K one can control of the filter response.

In order to avoid oscillation due to the positive feedback, the value of K should be less than unity. The value $(1 - K)^{-1}$ is normally equal to the number of pulses received from the target. For example, $K = 0.9$ corresponds to ten pulses, while $K = 0.98$ corresponds to about fifty pulses.

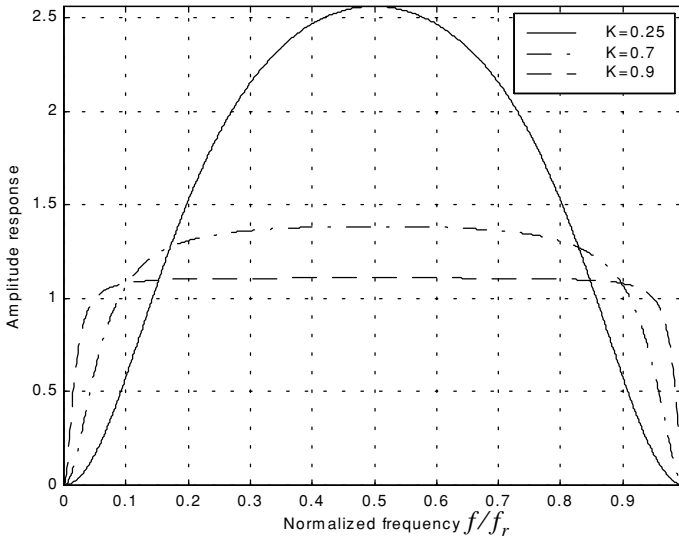


Figure 9.15. Frequency response corresponding to Eq. (9.56). This plot can be reproduced using MATLAB program “fig9_15.m” given in Listing 9.3 in Section 9.14.

9.10. PRF Staggering

Blind speeds can pose serious limitations on the performance of MTI radars and their ability to perform adequate target detection. Using PRF agility by changing the pulse repetition interval between consecutive pulses can extend

the first blind speed to tolerable values. In order to show how PRF staggering can alleviate the problem of blind speeds, let us first assume that two radars with distinct PRFs are utilized for detection. Since blind speeds are proportional to the PRF, the blind speeds of the two radars would be different. However, using two radars to alleviate the problem of blind speeds is a very costly option. A more practical solution is to use a single radar with two or more different PRFs.

For example, consider a radar system with two interpulse periods T_1 and T_2 , such that

$$\frac{T_1}{T_2} = \frac{n_1}{n_2} \quad (9.57)$$

where n_1 and n_2 are integers. The first true blind speed occurs when

$$\frac{n_1}{T_1} = \frac{n_2}{T_2} \quad (9.58)$$

This is illustrated in Fig. 9.16 for $n_1 = 4$ and $n_2 = 5$. Note that if $n_2 = n_1 + 1$, then the process of PRF staggering is similar to that discussed in Chapter 3.

The ratio

$$k_s = \frac{n_1}{n_2} \quad (9.59)$$

is known as the stagger ratio. Using staggering ratios closer to unity pushes the first true blind speed farther out. However, the dip in the vicinity of $1/T_1$ becomes deeper, as illustrated in Fig. 9.17 for stagger ratio $k_s = 63/64$. In general, if there are N PRFs related by

$$\frac{n_1}{T_1} = \frac{n_2}{T_2} = \dots = \frac{n_N}{T_N} \quad (9.60)$$

and if the first blind speed to occur for any of the individual PRFs is v_{blind1} , then the first true blind speed for the staggered waveform is

$$v_{blind} = \frac{n_1 + n_2 + \dots + n_N}{N} v_{blind1} \quad (9.61)$$

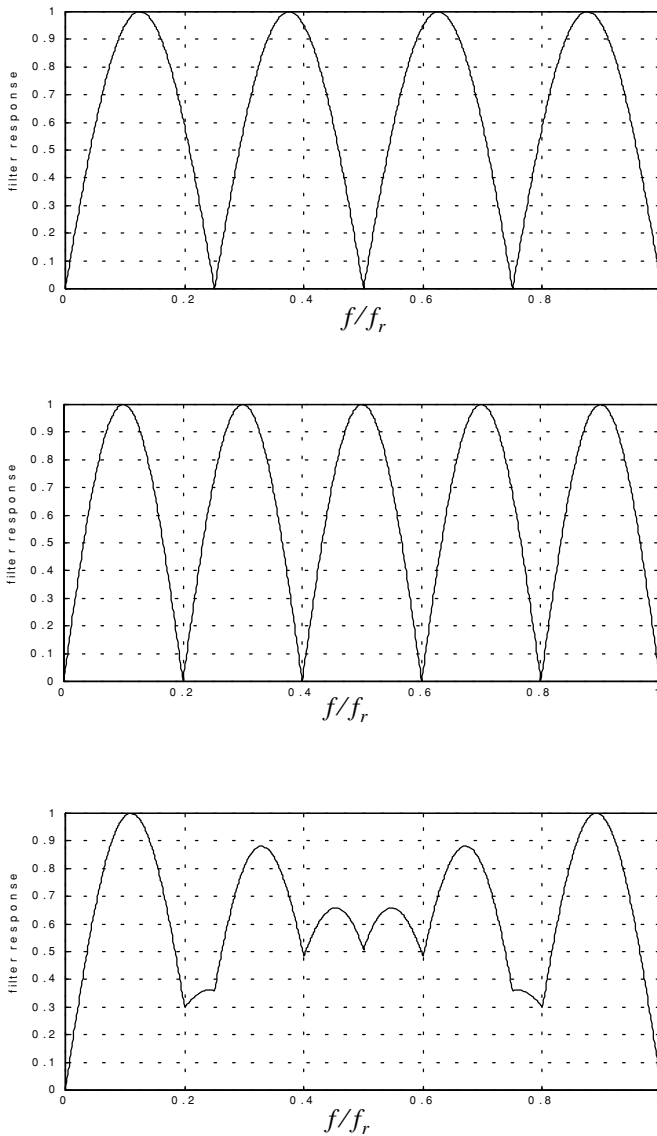


Figure 9.16. Frequency responses of a single canceler. Top plot corresponds to T_1 , middle plot corresponds to T_2 , bottom plot corresponds to stagger ratio $T_1/T_2 = 4/3$. This plot can be reproduced using MATLAB program “fig9_16.m” given in Listing 9.4 in Section 9.14.

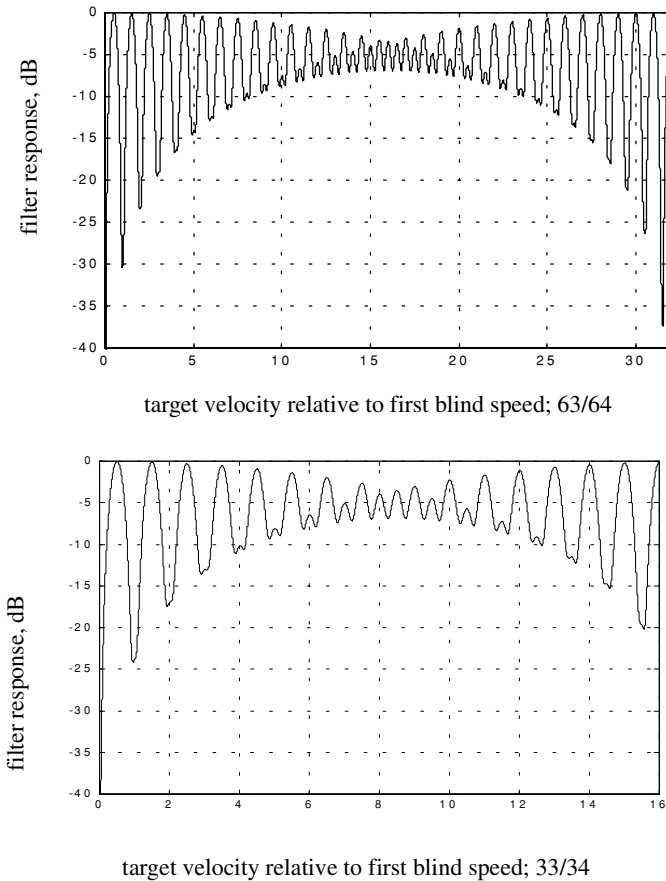


Figure 9.17. MTI responses, staggering ratio 63/64. This plot can be reproduced using MATLAB program “fig9_17.m” given in Listing 9.5 in Section 9.14.

9.11. MTI Improvement Factor

In this section two quantities that are normally used to define the performance of MTI systems are introduced. They are “Clutter Attenuation (CA)” and the MTI “Improvement Factor.” The MTI CA is defined as the ratio between the MTI filter input clutter power C_i to the output clutter power C_o ,

$$CA = C_i / C_o \quad (9.62)$$

The MTI improvement factor is defined as the ratio of the Signal to Clutter (SCR) at the output to the SCR at the input,

$$I = \left(\frac{S_o}{C_o}\right) / \left(\frac{S_i}{C_i}\right) \quad (9.63)$$

which can be rewritten as

$$I = \frac{S_o}{S_i} CA \quad (9.64)$$

The ratio S_o/S_i is the average power gain of the MTI filter, and it is equal to $|H(\omega)|^2$. In this section, a closed form expression for the improvement factor using a Gaussian-shaped power spectrum is developed. A Gaussian-shaped clutter power spectrum is given by

$$W(f) = \frac{P_c}{\sqrt{2\pi} \sigma_c} \exp(-f^2/2\sigma_c^2) \quad (9.65)$$

where P_c is the clutter power (constant), and σ_c is the clutter rms frequency and is given by

$$\sigma_c = 2\sigma_v/\lambda \quad (9.66)$$

where λ is the wavelength, and σ_v is the rms wind velocity, since wind is the main reason for clutter frequency spreading. Substituting Eq. (9.66) into Eq. (9.65) yields

$$W(f) = \frac{\lambda P_c}{2\sqrt{2\pi} \sigma_v} \exp\left(-\frac{f^2 \lambda^2}{8\sigma_v^2}\right) \quad (9.67)$$

The clutter power at the input of an MTI filter is

$$C_i = \int_{-\infty}^{\infty} \frac{P_c}{\sqrt{2\pi} \sigma_c} \exp\left(-\frac{f^2}{2\sigma_c^2}\right) df \quad (9.68)$$

Factoring out the constant P_c yields

$$C_i = P_c \int_{-\infty}^{\infty} \frac{1}{\sqrt{2\pi} \sigma_c} \exp\left(-\frac{f^2}{2\sigma_c^2}\right) df \quad (9.69)$$

It follows that (Why?)

$$C_i = P_c \quad (9.70)$$

The clutter power at the output of an MTI is

$$C_o = \int_{-\infty}^{\infty} W(f) |H(f)|^2 df \quad (9.71)$$

We will continue the analysis using a single delay line canceler. The frequency response for a single delay line canceler is given by Eq. (9.38). The single canceler power gain is given in Eq. (9.42), which will be repeated here, in terms of f rather than ω , as Eq. (9.72),

$$|H(f)|^2 = 4 \left(\sin \left(\frac{\pi f}{f_r} \right) \right)^2 \quad (9.72)$$

It follows that

$$C_o = \int_{-\infty}^{\infty} \frac{P_c}{\sqrt{2\pi} \sigma_c} \exp \left(- \frac{f^2}{2\sigma_c^2} \right) 4 \left(\sin \left(\frac{\pi f}{f_r} \right) \right)^2 df \quad (9.73)$$

Now, since clutter power will only be significant for small f , then the ratio f/f_r is very small (i.e., $\sigma_c \ll f_r$). Consequently, by using the small angle approximation Eq. (9.73) is approximated by

$$C_o \approx \int_{-\infty}^{\infty} \frac{P_c}{\sqrt{2\pi} \sigma_c} \exp \left(- \frac{f^2}{2\sigma_c^2} \right) 4 \left(\frac{\pi f}{f_r} \right)^2 df \quad (9.74)$$

which can be rewritten as

$$C_o = \frac{4P_c \pi^2}{f_r^2} \int_{-\infty}^{\infty} \frac{1}{\sqrt{2\pi} \sigma_c} \exp \left(- \frac{f^2}{2\sigma_c^2} \right) f^2 df \quad (9.75)$$

The integral part in Eq. (9.75) is the second moment of a zero mean Gaussian distribution with variance σ_c^2 . Replacing the integral in Eq. (9.75) by σ_c^2 yields

$$C_o = \frac{4P_c \pi^2}{f_r^2} \sigma_c^2 \quad (9.76)$$

Substituting Eqs. (9.76) and (9.70) into Eq. (9.62) produces

$$CA = \frac{C_i}{C_o} = \left(\frac{f_r}{2\pi\sigma_c} \right)^2 \quad (9.77)$$

It follows that the improvement factor for a single canceler is

$$I = \left(\frac{f_r}{2\pi\sigma_c} \right)^2 \frac{S_o}{S_i} \quad (9.78)$$

The power gain ratio for a single canceler is (remember that $|H(f)|$ is periodic with period f_r)

$$\frac{S_o}{S_i} = |H(f)|^2 = \frac{1}{f_r} \int_{-f_r/2}^{f_r/2} 4 \left(\sin \frac{\pi f}{f_r} \right)^2 df \quad (9.79)$$

Using the trigonometric identity $(2 - 2\cos 2\vartheta) = 4(\sin \vartheta)^2$ yields

$$|H(f)|^2 = \frac{1}{f_r} \int_{-f_r/2}^{f_r/2} \left(2 - 2\cos \frac{2\pi f}{f_r} \right) df = 2 \quad (9.80)$$

It follows that

$$I = 2(f_r/(2\pi\sigma_c))^2 \quad (9.81)$$

The expression given in Eq. (9.81) is an approximation valid only for $\sigma_c \ll f_r$. When the condition $\sigma_c \ll f_r$ is not true, then the autocorrelation function needs to be used in order to develop an exact expression for the improvement factor.

Example 9.3: A certain radar has $f_r = 800\text{Hz}$. If the clutter rms is $\sigma_c = 6.4\text{Hz}$ (wooded hills with $\sigma_v = 1.16311\text{Km/hr}$), find the improvement factor when a single delay line canceler is used.

Solution: The clutter attenuation CA is

$$CA = \left(\frac{f_r}{2\pi\sigma_c} \right)^2 = \left(\frac{800}{(2\pi)(6.4)} \right)^2 = 395.771 = 25.974\text{dB}$$

and since $S_o/S_i = 2 = 3\text{dB}$ we get

$$I_{dB} = (CA + S_o/S_i)_{dB} = 3 + 25.97 = 28.974\text{dB}.$$

9.12. Subclutter Visibility (SCV)

The phrase Subclutter Visibility (SCV) describes the radar's ability to detect non-stationary targets embedded in a strong clutter background, for some

probabilities of detection and false alarm. It is often used as a measure of MTI performance. For example, a radar with 10dB subclutter visibility will be able to detect moving targets whose returns are ten times smaller than those of clutter. A sketch illustrating the concept of SCV is shown in Fig. 9.18.

If a radar system can resolve the areas of strong and weak clutter within its field of view, then the phrase Interclutter Visibility (ICV) describes the radar's ability to detect non-stationary targets between strong clutter points. The subclutter visibility is expressed as the ratio of the improvement factor to the minimum MTI output SCR required for proper detection for a given probability of detection. More precisely,

$$SCV = I / (SCR)_o \tag{9.82}$$

When comparing different radar systems' performances on the basis of SCV, one should use caution since the amount of clutter power is dependent on the radar resolution cell (or volume), which may be different from one radar to another. Thus, only if the different radars have the same beam widths and the same pulse widths can SCV be used as a basis of performance comparison.

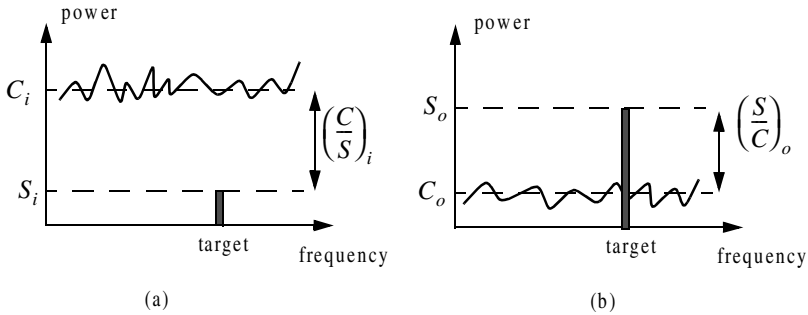


Figure 9.18. Illustration of SCV. (a) MTI input. (b) MTI output.

9.13. Delay Line Cancelers with Optimal Weights

The delay line cancelers discussed in this chapter belong to a family of transversal Finite Impulse Response (FIR) filters widely known as the "tapped delay line" filters. Fig. 9.19 shows an N-stage tapped delay line implementation.

When the weights are chosen such that they are the binomial coefficients (coefficients of the expansion $(1 - x)^N$) with alternating signs, then the resultant MTI filter is equivalent to N-stage cascaded single line cancelers. This is illustrated in Fig. 9.20 for $N = 4$. In general, the binomial coefficients are given by

$$w_i = (-1)^{i-1} \frac{N!}{(N-i+1)!(i-1)!} ; i = 1, \dots, N+1 \quad (9.83)$$

Using the binomial coefficients with alternating signs produces an MTI filter that closely approximates the optimal filter in the sense that it maximizes the improvement factor, as well as the probability of detection. In fact, the difference between an optimal filter and one with binomial coefficients is so small that the latter one is considered to be optimal by most radar designers. However, being optimal in the sense of the improvement factor does not guarantee a deep notch, nor a flat pass-band in the MTI filter response. Consequently, many researchers have been investigating other weights that can produce a deeper notch around DC, as well as a better pass-band response.

In general, the average power gain for an N-stage delay line canceler is

$$\frac{S_o}{S_i} = \prod_{i=1}^N |H_1(f)|^2 = \prod_{i=1}^N 4 \left(\sin \left(\frac{\pi f}{f_r} \right) \right)^2 \quad (9.84)$$

where $|H_1(f)|^2$ is given in Eq. (9.72). For example, $N = 2$ (double delay line canceler) gives

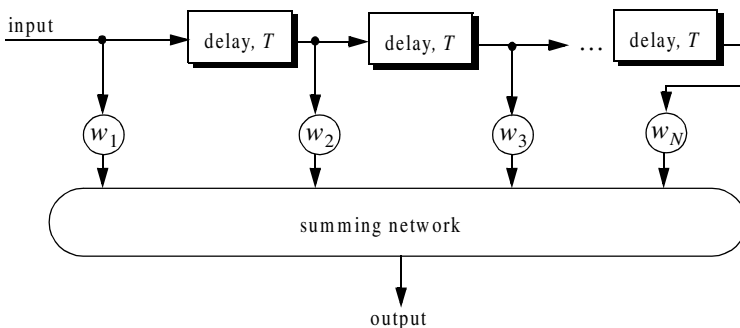


Figure 9.19. N-stage tapped delay line filter.

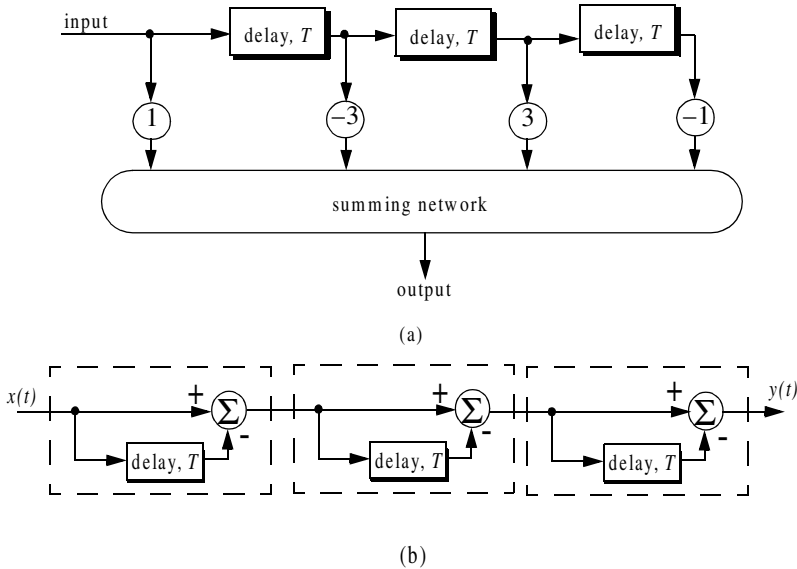


Figure 9.20. Two equivalent three delay line cancelers.
(a) Tapped delay line.
(b) Three cascaded single line cancelers.

$$\frac{S_o}{S_i} = 16 \left(\sin \left(\frac{\pi f}{f_r} \right) \right)^4 \tag{9.85}$$

Equation (9.84) can be rewritten as

$$\frac{S_o}{S_i} = |H_1(f)|^{2N} = 2^{2N} \left(\sin \left(\frac{\pi f}{f_r} \right) \right)^{2N} \tag{9.86}$$

As indicated by Eq. (9.86), blind speeds for an N-stage delay canceler are identical to those of a single canceler. It follows that blind speeds are independent from the number of cancelers used. It is possible to show that Eq. (9.86) can be written as

$$\frac{S_o}{S_i} = 1 + N^2 + \left(\frac{N(N-1)}{2!} \right)^2 + \left(\frac{N(N-1)(N-2)}{3!} \right)^2 + \dots \tag{9.87}$$

A general expression for the improvement factor of an N-stage tapped delay line canceler is reported by Nathanson¹ to be

1. Nathanson, F. E., *Radar Design Principles*, second edition, McGraw-Hill, Inc., 1991.

$$I = \frac{(S_o/S_i)}{N \sum_{k=1}^N \sum_{j=1}^N w_k w_j^* \rho\left(\frac{(k-j)}{f_r}\right)} \quad (9.88)$$

where the weights w_k and w_j are those of a tapped delay line canceler, and $\rho((k-j)/f_r)$ is the correlation coefficient between the k th and j th samples. For example, $N = 2$ produces

$$I = \frac{1}{1 - \frac{4}{3}\rho T + \frac{1}{3}\rho^2 2T} \quad (9.89)$$

9.14. MATLAB Program/Function Listings

This section contains listings of all MATLAB programs and functions used in this chapter. Users are encouraged to rerun these codes with different inputs in order to enhance their understanding of the theory.

Listing 9.1. MATLAB Function “single_canceler.m”

```
function [resp] = single_canceler (fofr1)
eps = 0.00001;
fofr = 0:0.01:fofr1;
arg1 = pi .* fofr;
resp = 4.0 .* ((sin(arg1)).^2);
max1 = max(resp);
resp = resp ./ max1;
subplot(2,1,1)
plot(fofr,resp,'k')
xlabel ('Normalized frequency - f/fr')
ylabel ('Amplitude response - Volts')
grid
subplot(2,1,2)
resp=10.*log10(resp+eps);
plot(fofr,resp,'k');
axis tight
grid
xlabel ('Normalized frequency - f/fr')
ylabel ('Amplitude response - dB')
```

Listing 9.2. MATLAB Function “double_canceler.m”

```
function [resp] = double_canceler(fofr1)
eps = 0.00001;
fofr = 0:0.01:fofr1;
arg1 = pi .* fofr;
resp = 4.0 .* ((sin(arg1)).^2);
max1 = max(resp);
resp = resp ./ max1;
resp2 = resp .* resp;
subplot(2,1,1);
plot(fofr,resp,'k--',fofr,resp2,'k');
ylabel('Amplitude response - Volts')
resp2 = 20. .* log10(resp2+eps);
resp1 = 20. .* log10(resp+eps);
subplot(2,1,2)
plot(fofr,resp1,'k--',fofr,resp2,'k');
legend('single canceler','double canceler')
xlabel('Normalized frequency f/fofr')
ylabel('Amplitude response - Volts')
```

Listing 9.3. MATLAB Program “fig9_15.m”

```
clear all
fofr = 0:0.001:1;
arg = 2.*pi.*fofr;
nume = 2.*(1.-cos(arg));
den11 = (1. + 0.25 * 0.25);
den12 = (2. * 0.25) .* cos(arg);
den1 = den11 - den12;
den21 = 1.0 + 0.7 * 0.7;
den22 = (2. * 0.7) .* cos(arg);
den2 = den21 - den22;
den31 = (1.0 + 0.9 * 0.9);
den32 = ((2. * 0.9) .* cos(arg));
den3 = den31 - den32;
resp1 = nume ./ den1;
resp2 = nume ./ den2;
resp3 = nume ./ den3;
plot(fofr,resp1,'k',fofr,resp2,'k-',fofr,resp3,'k--');
xlabel('Normalized frequency')
ylabel('Amplitude response')
legend('K=0.25','K=0.7','K=0.9')
grid
axis tight
```

Listing 9.4. MATLAB Program “fig9_16.m”

```
clear all
fofr = 0:0.001:1;
f1 = 4.0 .* fofr;
f2 = 5.0 .* fofr;
arg1 = pi .* f1;
arg2 = pi .* f2;
resp1 = abs(sin(arg1));
resp2 = abs(sin(arg2));
resp = resp1+resp2;
max1 = max(resp);
resp = resp./max1;
plot(fofr,resp1,fofr,resp2,fofr,resp);
xlabel('Normalized frequency f/fr')
ylabel('Filter response')
```

Listing 9.5. MATLAB Program “fig9_17.m”

```
clear all
fofr = 0.01:0.001:32;
a = 63.0 / 64.0;
term1 = (1. - 2.0 .* cos(a*2*pi*fofr) + cos(4*pi*fofr)).^2;
term2 = (-2. .* sin(a*2*pi*fofr) + sin(4*pi*fofr)).^2;
resp = 0.25 .* sqrt(term1 + term2);
resp = 10. .* log(resp);
plot(fofr,resp);
axis([0 32 -40 0]);
grid
```

Problems

9.1. Compute the signal-to-clutter ratio (SCR) for the radar described in Example 9.1. In this case, assume antenna 3dB beam width $\theta_{3dB} = 0.03rad$, pulse width $\tau = 10\mu s$, range $R = 50Km$, grazing angle $\psi_g = 15^\circ$, target RCS $\sigma_t = 0.1m^2$, and clutter reflection coefficient $\sigma^0 = 0.02(m^2/m^2)$.

9.2. Repeat Example 9.2 for target RCS $\sigma_t = 0.15m^2$, pulse width $\tau = 0.1\mu s$, antenna beam width $\theta_a = \theta_e = 0.03radians$; the detection range is $R = 100Km$, and $\sum \sigma_i = 1.6 \times 10^{-9}(m^2/m^3)$.

9.3. The quadrature components of the clutter power spectrum are, respectively, given by

$$\bar{S}_I(f) = \delta(f) + \frac{C}{\sqrt{2\pi}\sigma_c} \exp(-f^2/2\sigma_c^2)$$

$$\bar{S}_Q(f) = \frac{C}{\sqrt{2\pi}\sigma_c} \exp(-f^2/2\sigma_c^2)$$

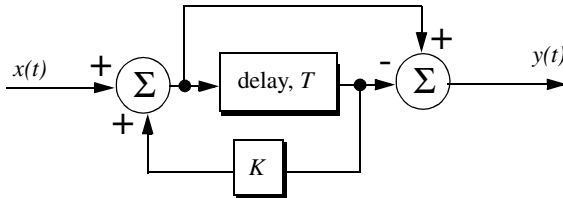
Compute the D.C. and A.C. power of the clutter. Let $\sigma_c = 10Hz$.

9.4. A certain radar has the following specifications: pulse width $\tau' = 1\mu s$, antenna beam width $\Omega = 1.5^\circ$, and wavelength $\lambda = 3cm$. The radar antenna is $7.5m$ high. A certain target is simulated by two point targets (scatterers). The first scatterer is $4m$ high and has RCS $\sigma_1 = 20m^2$. The second scatterer is $12m$ high and has RCS $\sigma_2 = 1m^2$. If the target is detected at $10Km$, compute (a) SCR when both scatterers are observed by the radar; (b) the SCR when only the first scatterer is observed by the radar. Assume a reflection coefficient of -1 , and $\sigma^0 = -30dB$.

9.5. A certain radar has range resolution of $300m$ and is observing a target somewhere in a line of high towers each having RCS $\sigma_{tower} = 10^6m^2$. If the target has RCS $\sigma_t = 1m^2$, (a) How much signal-to-clutter ratio should the radar have? (b) Repeat part a for range resolution of $30m$.

9.6. (a) Derive an expression for the impulse response of a single delay line canceler. (b) Repeat for a double delay line canceler.

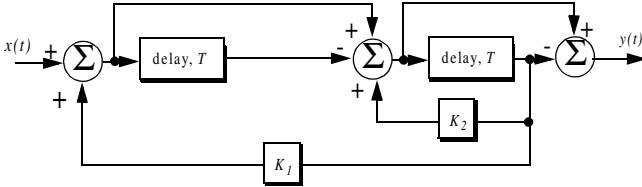
9.7. One implementation of a single delay line canceler with feedback is shown below:



(a) What is the transfer function, $H(z)$? (b) If the clutter power spectrum is $W(f) = w_0 \exp(-f^2/2\sigma_c^2)$, find an exact expression for the filter power gain. (c) Repeat part b for small values of frequency, f . (d) Compute the clutter attenuation and the improvement factor in terms of K and σ_c .

9.8. Plot the frequency response for the filter described in the previous problem for $K = -0.5, 0,$ and 0.5 .

9.9. An implementation of a double delay line canceler with feedback is shown below:



(a) What is the transfer function, $H(z)$? (b) Plot the frequency response for $K_1 = 0 = K_2$, and $K_1 = 0.2, K_2 = 0.5$.

9.10. Consider a single delay line canceler. Calculate the clutter attenuation and the improvement factor. Assume that $\sigma_c = 4Hz$ and a PRF $f_r = 450Hz$.

9.11. Develop an expression for the improvement factor of a double delay line canceler.

9.12. Repeat Problem 9.10 for a double delay line canceler.

9.13. An experimental expression for the clutter power spectrum density is $W(f) = w_0 \exp(-f^2/2\sigma_c^2)$, where w_0 is a constant. Show that using this expression leads to the same result obtained for the improvement factor as developed in Section 9.11.

9.14. Repeat Problem 9.13 for a double delay line canceler.

9.15. A certain radar uses two PRFs with stagger ratio 63/64. If the first PRF is $f_{r1} = 500Hz$, compute the blind speeds for both PRFs and for the resultant composite PRF. Assume $\lambda = 3cm$.

9.16. A certain filter used for clutter rejection has an impulse response $h(n) = \delta(n) - 3\delta(n-1) + 3\delta(n-2) - \delta(n-3)$. (a) Show an implementation of this filter using delay lines and adders. (b) What is the transfer function? (c) Plot the frequency response of this filter. (d) Calculate the output when the input is the unit step sequence.

9.17. The quadrature components of the clutter power spectrum are given in Problem 9.3. Let $\sigma_c = 10Hz$ and $f_r = 500Hz$. Compute the improvement of the signal-to-clutter ratio when a double delay line canceler is utilized.

9.18. Develop an expression for the clutter improvement factor for single and double line cancelers using the clutter autocorrelation function. Assume that the clutter power spectrum is as defined in Eq. (9.65).

An antenna is a radiating element which acts as a transducer between an electrical signal in a system and a propagating wave. The Institute of Electrical and Electronic Engineers (IEEE)'s Standard Definition of Terms for Antennas (IEEE std. 145-1973) defines an antenna as "a mean for radiating or receiving radio power."

10.1. Directivity, Power Gain, and Effective Aperture

Radar antennas can be characterized by the directive gain G_D , power gain G , and effective aperture A_e . Antenna gain is term used to describe the ability of an antenna to concentrate the transmitted energy in a certain direction. Directive gain, or simply directivity, is more representative of the antenna radiation pattern, while power gain is normally used in the radar equation. Plots of the power gain and directivity, when normalized to unity, are called *antenna radiation pattern*. The directivity of a transmitting antenna can be defined by

$$G_D = \frac{\text{maximum radiation intensity}}{\text{average radiation intensity}} \quad (10.1)$$

The radiation intensity is the power per unit solid angle in the direction (θ, ϕ) and denoted by $P(\theta, \phi)$. The average radiation intensity over 4π radians (solid angle) is the total power divided by 4π . Hence, Eq. (10.1) can be written as

$$G_D = \frac{4\pi(\text{maximum radiated power/unit solid angle})}{\text{total radiated power}} \quad (10.2)$$

It follows that

$$G_D = \frac{4\pi P(\beta, \phi)_{max}}{\iint P(\beta, \phi) d\beta d\phi} \quad (10.3)$$

As an approximation, it is customary to rewrite Eq. (10.3) as

$$G_D \approx \frac{4\pi}{\beta_3 \phi_3} \quad (10.4)$$

where β_3 and ϕ_3 are the antenna half-power (3-dB) beamwidths in either direction.

The antenna power gain and its directivity are related by

$$G = \rho_r G_D \quad (10.5)$$

where ρ_r is the radiation efficiency factor. In this book, the antenna power gain will be denoted as *gain*. The radiation efficiency factor accounts for the ohmic losses associated with the antenna. Therefore, the definition for the antenna gain is also given in Eq. (10.1). The antenna effective aperture A_e is related to gain by

$$A_e = \frac{G\lambda^2}{4\pi} \quad (10.6)$$

where λ is the wavelength. The relationship between the antenna's effective aperture A_e and the physical aperture A is

$$\begin{aligned} A_e &= \rho A \\ 0 &\leq \rho \leq 1 \end{aligned} \quad (10.7)$$

ρ is referred to as the aperture efficiency, and good antennas require $\rho \rightarrow 1$ (in this book $\rho = 1$ is always assumed, i.e., $A_e = A$).

Using simple algebraic manipulations of Eqs. (10.4) through (10.6) (assuming that $\rho_r = 1$) yields

$$G = \frac{4\pi A_e}{\lambda^2} \approx \frac{4\pi}{\beta_3 \phi_3} \quad (10.8)$$

Consequently, the angular cross section of the beam is

$$\beta_3 \phi_3 \approx \frac{\lambda^2}{A_e} \quad (10.9)$$

Eq. (10.9) indicates that the antenna beamwidth decreases as $\sqrt{A_e}$ increases. It follows that, in surveillance operations, the number of beam positions an antenna will take on to cover a volume V is

$$N_{Beams} > \frac{V}{\beta_3 \Phi_3} \quad (10.10)$$

and when V represents the entire hemisphere, Eq. (10.10) is modified to

$$N_{Beams} > \frac{2\pi}{\beta_3 \Phi_3} \approx \frac{2\pi A_e}{\lambda^2} \approx \frac{G}{2} \quad (10.11)$$

10.2. Near and Far Fields

The electric field intensity generated from the energy emitted by an antenna is a function of the antenna physical aperture shape and the electric current amplitude and phase distribution across the aperture. Plots of the modulus of the electric field intensity of the emitted radiation, $|E(\beta, \phi)|$, are referred to as the *intensity pattern* of the antenna. Alternatively, plots of $|E(\beta, \phi)|^2$ are called the *power radiation pattern* (the same as $P(\beta, \phi)$).

Based on the distance away from the face of the antenna, where the radiated electric field is measured, three distinct regions are identified. They are the near field, Fresnel, and the Fraunhofer regions. In the near field and the Fresnel regions, rays emitted from the antenna have spherical wavefronts (equi-phase fronts). In the Fraunhofer regions the wavefronts can be locally represented by plane waves. The near field and the Fresnel regions are normally of little interest to most radar applications. Most radar systems operate in the Fraunhofer region, which is also known as the far field region. In the far field region, the electric field intensity can be computed from the aperture Fourier transform.

Construction of the far criterion can be developed with the help of Fig. 10.1. Consider a radiating source at point O that emits spherical waves. A receiving antenna of length d is at distance r away from the source. The phase difference between a spherical wave and a locally plane wave at the receiving antenna can be expressed in terms of the distance δr . The distance δr is given by

$$\delta r = \overline{AO} - \overline{OB} = \sqrt{r^2 + \left(\frac{d}{2}\right)^2} - r \quad (10.12)$$

and since in the far field $d \ll r$, Eq. (10.12) is approximated via binomial expansion by

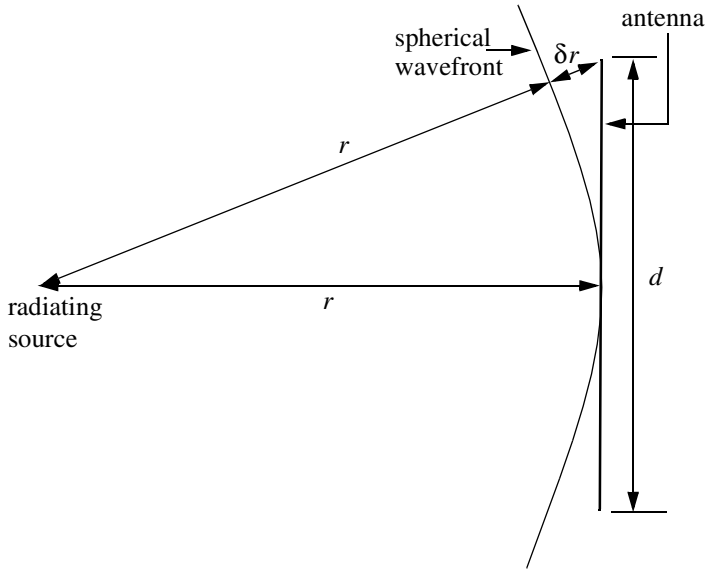


Figure 10.1. Construction for far field criterion.

$$\delta r = r \left(\sqrt{1 + \left(\frac{d}{2r} \right)^2} - 1 \right) \approx \frac{d^2}{8r} \quad (10.13)$$

It is customary to assume far field when the distance δr corresponds to less than $1/16$ of a wavelength (i.e., 22.5°). More precisely, if

$$\delta r = d^2/8r \leq \lambda/16 \quad (10.14)$$

then a useful expression for far field is

$$r \geq 2d^2/\lambda \quad (10.15)$$

Note that far field is a function of both the antenna size and the operating wavelength.

10.3. Circular Dish Antenna Pattern

Circular dish reflectors are widely used in microwave and radar applications because of their simplicity in design and fabrication. Additionally, closed form far field expressions can be easily computed for all existing modes over the

circular aperture. Fig. 10.2 shows the geometry associated with a circular aperture. Denote the aperture radius as r . A far field observation point P is defined by range R and angular position (β, ϕ) . The aperture factor at P is given by

$$E(\beta, \phi) = \int_{\text{aperture}} D(x', y') e^{j\Psi(x', y')} dx' dy' \quad (10.16)$$

$$\Psi(x', y') = k(x' \sin\beta \cos\phi + y' \sin\beta \sin\phi) \quad (10.17)$$

where $k = (2\pi)/\lambda$, λ is the wavelength, and $D(x', y')$ is the current distribution over the aperture. Due to the circular nature of the aperture, it is more convenient to adopt cylindrical coordinates. It follows that

$$\begin{aligned} x' &= \rho \cos\phi' \\ y' &= \rho \sin\phi' \end{aligned} \quad (10.18)$$

$$x' \sin\beta \cos\phi + y' \sin\beta \sin\phi = \rho \sin\beta \cos(\phi - \phi') \quad (10.19)$$

$$dx' dy' = \rho d\rho d\phi' \quad (10.20)$$

$$E(\beta, \phi) = \int_0^r \rho d\rho \int_0^{2\pi} e^{jk\rho \sin\beta \cos(\phi - \phi')} d\phi' \quad (10.21)$$

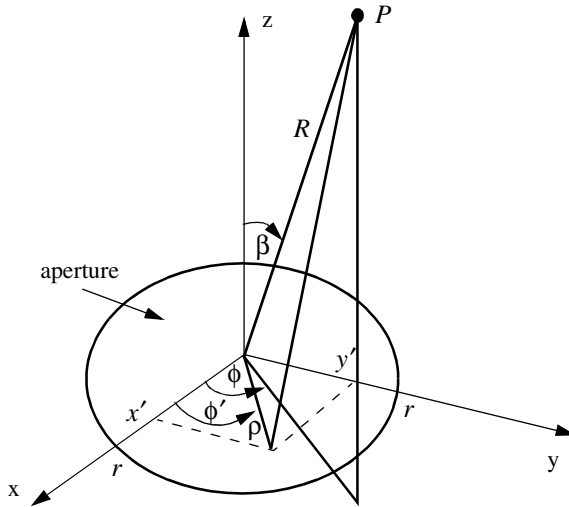


Figure 10.2. Circular aperture geometry.

where the current distribution over the aperture is assumed to be unity. The second integral in Eq. (10.21) is of the form

$$\int_0^{2\pi} e^{jz \cos \zeta} d\zeta = 2\pi J_0(z) \quad (10.22)$$

where J_0 is the Bessel function of the first kind of order zero. Because of the circular symmetry over the aperture, the electric field is independent of ϕ . Hence, $E(\beta, \phi) = E(\beta)$, and Eq. (10.21) can now be rewritten as

$$E(\beta) = 2\pi \int_0^r \rho J_0(k\rho \sin \beta) d\rho \quad (10.23)$$

Using the Bessel function identity

$$\int_0^r \rho J_0(q\rho) d\rho = \frac{r}{q} J_1(qr) \quad (10.24)$$

leads to the following expression for the aperture factor

$$E(\beta) = \pi r^2 \frac{2J_1(kr \sin \beta)}{kr \sin \beta} \quad (10.25)$$

The far field circular dish antenna pattern is computed as the modulus of the aperture factor defined in Eq. (10.25). The first null occurs when the Bessel function is zero. More precisely,

$$\frac{2\pi r}{\lambda} \sin \beta_{n1} = 1.22\pi \Rightarrow \beta_{n1} \approx 1.22 \frac{\lambda}{2r} \quad (10.26)$$

Through tapering (windowing) the current distribution across the aperture, one can significantly reduce the side lobe levels.

MATLAB Function “*circ_aperture.m*”

The function “*circ_aperture.m*” computes and plots the antenna patter for a circular aperture of diameter d . It is given in Listing 10.1 in Section 10.9. The syntax is as follows:

$$[emod] = circ_aperture(\lambda, d)$$

where λ is the wavelength and d is the aperture diameter; both parameters should be in meters. Fig. 10.3 shows typical outputs produced using this function. In this example, $d = 0.3m$ and $\lambda = 0.1m$.

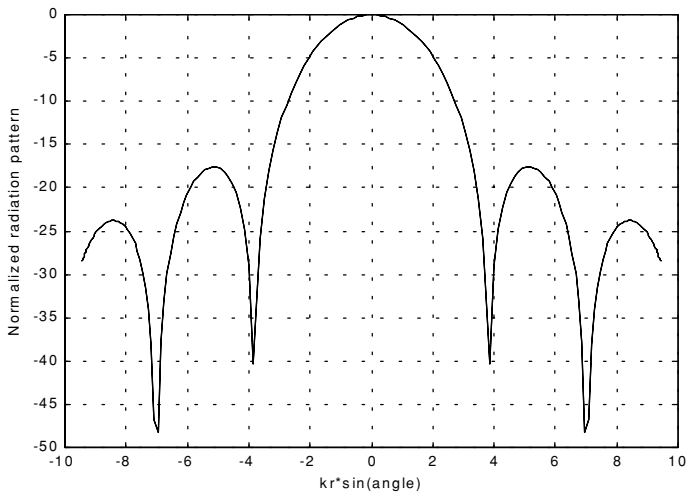


Figure 10.3a. Circular aperture radiation pattern. Typical output produced by “*circ_aperture.m*”. $d = 0.3m$; $\lambda = 0.1m$.

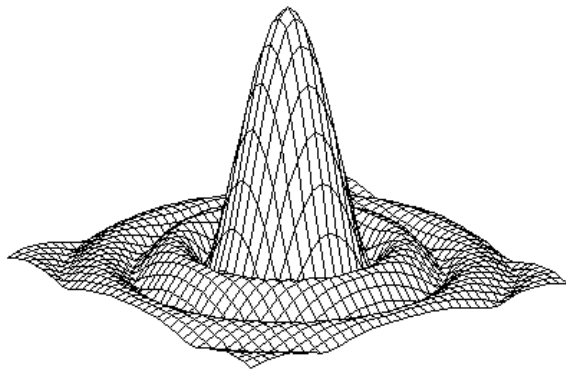


Figure 10.3b. Three-dimensional array pattern corresponding to Fig. 10.3a. Typical output produced by “*circ_aperture.m*”. $d = 0.3m$; $\lambda = 0.1m$.

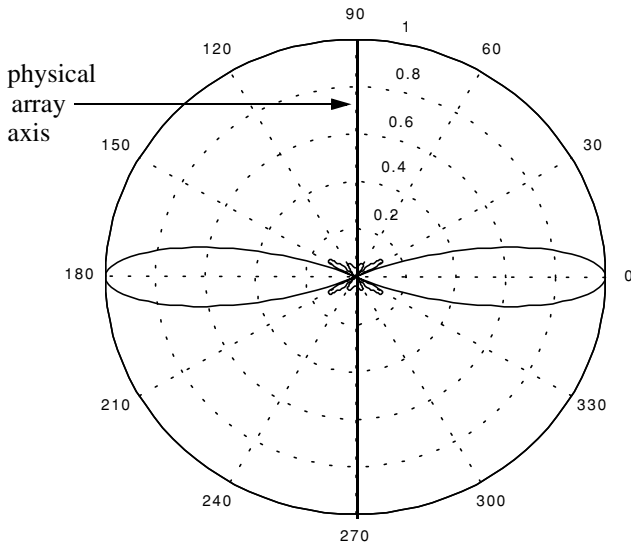


Figure 10.3c. Polar plot for a circular aperture. Typical output produced by “*circ_aperture.m*”. $d = 0.3m$; $\lambda = 0.1m$.

10.4. Array Antennas

An array is a composite antenna formed from two or more basic radiators. Each radiator is denoted as an element. The elements forming an array could be dipoles, dish reflectors, slots in a wave guide, or any other type of radiator. Array antennas synthesize narrow directive beams that may be steered, mechanically or electronically, in many directions. Electronic steering is achieved by controlling the phase of the current feeding the array elements. Arrays with electronic beam steering capability are called phased arrays. Phased array antennas when compared to other simple antennas such as dish reflectors, are costly and complicated to design. However, the inherent flexibility of phased array antennas to steer the beam electronically and also the need for specialized multi-function radar systems have made phased array antennas attractive for radar applications.

10.4.1. Linear Array Antennas

Fig.10.4 shows a linear array antenna consisting of N identical elements. The element spacing is d (normally measured in wavelength units). The combined electric field measured at a far field observation point P is computed as the product between the array factor and the element pattern,

$$E(P) = E(\text{one element})(\text{array factor}) \quad (10.27)$$

The array factor is a general function of the number of elements, their spacing, and their relative phases and magnitudes.

Consider the linear array shown in Fig. 10.4. Let element #1 serve as a phase reference for the array. From the geometry, it is clear that an outgoing wave at the n th element leads the phase at the $(n + 1)$ th element by $kd\sin\beta$, where $k = 2\pi/\lambda$. The electric field at a far field observation point with direction-sine equal to $\sin\beta$ (assuming isotropic elements) is

$$E(\sin\beta) = \sum_{i=1}^N e^{j(i-1)(kd\sin\beta)} \quad (10.28)$$

Expanding the summation in Eq. (10.28) yields

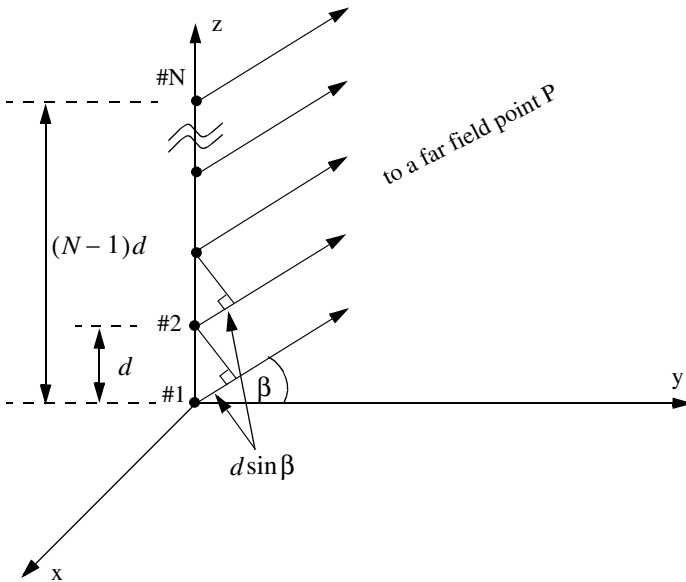


Figure 10.4. Linear array of equally spaced elements.

$$E(\sin\beta) = 1 + e^{jkd\sin\beta} + \dots + e^{j(N-1)(kd\sin\beta)} \quad (10.29)$$

The right-hand side of Eq. (10.29) is a geometric series, which can be expressed in the form

$$1 + a + a^2 + a^3 + \dots + a^{(N-1)} = \frac{1 - a^N}{1 - a} \quad (10.30)$$

Replacing a by $e^{jkd\sin\beta}$ yields

$$E(\sin\beta) = \frac{1 - e^{jNkd\sin\beta}}{1 - e^{jkd\sin\beta}} = \frac{1 - \cos Nkd\sin\beta - j\sin Nkd\sin\beta}{1 - \cos kd\sin\beta - j\sin kd\sin\beta} \quad (10.31)$$

The far field array intensity pattern is then given by

$$|E(\sin\beta)| = \sqrt{E(\sin\beta)E^*(\sin\beta)} \quad (10.32)$$

Substituting Eq. (10.31) into Eq. (10.32) and collecting terms yield

$$\begin{aligned} |E(\sin\beta)| &= \sqrt{\frac{(1 - \cos Nkd\sin\beta)^2 + (\sin Nkd\sin\beta)^2}{(1 - \cos kd\sin\beta)^2 + (\sin kd\sin\beta)^2}} \\ &= \sqrt{\frac{1 - \cos Nkd\sin\beta}{1 - \cos kd\sin\beta}} \end{aligned} \quad (10.33)$$

and using the trigonometric identity $1 - \cos\theta = 2(\sin\theta/2)^2$ yields

$$|E(\sin\beta)| = \left| \frac{\sin(Nkd\sin\beta/2)}{\sin(kd\sin\beta/2)} \right| \quad (10.34)$$

which is a periodic function of $kd\sin\beta$, and its period is equal to 2π .

The maximum value of $|E(\sin\beta)|$ occurs at $\beta = 0$, and it is equal to N . It follows that the normalized intensity pattern is equal to

$$|E_n(\sin\beta)| = \frac{1}{N} \left| \frac{\sin((Nkd\sin\beta)/2)}{\sin((kd\sin\beta)/2)} \right| \quad (10.35)$$

The normalized two-way array pattern (radiation pattern) is given by

$$G(\sin\beta) = |E_n(\sin\beta)|^2 = \frac{1}{N^2} \left(\frac{\sin((Nkd\sin\beta)/2)}{\sin((kd\sin\beta)/2)} \right)^2 \quad (10.36)$$

Fig. 10.5 shows a plot of Eq. (10.36) versus $\sin\beta$ for $N = 8$. The radiation pattern $G(\sin\beta)$ has cylindrical symmetry about its axis ($\sin\beta = 0$), and it is independent of the azimuth angle. Thus, it is completely determined by its values within the interval $(0 < \beta < \pi)$. This plot can be reproduced using MATLAB program “fig10_5.m” given in Listing 10.2 in Section 10.9.

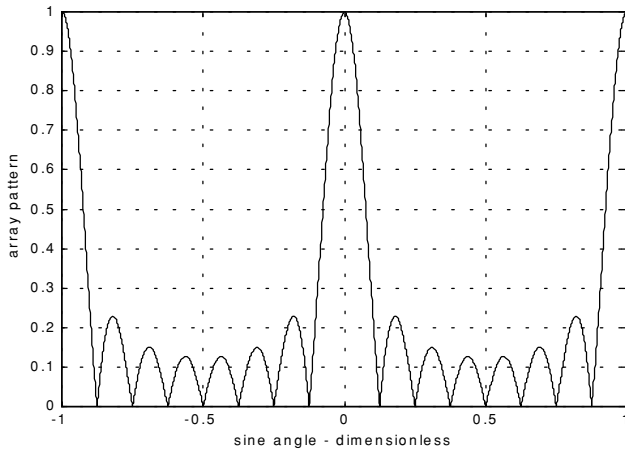


**Figure 10.5a. Normalized radiation pattern for a linear array;
 $N = 8$ and $d = \lambda$.**

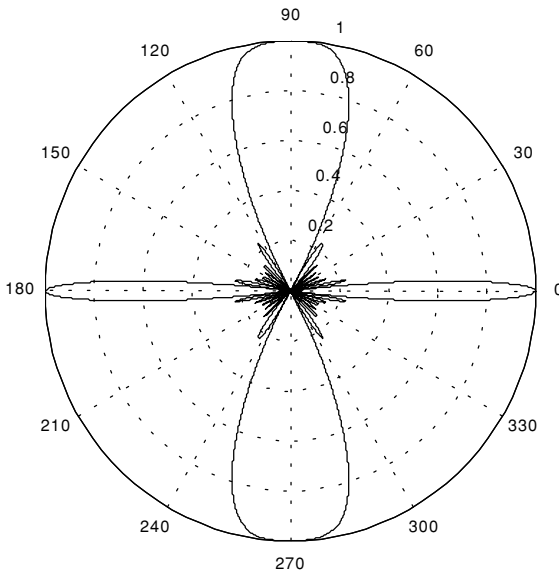


Figure 10.5b. Polar plot for the radiation pattern in Fig. 10.5a.

The main beam of an array can be steered electronically by varying the phase of the current applied to each array element. Steering the main beam into the direction-sine $\sin\beta_0$ is accomplished by making the phase difference between any two adjacent elements equal to $kd\sin\beta_0$. In this case, the normalized radiation pattern can be written as

$$G(\sin\beta) = \frac{1}{N^2} \left(\frac{\sin[(Nkd/2)(\sin\beta - \sin\beta_0)]}{\sin[(kd/2)(\sin\beta - \sin\beta_0)]} \right)^2 \quad (10.37)$$

If $\beta_0 = 0$ then the main beam is perpendicular to the array axis, and the array is said to be a broadside array. Alternatively, the array is called an endfire array when the main beam points along the array axis.

The radiation pattern maxima are computed using L'Hopital's rule when both the denominator and numerator of Eq. (10.36) are zeros. More precisely,

$$\frac{kdsin\beta}{2} = \pm m\pi \quad ; \quad m = 0, 1, 2, \dots \quad (10.38)$$

Solving for β yields

$$\beta_m = \text{asin}\left(\pm \frac{\lambda m}{d}\right) \quad ; \quad m = 0, 1, 2, \dots \quad (10.39)$$

where the subscript m is used as a maxima indicator. The first maximum occurs at $\beta_0 = 0$, and is denoted as the main beam (lobe). Other maxima occurring at $|m| \geq 1$ are called grating lobes. Grating lobes are undesirable and must be suppressed. The grating lobes occur at non-real angles when the absolute value of the arc-sine argument in Eq. (10.39) is greater than unity; it follows that $d < \lambda$. Under this condition, the main lobe is assumed to be at $\beta = 0$ (broadside array). Alternatively, when electronic beam steering is considered, the grating lobes occur at

$$|\sin\beta - \sin\beta_0| = \pm \frac{\lambda n}{d} \quad ; \quad n = 1, 2, \dots \quad (10.40)$$

Thus, in order to prevent the grating lobes from occurring between $\pm 90^\circ$, the element spacing should be $d < \lambda/2$.

The radiation pattern attains secondary maxima (side lobes). These secondary maxima occur when the numerator of Eq. (10.36) is maximum, or equivalently

$$\frac{Nkdsin\beta}{2} = \pm(2l+1)\frac{\pi}{2} \quad ; \quad l = 1, 2, \dots \quad (10.41)$$

Solving for β yields

$$\beta_l = \text{asin}\left(\pm \frac{\lambda}{2d} \frac{2l+1}{N}\right) \quad ; \quad l = 1, 2, \dots \quad (10.42)$$

where the subscript l is used as an indication of side lobe maxima. The nulls of the radiation pattern occur when only the numerator of Eq. (10.36) is zero. More precisely,

$$\frac{N}{2}kd\sin\beta = \pm n\pi \quad ; \quad \begin{array}{l} n = 1, 2, \dots \\ n \neq N, 2N, \dots \end{array} \quad (10.43)$$

Again solving for β yields

$$\beta_n = \text{asin}\left(\pm \frac{\lambda n}{dN}\right) \quad ; \quad \begin{array}{l} n = 1, 2, \dots \\ n \neq N, 2N, \dots \end{array} \quad (10.44)$$

where the subscript n is used as a null indicator. Define the angle which corresponds to the half power point as β_h . It follows that the half power (3 dB) beam width is $2|\beta_m - \beta_h|$. This occurs when

$$\frac{N}{2}kd\sin\beta_h = 1.391 \text{ radians} \Rightarrow \beta_h = \text{asin}\left(\frac{\lambda}{2\pi d} \frac{2.782}{N}\right) \quad (10.45)$$

MATLAB Function “linear_array.m”

The function “linear_array.m” computes and plots the linear array radiation pattern, in linear and polar coordinates. This function is given in Listing 10.3 in Section 10.9. The syntax is as follows:

$$[emod] = \text{linear_array}(ne, d, beta0)$$

where

Symbol	Description	Units	Status
ne	<i>number of elements in array</i>	<i>none</i>	<i>input</i>
d	<i>element spacing (e.g., $d = \lambda$; $d = \lambda/2$)</i>	<i>wavelengths</i>	<i>input</i>
$beta0$	<i>steering angle</i>	<i>degrees</i>	<i>input</i>
$emod$	<i>radiation pattern vector</i>	<i>dB</i>	<i>output</i>

Fig. 10.6 shows typical outputs produced using this function. In this example, $ne = 8$, $d = \lambda/2$, and $beta0 = 30^\circ$. The array axis is assumed to be aligned with the line passing through the 90-to-270 degrees line. Fig. 10.7 is similar to Fig. 10.6 except in this case $d = \lambda$ and $beta0 = 0^\circ$. Note how the grating lobes get closer to the main beam as the element spacing is increased, thus, limiting the electronic steering capability of the array to within the first pair of grating lobes.

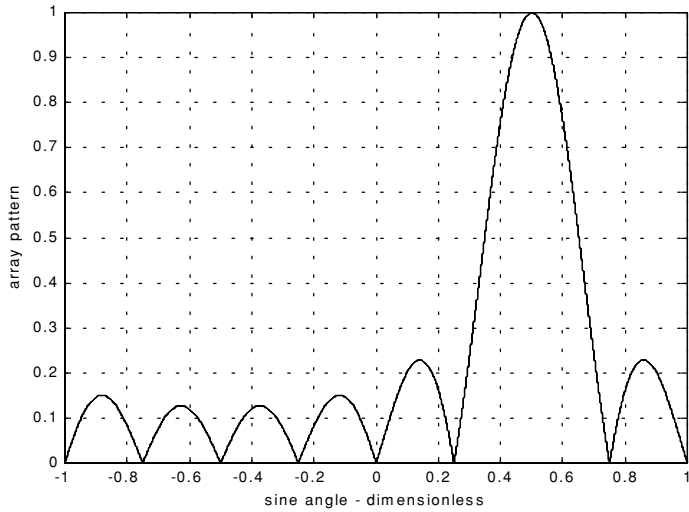


Figure 10.6a. Normalized radiation pattern for a linear array. $N = 8$, $d = \lambda/2$, and $\beta_0 = 30^\circ$.

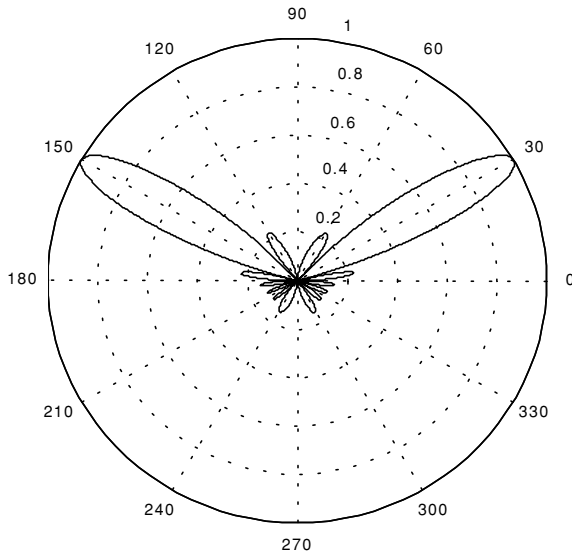


Figure 10.6b. Polar plot corresponding to [Fig. 10.6a](#).

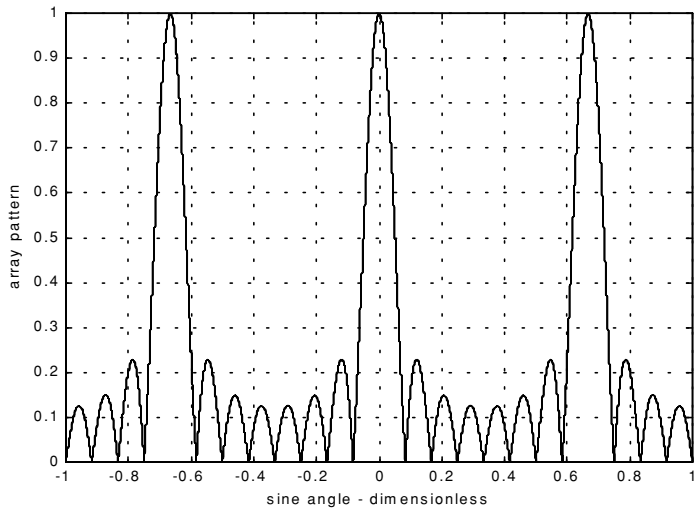


Figure 10.7a. Normalized radiation pattern for a linear array. $N = 8$, $d = 1.5\lambda$, and $\beta_0 = 0^\circ$.

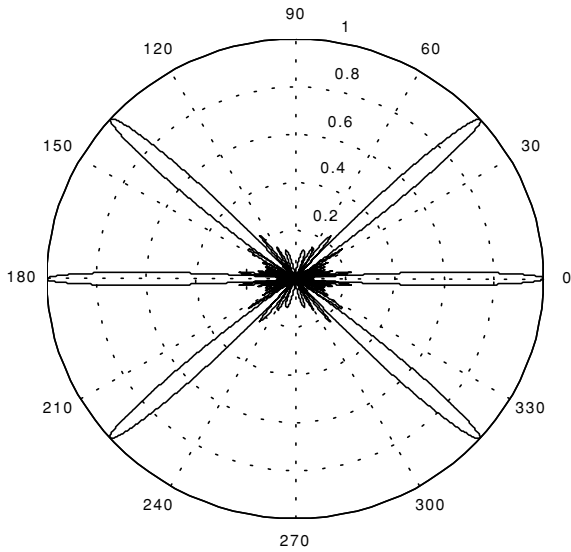


Figure 10.7b. Polar plot corresponding to [Fig. 10.7a](#).

10.5. Array Tapering

Fig. 10.8 shows a normalized two-way radiation pattern of a uniformly excited linear array of size $N = 8$, element spacing $d = \lambda/2$. The first side lobe is about 13.46 dB below the main lobe, and for most radar applications this may not be sufficient.

In order to reduce the side lobe levels, the array must be designed to radiate more power towards the center, and much less at the edges. This can be achieved through tapering (windowing) the current distribution over the face of the array. There are many possible tapering sequences that can be used for this purpose. However, as known from spectral analysis, windowing reduces side lobe levels at the expense of widening the main beam. Thus, for a given radar application, the choice of the tapering sequence must be based on the trade-off between side lobe reduction and main beam widening.

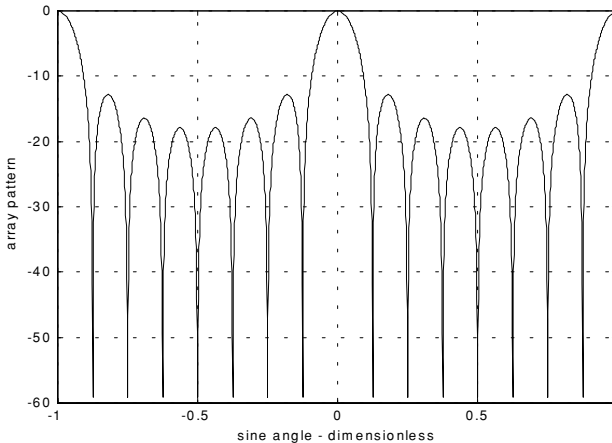


Figure 10.8. Normalized radiation pattern for a linear array.
 $N = 8$ and $d = \lambda/2$.

10.6. Computation of the Radiation Pattern via the DFT

Fig. 10.9 shows a linear array of size N , element spacing d , and wavelength λ . The radiators are circular dishes of diameter $D = d$. Let $w(n)$ and $\psi(n)$, respectively, denote the tapering and phase shifting sequences. The normalized electric field at a far field point in the direction-sine $\sin\beta$ is

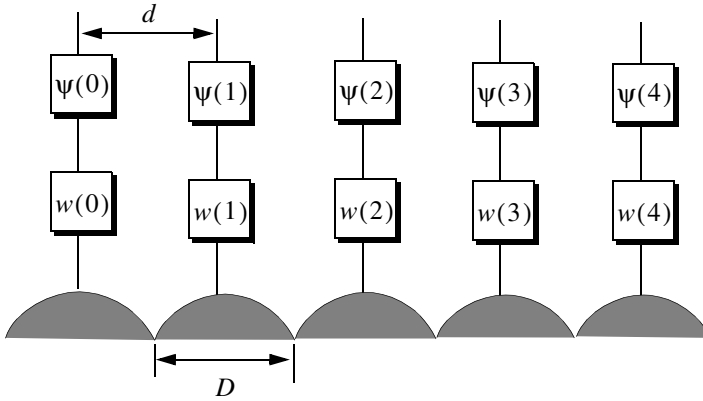


Figure 10.9. Linear array of size 5, with tapering and phase shifting hardware.

$$E(\sin\beta) = \sum_{n=0}^{N-1} w(n)e^{j\Delta\phi\left(n - \left(\frac{N-1}{2}\right)\right)} \quad (10.46)$$

where in this case the phase reference is taken as the physical center of the array, and

$$\Delta\phi = \frac{2\pi d}{\lambda} \sin\beta \quad (10.47)$$

Expanding Eq. (10.46) and factoring the common phase term $\exp[j(N-1)\Delta\phi/2]$ yield

$$E(\sin\beta) = e^{j(N-1)\Delta\phi/2} \{w(0)e^{-j(N-1)\Delta\phi} + w(1)e^{-j(N-2)\Delta\phi} + \dots + w(N-1)\} \quad (10.48)$$

By using the symmetry property of a window sequence (remember that a window must be symmetrical about its central point), we can rewrite Eq. (10.48) as

$$E(\sin\beta) = e^{j\phi_0} \{w(N-1)e^{-j(N-1)\Delta\phi} + w(N-2)e^{-j(N-2)\Delta\phi} + \dots + w(0)\} \quad (10.49)$$

where $\phi_0 = (N-1)\Delta\phi/2$.

Define $\{V_1^n = \exp(-j\Delta\phi n); n = 0, 1, \dots, N-1\}$. It follows that

$$\begin{aligned}
 E(\sin\beta) &= e^{j\phi_0} [w(0) + w(1)V_1^1 + \dots + w(N-1)V_1^{N-1}] \quad (10.50) \\
 &= e^{j\phi_0} \sum_{n=0}^{N-1} w(n)V_1^n
 \end{aligned}$$

The discrete Fourier transform of the sequence $w(n)$ is defined as

$$W(k) = \sum_{n=0}^{N-1} w(n)e^{-\frac{j2\pi nk}{N}} \quad ; \quad k = 0, 1, \dots, N-1 \quad (10.51)$$

The set $\{\sin\beta_k\}$ which makes V_1 equal to the DFT kernel is

$$\sin\beta_k = \frac{\lambda k}{Nd} \quad ; \quad k = 0, 1, \dots, N-1 \quad (10.52)$$

Then by using Eq. (10.52) in Eq. (10.51) yields

$$E(\sin\beta) = e^{j\phi_0} W(k) \quad (10.53)$$

The one-way array pattern is computed as the modulus of Eq. (10.53). It follows that the one-way radiation pattern of a tapered linear array of circular dishes is

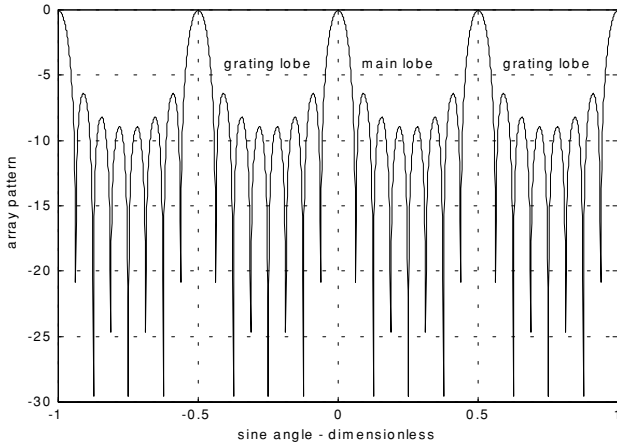
$$G(\sin\beta) = G_e\left(\frac{\lambda k}{Nd}\right) |W(k)| \quad (10.54)$$

where G_e is the element pattern. Fig. 10.10 shows the one-way array pattern for a linear array of size $N = 16$, element spacing $d = \lambda/2$, and the elements being circular dishes of diameter $D = d$; no tapering is utilized.

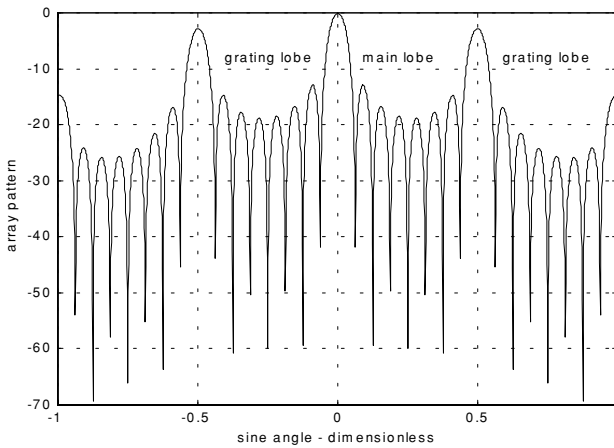
10.7. Array Pattern for Rectangular Planar Array

Fig. 10.11 shows a sketch of an $N \times N$ planar array formed from a rectangular grid. Other planar array configurations may be composed using a circular or hexagonal grid. Planar arrays can be steered electronically in both azimuth and elevation (β, ϕ) .

If the array were composed of only one line of elements distributed along the x-axis, then the electric field at a far field observation point defined by (β, ϕ) is



isotropic elements



circular dishes

Figure 10.10. Normalized one-way pattern for linear array of size 8, isotropic elements, and circular dishes. This plot can be reproduced using MATLAB program “fig10_10.m” given in Listing 10.4 in Section 10.9.

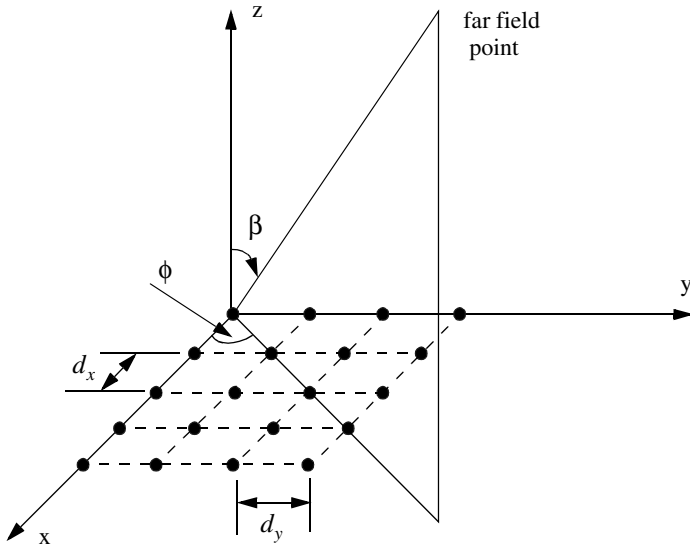


Figure 10.11. Planar array geometry.

$$E_x(\beta, \phi) = \sum_{n=1}^N e^{j(n-1)kd_x \sin\beta \cos\phi} \quad (10.55)$$

where d_x is the element spacing along the x -axis. Now, if N of these linear arrays are placed next to one another along the y -axis, a rectangular array would be formed. In this case, the total electric field at a far field observation point is computed as

$$E(\beta, \phi) = E_x(\beta, \phi)E_y(\beta, \phi) = \sum_{m=1}^N E_x(\beta, \phi) e^{j(m-1)kd_y \sin\beta \sin\phi} \quad (10.56)$$

where

$$E_y(\beta, \phi) = \sum_{m=1}^N e^{j(m-1)kd_y \sin\beta \sin\phi} \quad (10.57)$$

and d_y is the element spacing along the y -axis.

The rectangular array one-way intensity pattern is then equal to the product of the individual patterns. More precisely,

$$E(\beta, \phi) = \left| \frac{\sin((Nkd_x \sin \beta \cos \phi)/2)}{\sin((kd_x \sin \beta \cos \phi)/2)} \right| \left| \frac{\sin((Nkd_y \sin \beta \sin \phi)/2)}{\sin((kd_y \sin \beta \sin \phi)/2)} \right| \quad (10.58)$$

The radiation pattern maxima, nulls, side lobes, and grating lobes in both the x- and y-axis are computed in a similar fashion to the linear array case. Additionally, the same conditions for grating lobes control are applicable.

MATLAB Function “rect_array.m”

The function “rect_array.m” computes and plots the linear array radiation pattern, in linear and polar coordinates. This function is given in Listing 10.5 in Section 10.9. The syntax is as follows:

$$[emod] = \text{rect_array}(nex, ney, dx, dy)$$

where

Symbol	Description	Units	Status
<i>nex</i>	<i>number of elements in x-direction</i>	<i>none</i>	<i>input</i>
<i>ney</i>	<i>number of elements in y-direction</i>	<i>none</i>	<i>input</i>
<i>dx</i>	<i>element spacing in x-direction</i> <i>(e.g. $d = \lambda$; $d = \lambda/2$)</i>	<i>wavelengths</i>	<i>input</i>
<i>dy</i>	<i>element spacing in y-direction</i> <i>(e.g. $d = \lambda$; $d = \lambda/2$)</i>	<i>wavelengths</i>	<i>input</i>
<i>emod</i>	<i>radiation pattern vector</i>	<i>dB</i>	<i>output</i>

Fig. 10.12 shows a three-dimensional radiation pattern for a rectangular array of size 5×5 , element spacing $d_x = d_y = \lambda/2$, and isotropic elements.

10.8. Conventional Beamforming

Adaptive arrays are phased array antennas that are normally used to automatically sense and eliminate unwanted signals entering the radar's Field of View (FOV), while enhancing reception about the desired target returns. For this purpose, adaptive arrays utilize a rather complicated combination of hardware and require demanding levels of software implementation. Through feedback networks, a proper set of complex weights is computed and applied to each channel of the array. Adaptive array operation can be considered a special case of beamforming, where the basic idea is to enhance the signal in a certain direction while attenuating noise in all other directions.

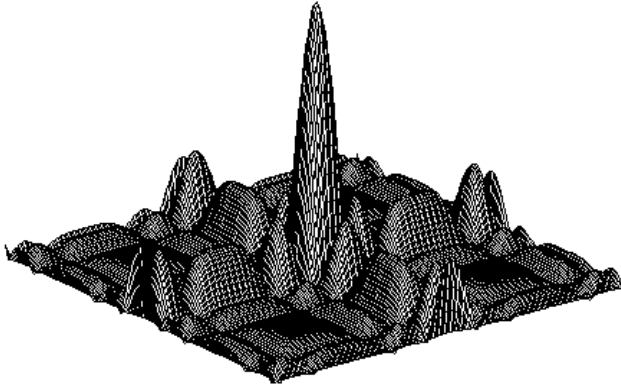


Figure 10.12a. Three-dimensional pattern for a rectangular array of size 5x5, and uniform element spacing.

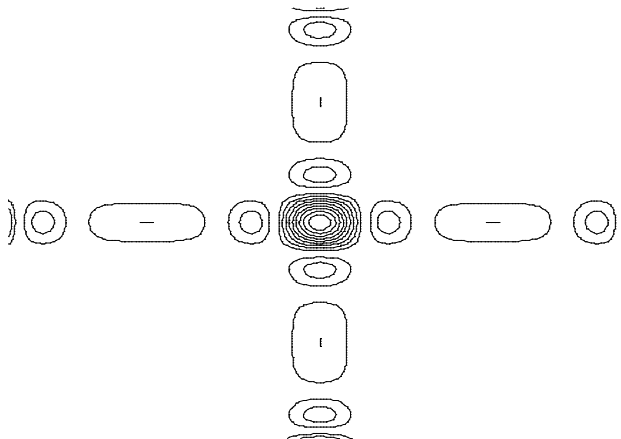


Figure 10.12b. Contour plot corresponding to [Fig. 10.12a](#).

Multiple beams can be formed at the transmitting or receiving modes. Also, it can be carried out at the RF, IF, base band, or digital levels. RF beamforming is the simplest and most common technique. In this case, multiple narrow beams are formed through the use of phase shifters. IF and base band beamforming require complex coherent hardware. However, the system is operated at lower frequencies where tolerance is not as critical. Digital beamforming is more flexible than RF, IF, or base band techniques, but it requires a demanding level of parallel VLSI processing hardware.

A successful implementation of adaptive arrays depends heavily on two factors: first, a proper choice of the reference signal, which is used for comparison against the received target/jammer returns. A good estimate of the reference signal makes the computation of the weights systematic and effective. On the other hand, a bad estimate of the reference signal increases the array's adapting time and limits the system to impractical (non-real time) situations. Second, a fast (real time) computation of the optimum weights is essential. There have been many algorithms developed for this purpose. Nevertheless, they all share a common problem, that is the computation of the inverse of a complex matrix. This drawback has limited the implementation of adaptive arrays to experimental systems or small arrays.

Consider a linear array of N equally spaced elements, and a plane wave incident on the aperture with direction-sine $\sin\beta$, as shown in Fig. 10.13. Conventional beamformers appropriately delay the outputs of each sensor to form a beam steered at angle β . The output of the beamformer is

$$y(t) = \sum_{n=0}^{N-1} x_n(t - \tau_n) \quad (10.59)$$

$$\tau_n = (N - 1 - n) \frac{d}{c} \sin\beta; \quad n = N - 1 \quad (10.60)$$

where d is the element spacing and c is the speed of light. Fourier transformation of Eq. (10.59) yields

$$Y(\omega) = \sum_{n=0}^{N-1} X_n(\omega) \exp(-j\omega\tau_n) \quad (10.61)$$

which can be written in vector form as

$$\vec{Y} = \vec{a} \vec{X} \quad (10.62)$$

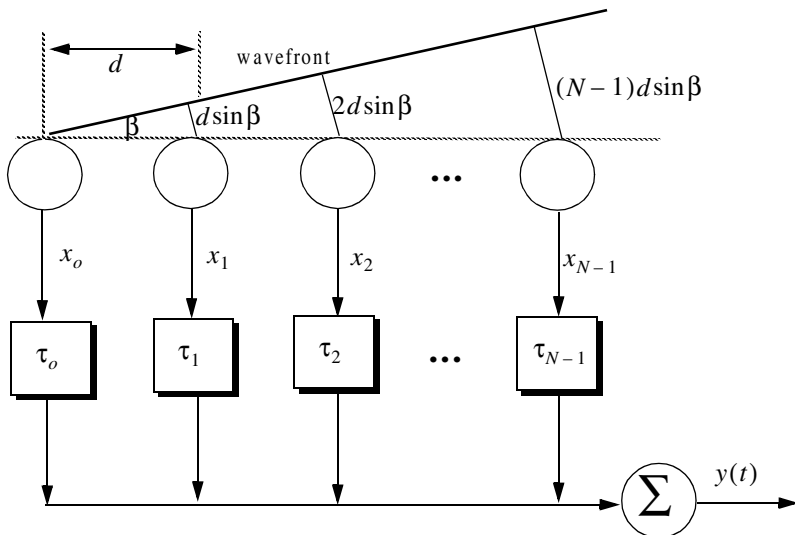


Figure 10.13. A linear array of size N , element spacing d , and an incident plane wave defined by $\sin \beta$.

$$\vec{a}^\dagger = [\exp(j\omega\tau_0) \exp(j\omega\tau_1) \dots \exp(j\omega\tau_{N-1})] \quad (10.63)$$

$$\vec{X}^\dagger = [X_0(\omega) X_1(\omega) \dots X_{N-1}(\omega)]^* \quad (10.64)$$

where the superscript \dagger indicates complex conjugate transpose.

Let A_1 be the amplitude of the wavefront defined by $\sin \beta_1$; it follows that the vector \vec{X} is given by

$$\vec{X} = A_1 \vec{s}_{k1}^* \quad (10.65)$$

where \vec{s}_{k1} is a steering vector, and in general \vec{s}_k is given by

$$\vec{s}_k^\dagger = [1 \cdot \exp(-jk) \cdot \dots \cdot \exp(-j(N-1)k)]; \quad k = \frac{2\pi d}{\lambda} \cdot \sin \beta \quad (10.66)$$

Ignoring the phase term $\exp(-j(N-1)k)$, we can write Eq. (10.63) as

$$\vec{a} = \vec{s}_k \quad (10.67)$$

and the beamformer output will be

$$\vec{Y} = \vec{a} \vec{X} = A_1 \vec{s}_{k_1} \vec{s}_{k_1}^\dagger \quad (10.68)$$

The array pattern of the beam steered at k_1 is computed as the expected value of \vec{Y} . In other words,

$$S(k) = E[\vec{Y} \vec{Y}^\dagger] = P_1 \vec{s}_{k_1} \vec{s}_{k_1}^\dagger \mathfrak{R} \quad (10.69)$$

where $P_1 = E[|A_1|^2]$ and \mathfrak{R} is the correlation matrix. If $\vec{X} = A_1 \vec{s}_{k_1}^*$, then the power spectrum is

$$S(k) = P_1 \vec{s}_{k_1} \vec{s}_{k_1}^\dagger \vec{s}_{k_1} \vec{s}_{k_1}^\dagger \quad (10.70)$$

Consider L incident plane waves with directions of arrival defined by

$$k_i = \frac{2\pi d}{\lambda} \sin \beta_i; \quad i = 1, L \quad (10.71)$$

The n^{th} sample at the output of the m^{th} sensor is

$$y_m(n) = v(n) + \sum_{i=1}^L A_i(n) \exp(-jmk_i); \quad m = 0, N-1 \quad (10.72)$$

where $A_i(n)$ is the amplitude of the i^{th} plane wave, and $v(n)$ is white, zero-mean noise with variance σ_v^2 , and it is assumed to be uncorrelated with the signals. Eq. (10.72) can be written in vector notation as

$$\vec{y}(n) = \vec{v}(n) + \sum_{i=1}^L A_i(n) \vec{s}_{k_i} \quad (10.73)$$

A set of L steering vectors is needed to simultaneously form L beams. Define the steering matrix \mathfrak{K} as

$$\mathfrak{K} = \begin{bmatrix} \vec{s}_{k_1} & \vec{s}_{k_2} & \dots & \vec{s}_{k_L} \end{bmatrix} \quad (10.74)$$

Then the autocorrelation matrix of the field measured by the array is

$$\mathfrak{R} = E\{\vec{y}_m(n) \vec{y}_m^\dagger(n)\} = \sigma_v^2 \mathbf{I} + \mathfrak{K} \mathbf{C} \mathfrak{K}^\dagger \quad (10.75)$$

where $\mathbf{C} = \text{diag}[P_1 \ P_2 \ \dots \ P_L]$, and \mathbf{I} is the identity matrix.

The array pattern can now be computed using standard spectral estimators. For example, using the Bartlett beamformer yields

$$\widehat{S}(k) = \sum_k^\dagger \Re s_k \quad (10.76)$$

The spectrum defined by Eq. (10.76) generates spectral peaks at angles β_i for each wavefront defined by k_i . Assuming the i^{th} wavefront, then the SNR is

$$SNR = N \left(\frac{P_i}{\sigma_v^2} \right) \quad (10.77)$$

10.9. MATLAB Programs and Functions

This section contains listings of all MATLAB programs and functions used in this chapter. Users are encouraged to rerun these codes with different inputs in order to enhance their understanding of the theory.

Listing 10.1. MATLAB Function “*circ_aperture.m*”

```
function [emod] = circ_aperture (lambda, d)
eps = 0.000001;
k = 2. * pi / lambda;
r = d / 2.;
beta = -pi:pi/200.:pi;
sinbet = sin(beta);
var = k * r .* sinbet; %2.0 * pi * (-2:0.001:2);
pattern = (2. * r^2) .* besselj(1,var) ./ (var);
maxval = max(abs(pattern));
pattern = pattern ./ maxval;
emod = 20. * log10(abs(pattern));
figure(1)
plot(var,emod,'k')
grid;
xlabel('kr*sin(angle)')
ylabel('Normalized radiation pattern');
minval = fix(min(var));
maxval = fix(max(var));
var3d = minval:.5:maxval;
[X,Y] = meshgrid(var3d,var3d);
U = sqrt(X.^2 + Y.^2) + eps;
z = 2. * besselj(1,U) ./ U;
figure (2)
mesh(abs(z))
axis off
figure(3)
```

polar(beta,pattern,'k')

Listing 10.2. MATLAB Program “fig10_5.m”

```
clear all
eps = 0.0000001;
beta = -pi : pi / 10791 : pi;
var = sin(beta);
%var = -1.:0.00101:1.;
num = sin((8. * 2. * pi * 0.5) .* var);
if(abs(num) <= eps)
    num = eps;
end
den = sin((2. * pi * 0.5) .* var);
if(abs(den) <= eps)
    den = eps;
end
pattern = num ./ den;
maxval = max(abs(pattern));
pattern = abs(pattern) ./ maxval;
i=0;
mod=abs(pattern);
figure (1)
plot(var,mod,'k');
grid;
xlabel('sine angle - dimensionless')
ylabel('array pattern')
figure(2)
polar(beta,abs(pattern),'k')
```

Listing 10.3. MATLAB Function “linear_array.m”

```
function [emod] = linear_array (ne, d, beta0)
eps = 0.0000001;
beta = 0 : pi / 10791 : 2.*pi;
beta0 = beta0 * pi /180.;
var = sin(beta) - sin(beta0);
num = sin((0.5 * ne * 2. * pi * d) .* var);
if(abs(num) <= eps)
    num = eps;
end
den = sin((0.5 * 2. * pi * d) .* var);
if(abs(den) <= eps)
    den = eps;
```

```

end
pattern = num ./ den;
maxval = max(abs(pattern));
pattern = abs(pattern ./ maxval);
emod=abs(pattern);
figure(1)
plot(sin(beta),emod,'k');
grid;
xlabel('sine angle - dimensionless')
ylabel('array pattern')
figure(2)
polar(beta,abs(pattern),'k')

```

Listing 10.4. MATLAB Program “fig10_10.m”

```

pattern = num ./ den;
maxval = max(abs(pattern));
pattern = abs(pattern ./ maxval);
i = 0.;
for ii=-1:0.001:1
i = i + 1.;
if(pattern(i) < 0.001)
    pattern(i) = 0.0011;
end
end
mod = abs(pattern);
subplot(2,1,1);
plot(var,20.0 .* log10(mod),'k');
grid;
xlabel('sine angle - dimensionless')
ylabel('array pattern')
gtext('main lobe');
gtext('grating lobe');
gtext('grating lobe');
var1 = 1. * pi . * var;
patternj = 2. .* besselj(1,var1) ./ var1;
mod = abs(pattern) .* abs(patternj);
subplot(2,1,2);
plot(var,20.0 .* log10(mod),'k');
grid;
xlabel('sine angle - dimensionless')
ylabel('array pattern')
gtext('main lobe');
gtext('grating lobe');

```

gtext('grating lobe');

Listing 10.5. MATLAB Function “rect_array.m”

```
function emod = rect_array(nex,ney,dx,dy)
eps = 0.0000001;
factx = nex * 2. * pi * 0.5 * dx ;
facty = ney * 2. * pi * 0.5 * dy ;
ii = 0.;
delpi = pi / 10.;
for betax = 0.+delpi : pi/101 : 2.*pi-delpi
    ii = ii + 1.;
    numx = sin(factx * sin(betax));
    if(abs(numx) <= eps)
        numx = eps;
    end
    denx = sin(factx * sin(betax) / nex);
    if(abs(denx) <= eps)
        denx = eps;
    end
    jj = 0.;
    for betay = 0.+delpi : pi/101 : 2.*pi-delpi
        jj = jj + 1.;
        numy = sin(facty * sin(betay));
        if(abs(numy) <= eps)
            numy = eps;
        end
        deny = sin(facty * sin(betay) / ney);
        if(abs(deny) <= eps)
            deny = eps;
        end
        emod(ii,jj) = abs(numx / denx) * abs(numy / deny);
    end
end
maxval = max(max(emod));
emod = emod ./ maxval;
figure(1)
mesh(emod)
figure(2)
contour(emod)
```

Problems

10.1. Consider an antenna whose diameter is $d = 3m$. What is the far field requirement for an X-band or an L-band radar that is using this antenna?

10.2. Consider an antenna with electric field intensity in the xy -plane $E(\zeta)$. This electric field is generated by a current distribution $D(y)$ in the yz -plane. The electric field intensity is computed using the integral

$$E(\zeta) = \int_{-r/2}^{r/2} D(y) \exp\left(2\pi j \frac{y}{\lambda} \sin \zeta\right) dy$$

where λ is the wavelength and r is the aperture. (a) Write an expression for $E(\zeta)$ when $D(Y) = d_0$ (a constant). (b) Write an expression for the normalized power radiation pattern and plot it in dB.

10.3. A linear phased array consists of 50 elements with $\lambda/2$ element spacing. (a) Compute the 3dB beam width when the main beam steering angle is 0° and 45° . (b) Compute the electronic phase difference for any two consecutive elements for steering angle 60° .

10.4. A linear phased array antenna consists of eight elements spaced with $d = \lambda$ element spacing. (a) Give an expression for the antenna gain pattern (assume no steering and uniform aperture weighting). (b) Sketch the gain pattern versus sine of the off boresight angle β . What problems do you see using $d = \lambda$ rather than $d = \lambda/2$?

10.5. In Section 10.6 we showed how a DFT can be used to compute the radiation pattern of a linear phased array. Consider a linear of 64 elements at half wavelength spacing, where an FFT of size 512 is used to compute the pattern. What are the FFT bins that correspond to steering angles $\beta = 30^\circ, 45^\circ$?

Part I: Single Target Tracking

Tracking radar systems are used to measure the target's relative position in range, azimuth angle, elevation angle, and velocity. Then, by using and keeping track of these measured parameters the radar can predict their future values. Target tracking is important to military radars as well as to most civilian radars. In military radars, tracking is responsible for fire control and missile guidance; in fact, missile guidance is almost impossible without proper target tracking. Commercial radar systems, such as civilian airport traffic control radars, may utilize tracking as a means of controlling incoming and departing airplanes.

Tracking techniques can be divided into range/velocity tracking and angle tracking. It is also customary to distinguish between continuous single-target tracking radars and multi-target track-while-scan (TWS) radars. Tracking radars utilize pencil beam (very narrow) antenna patterns. It is for this reason that a separate search radar is needed to facilitate target acquisition by the tracker. Still, the tracking radar has to search the volume where the target's presence is suspected. For this purpose, tracking radars use special search patterns, such as helical, T.V. raster, cluster, and spiral patterns, to name a few.

11.1. Angle Tracking

Angle tracking is concerned with generating continuous measurements of the target's angular position in the azimuth and elevation coordinates. The accuracy of early generation angle tracking radars depended heavily on the size of the pencil beam employed. Most modern radar systems achieve very fine angular measurements by utilizing monopulse tracking techniques.

Tracking radars use the angular deviation from the antenna main axis of the target within the beam to generate an error signal. This deviation is normally measured from the antenna's main axis. The resultant error signal describes how much the target has deviated from the beam main axis. Then, the beam position is continuously changed in an attempt to produce a zero error signal. If the radar beam is normal to the target (maximum gain), then the target angular position would be the same as that of the beam. In practice, this is rarely the case.

In order to be able to quickly achieve changing the beam position, the error signal needs to be a linear function of the deviation angle. It can be shown that this condition requires the beam's axis to be squinted by some angle (squint angle) off the antenna's main axis.

11.1.1. Sequential Lobing

Sequential lobing is one of the first tracking techniques that was utilized by the early generation of radar systems. Sequential lobing is often referred to as lobe switching or sequential switching. It has a tracking accuracy that is limited by the pencil beam width used and by the noise caused by either mechanical or electronic switching mechanisms. However, it is very simple to implement. The pencil beam used in sequential lobing must be symmetrical (equal azimuth and elevation beam widths).

Tracking is achieved (in one coordinate) by continuously switching the pencil beam between two pre-determined symmetrical positions around the antenna's Line of Sight (LOS) axis. Hence, the name sequential lobing is adopted. The LOS is called the radar tracking axis, as illustrated in [Fig. 11.1](#).

As the beam is switched between the two positions, the radar measures the returned signal levels. The difference between the two measured signal levels is used to compute the angular error signal. For example, when the target is tracked on the tracking axis, as the case in [Fig. 11.1a](#), the voltage difference is zero and, hence, is also the error signal. However, when the target is off the tracking axis, as in [Fig. 11.1b](#), a nonzero error signal is produced. The sign of the voltage difference determines the direction in which the antenna must be moved. Keep in mind, the goal here is to make the voltage difference be equal to zero.

In order to obtain the angular error in the orthogonal coordinate, two more switching positions are required for that coordinate. Thus, tracking in two coordinates can be accomplished by using a cluster of four antennas (two for each coordinate) or by a cluster of five antennas. In the latter case, the middle antenna is used to transmit, while the other four are used to receive.

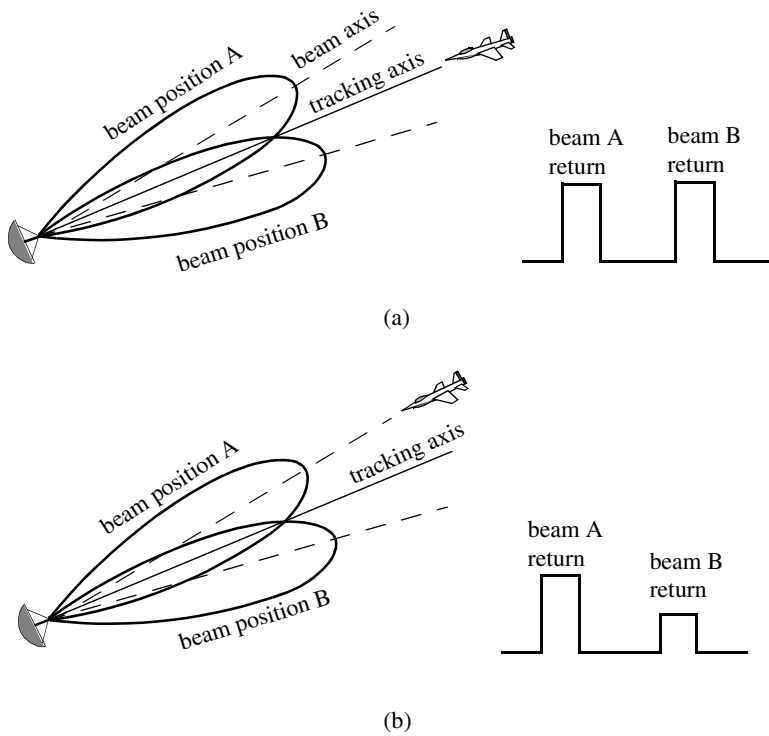


Figure 11.1. Sequential lobing. (a) Target is located on track axis. (b) Target is off track axis.

11.1.2. Conical Scan

Conical scan is a logical extension of sequential lobing where, in this case, the antenna is continuously rotated at an offset angle, or has a feed that is rotated about the antenna's main axis. Fig. 11.2 shows a typical conical scan beam. The beam scan frequency, in radians per second, is denoted as ω_s . The angle between the antenna's LOS and the rotation axis is the squint angle ϕ . The antenna's beam position is continuously changed so that the target will always be on the tracking axis.

Fig. 11.3 shows a simplified conical scan radar system. The envelope detector is used to extract the return signal amplitude and the Automatic Gain Control (AGC) tries to hold the receiver output to a constant value. Since the AGC operates on large time constants, it can hold the average signal level constant and still preserve the signal rapid scan variation. It follows that the tracking

error signals (azimuth and elevation) are functions of the target's RCS; they are functions of its angular position with the main beam axis.

In order to illustrate how conical scan tracking is achieved, we will first consider the case shown in Fig. 11.4. In this case, as the antenna rotates around the tracking axis all target returns have the same amplitude (zero error signal). Thus, no further action is required.

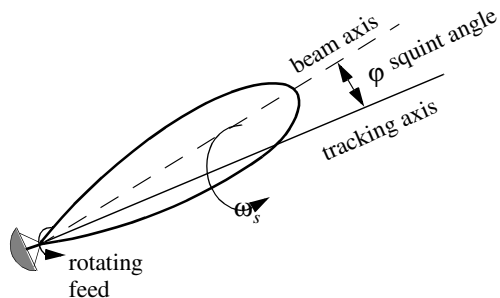


Figure 11.2. Conical scan beam.

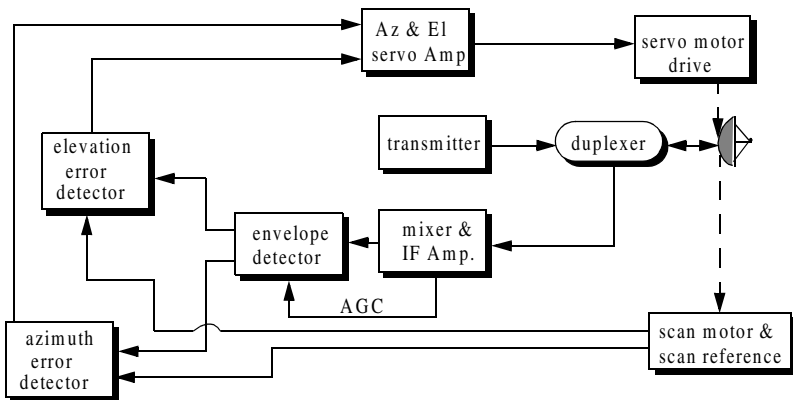


Figure 11.3. Simplified conical scan radar system.

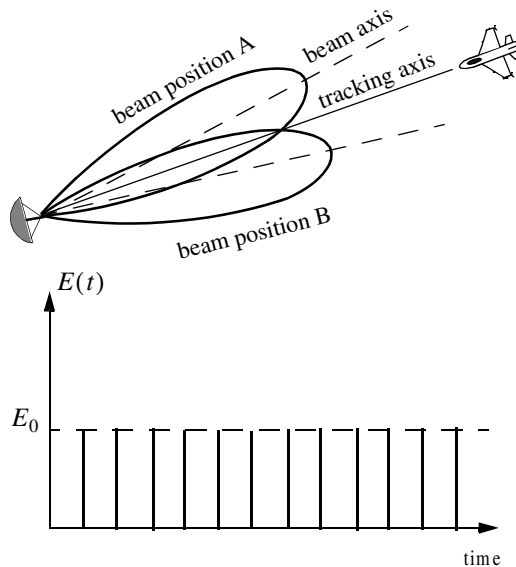


Figure 11.4. Error signal produced when the target is on the tracking axis for conical scan.

Next, consider the case depicted by Fig. 11.5. Here, when the beam is at position B, returns from the target will have maximum amplitude. And when the antenna is at position A, returns from the target have minimum amplitude. Between those two positions, the amplitude of the target returns will vary between the maximum value at position B, and the minimum value at position A. In other words, Amplitude Modulation (AM) exists on top of the returned signal. This AM envelope corresponds to the relative position of the target within the beam. Thus, the extracted AM envelope can be used to derive a servo-control system in order to position the target on the tracking axis.

Now, let us derive the error signal expression that is used to drive the servo-control system. Consider the top view of the beam axis location shown in Fig. 11.6. Assume that $t = 0$ is the starting beam position. The locations for maximum and minimum target returns are also identified. The quantity ϵ defines the distance between the target location and the antenna's tracking axis. It follows that the azimuth and elevation errors are, respectively, given by

$$\epsilon_a = \epsilon \sin \phi \quad (11.1)$$

$$\epsilon_e = \epsilon \cos \phi \quad (11.2)$$

These are the error signals that the radar uses to align the tracking axis on the target.

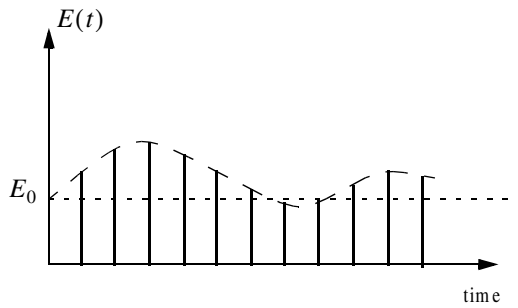
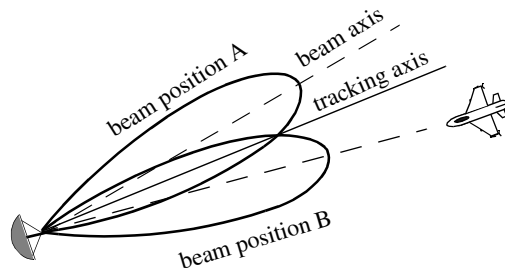


Figure 11.5. Error signal produced when the target is off the tracking axis for conical scan.

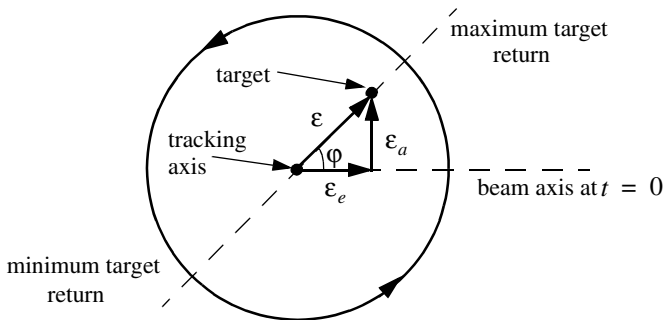


Figure 11.6. Top view of beam axis for a complete scan.

The AM signal $E(t)$ can then be written as

$$E(t) = E_0 \cos(\omega_s t - \varphi) = E_0 \varepsilon_e \cos \omega_s t + E_0 \varepsilon_a \sin \omega_s t \quad (11.3)$$

where E_0 is a constant called the error slope, ω_s is the scan frequency in radians per seconds, and φ is the angle already defined. The scan reference is the signal that the radar generates to keep track of the antenna's position around a complete path (scan). The elevation error signal is obtained by mixing the signal $E(t)$ with $\cos \omega_s t$ (the reference signal) followed by low pass filtering. More precisely,

$$E_e(t) = E_0 \cos(\omega_s t - \varphi) \cos \omega_s t = -\frac{1}{2} E_0 \cos \varphi + \frac{1}{2} \cos(2\omega_s t - \varphi) \quad (11.4)$$

and after low pass filtering we get

$$E_e(t) = -\frac{1}{2} E_0 \cos \varphi \quad (11.5)$$

Negative elevation error drives the antenna beam downward, while positive elevation error drives the antenna beam upward. Similarly, the azimuth error signal is obtained by multiplying $E(t)$ by $\sin \omega_s t$ followed by low pass filtering. It follows that

$$E_a(t) = \frac{1}{2} E_0 \sin \varphi \quad (11.6)$$

The antenna scan rate is limited by the scanning mechanism (mechanical or electronic), where electronic scanning is much faster and more accurate than mechanical scan. In either case, the radar needs at least four target returns to be able to determine the target azimuth and elevation coordinates (two returns per coordinate). Therefore, the maximum conical scan rate is equal to one fourth of the PRF. Rates as high as 30 scans per seconds are commonly used.

The conical scan squint angle needs to be large enough so that a good error signal can be measured. However, due to the squint angle, the antenna gain in the direction of the tracking axis is less than maximum. Thus, when the target is in track (located on the tracking axis), the SNR suffers a loss equal to the drop in the antenna gain. This loss is known as the squint or crossover loss. The squint angle is normally chosen such that the two-way (transmit and receive) crossover loss is less than a few decibels.

11.2. Amplitude Comparison Monopulse

Amplitude comparison monopulse tracking is similar to lobing in the sense that four squinted beams are required to measure the target's angular position. The difference is that the four beams are generated simultaneously rather than

sequentially. For this purpose, a special antenna feed is utilized such that the four beams are produced using a single pulse, hence the name “monopulse.” Additionally, monopulse tracking is more accurate and is not susceptible to lobing anomalies, such as AM jamming and gain inversion ECM. Finally, in sequential and conical lobing variations in the radar echoes degrade the tracking accuracy; however, this is not a problem for monopulse techniques since a single pulse is used to produce the error signals. Monopulse tracking radars can employ both antenna reflectors as well as phased array antennas.

Fig. 11.7 show a typical monopulse antenna pattern. The four beams A, B, C, and D represent the four conical scan beam positions. Four feeds, mainly horns, are used to produce the monopulse antenna pattern. Amplitude monopulse processing requires that the four signals have the same phase and different amplitudes.

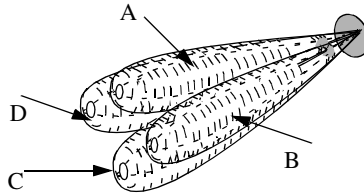


Figure 11.7. Monopulse antenna pattern.

A good way to explain the concept of amplitude monopulse technique is to represent the target echo signal by a circle centered at the antenna’s tracking axis, as illustrated by Fig. 11.8a, where the four quadrants represent the four beams. In this case, the four horns receive an equal amount of energy, which indicates that the target is located on the antenna’s tracking axis. However, when the target is off the tracking axis (Figs. 11.8b-d), an unbalance of energy occurs in the different beams. This unbalance of energy is used to generate an error signal that drives the servo-control system. Monopulse processing consists of computing a sum Σ and two difference Δ (azimuth and elevation) antenna patterns. Then by dividing a Δ channel voltage by the Σ channel voltage, the angle of the signal can be determined.

The radar continuously compares the amplitudes and phases of all beam returns to sense the amount of target displacement off the tracking axis. It is critical that the phases of the four signals be constant in both transmit and receive modes. For this purpose, either digital networks or microwave comparator circuitry are utilized. Fig. 11.9 shows a block diagram for a typical microwave comparator, where the three receiver channels are declared as the sum channel, elevation angle difference channel, and azimuth angle difference channel.

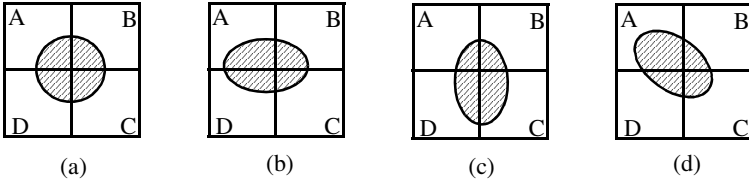


Figure 11.8. Illustration of monopulse concept. (a) Target is on the tracking axis. (b) - (d) Target is off the tracking axis.

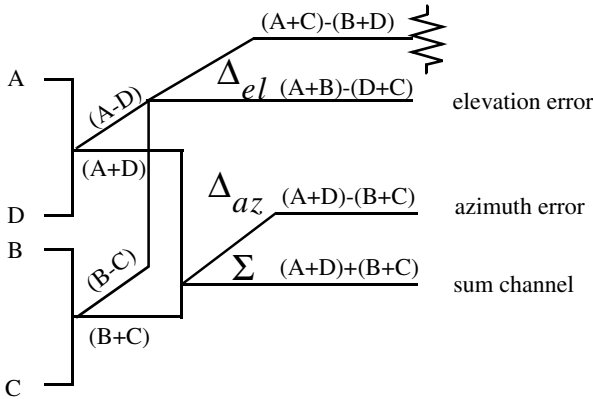


Figure 11.9. Monopulse comparator.

To generate the elevation difference beam, one can use the beam difference $(A-D)$ or $(B-C)$. However, by first forming the sum patterns $(A+B)$ and $(D+C)$ and then computing the difference $(A+B)-(D+C)$, we achieve a stronger elevation difference signal, Δ_{el} . Similarly, by first forming the sum patterns $(A+D)$ and $(B+C)$ and then computing the difference $(A+D)-(B+C)$, a stronger azimuth difference signal, Δ_{az} , is produced.

A simplified monopulse radar block diagram is shown in Fig. 11.10. The sum channel is used for both transmit and receive. In the receiving mode the sum channel provides the phase reference for the other two difference channels. Range measurements can also be obtained from the sum channel. In order to illustrate how the sum and difference antenna patterns are formed, we will assume a $\sin\varphi/\varphi$ single element antenna pattern and squint angle φ_0 . The sum signal in one coordinate (azimuth or elevation) is then given by

$$\Sigma(\varphi) = \frac{\sin(\varphi - \varphi_0)}{(\varphi - \varphi_0)} + \frac{\sin(\varphi + \varphi_0)}{(\varphi + \varphi_0)} \quad (11.7)$$

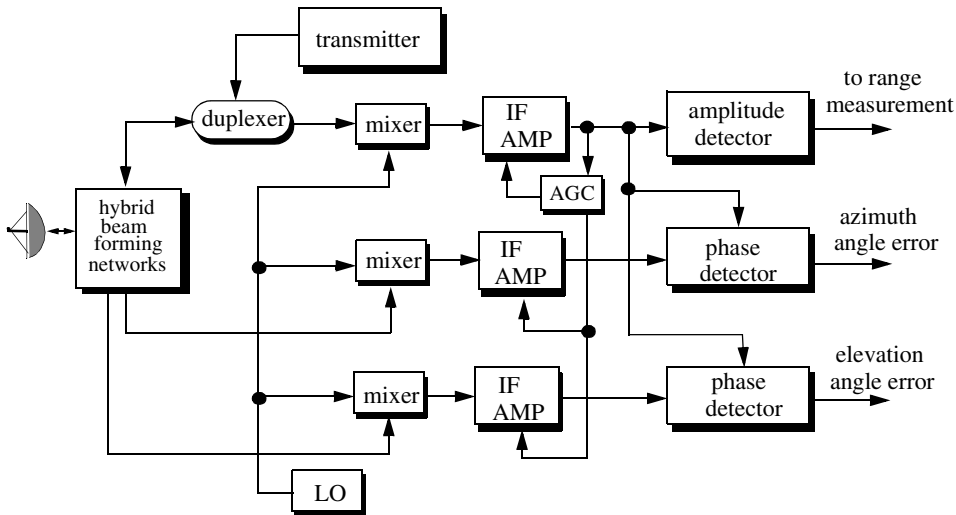


Figure 11.10. Simplified amplitude comparison monopulse radar block diagram.

and a difference signal in the same coordinate is

$$\Delta(\varphi) = \frac{\sin(\varphi - \varphi_0)}{(\varphi - \varphi_0)} - \frac{\sin(\varphi + \varphi_0)}{(\varphi + \varphi_0)} \quad (11.8)$$

MATLAB Function “mono_pulse.m”

The function “mono_pulse.m” implements Eqs. (11.7) and (11.8). Its output includes plots of the sum and difference antenna patterns as well as the difference-to-sum ratio. It is given in Listing 11.1 in Section 11.10. The syntax is as follows:

mono_pulse(phi0)

where *phi0* is the squint angle in radians.

Fig. 11.11 (a-c) shows the corresponding plots for the sum and difference patterns for $\varphi_0 = 0.15$ radians. Fig. 11.12 (a-c) is similar to Fig. 11.11, except in this case $\varphi_0 = 0.75$ radians. Clearly, the sum and difference patterns depend heavily on the squint angle. Using a relatively small squint angle produces a better sum pattern than that resulting from a larger angle. Additionally, the difference pattern slope is steeper for the small squint angle.

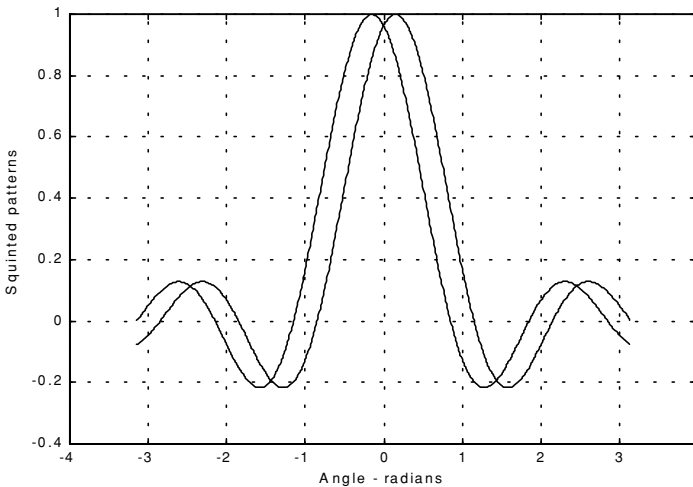


Figure 11.11a. Two squinted patterns. Squint angle is $\varphi_0 = 0.15$ radians.

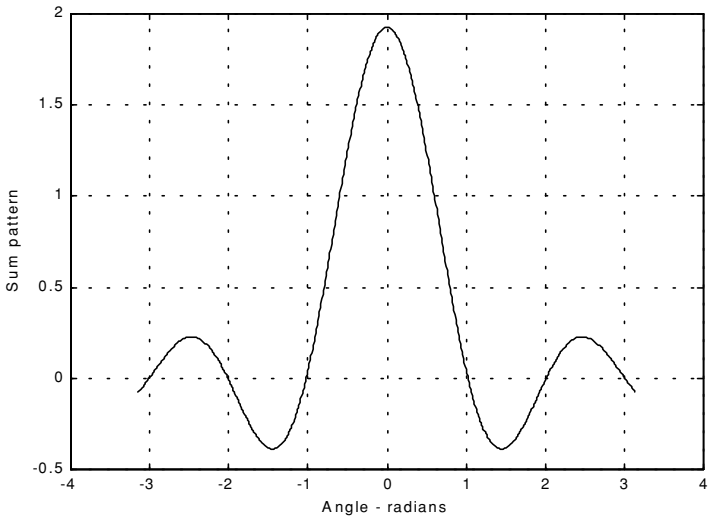


Figure 11.11b. Sum pattern corresponding to [Fig. 11.11a](#).

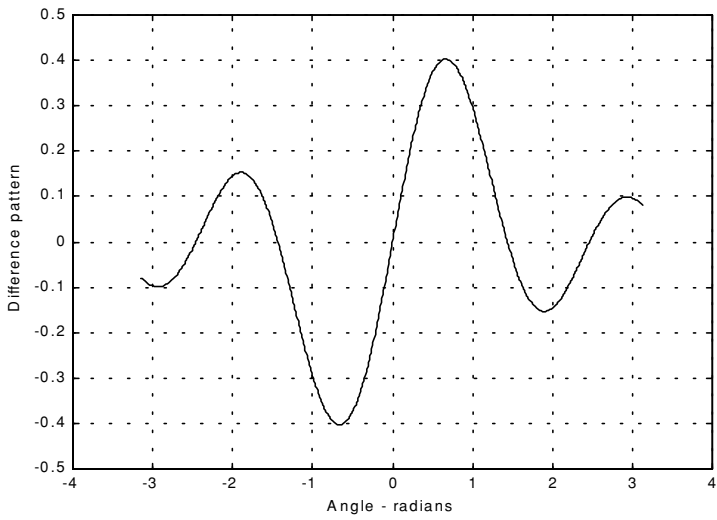


Figure 11.11c. Difference pattern corresponding to [Fig. 11.11a](#).

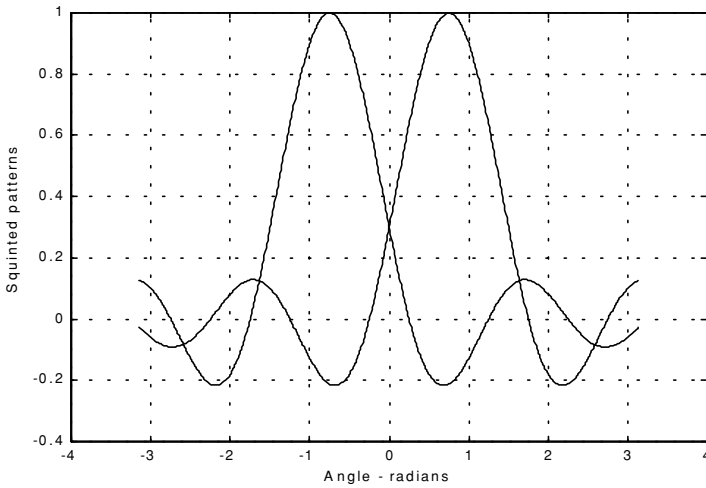


Figure 11.12a. Two squinted patterns. Squint angle is $\phi_0 = 0.75$ radians.

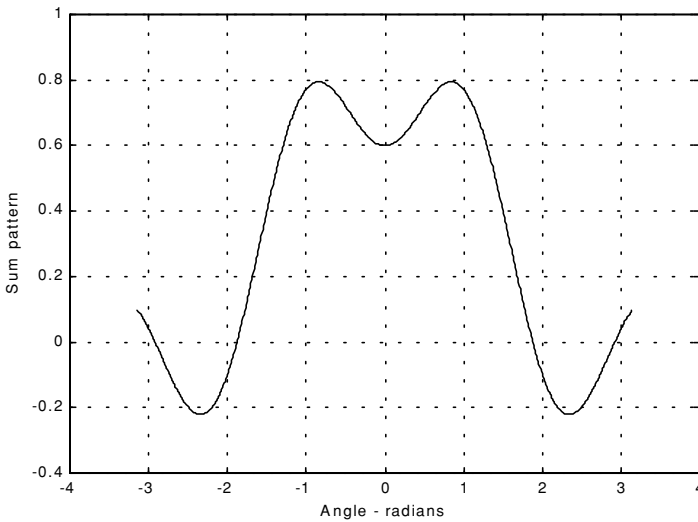


Figure 11.12b. Sum pattern corresponding to [Fig. 11.12a](#).

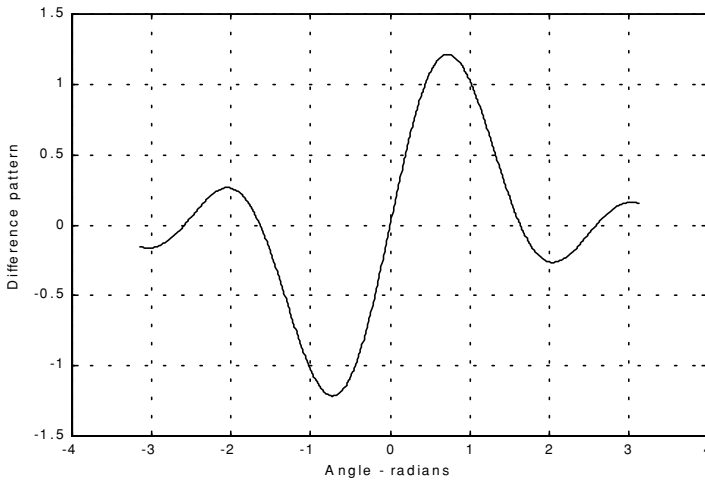


Figure 11.12c. Difference pattern corresponding to Fig. 11.12a.

The difference channels give us an indication of whether the target is on or off the tracking axis. However, this signal amplitude depends not only on the target angular position, but also on the target's range and RCS. For this reason the ratio Δ/Σ (delta over sum) can be used to accurately estimate the error angle that only depends on the target's angular position.

Let us now address how the error signals are computed. First, consider the azimuth error signal. Define the signals S_1 and S_2 as

$$S_1 = A + D \quad (11.9)$$

$$S_2 = B + C \quad (11.10)$$

The sum signal is $\Sigma = S_1 + S_2$, and the azimuth difference signal is $\Delta_{az} = S_1 - S_2$. If $S_1 \geq S_2$, then both channels have the same phase 0° (since the sum channel is used for phase reference). Alternatively, if $S_1 < S_2$, then the two channels are 180° out of phase. Similar analysis can be done for the elevation channel, where in this case $S_1 = A + B$ and $S_2 = D + C$. Thus, the error signal output is

$$\varepsilon_\varphi = \frac{|\Delta|}{|\Sigma|} \cos \xi \quad (11.11)$$

where ξ is the phase angle between the sum and difference channels and it is equal to 0° or 180° . More precisely, if $\xi = 0$, then the target is on the tracking axis; otherwise it is off the tracking axis. Fig. 11.13 (a,b) shows a plot for the ratio Δ/Σ for the monopulse radar whose sum and difference patterns are in Figs. 11.11 and 11.12.

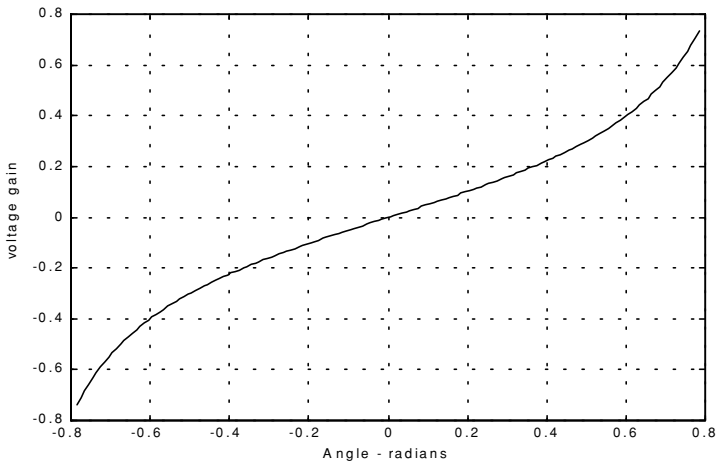


Figure 11.13a. Difference-to-sum ratio corresponding to Fig. 11.11a.

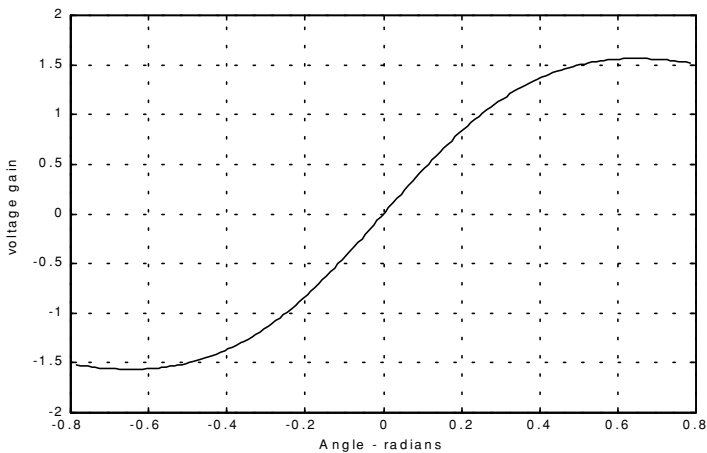


Figure 11.13b. Difference-to-sum ratio corresponding to Fig. 11.12a.

11.3. Phase Comparison Monopulse

Phase comparison monopulse is similar to amplitude comparison monopulse in the sense that the target angular coordinates are extracted from one sum and two difference channels. The main difference is that the four signals produced in amplitude comparison monopulse will have similar phases but different amplitudes; however, in phase comparison monopulse the signals have the same amplitude and different phases. Phase comparison monopulse tracking radars use a minimum of a two-element array antenna for each coordinate (azimuth and elevation), as illustrated in Fig. 11.14. A phase error signal (for each coordinate) is computed from the phase difference between the signals generated in the antenna elements.

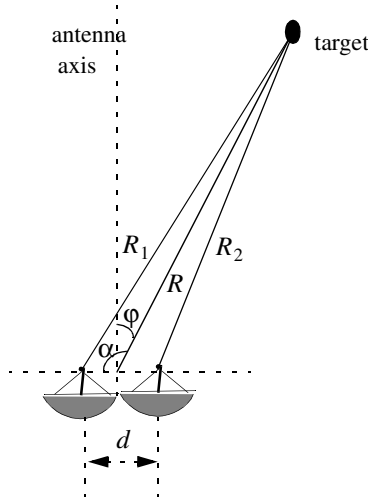


Figure 11.14. Single coordinate phase comparison monopulse antenna.

Consider Fig. 11.14; since the angle α is equal to $\phi + \pi/2$, it follows that

$$\begin{aligned} R_1^2 &= R^2 + \left(\frac{d}{2}\right)^2 - 2\frac{d}{2}R\cos\left(\phi + \frac{\pi}{2}\right) \\ &= R^2 + \frac{d^2}{4} - dR\sin\phi \end{aligned} \quad (11.12)$$

and since $d \ll R$ we can use the binomial series expansion to get

$$R_1 \approx R \left(1 + \frac{d}{2R} \sin \varphi \right) \quad (11.13)$$

Similarly,

$$R_2 \approx R \left(1 - \frac{d}{2R} \sin \varphi \right) \quad (11.14)$$

The phase difference between the two elements is then given by

$$\phi = \frac{2\pi}{\lambda} (R_1 - R_2) = \frac{2\pi}{\lambda} d \sin \varphi \quad (11.15)$$

where λ is the wavelength. The phase difference ϕ is used to determine the angular target location. Note that if $\phi = 0$, then the target would be on the antenna's main axis. The problem with this phase comparison monopulse technique is that it is quite difficult to maintain a stable measurement of the off-boresight angle φ , which causes serious performance degradation. This problem can be overcome by implementing a phase comparison monopulse system as illustrated in Fig. 11.15.

The (single coordinate) sum and difference signals are, respectively, given by

$$\Sigma(\varphi) = S_1 + S_2 \quad (11.16)$$

$$\Delta(\varphi) = S_1 - S_2 \quad (11.17)$$

where the S_1 and S_2 are the signals in the two elements. Now, since S_1 and S_2 have similar amplitude and are different in phase by ϕ , we can write

$$S_1 = S_2 e^{-j\phi} \quad (11.18)$$

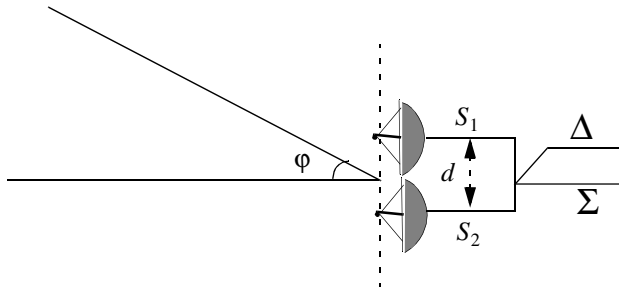


Figure 11.15. Single coordinate phase monopulse antenna, with sum and difference channels.

It follows that

$$\Delta(\varphi) = S_2(1 - e^{-j\phi}) \quad (11.19)$$

$$\Sigma(\varphi) = S_2(1 + e^{-j\phi}) \quad (11.20)$$

The phase error signal is computed from the ratio Δ/Σ . More precisely,

$$\frac{\Delta}{\Sigma} = \frac{1 - e^{-j\phi}}{1 + e^{-j\phi}} = j \tan\left(\frac{\phi}{2}\right) \quad (11.21)$$

which is purely imaginary. The modulus of the error signal is then given by

$$\frac{|\Delta|}{|\Sigma|} = \tan\left(\frac{\phi}{2}\right) \quad (11.22)$$

This kind of phase comparison monopulse tracker is often called the half-angle tracker.

11.4. Range Tracking

Target range is measured by estimating the round-trip delay of the transmitted pulses. The process of continuously estimating the range of a moving target is known as range tracking. Since the range to a moving target is changing with time, the range tracker must be constantly adjusted to keep the target locked in range. This can be accomplished using a split gate system, where two range gates (early and late) are utilized. The concept of split gate tracking is illustrated in Fig. 11.16, where a sketch of a typical pulsed radar echo is shown in the figure. The early gate opens at the anticipated starting time of the radar echo and lasts for half its duration. The late gate opens at the center and closes at the end of the echo signal. For this purpose, good estimates of the echo duration and the pulse centertime must be reported to the range tracker so that the early and late gates can be placed properly at the start and center times of the expected echo. This reporting process is widely known as the “designation process.”

The early gate produces positive voltage output while the late gate produces negative voltage output. The outputs of the early and late gates are subtracted, and the difference signal is fed into an integrator to generate an error signal. If both gates are placed properly in time, the integrator output will be equal to zero. Alternatively, when the gates are not timed properly, the integrator output is not zero, which gives an indication that the gates must be moved in time, left or right depending on the sign of the integrator output.

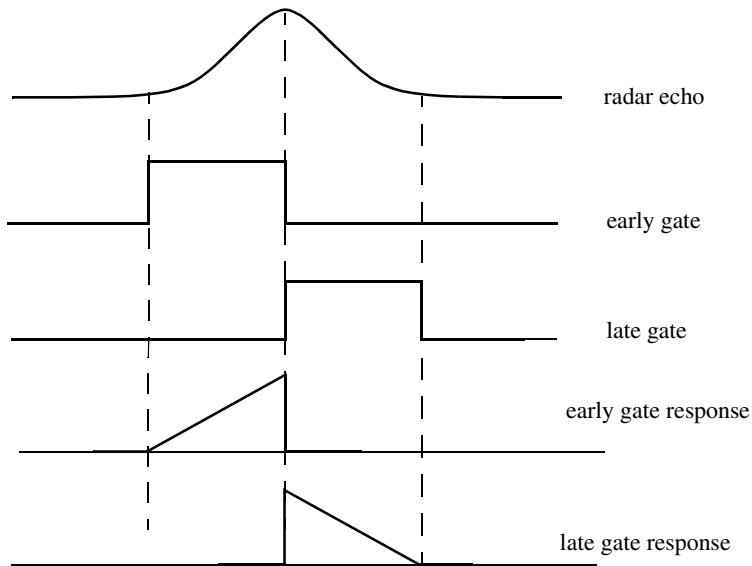


Figure 11.16. Illustration of split-range gate.

Part II: Multiple Target Tracking

Track-while-scan radar systems sample each target once per scan interval, and use sophisticated smoothing and prediction filters to estimate the target parameters between scans. To this end, the Kalman filter and the Alpha-Beta-Gamma ($\alpha\beta\gamma$) filter are commonly used. Once a particular target is detected, the radar may transmit up to a few pulses to verify the target parameters, before it establishes a track file for that target. Target position, velocity, and acceleration comprise the major components of the data maintained by a track file.

The principles of recursive tracking and prediction filters are presented in this part. First, an overview of state representation for Linear Time Invariant (LTI) systems is discussed. Then, second and third order one-dimensional fixed gain polynomial filter trackers are developed. These filters are, respectively, known as the $\alpha\beta$ and $\alpha\beta\gamma$ filters (also known as the g-h and g-h-k filters). Finally, the equations for an n-dimensional multi-state Kalman filter is introduced and analyzed. As a matter of notation, small case letters, with an underneath bar, are used.

11.5. Track-While-Scan (TWS)

Modern radar systems are designed to perform multi-function operations, such as detection, tracking, and discrimination. With the aid of sophisticated computer systems, multi-function radars are capable of simultaneously tracking many targets. In this case, each target is sampled once (mainly range and angular position) during a dwell interval (scan). Then, by using smoothing and prediction techniques future samples can be estimated. Radar systems that can perform multi-tasking and multi-target tracking are known as Track-While-Scan (TWS) radars.

Once a TWS radar detects a new target it initiates a separate track file for that detection; this ensures that sequential detections from that target are processed together to estimate the target's future parameters. Position, velocity, and acceleration comprise the main components of the track file. Typically, at least one other confirmation detection (verify detection) is required before the track file is established.

Unlike single target tracking systems, TWS radars must decide whether each detection (observation) belongs to a new target or belongs to a target that has been detected in earlier scans. And in order to accomplish this task, TWS radar systems utilize correlation and association algorithms. In the correlation process each new detection is correlated with all previous detections in order to avoid establishing redundant tracks. If a certain detection correlates with more than one track, then a pre-determined set of association rules are exercised so

that the detection is assigned to the proper track. A simplified TWS data processing block diagram is shown in Fig. 11.17.

Choosing a suitable tracking coordinate system is the first problem a TWS radar has to confront. It is desirable that a fixed reference of an inertial coordinate system be adopted. The radar measurements consist of target range, velocity, azimuth angle, and elevation angle. The TWS system places a gate around the target position and attempts to track the signal within this gate. The gate dimensions are normally azimuth, elevation, and range. Because of the uncertainty associated with the exact target position during the initial detections, a gate has to be large enough so that targets do not move appreciably from scan to scan; more precisely, targets must stay within the gate boundary during successive scans. After the target has been observed for several scans the size of the gate is reduced considerably.

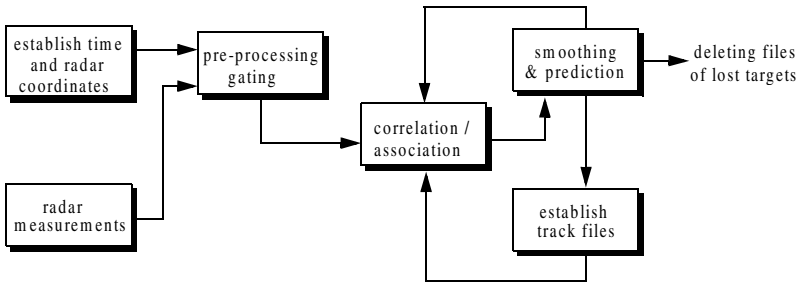


Figure. 11.17. Simplified block diagram of TWS data processing.

Gating is used to decide whether an observation is assigned to an existing track file, or to a new track file (new detection). Gating algorithms are normally based on computing a statistical error distance between a measured and an estimated radar observation. For each track file, an upper bound for this error distance is normally set. If the computed difference for a certain radar observation is less than the maximum error distance of a given track file, then the observation is assigned to that track.

All observations that have an error distance less than the maximum distance of a given track are said to correlate with that track. For each observation that does not correlate with any existing tracks, a new track file is established accordingly. Since new detections (measurements) are compared to all existing track files, a track file may then correlate with no observations or with one or more observations. The correlation between observations and all existing track files is identified using a correlation matrix. Rows of the correlation matrix

represent radar observations, while columns represent track files. In cases where several observations correlate with more than one track file, a set of pre-determined association rules can be utilized so that a single observation is assigned to a single track file.

11.6. State Variable Representation of an LTI System

Linear time invariant system (continuous or discrete) can be describe mathematically using three variables. They are the input, output, and the state variables. In this representation, any LTI system has observable or measurable objects (abstracts). For example, in the case of a radar system, range may be an object measured or observed by the radar tracking filter. States can be derived in many different ways. For the scope of this book, states of an object or an abstract are the components of the vector that contains the object and its time derivatives. For example, a third-order one-dimensional (in this case range) state vector representing range can be given by

$$\underline{x} = \begin{bmatrix} R \\ \dot{R} \\ \ddot{R} \end{bmatrix} \quad (11.23)$$

where R , \dot{R} , and \ddot{R} are, respectively, the range measurement, range rate (velocity), and acceleration. The state vector defined in Eq. (11.23) can be representative of continuous or discrete states. In this book, the emphasis is on discrete time representation, since most radar signal processing is executed using digital computers. For this purpose, an n -dimensional state vector has the following form:

$$\underline{x} = \left[x_1 \dot{x}_1 \dots x_2 \dot{x}_2 \dots x_n \dot{x}_n \dots \right]^t \quad (11.24)$$

where the superscript indicates the transpose operation.

The LTI system of interest can be represented using the following state equations:

$$\dot{\underline{x}}(t) = \underline{A} \underline{x}(t) + \underline{B}\underline{w}(t) \quad (11.25)$$

$$\underline{y}(t) = \underline{C} \underline{x}(t) + \underline{D}\underline{w}(t) \quad (11.26)$$

where: $\dot{\underline{x}}$ is the value of the $n \times 1$ state vector; \underline{y} is the value of the $p \times 1$ output vector; \underline{w} is the value of the $m \times 1$ input vector; \underline{A} is an $n \times n$ matrix; \underline{B} is an $n \times m$ matrix; \underline{C} is $p \times n$ matrix; and \underline{D} is an $p \times m$ matrix. The

homogeneous solution (i.e., $\underline{w} = \underline{0}$) to this linear system, assuming known initial condition $\underline{x}(0)$ at time t_0 , has the form

$$\underline{x}(t) = \underline{\Phi}(t - t_0)\underline{x}(t - t_0) \quad (11.27)$$

The matrix $\underline{\Phi}$ is known as the state transition matrix, or fundamental matrix, and is equal to

$$\underline{\Phi}(t - t_0) = e^{\underline{A}(t - t_0)} \quad (11.28)$$

Eq. (11.28) can be expressed in series format as

$$\underline{\Phi}(t - t_0)\big|_{t_0=0} = e^{\underline{A}t} = \underline{I} + \underline{A}t + \underline{A}^2 \frac{t^2}{2!} + \dots = \sum_{k=0}^{\infty} \underline{A}^k \frac{t^k}{k!} \quad (11.29)$$

Example 11.1: Compute the state transition matrix for an LTI system when

$$\underline{A} = \begin{bmatrix} 0 & 1 \\ -0.5 & -1 \end{bmatrix}$$

Solution:

The state transition matrix can be computed using Eq. (11.29). For this purpose, compute \underline{A}^2 and \underline{A}^3 It follows

$$\underline{A}^2 = \begin{bmatrix} -\frac{1}{2} & -1 \\ \frac{1}{2} & \frac{1}{2} \end{bmatrix} \quad \underline{A}^3 = \begin{bmatrix} \frac{1}{2} & \frac{1}{2} \\ -\frac{1}{4} & 0 \end{bmatrix} \quad \dots$$

Therefore,

$$\underline{\Phi} = \begin{bmatrix} 1 + 0t - \frac{1}{2}t^2 + \frac{1}{2}t^3 + \dots & 0 + t - \frac{t^2}{2!} + \frac{1}{2}t^3 + \dots \\ 0 - \frac{1}{2}t + \frac{1}{2}t^2 - \frac{1}{4}t^3 + \dots & 1 - t + \frac{t^2}{2!} + \frac{0t^3}{3!} + \dots \end{bmatrix}$$

The state transition matrix has the following properties (the proof is left as an exercise):

1. *Derivative property*

$$\frac{\partial}{\partial t} \underline{\Phi}(t-t_0) = \underline{A} \underline{\Phi}(t-t_0) \quad (11.30)$$

2. Identity property

$$\underline{\Phi}(t_0-t_0) = \underline{\Phi}(0) = \underline{I} \quad (11.31)$$

3. Initial value property

$$\left. \frac{\partial}{\partial t} \underline{\Phi}(t-t_0) \right|_{t=t_0} = \underline{A} \quad (11.32)$$

4. Transition property

$$\underline{\Phi}(t_2-t_0) = \underline{\Phi}(t_2-t_1) \underline{\Phi}(t_1-t_0) \quad ; \quad t_0 \leq t_1 \leq t_2 \quad (11.33)$$

5. Inverse property

$$\underline{\Phi}(t_0-t_1) = \underline{\Phi}^{-1}(t_1-t_0) \quad (11.34)$$

6. Separation property

$$\underline{\Phi}(t_1-t_0) = \underline{\Phi}(t_1) \underline{\Phi}^{-1}(t_0) \quad (11.35)$$

The general solution to the system defined in Eq. (11.25) can be written as

$$\underline{x}(t) = \underline{\Phi}(t-t_0) \underline{x}(t_0) + \int_{t_0}^t \underline{\Phi}(t-\tau) \underline{B} \underline{w}(\tau) d\tau \quad (11.36)$$

The first term of the right-hand side of Eq. (11.36) represents the contribution from the system response to the initial condition. The second term is the contribution due to the driving force \underline{w} . By combining Eqs. (11.26) and (11.36) an expression for the output is computed as

$$\underline{y}(t) = \underline{C} e^{\underline{A}(t-t_0)} \underline{x}(t_0) + \int_{t_0}^t [\underline{C} e^{\underline{A}(t-\tau)} \underline{B} - \underline{D} \delta(t-\tau)] \underline{w}(\tau) d\tau \quad (11.37)$$

Note that the system impulse response is equal to $\underline{C} e^{\underline{A}t} \underline{B} - \underline{D} \delta(t)$.

The difference equations describing a discrete time system, equivalent to Eqs. (11.25) and (11.26), are

$$\underline{x}(n+1) = \underline{A} \underline{x}(n) + \underline{B}\underline{w}(n) \quad (11.38)$$

$$\underline{y}(n) = \underline{C} \underline{x}(n) + \underline{D}\underline{w}(n) \quad (11.39)$$

where n defines the discrete time nT and T is the sampling interval. All other vectors and matrices were defined earlier. The homogeneous solution to the system defined in Eq. (11.38), with initial condition $\underline{x}(n_0)$, is

$$\underline{x}(n) = \underline{A}^{n-n_0} \underline{x}(n_0) \quad (11.40)$$

In this case the state transition matrix is an $n \times n$ matrix given by

$$\underline{\Phi}(n, n_0) = \underline{\Phi}(n - n_0) = \underline{A}^{n-n_0} \quad (11.41)$$

The following is the list of properties associated with the discrete transition matrix

$$\underline{\Phi}(n+1 - n_0) = \underline{A}\underline{\Phi}(n - n_0) \quad (11.42)$$

$$\underline{\Phi}(n_0 - n_0) = \underline{\Phi}(0) = \underline{I} \quad (11.43)$$

$$\underline{\Phi}(n_0 + 1 - n_0) = \underline{\Phi}(1) = \underline{A} \quad (11.44)$$

$$\underline{\Phi}(n_2 - n_0) = \underline{\Phi}(n_2 - n_1)\underline{\Phi}(n_1 - n_0) \quad (11.45)$$

$$\underline{\Phi}(n_0 - n_1) = \underline{\Phi}^{-1}(n_1 - n_0) \quad (11.46)$$

$$\underline{\Phi}(n_1 - n_0) = \underline{\Phi}(n_1)\underline{\Phi}^{-1}(n_0) \quad (11.47)$$

The solution to the general case (i.e., non-homogeneous system) is given by

$$\underline{x}(n) = \underline{\Phi}(n - n_0)\underline{x}(n_0) + \sum_{m=n_0}^{n-1} \underline{\Phi}(n - m - 1)\underline{B}\underline{w}(m) \quad (11.48)$$

It follows that the output is given by

$$\underline{y}(n) = \underline{C}\underline{\Phi}(n - n_0)\underline{x}(n_0) + \sum_{m=n_0}^{n-1} \underline{C} \underline{\Phi}(n - m - 1)\underline{B}\underline{w}(m) + \underline{D}\underline{w}(n) \quad (11.49)$$

where the system impulse response is given by

$$\underline{h}(n) = \sum_{m=n_0}^{n-1} \underline{C} \underline{\Phi}(n-m-1) \underline{B} \underline{\delta}(m) + \underline{D} \underline{\delta}(n) \quad (11.50)$$

Taking the Z-transform for Eqs. (11.38) and (11.39) yields

$$z\underline{x}(z) = \underline{A}\underline{x}(z) + \underline{B}\underline{w}(z) + z\underline{x}(0) \quad (11.51)$$

$$\underline{y}(z) = \underline{C}\underline{x}(z) + \underline{D}\underline{w}(z) \quad (11.52)$$

Manipulating Eqs. (11.51) and (11.52) yields

$$\underline{x}(z) = [z\underline{I} - \underline{A}]^{-1} \underline{B}\underline{w}(z) + [z\underline{I} - \underline{A}]^{-1} z\underline{x}(0) \quad (11.53)$$

$$\underline{y}(z) = \{ \underline{C}[z\underline{I} - \underline{A}]^{-1} \underline{B} + \underline{D} \} \underline{w}(z) + \underline{C}[z\underline{I} - \underline{A}]^{-1} z\underline{x}(0) \quad (11.54)$$

It follows that the state transition matrix is

$$\underline{\Phi}(z) = z[z\underline{I} - \underline{A}]^{-1} = [\underline{I} - z^{-1}\underline{A}]^{-1} \quad (11.55)$$

and the system impulse response in the z-domain is

$$\underline{h}(z) = \underline{C}\underline{\Phi}(z)z^{-1}\underline{B} + \underline{D} \quad (11.56)$$

11.7. The LTI System of Interest

For the purpose of establishing the framework necessary for the Kalman filter development, consider the LTI system shown in Fig. 11.18. This system (which is a special case of the system described in the previous section) can be described by the following first order differential vector equations

$$\dot{\underline{x}}(t) = \underline{A} \underline{x}(t) + \underline{u}(t) \quad (11.57)$$

$$\underline{y}(t) = \underline{G} \underline{x}(t) + \underline{v}(t) \quad (11.58)$$

where \underline{y} is the observable part of the system (i.e., output), \underline{u} is a driving force, and \underline{v} is the measurement noise. The matrices \underline{A} and \underline{G} vary depending on the system. The noise observation \underline{v} is assumed to be uncorrelated. If the initial condition vector is $\underline{x}(t_0)$, then from Eq. (11.36) we get

$$\underline{x}(t) = \underline{\Phi}(t-t_0)\underline{x}(t_0) + \int_{t_0}^t \underline{\Phi}(t-\tau)\underline{u}(\tau)d\tau \quad (11.59)$$

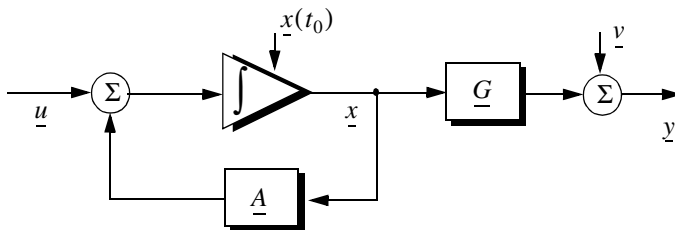


Figure 11.18. An LTI system.

The object (abstract) is observed only at discrete times determined by the system. These observation times are declared by discrete time nT where T is the sampling interval. Using the same notation adopted in the previous section, the discrete time representations of Eqs. (11.57) and (11.58) are

$$\underline{x}(n) = \underline{A} \underline{x}(n-1) + \underline{u}(n) \quad (11.60)$$

$$\underline{y}(n) = \underline{G} \underline{x}(n) + \underline{v}(n) \quad (11.61)$$

The homogeneous solution to this system is given in Eq. (11.27) for continuous time, and in Eq. (11.40) for discrete time.

The state transition matrix corresponding to this system can be obtained using Taylor series expansion of the vector \underline{x} . More precisely,

$$\begin{aligned} \underline{x} &= \underline{x} + T\dot{\underline{x}} + \frac{T^2}{2!}\ddot{\underline{x}} + \dots \\ \dot{\underline{x}} &= \dot{\underline{x}} + T\ddot{\underline{x}} + \dots \\ \ddot{\underline{x}} &= \ddot{\underline{x}} + \dots \end{aligned} \quad (11.62)$$

It follows that the elements of the state transition matrix are defined by

$$\underline{\Phi}[ij] = \begin{cases} T^{j-i} / (j-i)! & 1 \leq i, j \leq n \\ 0 & j < i \end{cases} \quad (11.63)$$

Using matrix notation, the state transition matrix is then given by

$$\underline{\Phi} = \begin{bmatrix} 1 & T & \frac{T^2}{2!} & \dots \\ 0 & 1 & T & \dots \\ 0 & 0 & 1 & \dots \\ \dots & \dots & \dots & \dots \end{bmatrix} \quad (11.64)$$

The matrix given in Eq. (11.64) is often called the Newtonian matrix.

11.8. Fixed-Gain Tracking Filters

This class of filters (or estimators) is also known as “Fixed-Coefficient” filters. The most common examples of this class of filters are the $\alpha\beta$ and $\alpha\beta\gamma$ filters and their variations. The $\alpha\beta$ and $\alpha\beta\gamma$ trackers are one-dimensional second and third order filters, respectively. They are equivalent to special cases of the one-dimensional Kalman filter. The general structure of this class of estimators is similar to that of the Kalman filter.

The standard $\alpha\beta\gamma$ filter provides smoothed and predicted data for target position, velocity (Doppler), and acceleration. It is a polynomial predictor/corrector linear recursive filter. This filter can reconstruct position, velocity, and constant acceleration based on position measurements. The $\alpha\beta\gamma$ filter can also provide a smoothed (corrected) estimate of the present position which can be used in guidance and fire control operations.

Notation:

For the purpose of the discussion presented in the remainder of this chapter, the following notation is adopted: $\underline{x}(n|m)$ represents the estimate during the n th sampling interval, using all data up to and including the m th sampling interval; y_n is the n th measured value; and e_n is the n th residual (error).

The fixed-gain filter equation is given by

$$\underline{x}(n|n) = \underline{\Phi}\underline{x}(n-1|n-1) + \underline{K}[y_n - \underline{G}\underline{\Phi}\underline{x}(n-1|n-1)] \quad (11.65)$$

Since the transition matrix assists in predicting the next state,

$$\underline{x}(n+1|n) = \underline{\Phi}\underline{x}(n|n) \quad (11.66)$$

Substituting Eq. (11.66) into Eq. (11.65) yields

$$\underline{x}(n|n) = \underline{x}(n|n-1) + \underline{K}[y_n - \underline{G}\underline{x}(n|n-1)] \quad (11.67)$$

The term enclosed within the brackets on the right hand side of Eq. (11.67) is often called the residual (error) which is the difference between the measured input and predicted output. Eq. (11.67) means that the estimate of $\underline{x}(n)$ is the sum of the prediction and the weighted residual. The term $\underline{G}\underline{x}(n|n-1)$ represents the prediction state. In the case of the $\alpha\beta\gamma$ estimator, \underline{G} is row vector given by

$$\underline{G} = [1 \ 0 \ 0 \ \dots] \quad (11.68)$$

and the gain matrix \underline{K} is given by

$$\underline{K} = \begin{bmatrix} \alpha \\ \beta/T \\ \gamma/T^2 \end{bmatrix} \quad (11.69)$$

One of the main objectives of a tracking filter is to decrease the effect of the noise observation on the measurement. For this purpose the noise covariance matrix is calculated. More precisely, the noise covariance matrix is

$$\underline{C}(n|n) = E\{(\underline{x}(n|n) - \underline{x}^t(n|n))(\underline{x}(n|n) - \underline{x}^t(n|n))^t\} \quad ; \quad y_n = v_n \quad (11.70)$$

where E indicates the expected value operator. Noise is assumed to be a zero mean random process with variance equal to σ_v^2 . Additionally, noise measurements are also assumed to be uncorrelated,

$$E\{v_n v_m\} = \begin{cases} \delta\sigma_v^2 & n = m \\ 0 & n \neq m \end{cases} \quad (11.71)$$

Eq. (11.65) can be written as

$$\underline{x}(n|n) = \underline{A}\underline{x}(n-1|n-1) + \underline{K}y_n \quad (11.72)$$

where

$$\underline{A} = (\underline{I} - \underline{K}\underline{G})\underline{\Phi} \quad (11.73)$$

Substituting Eqs. (11.72) and (11.73) into Eq. (11.70) yields

$$\underline{C}(n|n) = E\{(\underline{A}\underline{x}(n-1|n-1) + \underline{K}y_n)(\underline{A}\underline{x}(n-1|n-1) + \underline{K}y_n)^t\} \quad (11.74)$$

Expanding the right hand side of Eq. (11.74) and using Eq. (11.71) give

$$\underline{C}(n|n) = \underline{A}\underline{C}(n-1|n-1)\underline{A}^t + \underline{K}\underline{\sigma}_v^2\underline{K}^t \quad (11.75)$$

Under the steady state condition, Eq. (11.75) collapses to

$$\underline{C}(n|n) = \underline{A}\underline{C}\underline{A}^t + \underline{K}\underline{\sigma}_v^2\underline{K}^t \quad (11.76)$$

where \underline{C} is the steady state noise covariance matrix. In the steady state,

$$\underline{C}(n|n) = \underline{C}(n-1|n-1) = \underline{C} \quad \text{for any } n \quad (11.77)$$

Several criteria can be used to establish the performance of fixed-gain tracking filter. The most commonly used technique is to compute the Variance Reduction Ratio (VRR). The VRR is defined only when the input to the tracker is noise measurements. It follows that in the steady state case, the VRR is the steady state ratio of the output variance (auto-covariance) to the input measurement variance.

In order to determine the stability of the tracker under consideration, consider the Z-transform for Eq. (11.72),

$$\underline{x}(z) = \underline{A}z^{-1}\underline{x}(z) + \underline{K}y_n(z) \quad (11.78)$$

Rearranging Eq. (11.78) yields the following system transfer functions:

$$\underline{h}(z) = \frac{\underline{x}(z)}{y_n(z)} = (\underline{I} - \underline{A}z^{-1})^{-1}\underline{K} \quad (11.79)$$

where $(\underline{I} - \underline{A}z^{-1})$ is called the characteristic matrix. Note that the system transfer functions can exist only when the characteristic matrix is a non-singular matrix. Additionally, the system is stable if and only if the roots of the characteristic equation are within the unit circle in the z-plane,

$$|(\underline{I} - \underline{A}z^{-1})| = 0 \quad (11.80)$$

The filter's steady state errors can be determined with the help of Fig. 11.19. The error transfer function is

$$\underline{e}(z) = \frac{y(z)}{1 + \underline{h}(z)} \quad (11.81)$$

and by using Abel's theorem, the steady state error is

$$\underline{e}_\infty = \lim_{t \rightarrow \infty} \underline{e}(t) = \lim_{z \rightarrow 1} \left(\frac{z-1}{z} \right) \underline{e}(z) \quad (11.82)$$

Substituting Eq. (11.82) into (11.81) yields

$$e_{\infty} = \lim_{z \rightarrow 1} \frac{z-1}{z} \frac{\underline{y}(z)}{1 + \underline{h}(z)} \quad (11.83)$$

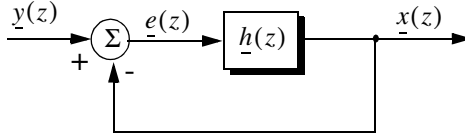


Figure 11.19. Steady state errors computation.

11.8.1. The $\alpha\beta$ Filter

The $\alpha\beta$ tracker produces, on the n th observation, smoothed estimates for position and velocity, and a predicted position for the $(n + 1)$ th observation. Fig. 11.20 shows an implementation of this filter. Note that the subscripts “ p ” and “ s ” are used to indicate, respectively, the predicted and smoothed values. The $\alpha\beta$ tracker can follow an input ramp (constant velocity) with no steady state errors. However, a steady state error will accumulate when constant acceleration is present in the input. Smoothing is done to reduce errors in the predicted position through adding a weighted difference between the measured and predicted values to the predicted position, as follows:

$$x_s(n) = x(n|n) = x_p(n) + \alpha(x_0(n) - x_p(n)) \quad (11.84)$$

$$\dot{x}_s(n) = \dot{x}'(n|n) = \dot{x}_s(n-1) + \frac{\beta}{T} (x_0(n) - x_p(n)) \quad (11.85)$$

x_0 is the position input samples. The predicted position is given by

$$x_p(n) = x_s(n|n-1) = x_s(n-1) + T\dot{x}_s(n-1) \quad (11.86)$$

The initialization process is defined by

$$\begin{aligned} x_s(1) &= x_p(2) = x_0(1) \\ \dot{x}_s(1) &= 0 \\ \dot{x}_s(2) &= \frac{x_0(2) - x_0(1)}{T} \end{aligned}$$

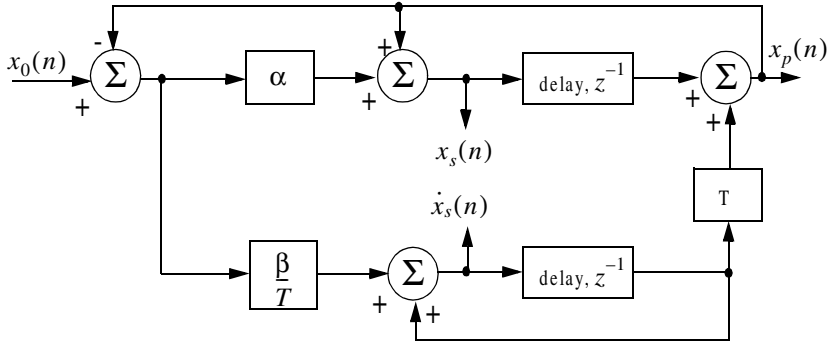


Figure 11.20. An implementation for an $\alpha\beta$ tracker.

A general form for the covariance matrix was developed in the previous section, and is given in Eq. (11.75). In general, a second order one-dimensional covariance matrix (in the context of the $\alpha\beta$ filter) can be written as

$$\underline{C}(n|n) = \begin{bmatrix} C_{xx} & C_{xx'} \\ C_{x'x} & C_{x'x'} \end{bmatrix} \quad (11.87)$$

where, in general, C_{xy} is

$$C_{xy} = E\{xy^t\} \quad (11.88)$$

By inspection, the $\alpha\beta$ filter has

$$\underline{A} = \begin{bmatrix} 1 - \alpha & (1 - \alpha)T \\ -\beta/T & (1 - \beta) \end{bmatrix} \quad (11.89)$$

$$\underline{K} = \begin{bmatrix} \alpha \\ \beta/T \end{bmatrix} \quad (11.90)$$

$$\underline{G} = \begin{bmatrix} 1 & 0 \end{bmatrix} \quad (11.91)$$

$$\underline{\Phi} = \begin{bmatrix} 1 & T \\ 0 & 1 \end{bmatrix} \quad (11.92)$$

Finally, by using Eqs. (11.89) through (11.92) in Eq. (11.72) yields the steady state noise covariance matrix,

$$\underline{C} = \frac{\sigma_v^2}{\alpha(4-2\alpha-\beta)} \begin{bmatrix} 2\alpha^2 - 3\alpha\beta + 2\beta & \frac{\beta(2\alpha-\beta)}{T} \\ \frac{\beta(2\alpha-\beta)}{T} & \frac{2\beta^2}{T^2} \end{bmatrix} \quad (11.93)$$

It follows that the position and velocity VRR ratios are, respectively, given by

$$(VRR)_x = C_{xx}/\sigma_v^2 = \frac{2\alpha^2 - 3\alpha\beta + 2\beta}{\alpha(4-2\alpha-\beta)} \quad (11.94)$$

$$(VRR)_v = C_{vv}/\sigma_v^2 = \frac{1}{T^2} \frac{2\beta^2}{\alpha(4-2\alpha-\beta)} \quad (11.95)$$

The stability of the $\alpha\beta$ filter is determined from its system transfer functions. For this purpose, compute the roots for Eq. (11.80) with \underline{A} from Eq. (11.89),

$$\left| \underline{I} - \underline{A}z^{-1} \right| = 1 - (2 - \alpha - \beta)z^{-1} + (1 - \alpha)z^{-2} = 0 \quad (11.96)$$

Solving Eq. (11.96) for z yields

$$z_{1,2} = 1 - \frac{\alpha + \beta}{2} \pm \frac{1}{2} \sqrt{(\alpha - \beta)^2 - 4\beta} \quad (11.97)$$

and in order to guarantee stability

$$|z_{1,2}| < 1 \quad (11.98)$$

Two cases are analyzed. First, $z_{1,2}$ are real. In this case (the details are left as an exercise),

$$\beta > 0 \quad ; \quad \alpha > -\beta \quad (11.99)$$

The second case is when the roots are complex; in this case we find

$$\alpha > 0 \quad (11.100)$$

The system transfer functions can be derived by using Eqs. (11.79), (11.89), and (11.90),

$$\begin{bmatrix} h_x(z) \\ h_v(z) \end{bmatrix} = \frac{1}{z^2 - z(2 - \alpha - \beta) + (1 - \alpha)} \begin{bmatrix} \alpha z \left(z - \frac{(\alpha - \beta)}{\alpha} \right) \\ \frac{\beta z(z - 1)}{T} \end{bmatrix} \quad (11.101)$$

Up to this point all relevant relations concerning the $\alpha\beta$ filter were made with no regard to how to choose the gain coefficients (α and β). Before considering the methodology of selecting these coefficients, consider the main objective behind using this filter. The purpose of the $\alpha\beta$ tracker can be described twofold:

1. *The tracker must reduce the measurement noise as much as possible.*
2. *The filter must be able to track maneuvering targets, with as little residual (tracking error) as possible.*

The reduction of measurement noise reduction is normally determined by the VRR ratios. However, the maneuverability performance of the filter depends heavily on the choice of the parameters α and β .

A special variation of the $\alpha\beta$ filter was developed by Benedict and Bordner¹, and is often referred to as the Benedict-Bordner filter. The main advantage of the Benedict-Bordner is reducing the transient errors associated with the $\alpha\beta$ tracker. This filter uses both the position and velocity VRR ratios as measure of performance. It computes the sum of the squared differences between the input (position) and the output when the input has a unit step velocity at time zero. Additionally, it computes the squared differences between the real velocity and the velocity output when the input is as described earlier. Both error differences are minimized when

$$\beta = \frac{\alpha^2}{2 - \alpha} \quad (11.102)$$

In this case, the position and velocity VRR ratios are, respectively, given by

$$(VRR)_x = \frac{\alpha(6 - 5\alpha)}{\alpha^2 - 8\alpha + 8} \quad (11.103)$$

$$(VRR)_v = \frac{2}{T^2} \frac{\alpha^3 / (2 - \alpha)}{\alpha^2 - 8\alpha + 8} \quad (11.104)$$

Another important sub-class of the $\alpha\beta$ tracker is the critically damped filter, often called the fading memory filter. In this case, the filter coefficients are chosen on the basis of a smoothing factor ξ , where $0 \leq \xi \leq 1$. The gain coefficients are given by

$$\alpha = 1 - \xi^2 \quad (11.105)$$

1. Benedict, T. R. and Bordner, G. W., Synthesis of an Optimal Set of Radar Track-While-Scan Smoothing Equations. *IRE Transaction on Automatic Control*, AC-7, July 1962, pp. 27-32.

$$\beta = (1 - \xi)^2 \tag{11.106}$$

Heavy smoothing means $\xi \rightarrow 1$ and little smoothing means $\xi \rightarrow 0$. The elements of the covariance matrix for a fading memory filter are

$$C_{xx} = \frac{1 - \xi}{(1 + \xi)^3} (1 + 4\xi + 5\xi^2) \sigma_v^2 \tag{11.107}$$

$$C_{\dot{x}\dot{x}} = C_{\dot{x}\dot{x}} = \frac{1}{T} \frac{1 - \xi}{(1 + \xi)^3} (1 + 2\xi + 3\xi^2) \sigma_v^2 \tag{11.108}$$

$$C_{\ddot{x}\ddot{x}} = \frac{2}{T^2} \frac{1 - \xi}{(1 + \xi)^3} (1 - \xi)^2 \sigma_v^2 \tag{11.109}$$

11.8.2. The $\alpha\beta\gamma$ Filter

The $\alpha\beta\gamma$ tracker produces, for the n th observation, smoothed estimates of position, velocity, and acceleration. It also produces predicted position and velocity for the $(n + 1)$ th observation. An implementation of the $\alpha\beta\gamma$ tracker is shown in Fig. 11.21.

The $\alpha\beta\gamma$ tracker will follow an input whose acceleration is constant with no steady state errors. Again, in order to reduce the error at the output of the tracker, a weighted difference between the measured and predicted values is used in estimating the smoothed position, velocity, and acceleration as follows:

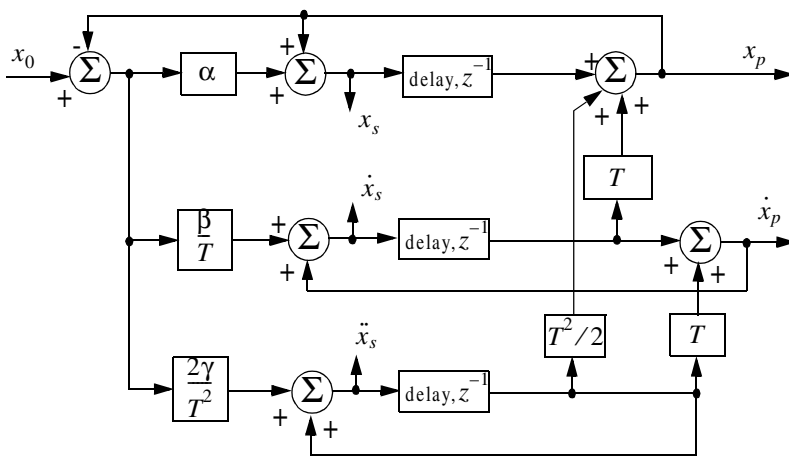


Figure 11.21. An implementation for an $\alpha\beta\gamma$ tracker.

$$x_s(n) = x_p(n) + \alpha(x_0(n) - x_p(n)) \quad (11.110)$$

$$\dot{x}_s(n) = \dot{x}_s(n-1) + T\ddot{x}_s(n-1) + \frac{\beta}{T} (x_0(n) - x_p(n)) \quad (11.111)$$

$$\ddot{x}_s(n) = \ddot{x}_s(n-1) + \frac{2\gamma}{T^2} (x_0(n) - x_p(n)) \quad (11.112)$$

$$x_p(n+1) = x_s(n) + T \dot{x}_s(n) + \frac{T^2}{2} \ddot{x}_s(n) \quad (11.113)$$

and the initialization process is

$$\begin{aligned} x_s(1) &= x_p(2) = x_0(1) \\ \dot{x}_s(1) &= \ddot{x}_s(1) = \ddot{x}_s(2) = 0 \\ \dot{x}_s(2) &= \frac{x_0(2) - x_0(1)}{T} \\ \ddot{x}_s(3) &= \frac{x_0(3) + x_0(1) - 2x_0(2)}{T^2} \end{aligned}$$

Using Eq. (11.63) the state transition matrix for the $\alpha\beta\gamma$ filter is

$$\underline{\Phi} = \begin{bmatrix} 1 & T & \frac{T^2}{2} \\ 0 & 1 & T \\ 0 & 0 & 1 \end{bmatrix} \quad (11.114)$$

The covariance matrix (which is symmetric) can be computed from Eq. (11.76). For this purpose, note that

$$\underline{K} = \begin{bmatrix} \alpha \\ \beta/T \\ \gamma/T^2 \end{bmatrix} \quad (11.115)$$

$$\underline{G} = \begin{bmatrix} 1 & 0 & 0 \end{bmatrix} \quad (11.116)$$

and

$$\underline{A} = (\underline{I} - \underline{K}\underline{G})\underline{\Phi} = \begin{bmatrix} 1 - \alpha & (1 - \alpha)T & (1 - \alpha)T^2/2 \\ -\beta/T & -\beta + 1 & (1 - \beta/2)T \\ -2\gamma/T^2 & -2\gamma/T & (1 - \gamma) \end{bmatrix} \quad (11.117)$$

Substituting Eq. (11.117) into (11.76) and collecting terms the VRR ratios are computed as

$$(VRR)_x = \frac{2\beta(2\alpha^2 + 2\beta - 3\alpha\beta) - \alpha\gamma(4 - 2\alpha - \beta)}{(4 - 2\alpha - \beta)(2\alpha\beta + \alpha\gamma - 2\gamma)} \quad (11.118)$$

$$(VRR)_x = \frac{4\beta^3 - 4\beta^2\gamma + 2\gamma^2(2 - \alpha)}{T^2(4 - 2\alpha - \beta)(2\alpha\beta + \alpha\gamma - 2\gamma)} \quad (11.119)$$

$$(VRR)_x = \frac{4\beta\gamma^2}{T^4(4 - 2\alpha - \beta)(2\alpha\beta + \alpha\gamma - 2\gamma)} \quad (11.120)$$

As in the case of any discrete time system, this filter will be stable if and only if all of its poles fall within the unit circle in the z -plane.

The $\alpha\beta\gamma$ characteristic equation is computed by setting

$$|I - Az^{-1}| = 0 \quad (11.121)$$

Substituting Eq. (11.117) into (11.121) and collecting terms yield the following characteristic function:

$$f(z) = z^3 + (-3\alpha + \beta + \gamma)z^2 + (3 - \beta - 2\alpha + \gamma)z - (1 - \alpha) \quad (11.122)$$

The $\alpha\beta\gamma$ becomes a Benedict-Bordner filter when

$$2\beta - \alpha\left(\alpha + \beta + \frac{\gamma}{2}\right) = 0 \quad (11.123)$$

Note that for $\gamma = 0$ Eq. (11.123) reduces to Eq. (11.102). For a critically damped filter the gain coefficients are

$$\alpha = 1 - \xi^3 \quad (11.124)$$

$$\beta = 1.5(1 - \xi^2)(1 - \xi) = 1.5(1 - \xi)^2(1 + \xi) \quad (11.125)$$

$$\gamma = (1 - \xi)^3 \quad (11.126)$$

Note that heavy smoothing takes place when $\xi \rightarrow 1$, while $\xi = 0$ means that no smoothing is present.

MATLAB Function “ghk_tracker.m”

The function “ghk_tracker.m”¹ implements the steady state $\alpha\beta\gamma$ filter. It is given in Listing 11.2 in Section 11.10. The syntax is as follows:

$$[residual, estimate] = ghk_tracker(X0, smooconf, inp, npts, T, nvar)$$

where

Symbol	Description	Status
<i>X0</i>	<i>initial state vector</i>	<i>input</i>
<i>smooconf</i>	<i>desired smoothing coefficient</i>	<i>input</i>
<i>inp</i>	<i>array of position measurements</i>	<i>input</i>
<i>npts</i>	<i>number of points in input position</i>	<i>input</i>
<i>T</i>	<i>sampling interval</i>	<i>input</i>
<i>nvar</i>	<i>desired noise variance</i>	<i>input</i>
<i>residual</i>	<i>array of position error (residual)</i>	<i>output</i>
<i>estimate</i>	<i>array of predicted position</i>	<i>output</i>

Note that “ghk_tracker.m” uses MATLAB’s function “normrnd.m” to generate zero mean Gaussian noise, which is part of MATLAB’s Statistics Toolbox. If this toolbox is not available to the user, then “ghk_tracker.m” function-call must be modified to

$$[residual, estimate] = ghk_tracker1(X0, smooconf, inp, npts, T)$$

which is also part of Listing 11.2. In this case, noise measurements are either to be considered unavailable or are part of the position input array.

To illustrate how to use the functions *ghk_tracker.m* and *ghk_tracker.m1*, consider the inputs shown in Figs. 11.22 and 11.23. Fig. 11.22 assumes an input with lazy maneuvering, while Fig. 11.23 assumes an aggressive maneuvering case. For this purpose, the program called “fig11_21.m” was written. It is given in Listing 11.3 in Section 11.10.

Figs. 11.24 and 11.25 show the residual error and predicted position corresponding (generated using the program “fig11_21.m”) to Fig. 11.22 for two cases: heavy smoothing and little smoothing with and without noise. The noise is white Gaussian with zero mean and variance of $\sigma_v^2 = 0.05$. Figs. 11.26 and 11.27 show the residual error and predicted position corresponding (generated using the program “fig11_20.m”) to Fig. 11.23 with and without noise.

1. This function was written by Mr. Edward Shamsi of COLSA Corporation in Huntsville, AL.

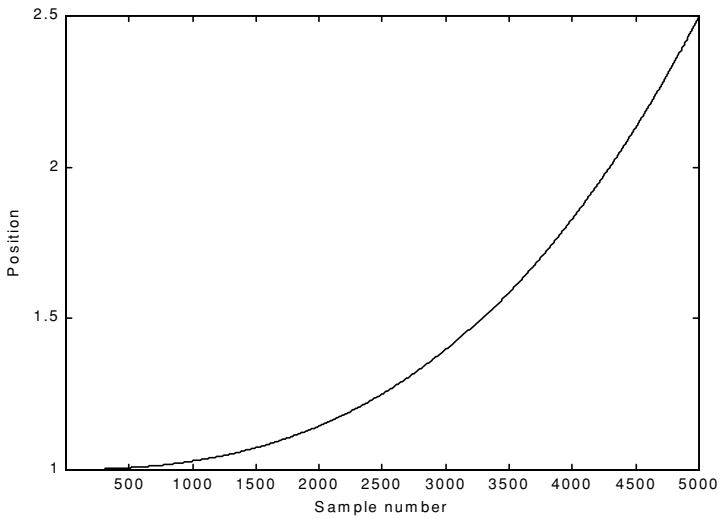


Figure 11.22. Position (truth-data); lazy maneuvering.

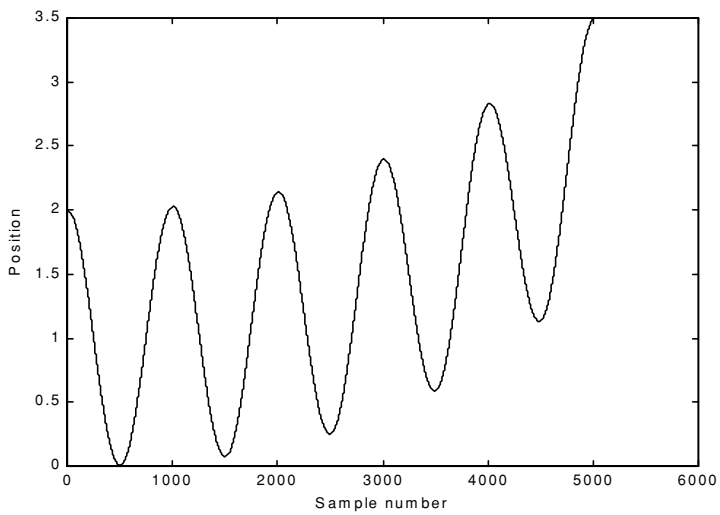


Figure 11.23. Position (truth-data); aggressive maneuvering.

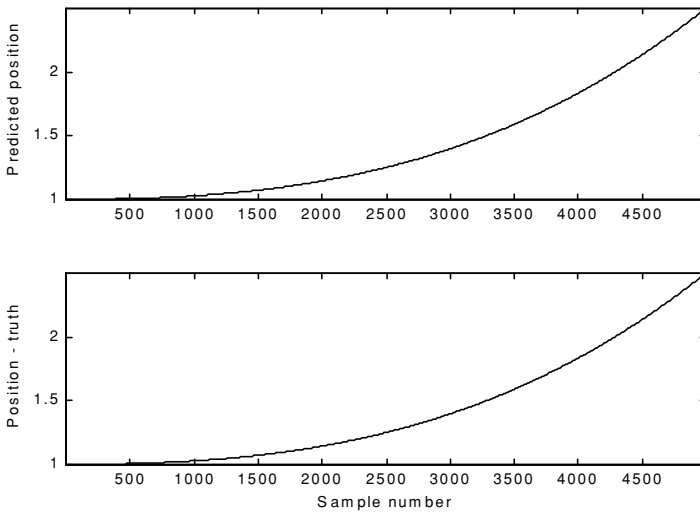


Figure 11.24a-1. Predicted and true position. $\xi = 0.1$ (i.e., large gain coefficients). No noise present.

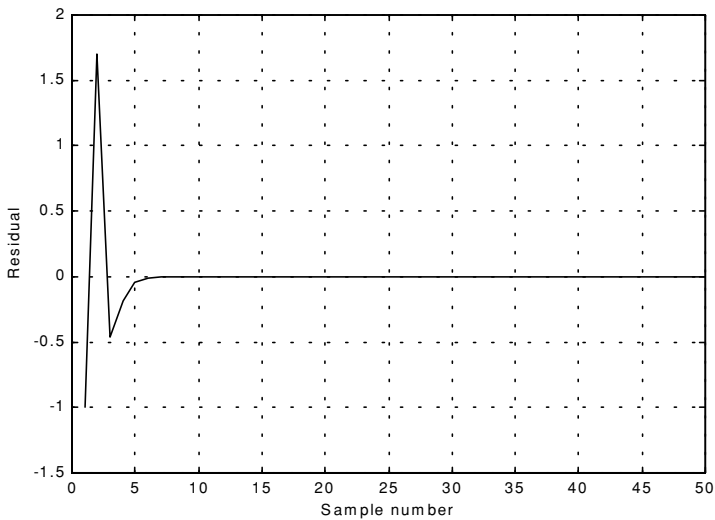


Figure 11.24a-2. Position residual (error). Large gain coefficients. No noise. The error settles to zero fairly quickly.

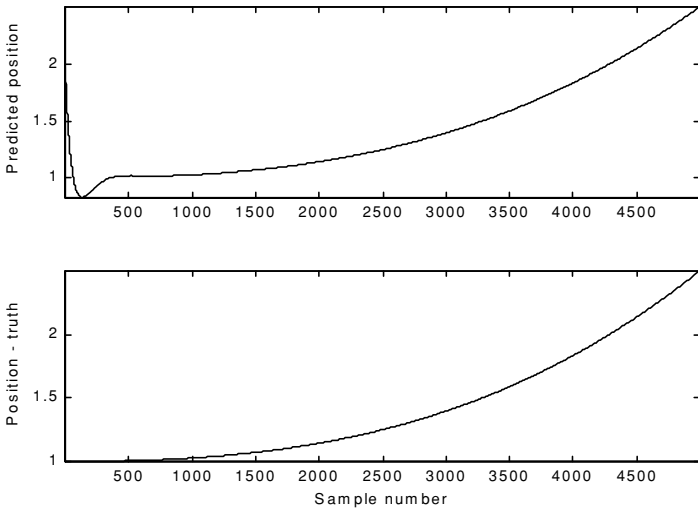


Figure 11.24b-1. Predicted and true position. $\xi = 0.9$ (i.e., small gain coefficients). No noise present.

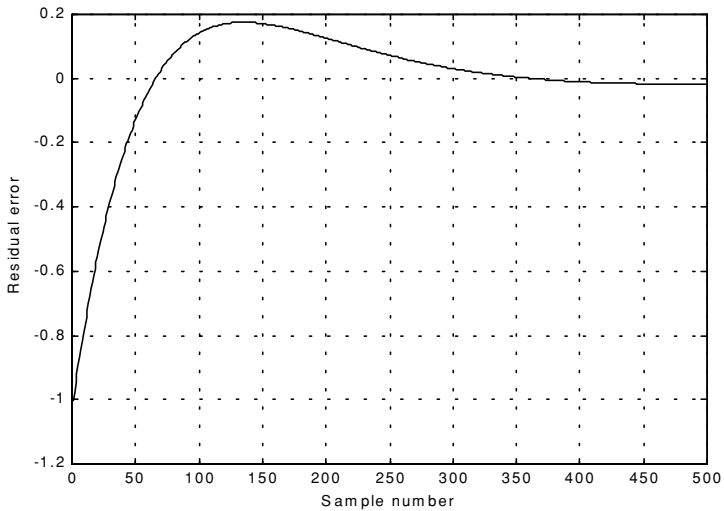


Figure 11.24b-2. Position residual (error). Small gain coefficients. No noise. It takes the filter longer time for the error to settle down.

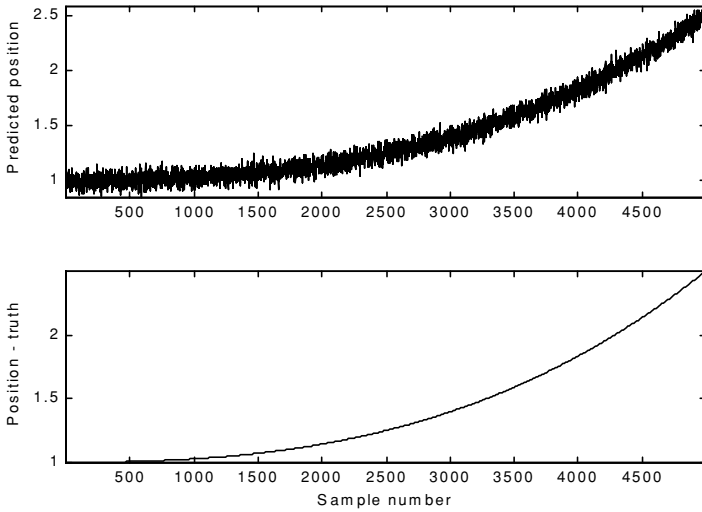


Figure 11.25a-1. Predicted and true position. $\xi = 0.1$ (i.e., large gain coefficients). Noise is present.

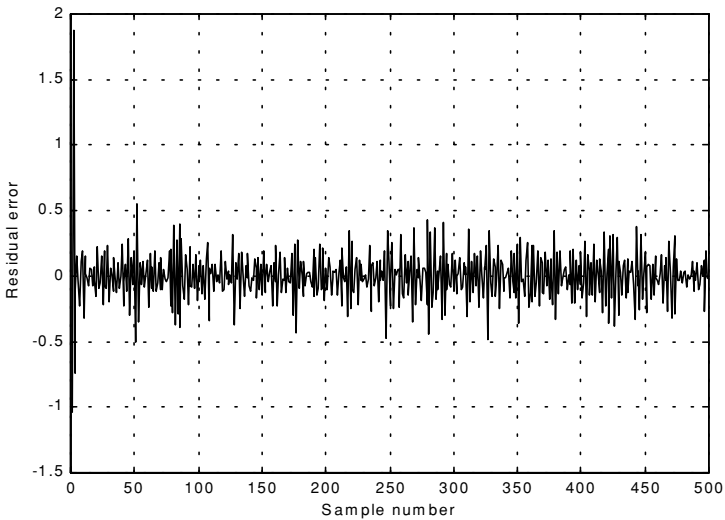


Figure 11.25a-2. Position residual (error). Large gain coefficients. Noise present. The error settles down quickly. The variation is due to noise.

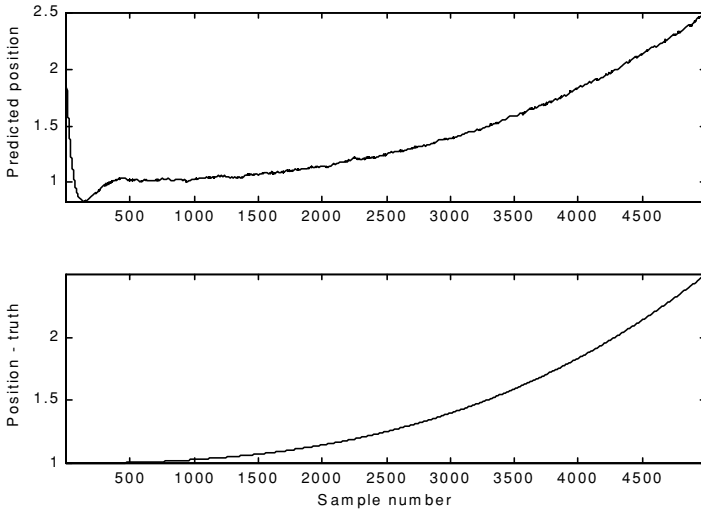


Figure 11.25b-1. Predicted and true position. $\xi = 0.9$ (i.e., small gain coefficients). Noise is present.

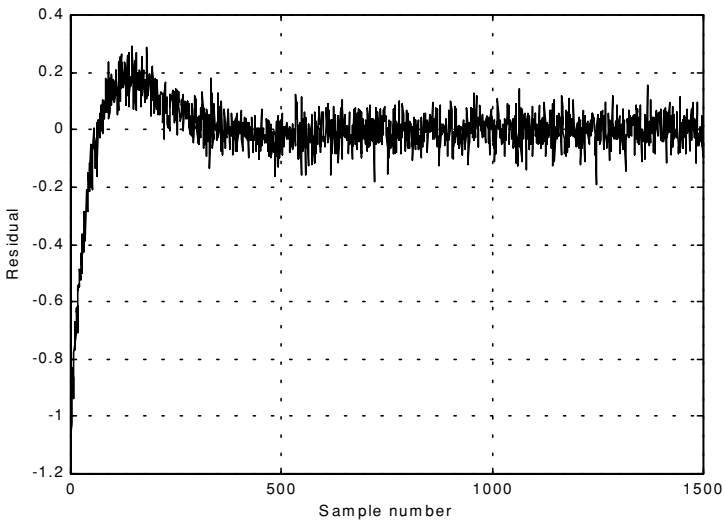


Figure 11.25b-2. Position residual (error). Small gain coefficients. Noise present. The error requires more time before settling down. The variation is due to noise.

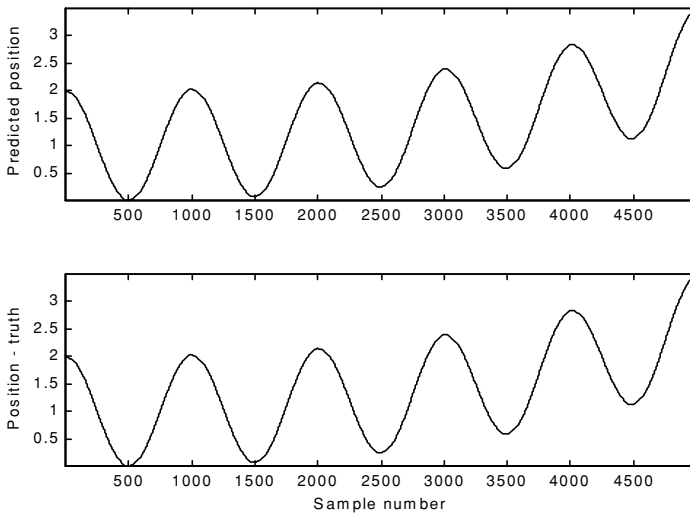


Figure 11.26a. Predicted and true position. $\xi = 0.1$ (i.e., large gain coefficients). Noise is present.

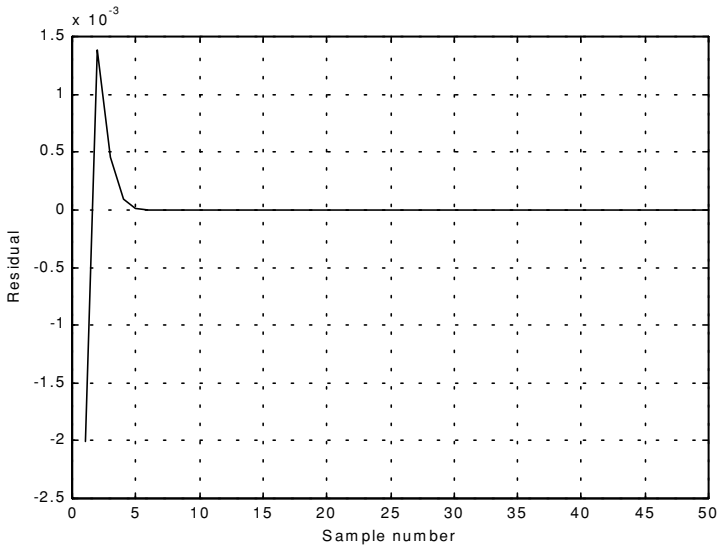


Figure 11.26b. Position residual (error). Large gain coefficients. No noise. The error settles down quickly.

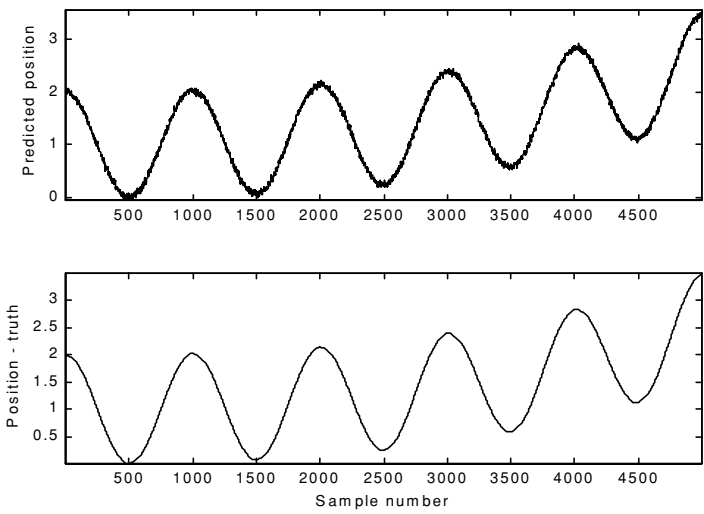


Figure 11.27a. Predicted and true position. $\xi = 0.8$ (i.e., small gain coefficients). Noise is present.

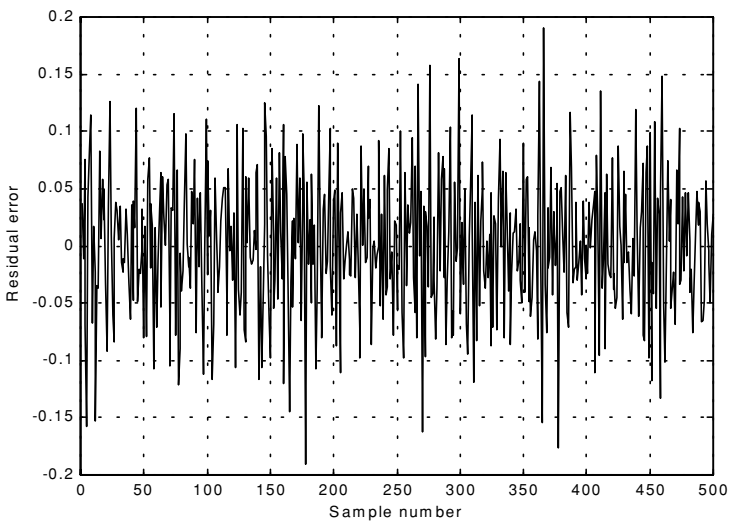


Figure 11.27b. Position residual (error). Small gain coefficients. Noise present. The error stays fairly large; however, its average is around zero. The variation is due to noise.

11.9. The Kalman Filter

The Kalman filter is a linear estimator that minimizes the mean squared error as long as the target dynamics are modeled accurately. All other recursive filters, such as the $\alpha\beta\gamma$ and the Benedict-Bordner filters, are special cases of the general solution provided by the Kalman filter for the mean squared estimation problem. Additionally, the Kalman filter has the following advantages:

1. *The gain coefficients are computed dynamically. This means that the same filter can be used for a variety of maneuvering target environments.*
2. *The Kalman filter gain computation adapts to varying detection histories, including missed detections.*
3. *The Kalman filter provides an accurate measure of the covariance matrix. This allows for better implementation of the gating and association processes.*
4. *The Kalman filter makes it possible to partially compensate for the effects of miss-correlation and miss-association.*

Many derivations of the Kalman filter exist in the literature; only results are provided in this chapter. Fig. 11.28 shows a block diagram for the Kalman filter. The Kalman filter equations can be deduced from Fig. 11.28. The filtering equation is

$$\underline{x}(n|n) = \underline{x}_s(n) = \underline{x}(n|n-1) + K(n)[\underline{y}(n) - \underline{G}\underline{x}(n|n-1)] \quad (11.127)$$

The measurement vector is

$$\underline{y}(n) = \underline{G}\underline{x}(n) + \underline{v}(n) \quad (11.128)$$

where $\underline{v}(n)$ is zero mean, white Gaussian noise with covariance \mathfrak{R}_c ,

$$\mathfrak{R}_c = E\{\underline{v}(n) \underline{v}^t(n)\} \quad (11.129)$$

The gain (weights) vector is dynamically computed as

$$\underline{K}(n) = \underline{P}(n|n-1)\underline{G}^t[\underline{G}\underline{P}(n|n-1)\underline{G}^t + \mathfrak{R}_c]^{-1} \quad (11.130)$$

where the measurement noise matrix \underline{P} represents the predictor covariance matrix, and is equal to

$$\underline{P}(n+1|n) = E\{\underline{x}_s(n+1)\underline{x}_s^*(n)\} = \underline{\Phi}\underline{P}(n|n)\underline{\Phi}^t + \underline{Q} \quad (11.131)$$

where \underline{Q} is the covariance matrix for the input \underline{u} ,

$$\underline{Q} = E\{\underline{u}(n) \underline{u}'(n)\} \quad (11.132)$$

The corrector equation (covariance of the smoothed estimate) is

$$\underline{P}(n|n) = [\underline{I} - \underline{K}(n)\underline{G}]\underline{P}(n|n-1) \quad (11.133)$$

Finally, the predictor equation is

$$\underline{x}(n+1|n) = \underline{\Phi}\underline{x}(n|n) \quad (11.134)$$

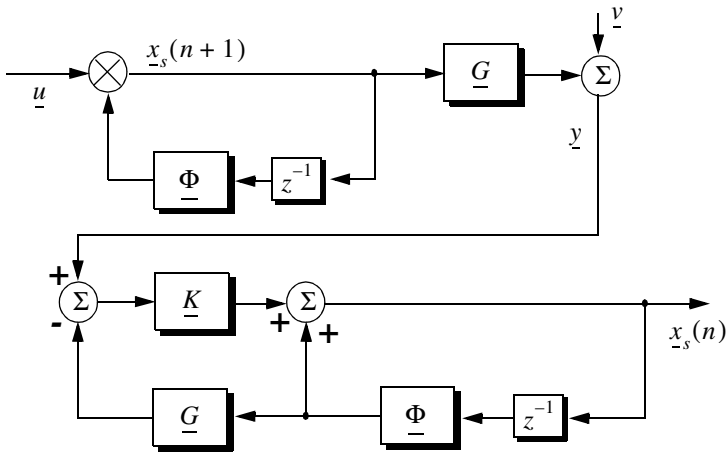


Figure 11.28. Structure of the Kalman filter.

11.9.1. The Singer $\alpha\beta\gamma$ -Kalman Filter

The Singer¹ filter is a special case of the Kalman where the filter is governed by a specified target dynamic model whose acceleration is a random process with autocorrelation function given by

$$E\{\ddot{x}(t) \ddot{x}(t+t_1)\} = \sigma_a^2 e^{-\frac{|t_1|}{\tau_m}} \quad (11.135)$$

1. Singer, R. A., Estimating Optimal Tracking Filter Performance for Manned Maneuvering Targets, *IEEE Transaction on aerospace and Electronics*, AES-5, July, 1970, pp. 473-483.

where τ_m is the correlation time of the acceleration due to target maneuver or atmospheric turbulence. The correlation time τ_m may vary from as low as 10 seconds for aggressive maneuvering to as large as 60 seconds for lazy maneuver cases.

Singer defined the random target acceleration model by a first order Markov process given by

$$\ddot{x}(n+1) = \rho_m \ddot{x}(n) + \sqrt{1-\rho_m^2} \sigma_m w(n) \quad (11.136)$$

where $w(n)$ is a zero mean, Gaussian random variable with unity variance, σ_m is the maneuver standard deviation, and the maneuvering correlation coefficient ρ_m is given by

$$\rho_m = e^{-\frac{T}{\tau_m}} \quad (11.137)$$

The continuous time domain system that corresponds to these conditions is as the Wiener-Kolmogorov whitening filter which is defined by the differential equation

$$\frac{d}{dt}v(t) = -\beta_m v(t) + w(t) \quad (11.138)$$

where β_m is equal to $1/\tau_m$. The maneuvering variance using Singer's model is given by

$$\sigma_m^2 = \frac{A_{max}^2}{3} [1 + 4P_{max} - P_0] \quad (11.139)$$

A_{max} is the maximum target acceleration with probability P_{max} and the term P_0 defines the probability that the target has no acceleration.

The transition matrix that corresponds to the Singer filter is given by

$$\underline{\Phi} = \begin{bmatrix} 1 & T & \frac{1}{\beta_m^2}(-1 + \beta_m T + \rho_m) \\ 0 & 1 & \frac{1}{\beta_m}(1 - \rho_m) \\ 0 & 0 & \rho_m \end{bmatrix} \quad (11.140)$$

Note that when $T\beta_m = T/\tau_m$ is small (the target has constant acceleration), then Eq. (11.140) reduces to Eq. (11.114). Typically, the sampling interval T is much less than the maneuver time constant τ_m ; hence, Eq. (11.140) can be accurately replaced by its second order approximation. More precisely,

$$\underline{\Phi} = \begin{bmatrix} 1 & T & T^2/2 \\ 0 & 1 & T(1 - T/2\tau_m) \\ 0 & 0 & \rho_m \end{bmatrix} \quad (11.141)$$

The covariance matrix was derived by Singer, and it is equal to

$$\underline{C} = \frac{2\sigma_m^2}{\tau_m} \begin{bmatrix} C_{11} & C_{12} & C_{13} \\ C_{21} & C_{22} & C_{23} \\ C_{31} & C_{32} & C_{33} \end{bmatrix} \quad (11.142)$$

where

$$C_{11} = \sigma_x^2 = \frac{1}{2\beta_m^5} \left[1 - e^{-2\beta_m T} + 2\beta_m T + \frac{2\beta_m^3 T^3}{3} - 2\beta_m^2 T^2 - 4\beta_m T e^{-\beta_m T} \right] \quad (11.143)$$

$$C_{12} = C_{21} = \frac{1}{2\beta_m^4} \left[e^{-2\beta_m T} + 1 - 2e^{-\beta_m T} + 2\beta_m T e^{-\beta_m T} - 2\beta_m T + \beta_m^2 T^2 \right] \quad (11.144)$$

$$C_{13} = C_{31} = \frac{1}{2\beta_m^3} \left[1 - e^{-2\beta_m T} - 2\beta_m T e^{-\beta_m T} \right] \quad (11.145)$$

$$C_{22} = \frac{1}{2\beta_m^3} \left[4e^{-\beta_m T} - 3 - e^{-2\beta_m T} + 2\beta_m T \right] \quad (11.146)$$

$$C_{23} = C_{32} = \frac{1}{2\beta_m^2} \left[e^{-2\beta_m T} + 1 - 2e^{-\beta_m T} \right] \quad (11.147)$$

$$C_{33} = \frac{1}{2\beta_m} \left[1 - e^{-2\beta_m T} \right] \quad (11.148)$$

Two limiting cases are of interest:

1. *The short sampling interval case* ($T \ll \tau_m$),

$$\lim_{\beta_m T \rightarrow 0} \underline{C} = \frac{2\sigma_m^2}{\tau_m} \begin{bmatrix} T^5/20 & T^4/8 & T^3/6 \\ T^4/8 & T^3/3 & T^2/2 \\ T^3/6 & T^2/2 & T \end{bmatrix} \quad (11.149)$$

and the state transition matrix is computed from Eq. (11.141) as

$$\lim_{\beta_m T \rightarrow 0} \underline{\Phi} = \begin{bmatrix} 1 & T & T^2/2 \\ 0 & 1 & T \\ 0 & 0 & 1 \end{bmatrix} \quad (11.150)$$

which is the same as the case for the $\alpha\beta\gamma$ filter (constant acceleration).

2. *The long sampling interval ($T \gg \tau_m$). This condition represents the case when acceleration is a white noise process. The corresponding covariance and transition matrices are, respectively, given by*

$$\lim_{\beta_m T \rightarrow \infty} \underline{C} = \sigma_m^2 \begin{bmatrix} \frac{2T^3\tau_m}{3} & T^2\tau_m & \tau_m^2 \\ T^2\tau_m & 2T\tau_m & \tau_m \\ \tau_m^2 & \tau_m & 1 \end{bmatrix} \quad (11.151)$$

$$\lim_{\beta_m T \rightarrow \infty} \underline{\Phi} = \begin{bmatrix} 1 & T & T\tau_m \\ 0 & 1 & \tau_m \\ 0 & 0 & 0 \end{bmatrix} \quad (11.152)$$

Note that under the condition that $T \gg \tau_m$, the cross correlation terms C_{13} and C_{23} become very small. It follows that estimates of acceleration are no longer available, and thus a two state filter model can be used to replace the three state model. In this case,

$$\underline{C} = 2\sigma_m^2\tau_m \begin{bmatrix} T^3/3 & T^2/2 \\ T^2/2 & T \end{bmatrix} \quad (11.153)$$

$$\underline{\Phi} = \begin{bmatrix} 1 & T \\ 0 & 1 \end{bmatrix} \quad (11.154)$$

11.9.2. Relationship between Kalman and $\alpha\beta\gamma$ Filters

The relationship between the Kalman filter and the $\alpha\beta\gamma$ filters can be easily obtained by using the appropriate state transition matrix $\underline{\Phi}$, and gain vector \underline{K} corresponding to the $\alpha\beta\gamma$ in Eq. (11.127). Thus,

$$\begin{bmatrix} x(n|n) \\ \dot{x}(n|n) \\ \ddot{x}(n|n) \end{bmatrix} = \begin{bmatrix} x(n|n-1) \\ \dot{x}(n|n-1) \\ \ddot{x}(n|n-1) \end{bmatrix} + \begin{bmatrix} k_1(n) \\ k_2(n) \\ k_3(n) \end{bmatrix} [x_0(n) - x(n|n-1)] \quad (11.155)$$

with (see Fig. 11.21)

$$x(n|n-1) = x_s(n-1) + T \dot{x}_s(n-1) + \frac{T^2}{2} \ddot{x}_s(n-1) \quad (11.156)$$

$$\dot{x}(n|n-1) = \dot{x}_s(n-1) + T \ddot{x}_s(n-1) \quad (11.157)$$

$$\ddot{x}(n|n-1) = \ddot{x}_s(n-1) \quad (11.158)$$

Comparing the previous three equations with the $\alpha\beta\gamma$ filter equations yields,

$$\begin{bmatrix} \alpha \\ \beta \\ T \\ \gamma \\ T^2 \end{bmatrix} = \begin{bmatrix} k_1 \\ k_2 \\ k_3 \end{bmatrix} \quad (11.159)$$

Additionally, the covariance matrix elements are related to the gain coefficients by

$$\begin{bmatrix} k_1 \\ k_2 \\ k_3 \end{bmatrix} = \frac{1}{C_{11} + \sigma_v^2} \begin{bmatrix} C_{11} \\ C_{12} \\ C_{13} \end{bmatrix} \quad (11.160)$$

Eq. (11.160) indicates that the first gain coefficient depends on the estimation error variance to the total residual variance, while the other two gain coefficients are calculated through the covariances between the second and third states and the first observed state.

MATLAB Function “kalman_filter.m”

The function “kalman_filter.m”¹ implements the Singer- $\alpha\beta\gamma$ Kalman filter. It is given in Listing 11.4 in Section 11.10. The syntax is as follows:

$$[residual, estimate] = kalman_filter(npts, T, X0, inp, R, nvar)$$

1. This function was written by Mr. Edward Shamsi of COLSA Corporation in Huntsville, AL.

where

Symbol	Description	Status
$npts$	number of points in input position	input
T	sampling interval	input
$X0$	initial state vector	input
inp	input array	input
R	noise variance see Eq. (11-129)	input
$nvar$	desired state noise variance	input
$residual$	array of position error (residual)	output
$estimate$	array of predicted position	output

Note that “*kalman_filter.m*” uses MATLAB’s function “*normrnd.m*” to generate zero mean Gaussian noise, which is part of MATLAB’s Statistics Toolbox.

To illustrate how to use the functions “*kalman_filter.m*”, consider the inputs shown in Figs. 11.22 and 11.23. Figs. 11.29 and 11.30 show the residual error and predicted position corresponding to Figs. 11.22 and 11.23. These plots can be reproduced using the program “*fig11_28.m*” given in Listing 11.5 in Section 11.10.

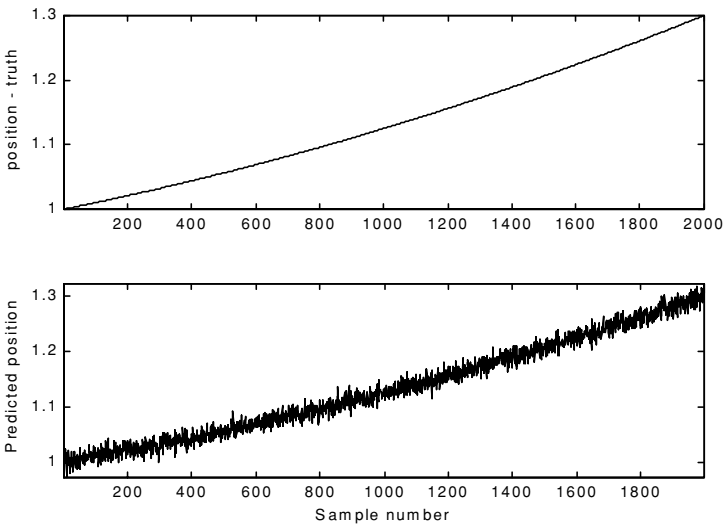


Figure 11.29a. True and predicted positions. Lazy maneuvering. Plot produced using the function “*kalman_filter.m*”.

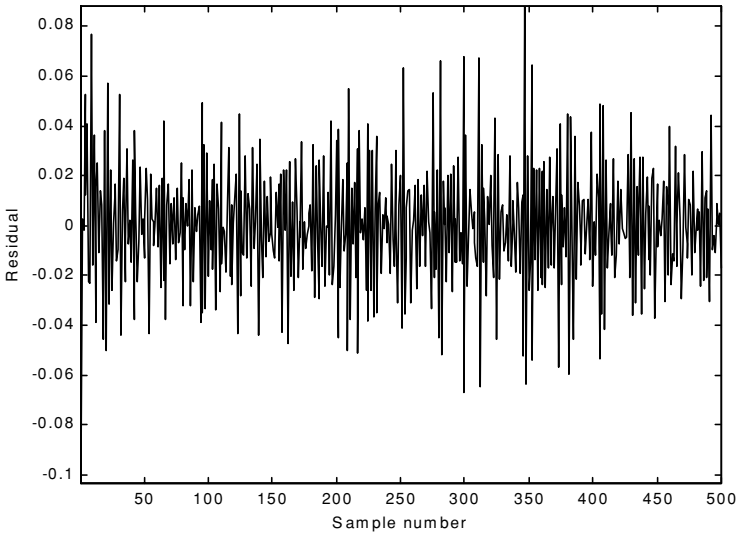


Figure 11.29b. Residual corresponding to [Fig. 11.29a](#).

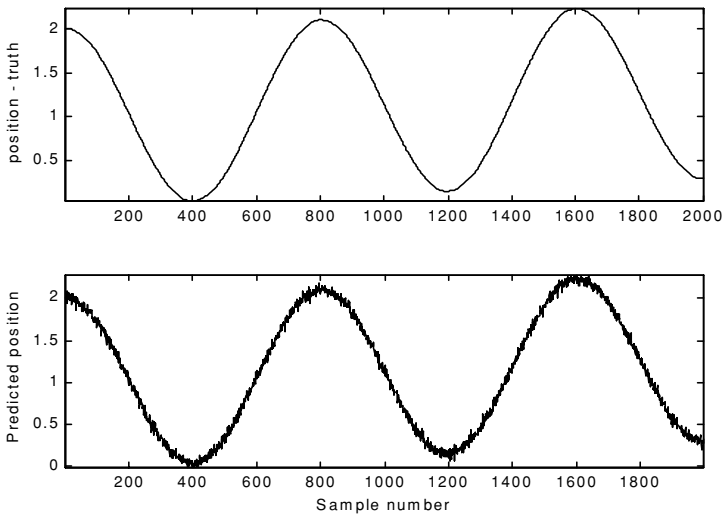


Figure 11.30a. True and predicted positions. Aggressive maneuvering. Plot produced using the function “*kalman_filter.m*”.

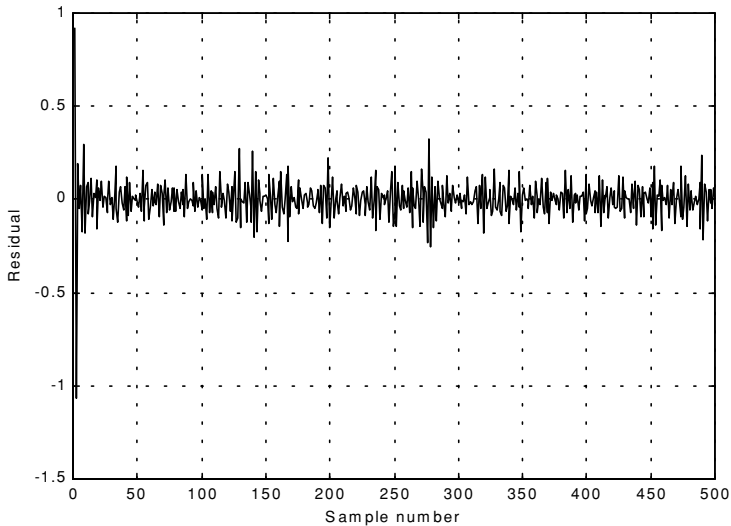


Figure 11.30b. Residual corresponding to Fig. 11.30a.

11.10. MATLAB Programs and Functions

This section contains listings of all MATLAB programs and functions used in this chapter. Users are encouraged to rerun these codes with different inputs in order to enhance their understanding of the theory.

Listing 11.1. MATLAB Function “mono_pulse.m”

```
function mono_pulse(phi0)
eps = 0.0000001;
angle = -pi:0.01:pi;
y1 = sinc(angle + phi0);
y2 = sinc((angle - phi0));
ysum = y1 + y2;
ydif = -y1 + y2;
figure (1)
plot (angle,y1,'k',angle,y2,'k');
grid;
xlabel ('Angle - radians')
ylabel ('Squinted patterns')
figure (2)
plot(angle,ysum,'k');
```

```

grid;
xlabel ('Angle - radians')
ylabel ('Sum pattern')
figure (3)
plot (angle,ydif,'k');
grid;
xlabel ('Angle - radians')
ylabel ('Difference pattern')
angle = -pi/4:0.01:pi/4;
y1 = sinc(angle + phi0);
y2 = sinc((angle - phi0));
ydif = -y1 + y2;
ysum = y1 + y2;
dovrs = ydif ./ ysum;
figure(4)
plot (angle,dovrs,'k');
grid;
xlabel ('Angle - radians')
ylabel ('voltage gain')

```

Listing 11.2. MATLAB Function “ghk_tracker.m”

```

function [residual, estimate] = ghk_tracker (X0, smoocof, inp, npts, T, nvar)
rn = 1.;
% read the initial estimate for the state vector
X = X0;
theta = smoocof;
%compute values for alpha, beta, gamma
w1 = 1. - (theta^3);
w2 = 1.5 * (1. + theta) * ((1. - theta)^2) / T;
w3 = ((1. - theta)^3) / (T^2);
% setup the transition matrix PHI
PHI = [1. T (T^2)/2.; 0. 1. T; 0. 0. 1.];
while rn < npts ;
    %use the transition matrix to predict the next state
    XN = PHI * X;
    error = (inp(rn) + normrnd(0,nvar)) - XN(1);
    residual(rn) = error;
    tmp1 = w1 * error;
    tmp2 = w2 * error;
    tmp3 = w3 * error;
    % compute the next state
    X(1) = XN(1) + tmp1;
    X(2) = XN(2) + tmp2;
    X(3) = XN(3) + tmp3;
    estimate(rn) = X(1);
    rn = rn + 1.;
end

```

```
return
```

MATLAB Function “ghk_tracker1.m”

```
function [residual, estimate] = ghk_tracker1 (X0, smoocof, inp, npts, T)
rn = 1.;
% read the initial estimate for the state vector
X = X0;
theta = smoocof;
%compute values for alpha, beta, gamma
w1 = 1. - (theta^3);
w2 = 1.5 * (1. + theta) * ((1. - theta)^2) / T;
w3 = ((1. - theta)^3) / (T^2);
% setup the transition matrix PHI
PHI = [1. T (T^2)/2.; 0. 1. T; 0. 0. 1.];
while rn < npts ;
    %use the transition matrix to predict the next state
    XN = PHI * X;
    error = inp(rn) - XN(1);
    residual(rn) = error;
    tmp1 = w1 * error;
    tmp2 = w2 * error;
    tmp3 = w3 * error;
    % compute the next state
    X(1) = XN(1) + tmp1;
    X(2) = XN(2) + tmp2;
    X(3) = XN(3) + tmp3;
    estimate(rn) = X(1);
    rn = rn + 1.;
end
return
```

Listing 11.3. MATLAB Program “fig11_21.m”

```
clear all
eps = 0.0000001;
npts = 5000;
del = 1./ 5000.;
t = 0. : del : 1.;
% generate input sequence
inp = 1. + t.^3 + .5 .*t.^2 + cos(2.*pi*10 .* t) ;
% read the initial estimate for the state vector
X0 = [2,.,1,.,01]';
% this is the update interval in seconds
T = 100. * del;
% this is the value of the smoothing coefficient
xi = .91;
[residual, estimate] = ghk_tracker (X0, xi, inp, npts, T, .01);
```

```

figure(1)
plot (residual(1:500))
xlabel ('Sample number')
ylabel ('Residual error')
grid
figure(2)
NN = 4999.;
n = 1:NN;
plot (n,estimate(1:NN),'b',n,inp(1:NN),'r')
xlabel ('Sample number')
ylabel ('Position')
legend ('Estimated','Input')

```

Listing 11.4. MATLAB Function “kalman_filter.m”

```

function [residual, estimate] = kalman_filter(npts, T, X0, inp, R, nvar)
N = npts;
rn=1;
% read the initial estimate for the state vector
X = X0;
% it is assumed that the measurmeny vector H=[1,0,0]
% this is the state noise variance
VAR = nvar;
% setup the initial value for the predication covariance.
S = [1. 1. 1.; 1. 1. 1.; 1. 1. 1.];
% setup the transition matrix PHI
PHI = [1. T (T^2)/2.; 0. 1. T; 0. 0. 1.];
% setup the state noise covariance matrix
Q(1,1) = (VAR * (T^5)) / 20.;
Q(1,2) = (VAR * (T^4)) / 8.;
Q(1,3) = (VAR * (T^3)) / 6.;
Q(2,1) = Q(1,2);
Q(2,2) = (VAR * (T^3)) / 3.;
Q(2,3) = (VAR * (T^2)) / 2.;
Q(3,1) = Q(1,3);
Q(3,2) = Q(2,3);
Q(3,3) = VAR * T;
while rn < N ;
    %use the transition matrix to predict the next state
    XN = PHI * X;
    % Perform error covariance extrapolation
    S = PHI * S * PHI' + Q;
    % compute the Kalman gains
    ak(1) = S(1,1) / (S(1,1) + R);
    ak(2) = S(1,2) / (S(1,1) + R);
    ak(3) = S(1,3) / (S(1,1) + R);
    %perform state estimate update:
    error = inp(rn) + normrnd(0,R) - XN(1);

```

```

residual(rn) = error;
tmp1 = ak(1) * error;
tmp2 = ak(2) * error;
tmp3 = ak(3) * error;
X(1) = XN(1) + tmp1;
X(2) = XN(2) + tmp2;
X(3) = XN(3) + tmp3;
estimate(rn) = X(1);
% update the error covariance
S(1,1) = S(1,1) * (1. -ak(1));
S(1,2) = S(1,2) * (1. -ak(1));
S(1,3) = S(1,3) * (1. -ak(1));
S(2,1) = S(1,2);
S(2,2) = -ak(2) * S(1,2) + S(2,2);
S(2,3) = -ak(2) * S(1,3) + S(2,3);
S(3,1) = S(1,3);
S(3,3) = -ak(3) * S(1,3) + S(3,3);
rn = rn + 1.;
end

```

Listing 11.5. MATLAB Program “fig11_28.m”

```

clear all
npts = 2000;
del = 1/2000;
t = 0:del:1;
inp = (1+.2 .* t + .1 .*t.^2) + cos(2. * pi * 2.5 .* t);
X0 = [1,.,.01]';
% it is assumed that the measurmeny vector H=[1,0,0]
% this is the update interval in seconds
T = 1.;
% enter the measurement noise variance
R = .035;
% this is the state noise variance
nvar = .5;
[residual, estimate] = kalman_filter(npts, T, X0, inp, R, nvar);
figure(1)
plot(residual)
xlabel ('Sample number')
ylabel ('Residual')
figure(2)
subplot(2,1,1)
plot(inp)
axis tight
ylabel ('position - truth')
subplot(2,1,2)
plot(estimate)
axis tight

```


xlabel ('Sample number')
ylabel ('Predicted position')

Problems

11.1. Show that in order to be able to quickly achieve changing the beam position the error signal needs to be a linear function of the deviation angle.

11.2. Prepare a short report on the vulnerability of conical scan to amplitude modulation jamming. In particular consider the self-protecting technique called "Gain Inversion."

11.3. Consider a conical scan radar. The pulse repetition interval is $10\mu s$. Calculate the scan rate so that at least ten pulses are emitted within one scan.

11.4. Consider a conical scan antenna whose rotation around the tracking axis is completed in 4 seconds. If during this time 20 pulses are emitted and received, calculate the radar PRF and the unambiguous range.

11.5. Reproduce Fig. 11.11 for $\varphi_0 = 0.05, 0.1, 0.15$ radians.

11.6. Reproduce Fig. 11.13 for the squint angles defined in the previous problem.

11.7. Derive Eq. (11.33) and Eq. (11.34).

11.8. Consider a monopulse radar where the input signal is comprised of both target return and additive white Gaussian noise. Develop an expression for the complex ratio Σ/Δ .

11.9. Consider the sum and difference signals defined in Eqs. (11.7) and (11.8). What is the squint angle φ_0 that maximizes $\Sigma(\varphi = 0)$?

11.10. A certain system is defined by the following difference equation:

$$y(n) + 4y(n-1) + 2y(n-2) = w(n)$$

Find the solution to this system for $n > 0$ and $w = \delta$.

11.11. Prove the state transition matrix properties (i.e., Eqs. (11.30) through (11.36)).

11.12. Suppose that the state equations for a certain discrete time LTI system are

$$\begin{bmatrix} x_1(n+1) \\ x_2(n+1) \end{bmatrix} = \begin{bmatrix} 0 & 1 \\ -2 & -3 \end{bmatrix} \begin{bmatrix} x_1(n) \\ x_2(n) \end{bmatrix} + \begin{bmatrix} 0 \\ 1 \end{bmatrix} w(n)$$

If $y(0) = y(1) = 1$, find $y(n)$ when the input is a step function.

11.13. Derive Eq. (11.55).

11.14. Derive Eq. (11.75).

11.15. Using Eq. (11.83), compute a general expression (in terms of the transfer function) for the steady state errors when the input sequence is:

$$u1 = \{0, 1, 1, 1, 1, \dots\}$$

$$u2 = \{0, 1, 2, 3, \dots\}$$

$$u3 = \{0, 1^2, 2^2, 3^2, \dots\}$$

$$u4 = \{0, 1^3, 2^3, 3^3, \dots\}$$

11.16. Verify the results in Eqs. (11.99) and (11.100).

11.17. Develop an expression for the steady state error transfer function for an $\alpha\beta$ tracker.

11.18. Using the result of the previous problem and Eq. (11.83), compute the steady-state errors for the $\alpha\beta$ tracker with the inputs defined in Problem 11.13.

11.19. Design a critically damped $\alpha\beta$, when the measurement noise variance associated with position is $\sigma_v^2 = 50m$ and when the desired standard deviation of the filter prediction error is $5.5m$.

11.20. Derive Eqs. (11.118) through (11.120).

11.21. Derive Eq. (11.122).

11.22. Consider a $\alpha\beta\gamma$ filter. We can define six transfer functions: $H_1(z)$, $H_2(z)$, $H_3(z)$, $H_4(z)$, $H_5(z)$, and $H_6(z)$ (predicted position, predicted velocity, predicted acceleration, smoothed position, smoothed velocity, and smoothed acceleration). Each transfer function has the form

$$H(z) = \frac{a_3 + a_2z^{-1} + a_1z^{-2}}{1 + b_2z^{-1} + b_1z^{-2} + b_0z^{-3}}$$

The denominator remains the same for all six transfer functions. Compute all the relevant coefficients for each transfer function.

11.23. Verify the results obtained for the two limiting cases of the Singer-Kalman filter.

11.24. Verify Eq. (11.160).

12.1. Introduction

Modern airborne radar systems are designed to perform a large number of functions which range from detection and discrimination of targets to mapping large areas of ground terrain. This mapping can be performed by the Synthetic Aperture Radar (SAR). Through illuminating the ground with coherent radiation and measuring the echo signals, SAR can produce high resolution two-dimensional (and in some cases three-dimensional) imagery of the ground surface. The quality of ground maps generated by SAR is determined by the size of the resolution cell. A resolution cell is specified by range and azimuth resolutions of the system. Other factors affecting the size of the resolution cells are (1) size of the processed map and the amount of signal processing involved; (2) cost consideration; and (3) size of the objects that need to be resolved in the map. For example, mapping gross features of cities and coastlines does not require as much resolution when compared to resolving houses, vehicles, and streets.

SAR systems can produce maps of reflectivity versus range and Doppler (cross range). Range resolution is accomplished through range gating. Fine range resolution can be accomplished by using pulse compression techniques. The azimuth resolution depends on antenna size and radar wavelength. Fine azimuth resolution is enhanced by taking advantage of the radar motion in order to synthesize a larger antenna aperture. Let N_r denote the number of range bins and let N_a denote the number of azimuth cells. It follows that the total number of resolution cells in the map is $N_r N_a$. SAR systems that are

generally concerned with improving azimuth resolution are often referred to as Doppler Beam-Sharpening (DBS) SARs. In this case, each range bin is processed to resolve targets in Doppler which correspond to azimuth. This chapter is presented in the context of DBS.

Due to the large amount of signal processing required in SAR imagery, the early SAR designs implemented optical processing techniques. Although such optical processors can produce high quality radar images, they have several shortcomings. They can be very costly and are, in general, limited to making strip maps. Motion compensation is not easy to implement for radars that utilize optical processors. With the recent advances in solid state electronics and Very Large Scale Integration (VLSI) technologies, digital signal processing in real time has been made possible in SAR systems.

12.2. Real Versus Synthetic Arrays

A linear array of size N , element spacing d , isotropic elements, and wavelength λ is shown in Fig. 12.1. A synthetic linear array is formed by linear motion of a single element, transmitting and receiving from distinct positions that correspond to the element locations in a real array. Thus, synthetic array geometry is similar to that of a real array, with the exception that the array exists only at a single element position at a time.

The two-way radiation pattern (in the direction-sine $\sin\beta$) for a real linear array was developed in Chapter 10; it is repeated here as Eq. (12.1):

$$G(\sin\beta) = \left(\frac{\sin((Nkd\sin\beta)/2)}{\sin((kd\sin\beta)/2)} \right)^2 \quad (12.1)$$

Since a synthetic array exists only at a single location at a time, the array transmission is sequential with only one element receiving. Therefore, the returns received by the successive array positions differ in phase by $\delta = k\Delta r$, where $k = 2\pi/\lambda$, and $\Delta r = 2d\sin\beta$ is the round-trip path difference between contiguous element positions. The two-way array pattern for a synthetic array is the coherent sum of the returns at all the array positions.

Thus, the overall two-way electric field for the synthetic array is

$$E(\sin\beta) = 1 + e^{-j2\delta} + e^{-j4\delta} + \dots + e^{-j2(N-1)\delta} = \sum_{n=1}^N e^{-j2(n-1)k d \sin\beta} \quad (12.2)$$

By using similar analysis as in Section 10.4, the two-way electric field for a synthetic array can be expressed as

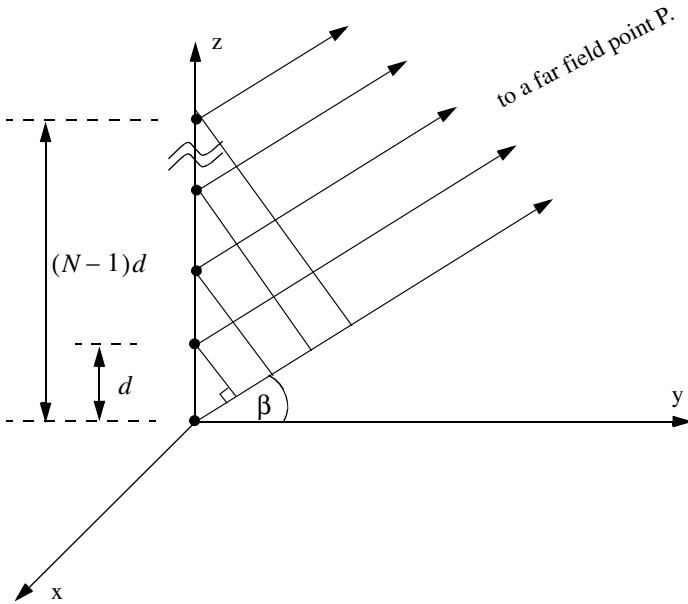


Figure 12.1. Geometry of real or synthetic array.

$$E(\sin \beta) = \frac{\sin(Nkd \sin \beta)}{\sin(kd \sin \beta)} \quad (12.3)$$

and the two-way radiation pattern is

$$G(\sin \beta) = |E(\sin \beta)| = \left| \frac{\sin(Nkd \sin \beta)}{\sin(kd \sin \beta)} \right| \quad (12.4)$$

Comparison of Eq. (12.4) and Eq. (12.1) indicates that the two-way radiation pattern for a real array is of the form $(\sin \theta / \theta)^2$, while it is of the form $\sin 2\theta / 2\theta$ for the synthetic array. Consequently, for the same size aperture, the main beam of the synthetic array is twice as narrow as that for the real array. Or equivalently, the resolution of a synthetic array of length L (aperture size) is equal to that of a real array with twice the aperture size ($2L$), as illustrated in Fig. 12.2.

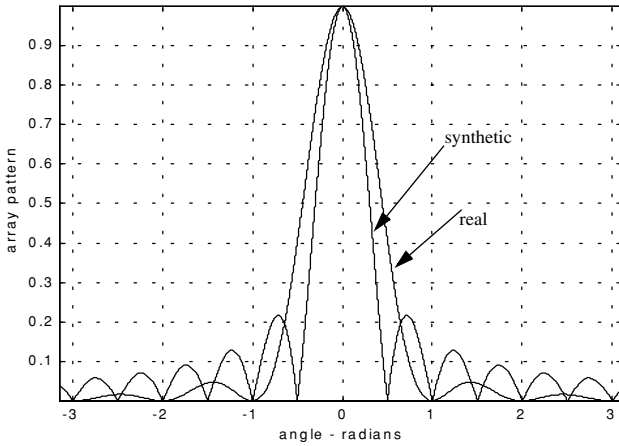


Figure 12.2. Pattern difference between real and synthetic arrays. This plot can be reproduced using MATLAB program “fig12_2.m” given in Listing 12.1 in Section 12.12.

12.3. Side Looking SAR Geometry

Fig. 12.3 shows the geometry for the standard side looking SAR. We will assume that the platform carrying the radar maintains both fixed altitude h and velocity v . The antenna $3dB$ beam width is θ , and the elevation angle (measured from the z -axis to the antenna axis) is β . The intersection of the antenna beam with the ground defines a footprint. As the platform moves, the footprint scans a swath on the ground.

The radar position with respect to the absolute origin $\vec{O} = (0, 0, 0)$, at any time is the vector $\vec{a}(t)$. The velocity vector $\vec{a}'(t)$ is

$$\vec{a}'(t) = 0 \times \hat{a}_x + v \times \hat{a}_y + 0 \times \hat{a}_z \quad (12.5)$$

The Line of Sight (LOS) for the current footprint centered at $\vec{q}(t_c)$ is defined by the vector $\vec{R}(t_c)$, where t_c denotes the central time of the observation interval T_{ob} (coherent integration interval). More precisely,

$$(t = t_a + t_c) ; -\frac{T_{ob}}{2} \leq t \leq \frac{T_{ob}}{2} \quad (12.6)$$

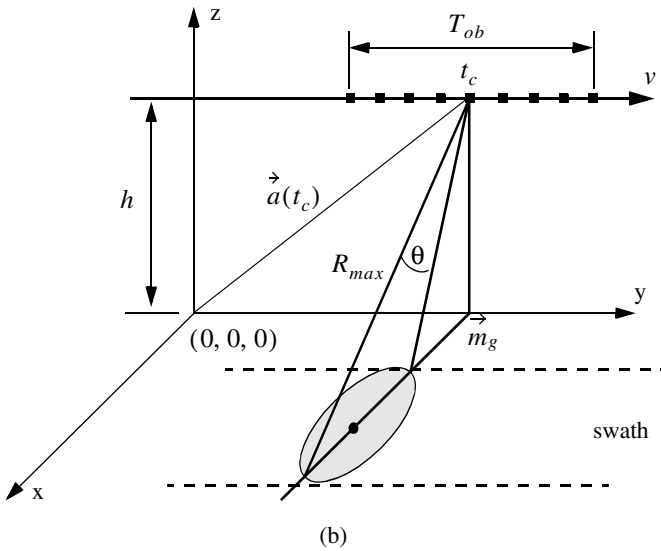
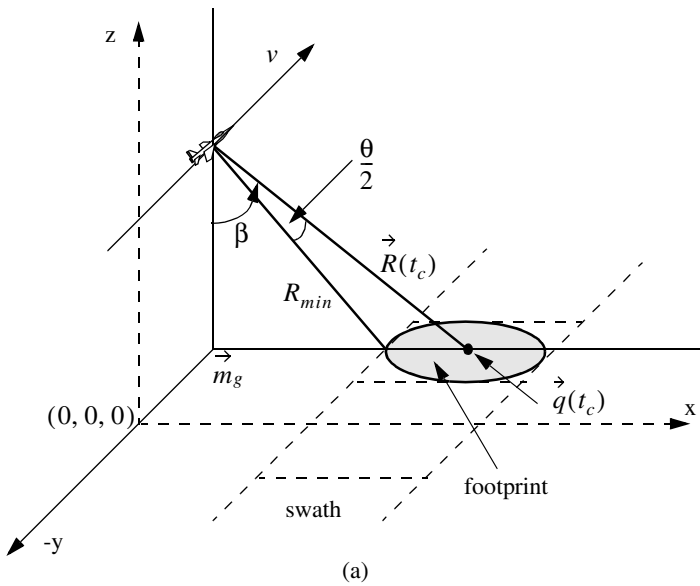


Figure 12.3. Side looking SAR geometry.

where t_a and t are the absolute and relative times, respectively. The vector \vec{m}_g defines the ground projection of the antenna at central time. The minimum slant range to the swath is R_{min} , and the maximum range is denoted R_{max} , as illustrated by Fig. 12.4. It follows that

$$\begin{aligned} R_{min} &= h / \cos(\beta - \theta/2) \\ R_{max} &= h / \cos(\beta + \theta/2) \end{aligned} \tag{12.7}$$

$$\left| \vec{R}(t_c) \right| = h / \cos \beta$$

Notice that the elevation angle β is equal to

$$\beta = 90 - \psi_g \tag{12.8}$$

where ψ_g is the grazing angle. The size of the footprint is a function of the grazing angle and the antenna beam width, as illustrated in Fig. 12.5. The SAR geometry described in this section is referred to as SAR “strip mode” of operation. Another SAR mode of operation, which will not be discussed in this chapter, is called “spot-light mode,” where the antenna is steered (mechanically or electronically) to continuously illuminate one spot (footprint) on the ground. In this case, one high resolution image of the current footprint is generated during an observation interval.

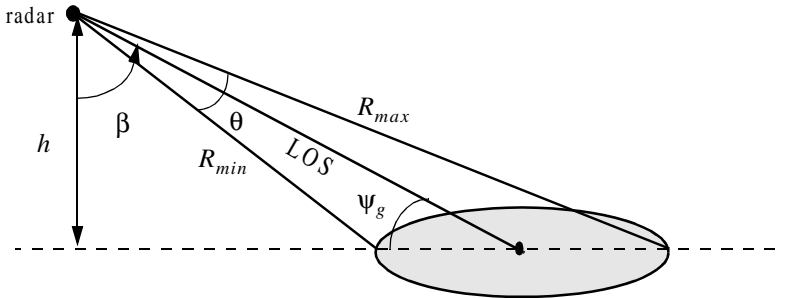


Figure 12.4. Definition of minimum and maximum range.

12.4. SAR Design Considerations

The quality of SAR images is heavily dependent on the size of the map resolution cell shown in Fig. 12.6. The range resolution, ΔR , is computed on the beam LOS, and is given by

$$\Delta R = (c\tau)/2 \tag{12.9}$$

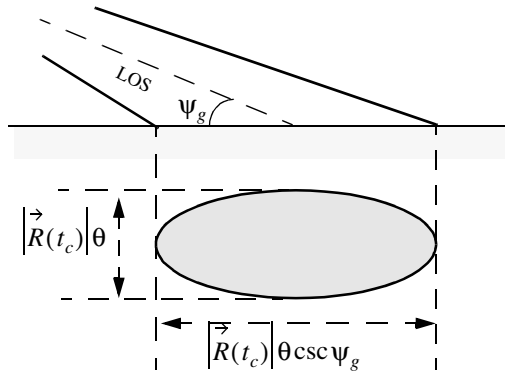


Figure 12.5. Footprint definition.

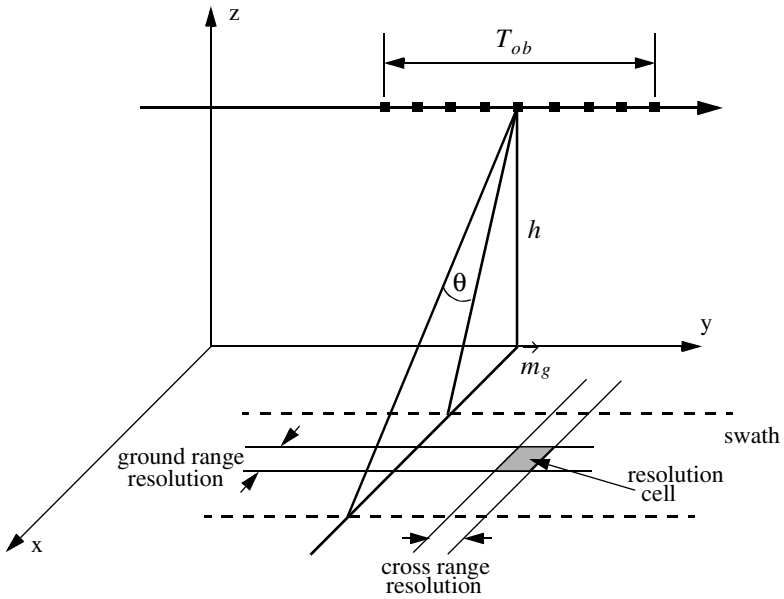


Figure 12.6. Definition of a resolution cell.

where τ is the pulse width. From the geometry in Fig. 12.7 the extent of the range cell ground projection ΔR_g is computed as

$$\Delta R_g = \frac{c\tau}{2} \sec \psi_g \quad (12.10)$$

The azimuth or cross range resolution for a real antenna with a $3dB$ beam width θ (radians) at range R is

$$\Delta A_r = \theta R \quad (12.11)$$

However, the antenna beam width is proportional to the aperture size,

$$\theta \approx \frac{\lambda}{L} \quad (12.12)$$

where λ is the wavelength and L is the aperture length. It follows that

$$\Delta A_r = \frac{\lambda R}{L} \quad (12.13)$$

And since the effective synthetic aperture size is twice that of a real array, the azimuth resolution for a synthetic array is then given by

$$\Delta A = \frac{\lambda R}{2L} \quad (12.14)$$

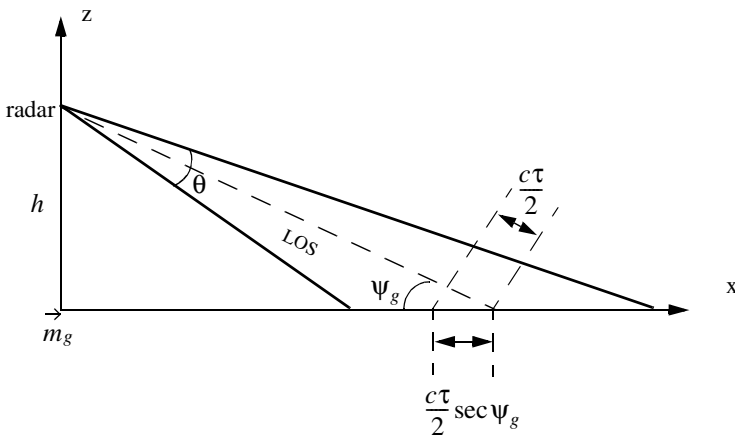


Figure 12.7. Definition of a range cell on the ground.

Furthermore, since the synthetic aperture length L is equal to vT_{ob} , Eq. (12.14) can be rewritten as

$$\Delta A = \frac{\lambda R}{2vT_{ob}} \quad (12.15)$$

The azimuth resolution can be greatly improved by taking advantage of the Doppler variation within a footprint (or a beam). As the radar travels along its flight path the radial velocity to a ground scatterer (point target) within a footprint varies as a function of the radar radial velocity in the direction of that scatterer. The variation of Doppler frequency for a certain scatterer is called the ‘‘Doppler history.’’

Let $R(t)$ denote range to a scatterer at time t , and v_r be the corresponding radial velocity; thus the Doppler shift is

$$f_d = - \frac{2R'(t)}{\lambda} = \frac{2v_r}{\lambda} \quad (12.16)$$

where $R'(t)$ is the range rate to the scatterer. Let t_1 and t_2 be the times when the scatterer enters and leaves the radar beam, respectively, and let t_c be the time that corresponds to minimum range. Fig. 12.8 shows a sketch of the corresponding $R(t)$ (see Eq. (12.16)). Since the radial velocity can be computed as the derivative of $R(t)$ with respect to time, one can clearly see that Doppler frequency is maximum at t_1 , zero at t_c , and minimum at t_2 , as illustrated in Fig. 12.9.

In general, the radar maximum PRF, $f_{r_{max}}$, must be low enough to avoid range ambiguity. Alternatively, the minimum PRF, $f_{r_{min}}$, must be high enough to avoid Doppler ambiguity. SAR unambiguous range must be at least as wide as the extent of a footprint. More precisely, since target returns from maximum range due to the current pulse must be received by the radar before the next pulse is transmitted, it follows that SAR unambiguous range is given by

$$R_u = R_{max} - R_{min} \quad (12.17)$$

An expression for unambiguous range was derived in Chapter 1, and is repeated here as Eq. (12.18),

$$R_u = \frac{c}{2f_r} \quad (12.18)$$

Combining Eq. (12.18) and Eq. (12.17) yields

$$f_{r_{max}} \leq \frac{c}{2(R_{max} - R_{min})} \quad (12.19)$$

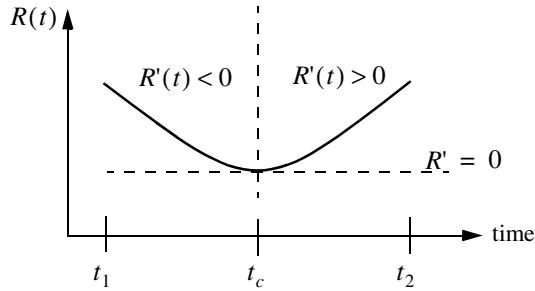


Figure 12.8. Sketch of range versus time for a scatterer.

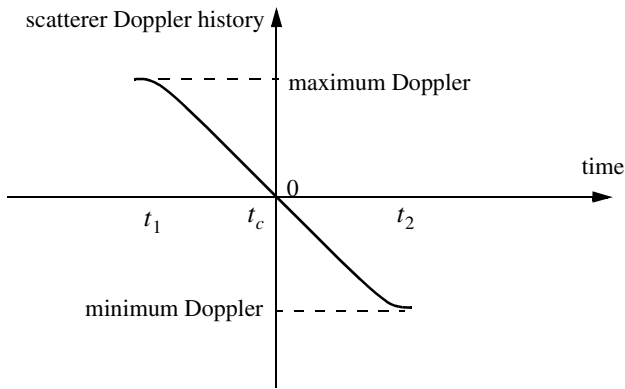
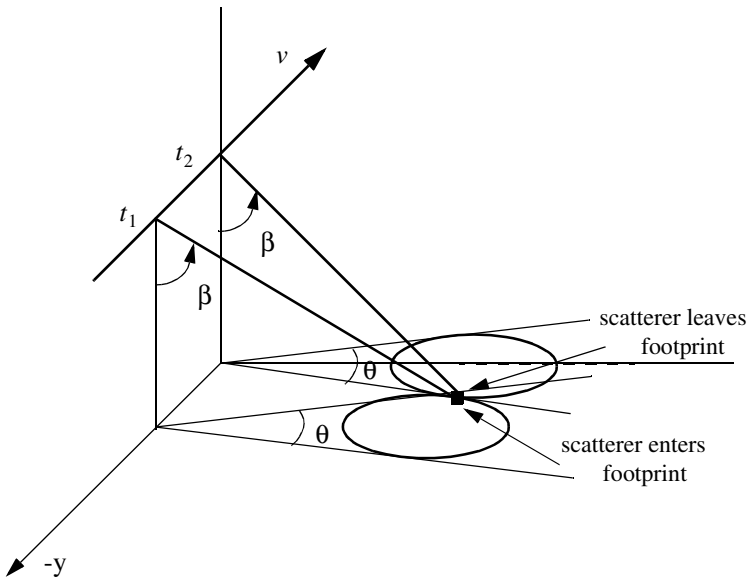


Figure 12.9. Point scatterer Doppler history.

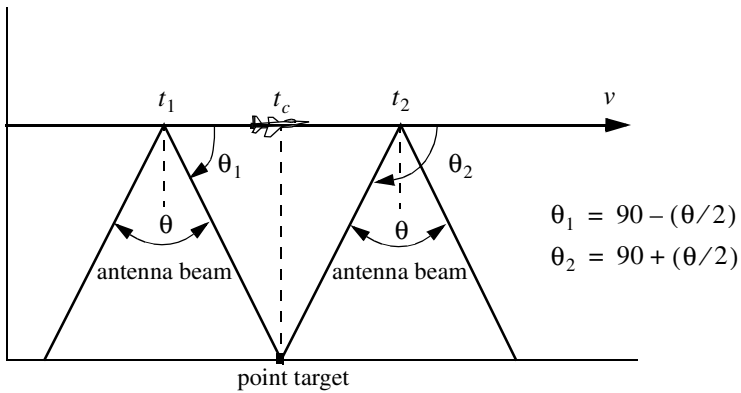
SAR minimum PRF, $f_{r_{min}}$, is selected so that Doppler ambiguity is avoided. In other words, $f_{r_{min}}$ must be greater than the maximum expected Doppler spread within a footprint. From the geometry of Fig. 12.10, the maximum and minimum Doppler frequencies are, respectively, given by

$$\left(f_{d_{max}} = \frac{2v}{\lambda} \cos\left(90 - \frac{\theta}{2}\right) \sin\beta \right) ; \text{ at } t_1 \quad (12.20)$$

$$\left(f_{d_{min}} = \frac{2v}{\lambda} \cos\left(90 + \frac{\theta}{2}\right) \sin\beta \right) ; \text{ at } t_2 \quad (12.21)$$



(a)



(b)

Figure 12.10. Doppler history computation. (a) Full view; (b) top view.

It follows that the maximum Doppler spread is

$$\Delta f_d = f_{d_{max}} - f_{d_{min}} \quad (12.22)$$

Substituting Eqs. (11.20) and (11.21) into Eq. (12.22) and applying the proper trigonometric identities yield

$$\Delta f_d = \frac{4v}{\lambda} \sin \frac{\theta}{2} \sin \beta \quad (12.23)$$

Finally, by using the small angle approximation we get

$$\Delta f_d \approx \frac{4v}{\lambda} \frac{\theta}{2} \sin \beta = \frac{2v}{\lambda} \theta \sin \beta \quad (12.24)$$

Therefore, the minimum PRF is

$$f_{r_{min}} \geq \frac{2v}{\lambda} \theta \sin \beta \quad (12.25)$$

Combining Eqs. (11.19) and (11.25) we get

$$\frac{c}{2(R_{max} - R_{min})} \geq f_r \geq \frac{2v}{\lambda} \theta \sin \beta \quad (12.26)$$

It is possible to resolve adjacent scatterers at the same range within a footprint based only on the difference of their Doppler histories. For this purpose, assume that the two scatterers are within the k th range bin. Denote their angular displacement as $\Delta\theta$, and let $\Delta f_{d_{min}}$ be the minimum Doppler spread between the two scatterers such that they will appear in two distinct Doppler filters. Using the same methodology that led to Eq. (12.24) we get

$$\Delta f_{d_{min}} = \frac{2v}{\lambda} \Delta\theta \sin \beta_k \quad (12.27)$$

where β_k is the elevation angle corresponding to the k th range bin.

The bandwidth of the individual Doppler filters must be equal to the inverse of the coherent integration interval T_{ob} (i.e., $\Delta f_{d_{min}} = 1/T_{ob}$). It follows that

$$\Delta\theta = \frac{\lambda}{2vT_{ob} \sin \beta_k} \quad (12.28)$$

Substituting L for vT_{ob} yields

$$\Delta\theta = \frac{\lambda}{2L\sin\beta_k} \quad (12.29)$$

Therefore, the SAR azimuth resolution (within the k th range bin) is

$$\Delta A_g = \Delta\theta R_k = R_k \frac{\lambda}{2L\sin\beta_k} \quad (12.30)$$

Note that when $\beta_k = 90^\circ$, Eq. (12.30) is identical to Eq. (12.14).

12.5. SAR Radar Equation

The single pulse radar equation was derived in Chapter 1, and is repeated here as Eq. (12.31),

$$SNR = \frac{P_t G^2 \lambda^2 \sigma}{(4\pi)^3 R_k^4 k T_0 B L_{Loss}} \quad (12.31)$$

where: P_t is peak power; G is antenna gain; λ is wavelength; σ is radar cross section; R_k is radar slant range to the k th range bin; k is Boltzman's constant; T_0 is receiver noise temperature; B is receiver bandwidth; and L_{Loss} is radar losses. The radar cross section is a function of the radar resolution cell and terrain reflectivity. More precisely,

$$\sigma = \sigma^0 \Delta R_g \Delta A_g = \sigma^0 \Delta A_g \frac{c\tau}{2} \sec\Psi_g \quad (12.32)$$

where σ^0 is the clutter scattering coefficient, ΔA_g is the azimuth resolution, and Eq. (12.10) was used to replace the ground range resolution. The number of coherently integrated pulses within an observation interval is

$$n = f_r T_{ob} = \frac{f_r L}{v} \quad (12.33)$$

where L is the synthetic aperture size. Using Eq. (12.30) in Eq. (12.33) and rearranging terms yield

$$n = \frac{\lambda R f_r}{2 \Delta A_g v} \csc\beta_k \quad (12.34)$$

The radar average power over the observation interval is

$$P_{av} = (P_t/B) f_r \quad (12.35)$$

The SNR for n coherently integrated pulses is then

$$(SNR)_n = nSNR = n \frac{P_i G^2 \lambda^2 \sigma}{(4\pi)^3 R_k^4 k T_0 B L_{Loss}} \quad (12.36)$$

Substituting Eqs. (11.35), (11.34), and (11.32) into Eq. (12.36) and performing some algebraic manipulations give the SAR radar equation,

$$(SNR)_n = \frac{P_{av} G^2 \lambda^3 \sigma^0}{(4\pi)^3 R_k^3 k T_0 L_{Loss}} \frac{\Delta R_g}{2v} \csc \beta_k \quad (12.37)$$

Eq. (12.37) leads to the conclusion that in SAR systems the SNR is (1) inversely proportional to the third power of range; (2) independent of azimuth resolution; (3) function of the ground range resolution; (4) inversely proportional to the velocity v ; and (5) proportional to the third power of wavelength.

12.6. SAR Signal Processing

There are two signal processing techniques to sequentially produce a SAR map or image; they are line-by-line processing and Doppler processing. The concept of SAR line-by-line processing is as follows. Through the radar linear motion a synthetic array is formed, where the elements of the current synthetic array correspond to the position of the antenna transmissions during the last observation interval. Azimuth resolution is obtained by forming narrow synthetic beams through combination of the last observation interval returns. Fine range resolution is accomplished in real time by utilizing range gating and pulse compression. For each range bin and each of the transmitted pulses during the last observation interval, the returns are recorded in a two-dimensional array of data that is updated for every pulse. Denote the two-dimensional array of data as *MAP*.

To further illustrate the concept of line-by-line processing, consider the case where a map of size $N_a \times N_r$ is to be produced, N_a is the number of azimuth cells, and N_r is the number of range bins. Hence, *MAP* is of size $N_a \times N_r$, where the columns refer to range bins, and the rows refer to azimuth cells. For each transmitted pulse, the echoes from consecutive range bins are recorded sequentially in the first row of *MAP*. Once the first row is completely filled (i.e., returns from all range bins have been received), all data (in all rows) are shifted downward one row before the next pulse is transmitted. Thus, one row of *MAP* is generated for every transmitted pulse. Consequently, for the current observation interval, returns from the first transmitted pulse will be located in the bottom row of *MAP*, and returns from the last transmitted pulse will be in the first row of *MAP*.

In SAR Doppler processing, the array MAP is updated once every N pulses so that a block of N columns is generated simultaneously. In this case, N refers to the number of transmissions during an observation interval (i.e., size of the synthetic array). From an antenna point of view, this is equivalent to having N adjacent synthetic beams formed in parallel through electronic steering.

12.7. Side Looking SAR Doppler Processing

Consider the geometry shown in Fig. 12.11, and assume that the scatterer C_i is located within the k th range bin. The scatterer azimuth and elevation angles are μ_i and β_i , respectively. The scatterer elevation angle β_i is assumed to be equal to β_k , the range bin elevation angle. This assumption is true if the ground range resolution, ΔR_g , is small; otherwise, $\beta_i = \beta_k + \epsilon_i$ for some small ϵ_i ; in this chapter $\epsilon_i = 0$.

The normalized transmitted signal can be represented by

$$s(t) = \cos(2\pi f_0 t - \xi_0) \tag{12.38}$$

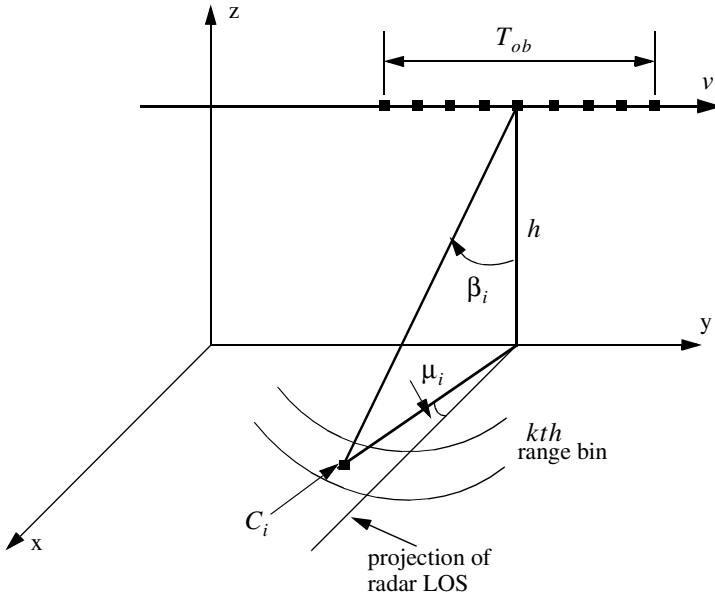


Figure 12.11. A scatterer C_i within the k th range bin.

where f_0 is the radar operating frequency, and ξ_0 denotes the transmitter phase. The returned radar signal from C_i is then equal to

$$s_i(t, \mu_i) = A_i \cos[2\pi f_0(t - \tau_i(t, \mu_i)) - \xi_0] \quad (12.39)$$

where $\tau_i(t, \mu_i)$ is the round-trip delay to the scatterer, and A_i includes scatterer strength, range attenuation, and antenna gain. The round-trip delay is

$$\tau_i(t, \mu_i) = \frac{2r_i(t, \mu_i)}{c} \quad (12.40)$$

where c is the speed of light and $r_i(t, \mu_i)$ is the scatterer slant range. From the geometry in Fig. 12.11, one can write the expression for the slant range to the i th scatterer within the k th range bin as

$$r_i(t, \mu_i) = \frac{h}{\cos \beta_i} \sqrt{1 - \frac{2vt}{h} \cos \beta_i \cos \mu_i \sin \beta_i + \left(\frac{vt}{h} \cos \beta_i\right)^2} \quad (12.41)$$

And by using Eq. (12.40) the round-trip delay can be written as

$$\tau_i(t, \mu_i) = \frac{2}{c} \frac{h}{\cos \beta_i} \sqrt{1 - \frac{2vt}{h} \cos \beta_i \cos \mu_i \sin \beta_i + \left(\frac{vt}{h} \cos \beta_i\right)^2} \quad (12.42)$$

The round-trip delay can be approximated using a two-dimensional second order Taylor series expansion about the reference state $(t, \mu) = (0, 0)$. Performing this Taylor series expansion yields

$$\tau_i(t, \mu_i) \approx \bar{\tau} + \bar{\tau}_{t\mu} \mu_i t + \bar{\tau}_{tt} \frac{t^2}{2} \quad (12.43)$$

where the over-bar indicates evaluation at the state $(0, 0)$, and the subscripts denote partial derivatives. For example, $\tau_{t\mu}$ means

$$\bar{\tau}_{t\mu} = \frac{\partial^2}{\partial t \partial \mu} \tau_i(t, \mu_i) \Big|_{(t, \mu) = (0, 0)} \quad (12.44)$$

The Taylor series coefficients are (see Problem 11.6)

$$\bar{\tau} = \left(\frac{2h}{c}\right) \frac{1}{\cos \beta_i} \quad (12.45)$$

$$\bar{\tau}_{t\mu} = \left(\frac{2v}{c}\right) \sin \beta_i \quad (12.46)$$

$$\bar{\tau}_{it} = \left(\frac{2v^2}{hc}\right)\cos\beta_i \quad (12.47)$$

Note that other Taylor series coefficients are either zeros or very small, hence they are neglected. Finally, by substituting Eqs. (12.45) through (12.47) into Eq. (12.43), we can rewrite the returned radar signal as

$$s_i(t, \mu_i) = A_i \cos[\psi_i(t, \mu_i) - \xi_0] \quad (12.48)$$

$$\hat{\psi}_i(t, \mu_i) = 2\pi f_0 \left[(1 - \bar{\tau}_{it}\mu_i)t - \bar{\tau} - \bar{\tau}_{it}\frac{t^2}{2} \right]$$

Observation of Eq. (12.48) indicates that the instantaneous frequency for the *i*th scatterer varies as a linear function of time due to the second order phase term $2\pi f_0(\bar{\tau}_{it}t^2/2)$ (this confirms the result we concluded about a scatterer Doppler history). Furthermore, since this phase term is range-bin dependent and not scatterer dependent, all scatterers within the same range bin produce this exact second order phase term. It follows that scatterers within a range bin have identical Doppler histories. These Doppler histories are separated by the time delay required to fly between them, as illustrated in Fig. 12.12.

Suppose that there are *I* scatterers within the *k*th range bin. In this case, the combined returns for this cell are the sum of the individual returns due to each scatterer as defined by Eq. (12.48). In other words, superposition holds, and the overall echo signal is

$$s_r(t) = \sum_{i=1}^I s_i(t, \mu_i) \quad (12.49)$$

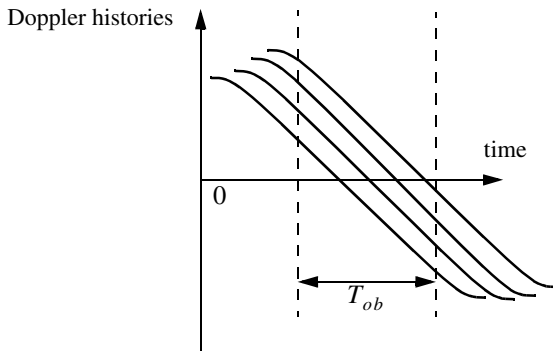


Figure 12.12. Doppler histories for several scatterers within the same range bin.

A signal processing block diagram for the k th range bin is illustrated in Fig. 12.13. It consists of the following steps. First, heterodyning with carrier frequency is performed to extract the quadrature components.

This is followed by LP filtering and A/D conversion. Next, deramping or focusing to remove the second order phase term of the quadrature components is carried out using a phase rotation matrix. The last stage of the processing includes windowing, performing FFT on the windowed quadrature components, and scaling of the amplitude spectrum to account for range attenuation and antenna gain.

The discrete quadrature components are

$$\begin{aligned}\tilde{x}_I(t_n) &= \tilde{x}_I(n) = A_i \cos[\tilde{\Psi}_i(t_n, \mu_i) - \xi_0] \\ \tilde{x}_Q(t_n) &= \tilde{x}_Q(n) = A_i \sin[\tilde{\Psi}_i(t_n, \mu_i) - \xi_0]\end{aligned}\tag{12.50}$$

$$\tilde{\Psi}_i(t_n, \mu_i) = \hat{\Psi}_i(t_n, \mu_i) - 2\pi f_0 t_n\tag{12.51}$$

and t_n denotes the n th sampling time (remember that $-T_{ob}/2 \leq t_n \leq T_{ob}/2$). The quadrature components after deramping (i.e., removal of the phase $\psi = -\pi f_0 \tilde{\tau}_i t_n^2$) are given by

$$\begin{bmatrix} x_I(n) \\ x_Q(n) \end{bmatrix} = \begin{bmatrix} \cos \psi & -\sin \psi \\ \sin \psi & \cos \psi \end{bmatrix} \begin{bmatrix} \tilde{x}_I(n) \\ \tilde{x}_Q(n) \end{bmatrix}\tag{12.52}$$

12.8. SAR Imaging Using Doppler Processing

It was mentioned earlier that SAR imaging is performed using two orthogonal dimensions (range and azimuth). Range resolution is controlled by the receiver bandwidth and pulse compression. Azimuth resolution is limited by the antenna beam width. A one-to-one correspondence between the FFT bins and the azimuth resolution cells can be established by utilizing the signal model described in the previous section. Therefore, the problem of target detection is transformed into a spectral analysis problem, where detection is based on the amplitude spectrum of the returned signal. The FFT frequency resolution Δf is equal to the inverse of the observation interval T_{ob} . It follows that a peak in the amplitude spectrum at $k_1 \Delta f$ indicates the presence of a scatterer at frequency $f_{d1} = k_1 \Delta f$.

For an example, consider the scatterer C_i within the k th range bin. The instantaneous frequency f_{di} corresponding to this scatterer is

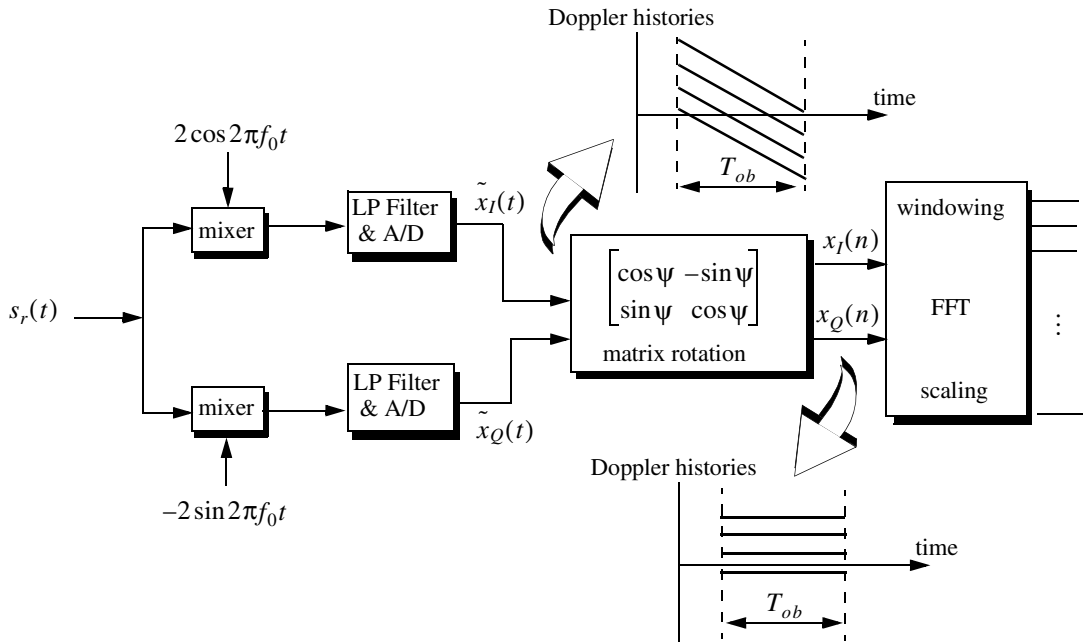


Figure 12.13. Signal processing block diagram for the k th range bin.

$$f_{di} = \frac{1}{2\pi} \frac{d\psi}{dt} = f_0 \bar{\tau}_{r\mu} \mu_i = \frac{2v}{\lambda} \sin\beta_i \mu_i \quad (12.53)$$

which is the same result derived in Eq. (12. 27), where $\mu_i = \Delta\theta$. Therefore, the scatterers separated in Doppler by a frequency greater than Δf can then be resolved.

12.9. Range Walk

As shown earlier SAR Doppler processing is achieved in two steps: first, range gating and second, azimuth compression within each bin at the end of the observation interval. For this purpose, azimuth compression assumes that each scatterer remains within the same range bin during the observation interval. However, since the range gates are defined with respect to a radar that is moving, the range gate grid is also moving relative to the ground. As a result a scatterer appears to be moving within its range bin. This phenomenon is known as range walk. A small amount of range walk does not bother Doppler processing as long as the scatterer remains within the same range bin. However, range walk over several range bins can constitute serious problems, where in this case Doppler processing is meaningless.

12.10. Case Study

Table 12.1 lists the selected design system parameters. The 3 dB element beamwidth is $\theta = 63.75$ milliradians. The maximum range interval spanned by the central footprint is

$$R_{span} = R_{mx} - R_{mn} \quad (12.54)$$

$$R_{mx} = h / \cos(\beta^* + \theta/2) \quad (12.55)$$

$$R_{mn} = h / \cos(\beta^* - \theta/2) \quad (12.56)$$

Substituting the proper values from Table 12.1 into Eqs. (12.54), (12.55), and (12.56) yields

$$\{R_{span}, R_{mx}, R_{mn}\} = \{81.448, 1315.538, 1234.090\}m \quad (12.57)$$

which indicates that the system should have a total of 82 range bins. Doppler shift over the footprint is proportional to the radial velocity. It is given by

$$\frac{2v}{\lambda} \cos(90 + \theta/2) \sin\beta^* < f < \frac{2v}{\lambda} \cos(90 - \theta/2) \sin\beta^* \quad (12.58)$$

For this example, f_d is

TABLE 12.1. List of selected system parameters.

Parameter	Symbol	Value
<i># subintervals</i>	M	64
<i>size of array</i>	N	32
<i>wavelength</i>	λ	3.19mm
<i>element spacing</i>	d	16λ
<i>velocity</i>	v	65m/s
<i>height</i>	h	900m
<i>elevation angle</i>	β^*	35°
<i>range resolution</i>	d_r	1m
<i>observation interval</i>	D_{ob}	20ms

$$-1489.88\text{Hz} < f_d < 1489.88\text{Hz} \quad (12.59)$$

To avoid range and Doppler ambiguities the Pulse Repetition Frequency (PRF) should be

$$\frac{2v}{\lambda}\theta \leq PRF \leq \frac{c}{2R_{span}} \quad (12.60)$$

Using the system parameters defined in [Table 12.1](#), we find $5.995\text{KHz} \leq PRF \leq 1.31579\text{MHz}$. The DFT frequency resolution Δf is computed as the inverse of the observation interval, and it is equal to 50Hz . The size of the DFT, denoted as $NFFT$, is equal to the number of positions the antenna takes on along the flight path. The maximum Doppler variation resolved by this DFT is less than or equal to $\Delta f \times NFFT / 2$.

12.11. Arrays in Sequential Mode Operation

Standard Synthetic Aperture Radar (SAR) imaging systems are generally used to generate high resolution two-dimensional (2-D) images of ground terrain. Range gating determines resolution along the first dimension. Pulse compression techniques are usually used to achieve fine range resolution. Such techniques require the use of wide band receiver and display devices in order to resolve the time structure in the returned signals. The width of azimuth cells

provides resolution along the other dimension. Azimuth resolution is limited by the duration of the observation interval.

An approach for multiple target detection using linear arrays operated in sequential mode was previously presented by Mahafza. This technique is based on Discrete Fourier Transform (DFT) processing of equiphase data collected in sequential mode (DFTSQM). DFTSQM processing was also developed for 2-D real and synthetic arrays to include applications such as SAR imaging. The Field of View (FOV) of an array utilizing DFTSQM operation and signal processing is defined by the 3 dB beamwidth of a single element. Advantages of DFTSQM are (1) simultaneous detection of targets within the array's FOV without using any phase shifting hardware; and (2) the two-way array pattern is improved due to the coherent integration of equiphase returns. More specifically, the main lobe resolution is doubled while achieving a 27 dB sidelobe attenuation. However, the time required for transmission and processing may become a limitation when using this technique. A brief description of DFTSQM is presented in the next section.

12.11.1. Linear Arrays

Consider a linear array of size N , uniform element spacing d , and wavelength λ . Assume a far field scatterer P located at direction-sine $\sin\beta_l$. DFTSQM operation for this array can be described as follows. The elements are fired sequentially, one at a time, while all elements receive in parallel. The echoes are collected and integrated coherently on the basis of equal phase to compute a complex information sequence $\{b(m); m = 0, 2N - 1\}$. The x -coordinates, in d -units, of the x_n^{th} element with respect to the center of the array are

$$x_n = \left(-\frac{N-1}{2} + n\right); \quad n = 0, N-1. \quad (12.61)$$

The electric field received by the x_2^{th} element due to the firing of the x_1^{th} , and reflection by the l^{th} far field scatterer P is

$$E(x_1, x_2; s_l) = G^2(s_l) \left(\frac{R_0}{R}\right)^4 \sqrt{\sigma_l} \exp(j\phi(x_1, x_2; s_l)) \quad (12.62)$$

$$\phi(x_1, x_2; s_l) = \frac{2\pi}{\lambda}(x_1 + x_2)(s_l) \quad (12.63)$$

$$s_l = \sin\beta_l \quad (12.64)$$

where $\sqrt{\sigma_l}$ is the target cross section, $G^2(s_l)$ is the two-way element gain, and $(R_0/R)^4$ is the range attenuation with respect to reference range R_0 . The scatterer phase is assumed to be zero, however it could be easily included.

Assuming multiple scatterers in the array's FOV, the cumulative electric field in the path $x_1 \Rightarrow x_2$ due to reflection from all scatterers is

$$E(x_1, x_2) = \sum_{\text{all } l} [E_I(x_1, x_2; s_l) + jE_Q(x_1, x_2; s_l)] \quad (12.65)$$

where the subscripts (I, Q) denote the quadrature components. Note that the variable part of the phase given in Eq. (12.63) is proportional to the integers resulting from the sums $\{(x_{n1} + x_{n2}); (n1, n2) = 0, N-1\}$. In the far field operation there are a total of $(2N-1)$ distinct $(x_{n1} + x_{n2})$ sums. Therefore, the electric fields with paths of the same $(x_{n1} + x_{n2})$ sums can be collected coherently. In this manner the information sequence $\{b(m); m = 0, 2N-1\}$ is computed, where $b(2N-1)$ is set to equal zero. At the same time one forms the sequence $\{c(m); m = 0, 2N-2\}$ which keeps track of the number of returns that have the same $(x_{n1} + x_{n2})$ sum. More precisely, for $m = n1 + n2; (n1, n2) = 0, N-1$

$$b(m) = b(m) + E(x_{n1}, x_{n2}) \quad (12.66)$$

$$c(m) = c(m) + 1 \quad (12.67)$$

It follows that

$$\{c(m); m = 0, 2N-2\} = \left\{ \begin{array}{ll} m+1 & ; m = 0, N-2 \\ N & ; m = N-1 \\ 2N-1-m & m = N, 2N-2 \end{array} \right\} \quad (12.68)$$

which is a triangular shape sequence.

The processing of the sequence $\{b(m)\}$ is performed as follows: (1) the weighting takes the sequence $\{c(m)\}$ into account; (2) the complex sequence $\{b(m)\}$ is extended to size N_F , a power integer of two, by zero padding; (3) the DFT of the extended sequence $\{b'(m); m = 0, N_F-1\}$ is computed,

$$B(q) = \sum_{m=0}^{N_F-1} b'(m) \cdot \exp\left(-j\frac{2\pi qm}{N_F}\right); \quad q = 0, N_F-1 \quad (12.69)$$

and (4) after compensation for antenna gain and range attenuation, scatterers are detected as peaks in the amplitude spectrum $|B(q)|$. Note that step (4) is true only when

$$\sin\beta_q = \frac{\lambda q}{2Nd} \quad ; \quad q = 0, 2N-1 \quad (12.70)$$

where $\sin\beta_q$ denotes the direction-sine of the q^{th} scatterer, and $N_F = 2N$ is implied in Eq. (12.70).

The classical approach to multiple target detection is to use a phased array antenna with phase shifting and tapering hardware. The array beamwidth is proportional to (λ/Nd) , and the first sidelobe is at about -13 dB. On the other hand, multiple target detection using DFTSQM provides a beamwidth proportional to $(\lambda/2Nd)$ as indicated by Eq. (12.70), which has the effect of doubling the array's resolution. The first sidelobe is at about -27 dB due the triangular sequence $\{c(m)\}$. Additionally, no phase shifting hardware is required for detection of targets within a single element field of view.

12.11.2. Rectangular Arrays

DFTSQM operation and signal processing for 2-D arrays can be described as follows. Consider an $N_x \times N_y$ rectangular array. All $N_x N_y$ elements are fired sequentially, one at a time; after each firing, all the $N_x N_y$ array elements receive in parallel. Thus, $N_x N_y$ samples of the quadrature components are collected after each firing, and a total of $(N_x N_y)^2$ samples will be collected. However, in the far field operation, there are only $(2N_x - 1) \times (2N_y - 1)$ distinct equiphase returns. Therefore, the collected data can be added coherently to form a 2-D information array of size $(2N_x - 1) \times (2N_y - 1)$. The two-way radiation pattern is computed as the modulus of the 2-D amplitude spectrum of the information array. The processing includes 2-D windowing, 2-D Discrete Fourier Transformation, antenna gain, and range attenuation compensation. The field of view of the 2-D array is determined by the 3 dB pattern of a single element. All the scatterers within this field will be detected simultaneously as peaks in the amplitude spectrum.

Consider a rectangular array of size $N \times N$, with uniform element spacing $d_x = d_y = d$, and wavelength λ . The coordinates of the n^{th} element, in d -units, are

$$x_n = \left(-\frac{N-1}{2} + n \right) \quad ; \quad n = 0, N-1 \quad (12.71)$$

$$y_n = \left(-\frac{N-1}{2} + n \right) \quad ; \quad n = 0, N-1 \quad (12.72)$$

Assume a far field point P defined by the azimuth and elevation angles (α, β) . In this case, the one-way geometric phase for an element is

$$\varphi'(x, y) = \frac{2\pi}{\lambda} [x \sin \beta \cos \alpha + y \sin \beta \sin \alpha] \quad (12.73)$$

Therefore, the two-way geometric phase between the (x_1, y_1) and (x_2, y_2) elements is

$$\varphi(x_1, y_1, x_2, y_2) = \frac{2\pi}{\lambda} \sin \beta [(x_1 + x_2) \cos \alpha + (y_1 + y_2) \sin \alpha] \quad (12.74)$$

The two-way electric field for the l^{th} scatterer at (α_l, β_l) is

$$E(x_1, x_2, y_1, y_2; \alpha_l, \beta_l) = G^2(\beta_l) \left(\frac{R_0}{R}\right)^4 \sqrt{\sigma_l} \exp[j(\varphi(x_1, y_1, x_2, y_2))] \quad (12.75)$$

Assuming multiple scatterers within the array's FOV, then the cumulative electric field for the two-way path $(x_1, y_1) \Rightarrow (x_2, y_2)$ is given by

$$E(x_1, x_2, y_1, y_2) = \sum_{\text{all scatterers}} E(x_1, x_2, y_1, y_2; \alpha_l, \beta_l) \quad (12.76)$$

All formulas for the 2-D case reduce to those of a linear array case by setting $N_y = 1$ and $\alpha = 0$.

The variable part of the phase given in Eq. (12.74) is proportional to the integers $(x_1 + x_2)$ and (y_1, y_2) . Therefore, after completion of the sequential firing, electric fields with paths of the same (i, j) sums, where

$$\{i = x_{n1} + x_{n2}; i = -(N-1), (N-1)\} \quad (12.77)$$

$$\{j = y_{n1} + y_{n2}; j = -(N-1), (N-1)\} \quad (12.78)$$

can be collected coherently. In this manner the 2-D information array $\{b(m_x, m_y); (m_x, m_y) = 0, 2N-1\}$ is computed. The coefficient sequence $\{c(m_x, m_y); (m_x, m_y) = 0, 2N-2\}$ is also computed. More precisely,

$$\text{for } m_x = n1 + n2 \text{ and } m_y = n1 + n2; \quad (12.79) \\ n1 = 0, N-1, \text{ and } n2 = 0, N-1$$

$$b(m_x, m_y) = b(m_x, m_y) + E(x_{n1}, y_{n1}, x_{n2}, y_{n2}) \quad (12.80)$$

It follows that

$$c(m_x, m_y) = (N_x - |m_x - (N_x - 1)|) \times (N_y - |m_y - (N_y - 1)|) \quad (12.81)$$

The processing of the complex 2-D information array $\{b(m_x, m_y)\}$ is similar to that of the linear case with the exception that one should use a 2-D DFT. After antenna gain and range attenuation compensation, scatterers are detected as peaks in the 2-D amplitude spectrum of the information array. A scatterer located at angles (α_l, β_l) will produce a peak in the amplitude spectrum at DFT indexes (p_l, q_l) , where

$$\alpha_l = \text{atan}\left(\frac{q_l}{p_l}\right) \quad (12.82)$$

$$\sin\beta_l = \frac{\lambda p_l}{2Nd\cos\alpha_l} = \frac{\lambda q_l}{2Nd\sin\alpha_l} \quad (12.83)$$

In order to prove Eq. (12.82), consider a rectangular array of size $N \times N$, with uniform element spacing $d_x = d_y = d$, and wavelength λ . Assume sequential mode operation where elements are fired sequentially, one at a time, while all elements receive in parallel. Assuming far field observation defined by azimuth and elevation angles (α, β) . The unit vector \vec{u} on the line of sight, with respect to \vec{O} , is given by

$$\vec{u} = \sin\beta\cos\alpha\vec{a}_x + \sin\beta\sin\alpha\vec{a}_y + \cos\beta\vec{a}_z \quad (12.84)$$

The $(n_x, n_y)^{th}$ element of the array can be defined by the vector

$$\vec{e}(n_x, n_y) = \left(n_x - \frac{N-1}{2}\right)d\vec{a}_x + \left(n_y - \frac{N-1}{2}\right)d\vec{a}_y \quad (12.85)$$

where $(n_x, n_y = 0, N-1)$. The one-way geometric phase for this element is

$$\varphi'(n_x, n_y) = k(\vec{u} \bullet \vec{e}(n_x, n_y)) \quad (12.86)$$

where $k = 2\pi/\lambda$ is the wave-number, and the operator (\bullet) indicates dot product. Therefore, the two-way geometric phase between the (n_{x1}, n_{y1}) and (n_{x2}, n_{y2}) elements is

$$\varphi(n_{x1}, n_{y1}, n_{x2}, n_{y2}) = k[\vec{u} \bullet \{\vec{e}(n_{x1}, n_{y1}) + \vec{e}(n_{x2}, n_{y2})\}] \quad (12.87)$$

The cumulative two-way normalized electric due to all transmissions in the direction (α, β) is

$$E(\vec{u}) = E_t(\vec{u})E_r(\vec{u}) \quad (12.88)$$

where the subscripts t and r , respectively, refer to the transmitted and received electric fields. More precisely,

$$E_t(\vec{u}) = \sum_{n_{xt}=0}^{N-1} \sum_{n_{yt}=0}^{N-1} w(n_{xt}, n_{yt}) \exp[jk\{\vec{u} \bullet \vec{e}(n_{xt}, n_{yt})\}] \quad (12.89)$$

$$E_r(\vec{u}) = \sum_{n_{xr}=0}^{N-1} \sum_{n_{yr}=0}^{N-1} w(n_{xr}, n_{yr}) \exp[jk\{\vec{u} \bullet \vec{e}(n_{xr}, n_{yr})\}] \quad (12.90)$$

In this case, $w(n_x, n_y)$ denotes the tapering sequence. Substituting Eqs. (12.87), (12.89), and (12.90) into Eq. (12.88) and grouping all fields with the same two-way geometric phase yield

$$E(\vec{u}) = e^{j\delta} \sum_{m=0}^{N_a-1} \sum_{n=0}^{N_a-1} w'(m, n) \exp[jkd \sin \beta (m \cos \alpha + n \sin \alpha)] \quad (12.91)$$

$$N_a = 2N - 1 \quad (12.92)$$

$$m = n_{xt} + n_{xr}; m = 0, 2N - 2 \quad (12.93)$$

$$n = n_{yt} + n_{yr}; n = 0, 2N - 2 \quad (12.94)$$

$$\delta = \left(\frac{-d \sin \beta}{2} \right) (N - 1) (\cos \alpha + \sin \alpha) \quad (12.95)$$

The two-way array pattern is then computed as

$$|E(\vec{u})| = \left| \sum_{m=0}^{N_a-1} \sum_{n=0}^{N_a-1} w'(m, n) \exp[jkd \sin \beta (m \cos \alpha + n \sin \alpha)] \right| \quad (12.96)$$

Consider the two-dimensional DFT transform, $W'(p, q)$, of the array $w'(n_x, n_y)$

$$W'(p, q) = \sum_{m=0}^{N_a-1} \sum_{n=0}^{N_a-1} w'(m, n) e^{-j \frac{2\pi}{N_a} (pm + qn)} ; (p, q) = 0, N_a - 1 \quad (12.97)$$

Comparison of Eq. (12.96) and (12.97) indicates that $|E(\vec{u})|$ is equal to $|W(p, q)|$ if

$$-\left(\frac{2\pi}{N_a}\right)p = \frac{2\pi}{\lambda}d\sin\beta\cos\alpha \quad (12.98)$$

$$-\left(\frac{2\pi}{N_a}\right)q = \frac{2\pi}{\lambda}d\sin\beta\sin\alpha \quad (12.99)$$

It follows that

$$\alpha = \tan^{-1}\left(\frac{q}{p}\right) \quad (12.100)$$

which is the same as Eq. (12.82).

12.12. MATLAB Programs

This section contains the MATLAB programs used in this chapter.

Listing 12.1. MATLAB Program “fig12_2.m”

```
clear all
var = -pi:0.001:pi;
y1 = (sinc(var)).^2;
y2 = abs(sinc(2.0 * var));
plot (var,y1,var,y2);
axis tight
grid;
xlabel ('angle - radians');
ylabel ('array pattern');
```

Problems

12.1. A side looking SAR is traveling at an altitude of 15 Km ; the elevation angle is $\beta = 15^\circ$. If the aperture length is $L = 5\text{ m}$, the pulse width is $\tau = 20\mu\text{ s}$ and the wavelength is $\lambda = 3.5\text{ cm}$. (a) Calculate the azimuth resolution. (b) Calculate the range and ground range resolutions.

12.2. A MMW side looking SAR has the following specifications: radar velocity $v = 70\text{ m/s}$, elevation angle $\beta = 35^\circ$, operating frequency $f_0 = 94\text{ GHz}$, and antenna 3dB beam width $\theta_{3dB} = 65\text{ mrad}$. (a) Calculate

the footprint dimensions. (b) Compute the minimum and maximum ranges. (c) Compute the Doppler frequency span across the footprint. (d) Calculate the minimum and maximum PRFs.

12.3. A side looking SAR takes on eight positions within an observation interval. In each position the radar transmits and receives one pulse. Let the distance between any two consecutive antenna positions be d , and define

$\delta = 2\pi\frac{d}{\lambda}(\sin\beta - \sin\beta_0)$ to be the one-way phase difference for a beam steered

at angle β_0 . (a) In each of the eight positions a sample of the phase pattern is obtained after heterodyning. List the phase samples. (b) How will you process the sequence of samples using an FFT (do not forget windowing)? (c) Give a formula for the angle between the grating lobes.

12.4. Consider a synthetic aperture radar. You are given the following Doppler history for a scatterer: $\{1000Hz, 0, -1000HZ\}$ which corresponds to times $\{-10ms, 0, 10ms\}$. Assume that the observation interval is $T_{ob} = 20ms$, and a platform velocity $v = 200m/s$. (a) Show the Doppler history for another scatterer which is identical to the first one except that it is located in azimuth $1m$ earlier. (b) How will you perform deramping on the quadrature components (show only the general approach)? (c) Show the Doppler history for both scatterers after deramping.

12.5. You want to design a side looking synthetic aperture Ultrasonic radar operating at $f_0 = 60KHz$ and peak power $P_t = 2W$. The antenna beam is conical with 3dB beam width $\theta_{3dB} = 5^\circ$. The maximum gain is 16. The radar is at a constant altitude $h = 15m$ and is moving at a velocity of $10m/s$. The elevation angle defining the footprint is $\beta = 45^\circ$. (a) Give an expression for the antenna gain assuming a Gaussian pattern. (b) Compute the pulse width corresponding to range resolution of $10mm$. (c) What are the footprint dimensions? (d) Compute and plot the Doppler history for a scatterer located on the central range bin. (e) Calculate the minimum and maximum PRFs; do you need to use more than one PRF? (f) How will you design the system in order to achieve an azimuth resolution of $10mm$?

12.6. Derive Eq. (12.45) through Eq. (12.47).

12.7. In Section 12.7 we assumed the elevation angle increment ϵ is equal to zero. Develop an equivalent to Eq. (12.43) for the case when $\epsilon \neq 0$. You need to use a third order three-dimensional Taylor series expansion about the state $(t, \mu, \epsilon) = (0, 0, 0)$ in order to compute the new round-trip delay expression.

13.1. Signal and System Classifications

In general, electrical signals can represent either current or voltage, and may be classified into two main categories: energy signals and power signals. Energy signals can be deterministic or random, while power signals can be periodic or random. A signal is said to be random if it is a function of a random parameter (such as random phase or random amplitude). Additionally, signals may be divided into low pass or band pass signals. Signals that contain very low frequencies (close to DC) are called low pass signals; otherwise they are referred to as band pass signals. Through modulation, low pass signals can be mapped into band pass signals.

The average power P for the current or voltage signal $x(t)$ over the interval (t_1, t_2) across a 1Ω resistor is

$$P = \frac{1}{t_2 - t_1} \int_{t_1}^{t_2} |x(t)|^2 dt \quad (13.1)$$

The signal $x(t)$ is said to be a power signal over a very large interval $T = t_2 - t_1$, if and only if it has finite power; it must satisfy the following relation:

$$0 < \lim_{T \rightarrow \infty} \frac{1}{T} \int_{-T/2}^{T/2} |x(t)|^2 dt < \infty \quad (13.2)$$

Using Parseval's theorem, the energy E dissipated by the current or voltage signal $x(t)$ across a 1Ω resistor, over the interval (t_1, t_2) , is

$$E = \int_{t_1}^{t_2} |x(t)|^2 dt \quad (13.3)$$

The signal $x(t)$ is said to be an energy signal if and only if it has finite energy,

$$E = \int_{-\infty}^{\infty} |x(t)|^2 dt < \infty \quad (13.4)$$

A signal $x(t)$ is said to be periodic with period T if and only if

$$x(t) = x(t + nT) \quad \text{for all } t \quad (13.5)$$

where n is an integer.

Example 13.1: Classify each of the following signals as an energy signal, as a power signal, or as neither. All signals are defined over the interval $(-\infty < t < \infty)$: $x_1(t) = \cos t + \cos 2t$, $x_2(t) = \exp(-\alpha^2 t^2)$.

Solution:

$$P_{x_1} = \frac{1}{T} \int_{-T/2}^{T/2} (\cos t + \cos 2t)^2 dt = 1 \Rightarrow \text{power signal}$$

Note that since the cosine function is periodic, the limit is not necessary.

$$E_{x_2} = \int_{-\infty}^{\infty} (e^{-\alpha^2 t^2})^2 dt = 2 \int_0^{\infty} e^{-2\alpha^2 t^2} dt = 2 \frac{\sqrt{\pi}}{2\sqrt{2}\alpha} = \frac{1}{\alpha} \frac{\sqrt{\pi}}{\sqrt{2}} \Rightarrow \text{energy signal}.$$

Electrical systems can be linear or nonlinear. Furthermore, linear systems may be divided into continuous or discrete. A system is linear if the input signal $x_1(t)$ produces $y_1(t)$ and $x_2(t)$ produces $y_2(t)$; then for some arbitrary constants a_1 and a_2 the input signal $a_1x_1(t) + a_2x_2(t)$ produces the output $a_1y_1(t) + a_2y_2(t)$. A linear system is said to be shift invariant (or time invariant) if a time shift at its input produces the same shift at its output. More precisely, if the input signal $x(t)$ produces $y(t)$ then the delayed signal $x(t - t_0)$ produces the output $y(t - t_0)$. The impulse response of a Linear Time Invariant (LTI) system, $h(t)$, is defined to be the system's output when the input is an impulse (delta function).

13.2. The Fourier Transform

The Fourier Transform (FT) of the signal $x(t)$ is

$$F\{x(t)\} = X(\omega) = \int_{-\infty}^{\infty} x(t)e^{-j\omega t} dt \quad (13.6)$$

or

$$F\{x(t)\} = X(f) = \int_{-\infty}^{\infty} x(t)e^{-j2\pi ft} dt \quad (13.7)$$

and the Inverse Fourier Transform (IFT) is

$$F^{-1}\{X(\omega)\} = x(t) = \frac{1}{2\pi} \int_{-\infty}^{\infty} X(\omega)e^{j\omega t} d\omega \quad (13.8)$$

or

$$F^{-1}\{X(f)\} = x(t) = \int_{-\infty}^{\infty} X(f)e^{j2\pi ft} df \quad (13.9)$$

where, in general, t represents time, while $\omega = 2\pi f$ and f represent frequency in radians per second and Hertz, respectively. In this book we will use both notations for the transform, as appropriate (i.e., $X(\omega)$ and $X(f)$).

A detailed table of the FT pairs is listed in Appendix C. The FT properties are (the proofs are left as an exercise):

1. *Linearity:*

$$F\{a_1x_1(t) + a_2x_2(t)\} = a_1X_1(\omega) + a_2X_2(\omega) \quad (13.10)$$

2. *Symmetry:* If $F\{x(t)\} = X(\omega)$ then

$$2\pi X(-\omega) = \int_{-\infty}^{\infty} X(t)e^{-j\omega t} dt \quad (13.11)$$

3. *Shifting:* For any real time t_0

$$F\{x(t \pm t_0)\} = e^{\pm j\omega t_0} X(\omega) \quad (13.12)$$

4. *Scaling: If $F\{x(t)\} = X(\omega)$ then*

$$F\{x(at)\} = \frac{1}{|a|} X\left(\frac{\omega}{a}\right) \quad (13.13)$$

5. *Central Ordinate:*

$$X(0) = \int_{-\infty}^{\infty} x(t) dt \quad (13.14)$$

$$x(0) = \frac{1}{2\pi} \int_{-\infty}^{\infty} X(\omega) d\omega \quad (13.15)$$

6. *Frequency Shift: If $F\{x(t)\} = X(\omega)$ then*

$$F\{e^{\pm j\omega_0 t} x(t)\} = X(\omega \mp \omega_0) \quad (13.16)$$

7. *Modulation: If $F\{x(t)\} = X(\omega)$ then*

$$F\{x(t) \cos \omega_0 t\} = \frac{1}{2} [X(\omega + \omega_0) + X(\omega - \omega_0)] \quad (13.17)$$

$$F\{x(t) \sin(\omega_0 t)\} = \frac{1}{2j} [X(\omega - \omega_0) - X(\omega + \omega_0)] \quad (13.18)$$

8. *Derivatives:*

$$F\left\{\frac{d^n}{dt^n} (x(t))\right\} = (j\omega)^n X(\omega) \quad (13.19)$$

9. *Time Convolution: if $x(t)$ and $h(t)$ have Fourier transforms $X(\omega)$ and $H(\omega)$, respectively, then*

$$F\left\{\int_{-\infty}^{\infty} x(\tau) h(t - \tau) d\tau\right\} = X(\omega) H(\omega) \quad (13.20)$$

10. Frequency Convolution:

$$F\{x(t)h(t)\} = \frac{1}{2\pi} \int_{-\infty}^{\infty} X(\tau)H(\omega - \tau)d\tau \quad (13.21)$$

11. Autocorrelation:

$$F\left\{ \int_{-\infty}^{\infty} x(\tau)x^*(\tau - t)d\tau \right\} = X(\omega)X^*(\omega) = |X(\omega)|^2 \quad (13.22)$$

12. Parseval's Theorem: The energy associated with the signal $x(t)$ is

$$E = \int_{-\infty}^{\infty} |x(t)|^2 dt = \int_{-\infty}^{\infty} |X(\omega)|^2 d\omega \quad (13.23)$$

13. Moments: The n th moment is

$$m_n = \int_0^{\infty} t^n x(t) dt = \frac{d^n}{d\omega^n} X(\omega) \Big|_{\omega=0} \quad (13.24)$$

13.3. The Fourier Series

A set of functions $S = \{\phi_n(t) ; n= 1, \dots, N\}$ is said to be orthogonal over the interval (t_1, t_2) if and only if

$$\int_{t_1}^{t_2} \phi_i^*(t)\phi_j(t)dt = \int_{t_1}^{t_2} \phi_i(t)\phi_j^*(t)dt = \begin{cases} 0 & i \neq j \\ \lambda_i & i = j \end{cases} \quad (13.25)$$

where the asterisk indicates complex conjugate, and λ_i are constants. If $\lambda_i = 1$ for all i , then the set S is said to be an orthonormal set.

An electrical signal $x(t)$ can be expressed over the interval (t_1, t_2) as a weighted sum of a set of orthogonal functions as

$$x(t) \approx \sum_{n=1}^N X_n \phi_n(t) \quad (13.26)$$

where X_n are, in general, complex constants, and the orthogonal functions $\varphi_n(t)$ are called basis functions. If the integral-square error over the interval (t_1, t_2) is equal to zero as N approaches infinity, i.e.,

$$\lim_{N \rightarrow \infty} \int_{t_1}^{t_2} \left| x(t) - \sum_{n=1}^N X_n \varphi_n(t) \right|^2 dt = 0 \quad (13.27)$$

then the set $S = \{\varphi_n(t)\}$ is said to be complete, and Eq. (13.12) becomes an equality. The constants X_n are computed as

$$X_n = \frac{\int_{t_1}^{t_2} x(t) \varphi_n^*(t) dt}{\int_{t_1}^{t_2} |\varphi_n(t)|^2 dt} \quad (13.28)$$

Let the signal $x(t)$ be periodic with period T , and let the complete orthogonal set S be

$$S = \left\{ e^{\frac{j2\pi n t}{T}} ; n = -\infty, \infty \right\} \quad (13.29)$$

Then the complex exponential Fourier series of $x(t)$ is

$$x(t) = \sum_{n=-\infty}^{\infty} X_n e^{\frac{j2\pi n t}{T}} \quad (13.30)$$

Using Eq. (13.28) yields

$$X_n = \frac{1}{T} \int_{-T/2}^{T/2} x(t) e^{-\frac{j2\pi n t}{T}} dt \quad (13.31)$$

The FT of Eq. (13.30) is given by

$$X(\omega) = 2\pi \sum_{n=-\infty}^{\infty} X_n \delta\left(\omega - \frac{2\pi n}{T}\right) \quad (13.32)$$

where $\delta(\cdot)$ is delta function. When the signal $x(t)$ is real we can compute its trigonometric Fourier series from Eq. (13.30) as

$$x(t) = a_0 + \sum_{n=1}^{\infty} a_n \cos\left(\frac{2\pi nt}{T}\right) + \sum_{n=1}^{\infty} b_n \sin\left(\frac{2\pi nt}{T}\right) \quad (13.33)$$

$$a_0 = X_0$$

$$a_n = \frac{1}{T} \int_{-T/2}^{T/2} x(t) \cos\left(\frac{2\pi nt}{T}\right) dt \quad (13.34)$$

$$b_n = \frac{1}{T} \int_{-T/2}^{T/2} x(t) \sin\left(\frac{2\pi nt}{T}\right) dt$$

The coefficients a_n are all zeros when the signal $x(t)$ is an odd function of time. Alternatively, when the signal is an even function of time, then all b_n are equal to zero.

Consider the periodic energy signal defined in Eq. (13.33). The total energy associated with this signal is then given by

$$E = \frac{1}{T} \int_{t_0}^{t_0+T} |x(t)|^2 dt = \frac{a_0^2}{4} + \sum_{n=1}^{\infty} \left(\frac{a_n^2}{2} + \frac{b_n^2}{2} \right) \quad (13.35)$$

13.4. Convolution and Correlation Integrals

The convolution $\phi_{xh}(t)$ between the signals $x(t)$ and $h(t)$ is defined by

$$\phi_{xh}(t) = x(t) \bullet h(t) = \int_{-\infty}^{\infty} x(\tau) h(t - \tau) d\tau \quad (13.36)$$

where τ is a dummy variable, and the operator \bullet is used to symbolically describe the convolution integral. Convolution is commutative, associative, and distributive. More precisely,

$$\begin{aligned} x(t) \bullet h(t) &= h(t) \bullet x(t) \\ x(t) \bullet h(t) \bullet g(t) &= (x(t) \bullet h(t)) \bullet g(t) = x(t) \bullet (h(t) \bullet g(t)) \end{aligned} \quad (13.37)$$

For the convolution integral to be finite at least one of the two signals must be an energy signal. The convolution between two signals can be computed using the FT

$$\phi_{xh}(t) = F^{-1}\{X(\omega)H(\omega)\} \quad (13.38)$$

Consider an LTI system with impulse response $h(t)$ and input signal $x(t)$. It follows that the output signal $y(t)$ is equal to the convolution between the input signal and the system impulse response,

$$y(t) = \int_{-\infty}^{\infty} x(\tau)h(t - \tau)d\tau = \int_{-\infty}^{\infty} h(\tau)x(t - \tau)d\tau \quad (13.39)$$

The cross-correlation function between the signals $x(t)$ and $g(t)$ is defined as

$$R_{xg}(t) = \int_{-\infty}^{\infty} x^*(\tau)g(t + \tau)d\tau \quad (13.40)$$

Again, at least one of the two signals should be an energy signal for the correlation integral to be finite. The cross-correlation function measures the similarity between the two signals. The peak value of $R_{xg}(t)$ and its spread around this peak are an indication of how good this similarity is. The cross-correlation integral can be computed as

$$R_{xg}(t) = F^{-1}\{X^*(\omega)G(\omega)\} \quad (13.41)$$

When $x(t) = g(t)$ we get the autocorrelation integral,

$$R_x(t) = \int_{-\infty}^{\infty} x^*(\tau)x(t + \tau)d\tau \quad (13.42)$$

Note that the autocorrelation function is denoted by $R_x(t)$ rather than $R_{xx}(t)$. When the signals $x(t)$ and $g(t)$ are power signals, the correlation integral becomes infinite and thus, time averaging must be included. More precisely,

$$\bar{R}_{xg}(t) = \lim_{T \rightarrow \infty} \frac{1}{T} \int_{-T/2}^{T/2} x^*(\tau)g(t + \tau)d\tau \quad (13.43)$$

13.5. Energy and Power Spectrum Densities

Consider an energy signal $x(t)$. From Parseval's theorem, the total energy associated with this signal is

$$E = \int_{-\infty}^{\infty} |x(t)|^2 dt = \frac{1}{2\pi} \int_{-\infty}^{\infty} |X(\omega)|^2 d\omega \quad (13.44)$$

When $x(t)$ is a voltage signal, the amount of energy dissipated by this signal when applied across a network of resistance R is

$$E = \frac{1}{R} \int_{-\infty}^{\infty} |x(t)|^2 dt = \frac{1}{2\pi R} \int_{-\infty}^{\infty} |X(\omega)|^2 d\omega \quad (13.45)$$

Alternatively, when $x(t)$ is a current signal we get

$$E = R \int_{-\infty}^{\infty} |x(t)|^2 dt = \frac{R}{2\pi} \int_{-\infty}^{\infty} |X(\omega)|^2 d\omega \quad (13.46)$$

The quantity $\int |X(\omega)|^2 d\omega$ represents the amount of energy spread per unit frequency across a 1Ω resistor; therefore, the Energy Spectrum Density (ESD) function for the energy signal $x(t)$ is defined as

$$ESD = |X(\omega)|^2 \quad (13.47)$$

The ESD at the output of an LTI system when $x(t)$ is at its input is

$$|Y(\omega)|^2 = |X(\omega)|^2 |H(\omega)|^2 \quad (13.48)$$

where $H(\omega)$ is the FT of the system impulse response, $h(t)$. It follows that the energy present at the output of the system is

$$E_y = \frac{1}{2\pi} \int_{-\infty}^{\infty} |X(\omega)|^2 |H(\omega)|^2 d\omega \quad (13.49)$$

Example 13.2: The voltage signal $x(t) = e^{-5t}$; $t \geq 0$ is applied to the input of a low pass LTI system. The system bandwidth is 5Hz , and its input resistance is 5Ω . If $H(\omega) = 1$ over the interval $(-10\pi < \omega < 10\pi)$ and zero elsewhere, compute the energy at the output.

Solution: From Eqs. (13.45) and (13.49) we get

$$E_y = \frac{1}{2\pi R} \int_{\omega = -10\pi}^{10\pi} |X(\omega)|^2 |H(\omega)|^2 d\omega$$

Using Fourier transform tables and substituting $R = 5$ yield

$$E_y = \frac{1}{5\pi} \int_0^{10\pi} \frac{1}{\omega^2 + 25} d\omega$$

Completing the integration yields

$$E_y = \frac{1}{25\pi} [\operatorname{atanh}(2\pi) - \operatorname{atanh}(0)] = 0.01799 \text{ Joules}$$

Note that an infinite bandwidth would give $E_y = 0.02$, only 11% larger.

The total power associated with a power signal $g(t)$ is

$$P = \lim_{T \rightarrow \infty} \frac{1}{T} \int_{-T/2}^{T/2} |g(t)|^2 dt \quad (13.50)$$

Define the Power Spectrum Density (PSD) function for the signal $g(t)$ as $S_g(\omega)$, where

$$P = \lim_{T \rightarrow \infty} \frac{1}{T} \int_{-T/2}^{T/2} |g(t)|^2 dt = \frac{1}{2\pi} \int_{-\infty}^{\infty} S_g(\omega) d\omega \quad (13.51)$$

It can be shown that (see Problem 1.13)

$$S_g(\omega) = \lim_{T \rightarrow \infty} \frac{|G(\omega)|^2}{T} \quad (13.52)$$

Let the signals $x(t)$ and $g(t)$ be two periodic signals with period T . The complex exponential Fourier series expansions for those signals are, respectively, given by

$$x(t) = \sum_{n=-\infty}^{\infty} X_n e^{\frac{j2\pi n t}{T}} \quad (13.53)$$

$$g(t) = \sum_{m=-\infty}^{\infty} G_m e^{\frac{j2\pi m t}{T}} \quad (13.54)$$

The power cross-correlation function $\bar{R}_{gx}(t)$ was given in Eq. (13.43), and is repeated here as Eq. (13.55),

$$\bar{R}_{gx}(t) = \frac{1}{T} \int_{-T/2}^{T/2} g^*(\tau)x(t+\tau)d\tau \quad (13.55)$$

Note that because both signals are periodic the limit is no longer necessary. Substituting Eqs. (13.53) and (13.54) into Eq. (13.55), collecting terms, and using the definition of orthogonality, we get

$$\bar{R}_{gx}(t) = \sum_{n=-\infty}^{\infty} G_n^* X_n e^{\frac{j2n\pi t}{T}} \quad (13.56)$$

When $x(t) = g(t)$, Eq. (13.56) becomes the power autocorrelation function,

$$\bar{R}_x(t) = \sum_{n=-\infty}^{\infty} |X_n|^2 e^{\frac{j2n\pi t}{T}} = |X_0|^2 + 2 \sum_{n=1}^{\infty} |X_n|^2 e^{\frac{j2n\pi t}{T}} \quad (13.57)$$

The power spectrum and cross-power spectrum density functions are then computed as the FT of Eqs. (13.57) and (13.56), respectively. More precisely,

$$\begin{aligned} \bar{S}_x(\omega) &= 2\pi \sum_{n=-\infty}^{\infty} |X_n|^2 \delta\left(\omega - \frac{2n\pi}{T}\right) \\ \bar{S}_{gx}(\omega) &= 2\pi \sum_{n=-\infty}^{\infty} G_n^* X_n \delta\left(\omega - \frac{2n\pi}{T}\right) \end{aligned} \quad (13.58)$$

The line (or discrete) power spectrum is defined as the plot of $|X_n|^2$ versus n , where the lines are $\Delta f = 1/T$ apart. The DC power is $|X_0|^2$, and the total

power is $\sum_{n=-\infty}^{\infty} |X_n|^2$.

13.6. Random Variables

Consider an experiment with outcomes defined by a certain sample space. The rule or functional relationship that maps each point in this sample space into a real number is called “random variable.” Random variables are designated by capital letters (e.g., X, Y, \dots), and a particular value of a random variable is denoted by a lowercase letter (e.g., x, y, \dots).

The Cumulative Distribution Function (*cdf*) associated with the random variable X is denoted as $F_X(x)$, and is interpreted as the total probability that the random variable X is less or equal to the value x . More precisely,

$$F_X(x) = Pr\{X \leq x\} \quad (13.59)$$

The probability that the random variable X is in the interval (x_1, x_2) is then given by

$$F_X(x_2) - F_X(x_1) = Pr\{x_1 \leq X \leq x_2\} \quad (13.60)$$

The *cdf* has the following properties:

$$\begin{aligned} 0 &\leq F_X(x) \leq 1 \\ F_X(-\infty) &= 0 \\ F_X(\infty) &= 1 \\ F_X(x_1) \leq F_X(x_2) &\Leftrightarrow x_1 \leq x_2 \end{aligned} \quad (13.61)$$

It is often practical to describe a random variable by the derivative of its *cdf*, which is called the Probability Density Function (*pdf*). The *pdf* of the random variable X is

$$f_X(x) = \frac{d}{dx}F_X(x) \quad (13.62)$$

or, equivalently,

$$F_X(x) = Pr\{X \leq x\} = \int_{-\infty}^x f_X(\lambda) d\lambda \quad (13.63)$$

The probability that a random variable X has values in the interval (x_1, x_2) is

$$F_X(x_2) - F_X(x_1) = Pr\{x_1 \leq X \leq x_2\} = \int_{x_1}^{x_2} f_X(x) dx \quad (13.64)$$

Define the *n*th moment for the random variable X as

$$E[X^n] = \overline{X^n} = \int_{-\infty}^{\infty} x^n f_X(x) dx \quad (13.65)$$

The first moment, $E[X]$, is called the mean value, while the second moment, $E[X^2]$, is called the mean squared value. When the random variable X

represents an electrical signal across a 1Ω resistor, then $E[X]$ is the DC component, and $E[X^2]$ is the total average power.

The n th central moment is defined as

$$E[(X - \bar{X})^n] = \overline{(X - \bar{X})^n} = \int_{-\infty}^{\infty} (x - \bar{x})^n f_X(x) dx \quad (13.66)$$

and thus, the first central moment is zero. The second central moment is called the variance and is denoted by the symbol σ_X^2 ,

$$\sigma_X^2 = \overline{(X - \bar{X})^2} \quad (13.67)$$

Appendix E has some common *pdfs* and their means and variances.

In practice, the random nature of an electrical signal may need to be described by more than one random variable. In this case, the joint *cdf* and *pdf* functions need to be considered. The joint *cdf* and *pdf* for the two random variables X and Y are, respectively, defined by

$$F_{XY}(x, y) = Pr\{X \leq x; Y \leq y\} \quad (13.68)$$

$$f_{XY}(x, y) = \frac{\partial^2}{\partial x \partial y} F_{XY}(x, y) \quad (13.69)$$

The marginal *cdfs* are obtained as follows:

$$F_X(x) = \int_{-\infty}^{\infty} \int_{-\infty}^x f_{UV}(u, v) du dv = F_{XY}(x, \infty) \quad (13.70)$$

$$F_Y(y) = \int_{-\infty}^{\infty} \int_{-\infty}^y f_{UV}(u, v) dv du = F_{XY}(\infty, y)$$

If the two random variables are statistically independent, then the joint *cdfs* and *pdfs* are, respectively, given by

$$F_{XY}(x, y) = F_X(x)F_Y(y) \quad (13.71)$$

$$f_{XY}(x, y) = f_X(x)f_Y(y) \quad (13.72)$$

Let us now consider a case when the two random variables X and Y are mapped into two new variables U and V through some transformations T_1 and T_2 defined by

$$\begin{aligned} U &= T_1(X, Y) \\ V &= T_2(X, Y) \end{aligned} \tag{13.73}$$

The joint *pdf*, $f_{UV}(u, v)$, may be computed based on the invariance of probability under the transformation. One must first compute the matrix of derivatives; then the new joint *pdf* is computed as

$$f_{UV}(u, v) = f_{XY}(x, y)|J| \tag{13.74}$$

$$|J| = \begin{vmatrix} \frac{\partial x}{\partial u} & \frac{\partial x}{\partial v} \\ \frac{\partial y}{\partial u} & \frac{\partial y}{\partial v} \end{vmatrix} \tag{13.75}$$

where the determinant of the matrix of derivatives $|J|$ is called the Jacobian.

The characteristic function for the random variable X is defined as

$$C_X(\omega) = E[e^{j\omega X}] = \int_{-\infty}^{\infty} f_X(x)e^{j\omega x} dx \tag{13.76}$$

The characteristic function can be used to compute the *pdf* for a sum of independent random variables. More precisely, let the random variable Y be equal to

$$Y = X_1 + X_2 + \dots + X_N \tag{13.77}$$

where $\{X_i ; i = 1, \dots, N\}$ is a set of independent random variables. It can be shown that

$$C_Y(\omega) = C_{X_1}(\omega)C_{X_2}(\omega)\dots C_{X_N}(\omega) \tag{13.78}$$

and the *pdf* $f_Y(y)$ is computed as the inverse Fourier transform of $C_Y(\omega)$ (with the sign of y reversed),

$$f_Y(y) = \frac{1}{2\pi} \int_{-\infty}^{\infty} C_Y(\omega)e^{-j\omega y} d\omega \tag{13.79}$$

The characteristic function may also be used to compute the n th moment for the random variable X as

$$E[X^n] = (-j)^n \frac{d^n}{d\omega^n} C_X(\omega) \Big|_{\omega=0} \quad (13.80)$$

13.7. Multivariate Gaussian Distribution

Consider a joint probability for m random variables, X_1, X_2, \dots, X_m . These variables can be represented as components of an $m \times 1$ random column vector, \underline{X} . More precisely,

$$\underline{X}^t = [X_1 \ X_2 \ \dots \ X_m] \quad (13.81)$$

where the superscript indicates the transpose operation. The joint *pdf* for the vector \underline{X} is

$$f_{\underline{x}}(\underline{x}) = f_{x_1, x_2, \dots, x_m}(x_1, x_2, \dots, x_m) \quad (13.82)$$

The mean vector is defined as

$$\underline{\mu}_x = [E[X_1] \ E[X_2] \ \dots \ E[X_m]]^t \quad (13.83)$$

and the covariance is an $m \times m$ matrix given by

$$C_x = E[\underline{X} \ \underline{X}^t] - \underline{\mu}_x \ \underline{\mu}_x^t \quad (13.84)$$

Note that if the elements of the vector \underline{X} are independent, then the covariance matrix is a diagonal matrix.

By definition a random vector \underline{X} is multivariate Gaussian if its *pdf* has the form

$$f_{\underline{x}}(\underline{x}) = [(2\pi)^{m/2} |C_x|^{1/2}]^{-1} \exp\left(-\frac{1}{2}(\underline{x} - \underline{\mu}_x)^t C_x^{-1} (\underline{x} - \underline{\mu}_x)\right) \quad (13.85)$$

where $\underline{\mu}_x$ is the mean vector, C_x is the covariance matrix, C_x^{-1} is inverse of the covariance matrix and $|C_x|$ is its determinant, and \underline{X} is of dimension m . If \underline{A} is a $k \times m$ matrix of rank k , then the random vector $\underline{Y} = \underline{A}\underline{X}$ is a k -variate Gaussian vector with

$$\underline{\mu}_y = \underline{A}\underline{\mu}_x \quad (13.86)$$

and

$$C_y = \underline{A} C_x \underline{A}^t \quad (13.87)$$

The characteristic function for a multivariate Gaussian *pdf* is defined by

$$C_{\underline{X}} = E[\exp\{j(\omega_1 X_1 + \omega_2 X_2 + \dots + \omega_m X_m)\}] = \quad (13.88)$$

$$\exp\left\{j\mu_x' \underline{\omega} - \frac{1}{2} \underline{\omega}' C_x \underline{\omega}\right\}$$

Then the moments for the joint distribution can be obtained by partial differentiation. For example,

$$E[X_1 X_2 X_3] = \frac{\partial^3}{\partial \omega_1 \partial \omega_2 \partial \omega_3} C_{\underline{X}}(\omega_1, \omega_2, \omega_3) \quad \text{at} \quad \underline{\omega} = \underline{0} \quad (13.89)$$

Example 13.3: The vector \underline{X} is a 4-variate Gaussian with

$$\mu_x = [2 \ 1 \ 1 \ 0]^t$$

$$C_x = \begin{bmatrix} 6 & 3 & 2 & 1 \\ 3 & 4 & 3 & 2 \\ 2 & 3 & 4 & 3 \\ 1 & 2 & 3 & 3 \end{bmatrix}$$

Define

$$\underline{X}_1 = \begin{bmatrix} X_1 \\ X_2 \end{bmatrix} \quad \underline{X}_2 = \begin{bmatrix} X_3 \\ X_4 \end{bmatrix}$$

Find the distribution of \underline{X}_1 and the distribution of

$$\underline{Y} = \begin{bmatrix} 2X_1 \\ X_1 + 2X_2 \\ X_3 + X_4 \end{bmatrix}$$

Solution:

\underline{X}_1 has a bivariate Gaussian distribution with

$$\mu_{x_1} = \begin{bmatrix} 2 \\ 1 \end{bmatrix} \quad C_{x_1} = \begin{bmatrix} 6 & 3 \\ 3 & 4 \end{bmatrix}$$

The vector \underline{Y} can be expressed as

$$\underline{Y} = \begin{bmatrix} 2 & 0 & 0 & 0 \\ 1 & 2 & 0 & 0 \\ 0 & 0 & 1 & 1 \end{bmatrix} \begin{bmatrix} X_1 \\ X_2 \\ X_3 \\ X_4 \end{bmatrix} = \underline{A}\underline{X}$$

It follows that

$$\mu_y = \underline{A}\mu_x = [4 \ 4 \ 1]^t$$

$$C_y = \underline{A}C_x\underline{A}^t = \begin{bmatrix} 24 & 24 & 6 \\ 24 & 34 & 13 \\ 6 & 13 & 13 \end{bmatrix}$$

13.8. Random Processes

A random variable X is by definition a mapping of all possible outcomes of a random experiment to numbers. When the random variable becomes a function of both the outcomes of the experiment as well as time, it is called a random process and is denoted by $X(t)$. Thus, one can view a random process as an ensemble of time domain functions that are the outcome of a certain random experiment, as compared to single real numbers in the case of a random variable.

Since the *cdf* and *pdf* of a random process are time dependent, we will denote them as $F_X(x;t)$ and $f_X(x;t)$, respectively. The n th moment for the random process $X(t)$ is

$$E[X^n(t)] = \int_{-\infty}^{\infty} x^n f_X(x;t) dx \quad (13.90)$$

A random process $X(t)$ is referred to as stationary to order one if all its statistical properties do not change with time. Consequently, $E[X(t)] = \bar{X}$, where \bar{X} is a constant. A random process $X(t)$ is called stationary to order two (or wide sense stationary) if

$$f_{\bar{X}}(x_1, x_2; t_1, t_2) = f_{\bar{X}}(x_1, x_2; t_1 + \Delta t, t_2 + \Delta t) \quad (13.91)$$

for all t_1, t_2 and Δt .

Define the statistical autocorrelation function for the random process $X(t)$ as

$$\mathfrak{R}_X(t_1, t_2) = E[X(t_1)X(t_2)] \quad (13.92)$$

The correlation $E[X(t_1)X(t_2)]$ is, in general, a function of (t_1, t_2) . As a consequence of the wide sense stationary definition, the autocorrelation function depends on the time difference $\tau = t_2 - t_1$, rather than on absolute time; and thus, for a wide sense stationary process we have

$$\begin{aligned} E[X(t)] &= \bar{X} \\ \mathfrak{R}_X(\tau) &= E[X(t)X(t + \tau)] \end{aligned} \quad (13.93)$$

If the time average and time correlation functions are equal to the statistical average and statistical correlation functions, the random process is referred to as an ergodic random process. The following is true for an ergodic process:

$$\lim_{T \rightarrow \infty} \frac{1}{T} \int_{-T/2}^{T/2} x(t) dt = E[X(t)] = \bar{X} \quad (13.94)$$

$$\lim_{T \rightarrow \infty} \frac{1}{T} \int_{-T/2}^{T/2} x^*(t)x(t + \tau) dt = \mathfrak{R}_X(\tau) \quad (13.95)$$

The covariance of two random processes $X(t)$ and $Y(t)$ is defined by

$$C_{XY}(t, t + \tau) = E[\{X(t) - E[X(t)]\}\{Y(t + \tau) - E[Y(t + \tau)]\}] \quad (13.96)$$

which can be written as

$$C_{XY}(t, t + \tau) = \mathfrak{R}_{XY}(\tau) - \bar{X}\bar{Y} \quad (13.97)$$

13.9. Sampling Theorem

Most modern communication and radar systems are designed to process discrete samples of signals bearing information. In general, we would like to determine the necessary condition such that a signal can be fully reconstructed from its samples by filtering, or data processing in general. The answer to this question lies in the sampling theorem which may be stated as follows: let the signal $x(t)$ be real-valued and band-limited with bandwidth B ; this signal can be fully reconstructed from its samples if the time interval between samples is no greater than $1/(2B)$.

Fig. 13.1 illustrates the sampling process concept. The sampling signal $p(t)$ is periodic with period T_s , which is called the sampling interval. The Fourier series expansion of $p(t)$ is

$$p(t) = \sum_{n=-\infty}^{\infty} P_n e^{j\frac{2\pi n t}{T_s}} \quad (13.98)$$

The sampled signal $x_s(t)$ is then given by

$$x_s(t) = \sum_{n=-\infty}^{\infty} x(t) P_n e^{j\frac{2\pi n t}{T_s}} \quad (13.99)$$

Taking the FT of Eq. (13.99) yields

$$X_s(\omega) = \sum_{n=-\infty}^{\infty} P_n X\left(\omega - \frac{2\pi n}{T_s}\right) = P_0 X(\omega) + \sum_{\substack{n=-\infty \\ n \neq 0}}^{\infty} P_n X\left(\omega - \frac{2\pi n}{T_s}\right) \quad (13.100)$$

where $X(\omega)$ is the FT of $x(t)$.

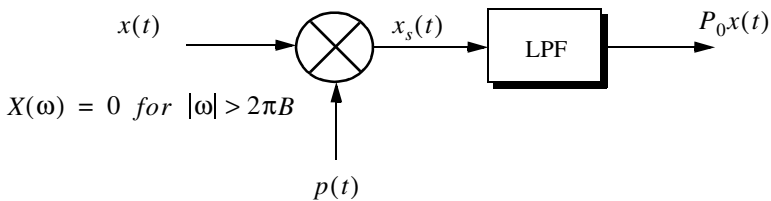


Figure 13.1. Concept of sampling.

Therefore, we conclude that the spectral density, $X_s(\omega)$, consists of replicas of $X(\omega)$ spaced $(2\pi/T_s)$ apart and scaled by the Fourier series coefficients P_n . A Low Pass Filter (LPF) of bandwidth B can then be used to recover the original signal $x(t)$.

When the sampling rate is increased (i.e., T_s decreases), the replicas of $X(\omega)$ move farther apart from each other. Alternatively, when the sampling rate is decreased (i.e., T_s increases), the replicas get closer to one another. The value of T_s such that the replicas are tangent to one another defines the minimum required sampling rate so that $x(t)$ can be recovered from its samples by using an LPF. It follows that

$$\frac{2\pi}{T_s} = 2\pi(2B) \Leftrightarrow T_s = \frac{1}{2B} \quad (13.101)$$

The sampling rate defined by Eq. (13.101) is known as the Nyquist sampling rate. When $T_s > (1/2B)$, the replicas of $X(\omega)$ overlap and thus, $x(t)$ cannot be recovered cleanly from its samples. This is known as aliasing. In practice, ideal LPF cannot be implemented; hence, practical systems tend to over-sample in order to avoid aliasing.

Example 13.4: Assume that the sampling signal $p(t)$ is given by

$$p(t) = \sum_{n=-\infty}^{\infty} \delta(t - nT_s)$$

Compute an expression for $X_s(\omega)$.

Solution: The signal $p(t)$ is called the Comb function. Its exponential Fourier series is

$$p(t) = \sum_{n=-\infty}^{\infty} \frac{1}{T_s} e^{\frac{2\pi n t}{T_s}}$$

It follows that

$$x_s(t) = \sum_{n=-\infty}^{\infty} x(t) \frac{1}{T_s} e^{\frac{2\pi n t}{T_s}}$$

Taking the Fourier transform of this equation yields

$$X_s(\omega) = \frac{2\pi}{T_s} \sum_{n=-\infty}^{\infty} X\left(\omega - \frac{2\pi n}{T_s}\right).$$

Before proceeding to the next section, we will establish the following notation: samples of the signal $x(t)$ are denoted by $x(n)$ and referred to as a discrete time domain sequence, or simply a sequence. If the signal $x(t)$ is periodic, we will denote its sample by the periodic sequence $x(n)$.

13.10. The Z-Transform

The Z-transform is a transformation that maps samples of a discrete time domain sequence into a new domain known as the z-domain. It is defined as

$$Z\{x(n)\} = X(z) = \sum_{n=-\infty}^{\infty} x(n)z^{-n} \quad (13.102)$$

where $z = re^{j\omega}$, and for most cases, $r = 1$. It follows that Eq. (13.102) can be rewritten as

$$X(e^{j\omega}) = \sum_{n=-\infty}^{\infty} x(n)e^{-jn\omega} \quad (13.103)$$

In the z-domain, the region over which $X(z)$ is finite is called the Region of Convergence (ROC). Appendix D has a list of most common Z-transform pairs. The Z-transform properties are (the proofs are left as an exercise):

1. *Linearity:*

$$Z\{ax_1(n) + bx_2(n)\} = aX_1(z) + bX_2(z) \quad (13.104)$$

2. *Right-Shifting Property:*

$$Z\{x(n-k)\} = z^{-k}X(z) \quad (13.105)$$

3. *Left-Shifting Property:*

$$Z\{x(n+k)\} = z^kX(z) - \sum_{n=0}^{k-1} x(n)z^{k-n} \quad (13.106)$$

4. *Time Scaling:*

$$Z\{a^n x(n)\} = X(a^{-1}z) = \sum_{n=0}^{\infty} (a^{-1}z)^{-n} x(n) \quad (13.107)$$

5. *Periodic Sequences:*

$$Z\{x(n)\} = \frac{z^N}{z^N - 1} Z\{x(n)\} \quad (13.108)$$

where N is the period.

6. *Multiplication by n :*

$$Z\{nx(n)\} = -z \frac{d}{dz} X(z) \quad (13.109)$$

7. *Division by $n + a$; a is a real number:*

$$Z\left\{\frac{x(n)}{n+a}\right\} = \sum_{n=0}^{\infty} x(n) z^a \left(-\int_0^z u^{-k-a-1} du \right) \quad (13.110)$$

8. *Initial Value:*

$$x(n_0) = z^{n_0} X(z) \Big|_{z \rightarrow \infty} \quad (13.111)$$

9. *Final Value:*

$$\lim_{n \rightarrow \infty} x(n) = \lim_{z \rightarrow 1} (1 - z^{-1}) X(z) \quad (13.112)$$

10. *Convolution:*

$$Z\left\{\sum_{k=0}^{\infty} h(n-k)x(k)\right\} = H(z)X(z) \quad (13.113)$$

11. *Bilateral Convolution:*

$$Z\left\{\sum_{k=-\infty}^{\infty} h(n-k)x(k)\right\} = H(z)X(z) \quad (13.114)$$

Example 13.5: Prove Eq. (13.109).

Solution: Starting with the definition of the Z-transform,

$$X(z) = \sum_{n=-\infty}^{\infty} x(n)z^{-n}$$

Taking the derivative, with respect to z , of the above equation yields

$$\begin{aligned} \frac{d}{dz}X(z) &= \sum_{n=-\infty}^{\infty} x(n)(-n)z^{-n-1} \\ &= (-z^{-1}) \sum_{n=-\infty}^{\infty} nx(n)z^{-n} \end{aligned}$$

It follows that

$$Z\{nx(n)\} = (-z)\frac{d}{dz}X(z)$$

In general, a discrete LTI system has a transfer function $H(z)$ which describes how the system operates on its input sequence $x(n)$ in order to produce the output sequence $y(n)$. The output sequence $y(n)$ is computed from the discrete convolution between the sequences $x(n)$ and $h(n)$,

$$y(n) = \sum_{m=-\infty}^{\infty} x(m)h(n-m) \quad (13.115)$$

However, since practical systems require that the sequence $x(n)$ be of finite length, we can rewrite Eq. (13.115) as

$$y(n) = \sum_{m=0}^N x(m)h(n-m) \quad (13.116)$$

where N denotes the input sequence length. Taking the Z-transform of Eq. (13.116) yields

$$Y(z) = X(z)H(z) \quad (13.117)$$

and the discrete system transfer function is

$$H(z) = \frac{Y(z)}{X(z)} \quad (13.118)$$

Finally, the transfer function $H(z)$ can be written as

$$H(z)\Big|_{z=e^{j\omega}} = |H(e^{j\omega})|e^{\angle H(e^{j\omega})} \quad (13.119)$$

where $|H(e^{j\omega})|$ is the amplitude response, and $\angle H(e^{j\omega})$ is the phase response.

13.11. The Discrete Fourier Transform

The Discrete Fourier Transform (DFT) is a mathematical operation that transforms a discrete sequence, usually from the time domain into the frequency domain, in order to explicitly determine the spectral information for the sequence. The time domain sequence can be real or complex. The DFT has finite length N , and is periodic with period equal to N .

The discrete Fourier transform for the finite sequence $x(n)$ is defined by

$$\tilde{X}(k) = \sum_{n=0}^{N-1} x(n)e^{-\frac{j2\pi nk}{N}} \quad ; \quad k = 0, \dots, N-1 \quad (13.120)$$

The inverse DFT is given by

$$\tilde{x}(n) = \frac{1}{N} \sum_{k=0}^{N-1} \tilde{X}(k)e^{\frac{j2\pi nk}{N}} \quad ; \quad n = 0, \dots, N-1 \quad (13.121)$$

The Fast Fourier Transform (FFT) is not a new kind of transform different from the DFT. Instead, it is an algorithm used to compute the DFT more efficiently. There are numerous FFT algorithms that can be found in the literature. In this book we will interchangeably use the DFT and the FFT to mean the same. Furthermore, we will assume radix-2 FFT algorithm, where the FFT size is equal to $N = 2^m$ for some integer m .

13.12. Discrete Power Spectrum

Practical discrete systems utilize DFTs of finite length as a means of numerical approximation for the Fourier transform. It follows that input signals must be truncated to a finite duration (denoted by T) before they are sampled. This is necessary so that a finite length sequence is generated prior to signal processing. Unfortunately, this truncation process may cause some serious problems.

To demonstrate this difficulty, consider the time domain signal $x(t) = \sin 2\pi f_0 t$. The spectrum of $x(t)$ consists of two spectral lines at $\pm f_0$. Now, when $x(t)$ is truncated to length T seconds and sampled at a rate $T_s = T/N$, where N is the number of desired samples, we produce the sequence $\{x(n) ; n = 0, 1, \dots, N-1\}$. The spectrum of $x(n)$ would still be composed of the same spectral lines if T is an integer multiple of T_s and if the DFT frequency resolution Δf is an integer multiple of f_0 . Unfortunately, those two conditions are rarely met and as a consequence, the spectrum of $x(n)$ spreads over several lines (normally the spread may extend up to three lines). This is known as spectral leakage. Since f_0 is normally unknown, this discontinuity caused by an arbitrary choice of T cannot be avoided. Windowing techniques can be used to mitigate the effect of this discontinuity by applying smaller weights to samples close to the edges.

A truncated sequence $x(n)$ can be viewed as one period of some periodic sequence $x(n)$ with period N . The discrete Fourier series expansion of $x(n)$ is

$$x(n) = \sum_{k=0}^{N-1} X_k e^{j2\pi nk/N} \quad (13.122)$$

It can be shown that the coefficients X_k are given by

$$X_k = \frac{1}{N} \sum_{n=0}^{N-1} x(n) e^{-j2\pi nk/N} = \frac{1}{N} X(k) \quad (13.123)$$

where $X(k)$ is the DFT of $x(n)$. Therefore, the Discrete Power Spectrum (DPS) for the band limited sequence $x(n)$ is the plot of $|X_k|^2$ versus k , where the lines are Δf apart,

$$P_0 = \frac{1}{N^2} |X(0)|^2$$

$$P_k = \frac{1}{N^2} \{ |X(k)|^2 + |X(N-k)|^2 \} \quad ; \quad k = 1, 2, \dots, \frac{N}{2} - 1 \quad (13.124)$$

$$P_{N/2} = \frac{1}{N^2} |X(N/2)|^2$$

Before proceeding to the next section, we will show how to select the FFT parameters. For this purpose, consider a band limited signal $x(t)$ with bandwidth B . If the signal is not band limited, a LPF can be used to eliminate

frequencies greater than B . In order to satisfy the sampling theorem, one must choose a sampling frequency $f_s = 1/T_s$, such that

$$f_s \geq 2B \quad (13.125)$$

The truncated sequence duration T and the total number of samples N are related by

$$T = NT_s \quad (13.126)$$

or equivalently,

$$f_s = \frac{N}{T} \quad (13.127)$$

It follows that

$$f_s = \frac{N}{T} \geq 2B \quad (13.128)$$

and the frequency resolution is

$$\Delta f = \frac{1}{NT_s} = \frac{f_s}{N} = \frac{1}{T} \geq \frac{2B}{N} \quad (13.129)$$

13.13. Windowing Techniques

Truncation of the sequence $x(n)$ can be accomplished by computing the product,

$$x_w(n) = x(n)w(n) \quad (13.130)$$

where

$$w(n) = \left\{ \begin{array}{ll} f(n) & ; n = 0, 1, \dots, N-1 \\ 0 & otherwise \end{array} \right\} \quad (13.131)$$

where $f(n) \leq 1$. The finite sequence $w(n)$ is called a windowing sequence, or simply a window. The windowing process should not impact the phase response of the truncated sequence. Consequently, the sequence $w(n)$ must retain linear phase. This can be accomplished by making the window symmetrical with respect to its central point.

If $f(n) = 1$ for all n we have what is known as the rectangular window. It leads to the Gibbs phenomenon which manifests itself as an overshoot and a

ripple before and after a discontinuity. Fig. 13.2 shows the amplitude spectrum of a rectangular window. Note that the first side lobe is about $-13.46dB$ below the main lobe. Windows that place smaller weights on the samples near the edges will have lesser overshoot at the discontinuity points (lower side lobes); hence, they are more desirable than a rectangular window. However, side lobes reduction is offset by a widening of the main lobe (loss of resolution). Therefore, the proper choice of a windowing sequence is continuous trade-off between side lobe reduction and main lobe widening.

The multiplication process defined in Eq. (13.131) is equivalent to cyclic convolution in the frequency domain. It follows that $X_w(k)$ is a smeared (distorted) version of $X(k)$. To minimize this distortion, we would seek windows that have a narrow main lobe and small side lobes. Additionally, using a window other than a rectangular window reduces the power by a factor P_w , where

$$P_w = \frac{1}{N} \sum_{n=0}^{N-1} w^2(n) = \sum_{k=0}^{N-1} |W(k)|^2 \quad (13.132)$$

It follows that the DPS for the sequence $x_w(n)$ is now given by

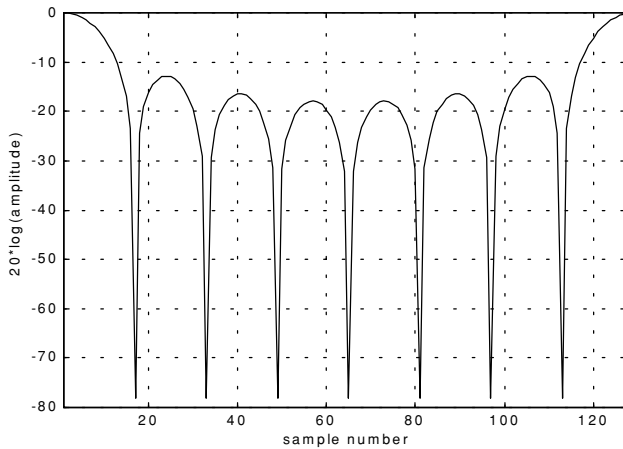


Figure 13.2. Normalized amplitude spectrum for rectangular window.

$$P_0^w = \frac{1}{P_w N^2} |X(0)|^2$$

$$P_k^w = \frac{1}{P_w N^2} \{ |X(k)|^2 + |X(N-k)|^2 \} \quad ; \quad k = 1, 2, \dots, \frac{N}{2} - 1 \quad (13.133)$$

$$P_{N/2}^w = \frac{1}{P_w N^2} |X(N/2)|^2$$

where P_w is defined in Eq. (13.133). [Table 13.1](#) lists some common windows. [Figs. 13.3](#) through [13.5](#) show the frequency domain characteristics for these windows.

TABLE 13.1. Some common windows. $n = 0, N-1$.

Window	Expression	First side lobe	Main lobe width
rectangular	$w(n) = 1$	-13.46dB	1
Hamming	$w(n) = 0.54 - 0.46 \cos\left(\frac{2\pi n}{N-1}\right)$	-41dB	2
Hanning	$w(n) = 0.5 \left[1 - \cos\left(\frac{2\pi n}{N-1}\right) \right]$	-32dB	2
Kaiser	$w(n) = \frac{I_0[\beta \sqrt{1 - (2n/N)^2}]}{I_0(\beta)}$ I_0 is the zero-order modified Bessel function of the first kind	-46dB for $\beta = 2\pi$	$\sqrt{5}$ for $\beta = 2\pi$

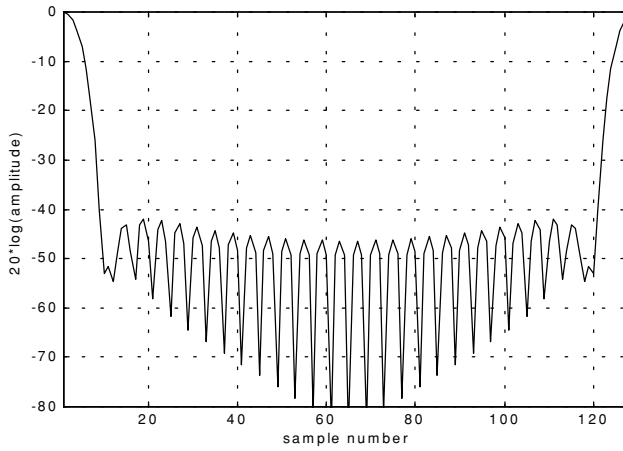


Figure 13.3. Normalized amplitude spectrum for Hamming window.

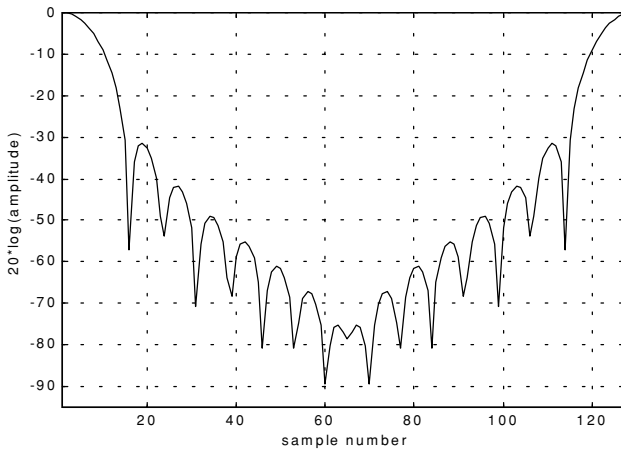


Figure 13.4. Normalized amplitude spectrum for Hanning window.

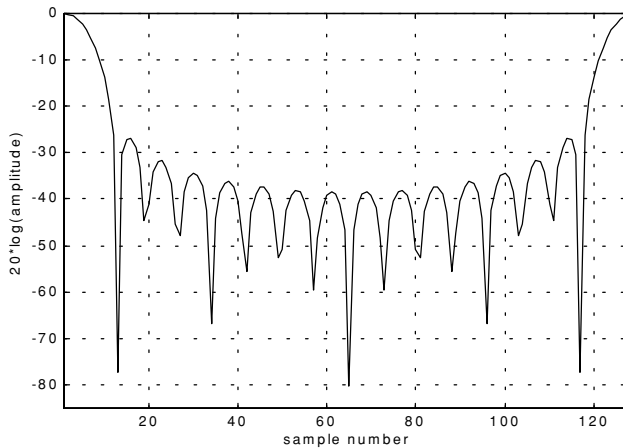


Figure 13.5. Normalized amplitude spectrum for Kaiser window (parameter π).

Problems

13.1. Classify each of the following signals as an energy signal, as a power signal, or as neither. (a) $\exp(0.5t)$ ($t \geq 0$); (b) $\exp(-0.5t)$ ($t \geq 0$); (c) $\cos t + \cos 2t$ ($-\infty < t < \infty$); (d) $e^{-a|t|}$ ($a > 0$).

13.2. Compute the energy associated with the signal $x(t) = A \text{Rect}(t/\tau)$.

13.3. (a) Prove that $\phi_1(t)$ and $\phi_2(t)$, shown in Fig. P13.3, are orthogonal over the interval $(-2 \leq t \leq 2)$. (b) Express the signal $x(t) = t$ as a weighted sum of $\phi_1(t)$ and $\phi_2(t)$ over the same time interval.

13.4. A periodic signal $x_p(t)$ is formed by repeating the pulse $x(t) = 2\Delta((t-3)/5)$ every 10 seconds. (a) What is the Fourier transform of $x(t)$. (b) Compute the complex Fourier series of $x_p(t)$? (c) Give an expression for the autocorrelation function $\bar{R}_{x_p}(t)$ and the power spectrum density $\bar{S}_{x_p}(\omega)$.

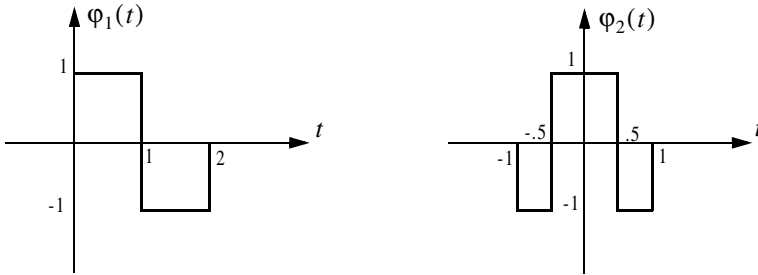


Figure P13.3

13.5. If the Fourier series is

$$x(t) = \sum_{n=-\infty}^{\infty} X_n e^{j2\pi nt/T}$$

define $y(t) = x(t - t_0)$. Compute an expression for the complex Fourier series expansion of $y(t)$.

13.6. Show that (a) $\bar{R}_x(-t) = \bar{R}_x^*(t)$. (b) If $x(t) = f(t) + m_1$ and $y(t) = g(t) + m_2$, then $\bar{R}_{xy}(t) = m_1 m_2$, where the average values for $f(t)$ and $g(t)$ are zeroes.

13.7. What is the power spectral density for the signal

$$x(t) = A \cos(2\pi f_0 t + \theta_0)$$

13.8. A certain radar system uses linear frequency modulated waveforms of the form

$$x(t) = \text{Rect}\left(\frac{t}{\tau}\right) \cos\left(\omega_0 t + \mu \frac{t^2}{2}\right)$$

What are the quadrature components? Give an expression for both the modulation and instantaneous frequencies.

13.9. Consider the signal $x(t) = \text{Rect}(t/\tau) \cos(\omega_0 t - Bt^2/2\tau)$ and let $\tau = 15\mu\text{s}$ and $B = 10\text{MHz}$. What are the quadrature components?

13.10. Determine the quadrature components for the signal

$$h(t) = \delta(t) - \left(\frac{\omega_0}{\omega_d}\right) e^{-2t} \sin \omega_0 t u(t).$$

13.11. If $x(t) = x_1(t) - 2x_1(t-5) + x_1(t-10)$, determine the autocorrelation functions $R_{x_1}(t)$ and $R_x(t)$ when $x_1(t) = \exp(-t^2/2)$.

13.12. Write an expression for the autocorrelation function $R_y(t)$, where

$$y(t) = \sum_{n=1}^5 Y_n \text{Rect}\left(\frac{t-n5}{2}\right)$$

and $\{Y_n\} = \{0.8, 1, 1, 1, 0.8\}$. Give an expression for the density function $S_y(\omega)$.

13.13. Derive Eq. (13.52).

13.14. An LTI system has impulse response

$$h(t) = \begin{cases} \exp(-2t) & t \geq 0 \\ 0 & t < 0 \end{cases}$$

(a) Find the autocorrelation function $R_h(\tau)$. (b) Assume the input of this system is $x(t) = 3 \cos(100t)$. What is the output?

13.15. Suppose you want to determine an unknown DC voltage v_{dc} in the presence of additive white Gaussian noise $n(t)$ of zero mean and variance σ_n^2 . The measured signal is $x(t) = v_{dc} + n(t)$. An estimate of v_{dc} is computed by making three independent measurements of $x(t)$ and computing the arithmetic mean, $\widehat{v}_{dc} \approx (x_1 + x_2 + x_3)/3$. (a) Find the mean and variance of the random variable \widehat{v}_{dc} . (b) Does the estimate of v_{dc} get better by using ten measurements instead of three? Why?

13.16. Consider the network shown in Fig. P13.16, where $x(t)$ is a random voltage with zero mean and autocorrelation function $\mathfrak{R}_x(\tau) = 1 + \exp(-a|\tau|)$. Find the power spectrum $S_x(\omega)$. What is the transfer function? Find the power spectrum $S_v(\omega)$.

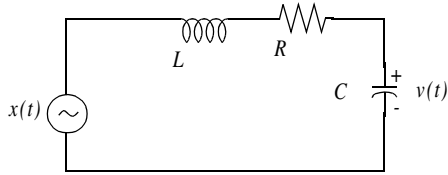


Figure P13.16.

13.17. (a) A random voltage $v(t)$ has an exponential distribution function $f_V(v) = a \exp(-av)$ where $(a > 0); (0 \leq v < \infty)$. The expected value $E[V] = 0.5$. Determine $Pr\{V > 0.5\}$.

13.18. Assume the X and Y miss distances of darts thrown at a bulls-eye dart board are Gaussian with zero mean and variance σ^2 . (a) Determine the probability that a dart will fall between 0.8σ and 1.2σ . (b) Determine the radius of a circle about the bulls-eye that contains 80% of the darts thrown. (c) Consider a square with side s in the first quadrant of the board. Determine s so that the probability that a dart will fall within the square is 0.07.

13.19. Let $\bar{S}_X(\omega)$ be the PSD function for the stationary random process $X(t)$. Compute an expression for the PSD function of $Y(t) = X(t) - 2X(t - T)$.

13.20. Let X be a random variable with

$$f_X(x) = \begin{cases} \frac{1}{\sigma} t^3 e^{-t} & t \geq 0 \\ 0 & \text{elsewhere} \end{cases}$$

(a) Determine the characteristic function $C_X(\omega)$. (b) Using $C_X(\omega)$, validate that $f_X(x)$ is a proper *pdf*. (c) Use $C_X(\omega)$ to determine the first two moments of X . (d) Calculate the variance of X .

13.21. Let $X(t)$ be a stationary random process, $E[X(t)] = 1$ and the autocorrelation $\mathfrak{R}_X(\tau) = 3 + \exp(-|\tau|)$. Define a new random variable

$$Y = \int_0^2 x(t) dt$$

Compute $E[Y(t)]$ and σ_Y^2 .

13.22. In Fig. 13.1, let

$$p(t) = \sum_{n=-\infty}^{\infty} A \operatorname{Rect}\left(\frac{t-nT}{\tau}\right)$$

Give an expression for $X_s(\omega)$.

13.23. Compute the Z-transform for

$$(a) x_1(n) = \frac{1}{n!}u(n); \quad (b) x_2(n) = \frac{1}{(-n)!}u(-n).$$

13.24. (a) Write an expression for the Fourier transform of

$$x(t) = \operatorname{Rect}(t/3)$$

(b) Assume that you want to compute the modulus of the Fourier transform using a DFT of size 512 with a sampling interval of 1 second. Evaluate the modulus at frequency $(80/512)Hz$. Compare your answer to the theoretical value and compute the error.

13.25. A certain band-limited signal has bandwidth $B = 20KHz$. Find the FFT size required so that the frequency resolution is $\Delta f = 50Hz$. Assume radix 2 FFT and record length of 1 second.

13.26. Assume that a certain sequence is determined by its FFT. If the record length is $2ms$ and the sampling frequency is $f_s = 10KHz$, find N .

Any signal other than the target returns in the radar receiver is considered as noise. This includes interfering signals from outside the radar and thermal noise generated within the receiver itself. Thermal noise (thermal agitation of electrons) and shot noise (variation in carrier density of a semiconductor) are the two main internal noise sources within a radar receiver.

The power spectral density of thermal noise is given by

$$S_n(\omega) = \frac{|\omega|h}{\pi \left[\exp\left(\frac{|\omega|h}{2\pi kT}\right) - 1 \right]} \quad (\text{A.1})$$

where $|\omega|$ is the absolute value of the frequency in radians per second, T is temperature of the conducting medium in degrees Kelvin, k is Boltzman's constant, and h is Plank's constant ($h = 6.625 \times 10^{-34}$ joule seconds). When the condition $|\omega| \ll 2\pi kT/h$ is true, it can be shown that Eq. (A.1) is approximated by

$$S_n(\omega) \approx 2kT \quad (\text{A.2})$$

This approximation is widely accepted, since, in practice, radar systems operate at frequencies less than 100 GHz; and, for example, if $T = 290K$, then $2\pi kT/h \approx 6000$ GHz.

The mean square noise voltage (noise power) generated across a 1 ohm resistance is then

$$\langle n^2 \rangle = \frac{1}{2\pi} \int_{-2\pi B}^{2\pi B} 2kT \, d\omega = 4kTB \quad (\text{A.3})$$

where B is the system bandwidth in hertz.

Any electrical system containing thermal noise and having input resistance R_{in} can be replaced by an equivalent noiseless system with a series combination of a noise equivalent voltage source and a noiseless input resistor R_{in} added at its input. This is illustrated in Fig. A.1.

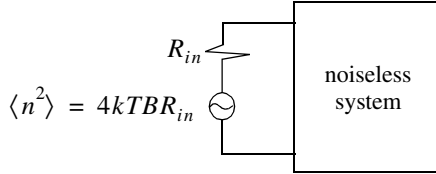


Figure A.1. Noiseless system with an input noise voltage source.

The amount of noise power that can physically be extracted from $\langle n^2 \rangle$ is one fourth the value computed in Eq. (A.3). The proof is left as an exercise.

Consider a noisy system with power gain A_p , as shown in Fig. A.2.

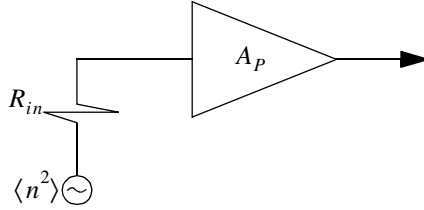


Figure A.2. Noisy amplifier replaced by its noiseless equivalent and an input voltage source in series with a resistor.

The noise figure is defined by

$$F_{dB} = 10 \log \frac{\text{total noise power out}}{\text{noise power out due to } R_{in} \text{ alone}} \quad (\text{A.4})$$

More precisely,

$$F_{dB} = 10 \log \frac{N_o}{N_i A_p} \quad (\text{A.5})$$

where N_o and N_i are, respectively, the noise power at the output and input of the system.

If we define the input and output signal power by S_i and S_o , respectively, then the power gain is

$$A_P = \frac{S_o}{S_i} \quad (\text{A.6})$$

It follows that

$$F_{dB} = 10 \log \left(\frac{S_i/N_i}{S_o/N_o} \right) = \left(\frac{S_i}{N_i} \right)_{dB} - \left(\frac{S_o}{N_o} \right)_{dB} \quad (\text{A.7})$$

where

$$\left(\frac{S_i}{N_i} \right)_{dB} > \left(\frac{S_o}{N_o} \right)_{dB} \quad (\text{A.8})$$

Thus, it can be said that the noise figure is the loss in the signal-to-noise ratio due to the added thermal noise of the amplifier ($(SNR)_o = (SNR)_i - F$ in dB).

We can also express the noise figure in terms of the system's effective temperature T_e . Consider the amplifier shown in Fig. A.2, and let its effective temperature be T_e . Assume the input noise temperature is T_o . Thus, the input noise power is

$$N_i = kT_o B \quad (\text{A.9})$$

and the output noise power is

$$N_o = kT_o B A_p + kT_e B A_p \quad (\text{A.10})$$

where the first term on the right-hand side of Eq. (A.10) corresponds to the input noise, and the latter term is due to thermal noise generated inside the system. It follows that the noise figure can be expressed as

$$F = \frac{(SNR)_i}{(SNR)_o} = \frac{S_i}{kT_o B} \frac{1}{kBA_p} \frac{T_o + T_e}{S_o} = 1 + \frac{T_e}{T_o} \quad (\text{A.11})$$

Equivalently, we can write

$$T_e = (F - 1)T_o \quad (\text{A.12})$$

Example A.1: An amplifier has a 4dB noise figure; the bandwidth is $B = 500$ KHz. Calculate the input signal power that yields a unity SNR at the output. Assume $T_o = 290$ degree Kelvin and an input resistance of one ohm.

Solution: The input noise power is

$$kT_oB = 1.38 \times 10^{-23} \times 290 \times 500 \times 10^3 = 2.0 \times 10^{-15} \text{ w}$$

Assuming a voltage signal, then the input noise mean squared voltage is

$$\langle n_i^2 \rangle = kT_oB = 2.0 \times 10^{-15} \text{ v}^2$$

$$F = 10^{0.4} = 2.51$$

From the noise figure definition we get

$$\frac{S_i}{N_i} = F \left(\frac{S_o}{N_o} \right) = F$$

and

$$\langle s_i^2 \rangle = F \langle n_i^2 \rangle = 2.51 \times 2.0 \times 10^{-15} = 5.02 \times 10^{-15} \text{ v}^2$$

Finally,

$$\sqrt{\langle s_i^2 \rangle} = 70.852 \text{ nV}$$

Consider a cascaded system as in Fig. A.3. Network 1 is defined by noise figure F_1 , power gain G_1 , bandwidth B , and temperature T_{e1} . Similarly, network 2 is defined by F_2 , G_2 , B , and T_{e2} . Assume the input noise has temperature T_0 .

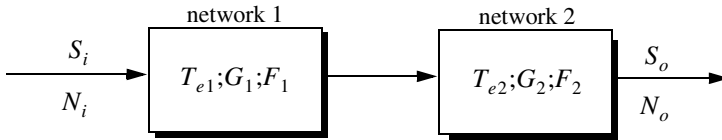


Figure A.3. Cascaded linear system.

The output signal power is

$$S_o = S_i G_1 G_2 \tag{A.13}$$

The input and output noise powers are, respectively, given by

$$N_i = kT_oB \tag{A.14}$$

$$N_o = kT_0BG_1G_2 + kT_{e1}BG_1G_2 + kT_{e2}BG_2 \quad (\text{A.15})$$

where the three terms on the right-hand side of Eq. (A.15), respectively, correspond to the input noise power, thermal noise generated inside network 1, and thermal noise generated inside network 2.

Now if we use the relation $T_e = (F - 1)T_0$ along with Eq. (A.13) and Eq. (A.14), we can express the overall output noise power as

$$N_o = F_1N_iG_1G_2 + (F_2 - 1)NiG_2 \quad (\text{A.16})$$

It follows that the overall noise figure for the cascaded system is

$$F = \frac{(S_i/N_i)}{(S_o/N_o)} = F_1 + \frac{F_2 - 1}{G_1} \quad (\text{A.17})$$

In general, for an n-stage system we get

$$F = F_1 + \frac{F_2 - 1}{G_1} + \frac{F_3 - 1}{G_1G_2} + \dots + \frac{F_n - 1}{G_1G_2G_3 \dots G_{n-1}} \quad (\text{A.18})$$

Also, the n-stage system effective temperatures can be computed as

$$T_e = T_{e1} + \frac{T_{e2}}{G_1} + \frac{T_{e3}}{G_1G_2} + \dots + \frac{T_{en}}{G_1G_2G_3 \dots G_{n-1}} \quad (\text{A.19})$$

As suggested by Eq. (A.18) and Eq. (A.19), the overall noise figure is mainly dominated by the first stage. Thus, radar receivers employ low noise power amplifiers in the first stage in order to minimize the overall receiver noise figure. However, for radar systems that are built for low RCS operations every stage should be included in the analysis.

Example A.2: A radar receiver consists of an antenna with cable loss $L = 1\text{dB} = F_1$, an RF amplifier with $F_2 = 6\text{dB}$, and gain $G_2 = 20\text{dB}$, followed by a mixer whose noise figure is $F_3 = 10\text{dB}$ and conversion loss $L = 8\text{dB}$, and finally, an integrated circuit IF amplifier with $F_4 = 6\text{dB}$ and gain $G_4 = 60\text{dB}$. Find the overall noise figure.

Solution:

From Eq. (A.18) we have

$$F = F_1 + \frac{F_2 - 1}{G_1} + \frac{F_3 - 1}{G_1G_2} + \frac{F_4 - 1}{G_1G_2G_3}$$

G_1	G_2	G_3	G_4	F_1	F_2	F_3	F_4
$-1dB$	$20dB$	$-8dB$	$60dB$	$1dB$	$6dB$	$10dB$	$6dB$
0.7943	100	0.1585	10^6	1.2589	3.9811	10	3.9811

It follows that

$$F = 1.2589 + \frac{3.9811 - 1}{0.7943} + \frac{10 - 1}{100 \times 0.7943} + \frac{3.9811 - 1}{0.158 \times 1000.7943} = 5.3628$$

$$F = 10\log(5.3628) = 7.294dB$$

Problems

A. 1. A source with equivalent temperature $T_e = 500K$ is followed by three amplifiers with specifications shown in the table below.

Amplifier	F, dB	G, dB	T_e
1	You must compute	12	350
2	10	22	
3	15	35	

Assume a bandwidth of $150KHz$. (a) Compute the noise figure for the three cascaded amplifiers. (b) Compute the effective temperature for the three cascaded amplifiers. (c) Compute the overall system noise figure.

A. 2. Derive Eq. (A.19).

The decibel, often called dB, is widely used in radar system analysis and design. It is a way of representing the radar parameters and relevant quantities in terms of logarithms. The unit dB is named after Alexander Graham Bell, who originated the unit as a measure of power attenuation in telephone lines. By Bell's definition, a unit of Bell gain is

$$\log\left(\frac{P_0}{P_i}\right) \quad (\text{B.1})$$

where the logarithm operation is base 10, P_0 is the output power of a standard telephone line (almost one mile long), and P_i is the input power to the line. If voltage (or current) ratios were used instead of the power ratio, then a unit Bell gain is defined as

$$\log\left(\frac{V_0}{V_i}\right)^2 \quad \text{or} \quad \log\left(\frac{I_0}{I_i}\right)^2 \quad (\text{B.2})$$

A decibel, dB, is 1/10 of a Bell (the prefix "deci" means 10^{-1}). It follows that a dB is defined as

$$10\log\left(\frac{P_0}{P_i}\right) = 10\log\left(\frac{V_0}{V_i}\right)^2 = 10\log\left(\frac{I_0}{I_i}\right)^2 \quad (\text{B.3})$$

The inverse dB is computed from the relations

$$\begin{aligned} P_0/P_i &= 10^{dB/10} \\ V_0/V_i &= 10^{dB/20} \\ I_0/I_i &= 10^{dB/20} \end{aligned} \quad (\text{B.4})$$

Decibels are widely used by radar designers and users for several reasons. Perhaps the most important of them all is that utilizing dBs drastically reduces the dynamic range that a designer or a user has to use. For example, an incoming radar signal may be as weak as $0.000000001 V$, which can be expressed in dBs as $10\log(0.000000001) = -90dB$. Alternatively, a target may be located at range $R = 1000000m = 1000Km$ which can be expressed in dBs as $60dB$.

Another advantage of using dB in radar analysis is to facilitate the arithmetic associated with calculating the different radar parameters. The reason for this is the following: when using logarithms, multiplication of two numbers is equivalent to adding their corresponding dBs, and their division is equivalent to subtraction of dBs. For example,

$$\frac{250 \times 0.0001}{455} = \tag{B.5}$$

$$[10\log(250) + 10\log(0.0001) - 10\log(455)]dB = -42.6dB$$

In general,

$$10\log\left(\frac{A \times B}{C}\right) = 10\log A + 10\log B - 10\log C \tag{B.6}$$

$$10\log A^q = q \times 10\log A \tag{B.7}$$

Other dB ratios that are often used in radar analysis include the dBsm (dB - squared meters). This definition is very important when referring to target RCS, whose units are in squared meters. More precisely, a target whose RCS is σm^2 can be expressed in dBsm as $10\log(\sigma m^2)$. For example, a $10m^2$ target is often referred to as $10dBsm$ target, and a target with RCS $0.01m^2$ is equivalent to a $-20dBsm$.

Finally, the units dBm and dBW are power ratios of dBs with reference to one milliwatt and one Watt, respectively.

$$dBm = 10\log\left(\frac{P}{1mW}\right) \tag{B.8}$$

$$dBW = 10\log\left(\frac{P}{1W}\right) \tag{B.9}$$

To find dBm from dBW, add 30 dB, and to find dBW from dBm, subtract 30 dB.

Appendix C

***Fourier Transform
Table***

$x(t)$	$X(\omega)$
$A \text{Rect}(t/\tau)$; rectangular pulse	$A\tau \text{Sinc}(\omega\tau/2)$
$A\Delta(t/\tau)$; triangular pulse	$A\frac{\tau}{2} \text{Sinc}^2(\tau\omega/4)$
$\frac{1}{\sqrt{2\pi}\sigma} \exp\left(-\frac{t^2}{2\sigma^2}\right)$; Gaussian pulse	$\exp\left(-\frac{\sigma^2\omega^2}{2}\right)$
$e^{-at} u(t)$	$1/(a + j\omega)$
$e^{-a t }$	$\frac{2a}{a^2 + \omega^2}$
$e^{-at} \sin\omega_0 t u(t)$	$\frac{\omega_0}{\omega_0^2 + (a + j\omega)^2}$
$e^{-at} \cos\omega_0 t u(t)$	$\frac{a + j\omega}{\omega_0^2 + (a + j\omega)^2}$
$\delta(t)$	1
1	$2\pi\delta(\omega)$
$u(t)$	$\pi\delta(\omega) + \frac{1}{j\omega}$
$\text{sgn}(t)$	$\frac{2}{j\omega}$

$x(t)$	$X(\omega)$
$\cos \omega_0 t$	$\pi[\delta(\omega - \omega_0) + \delta(\omega + \omega_0)]$
$\sin \omega_0 t$	$j\pi[\delta(\omega + \omega_0) - \delta(\omega - \omega_0)]$
$u(t) \cos \omega_0 t$	$\frac{\pi}{2}[\delta(\omega - \omega_0) + \delta(\omega + \omega_0)] + \frac{j\omega}{\omega_0^2 - \omega^2}$
$u(t) \sin \omega_0 t$	$\frac{\pi}{2j}[\delta(\omega + \omega_0) - \delta(\omega - \omega_0)] + \frac{\omega_0}{\omega_0^2 - \omega^2}$
$ t $	$\frac{-2}{\omega^2}$

Appendix D***Some Common
Probability Densities***

Chi-Square with N degrees of freedom

$$f_X(x) = \frac{x^{(N/2)-1}}{2^{N/2}\Gamma(N/2)} \exp\left\{\frac{-x}{2}\right\} ; x > 0$$

$$\bar{X} = N ; \sigma_X^2 = 2N$$

$$\text{gamma function} = \Gamma(z) = \int_0^{\infty} \lambda^{z-1} e^{-\lambda} d\lambda ; \text{Re}\{z\} > 0$$

Exponential

$$(f_X(x) = a \exp\{-ax\}) ; x > 0$$

$$\bar{X} = \frac{1}{a} ; \sigma_X^2 = \frac{1}{a^2}$$

Gaussian

$$f_X(x) = \frac{1}{\sqrt{2\pi}\sigma} \exp\left\{-\frac{1}{2}\left(\frac{x-x_m}{\sigma}\right)^2\right\} ; \bar{X} = x_m ; \sigma_X^2 = \sigma^2$$

Laplace

$$f_X(x) = \frac{\sigma}{2} \exp\{-\sigma|x-x_m|\}$$

$$\bar{X} = x_m ; \sigma_X^2 = \frac{2}{\sigma^2}$$

Log-Normal

$$f_X(x) = \frac{1}{x\sigma\sqrt{2\pi}} \exp\left(-\frac{(\ln x - \ln x_m)^2}{2\sigma^2}\right) ; x > 0$$

$$\bar{X} = \exp\left\{\ln x_m + \frac{\sigma^2}{2}\right\} ; \sigma_X^2 = [\exp\{2\ln x_m + \sigma^2\}][\exp\{\sigma^2\} - 1]$$

Rayleigh

$$f_X(x) = \frac{x}{\sigma^2} \exp\left\{-\frac{x^2}{2\sigma^2}\right\} ; x \geq 0$$

$$\bar{X} = \sqrt{\frac{\pi}{2}} \sigma ; \sigma_X^2 = \frac{\sigma^2}{2}(4 - \pi)$$

Uniform

$$f_X(x) = \frac{1}{b-a} ; a < b ; \bar{X} = \frac{a+b}{2} ; \sigma_X^2 = \frac{(b-a)^2}{12}$$

Weibull

$$f_X(x) = \frac{bx^{b-1}}{\bar{\sigma}_0} \exp\left(-\frac{(x)^b}{\bar{\sigma}_0}\right) ; (x, b, \bar{\sigma}_0) \geq 0$$

$$\bar{X} = \frac{\Gamma(1+b^{-1})}{1/(b\sqrt{\bar{\sigma}_0})} ; \sigma_X^2 = \frac{\Gamma(1+2b^{-1}) - [\Gamma(1+b^{-1})]^2}{1/[b\sqrt{(\bar{\sigma}_0)^2}]}$$

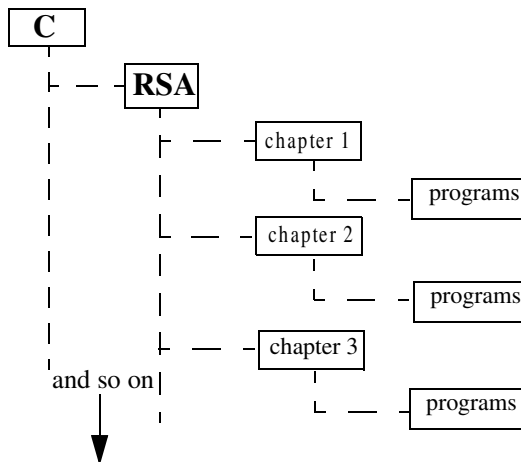
Appendix E
Z - Transform Table

$x(n); n \geq 0$	$X(z)$	ROC; $z > R$
$\delta(n)$	1	0
1	$\frac{z}{z-1}$	1
n	$\frac{z}{(z-1)^2}$	1
n^2	$\frac{z(z+1)}{(z-1)^3}$	1
a^n	$\frac{z}{z-a}$	$ a $
na^n	$\frac{az}{(z-a)^2}$	$ a $
$\frac{a^n}{n!}$	$e^{a/z}$	0
$(n+1)a^n$	$\frac{z^2}{(z-a)^2}$	$ a $
$\sin n\omega T$	$\frac{z \sin \omega T}{z^2 - 2z \cos \omega T + 1}$	1
$\cos n\omega T$	$\frac{z(z - \cos \omega T)}{z^2 - 2z \cos \omega T + 1}$	1

$x(n); n \geq 0$	$X(z)$	ROC; $z > R$
$a^n \sin n\omega T$	$\frac{az \sin \omega T}{z^2 - 2az \cos \omega T + a^2}$	$\frac{1}{ a }$
$a^n \cos n\omega T$	$\frac{z(z - a^2 \cos \omega T)}{z^2 - 2az \cos \omega T + a^2}$	$\frac{1}{ a }$
$\frac{n(n-1)}{2!}$	$\frac{z}{(z-1)^3}$	1
$\frac{n(n-1)(n-2)}{3!}$	$\frac{z}{(z-1)^4}$	1
$\frac{(n+1)(n+2)a^n}{2!}$	$\frac{z^3}{(z-a)^3}$	$ a $
$\frac{(n+1)(n+2)\dots(n+m)a^n}{m!}$	$\frac{z^{m+1}}{(z-a)^{m+1}}$	$ a $

Appendix F***MATLAB Program
and Function Name
List***

A MATLAB program and function¹ name list is provided in this appendix on a per-chapter basis. Programs and functions that have associated MATLAB GUI are identified. All these programs and functions can be downloaded from CRC Press Web site (www.crcpress.com). For this purpose, create the following directory in your C-drive: C:\RSA. Copy all programs into this directory. The path tree should be as shown in Fig. F.1. Users can execute a certain function / program GUI by typing: *file_name_driver*, where file names are as indicated in the left columns of the tables listed in this appendix.

**Figure F.1. Path tree.**

1. All MATLAB programs and functions provided in this book were developed using MATLAB 5.0 - R11 with the Signal Processing Toolbox, on a PC with Windows 98 operating system.

Chapter 1:

Name	Purpose
pulse_train	compute duty cycle, average power, pulse energy
range_resolution	compute range resolution
doppler_frequency	compute Doppler frequency
radar_equation	implement the radar equation - with GUI
lprf_req	implement the LPRF radar equation - with GUI
hprf_req	implement the HPRF radar equation - with GUI
power_aperture	implement the surveillance radar equation - with GUI
ssj_req	implement self-screening jammer radar equation - with GUI
soj_req	implement the stand-off jammer radar equation - with GUI
range_red_fac	compute and plot the range reduction factor associated with ECM - with GUI

Chapter 2:

Name	Purpose (all functions have associated GUI)
rsc_aspect	compute and plot RCS dependency on aspect angle
rsc_frequency	compute and plot RCS dependency on frequency
rsc_sphere	compute and plot RCS of a sphere
rsc_ellipsoid	compute and plot RCS of an ellipsoid
rsc_circ_plate	compute and plot RCS of a circular flat plate
rsc_frustum	compute and plot RCS of a truncated cone
rsc_cylinder	compute and plot RCS of a cylinder
rsc_rect_plate	compute and plot RCS of a rectangular flat plate
rsc_isoceles	compute and plot RCS of a triangular flat plate
rsc_cylinder_complex	reproduce Fig. 2.22
swerlin_models	reproduce Fig. 2.24

Chapter 3:

Name	Purpose
range_calc	perform radar range equation calculation - with MATLAB-based GUI

Chapter 4:

Name	Purpose
marcumsg	compute and plot single pulse probability of detection versus SNR
improv_fac	compute and plot non-coherent integration improvement factor
incomplete_gamma	compute and plot Incomplete Gamma function
threshold	compute appropriate threshold for probability of detection calculation
pd_swerling5	compute and plot probability of detection for Swerling 5 targets
pd_swerling1	compute and plot probability of detection for Swerling 1 targets
pd_swerling2	compute and plot probability of detection for Swerling 2 targets
pd_swerling3	compute and plot probability of detection for Swerling 3 targets
pd_swerling4	compute and plot probability of detection for Swerling 4 targets

Chapter 5:

Name	Purpose
fresnel	compute and plot Fresnel functions
hrr_profile	compute and plot High Range Resolution Profiles associated with Stepped Frequency waveforms

Chapter 6:

Name	Purpose
single_pulse_ambg	compute and plot single ambiguity function
fig6_3	reproduce Fig. 6.3
fig6_5	reproduce Fig. 6.5
lfm_ambg	compute and plot LFM ambiguity function, with GUI
fig6_6	reproduce Fig. 6.6
fig6_7	reproduce Fig. 6.7
train_ambg	compute and plot ambiguity function for a coherent pulse train
fig6-9a	reproduce Fig. 6.9a

Chapter 7:

Name	Purpose
matched_filter	Compute and plot compressed output from a matched filter
stretch	implements stretch pulse compression
fig7_10	reproduce Fig. 7.10

Chapter 8:

Name	Purpose
ref_coef	compute and plot reflection coefficient - vertical and horizontal

Chapter 9:

Name	Purpose
single_canceler	plot output from a single delay line canceler
double_canceler	plot output from a double delay line canceler
fig9_15	reproduce Fig. 9.15
fig9_16	reproduce Fig. 9.16
fig9_17	reproduce Fig. 9.17

Chapter 10:

Name	Purpose
circ_aperture	compute and plot antenna radiation pattern for a circular aperture, including 3-D
fig10_5	reproduce Fig. 10.5
fig10_10	reproduce Fig. 10.10
linear_array	compute and plot radiation pattern for a linear phased array
rect_array	compute and plot radiation pattern for a rectangular array

Chapter 11:

Name	Purpose
mono_pulse	compute and plot sum and difference patterns for monopulse antenna
ghk_tracker	implement ghk 3-state tracker
fig11_21	reproduce Fig. 11.21
kalaman_filter	implement a 3-state Kalman filter
fig11_28	reproduce Fig. 11.28

Chapter 12:

Name	Purpose
fig12_2	reproduce Fig. 12.2